Investigating disease mechanisms in autosomal dominant optic atrophy with retinal ganglion cells derived from induced pluripotent stem cells

Paul Edward Sladen

Thesis submitted for the degree of

Doctor of Philosophy

January 2021

UCL Institute of Ophthalmology

Faculty of Brain Sciences

University College London

Declaration

I, Paul Edward Sladen, confirm that the work presented in this thesis is my own. Where information has been derived from other sources, I confirm that this has been indicated in the thesis.

Acknowledgments

Firstly, I would like to thank my primary supervisor Professor Mike Cheetham for his supervisory advice, support and scientific expertise. Thank you for giving me the opportunity to explore a fantastic topic and allowing me to work within your research group. Also, thanks for providing me the experimental freedom to investigate and explore new and exciting topics. I am grateful for the time you have dedicated throughout my PhD and for your invaluable scientific input into this project.

Next, I would like to say thank you to my secondary supervisor, Dr Patrick Yu-Wai-Man. I am greatly thankful for your supervision; your enthusiasm and passion for the project has been infectious. We have not had nearly enough time to fully investigate half of the ideas we have had, hopefully this partnership will continue to blossom and we can finally tick off the long list of ideas. Again, thank you for introducing me to and providing me the opportunity to explore such a fantastic, complex topic that has become my passion.

I would also like to say thank you to Professor Alison Hardcastle, Dr Jacqui Van Der Spuy and Dr Alice Davidson for your contributions to this work throughout our weekly research update sessions. Having three extra pairs of eyes to scrutinise and question my work was excellent for my development and instrumental in driving this work forward.

Thank you to Naheed Kanuga, my PhD would not have been conceivable without your tireless support. Your ability to problem solve and fix lab issues as they arise made my PhD run as smoothly as possible. Thank you for always being there to deal with my lab demands, for managing the PhD finances, and for placing my endless orders.

I would also like to thank current and previous members of the Cheetham-Hardcastle group. Firstly, thanks to Christina Zarouchlioti, my PhD buddy. It's been great to have you alongside me this whole time to share the trials, tribulations, laughs and scientific revolutions we have both experienced. It has been a tough four years, but we've made it, and I'm incredibly proud of what we've achieved. To Katarina Jovanovic, thank you for being a great scientist, a great trouble shooter, a great friend and for allowing me to ask all the "dumb" questions. You have taught me a great deal; half this PhD would not exist without your help. Thanks must also go to Pedro Perdigao, the CRISPR expert. I learnt an incredible amount from you in such a short time, I wouldn't have completed the CRISPR work without you. Finally, thanks to the rest of the Cheetham-Hardcastle lab: Dr Amelia Lane, Dr Monica Aguila, Dr David Parfitt, Dr Daniele Ottaviani, Dr Kwan Hau, Dr Rosellina Guarascio, Dr Alessia Fiorentino, Dr Almudena Sacristan Reviriego, Dr Jim Bellingham, Dr Dimitra Athanasiou, Dr Jessica Gardner, Nathan Hafford Tear, Kelly Ziaka, Owen Fernando, and Amanda Sadan. I was incredibly lucky to find a lab with such

a brilliant group of scientists and have formed great friendships with many of you, thanks for all the beers in the pubs, help in the lab and laughs in the office.

I'd also like to thank Professor Paul Chapple for providing the opportunity to utilise the Seahorse machine at QMUL. In addition, thank you to the Chapple lab: Grace, Lisa and Tatiana for assisting me whenever I wanted to visit and run experiments. Thank you for your time and sorry for all the inconvenience I caused you.

Many thanks to Moorfields Eye Charity for providing my PhD funding. I'm very grateful to the generous donors and supporters of Moorfields Eye Charity for giving me the opportunity to pursue the research I love. The foundation for this work was tissue and cells generously donated from patients who have experienced the debilitating effects of DOA. I'd like to thank these people for their invaluable donations and hope that the research performed using their priceless gifts will one day help in developing treatments for the entire DOA community.

In addition, I extend thanks and love to all of my close friends from St Barts and Bath University for helping me to enjoy life outside of the lab. Especially thanks to Ben, Tim, Hector and Sarah who have had to live with me through these 4 challenging years. It has been a pleasure to live with you all, thanks for the chats, the beers and the memories.

To Bea, thank you for your never-ending support. The last four years have been a rollercoaster of highs and lows and you have been there every step of the way. You have been a ceaseless reassuring presence and constantly picked me up when times were tough. It has been a great joy to share this journey with you, and I can't thank you enough for providing me with kindness, love, laughter and happiness. Thank you.

Finally, I thank my fantastic family. First; Mum and Dad. Your support for me throughout this time has been immeasurable, I would not have made it this far through the education system without your generous love and encouragement. I appreciate everything you do for us. To my siblings; Joe and Liz, thanks for all the help you have given me and the reassurances when times were tough. You have both paved the way for me in life, constantly setting high targets and I wouldn't have made it this far without you. And to Tim and Claire, thanks for being part of our family, thanks for the support and the laughs even when we get a little weird at times. Gran, thank you for our light-hearted, walking-home chats, with offers to write my thesis. They allowed me to clear my head and put science aside for a short time. Thank you to all of you for everything over the past 4 years, this PhD would not have been possible without the lot of you.

Abstract

Dominant Optic Atrophy (DOA) is the most common inherited optic neuropathy in the UK, characterised by the preferential loss of retinal ganglion cells (RGCs) and progressive blindness. 60-70 % of DOA patients harbour mutations in the *OPA1* gene, encoding a mitochondrial protein that regulates mitochondrial morphology, bioenergetics and mitochondrial DNA (mtDNA) quality. Currently, DOA has no therapeutic options and the mechanisms driving RGC degeneration are poorly understood.

In this study, a biobank of induced pluripotent stem cells iPSCs (iPSCs) encompassing the clinical and genetic DOA spectrum was created using patient-derived *OPA1* mutant fibroblast cell lines, and CRISPR/Cas9 gene editing to generate isogenic cell lines. RGC differentiation was optimized and characterised in 2D and 3D *in vitro* methods, demonstrating expression of RGC-associated genes including *BRN3B* and *ISL1. OPA1* mutant iPSCs showed no differentiation deficit compared to wild-type control cell lines, exhibiting comparable expression of all relevant markers. 2D-RGCs demonstrated enrichment of neuronal associated markers, including *ELAVL3* and *TAU*, when compared to 3D retinal organoids. Phenotypic analysis demonstrated significant deficits in respiration, ATP production and increased mtDNA mutation in fibroblasts, iPSCs and 2D-RGCs compared to isogenic controls. Characterisation of mitochondrial stress through induction of stress associated gene expression demonstrated significant levels of upregulation in iPSCs, however, 3D- and 2D-RGCs exhibited fewer upregulated genes indicating that mitochondrial stress may be a cell type specific response. Importantly, correction of patient-derived iPSCs restored mitochondrial homeostasis, demonstrating that restoration of WT *OPA1* expression is able to mitigate mutant associated phenotypes.

Thus, an *OPA1* mutant iPSC biobank has been established encompassing the clinical disease spectrum, enabling effective *in vitro* modelling to establish RGC specific disease mechanisms. *OPA1* mutant RGCs demonstrate significant reductions in mitochondrial homeostasis, including reduced bioenergetic output and mtDNA quality. This work provides a platform for further investigation of *OPA1*-mediated disease mechanisms and therapeutic design.

Impact statement

Autosomal Dominant Optic Atrophy (DOA) is currently incurable. DOA results in the debilitating bilateral loss of sight by the 5th decade of life and is characterised by the preferential degeneration of retinal ganglion cells (RGCs) and the optic nerve. Prevalence estimates suggest that DOA effects between 1:10,000 and 1:50,000 people, making DOA the most common inherited optic neuropathy globally. Although approximately 60 % of DOA patients have mutations within the *OPA1* gene, an association identified over 2 decades ago, there are currently no treatments available that therefore places an unpreventable social and economic burden on both patients and communities. Current understanding of OPA1 function is mainly based on models that do not accurately represent the RGC morphological or functional niche. Therefore, the work in this thesis focused on increasing understanding of the primary pathological hallmark of DOA, RGC loss, by developing *in vitro* models of human RGCs to investigate OPA1 dysfunction disease mechanisms.

Initially, this study focused on the development of a comprehensive biobank of *OPA1* mutant iPSCs encompassing the range of clinical and genetic mutations associated with DOA, providing a near unlimited source of research material to facilitate the understanding of pathogenic disease mechanisms. Importantly, this work also generated isogenic mutant and wild-type cell lines using CRISPR/Cas9 gene editing technology that provide two clear benefits, enabling the specific study of *OPA1* mutations by removing genetic heterogeneity and providing a clear rescued phenotype for the direct comparison of therapeutics on mutant cell lines. Dissemination of this biobank to other research groups and collaborators will enable a greater depth of research into the impact *OPA1* mutation has on RGC biology and the disease mechanisms associated with DOA.

Complementing the biobank, this study also established the feasibility of understanding DOA through *in vitro* disease modelling, providing a clear demonstration of the knowledge that can be garnered from context specific modelling. Developing improved models of RGC biology is key to understanding why the retina is preferentially affected in DOA, whilst also being applicable to a wide-range of non-genetic, age related conditions. In addition to DOA, RGC health is severely affected in glaucoma, an incurable disease with typically sporadic onset that is predicted to globally affect approximately 110 million individuals by 2040. It is therefore hoped that this model may have benefits for those in both the academic and commercial world over a broad range of diseases, by providing a rapid, human-specific modelling resource to reduce the dependence on animal modelling and facilitate greater understanding of novel treatments through increased screening capacity.

To summarise, the work presented within this thesis develops our understanding of the disease mechanisms in DOA, the most common inherited optic neuropathy. The development of this OPA1 iPSC biobank, in collaboration with the developed methodology and disease characterisation will enable the future development of therapeutic strategies to reduce the burden on patients and public health systems.

Contents

List of figures

List of tables

Abbreviations

1334G>A – patient iPSCs carrying *OPA1* c.1334G>A mutation

1334>WT1 – patient iPSCs corrected with CRISPR/Cas9, line 1

1334>WT2 – patient iPSCs corrected with CRISPR/Cas9, line 2

2708del – patient iPSCs carrying *OPA1* c.2708delTTAG mutation

2D – two dimensional

2D-RGCs – retinal ganglion cells generated through 2D cultures

3D – three dimensional

A/A – antibiotic, antimycotic

AAV – Adeno-Associated Virus

acetyl-CoA – acetyl-coenzyme A

AD – Alzheimer's disease

ADP – adenosine diphosphate

ALS – Amyotrophic lateral sclerosis

ATP – adenosine tri-phosphate

BCA – bicinchoninic acid

bp – base pair

BSA – bovine serum albumin

Ca^{2+} – calcium

Cas9 – CRISPR associated protein 9

cDNA – complementary deoxyribonucleic acid

CJ – cristae junction

CM – cristae membrane

CRISPR – Clustered regularly interspaced short palindromic repeats

CRISPRa – CRISPR activation

CRISPRi – CRISPR interference

crRNA – CRISPR-RNA

Ct – cycle threshold value

D - day

DAPI – 4’,6-diamidino-2-phenylindole dilactate

ddH_2O – double-distilled water

D-loop – displacement loop

DMEM – Dulbecco’s Modified Eagle Medium

DMSO – dimethyl sulfoxide

DNA – deoxyribonucleic acid

dNTP – deoxynucleotide

DOA – dominant optic atrophy

DOA+ – dominant optic atrophy plus

DPBS – Dulbeccos phosphate buffered saline

dsDNA – double strand DNA

dsRGC - direction selective RGCs

E8F – essential 8 flex

EB – embryoid body

ECAR – Extracellular acidification rate

EFTF – eye field transcription factor

ESCs – embryonic stem cells

ETC – electron transport chain

FBS – foetal bovine serum

FCCP – carbonyl cyanide p-triflouromethoxyphenylhydrazone

fcut – fraction of cleaved PCR product

$FADH_2$ – flavin adenine dinucleotide

GCL – ganglion cell layer

gDNA – genomic DNA

GED - GTPase effector domain

gRNA – guide ribonucleic acid

H^+ – hydrogen ions

HDR – homology directed repair

HDRe – HDR enhancer

HDFn – human dermal fibroblasts, neonatal origin

hESC – human ESC

HRP – horseradish peroxidase

HSP7 – hereditary spastic paraplegia type 7

IBM – IMM boundary membrane

ICC – immunocytochemistry

ICL – inner cell layer

IHC – immunohistochemistry

IF – immunofluorescence

InDel – Insertion or deletion

IOP – intraocular pressure

iPSCs – induced pluripotent stem cells

ipRGC – Intrinsically photosensitive retinal ganglion cell

ISR – integrated stress response

K^+ - potassium ions

kb – kilobase

kDa – kilodalton

LCA – Leber Congenital Amaurosis

LGN – lateral geniculate nucleus

LHON – Leber hereditary optic neuropathy

L-OPA1 – OPA1 long isoform

LR-PCR – long range-PCR

MACS – magnetic-activated cell sorting

MEFs – mouse embryonic fibroblasts

MELAS – Mitochondrial encephalomyopathy, lactic acidosis, and stroke-like episodes

MiNa – mitochondrial network analysis

miRNA – microRNA

Mito-stress – mitochondrial stress

MPP – mitochondrial processing peptidase

mRNA – messenger ribonucleic acid

MRPs – mitochondrial ribosomal proteins

MS – multiple sclerosis

mtDNA – mitochondria DNA

MTS – mitochondrial targeting sequence

Na^+ - sodium ions

NADH – nicotinamide adenine dinucleotide

nDNA – nuclear DNA

NEAA – non-essential amino acids

NGS – next generation sequencing

NHEJ – non-homologous end joining

NIM – neural induction media

NMD – nonsense mediated decay

NPCs – neural precursor cells

nt – nucleotides

NTG – normal tension glaucoma

OCL – outer cell layer

OCR – Oxygen consumption rate

O.C.T – Optimal Cutting Temperature compound

OPA1+/- iPSCs – CRISPR/Cas9 edited, heterozygous OPA1 knockout iPSCs

$Opa1^{Q285STOP}$ – mice harbouring an *Opa1* c.1051C>T/p.(Q285STOP) mutation

Opa1^{delTTAG} – mice harbouring a human *Opa1* c.2708_2711delTTAG mutation

OVs – optic vesicle

OXPHOS – oxidative phosphorylation

PAM – protospacer adjacent motif

PBMCs – peripheral blood mononuclear cells

PBS – phosphate buffered saline

PBS-T - phosphate buffered saline with Tween 20

PCR – polymerase chain reaction

PD – Parkinson's disease

PFA – paraformaldehyde

PH domain – pleckstrin-homology domain

PIC – proteinase inhibitor cocktail

PMT – mitochondrial permeability transition

POAG – primary open angle glaucoma

P/S – penicillin and streptomycin

PTC – premature termination codon

qPCR – quantitative polymerase chain reaction

RDM – retinal differentiation media

RGCs – retinal ganglion cells

rhLaminin – recombinant human laminin

RIPA – radioimmunoprecipitation assay buffer

RMM – retina maturation media

RNA – ribonucleic acid

RNAi – RNA interference

RNase – ribonuclease

RNA-seq – RNA-sequencing

RNFL – retinal nerve fibre layer

RNP – ribonucleoprotein

ROCKi – ROCK inhibitor

ROS – reactive oxygen species

RPE – retinal pigmented epithelium

RPC – retinal precursor cell

RT – room temperature

RT-PCR – reverse transcriptase polymerase chain reaction

SEM – standard error of mean

SFEBq – serum-free floating culture of embryoid-body-like aggregates with quick reaggregation

shh – sonic hedgehog

ssDNA – single stranded deoxyribonucleic acid

siRNA – small interfering RNA

SNPs – single nucleotide polymorphisms

ssODN – single stranded oligodeoxynucleotide

S-OPA1 – OPA1 short isoform

TCA – the tricarboxylic acid cycle

tRNA – transfer RNA

v/v – volume by volume

WT – wild type

w/v – weight by volume

XLRP – X-linked retinitis pigmentosa

Chapter 1: Introduction

The vertebrate eye is a complex, multi-tissue organ that enables the perception of light and is believed to have evolved over 500 million years ago (Lamb *et al.* 2007). Today, vision is our most precious sense, integral to modern human life to facilitate the interactions that generate our intricate societies. However, within the UK, vision loss and blindness effects approximately 2 million people (Bosanquet and Mehta 2009), placing an unpreventable socioeconomic burden on both patients and their communities. Approximately half of all UK sight loss has an insidious onset, believed to have a preventable or treatable cause (Bosanquet *et al.* 2009). However, inherited ocular disorders are now believed to be the leading cause of visual impairment or sight loss in the working age population within the UK (Liew *et al.* 2014), whilst in developed countries approximately half of all childhood visual impairment or blindness is believed to have a genetic origin (Gillespie *et al.* 2014). Crucially, the genetic revolution has enabled rapid, cost effective genetic sequencing of visually impaired or blind patients to illuminate the mutational landscape of inherited eye diseases.

Principally, the eye is separated into three distinct layers that function synergistically in visual perception whilst also maintaining the structure, function and health of the eye. The outer fibrous region of the eye is composed of the sclera and the optically clear cornea (Figure 1.1), these two tissues primarily function to maintain the eye's shape whilst providing protection from internal and external forces. In addition, the cornea provides two thirds of the eye's refractive power, beginning the process of focusing light onto the retina. The middle vascular layer is composed of the iris, the ciliary body and the choroid (Figure 1.1), which regulate the size of the pupil, the shape of the lens and contain vasculature required for providing oxygen and nutrients to the retinal layers, respectively. Importantly, the middle layer further fine tunes the light refracted by the cornea, the iris regulates the levels of light entering the eye whilst the ciliary body suspends the lens, a crystalline epithelial tissue that further focuses light onto the retina. The inner most layer is composed solely of the retina, a complex layered neuronal tissue that captures and processes light (Figure 1.1; Galloway *et al.* 2006; Willoughby *et al.* 2010; Levin *et al.* 2011). Due to its complex physiology, genetic mutations throughout the ocular tissues and their associated processes are known to drive visual impairment (Farrar *et al.* 2017).

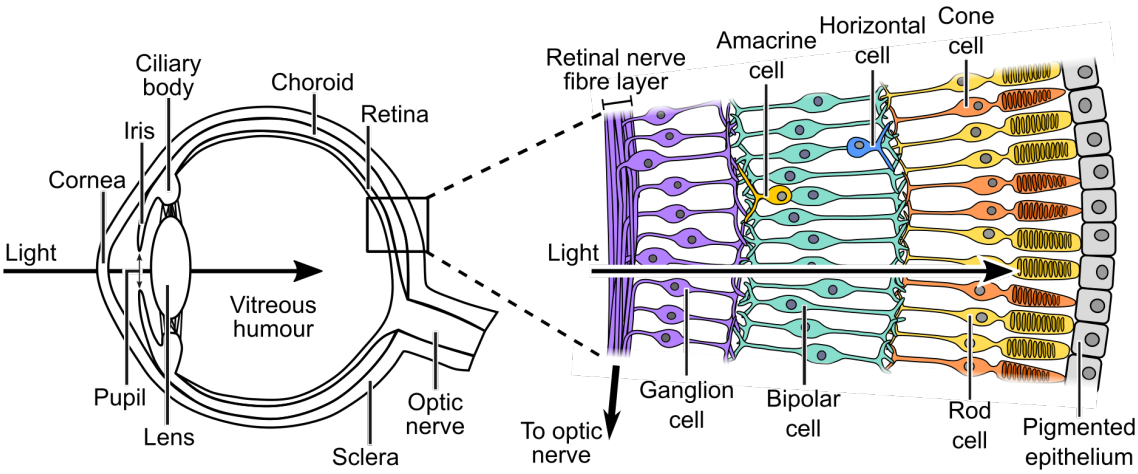

Figure 1.1. Schematic of the eye and retina.

The eye is principally composed of three layers, the outer fibrous layer (cornea and sclera), the middle vascularised layer (iris, ciliary body and choroid) and the inner neuronal layer (retina). Light initially enters the eye through the cornea and pupil before refraction and focus by the lens. Upon reaching the retina, light activates the light sensitive opsins within the rod and cone photoreceptors causing a neuronal signalling cascade: transmitting signals through bipolar cells to the retinal ganglion cells, which project axons forming the optic nerve and transmit visual information to the visual cortex.

Once light reaches the retina, it must initially pass through the retinal nerve fibre layer (RNFL), retinal ganglion cells (RGCs) and bipolar cells before reaching the photoreceptors. Here light activates the photosensitive opsins, inducing photoreceptor cell activation and initiating retinal signalling cascades through the bipolar cells and the RGCs, which project axons to form the optic nerve connecting to and activating the visual cortex and allowing us to see. Further refinement of the signalling cascade is controlled by the horizontal and amacrine cells within the bipolar layer, enabling precise, finetuning of light responses (Willoughby *et al.* 2010; Levin *et al.* 2011). Like the overall eye, mutations throughout the different retinal layers are associated with disease causation, with more than 250 genes known to be associated with retinal visual loss (Farrar *et al.* 2017; Pontikos *et al.* 2020).

1.1 Inherited optic neuropathies

The inherited optic neuropathies encompass a range of genetically diverse disorders that result in severe progressive visual impairment, globally afflicting approximately 1:10000 people. Although the spectrum of diseases is gradually expanding, autosomal dominant optic atrophy (DOA) and Leber hereditary optic neuropathy (LHON) account for the majority of clinically diagnosed conditions, sharing both clinical and pathological characteristics even though they are genetically distinct conditions (Yu-Wai-Man *et al.* 2014). DOA patients primarily carry nuclear encoded genetic abnormalities, whilst LHON cases originate due to mitochondrial DNA (mtDNA) mutations. Regardless of the genetic deficit, inherited optic neuropathies share remarkably similar clinical features, presenting

with degeneration of the optic nerve caused by the selective loss of RGCs (Newman and Biousse 2004; Yu-Wai-Man *et al.* 2016). Ultimately, RGC loss and the associated optic nerve degeneration results in the symmetrical, bilateral loss of central vision, which is typically progressive throughout life (Newman *et al.* 2004). However, in spite of understanding the pathological features and genetic causes behind this spectrum of diseases, the precise mechanisms causing the preferential loss of RGCs in inherited optic neuropathies remain elusive and require further investigating.

1.2 Embryonic retinal development

To understand the functional consequences of RGC loss, it is crucial to understand the complex physiology and development of the retina. Embryonic development of the functional vertebrate eye begins during the 4th week of embryogenesis. Developmentally the eye originates from multiple embryonic tissue layers; the neural retina, retinal pigmented epithelium (RPE) and iris structures are formed from the neuroectoderm; the lens and components of the cornea originate from surface ectoderm, whilst the neural crest gives rise to corneal endothelial cells, ciliary body and vascular choroid; finally the mesoderm contributes cells to the corneal Bowman's membrane and stroma, and angioblasts to the choroid (Chow and Lang 2001; Schoenwolf *et al.* 2009). Due to the diverse origins of the ocular tissues, eye development is a tightly coordinated process enabling the specific development of cells with diverse morphology and function, however, this section will primarily focus on the development of the retina and RGCs.

The early stages of retinal differentiation are governed through "progressive induction", in which sequential steps of gene activation and development govern the generation of the vertebrate eye (Heavner and Pevny 2012). Initially, neural induction drives the formation of the neural plate from dorsal ectoderm. Subsequently, the presumptive forebrain is specified within the cranial neural plate, a process coordinated by expression of *OTX2*, which primes the forebrain for eye development and specifies the eye field (Zuber *et al.* 2003; Schoenwolf *et al.* 2009). Expression of *OTX2* further specifies the eye field through induction of the eye field transcription factors (EFTFs), including *RAX*, *PAX6*, *SIX2* and *LHX2* (Zuber *et al.* 2003). Studies of EFTFs within model organisms have demonstrated their requirement for successful retinal development, with *Rax, Lhx2* and *Pax6* mutant mice demonstrating significant retinal developmental defects (Mathers and Jamrich 2000; Marquardt *et al.* 2001; Philips *et al.* 2005; Riesenberg *et al.* 2009; Tétreaulta *et al.* 2009), in particular, *Rax* knockout mice have no apparent eye field whilst over expression of *Rax* causes excessive proliferation of the neural retina (Mathers *et al.* 1997; Bailey *et al.* 2004). Conditional knockout of *Pax6* within the developing mouse retina limits retinal precursor cells (RPCs) to a single cell fate, that of amacrine interneurons (Marquardt *et al.* 2001). Similarly, misexpression of *Pax6* by microinjection

during *Xenopus* embryogenesis causes ectopic eye development, associated with upregulation of other EFTFs, including *Rax* (Chow *et al.* 1999), confirming its importance for retinogenesis and RPC competency.

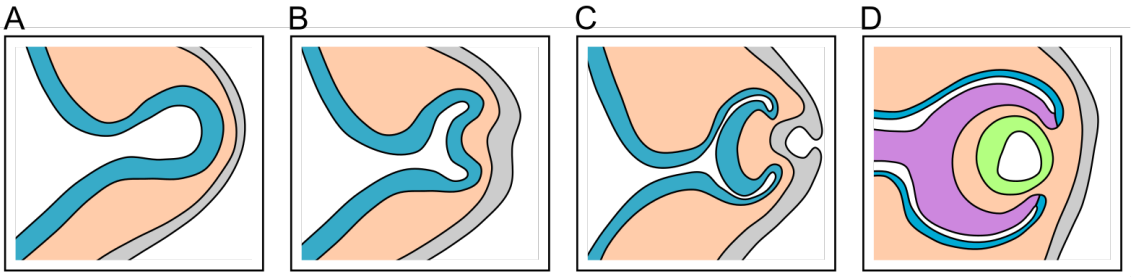

Figure 1.2. Initial stages of eye development during embryogenesis.

(A) After initial specification of the eye field in the neural plate, the neuroepithelium forms lateral protrusions known as optic vesicles (blue).

(B) Continued growth of the optic vesicle results in interactions with the surface ectoderm (grey), resulting in invagination of the optic vesicle to form the optic cup.

(C) Further invagination of the optic cup results in a bi-layered presumptive retinal structure, with outer (RPE) and inner (neural retina) layers, whilst the surface ectoderm begins invaginating to form the presumptive lens (green).

(D) The presumptive retina (purple) and RPE (blue) become further specified as the developing retina thickens, before the retina becomes stratified into neuroblastic layers for retinal cell development.

Inspired by Schoenwolf *et al.* (2009) and Zhao *et al.* (2017).

Once the eye field is defined, the optic vesicles develop as lateral bulges protruding from the forebrain, connected by the optic stalk, a structure required for optic nerve formation (Figure 1.2A; Schoenwolf *et al.* 2009; Graw 2010). Continual growth of the optic vesicle results in contact with surface ectoderm (Figure 1.2B), inducing the vesicle to invaginate and form the optic cup (Figure 1.2C), a structure composed of an inner neural retina and an outer RPE layer of cells (Figure 1.2D). Interactions with the surface ectoderm induces the expression of *VSX2* within the presumptive neural retina, required for maintaining the identity and causing the proliferation of RPCs (Chow *et al.* 2001; Zagozewski *et al.* 2014). Although, mutation to *VSX2* does not significantly impair retinal development, abnormal signalling of the EFTFs *Pax6* and *Lhx2*, results in poorly formed or absent optic cups, demonstrating their key requirement during eye development (Horsford *et al.* 2005; Adler and Canto-Soler 2007).

Following specification of the optic cup, at approximately six weeks of embryogenesis, the presumptive neural retina becomes patterned into two distinct layers, known as the outer and inner neuroblastic layers that are composed of multipotent retinal precursors that can differentiate into all retinal cells (Schoenwolf *et al.* 2009; Zagozewski *et al.* 2014).

1.2.1 Development of RGCs and the optic nerve

After initial specification, the presumptive retina develops six neuronal cell types and one glial cell type through an evolutionary conserved, temporal developmental process; the first cells to develop are the RGCs, cone photoreceptors and horizontal cells, followed by the amacrine cells and rod photoreceptors, and lastly the bipolar and Müller glia cells (Graw 2010; Heavner *et al.* 2012). The time at which retinal progenitors exit the cell cycle appears to facilitate their fate commitment, with progenitors that exit the cycle early able to develop into early born cell types (RGCs or bipolar cells) and the opposite for progenitors exiting the cell cycle late on in development. In addition, both intrinsic and extrinsic factors are known to regulate progenitor cell populations, controlling the pool of progenitors available for proliferation and defining those differentiating to a specific fate (Andreazzoli 2009). Furthermore, the differentiation of a number of retinal cell lineages, including RGCs, has been demonstrated to involve autonomous negative feedback loops, with the development of RGCs preventing their own over-development during retinogenesis (Andreazzoli 2009).

A number of studies have been conducted to determine the intrinsic transcription factors that govern RGC differentiation. The EFTF *PAX6* is known to be a key regulator within RGC development, fundamental to regulating the multipotent state of progenitor cells and the induction of downstream genes required for RGC differentiation, including the RGC transcription factor *ATOH7*, or the mouse ortholog *Math5*. Ablation of *Pax6* in mice prevents the induction of *Math5* and inhibits RGC generation during retinogenesis, whilst *Math5* mutant mice have significantly reduced RGC development (Marquardt *et al.* 2001; Wang *et al.* 2001; Yang *et al.* 2003). Furthermore, impaired *Math5* expression significantly reduces the expression of further downstream genes required for RGC specification (Brown *et al.* 2001).

Early studies of *in vivo* RGCs identified the *BRN3* family of transcription factors, comprising of *BRN3A*, *BRN3B* and *BRN3C*, to selectively identify the presence of RGCs within the retina (Xiang *et al.* 1993; Gan *et al.* 1999). Analysis of the developing chick retina confirmed the requirement of *ATOH7* for RGC development, identifying its expression within early differentiating RGCs. Forced expression of *ATOH7*, or *Math5*, induced the expression of *BRN3* isoforms, promoting the development of RGCs (Liu *et al.* 2001). Analysis of all three *BRN3* isoforms has highlighted their function during RGC development. *Brn3b* ablation within mice causes a significant reduction in RGC number, primarily due to the misspecification of precursor cells and impaired axon formation causing RGC apoptosis (Erkman *et al.* 1996; Xiang 1998; Gan *et al.* 1999; Wang *et al.* 2000; Qiu *et al.* 2008; Badea *et al.* 2009). Analysis of mice with *Brn3a* deletions demonstrated no notable RGC death but significantly impaired dendritic arbour

distribution (Badea *et al.* 2009), whilst in double *Brn3b* and *Brn3c* knockout mice, increased RGC loss is observed when compared to *Brn3b* knockout alone, coupled with further reductions in axonal projections forming the optic nerve (Wang *et al.* 2002). Thus, although *Brn3a* and *Brn3c* deletion does not cause significant developmental deficits, they are key to facilitating accurate RGC development during embryogenesis. Further analysis of *Brn3* genes within the developing chick retina demonstrated their involvement in maintaining RGC cell identity through self-regulatory feedback loops (Liu *et al.* 2001).

Although initial studies of RGCs focused on the use of the *BRN3* gene family, further genes have been identified that are required for their accurate differentiation. Temporal analysis of the gene *Isl1* throughout mouse development have established its requirement for proper retinal development, demonstrating expression within developing RGCs, amacrine and bipolar cells, which is maintained in mature RGCs (Elshatory *et al.* 2007). Subsequent studies have demonstrated that *ISL1* and *BRN3B* form molecular complexes to regulate gene expression within developing RGCs (Li *et al.* 2014). Deletion of *Isl1* in mice causes apoptosis of RGCs and optic nerve defects, which are further exacerbated in *Isl1* and *Brn3b* double null mutants (Pan *et al.* 2008). Furthermore, ectopic expression of both *Brn3b* and *Isl1* in *Math5* null mice, which exhibit reduced numbers of RGCs, restores the development of RGC and results in a near normal ganglion cell layer (GCL) in the mature retina (Wu *et al.* 2015), suggesting expression of *Isl1* and *Brn3b* alone can specify RGCs.

Following terminal differentiation, humans possess approximately 3.7 million RGCs that must extend axonal projections towards the visual cortex. These connections are subsequently fine-tuned, with humans retaining approximately 1.3 million RGCs at birth which form the optic nerve (Provis *et al.* 1985). Importantly, RGCs become polarised throughout embryonic development due to the presence of the basal lamina of the retina, ensuring axonal projections grow towards the RNFL (Halfter *et al.* 2001; Zolessi *et al.* 2006; Bao 2008). Initially RGCs project axons to the surface of the neural retina, developing into the RNFL and through “intraretinal axon targeting” project towards the head of the optic stalk, consequently known as the optic disc (Bao 2008). Following their exit of the eye at the optic disc, RGC axons project towards the optic chiasm where they interact with cells at the embryo midline, and those from the contralateral eye, to determine which side of the brain to project towards. Finally, the axons project to the visual cortex via the optic tract, ultimately terminating in the superior colliculus and lateral geniculate nucleus (LGN) in mammals (Erskine and Herrera 2007; Bao 2008).

Although the exact mechanisms that regulate the axonal guidance process are not fully understood, some of the molecular determinants required for correct axonal projection

are becoming clearer. Importantly, axonal guidance is primarily regulated through the axon growth cone, specialised structures at the leading tip of the axon that sense and respond to environmental signals (Oster and Sretavan 2003). Throughout the RGC axon development process, growth cones interact with extrinsic attractive and repulsive factors, that either inhibit or promote axonal growth (Erskine *et al.* 2007). Within the retina, inhibitory molecules within the SLIT family of proteins prevent axonal growth towards the retina periphery through interaction with the ROBO RGC receptors, whilst sonic hedgehog (shh), and the cell adhesion molecules L1 and Neurolin promote axonal growth towards the central retina and optic disc (Oster *et al.* 2003; Taylor 2005; Erskine *et al.* 2007). In addition, during development RGCs are born in a central to peripheral pattern, with the oldest RGCs closest to the optic disk and the youngest RGCs towards the retina's periphery. Crucially this enables new RGCs to utilise older RGCs as a growth scaffold for efficient axon guidance, due to expression of guidance cues on the RGC surface (Bodick and Levinthal 1980; Oster *et al.* 2003). Once RGC axons reach the optic disk, interaction with NETRIN-1 via the receptor DCC instructs the axonal projections to enter the presumptive optic nerve head (Oster *et al.* 2004; Erskine *et al.* 2007). After leaving the eye, axonal guidance is controlled through the expression of inhibitory Semaphorin and Slit proteins, promoting fasciculation into the optic nerve bundle, whilst both Slit and shh regulate axonal growth through the optic chiasm (Oster *et al.* 2003; Erskine *et al.* 2007). Finally, RGCs project to the visual cortex where signalling from gradients of the EPHRIN family of proteins regulates RGC axonal targeting, ensuring RGCs project to the correct region of the superior colliculus (Oster *et al.* 2003). Ultimately, projection of RGC axons and development of the optic nerve is a multifaceted and complex process requiring diverse signalling processes to correctly guide RGC axonal outgrowth.

1.2.1.1 RGC Subtypes

Although originating from the same pool of progenitor cells, traversing the same axonal tracts and connecting to similar axonal targets, extensive analysis has demonstrated an abundance of distinct RGC subtypes. The initial defining characteristics of RGCs within the retina are a cell soma located in the ganglion cell layer, dendritic arbours in the inner plexiform layer (the region between RGC cell soma and amacrine/bipolar cell nuclei), axons that traverse the optic nerve, generation of action potentials and release of glutamate from synaptic terminals (Sanes and Masland 2015). Classically, RGCs were characterised primarily due to their physiological properties in combination with their dendritic arbour morphology, however, advances in molecular characterisation has increased our ability to define RGCs by their molecular signatures, such as transcriptomic profiles (Van Wyk *et al.* 2009; Ecker *et al.* 2010; Sümbül *et al.* 2014;

Struebing *et al.* 2016; Jacoby and Schwartz 2017; Laboissonniere *et al.* 2019; Sweeney *et al.* 2019). As such, classification of RGCs now occurs due to four overarching criteria: morphology, gene expression, spacing, and physiology (Table 1.1; Sanes *et al.* 2015).

Table 1.1. Characteristics defining RGC subtypes.

Characterisitic	Defining features
Morphology	Consistent and uniform morphology (e.g. dendritic pattern)
Gene expression	Similar gene expression (e.g. unique sets of genes)
Spacing	Regular, consistent spacing.
Physiology	Unform physiological properties (e.g. receptive fields)

Current estimates suggest there at least 30 subtypes of mammalian RGC, with major categories including the intrinsic photosensitive RGCs (ipRGCs), ON-RGCs, OFF-RGCs, ON-OFF RGCs, direction selective RGCs (DS-RGCs), α-RGCs and local edge detector RGCs (LED-RGCs; Watanabe *et al.* 1993; Kay *et al.* 2011; Sümbül *et al.* 2014; Sanes *et al.* 2015; Sweeney *et al.* 2019). Although in-depth discussion of the different types of RGCs is beyond the scope of this thesis, understanding RGC subtypes is of importance as specific subtypes have been shown to resist extrinsic and intrinsic insults. Multiple studies have demonstrated the ability for ipRGCs to resist injury in models of glaucoma (Li *et al.* 2006; Li *et al.* 2008; Zhang *et al.* 2013; Struebing *et al.* 2016), optic nerve injury (Robinson and Madison 2004; Pérez de Sevilla Müller *et al.* 2014) and chemical excitotoxicity (DeParis *et al.* 2012). More importantly, analysis of post-mortem tissue derived from both LHON and DOA patients demonstrated preservation of ipRGC number when compared to the overall loss of total RGC number, suggesting a relative sparing of ipRGCs in neurodegenerative conditions associated with mitochondrial dysfunction (La Morgia *et al.* 2010). In addition, analysis of a mouse model of DOA further confirmed the survival of ipRGCs within the retina, with DOA mice demonstrating no significant circadian rhythm visual impairments (such as response to light/dark cycles) when compared to wildtype (WT) littermates (Perganta *et al.* 2013). Further investigation is therefore required to understand the roles different RGC subtypes have in inherited optic neuropathies, which will facilitate our understanding of both disease progression and potential therapeutic strategies.

1.3 Dominant Optic Atrophy

1.3.1 DOA epidemiology

Initially described in 1959 by Danish Ophthalmologist Poul Kjer (Kjer 1959), DOA is now regarded as the most prevalent inherited optic neuropathy within the UK, affecting approximately 1:35000 people (Yu-Wai-Man *et al.* 2014), with a prevalence as high as 1:12000 people in Denmark (Kjer *et al.* 1996). As with all inherited optic neuropathies,

DOA has an insidious onset during the first two decades of life, with a mean onset of 6 to 10 years of age, initially presenting as bilateral central vision loss and optic disk pallor due to RGC loss and optic nerve degeneration (Figure 1.3; Yu-Wai-Man *et al.* 2014; Yu-Wai-Man *et al.* 2016). However, DOA demonstrates incomplete penetrance and is a clinically heterogeneous disease, with notable inter- and intrafamilial variability in disease presentation and progression. As such, DOA displays a spectrum of symptoms, approximately 1 in 4 patients present as asymptomatic with near perfect central visual acuity, whilst others will have severe loss of vision (Eliott *et al.* 1993; Yu-Wai-Man *et al.* 2011; Chun and Rizzo III 2017). As with initial presentation in the clinic, the rate of visual decline is also incredibly variable amongst DOA patients, however, this is believed to be independent of the severity of the initial clinical diagnosis (Fraser *et al.* 2010; Yu-Wai-Man *et al.* 2011). When compared to other optic neuropathies, in general DOA is associated with a slower disease progression and the majority of patients will retain relatively good visual function until later in life. Nevertheless, irreversible visual decline occurs in approximately 50 – 75 % of patients, with approximately half of all patients ultimately registering as legally blind (Yu-Wai-Man *et al.* 2011; Yu-Wai-Man *et al*. 2016).

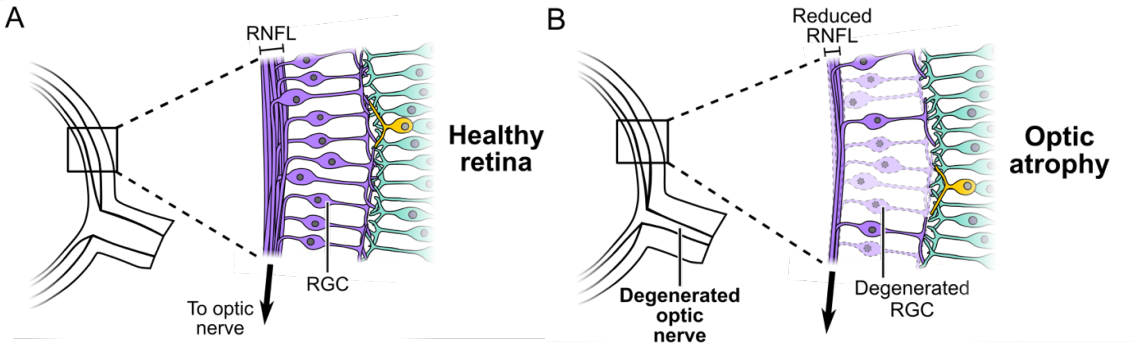

Figure 1.3. Schematic demonstrating physiological changes in the DOA retina.
RGCs in the healthy retina project axons, forming the retinal nerve fibre layer (RNFL) and the optic nerve **(A)**. In patients with optic atrophy, such as DOA, degeneration of RGCs resulting in thinning of the RNFL and degeneration of the optic nerve, and progressive vision loss **(B)**.

Visual field analysis of DOA patients typically reveals central, cecocentral (spreading from central vision to the blind spot) and paracentral scotomas, associated with preferential loss of RGCs within the papillomacular bundle, whilst the peripheral vision remains relatively unaffected (Lenears *et al.* 2012). Furthermore, assessment of DOA patients through retinal imaging techniques demonstrates significant pallor in the optic disk and significant thinning of the RNFL, both indicative of RGC axonal degeneration (Votruba *et al.* 2003; Ito *et al.* 2007; Milea *et al.* 2010; Yu-Wai-Man *et al.* 2010). In addition to loss of central vision, defects in colour vision are also widely reported with most patients exhibiting generalised dyschromatopsia (Fraser *et al.* 2010; Yu-Wai-Man *et al.* 2011).

Although optic atrophy is the fundamental characteristic of DOA, approximately 20 % of patients have a multi-system or syndromic form of the disease, known as DOA plus (DOA+), that presents with additional extraocular symptoms (Yu-Wai-Man *et al.* 2010). The most frequently diagnosed extraocular manifestation among DOA+ patients is bilateral sensorineural hearing loss, which is typically diagnosed in late childhood or early adulthood, and affects nearly two thirds of all DOA+ patients. In addition, progressive external ophthalmoplegia, ataxia, myopathy and peripheral neuropathy arise after the initial decrease in visual acuity, typically developing during the third decade of life (Votruba *et al.* 1998; Amati-Bonneau *et al.* 2005; Amati-Bonneau *et al.* 2008; Yu-Wai-Man *et al.* 2010; Lenears *et al.* 2012). In spite of the phenotypic heterogeneity, the primary pathological hallmark of DOA remains consistent: loss of RGCs and degradation of the optic nerve (Yu-Wai-Man *et al.* 2016).

1.3.2 Genetics of DOA

Understanding of the mechanisms causing DOA was accelerated through identification of its underlying pathogenic mutations. Initial chromosomal mapping identified a region on chromosome 3 (3q28-qter) associated with DOA (Eiberg *et al.* 1994; Kjer *et al.* 1996). Subsequent studies further refined the disease loci, enabling identification of the specific gene within the 3q28-qter region, termed as *Optic Atrophy 1* (*OPA1*), which targets to the mitochondria (Alexander *et al.* 2000; Delettre *et al.* 2000). Although mutations in *OPA1* were initially believed to be the sole disease causing genetic defect (Bonneau *et al.* 1995), more recent studies have further expanded the DOA genetic landscape, associating DOA with mutations in *OPA3*, *DNM1L* (*DRP1*), *WFS1*, *SSBP1*, *AFG3L2* and *SPG7* (Table 1.2; Kerrison *et al.* 1999; Reynier *et al.* 2004; Barbet *et al.* 2005; Eiberg *et al.* 2006; Carelli *et al.* 2011; Klebe *et al.* 2012; Charif *et al.* 2015; Colavito *et al.* 2017; Gerber *et al.* 2017; Jurkute *et al.* 2019). Interestingly, some of the newly identified genes related to DOA are functionally connected to OPA1 and play an important role in its processing. Both *AFG3L2* and *SPG7* encode mitochondrial proteases involved in the proteolytic cleavage of OPA1 (Klebe *et al.* 2012; Charif *et al.* 2015; Colavito *et al.* 2017), a process that is integral to its mitochondrial function. In addition, *SSBP1* is known to be integral for the maintenance of the mitochondrial genome (Jurkute *et al.* 2019), a role also commonly associated to OPA1 function (Song *et al.* 2007), potentially indicating an interplay between the two proteins. In spite of the growing list of genes, it is believed *OPA1* mutations cause approximately 60 – 70 % of all genetically confirmed DOA cases (Cohn *et al.* 2007; Yu-Wai-Man *et al.* 2016).

Table 1.2. Genetic loci associated with DOA.

Modified from Lenaers *et al.* 2012.

Locus	Chromosome	Gene	Mode of inheritance	Reference
OPA1	3q28-29	*OPA1*	Dominant	Eiberg *et al.* 1994; Kjer *et al.* 1996; Alexander *et al.* 2000; Delettre *et al.* 2000
OPA3	19q13.2-q13.3	*OPA3*	Dominant/Recessive	Reynier *et al.* 2004
OPA4	18q12.2-q12.3	-	Dominant	Kerrison *et al. 1999*
OPA5	22q12.1-q13.1	-	Dominant	Barbet *et al.* 2005
OPA8	16q21-q22	-	Dominant	Carelli *et al.* 2011
-	4p16.1	*WSF1*	Dominant	Eiberg *et al.* 2006
-	16q24.3	*SPG7*	Dominant	Klebe *et al.* 2012
-	18p11.21	*AFG3L2*	Dominant	Chariff *et al.* 2015; Colavito et al. 2017
-	12p11.21	*DNM1L*	Dominant	Gerber *et al.* 2017
-	7q33-q35	*SSBP1*	Dominant	Jurkute *et al.* 2019

OPA1 is a highly polymorphic gene with over 300 known genetic variants and 241 variants known to be pathogenic disease causing (Ferre *et al.* 2015). The majority of disease associated variants cluster within the dynamin central region (38 %) and GTPase domain (31 %; Ferre *et al.* 2015), whilst 27 % of the mutations are missense, 27 % cause splice variants, 23.5 % cause frame shifts, 16.5 % are nonsense and 6 % are deletions or duplications (Ferre *et al.* 2005; Lenears *et al.* 2012; Ferre *et al.* 2015). Although the mutational types are diverse, the bulk of mutations lead to premature termination codons (PTCs), mRNA decay and an approximate 50 % reduction in total protein, resulting in haploinsufficiency (Pesch *et al.* 2001; Marchbank *et al.* 2002; Schimpf *et al.* 2008; Ścieżyńska *et al.* 2017). Identification of multiple patients carrying large-scale deletions within *OPA1*, including deletion of the entire gene, further emphasized haploinsufficiency as a significant pathological disease mechanism driving DOA (Marchbank *et al.* 2002; Fuhrmann *et al.* 2009). Given the diverse range of mutations throughout the gene, there is no direct genotype-phenotype correlation (Puomila *et al.* 2005). However, it is believed that missense mutations, primarily within the GTPase domain, increase the risk of developing DOA+ likely due to exerting a dominant-negative protein effect (Olichon *et al.* 2007; Amati-Bonneau *et al.* 2008; Huang *et al.* 2009; Yu-Wai-Man *et al.* 2010; Barboni *et al.* 2014; Kane *et al.* 2017). More recent analysis suggests that patients with pure DOA are more likely to have mutations in *OPA1* exons 8 and 9, whilst mutations in exons 14, 15 and 17 increase the likelihood of developing DOA+ (Figure 1.4). Interestingly, maternally inherited *OPA1* mutations also further predispose patients to acquiring DOA+ phenotypes, due to the effects of *OPA1* mutation within oocyte mitochondria (Ham *et al.* 2019). The dominant-negative hypothesis was further supported through western blot analysis of two missense mutations, p.S545R and p.R445H, which demonstrated no significant reduction in OPA1 protein levels (Kane *et al.* 2017). More recently homozygous and compound heterozygous mutations within *OPA1* have been identified, however, these are

associated with more severe, multisystem developmental conditions rather than classical DOA or DOA+, with symptoms including encephalopathy and neuromuscular difficulties (Bonneau *et al.* 2014; Carelli *et al.* 2014; Spiegel *et al.* 2016; Nasca *et al.* 2017).

1.3.3 *OPA1* structure and expression

OPA1 is a 31-exon gene spanning approximately 60 kb of chromosome 3 (Figure 1.4A), which encodes an inner mitochondrial membrane (IMM) targeted 960 amino acid dynamin-related GTPase protein (Delettre *et al.* 2000). Within human tissues expression of *OPA1* is tightly regulated, with alternative splicing of exons 4, 4b and 5b generating 8 distinct splice isoforms (Figure 1.4B; Delettre *et al.* 2001). However, all isoforms are characterised by the presence of a highly conserved GTPase domain, required for GTP hydrolysis, and a middle or dynamin central region, involved in oligomerisation (Figure 1.4C; Delettre *et al.* 2000; Belenguer and Pellegrin 2013). In addition, *OPA1* encodes a mitochondrial targeting sequence (MTS) at the N-terminus of the protein to facilitate its mitochondrial localisation, a transmembrane domain for anchoring in the IMM, a pleckstrin-homology domain (PH domain) for lipid interaction and a GTPase effector domain (GED), to stimulate GTPase activity (Figure 1.4C; Olichon *et al.* 2007; Akepati *et al.* 2008; Li *et al.* 2019).

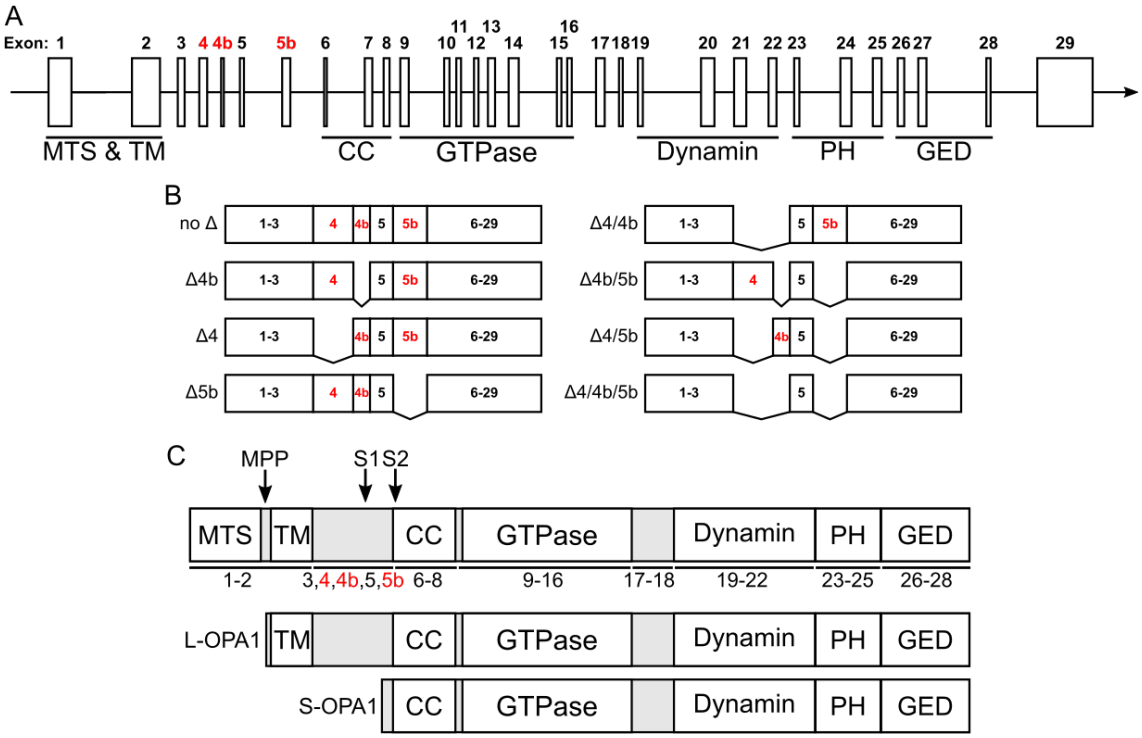

Figure 1.4. Schematic of *OPA1* genetic architecture.

(A) Representation of *OPA1* genetic structure in chromosome 3.

(B) Schematic representation of *OPA1* alternative splicing events. Inspired by Delettre *et al.* 2001.

(C) Schematic representation of OPA1 protein structure. The predominant features of OPA1 are a GTPase domain and dynamin middle domain. A mitochondrial targeting sequence (MTS) facilitates localisation of OPA1 to mitochondrial networks, before cleavage by mitochondrial processing peptidase (MPP arrow) into L-OPA1. The coil-coil (CC) domain, dynamin domain and pleckstrin-homology (PH) domain facilitate protein and lipid interactions. The GTPase effector domain (GED) stimulates GTPase function. *OPA1* exon 5 and 5b encode proteolytic cleavage sites S1 and S2 (S1 and S2 arrows), required for processing of L-OPA1 into S-OPA1 by proteases, including OMA1 and YME1L. *OPA1* exons are noted underneath protein schematic. Inspired by Belenguer and Pellegrin 2014, Yu-Wai-Man *et al.* 2010a, MacVicar and Lane 2014, and Li *et al.* 2019.

Alternatively spliced exons denoted in red.

Once targeted to the mitochondria through the MTS, OPA1 undergoes cleavage by mitochondrial processing peptidase (MPP) to remove the MTS, generating long isoforms of OPA1 (L-OPA1; Figure 1.4C; Akepati *et al.* 2008). In addition to MPP cleavage, molecular analysis has demonstrated that OPA1 contains 2 proteolytic cleavage sites (S1 and S2; Figure 1.4C), encoded by exon 5 and alternatively spliced exon 5b, required for further processing of L-OPA1. Cleavage at either S1 by OMA1 or S2 by the i-AAA protease YME1L removes the transmembrane domain required for anchoring L-OPA1 within the IMM, converting L-OPA1 into a shorter, soluble form (S-OPA1; Figure 1.4C) typically found within the inter-membrane space (Song *et al.* 2007; Anand *et al.* 2014; Mishra *et al.* 2014; MacVicar and Langer 2016). Importantly, L-OPA1 and S-OPA1 are believed to function both synergistically and individually within the mitochondrial network (Anand *et al.* 2014; Mishra *et al.* 2014; MacVicar *et al.* 2016; Del Dotto *et al.* 2017).

Further molecular analysis of *OPA1* has enabled the determination of its expression profile throughout the body. Perhaps one of the most perplexing aspects of DOA is that the primary genetic defect occurs in a protein that is constitutively expressed throughout the body, but when mutated causes the preferential loss of RGCs within the retina (Votruba *et al.* 1998). Thus, early studies aimed to establish the expression pattern of *OPA1* within the retina to determine if this was a driving force behind the loss of RGCs. Initial work by Delettre *et al.* (2003) established the variable splice patterns of *OPA1* throughout human tissues, whilst also establishing that the highest levels of *OPA1* expression occur within the retina, brain, heart and muscle. Interestingly, all four tissues had similarly high levels of expression of two isoforms, one containing exon 5b and the other containing exon 4. Furthermore, analysis of mouse, rat and human retinal tissue demonstrated that *OPA1* was expressed throughout the retinal layers, including the GCL, photoreceptor inner segments and RPE (Aijaz *et al.* 2004; Kamei *et al.* 2005), thus suggesting that it is not a specific isoform expression pattern that leads to RGC deficits. Further analysis of mouse *Opa1* isoform expression demonstrated that only exon 4b and 5b undergo alternative splicing in murine tissues, generating only 4 distinct transcripts compared to 8 in human tissues, and thus indicating a significant difference in the mouse models of DOA (Akepati *et al.* 2008). More recently, analysis of *in vitro* neuronal differentiation demonstrated a shift towards *OPA1* isoforms lacking exon 4b and 5b during neural differentiation (Caglayan *et al.* 2020). Importantly, developing our understanding of *OPA1* alternative splicing events has confirmed there is no specific isoform expressed in RGCs that leads to their preferential loss, and it further raises questions as to why only a small proportion of DOA patients experience a plus phenotype with extraocular features when other neuronal populations exhibit similar expression patterns to the retina.

1.4 Mitochondria in health and disease

Although classically referred to as “the powerhouse of the cell” and depicted as a single, bean shaped organelle, mitochondria are phenotypically heterogeneous and functionally diverse organelles essential to eukaryotic cell function (Tronstad *et al.* 2014; Spinelli and Haigis 2018). Thought to have originated over 1.6 billion years ago from the engulfment of α-proteobacteria (Taanman 1999; Kühlbrandt 2015; Wang and Wu 2015), mitochondria are essential for eukaryotic cell viability (Bulthuis *et al.* 2019). Like the cell nucleus, mitochondria are structurally composed of a double membrane, in which the IMM is encapsulated by the outer mitochondrial membrane (OMM; Figure 1.5A). The IMM surrounds the mitochondrial matrix and is further specialised into two distinct domains: an inner boundary membrane that is adjacent to and interacts with the OMM,

and distinct membrane folds, known as cristae, to enlarge the IMM surface area (Figure 1.5B,C; Pfanner *et al.* 2014; Bulthuis *et al.* 2019).

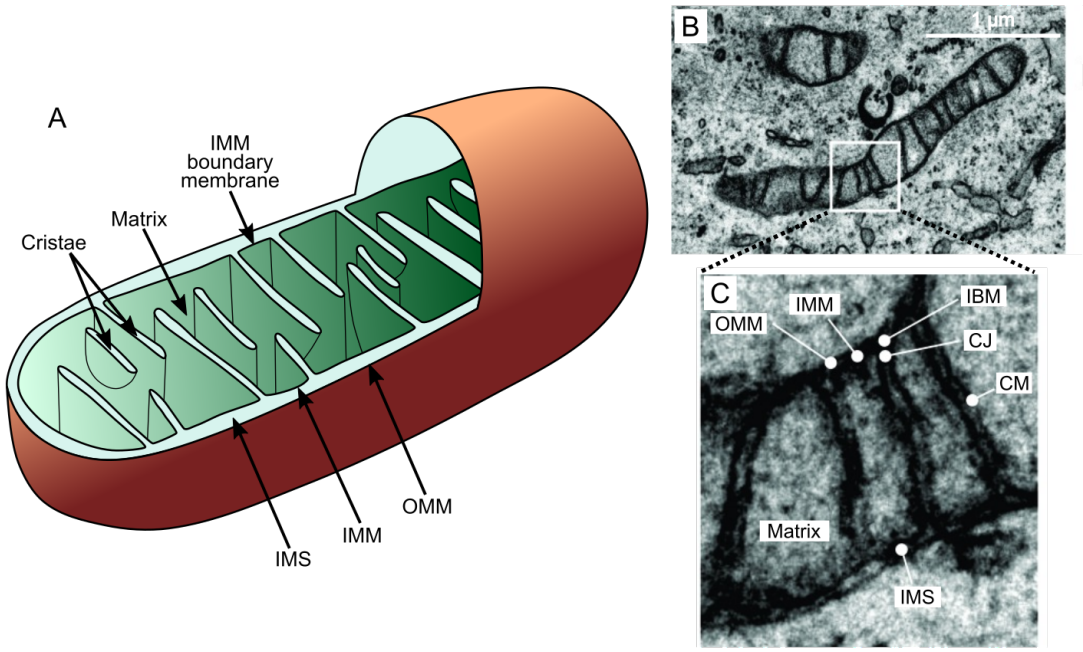

Figure 1.5. Mitochondrial structure.

(A) Schematic representation of mitochondrial structure. The outer mitochondrial membrane (OMM) encapsulates the inner mitochondrial membrane (IMM), creating the intermembrane space (IMS). The IMM is specialised into 2 distinct domains, the IMM boundary membrane and cristae, IMM folds required for mitochondrial function. The IMM encloses the mitochondrial matrix.

(B) Electron microscopy imaging depicting mitochondrial structure in HeLa cells. Scale bar represents 1 µm.

(C) Zoomed image taken from **(B)**. The mitochondrial structures are clearly defined, with the OMM encapsulating the IMS and IMM. The IMM boundary membrane (IBM), cristae membrane (CM) and cristae junction (CJ) required for cristae function are also depicted. The mitochondrial cristae form numerous folds protruding into the mitochondrial matrix.

B and **C** taken from Bulthuis *et al.* (2019) with minor modifications.

Importantly, both the IMM and OMM possess different functionality, specialised to their specific role in mitochondrial function. The OMM is highly permeable due to an abundance of porins, mitochondrial pore-forming membrane proteins that allow the free transfer of ions and uncharged molecules across the membrane (Young *et al.* 2007; Kühlbrandt 2015). Conversely, the IMM is highly impermeable to all ions and small molecules, which require molecule-specific transport proteins for transfer to the mitochondrial matrix; a characteristic essential to mitochondrial function, generating an electrochemical membrane potential required for ATP synthesis, protein import and mitochondrial quality control (Kühlbrandt 2015; Zorova *et al.* 2018). However, due to its specific membrane composition, and a number of unique characteristics that will subsequently be discussed, mitochondrial dysfunction is associated with a clinically heterogeneous group of pathological conditions, including neurodegeneration, cancer, diabetes and the inherited optic neuropathies (Alston *et al.* 2017; Bulthuis *et al.* 2019).

1.4.1 The mitochondrial genome

Mitochondria retain many characteristics of their evolutionary ancestors. Most notably, mitochondria contain a 16.6 kilobase (kb) circular genome, which utilises a mitochondrial specific triplet code and mitochondrial specific transfer RNAs (tRNAs) for protein synthesis (Taanman 1999; Shokolenko and Alexeyev 2017). Due to reductive evolution, the process of gene transfer from one genome to another, mtDNA only comprises approximately 0.0005 % of the human genome yet it encodes approximately 0.1 % of all human genes (Andersson and Kurland 1998; Holt *et al.* 2007). Structurally, the mammalian mitochondrial genome comprises a circular, double stranded DNA molecule that is arranged into nucleoprotein complexes, or nucleoids, consisting of 6-10 copies of mtDNA alongside proteins required for mtDNA structure, transcription and replication of the circular genome (Holt *et al.* 2007; Alexeyev *et al.* 2013). Unlike nuclear DNA, mtDNA contains virtually no non-coding regions and is transcribed as a single polycistronic transcript, which is later processed for gene expression. Crucially, mtDNA encodes key elements of transcription, translation and the respiratory chain, including core components of both complex I, complex IV and ATP synthase, and thus absence of mtDNA inhibits respiration and ATP synthesis entirely (Holt *et al.* 2007). Furthermore, mtDNA is wholly dependent on nuclear encoded proteins for DNA replication (Holt and Reyes 2012) and impaired maintenance of the mitochondrial genome has been implicated in a number of neurological diseases, including Parkinson's disease (PD), Alzheimer's disease (AD) and amyotrophic lateral sclerosis (ALS; de la Monte *et al.* 2000; Bender *et al.* 2006; Artuso *et al.* 2013). Furthermore, DOA shares many clinical features with LHON, a disease caused by specific mutations within the mitochondrial genome (Yu-Wai-Man *et al.* 2002), demonstrating how impaired mtDNA maintenance may contribute to the preferential loss of RGCs within DOA.

1.4.1.1 Effects of *OPA1* mutation on mtDNA maintenance

Early studies of yeast demonstrated that *Mgm1*, the yeast *OPA1* ortholog, was important for the segregation of mtDNA during cell division and *Mgm1* mutants resulted in cells devoid of mtDNA that were incapable of respiration (Jones and Fangman 1992; Guan *et al.* 1993). More recently, the precise mechanisms by which *OPA1* regulates mitochondrial genome stability are slowly becoming clear. Elachouri *et al.* (2011) initially provided a foundation for the interactions of OPA1 and mtDNA, demonstrating the requirement of *OPA1* exon 4b for maintaining mtDNA quality. Analysis of siRNAs targeted to *OPA1* alternatively spliced exons 4, 4b and 5b demonstrated that silencing of exon 4b isoforms significantly reduced mtDNA copy number when quantified by quantitative PCR (qPCR) and Southern blot. Furthermore, siRNA reduction of transcripts containing exon 4b caused reduced mtDNA replication alongside disturbed mtDNA

distribution throughout the mitochondrial network. Finally, Elachouri *et al.* demonstrated that *OPA1* isoforms containing exon 4b, which encodes a secondary TM domain, are embedded within the IMM where it can bind to mtDNA to facilitate its stabilisation. In addition, work by Song *et al.* (2007) demonstrated that OPA1 isoforms containing exon 4b are entirely processed by at the second cleavage site by YME1L, thus generating a small IMM bound protein containing exon 4b and S-OPA1. The requirement for OPA1 cleavage for mtDNA maintenance was further confirmed in studies of Mgm1 and Msp1p, yeast OPA1 orthologues. Ablation of Mgm1 and Msp1p processing peptides results in mtDNA depletion (Herlan *et al.* 2003; Sesaki *et al.* 2003; Diot *et al.* 2009).

More recently, Del Dotto *et al.* (2017) individually expressed each of the 8 human isoforms within OPA1 null MEFs, demonstrating rescue of mtDNA copy number when compared to the null cells. Furthermore, expression of constructs containing specific *OPA1* domains established that a functional OPA1 N-terminus and GTPase domain is required for the maintenance of mtDNA content. Yang *et al.* (2020) also established through CHiP-qPCR that OPA1 interacts with and regulates mtDNA quality through direct binding of exon 4b to the mtDNA displacement loop (*D-loop*); and when *OPA1* isoforms do not contain exon 4b there is significantly reduced enrichment of mtDNA genes including the mitochondrial *D-loop*, *MTND2*, and *MTND4* in qPCR analysis. Thus, there is clear evidence for the requirement of OPA1 to maintain the integrity of the mtDNA genome, coordinated by proteolytic cleavage and IMM localisation and interaction through exon 4b (Elachouri *et al.* 2011).

Interestingly, there are conflicting theories regarding how mutation in *OPA1* affects the quality and quantity of mtDNA. Analysis of *OPA1* siRNA treated cells, patient derived fibroblasts carrying biallelic *OPA1* mutations (*OPA1* c.2708_2711delTTAG/c.661G>A *&* *OPA1* c.2353delC/c.2869C>T) and cardiac tissue extracted from mutant *OPA1* mouse models suggest that *OPA1* mutation results in depleted mtDNA copy number (Kim *et al.* 2004; Chen *et al.* 2012; Kushnareva *et al.* 2013; Liao *et al.* 2017). In contrast, a number of studies demonstrate that mtDNA copy number is not reduced but increased, likely due to a proliferative response to mtDNA somatic mutations caused by OPA1 functional loss in an attempt to maintain wild type mtDNA (Zanna *et al.* 2008; Yu-Wai-Man *et al.* 2010), an effect also observed in the optic nerves of *Opa1* mutant mice carrying the human c.2708_2711delTTAG mutation ($Opa1^{delTTAG}$; Sarzi *et al.* 2012). However, proliferation of mtDNA was not replicated in mice carrying a heterozygous nonsense mutation in *Opa1* exon 8 resulting in a PTC (Yu-Wai-Man *et al.* 2009), further muddling the picture of *OPA1* role in mtDNA copy number maintenance.

Further to the effects on mtDNA copy number, analysis of DOA patient muscle biopsies demonstrated a requirement for functional OPA1 to maintain WT mtDNA copies. Long range-PCR (LR-PCR) and qPCR analysis of mtDNA demonstrated significantly reduced mtDNA WT levels for a range of *OPA1* mutation types, including frameshifts, premature stop codons and missense mutations, due to the accumulation of mtDNA mutations and deletions (Amati-Bonneau *et al.* 2008; Hudson *et al.* 2008; Yu-Wai-Man *et al.* 2010; Chen *et al.* 2012). Despite the conflicting evidence surrounding mtDNA copy number it is clear that OPA1 mutation results in mtDNA instability, and likely contributes to mitochondrial respiratory dysfunction due to the reduction of respiratory chain components encoded within mtDNA.

1.4.2 Fusion, fission and the mitochondrial network

The mitochondrial network is a morphologically dynamic system of organelles; constantly altering mitochondrial size, shape and quantity to accurately match the physiological needs of each individual cell (Santel and Fuller 2000; Tronstad *et al.* 2014). Crucially, dynamic changes to the network enable rapid responses to changing stimuli and intracellular metabolic demands, and is primarily governed by four mechanisms: mitochondrial transport, mitochondrial fission (the separation of tubular mitochondria into distinct parts; Figure 1.6), mitochondrial fusion (the joining of two individual mitochondria into one filamentous piece; Figure 1.6) and mitophagy (the specific degradation of mitochondria; Mishra and Chan 2016). Under physiological steady-state conditions both fission and fusion occur in equilibrium, which is integral to maintaining mitochondrial function and cellular homeostasis (Detmer and Chan 2007; Suárez-Rivero *et al.* 2017). Due to the central role both fission and fusion play in cell viability, studies have begun to reveal the molecular mechanisms regulating the fission and fusion processes and the physiological role these play in maintaining cell health.

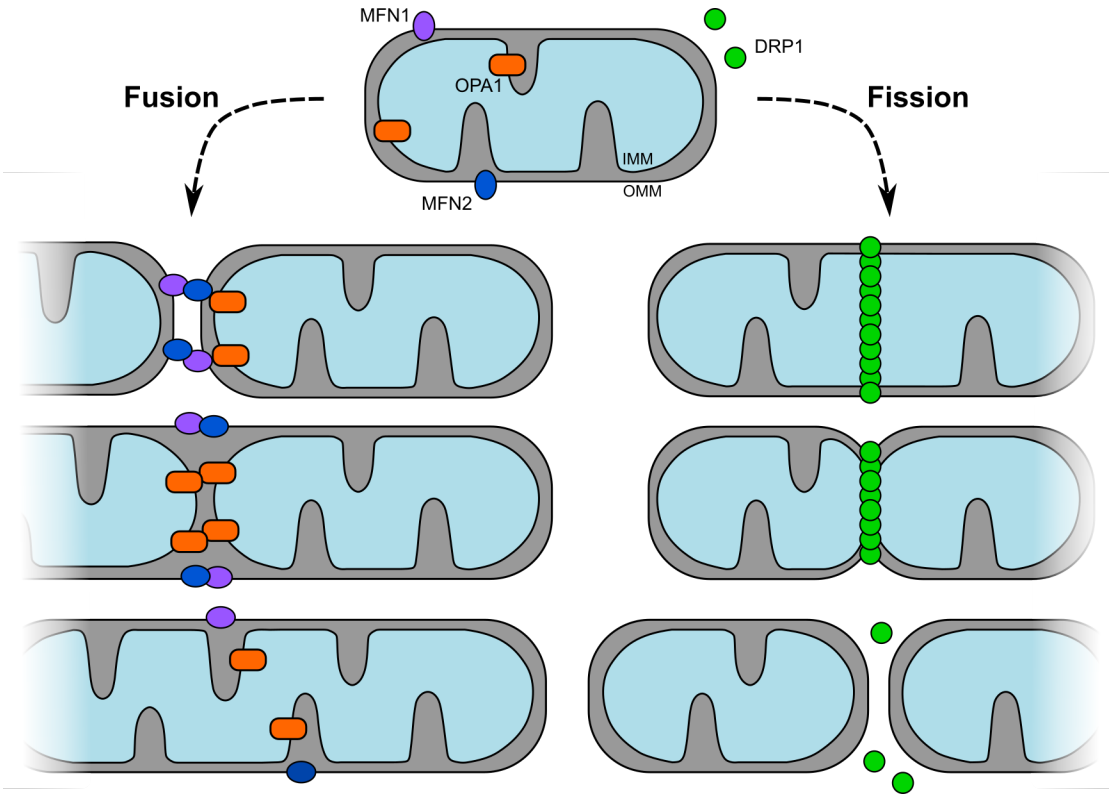

Figure 1.6. Mechanisms of mitochondrial fusion and fission.

Mitochondrial outer membrane (OMM) fusion is mediated by the mitofusins (MFN, purple and blue) before the inner membrane (IMM) is fused through OPA1 (orange) interactions. Mitochondrial fission is primarily governed by DRP1 (green).

Inspired by van der Bliek *et al.* (2013).

A number of plausible reasons have been hypothesised surrounding biological function of fission and fusion. Morphological changes to mitochondrial networks have been heavily linked with nutrient availability, regulating the energy production of cells through respiration (Liesa *et al.* 2009; Yu and Pekkurnaz 2018). Studies of HeLa cells demonstrated prominent mitochondrial reorganization in response to changes in energy substrate availability, increasing mitochondrial distribution in response to forced oxidative phosphorylation (OXPHOS; Rossignol *et al.* 2004). Importantly, starvation of cells was shown to drive mitochondrial fusion and thus elongation, preventing the degradation of mitochondria through mitophagy whilst maintaining ATP synthesis (Gomes *et al.* 2011; Rambold *et al.* 2011). Furthermore, induction of stress either via ultra-violet irradiation, serum or amino acid starvation induced mitochondria to hyper-fuse, forming a highly interconnected network, alongside significant increases in ATP production (Tondera *et al.* 2009). However, more recent analysis of cardiac energy demand in mice demonstrated increased mitochondrial fragmentation due to fission, alongside increased mitochondria function, in response to increased energy requirements (Coronado *et al.* 2018), suggesting mitochondrial morphology changes may be cell type specific.

Similarly, both fission and fusion can be seen as protective mechanism to prevent mitochondrial network dysfunction. Mitochondrial fusion is hypothesised to maintain mitochondrial homeostasis, allowing the diffusion of proteins and metabolites throughout the mitochondrial network to prevent mitochondrial heterogeneity and dysfunction (Liu *et al.* 2009; Chan 2020). This is of particular importance for mtDNA integrity, which is essential to mitochondrial function, and constantly undergoes sporadic mutation due to the production of free radicals (Harman 1992; Taylor and Turnbull 2005). Loss of fusion capability prevents the distribution of mtDNA throughout the mitochondrial network and also enables the accumulation of mtDNA mutations (Chen *et al.* 2007; Chen *et al.* 2010; Yu-Wai-Man *et al.* 2010; Chan 2020). Preventing the accumulation of mtDNA mutations through mitochondrial fusion thus prevents functional decline.

Furthermore, fission plays a central role in the segregation and removal of dysfunctional mitochondria from the cytoplasm through mitophagy. Fission and the inhibition of fusion initiates the process of mitochondrial segregation, preventing dysfunctional mitochondria from integrating back into the mitochondrial network. Fusion inhibition is primarily governed by reduction and/or inactivation of OPA1 protein, dependent on dysfunctional mitochondrial characteristics such as reduced membrane potential or inactive OXPHOS (Duvezin-Caube *et al.* 2006; Ishihara *et al.* 2006; Twig *et al.* 2008; Mishra *et al.* 2014). Alongside fusion inhibition, fission can induce mitochondrial fragmentation to facilitate the removal of mitochondria, which is a prominent response to mitochondrial stress (Lemasters 2005; Twig and Shirihai 2011; Wu *et al.* 2011; Frank *et al.* 2012; Toyama *et al.* 2016). Furthermore, IMM depolarisation causes stabilisation of PTEN-induced putative kinase 1 (PINK1) on the OMM, preventing its proteolytic degradation by the mitochondrial rhomboid protease, PARL (Matsuda *et al.* 2010; Twig *et al.* 2011; Kondapalli *et al.* 2012; Nguyen *et al.* 2016). PINK1 stabilisation subsequently causes the recruitment of cytosolic PARKIN, a ubiquitin E3 ligase, to the OMM (Kim *et al.* 2008; Matsuda *et al.* 2010; Twig *et al.* 2011; Kondapalli *et al.* 2012; Nguyen *et al.* 2016). Recruitment to the OMM and activation of PARKIN through phosphorylation subsequently causes poly-ubiquitylation of OMM proteins, including VDAC1 and the mitofusins, identifying mitochondria for degradation (Geisler *et al.* 2010; Ziviani *et al.* 2010). Ubiquitination of OMM proteins causes the recruitment of the autophagosome adaptor p62, which results in clustering of mitochondria targeted for degradation before engulfment by autophagosome (Geisler *et al.* 2010; Narendra *et al.* 2010; Deas *et al.* 2011). Mitophagy therefore represents a carefully coordinated process for the effective clearance of dysfunctional mitochondria to maintain mitochondrial homeostasis, which is governed by the synergistic mechanisms of fission and fusion.

Both fission and fusion are coordinated through separate members of dynamin-related superfamily of proteins, however, due to their double membrane composition, the fusion of two mitochondria requires a sequential, two-step mechanism. Early studies of both *Drosophila* and yeast demonstrated that GTPase proteins tethered to the OMM regulate mitochondrial fusion (Hermann *et al.* 1998). Further molecular analysis of the mammalian fusion process has revealed the core protein machinery required for the two-step process, with the synergistic cooperation of mitofusin 1 and 2 (MFN1 and MFN2) and OPA1. MFN1 and MFN2 are essential for the initial fusion of the OMM on two adjacent mitochondria through homotypic and heterotypic interactions (Figure 1.6; Santel *et al.* 2000; Chen *et al.* 2003). Following the discovery of OPA1 as a mitochondrial protein, studies have identified it as a regulator of mitochondrial network structure, functioning as a pro-fusion protein that facilitates the fusion of the IMM (Figure 1.6; Delettre *et al.* 2000; Cipolat *et al.* 2004; Davies *et al.* 2007). Although the mechanisms of OMM and IMM fusion are regulated by separate machinery, the two-process are strongly linked and it has been shown that OPA1 functionally requires MFN1, but not MFN2, for IMM fusion (Cipolat *et al.* 2004). Conversely, fission is coordinated primarily through mitochondrial recruitment of dynamin-related protein 1 (DRP1) from its cytosolic pool to the OMM surface (Chan 2020). Initial studies demonstrated that both DRP1 and Dnm1, the DRP1 yeast orthologue, form rings around mitochondria at division points to constrict the mitochondrial tubule and eventually cause mitochondrial scission (Figure 1.6; Bleazard *et al.* 1999; Smirnova *et al.* 2001). Follow up studies have further elaborated the components required for fission, demonstrating the requirement of OMM integral proteins Fis1, Mff, MiD49 and MiD51 for recruitment of DRP1 onto the OMM surface before the initiation of fission (Losón *et al.* 2013; Chan 2020).

Dysfunction of either OMM or IMM fusion and fission has downstream implications for mitochondrial dynamics, and genetic mutations within either mechanism are associated with disease. Two clinical studies have associated mutation in *DRP1* to microcephaly and abnormal brain development (Waterham *et al.* 2007), and epilepsy (Vanstone *et al.* 2016). Furthermore, mutations within *MFN2* were identified as a genetic cause of Charcot-Marie-Tooth neuropathy type 2 (Züchner *et al.* 2004), whilst aside from causing DOA (Alexander *et al.* 2000) mutations in *OPA1* are heavily linked to further neurological conditions; such as, PD (Carelli *et al.* 2015) and infantile mitochondrial encephalomyopathy (Spiegel *et al.* 2016).

1.4.2.1 *OPA1* mutations and mitochondrial fusion

The use of *OPA1* mutant cell lines in conjunction with RNA interference (RNAi) studies has developed the picture surrounding OPA1 dysfunction and mitochondrial fusion. DOA patient-derived fibroblasts with either *OPA1*: c.2708_2711delTTAG (p.R905*) and

OPA1: c.1334G>A (p.R445H) mutations, known to be the most prevalent mutation within the UK population (Yu-Wai-Man and Chinnery 2013) and associated with increased risk of developing DOA+ (Amati-Bonneau *et al.* 2003; Yu-Wai-Man *et al.* 2010) respectively, demonstrate a notable increase in mitochondrial fission, resulting in severe fragmentation of the mitochondrial network (Amati-Bonneau *et al.* 2005; Zanna *et al.* 2008), suggesting that both haploinsufficiency and dominant-negative mutations perturb mitochondrial dynamics. Similarly, reduction of OPA1 through RNAi in HeLa cells and Mouse Embryonic Fibroblasts (MEFs) impairs mitochondrial fusion, increases network fragmentation and ultimately creates punctate and dispersed mitochondria (Amati-Bonneau *et al.* 2005; Arnoult *et al.* 2005; Zanna *et al.* 2008; Kushnareva *et al.* 2013). Furthermore, generation of DOA mouse models through targeted *Opa1* mutation, resulting in heterozygous truncation of OPA1 and haploinsufficiency, further confirmed the effects seen in cell lines. In comparison to healthy controls, muscle explant cells from *Opa1+/-* mice had significantly higher levels of dispersed and punctate mitochondria than those of *Opa1+/+* mice (Davies *et al.* 2007). However, analysis of *ex vivo* rat RGCs treated for 3 day with *Opa1* small interfering RNA (siRNA) showed no clear morphological abnormalities in axonal mitochondria, with both the mitochondrial length and volume equal to those of scrambled siRNA controls (Kushnareva *et al.* 2013).

Importantly, experiments using OPA1 null cells have further illuminated the role OPA1 plays in mitochondrial fusion. *Opa1* null MEFs transfected with proteolytic cleavage resistant L-OPA1 isoforms suggested that the presence of both L-OPA1 and S-OPA1 is required for mitochondrial fusion, with little to no fusion activity when either OPA1 form is expressed alone (Song *et al.* 2007). More recently, molecular studies of membrane fusion models have further revealed the mechanisms surrounding OPA1 mediated mitochondrial fusion, demonstrating that L-OPA1 interacts with cardiolipin, a key inner membrane lipid, on opposing membranes to initiate membrane fusion. Addition of S-OPA1 within this system further accelerated membrane fusion, suggesting that the short isoform can facilitate L-OPA1 driven fusion (Ban *et al.* 2017). Interestingly, analysis of all *OPA1* mRNA isoforms suggested that transcripts that generate both L-OPA1 and S-OPA1 have substantially greater membrane fusion activity than those that are predominantly proteolytically cleaved into S-OPA1, reaffirming the hypothesis that both L-OPA1 and S-OPA1 are required fusion activity. Furthermore, the OPA1 isoforms that result in significant levels of cleavage, and have poor fusion activity all contain exon 4b, suggesting this exon may facilitate the regulation OPA1 proteolytic processing and fusion (Song *et al.* 2007). Further analysis of isolated S-OPA1 within the same membrane fusion model suggested it can facilitate membrane fusion, independent of L-OPA1, when both fusing membranes contain cardiolipin (Belenguer *et al.* 2013), however, when S-OPA1 isoforms are solely expressed within OPA1 null MEFs mitochondrial membrane

fusion is lost (Song *et al.* 2007). Thus, the true role of S-OPA1 in mitochondrial fusion remains unclear and requires further investigation.

In addition to regulating overall mitochondrial networks, OPA1 has also been shown to define the structure of the IMM required for mitochondrial function. Classically, the IMM is formed into multiple thin, well defined cristae structures that run perpendicular to the longitudinal mitochondrial axis. However, when mitochondria lose their ability to maintain IMM structure, cristae morphology becomes abnormal, with mitochondria presenting with disorganised, swollen cristae that can run parallel with the longitudinal axis or becoming devoid of cristae altogether (Agier *et al.* 2012). Knockdown of *OPA1* expression with siRNA causes severe disruption to mitochondria cristae structure, generating vesicular like structures rather than envelopes perpendicular to the outer membrane (Olichon *et al.* 2003; Song *et al.* 2007; Agier *et al.* 2012). Again, the generation of *Opa1* mutant mice carrying a splice site mutation that induces skipping of exon 10, and thus a deletion of 27 amino acids from the GTPase domain, further demonstrated the effects of *OPA1* mutation on mitochondrial morphology. Electron microscopy analysis of RGCs in mutant mice revealed abnormal cristae morphology, with severely disorganised IMM cristae structure when compared to WT mice. *Opa1* mutant mice exhibited mitochondria devoid of cristae structures, or with grossly abnormal morphology (e.g. swollen, wide cristae; Alavi *et al.* 2007). Additional analysis of both L- and S-OPA1 in MEFS further confirmed OPA1 function in cristae formation, demonstrating that both isoforms facilitate the structure of the IMM by creating tight cristae junctions (Frezza *et al.* 2006). Whilst in depth analysis of all OPA1 variants suggests that either L-OPA1 and S-OPA1 alone are sufficient to facilitate cristae formation, GTPase functionality is required to maintain cristae junction integrity as GTPase defective OPA1 variants exhibit morphologically abnormal cristae (Patten *et al.* 2014; Lee *et al.* 2017). Despite this depth of knowledge surrounding OPA1 function in mitochondrial network and morphological structure, no study has examined the impact OPA1 dysfunction has on human RGC mitochondrial networks as yet.

1.4.3 Mitochondrial function overview

The most prominent mitochondrial function is the generation of ATP through OXPHOS. Functionally, the OXPHOS system is composed of the electron transport chain (ETC) and ATP synthase (Figure 1.7), which are fuelled through the generation of reduced nicotinamide adenine dinucleotide (NADH) and flavin adenine dinucleotide ($FADH_2$) by glycolysis, the breakdown of glucose, and the tricarboxylic acid (TCA) cycle, the oxidation of acetyl-coenzyme A (acetyl-CoA). The ETC is primarily composed of multi-subunit protein complexes I-IV, in conjunction with Coenzyme Q10 and cytochrome *c* (Figure 1.7). Collectively the ETC functions to generate an electrochemical gradient by

simultaneously transferring electrons through the chain and shuttling hydrogen ions (H^+) into the mitochondrial intermembrane space (Figure 1.7). Lastly, ATP synthase (or complex V) utilises the generated electrochemical gradient for energy production, pumping H^+ into the mitochondria matrix to catalyse the reaction of adenosine diphosphate (ADP) to ATP, utilising approximately four H^+ to synthesise 1 molecule of ATP (Figure 1.7; Osellame *et al.* 2012; Chaban *et al.* 2014; Bulthuis *et al.* 2019). Mitochondrial membrane structure and morphology are tightly linked to the generation of energy through OXPHOS, with approximately 94 % of both complex III and ATP synthase embedded in the impermeable IMM cristae folds (Gilkerson *et al.* 2003). This relationship is further exemplified through analysis of ATP synthase structure, which demonstrated subunit involvement in generating cristae morphology (Paumard *et al.* 2002). Furthermore, IMM cristae structure is key to generating ETC respiratory supercomplexes, quaternary structures of multiple ETC components that increase respiratory efficiency (Cogliati *et al.* 2013).

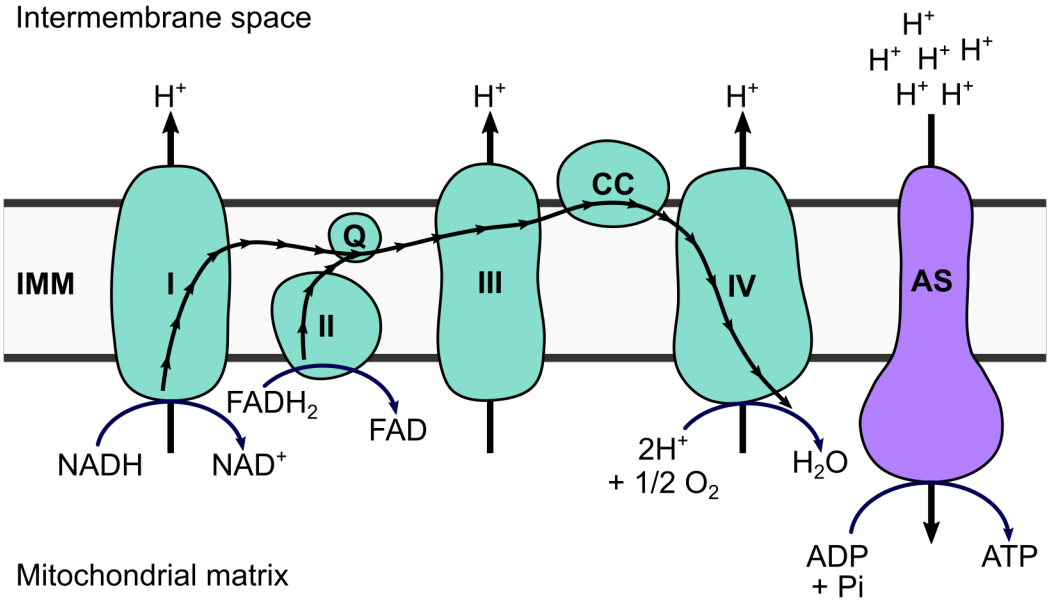

Figure 1.7. Electron transport chain and ATP synthase schematic.

Mitochondrial ATP is generated by the ETC and ATP synthase located in the IMM. Reduced nicotinamide adenine dinucleotide (NADH) and flavin adenine dinucleotide ($FADH_2$) are produced by glycolysis and the tricarboxylic acid (TCA). The ETC is composed of multi-subunit protein complexes I-IV (green) that work in conjunction with Coenzyme Q10 (Q) and cytochrome *c* (CC). The ETC generates an electrochemical gradient by transferring electrons through the chain and shuttling hydrogen ions (H^+) into the mitochondrial intermembrane space. Lastly, ATP synthase (AS; also known as complex V) utilises the electrochemical gradient for energy production, pumping H^+ into the mitochondria matrix to catalyse the reaction of ADP with inorganic phosphate (Pi) to ATP.

Inspired by from Osellame *et al.* (2012).

Although initially identified as the primary organelle for energy production, mitochondria are now known to play a central role in a diverse array of cellular functions beyond ATP synthesis. Most notably, mitochondria function in the regulation of calcium signalling, the initiation of metabolic biosynthetic pathways and regulating programmed cell death

(Osellame *et al.* 2012; Spinelli *et al.* 2018). The mitochondrial network is thus central to overall cellular health and mitochondrial dysfunction has downstream implications beyond energy deficiency.

In addition, mitochondria have been shown to function in cellular calcium (Ca^{2+}) signalling, a ubiquitous second messenger molecule, by regulating the availability of Ca^{2+} (Giorgi *et al.* 2018). Mitochondria possess a number of protein pores and transporters that function in Ca^{2+} uptake. Due to the OMMs inherent permeability, Ca^{2+} can readily traverse the OMM. Once located within the intermembrane space, mitochondria primarily transfer Ca^{2+} through the mitochondrial Ca^{2+} uniporter (MCU) complex (Giorgi *et al.* 2018). Uptake of Ca^{2+} by mitochondria is believed to play a number of key functions in cell function (Rizzuto *et al.* 2012). Ca^{2+} import is known to be a key modulator of OXPHOS activity, through activation of the three rate limiting steps in the TCA cycle, thus accelerating the generation of H^+ and electron donors for the ETC in the form of NADH. Increased turnover in the TCA cycle thus accelerates ETC function, ultimately increasing ATP output (Jouaville *et al.* 1999; Gunter *et al.* 2000; Osellame *et al.* 2012). Linking Ca^{2+} influx to energy production is believed to be central to cellular function due to the role of Ca^{2+} as a second messenger molecule. Cellular activation, such as neuronal stimulation or muscle contraction, that functions through Ca^{2+} and requires increased energy supply also induces increased mitochondrial output, thus coupling cellular stimulation to energy output (Pinton *et al.* 2008; Griffiths and Rutter 2009)

In addition, it is believed mitochondrial Ca^{2+} uptake regulates local and bulk cytoplasmic Ca^{2+} signalling pathways through modulating the amplitude of Ca^{2+} cascades (Gunter *et al.* 2000; Giorgi *et al.* 2018), a process examined closely in neuronal and cardiac cell populations (Werth and Thayer 1994; David and Barrett 2003; Maack *et al.* 2006; Drago *et al.* 2012; Fluegge *et al.* 2012). Furthermore, buffering cellular Ca^{2+} is known to be integral to cell viability, with high levels of intracellular Ca^{2+} known to be cytotoxic to cells (Sattler and Tymianski 2000; Rizzuto *et al.* 2003; Danese *et al.* 2017), with efflux of Ca^{2+} from the endoplasmic reticulum known to be an initiator of cell death pathways (Scorrano *et al.* 2003; Danese *et al.* 2017). However, prolonged mitochondrial Ca^{2+} overload is also pro-apoptotic through its induction of the mitochondrial permeability transition (PMT). Increased mitochondrial matrix Ca^{2+} induces the opening of permeability transition pores, abruptly increasing the permeability of the IMM (Pinton *et al.* 2008; Lemasters *et al.* 2009). PMT induces mitochondrial swelling, followed by membrane rupture and release of pro-apoptotic factors, including cytochrome *c* and apoptosis inducing factor (AIF), from the intermembrane space (Gunter *et al.* 2000; Pinton *et al.* 2008). This process is integral to induction of cell death as within the mitochondria these proteins perform important

functions, whereas in the cytosol they induce pro-death signalling cascades (Murphy *et al.* 2016) and ultimately induce cell death.

Further to the function as the site of OXPHOS and Ca^{2+} homeostasis, the mitochondrial network is involved in the initiation of metabolic biosynthetic pathways. The TCA cycle is a central pathway from which mitochondria contribute to macromolecule synthesis. Intermediates from the TCA cycle, including citrate and α-ketoglutarate, are shuttled from the mitochondrial matrix to enable the synthesis of lipids and amino acids (Ahn and Metallo 2015; Herst *et al.* 2017; Williams and O'Neill 2018). TCA metabolites are also required for post-translational modification of proteins, enabling cells to fine tune protein modifications for specific cell functions. For example, exported citrate can be converted into acetyl-CoA to provide acetyl groups for protein acetylation (Pietrocola *et al.* 2015; Martínez-Reyes and Chandel 2020). Furthermore, the synthesis of both purine and pyrimidine nucleotides is dependent on mitochondrial function. Pyrimidine synthesis relies on the activity of mitochondrially located dihydroorotate dehydrogenase (DHODH) for substrate conversion (Löffler *et al.* 2005; Ahn *et al.* 2015). Similarly, purine synthesis is dependent on the generation of formate from the catabolism of the amino acid serine, a reaction that predominantly occurs within the mitochondrial matrix (Ahn *et al.* 2015; Ben-Sahra *et al.* 2016). Additionally, mitochondrial are essential for the generation of steroid precursors within steroidogenic cells. The P450scc enzyme, which associates with the IMM, initiates the generation of steroids through the cleavage of cholesterol to generate the soluble steroid precursor pregnenolone (Jefcoate *et al.* 1992; Miller 2013). Thus, mitochondria are central to biosynthetic pathways within eukaryotic cells, coupled with their fundamental role in energy production, disruption of mitochondrial function has severe downstream impacts on cell viability.

1.4.3.1 OPA1 in mitochondrial function

As previously mentioned, control of mitochondrial dynamics is a central regulator of cellular bioenergetic output to match the demands of each individual cell (Westermann 2010; Suárez-Rivero *et al.* 2017), due to its role in mitochondrial dynamics, OPA1 can be seen as an important regulator of mitochondrial energy output. Unsurprisingly, OPA1 function in respiration regulation is directly coupled to its role regulating mitochondrial fusion and inner membrane morphology. When mitochondrial fusion is entirely inhibited through either targeted gene mutation or RNAi knockdown of pro-fusion genes, including both *MFN1*, *MFN2* and *OPA1*, cellular respiration is severely impaired. Restoration of gene function via exogenous gene expression restores mitochondrial fusion and thus respiratory function, suggesting that mitochondrial fusion directly impacts respiration (Chen *et al.* 2005).

OPA1 has also been shown to respond to changes in nutrient availability in order to regulate cristae structure and thus ATP synthesis. *In vitro* analysis of OPA1 function through cellular starvation of Opa1 null cells demonstrated that a fusion incompetent OPA1 mutant could rescue respiration through the tightening of cristae driven by increased OPA1 oligomerization at cristae junctions, potentially altering local substrate concentrations to support ETC function (Patten *et al.* 2014). Importantly, increased oligomerization was driven by OPA1 interactions with SLC25A transporters, a family of mitochondrial molecular transporters involved in sensing substrate availability and required for mitochondrial substrate transfer across the IMM (Gutiérrez-Aguilar and Baines 2013; Patten *et al.* 2014). Treating cells with molecules that mimic SLC25A transporter substrates reduces OPA1 oligomerisation and increases IMM cristae width, replicating the effect of nutrient rich conditions (Patten *et al.* 2014). In addition, analysis of cells with 2708del and 1334G>A mutations, alongside model cell lines, demonstrates that *OPA1* mutation results in reduced ATP synthesis via OXPHOS (Lodi *et al.* 2004; Amati-Bonneau *et al.* 2005; Zanna *et al.* 2008; Kushnareva *et al.* 2013). Analysis of *ex vivo* mouse cortical neurons treated with *Opa1* siRNA demonstrated significant reductions in maximal mitochondrial respiration and ATP synthesis, as determined by Seahorse bioenergetic analysis (Millet *et al.* 2016). In addition, analysis of *in vitro* differentiations has also confirmed the effect of OPA1 mutation on mitochondrial respiration, with both iPSC derived dopaminergic neurons (Jonikas *et al.* 2018) and iPSCs derived neural progenitor cells (NPCs; Iannielli *et al.* 2018) demonstrating reduced OXPHOS functionality with lower ATP synthesis. Recently it has been demonstrated that any splice isoform of human *OPA1* is capable of rescuing ATP synthesis within Opa1 null MEFs, a feature that was independent of their ability to rescue mitochondrial morphology, suggesting that functional fusion *per se* is not required for OPA1 regulation of energy output (Del Dotto *et al.* 2017).

However, reduced ATP synthesis is not thought to result from reduced assembly of the respiratory chain, but rather reduced enzyme stability, primarily of complex I, complex IV and ATP synthase, due to loss of cristae structure (Chevrollier *et al.* 2008; Zanna *et al.* 2008; Kushnareva *et al.* 2013; Patten *et al.* 2014). Furthermore, analysis of ATP synthase dimerization and oligomerization, which increases enzymatic efficiency, demonstrated reduced levels in OPA1 knockout cells when compared to WT counterparts (Gomes *et al.* 2011). Additionally, it has become evident that tight cristae junctions formed by OPA1 facilitate the assembly and stabilisation of respiratory chain supercomplexes. Loss of OPA1 dependent cristae structure results in the degradation of supercomplexes, reduced respiratory output and reduced cellular growth (Cogliati *et al.* 2013). This effect was further confirmed in *Opa1*^{delTTAG} mice, which exhibited reduced supercomplex stability and a greater quantity of monomeric ETC components (Sarzi *et*

al. 2012). It is thus clear that OPA1 plays a vital role in maintaining cellular bioenergetic output through regulation of mitochondrial cristae morphology and ETC components.

Although the predominant work on OPA1 function has focused on its effects on OXPHOS, given the central role of mitochondrial in cellular energy production, additional studies have identified further deficits in mitochondrial function caused by *OPA1* mutation. Analysis of the *Opa1*^{delTTAG} DOA mouse model identified female specific deficits in steroid synthesis. *Opa1* mutant mice exhibited increased steroid production within the blood and retina, which were implicated in impaired complex IV activity and increased RGC apoptosis (Sarzi *et al.* 2016). Furthermore, Kushnareva *et al.* (2013) demonstrated loss of *Opa1* in *ex vivo* RGCs through RNAi reduced the ability for mitochondrial to maintain Ca^{2+} homeostasis. Most notably, cells with *Opa1* knockdown exhibited reduced ability to buffer cellular Ca^{2+} levels due to an inability to retain Ca^{2+} within the mitochondrial matrix. In addition, *Opa1* knockdown cells exhibited a reduced level of TCA activation following induction of mitochondrial Ca^{2+} uptake, required for the Ca^{2+} induced energetic response to mitochondrial stimulation. More recently, metabolomic analysis of *Opa1* null MEFs revealed significant alterations to the metabolomic profiles, with a particular focus on the concentrations of key mitochondrial substrates. Ablation of Opa1 caused significant decreases in aspartate, glutamate and α-ketoglutarate in parallel with increased concentration of asparagine and glutamine, key metabolites in both the TCA cycle and amino acid and nucleotide biosynthesis (Bocca *et al.* 2018). This coincides with analysis of patient-derived plasma from the same research group, which demonstrated impairment of purine metabolism, including significant differences in aspartate and glutamate concentrations (Bocca *et al.* 2018). Ultimately, these deficits further confirm the impact *OPA1* mutation has on mitochondrial function, indicating how deficits in biosynthetic pathway may promote DOA progression.

1.4.4 The mitochondrial stress response

Although the direct function of OPA1 within mitochondria function is becoming ever clearer, the additional downstream effects of a mitochondrial aberrations, including network fragmentation, dysfunctional bioenergetics or disrupted molecular biosynthesis, are less well understood. Consequently, a dysfunctional mitochondrial network represents a significant source of intrinsic toxic insults, such as the generation of reactive oxygen species (ROS), the accumulation of mutated mtDNA or impaired Ca^{2+} flux (Amati-Bonneau *et al.* 2008; Yu-Wai-Man *et al.* 2010; Kushnareva *et al.* 2013; Chen *et al.* 2016). Although cells have the ability to clear dysfunctional mitochondria through autophagy, more recently it has become clear that cells possess distinct signalling pathways to regulate and prevent the accumulation of such cytotoxic insults, that may lead to cellular stress and ultimately cell death (Melber and Haynes 2018).

Initial demonstration of a mitochondrial specific stress response in mammalian cell lines, established that depletion of mtDNA through ethidium bromide treatment causes significant upregulation of both *HSP60* and *HSP10* through nuclear transcriptional changes, thus indicating mitochondrial-nuclear communication of stress (Martinus *et al.* 1996). Following this discovery, the molecular pathways required for the mitochondrial stress (mito-stress) response have been more extensively characterised within *Caenorhabditis elegans*. Importantly, the perturbation of numerous different mitochondrial components has been shown to activate the mitochondrial stress response, including mtDNA damage, inhibition of the respiratory chain complexes or inactivation of mitochondrial protein-handling machinery (Figure 1.8; Martinus *et al.* 1996; Yoneda *et al.* 2004; Baker *et al.* 2012; Runkel *et al.* 2013), characteristics commonly associated with *OPA1* mutation.

Within *C. elegans* the transcriptional alterations in response to mito-stress are primarily coordinated by the transcription factor 'activating transcription factor associated with stress–1' (ATFS-1), which is imported into the mitochondria under normal homeostatic conditions. However, under stress ATFS-1 mitochondrial import is inhibited leading to cytosolic accumulation, subsequent nuclear translocation and transcriptional activation of stress response genes, including protein chaperones and proteases (Nargund *et al.* 2012). Since the discovery of specific signalling factors coordinating mitochondrial-nuclear communication, extensive work has been completed to determine the proteins and transcription factors required for mammalian signalling. Initial experiments demonstrated that mito-stress, induced through accumulation of unfolded protein within the mitochondrial matrix, was coordinated through the transcription factor DDIT3 (also known as CHOP; Zhao *et al.* 2002). Zhao *et al.* (2002) demonstrate that overexpression of DDIT3 caused an approximate 2-fold increase in mitochondrial chaperones, however, dominant-negative DDIT3 mutants failed to induce expression of genes regulated by DDIT3. Interestingly, although DDIT3 is integral to the endoplasmic reticulum integrated stress response (ISR), Zhao *et al.* (2002) suggested that mitochondrial signalling is independent of ISR signalling, as mito-stress does not induce ISR downstream proteins. However, more recent data suggests that mito-stress, induced by rotenone inhibition of complex I, induces ISR associated genes and phosphorylation cascades, most notably that of protein kinase RNA (PKR)-like ER kinase (PERK) and eukaryotic translation initiation factor-2 phosphorylation (eIF2α; Silva *et al.* 2009; Quirós *et al.* 2017). Both PERK and eIF2α are integral to the ISR, increasing transcription of downstream response genes required for attenuating the stress insult (Pakos-Zebrucka *et al.* 2016). Furthermore, additional investigation of the DDIT3 activated mito-stress response demonstrated a requirement for CEBPB-DDIT3 dimerization for gene activation, which

actively target DDIT3 response elements upstream of response genes (Figure 1.8; Zhao *et al.* 2002; Aldridge *et al.* 2007).

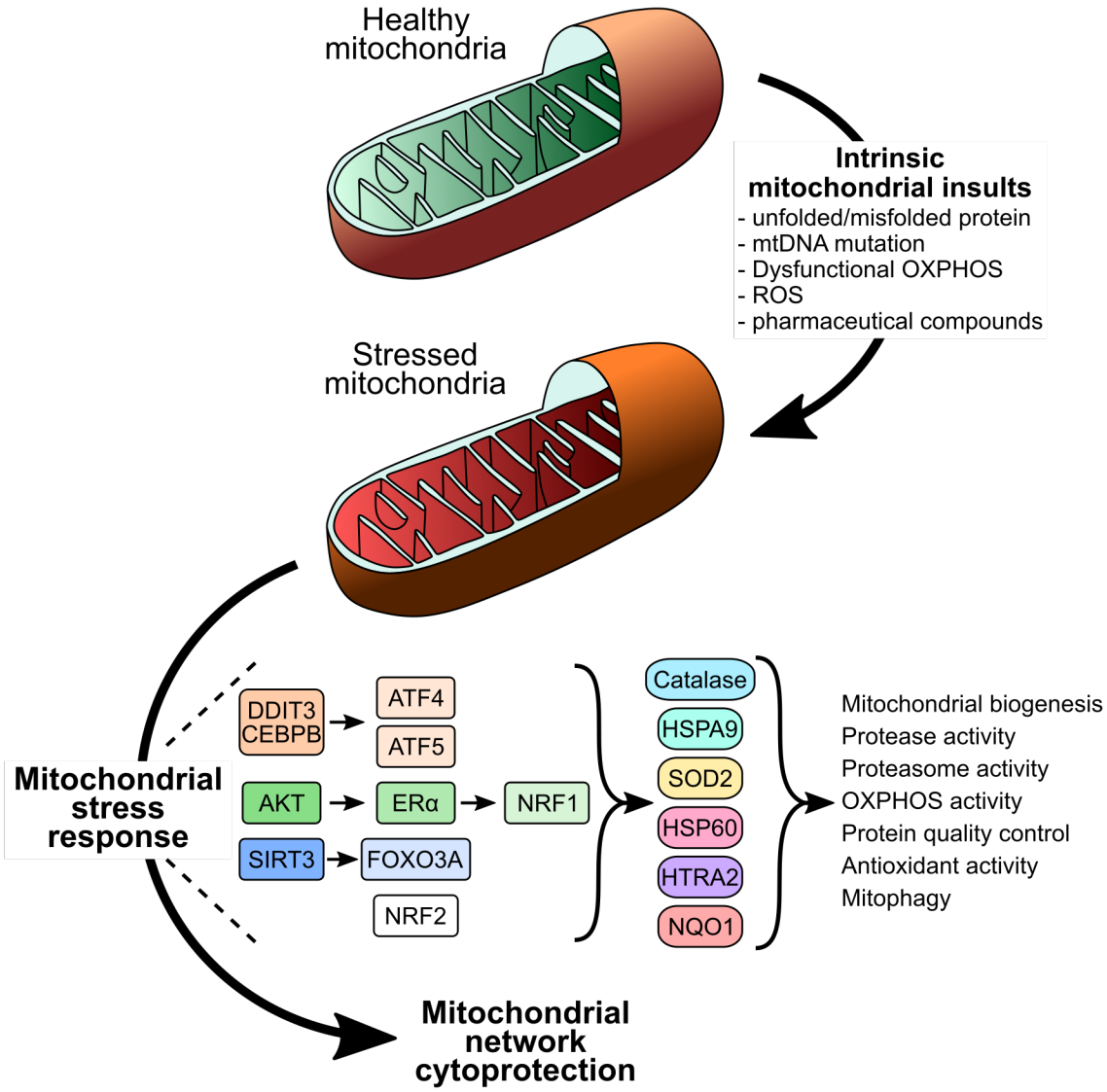

Figure 1.8. Mitochondrial stress response.

Schematic representation of mammalian mitochondrial stress response. Healthy mitochondria accumulate intrinsic insults, including reactive oxygen species (ROS), mtDNA mutations and misfolded proteins, which activates the mitochondrial stress response gene pathways. Activation of the mito-stress response causes DDIT3-CEBPB activation, followed by *ATF5* and *ATF4* induction. Accumulation of misfolded proteins causes phosphorylation of AKT, which in turn phosphorylates ERα and induces expression of *NRF1*. SIRT3 activation causes the relocalisation of FOXO3A to further modulate the mito-stress response. Activation of mito-stress signalling cascades causes upregulation of proteins, including HSPA9, HSP60 and NQO1, with chaperonin and antioxidant activity required for restoring mitochondrial homeostasis.

Inspired by Kenny *et al.* (2017) and Münch (2018).

More recently, ATF5 has been identified as the mammalian homologue of ATFS-1, acting downstream of DDIT3 (Figure 1.8; Kenny *et al.* 2017). Importantly, ATF5 has been shown to have similar regulation to ATFS-1, with import into the mitochondria under normal homeostatic conditions and nuclear translocation during mito-stress.

Furthermore, ATF5 could rescue mito-stress responses in ATFS-1 null *C. elegans* (Fiorese *et al.* 2016). ATF4 has also been identified as an integral signalling factor during mito-stress, upregulating genes required for cytoprotection and metabolic reprogramming through activation of core stress response pathways. Importantly, ATF4 reduces mitochondrial ribosomal proteins (MRPs) through reduced translation and thus attenuates mitochondrial translation to reduce protein synthesis during stress events, potentially reducing further production of cyto-toxic proteins (Silva *et al.* 2009; Quirós *et al.* 2017). Finally, the transcriptional mito-stress changes are also believed to be coordinated by the Mitochondrial unfolded protein response elements (MURE1 and MURE2), which have been identified in proximity to DDIT3 binding elements in mito-stress response genes, suggesting that there are additional signalling proteins that can regulate the mito-stress response (Aldridge *et al.* 2007).

Further to transcription factor coordinated responses to mito-stress, mammalian cells also possess responses primarily coordinated through protein activation. Accumulation of ROS or unfolded proteins within the intermembrane space has been shown to enhance the mammalian mito-stress response. Increased levels of misfolded proteins induce the phosphorylation of AKT, subsequently activating oestrogen receptor α (ERα) through phosphorylation and inducing expression of *NRF1* (Figure 1.8; Papa and Germain 2011). NRF1 facilitates the regulation of genes required for mitochondrial respiratory function and increases both proteasome and protease activity, including HTRA2, to increase the total level of cellular protein quality control (Scarpulla 2006; Radke *et al.* 2008; Papa *et al.* 2011; Münch 2018). Inhibition of ERα through RNAi prevents activation of NRF1, and subsequently inhibits activation of the mito-stress response (Papa *et al.* 2011). Furthermore, although there are conflicting reports regarding the effect of ERα activation on NRF2 activity (Namani *et al.* 2014; Oh *et al.* 2019), studies suggest that NRF2, a homologue to NRF1, is crucial to mitochondrial antioxidant response. During normal homeostatic conditions, NRF2 is rapidly cycled within the cytoplasm preventing its translocation to the nucleus, however, upon activation NRF2 translocates to the nucleus for gene induction (Shih *et al.* 2005; He *et al.* 2009; Kovac *et al.* 2015). Activated NRF2 binds to regulatory anti-oxidant response elements to activate downstream cytoprotective genes, including antioxidants such as heme oxygenase 1 (*HMOX1*), the versatile NAD(P)H quinone oxidoreductase 1 (*NQO1)*, and multiple glutathione S-transferase (GSTs) isoforms (He *et al.* 2009; Baird and Dinkova-Kostova 2011; Chau 2015; Kovac *et al.* 2015; Ross and Siegel 2017). Analysis of NRF2-KO cells further confirmed the importance of NRF2 in maintaining mitochondrial homeostasis, demonstrating significantly increased mitochondrial ROS production, reduced respiration and reduced ATP levels in KO cells when compared to WT cells (Holmström *et al.* 2013; Kovac *et al.* 2015).

Furthermore, analysis of ERα negative cell lines identified a further mito-stress response pathway coordinated by Sirtuin 3 (SIRT3) protein activity, a pathway independent of DDIT3 activation (Papa and Germain 2014; Kenny *et al.* 2017). During mito-stress, SIRT3 levels become elevated, which results in the activation of the transcription factor FOXO3a through deactylation, FOXO3a subsequently increase expression of mito-stress response genes (Figure 1.8; Papa *et al.* 2014). Similar pathways were subsequently identified within *C. elegans,* in which sirtuin deactylases regulate mitochondrial function through nuclear gene expression (Mouchiroud *et al.* 2013). Furthermore, SIRT3 has been shown to be sequestered by ATP synthase under normal homeostatic conditions, however, upon mitochondrial pH reduction and membrane depolarization SIRT3 dissociates to rapidly deacetylate proteins required for maintaining the membrane potential (Yang *et al.* 2016). Finally, SIRT3 has also been associated with maintenance of the mitochondrial genome. Analysis of SIRT3 knockout mice demonstrated increased mtDNA instability with age, whilst SIRT3 null MEFs demonstrated increased levels of mtDNA deletion after serial passage (Kim *et al.* 2010).

Although the signalling cascades required for the mito-stress response are still being delineated, it is clear that mammalian cells possess a number of methods to alleviate stress, including mitochondrial effector proteins required to reduce cytotoxic stimuli. The DDIT3-CEBPB axis of the mito-stress response is known to upregulate expression of mitochondrial proteases and chaperones, including *HSP60* and *HSP10* required for maintain mitochondrial proteostasis (Figure 1.8; Zhao *et al.* 2002; Münch 2018). Furthermore, activation of the mito-stress response with either paraquat or expression of mutant proteins causes induction of both *HSP60* and *HSPA9* (also known as mtHSP70) to promote correct protein folding, through ATF5 signalling (Fiorese *et al.* 2016). In addition, research suggests the response coordinated by ERα and NRF1 increases proteasome activity, reducing protein import, and induces expression of *HTRA2*, a mitochondrial serine protease involved in protein degradation, in order to increase the level of mitochondrial protein quality control (Papa *et al.* 2011). Furthermore, the SIRT3 coordinated mito-stress response orchestrates expression of key enzymes require for antioxidant activity, including SOD2 and catalase facilitating the removal of excess ROS from the cell matrix (Figure 1.8; Papa *et al.* 2014). Unsurprisingly, in addition to activating the expression of specific cytoprotective proteins, induction of the mito-stress response also alters diverse mitochondrial functions. Multi-omic analysis of mitochondrial stress demonstrated significant alterations to carbon metabolism, biosynthesis of amino acids and reduced mitochondrial translation and OXPHOS, primarily regulated through ATF4 (Bao *et al.* 2016; Münch and Harper 2016; Quirós *et al.* 2017).

1.4.4.1 OPA1 in the mito-stress response

Although the pathways regulating mito-stress have become clearer over the past decade, the effects of OPA1 dysfunction on the mitochondrial stress response are still poorly understood. Importantly, SIRT3 has been shown to deacetylate OPA1 within the GTPase domain, increasing the GTPase activity of OPA1, and within SIRT3 knockout cells mitochondrial fusion is significant reduced, due to the reduced deacetylation of OPA1 (Samant *et al.* 2014). Thus, during mito-stress SIRT3 may play a role in increasing OPA1 activity to promote mitochondrial fusion to restore mitochondrial homeostasis. Interestingly, analysis of 10-month old OPA1+/- mice demonstrated modulation of the SIRT3 mito-stress axis, with significantly increased levels of SOD2 protein within cortices. However, siRNA knockdown of OPA1 within primary cortical neurons present a more confusing picture, with no distinct change in expression of HSP60 or SOD2 but with increased levels of catalase driven by increased NRF2 activation and nuclear translocation (Millet *et al.* 2016). Furthermore, Millet *et al.* 2016 demonstrated that patient-derived *OPA1* mutant fibroblasts have heterogeneous levels of SOD2 and catalase, further muddying the picture. Furthermore, Tezze *et al*. (2017) demonstrated activation of the ISR response within inducible Opa1 null mouse cells, activation associated with increased expression of both DDIT3 and ATF4. However, the authors make no mention of the mito-stress response instead indicating ATF4 and DDIT3 levels are associated to the induction of the ISR response and analysis of mito-stress effector proteins was not shown. Thus, further investigation is required into the effect *OPA1* mutation has on mitochondrial stress and how it may impact the disease mechanisms associated with DOA.

1.5 DOA therapeutic strategies

Alongside developing greater understanding of the role OPA1 plays within mitochondrial biology, research has aimed to develop therapeutic strategies to reduce RGC death and prevent visual decline. Unfortunately, there are no treatments clinically available to DOA patients to ameliorate symptoms. However, a number of different clinical avenues are being explored due to the diverse genotypic spectrum associated with *OPA1* mutation.

The predominant focus of therapeutic development has been understanding the potential of the ubiquinone (cytochrome *c*) analogue, ibedenone. Ubiquinone is present at remarkably high concentrations within the IMM, where it functions to efficiently shuttle electrons from complex I and complex II to complex III within the ETC (Yu-Wai-Man *et al.* 2014; Yu-Wai-Man 2015). Due to the deficiencies of complex I within *OPA1* mutant cells (Zanna *et al.* 2008) supporting the function of the ETC through electron shuttling to promote ATP synthesis, and thus supporting mitochondrial function, may be of clinical

benefit (Yu-Wai-Man *et al.* 2014; Yu-Wai-Man 2015). Importantly, idebenone is approved for the treatment of LHON within the EU (Lyseng-Williamson 2016), demonstrating its clinical safety and efficacy, whilst multiple studies have demonstrated the effectiveness of treatment (Mashima *et al.* 2000; Carelli *et al.* 2011; Klopstock *et al.* 2011; Klopstock *et al.* 2013; Lloria *et al.* 2019; Zhao *et al.* 2020). However, within LHON patient-derived fibroblasts idebenone demonstrated inconsistent results, having both positive and negligible effects on the restoration of ATP synthesis (Yu-Wai-Man *et al.* 2017), whilst another small-scale clinical trial showed limited effectiveness (Barnils *et al.* 2007).

Following the promising effects of idebenone treatment in LHON patients, a number of small-scale studies have examined the effect in DOA patients. Initially, a small pilot clinical trial of seven *OPA1* DOA patients suggested some possible benefit, with treated patients showing significant levels of visual acuity stabilization when compared to untreated patients (Barboni *et al.* 2013). Furthermore, a more recent study of 87 DOA patients confirmed these effects, suggesting idebenone provides visual acuity stabilization or recovery when compared to untreated individuals (Romagnoli *et al.* 2020). However, Romagnoli *et al.* also noted that a number of treated patients still exhibited worsening visual acuity, suggesting idebenone is not applicable for treating all patients. Furthermore, a randomized placebo-controlled trial in a DOA mouse model, where mice carry a PTC in exon 8 resulting in an approximate 50 % reduction in protein, showed a more transient benefit that may be dependent on the timing of idebenone treatment. Crucially, early treatment of mice demonstrated moderate visual recovery for 3 weeks, however, this was not sustained to the final time point at 6 weeks and treatment of aged mice (12-14 months) showed no RGC or visual improvements (Smith *et al.* 2016).

More recently, gene therapy has been explored as a potential treatment strategy for DOA. Crucially, the majority of *OPA1* mutations associated with DOA result in haploinsufficiency (Schimpf *et al.* 2008; Ścieżyńska *et al.* 2017), and even dominant negative effects could be ameliorated by increasing expression of the wild-type gene, hypothetically diluting the availability of the mutated allele to increase WT function (Wilson and Wensel 2003). Sarzi *et al.* (2018) demonstrated the feasibility of *OPA1* gene therapy, treating *Opa1*^{delTTAG} mice with an Adeno-Associated Virus (AAV) containing human *OPA1* cDNA. Importantly, this study demonstrated mice treated with AAV-*OPA1* had increased RGC survival and improved visual function when compared to untreated controls. However, despite the clinically promising results for idebenone and demonstration of feasibility of gene therapy, patients remain without a viable therapeutic option.

1.6 Thesis aims

The past two decades have illuminated our understanding of DOA and the disease mechanisms associated with *OPA1* mutation, however, despite the promise of a number of therapeutic strategies patients remain without an effective clinical approach. To-date, research has demonstrated that *OPA1* has a multifaceted function within mitochondria, regulating mitochondrial network morphology, facilitating ATP synthesis through the ETC and maintaining the integrity of the mitochondrial genome. Thus, it stands to reason that mutation to *OPA1* results in significant impairment of mitochondrial function, yet, the majority of our knowledge surrounding *OPA1* mutation has originated from out of context disease models and whether these phenotypes are consistent within and effect the primary pathologically tissue, the retina and RGCs, remains unclear. Furthermore, although two previous studies have utilised patient tissue, this is remarkably rare to obtain (Johnston *et al.* 1979; Kjer *et al.* 1983) and can thus not be relied upon to illuminate the disease mechanisms associated with DOA. Therefore, understanding the pathogenic disease mechanisms associated with *OPA1* mutation in a physiologically relevant *in vitro* model may provide valuable insight into the disease mechanisms causing the preferential loss of RGCs, providing a foundation for developing further therapeutic strategies.

The work described in this thesis therefore primarily focuses on the use of *in vitro* models to develop our understanding of *OPA1* (Figure 1.9). The use of patient-derived cells will underpin this work, providing clinically relevant cell lines with a broad range of *OPA1* mutations. In addition, this thesis will describe the use of cutting-edge disease modelling methods, including cellular reprogramming and CRISPR/Cas9 gene editing technology, to further investigate the role of *OPA1* within mitochondrial function and its association to preferential RGC death in DOA.

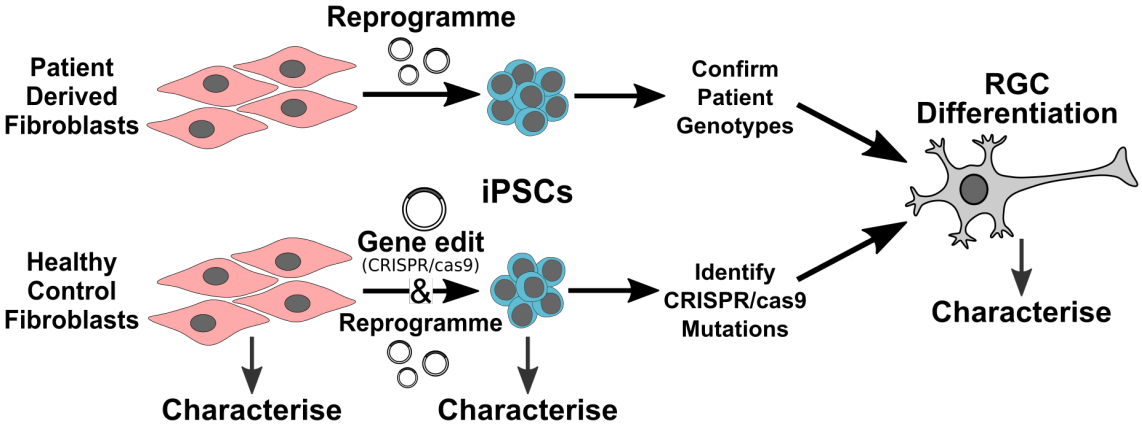

Figure 1.9. Overview of PhD work flow.

DOA patient-derived fibroblasts were reprogrammed to iPSCs through electroporation of Yamanaka factors. Simultaneously, health control fibroblasts were gene edited using CRISPR/Cas9 to generate *OPA1* knock-out cell lines. *OPA1* mutations were confirmed in all generated iPSCs before *in vitro* differentiation to RGCs. Fibroblasts, iPSCs and RGCs were characterised to determine the effects of *OPA1* mutation.

The primary aims of work described in this thesis were:

1. To establish a comprehensive biobank of induced pluripotent stem cell (iPSC) lines from DOA patients harbouring pathogenic *OPA1* mutations.

2. To optimise the differentiation of *OPA1*-mutant iPSC lines into retinal ganglion cells.

3. To further investigate the disease mechanisms by which *OPA1* mutations lead to RGC loss and progressive blindness in patients with DOA.

Chapter 2: Materials and methods

All materials and consumables are listed in supplementary materials (Appendix A).

2.1 General laboratory methods

2.1.1 Genomic DNA extraction

Total genomic DNA (gDNA) was extracted using the Wizard gDNA Purification Kit (Promega) following the manufacturers guidelines. Briefly, cells were washed with Dulbeccos phosphate buffered saline (DPBS; Gibco) and lysed with 250 µl Wizard SV Lysis Buffer. Sample lysates were transferred to individual Wizard SV Mini columns and centrifuged at 13,000 *g* for 3 minutes. Mini columns were then washed with Column Wash Solution and centrifuged at 13,000 *g* for 1 minute, repeated a total of four times. After washing, Mini columns were centrifuged for 2 minutes at 13000 *g* to dry the binding matrix. Finally, 200 µl of nuclease free water was added to the Mini column, incubated for 2 minutes at room temperature (RT) and gDNA eluted by centrifugation at 13000 *g* for 1 minute. Total DNA was quantified by spectrophotometry using a Nanodrop 2000 (ThermoFisher).

2.1.2 RNA extraction

Total RNA was extracted using the RNeasy Mini Kit (Qiagen) according to the manufacturers instructions. Samples were washed once with DPBS and lysed using RLT buffer containing 1 % (v/v) β-mercaptoethanol. Lysed samples were homogenised with a QIAshredder spin column (Qiagen) and centrifuged for 2 minutes at 16000 *g*. After homogenization, one volume of 70 % ethanol was added to each sample and mixed thoroughly. Homogenates were then added to a RNeasy spin column and centrifuged at 8000 *g* for 15-20 seconds to bind RNA. Spin columns were subsequently washed with 350 µl of RW1 buffer and centrifuged at 8000 *g* for 15-20 seconds. Following washing, contaminating gDNA was removed by use of the RNase-Free DNase kit (Qiagen); 80 µl of DNase I diluted in RDD buffer was directly added to each spin column membrane and incubated at RT for 15 minutes. After incubation DNase I was removed by washing with RW1 buffer. Subsequently spin columns were washed with 500 µl RPE wash buffer, first with a centrifugation at 8000 *g* for 15 seconds and secondly for 2 minutes at 8000 *g*. Afterwards spin columns were transferred to a fresh collection tube and centrifuged for 1 minute at 13000 *g* to remove all RPE buffer and dry the membrane. Finally, spin columns were transferred to a 1.5 ml collection tube, 50 µl of RNase-free water added directly to the membrane, incubated for 1 minute at RT and centrifuged for 1 minute at 8000 *g*. Total RNA was quantified using Nanodrop spectrophotometry and stored at -80°C before further experimentation.

2.1.3 cDNA synthesis

After total RNA extraction, first strand cDNA synthesis was performed using the Tetro cDNA synthesis kit (Bioline), as per the manufacturer's instructions. A reagent master mix was prepared by mixing the following components: 1 µl oligo $(dT)_{18}$ primer, 1 µl random hexamer primer, 1 µl 10 mM deoxynucleotides (dNTP) mix, 4 µl 5X reaction buffer, 1 µl RiboSafe RNase Inhibitor and 1 µl Tetro Reverse Transcriptase (200 U/µL). Master mix was combined with 50-300 ng of total RNA and DEPC-treated water was added to total 20 µl. Reactions were briefly vortexed to thoroughly mix components, centrifuged and incubated in a thermocycler using the following conditions:

1. 15 minutes at 25°C.
2. 45°C for 45 minutes.
3. 85°C for 5 minutes.

Reactions were subsequently diluted to a ratio of 50 ng of starting RNA per 100 µl H_2O and either immediately used for RT-PCR reactions or stored at –20°C.

2.1.4 Polymerase Chain Reaction (PCR) and Reverse Transcription PCR (RT-PCR)

Primers for DNA analysis were designed using Primer-BLAST (https://www.ncbi.nlm.nih.gov/tools/primer-blast). Amplification of DNA was completed using standard PCR techniques. A master mix was prepared using either 2X GoTaq green master mix (Promega) or 2X Q5® High-Fidelity DNA Polymerase (NEB), combined with 0.2 µM forward and reverse primers. A total of 100 ng of DNA was loaded per 25 µl reaction. PCR reactions were incubated in a thermocycler at the following conditions:

1. 2 min at 95°C.
2. 35 cycles: 30 seconds at 95°C.
   30 seconds at 60°C.
   72°C (30 seconds per 500 base pair (bp)).
3. 2 min at 72°C.

After amplification reactions were stored at 4°C until gel electrophoresis. Successful PCR amplification was confirmed by running 10 µl of PCR reaction on a 2 % (w/v) agarose (Bioline) gel containing 0.005 % (v/v) Safeview nucleic acid stain (NBS Biologicals) and visualised on a BioRad ChemiDoc XRS+ (BioRad) using ImageLab software (BioRad).

RT-PCR analysis of cDNA was conducted as above with minor modifications. A 15 µl master mix was prepared with 2X GoTaq green and 0.5 µM forward and reverse primers

(Table 2.1). cDNA was diluted with double-distilled water (ddH_2O) and 5 µl used per reaction. RT-PCR reactions were incubated in a thermocyler for a total of 28-35 cycles.

Table 2.1. RT-PCR primers.

Gene	Primer		Product size	Source
	Forward	Reverse		
ARR3	CAGCTCAGCCCCTACAACTC	ACTGCAAAGCTCTGGGAGAA	244	-
ACTIN	CCAACCGCGAGAAGATGA	CCAGAGGCGTACAGGGATAG	97	-
CRX	TTTGCCAAGACCCAGTACC	GTTCTTGAACCAAACCTGAACC	96	-
DCC	ACCCAAGCTGGCTTTTGTACT	TGTGACGGCATCAGAAGGTTC	124	PrimerBank: 260436868c1
ELAVL3 (*HUC*)	TCGAGTCCTGCAAGTTGGTTC	TGCATCATTGGGGTCAGAATAGT	86	Sluch et al (2015)
GAPDH	CCCCACCACACTGAATCTCC	GGTACTTTATTGATGGTACATGACAAG	105	-
GNAT1	CTGCTCACTCTGTCCCTTCG	TTGACGATGGTGCTCTTCCC	175	-
NEUN (*RBFOX3*)	CCAAGCGGCTACACGTCTC	CGTCCCATTCAGCTTCTCCC	191	PrimerBank: 128485755c1
NFL	TCAACGTGAAGATGGCTTTGGATA	AAGACCTGGGAGCTCTGGGAGTA	130	Tanaka et al (2015)
NFM	ACAACCACGACCTCAGCAGCTA	ATGACGAGCCATTTCCCACTTT	86	Tanaka et al (2015)
NR2E3	TGGTCCTCTTCAAGCCAGAGA	TTTCACCTCCACCCCCACTA	274	-
NRL	CACTGACCACATCCTCTCGG	GAGGGTTCCCGCTTTACCTC	141	-
NRP1	ACGTGGAAGTCTTCGATGGAG	CACCATGTGTTTCGTAGTCAGA	138	PrimerBank: 182509170c3
OPA1 AS	TGCCTGACATTGTGTGGGAAA	AACAACCCGTGGCAGATGAT	-	-
OPA1 ex2-6	ACATCTGGTTTCACGAAGCA	GCTCACCAAGCAGACCCTTT	542	-
OPA1 ex11-18	CCTCACCATGTGGCCCTATTT	GTCACTTGGTGTGCCTTTAGC	617	-
OPA1 ex23-29	GCAGGCTCGTCTCAAGGATAC	TCTCTAACTTTCTTGAGGTCTTCCG	576	-
RECOVERIN	AGCTCCTTCCAGACGATGAA	CAAACTGGATCAGTCGCAGA	150	-
RLBP1 (CRALBP)	GCTGCTGGAGAATGAGGAAACTC	GGCTGGTGGATGAAGTGGAT	174	-
ROBO2	CTCTGCTACACTCACCGTCC	GCTGCCTTCTTTCTGCCAAA	145	-
SNAP25	TCGTGTAGTGGACGAACGG	TCTCATTGCCCATATCCAGGG	158	PrimerBank: 341572584c2
STX1A	TAAAGAGCATCGAGCAGTCCA	GACATGACCTCCACAAACTTTCT	118	PrimerBank: 260166656c2
TAU	CCAAGTGTGGCTCATTAGGCA	CCAATCTTCGACTGGACTCTGT	106	PrimerBank: 294862264c1
TUBB3	TCAGCCGATGCGAAGGG	GGCCTCGTTGTAGTAGACGC	281	-
VAMP2	TTGAAACAAGCGCAGCCAAG	ATGATGAGGATGATGGCGCA	97	-

2.1.5 Quantitative PCR (qPCR)

qPCR was completed to determine relative levels of gene expression using SYBR green. A master mix was prepared containing 10 µl of 2X LabTAQ hi-rox green master mix, 0.8 µl of 10 µM forward and reverse primers and 3.4 µl ddH_2O, prepared in triplicate for each sample. Subsequently, cDNA was diluted and 5 µl added to each reaction well. Reactions were loaded into MicroAmp™ Optical 96-Well Reaction Plate (Thermofisher), centrifuged and placed into a Quantstudio 6 Flex real-time PCR system (Thermofisher), with reactions conducted at the following conditions:

1. 2 min at 95°C.
2. 40 cycles: 10 seconds at 95°C.
   25 seconds at 60°C.

Finally, amplified reactions were incubated at the following conditions for 30 cycles to generate a melt curve:

1. 15 seconds at 95°C.
2. 15 seconds at 60°C.

qPCR data was collected in QuantStudio Real-Time PCR software (Applied Biosystems) and raw data exported to Microsoft Excel (Microsoft).

2.1.5.1 Primer design and PCR amplicon validation

Primer pairs were designed for relative quantification of chosen target genes (Table 2.2), whereby the target gene is normalised to the geometric mean of reference gene (*ACTIN* and *GAPDH*) expression. Primer pairs were obtained from one of three sources: from PrimerBank (https://pga.mgh.harvard.edu/primerbank/), previously validated primers within the Cheetham lab or designed using PrimerBLAST. Manually designed primers were made using the following parameters where possible:

- ~50 % GC content.
- Exon spanning.
- Amplicon length: 80-190 bp.
- Minimal self- and hetero-dimers at predicted melting temperatures.

All primers were synthesised by Sigma-Aldrich and reconstituted to 100 µM in ddH_2O upon arrival.

Table 2.2. qPCR primers.

Gene	Primer		Product size	Source
	Forward	Reverse		
ACTIN	CCAACCGCGAGAAGATGA	CCAGAGGCGTACAGGGATAG	97	-
AP1	GAACTCGGACCTCCTCACCT	TCATCTGTCACGTTCTTGGGG	150	-
ATF4	GTTCTCCAGCGACAAGGCTA	ATCCTGCTTGCTGTTGTTGG	88	-
ATF5	AGAGACCAGAACAAGTCGGC	CGGGCCTTGTAAACCTCGAT	182	-
ATOH7	CTGCCTTCGACCGCTTACG	CAGAGCCATGATGTAGCTCAG	104	PrimerBank: 363543334c1
BRN3B (POU4F2)	CAAGCAGCGACGCATCAAG	GGGTTTGAGCGCGATCATATT	157	PrimerBank: 110347454c1
CEBPB	ACGAGTACAAGATCCGGCG	AACAAGTTCCGCAGGGTGC	178	-
DDIT3 (CHOP)	ACCAAGGGAGAACCAGGAAACG	TCACCATTCGGTCAATCAGAGC	201	-
GAPDH	CCCCACCACACTGAATCTCC	GGTACTTTATTGATGGTACATGACAAG	105	-
HSPA9 (mtHSP70)	CTTGGGGCACACAGCAAAAA	CCCGAAGCACATTCAGTCCA	113	-
HSPD1 (HSP60)	GCAGAGTTCCTCAGAAGTTGG	CAGCAGCATCCAATAAAGCA	116	-
HTRA2	TCTGCATCGTGGGGAAAAGAA	CCATGCTGAACATCGGGAAA	147	-
ISL1	GCGGAGTGTAATCAGTATTTGGA	CACACAGCGGAAACACTCGAT	102	PrimerBank: 115387113c1
LHX2	TCGGGACTTGGTTTATCACCT	GCAAGCGGCAGTAGACCAG	110	PrimerBank: 30795195c2
NRF1	GCTGATGAAGACTCGCCTTCT	TACATGAGGCCGTTTCCGTTT	171	PrimerBank: 93141038c2
OPA1	CGACCCCAATTAAGGACATCC	GCGAGGCTGGTAGCCATATTT	102	PrimerBank: 224831252c1
PAX6	TCAGCTCGGTGGTGTCTTTG	GTCTCGGATTTCCCAAGCAA	328	-
RAX	GTCTGTCGGTCCTGAGCAAA	ATATTGCGTCATGCCAGGGT	148	-
SNCG	TGAGCAGCGTCAACACTGTG	TGGCCTGTAGCCCTCTAGTC	187	-
SIRT3	CCCCAAGCCCTTTTTCACTTT	CGACACTCTCTCAAGCCCA	148	PrimerBank: 157671925c2
SOD2	GGAGAACCCAAAGGGGAGTTG	TTGAAACCAAGCCAACCCCAA	128	-
VSX2	GTGGCTACTGGGGATGCAC	TCCTGCTCCATCTTGTCGAG	108	-

Once reconstituted, primers were analysed by RT-PCR (Section 2.1.4) to confirm amplicon length and specificity at an equal annealing temperature, set at 60°C. After confirmation of specificity, primer efficiencies of both target genes and reference genes were tested by serial dilution qPCR. Serial dilutions of cDNA were prepared at the following concentrations: 1:5, 1:25, 1:50, 1:100 and 1:200, and combined with qPCR master mix. Subsequently, a standard curve was generated by plotting the threshold value (Ct; x) versus log cDNA dilution (y), to enable calculation of primer pair reaction efficiency (E) using the following equation:

$$E\ (\%) = (10^{-1/slope} - 1) \times 100.$$

This equation determines the ability of polymerase to amplify the target gene given the reaction conditions and specific primer sequences. As such, reaction efficiency should be 90-110 % to enable effective and accurate comparisons between qPCR genes. Finally, the delta Ct (ΔCt) for each primer set was calculated with the following equation:

$$\Delta Ct = Ct\ target\ gene - Ct\ reference\ gene.$$

The ΔCt values were subsequently plotted against the log of input cDNA to verify compatibility against reference genes, the slope of the plot verified to be <0.1.

2.1.5.2 qPCR analysis: relative quantification using the ΔΔCt method

Analysis of subsequent qPCR reactions was performed using the ΔΔCt method (Livak and Schmittgen 2001), which enables relative quantification of target genes against stably expressed reference genes. Initially, the ΔCt values were calculated for the target gene against the reference gene for all samples, using the following equation:

$$\Delta Ct = Ct\ target\ gene - Ct\ geometric\ mean\ of\ reference\ genes$$

Subsequently, the ΔΔCt was generated by comparing the expression of test samples vs that of a reference sample, as following:

$$\Delta\Delta Ct = \Delta Ct\ test\ samples - \Delta Ct\ reference\ sample$$

Finally, the fold change in expression of the target gene in each sample is calculated using the following equation:

$$\text{Fold change} = 2^{-\Delta\Delta Ct}$$

qPCR statistical analysis was completed on $\Delta\Delta Ct$ values and subsequently graphically plotted as average fold change with upper and lower limits defined by the standard error of the mean (SEM).

2.1.6 PCR reaction purification

2.1.6.1 Gel DNA extraction

Gel DNA extraction was performed using the QIAquick® Gel Extraction Kit (Qiagen) following the manufacturers instructions, all centrifugations were completed at 16000 *g*. Briefly, after gel electrophoresis PCR bands were excised using UV back lighting and a scalpel. Gel pieces were weighed and six volumes of buffer QG were added for 1 volume of PCR sample. Samples were incubated at 50°C for 10 minutes, with brief vortexing

ever 3 minutes. After the gel was dissolved 1 volume of isopropanol was added. Samples were loaded into QIAquick spin columns and centrifuged for 1 minute. Flow-through was discarded and 500 µl Buffer QG to the QIAquick column, followed by centrifugation for 1 minute. QIAquick columns were then washed with 750 µl Buffer PE with 1 minute centrifugation. Flow-through was discarded and column centrifuged for 1 minute to removal residual buffer. Spin columns were transferred to labelled 1.5 ml Eppendorf tubes, and 50 µl distilled water was added directly to each spin column membrane. Columns were incubated for two minutes at RT and finally centrifuged for 1 minute. Once eluted DNA was quantified via spectrophotometry and stored at -20°C before further use.

2.1.6.2 PCR product purification – Multiscreen filter plates

PCR products were purified using a MultiScreen® PCR µ96 Filter Plate (Millipore). Briefly, individual reactions were added to wells of the MultiScreen plate and the plate applied to a vacuum pump for 10 minutes at -60 kPa/457 mmHg. After binding of DNA plates were washed with 70 µl of nuclease free water and vacuumed again. Finally, DNA was eluted from the plate using nuclease free water with gentle shaking for 10 minutes at RT, before quantification.

2.1.7 Sequencing

All DNA samples were Sanger sequenced by Source Biosciences (Cambridge). Samples were sent at the following concentrations: plasmid DNA at 100 ng/µl and purified PCR products at 10 ng/µl, using 3.2 pmol/µl forward or reverse primers.

2.1.8 Protein extraction and quantification

Cell samples were washed with PBS and lysed in radioimmunoprecipitation buffer (RIPA; see Appendix A for formulation) containing 2 % (v/v) protease inhibitor cocktail (PIC; Sigma) on ice. Protein quantification was completed using the Pierce Bicinchoninic acid (BCA) Protein Assay (Thermofisher) following the manufacturers microplate procedure. After lysis 10-30 µl of sample solution was aliquoted in triplicate into individual wells of 96-well plate. Simultaneously, standards of known protein quantity (25-2000 µg/ml) were loaded in triplicate. Once loaded, samples and standards were mixed with 200 µl of BCA Working Reagent and incubated at 37°C for 30 minutes. Finally, absorbance at 562 nm of standards and samples was quantified using a spectrophotometer (Safire, Tecan). Following quantification, a protein standard curve with linear regression was generated to allow calculation of total protein per sample.

2.1.9 Western blot

Following protein extraction cell lysates were sonicated for 10s at 0.1 watts using an Ultrasonic Liquid Processor XL-2000 (Misonix Incorporated) and centrifuged at 13,000 *g* for 10min at 4°C to remove cellular debris. Supernatants were aliquoted into fresh 1.5 ml Eppendorf tubes and 30 µl was removed for protein quantification. Total protein was measured using the Pierce™ BCA Protein assay kit (ThermoFisher; Section 2.1.8). 10 % acrylamide gels (formulation in Appendix A) were loaded with PageRuler™ Plus Prestained Protein Ladder (ThermoFisher) followed by equal amounts of protein and run at 200 volts until the gel front ran off the bottom of the gel. Protein was transferred to nitrocellulose membranes via wet transfer using Transfer buffer (see appendix for formulation), run at 100 volts for one hour with cooling and stirring. Membranes were stained with Ponceau S stain (see materials appendix) to identify successful protein transfer. Following staining, membranes were washed with distilled water and blocked with 5 % (w/v) milk (Marvel) in PBS containing 0.1 % TWEEN-20 (PBS-T, Sigma). Blots were incubated with primary antibodies (Table 2.3), diluted in 5 % milk PBS-T, overnight at 4°C with shaking. The next day blots were washed three times in PBS-T, followed by a two-hour incubation with HRP-conjugated secondary antibody (Table 2.3), diluted in 2.5 % (w/v) milk PBS-T. Following secondary incubation membranes were washed with PBS-T three times and protein detected using Luminata Crescendo or Forte western HRP substrate (Millipore) and imaged with ImageLab on a BioRad ChemiDoc XRS+.

Table 2.3. Antibodies used for western blot analysis.

Antigen	Host	Clone	Isotype	Supplier/ Catalogue #	Working Concentration
β-TUBULIN	Mouse	TUB2.1	IgG1	Sigma T4026	300 ng/mL
OPA1	Mouse	1E81D9	IgG1	Abcam Ab119685	1 µg/mL
Mouse	Goat	HRP	IgG	ThermoFisher 31430	26 ng/mL

Following protein detection blots were re-incubated to determine protein loading by staining for control proteins. Blots were re-blocked in 5 % milk for 1 hour and incubated overnight with primary antibody (Table 2.3). The following day blots were washed and incubated for two-hours with horseradish peroxidase (HRP)-conjugated secondary antibody. Following secondary incubation membranes were washed with PBS-T and protein detected using either Luminata Crescendo or Forte substrate.

Quantification of western blots was performed with ImageLab software (bio-rad.com) and protein expression was normalised to control proteins before analysis.

2.1.10 Immunofluorescence

Cellular proteins were detected using indirect immunofluorescence analysis. Samples were washed with 1X Phosphate Buffered Saline (PBS; Oxoid) and fixed for 10 minutes at RT in 4 % paraformaldehyde (PFA, ThermoFisher) diluted in PBS. Subsequently cells were washed with PBS and permeabilised for 15 minutes at RT in PBS containing 0.1 % triton X-100 (Sigma). To reduce unspecific background staining cells were blocked at RT for at least 1 hour in PBS containing 10 % (v/v) donkey or goat serum (Sigma), depending on the intended species of the secondary antibody, and 0.3 % (w/v) bovine serum albumin (BSA, Sigma). Staining with primary antibodies was completed in blocking solution for either two hours at RT or overnight at 4°C, negative controls were performed without primary antibodies. After primary incubation slides were washed with PBS and incubated in secondary antibodies in diluted blocking solution (1:1 with PBS) for 2 hours at RT. A list of primary and secondary antibodies with their respective concentrations is given in Table 2.4 and Table 2.5. Finally, cells were washed three times with PBS and stained with 4 µg/ml 4',6-diamidino-2-phenylindole dilactate (DAPI, Sigma) diluted in PBS to identify nuclei. After staining cells were washed and mounted with Dako fluorescent mounting medium (Dako) or Vectorshield® Vibrance Antifade mounting medium (Vector Laboratories) and left to set over night at RT.

All images were obtained using Carl Zeiss LSM710 or LSM700 laser-scanning confocal microscope (Zeiss) or a Leica TCS SP8 MP confocal microscope (Leica Microsystems). For Zeiss microscopes, proteins were visualised using a HeNe laser with 546nm or 633nm excitation, a 488nm argon ion laser and a 405nm excitation diode laser. For Leica microscopes, proteins were visualised using a white light laser with excitation at 405 nm, 488 nm, 546nm and 633nm. Sections were observed at 20x and 63x magnification to allow for visualisation of whole fields and closer cellular protein localisation, scale bars are noted in all figures and accompanying legends. Fluorescent intensities were optimized to reduce photo bleaching and images captured using Z-stacks. Images were exported from Zen 2009 software and prepared using FIJI (imagej.net/Fiji) and InkScape (Inkscape.org).

Table 2.4. Primary antibodies used for immunohistochemistry.

Antigen	Host	Clone	Isotype	Supplier/ Catalogue #	Working Concentration
ATOH7	Rabbit	Polyclonal	IgG	Sigma AB5694	3.33 µg/ml
ATOH7	Rabbit	-	IgG	Stratech ORB373591-BOR	1 µg/ml
BRN3A	Goat	C-20	IgG	Santa Cruz Sc-31984	500 ng/ml
BRN3A	Mouse	14A6	IgG_{2B}	Santa Cruz Sc-8429	4 µg/ml
BRN3B	Rabbit	Polyclonal	IgG	Abcam Ab56026	5 µg/ml
βIII TUBULIN (Neuronal)	Mouse	2G10	IgG_{2A}	Abcam Ab78078	1 µg/ml
βIII TUBULIN	Rabbit	Poly-clonal	IgG	Abcam Ab18207	1 µg/ml
CRX	Mouse	4G11	IgG_{2A}	Abnova H00001406-M02	3.33 µg/ml
ISL1	Rabbit	Polyclonal	-	Millipore AB4326	1.6 µg/ml
ISL1	Rabbit	EP4182	IgG	Abcam Ab109517	4 µg/ml
NANOG	Mouse	23D23C6	IgG	Invitrogen MA1-017	6.6 µg/ml
Neurofilament 160/200	Mouse	RMdO20	IgG1	Sigma N2912	10 µg/ml
OCT4	Rabbit	Polyclonal	IgG	Abcam Ab19857	1 µg/ml
PAX6	Rabbit	Polyclonal	IgG	Thermofisher 42-6600	6.6 µg/ml
RAX	Rabbit	Polyclonal	IgG	Abcam Ab23340	5 µg/ml
SNCG	Rabbit	Poly-clonal	IgG	Abcam Ab55424	5 µg/ml
SSEA4	Mouse	MC813	IgG3	Cell Signalling Technologies 4755S	3.3 µg/ml
TOMM20	Mouse	F-10	IgG_{2A}	Santa Cruz Sc-17764	400 ng/ml
TRA-1-61	Mouse	cl.A	IgM	Invitrogen 411000	1 µg/ml
TRA-1-80	Mouse	cl.26	IgM	Invitrogen 411100	1 µg/ml
VSX2 (CHX10)	Sheep	Polyclonal	-	Millipore AB9014	10 µg/ml

Table 2.5. Secondary antibodies used for immunohistochemistry.

Antigen	Host	Fluorophore	Isotype	Supplier/ Catalogue #	Working Concentration
Goat	Donkey	488	IgG	Invitrogen A32814	4 µg/ml
Goat	Donkey	555	IgG	Invitrogen A32816	4 µg/ml
Mouse	Donkey	488	IgG	Invitrogen A-21202	4 µg/ml
Mouse	Donkey	555	IgG	Invitrogen A-31570	4 µg/ml
Rabbit	Donkey	488	IgG	Invitrogen A-21206	4 µg/ml
Rabbit	Donkey	555	IgG	Invitrogen A-31572	4 µg/ml

2.2 Cell culture

2.2.1 Maintenance, expansion and storage of fibroblasts

Control Human Dermal Fibroblasts of neonatal origin (HDFn) were purchased from Sigma. Patient fibroblasts were isolated from skin biopsies obtained by Dr Yu-Wai-Man after informed patient consent following the tenets of the Declaration of Helsinki and ethical approval by NRES Committee, Yorkshire and The Humber - Leeds Bradford Research Ethics Committee (REC 13/YH/0310). All fibroblast lines were maintained in fibroblast growth media consisting of DMEM + GlutaMAX (Gibco) with 10 % (v/v) foetal bovine serum (FBS, Lonza), 100 ug/ml penicillin and 100 U/ml streptomycin (P/S, Gibco) and 1 % (v/v) minimum essential medium non-essential amino acids (NEAA, Gibco). Fibroblasts were maintained at 37°C in 5 % CO_2 and passaged every 3-4 days, at approximately 70-90 % confluency, using a double DPBS wash followed by trypsinisation with 0.05 % Trypsin-EDTA (Gibco) and resuspension in fibroblast medium.

Once fibroblast cultures were established, a low passage bank of cells was prepared. One 80-90 % T75 flask of fibroblasts was trypsinised, the cells were pelleted at 0.8 *g* and resuspended in freezing medium, consisting of FBS with 10 % v/v Dimethyl sulfoxide (DMSO). Cells were then transferred to cryovials, with one T75 flask distributed into approximately four 1 ml cryovials, and frozen at -80°C in a Mr Frosty (Nalgene) for 24 hours before transfer to a liquid nitrogen storage tank. Frozen vials were defrosted as and when required by warming cryovials to RT and seeding cells in a T25 flask containing fibroblast growth media. A full media change was completed the following day to remove residual freezing medium from the culture.

2.2.2 Generation of iPSCs from patient-derived *OPA1* cell lines

Generation of patient-derived iPSC was completed as previously reported (Schwarz *et al.* 2015). On the day of reprogramming, fibroblasts were at approximately 90 % confluency and less than passage 15.

Generation of iPSCs was performed using integration-free episomal vectors: pCXLE-hOCT3/4-shp53-F (Addgene plasmid #27077), pCXLE-hSK (Addgene plasmid #27078), pCXLE-hUL (Addgene Plasmid #27080) and miRNA 302/367 plasmid (Gift from Dr J. A. Thomson, Regenerative Biology, Morgridge Institute for Research, Madison, Wisconsin, USA; Howden *et al.* 2015). Fibroblasts were dissociated with 0.05 % Trypsin-EDTA, centrifuged at 200 *g* for 5 minutes, and resuspended in DPBS before counting with a haemocytometer. Subsequently, 1×10^6 cells were isolated and centrifuged at 200 *g* for 4 minutes and thoroughly resuspended in 100 µl Nucleofector solution from the Cell Line Nucleofector Kit R (Lonza). During centrifugation 1 µg of each episomal plasmid was combined together into a master mix and subsequently mixed with the cellular suspension. Samples were transferred into a cuvette and electroporated using an Amaxa Nucleofector I device (Lonza), setting U-023.

Following electroporation, fibroblasts were plated onto a 0.1 % (v/v) gelatine (Sigma) coated 10 cm^2 culture dish and maintained in fibroblast growth media. 24 hours post electroporation; media was replaced with fresh fibroblast growth media containing 0.5 mM sodium butyrate (Sigma), changed daily. On day 7 of reprogramming, cells were dissociated with TrypLE Express (Gibco), plated into a 6-well plate pre-coated with 1 % (v/v) Geltrex LDEV-free reduced growth factor basement membrane matrix (Gibco) and maintained in fibroblast growth medium overnight. The following day media was replaced with Essential 8 flex (E8F) media (Gibco) plus 0.5 mM sodium butyrate, which was replaced daily until day 13 of reprogramming when media was changed to E8F only. Individual clonal iPSC colonies were identified by morphology, isolated by mechanical dissection and placed into individual Geltrex pre-coated 6 well plates. Clonal iPSC lines were then maintained in E8F media at 37°C in 5 % CO_2.

Pluritpotency and self-renewal capability were assessed through immunofluorescence and TaqMan® hPSC Scorecard™ Assay (as below; ThermoFisher).

2.2.3 Assessment of endogenous marker expression

To determine if reprogramming had efficiently activated endogenous pluripotency genes RNA was extracted from iPSC over multiple passages. cDNA was synthesised (Section 2.1.3) and RT-PCR conducted using endogenous and vector specific primers to determine expression of reprogramming episomal plasmids and endogenous genes

(Table 2.6). PCR reactions were analysed via gel electrophoresis to confirm expansion of the target genes.

Table 2.6. Primers for assessing episomal vector expression in iPSCs.

Gene	Primer		Product size
	Forward	Reverse	
LIN28 CDS	AGCCATATGGTAGCCTCATGTCCGC	TCAATTCTGTGCCTCCGGGAGCAGGGTAGG	129
LIN28 Plasmid	AGCCATATGGTAGCCTCATGTCCGC	TAGCGTAAAAGGAGCAACATAG	251
L-MYC CDS	GCGAACCCAAGACCCAGGCCTGCTCC	CAGGGGGTCTGCTCGCACCGTGATG	143
L-MYC Plasmid	GGCTGAGAAGAGGATGGCTAC	TTTGTTTGACAGGAGCGACAAT	122
OCT4 CDS	CCCCAGGGCCCCATTTTGGTACC	ACCTCAGTTTGAATGCATGGGAGAGC	143
OCT4 Plasmid	CATTCAAACTGAGGTAAGGG	TAGCGTAAAAGGAGCAACATAG	124
SOX2 CDS	TTCACATGTCCCAGCACTACCAGA	TCACATGTGTGAGAGGGGCAGTGTGC	80
SOX2 Plasmid	TTCACATGTCCCAGCACTACCAGA	TTTGTTTGACAGGAGCGACAAT	111

2.2.4 Confirmation of patient mutations within iPSC lines

To confirm that the original patient mutations were present within the generated patient-iPSC lines primers for exon 14 and exon 27 were designed centring on the mutation site (Table 2.7). PCR reactions were conducted (Section 2.1.4), to amplify the desired region of *OPA1*. Successful amplification of the target region was confirmed via gel electrophoresis. Following confirmation, the remaining PCR product was purified on a MultiScreen® PCR µ96 Filter Plate (Millipore) as previously described (Section 2.1.6.2). DNA was quantified via spectrophotometry and samples sent to Source Biosciences (Cambridge) for sequencing using forward primers. Sanger sequences were aligned to an *OPA1* reference sequence (Ensembl.org; ENST00000392438.7) using Benchling's alignment software (Benchling.com) and manually analysed for the presence of OPA1 mutations.

Table 2.7. Primers used for *OPA1* gDNA PCR expansion.

Gene	Primer		Product size	Source
	Forward	Reverse		
OPA1-ex2	GAGGTCTGCCAGTCTTTAGTG	TGTGTGAGAATGCCACCTGA	622	-
OPA1-ex14	GCATTTTTGCCTTCTCTTCGT	TGCTTTCCTTTTGGGAGTATG	732	-
OPA1-ex27	TGGGTGATAAAACATACCAGGAG	GGAAGCTGGGTCAGGTATTG	1073	-

2.2.5 Analysis of NMD - emetine treatment of cells

To determine if *OPA1* transcripts are degraded through NMD, fibroblasts and iPSCs were treated with 25 µM Emetine dihydrochloride hydrate (Sigma) for 4 hours at 37°C. Following treatment, RNA was extracted (Section 2.1.2) before first strand cDNA synthesis (Section 2.1.3) and PCR expansion of the target region using primers *OPA1* ex2-6 or *OPA1* ex23-29 (Table 2.1). After PCR expansion samples were either analysed via gel electrophoresis or sent for Sanger sequencing (Section 2.1.7) to determine to effect of *OPA1* mutation on transcript expression.

2.2.6 CRISPR/Cas9 genome engineering

2.2.6.1 Design and generation of CRISPR/Cas9 guide RNAs and plasmids for OPA1 knock-out

CRISPR guide RNAs (gRNA) specific to the *OPA1* exon 2 sequence were designed on the MIT CRISPR design tool (crispr.mit.edu), Benchling and validated on OffSpotter (cm.jefferson.edu/Off-Spotter). A reference sequence corresponding to *OPA1* was obtained from Ensembl (ENST00000392438.7) and uploaded to Benchling. Subsequently, the 150 base pairs surrounding the end of exon 2 were analysed for gRNAs using the Benchling CRISPR tool and the MIT CRISPR design tool. Once generated, gRNAs were further analysed with OffSpotter to determine potential off-target effects. From this collective analysis three gRNAs were selected with minimal off-target effects, high GC content (%) and high on-target cutting efficiency, as determined by the Benchling on-target score, and the CRISPR design tool quality score.

The designed gRNAs were modified with the addition of an overhang sequence to both the forward and reverse oligonucleotide according to the protocol provided by Ran *et al.* (2013) and synthesised by Sigma-Aldrich to enable successful incorporation into the pSpCas9(BB)-2A-GFP (PX458) plasmid (Addgene plasmid #48138; Appendix B), which encodes for both the Cas9 protein, trans-activating crRNA (tracrRNA; a gRNA scaffold), gRNAs and enhanced green fluorescent protein (eGFP).

Generation of the gRNA-pSpCas9 plasmid was also completed following the protocol provided by Ran *et al*. (2013). Briefly, each pair of gRNA oligonucleotides were phosphorylated using a T4 polynucleotide kinase and annealed in a thermocycler with the following parameters: 37°C for 30 minutes, 95°C for 5 minutes then ramped down to 25°C at 5°C min^{-1}. Following annealing, gRNAs were ligated into *Bbs*I digested PX458 plasmid using T7 DNA ligase (NEB) via thermocycler incubation with the following conditions: 37°C for 5 min, 21°C for 5 min for a total of 1 hour. Ligated plasmids were subsequently transformed into NEB 5α competent *Escherichia coli* (NEB), a derivative of DH5α *E. coli*, with standard heat-shock procedures. Briefly, 2 µl of ligation reaction was added to 50 µl of *E. coli* and incubated for 10 minutes on ice followed by 45 seconds at 42°C and finally 2 minutes on ice. Following heat-shock 150 µl of SOC media (NEB) was added to *E. coli* and plated onto lysogeny broth (LB, Sigma) agar (see Appendix A for formulation) plates containing 100 µg/ml ampicillin. Plates were incubated overnight at 37°C. The following day individual colonies were picked using a sterile inoculation loop and added to 3 ml of LB broth (see materials appendix for recipe) containing 100 µg/ml ampicillin (Sigma). Bacteria cultures were incubated overnight at 37°C with shaking at 250 RPM.

Plasmid DNA was extracted from overnight cultures using the Wizard Plus SV Miniprep DNA Purification System (Promega). Briefly, bacteria were pelleted for 5 minutes at 16000 *g*, resuspended in Cell Resuspension Solution and lysed with Cell Lysis Solution to extract DNA. Lysates were centrifuged at 16000 *g* for 10 minutes at RT. Supernatants were then transferred to a Miniprep spin column and centrifuged at 16000 *g* for 1 minute to bind plasmid DNA. After binding, columns were washed twice with Column Wash Solution before DNA elution in 100 µl of nuclease-free water. Plasmid DNA was quantified by spectrophotometry and then sent to for Sanger sequencing using the U6 forward primer (Table 2.8). To confirm correct insertion of gRNAs, plasmids were aligned to the PX458 reference sequence on Benchling.

Table 2.8. PX458 sequencing primer.

Target	Primer
U6 forward primer	GGACTATCATATGCTTACCGTAACTTGA

2.2.6.2 T7 endonuclease I assay for genome modification

The efficiency of *OPA1* target gRNAs was confirmed via transfection of Human Embryonic Kidney (HEK) cell line 293. Cells were maintained in fibroblast growth media and seeded onto 24-well plates at a density of 150,000 cells/well, 24 hours before transfection. Upon reaching 80-90 % confluency cells were transfected using Mirus TransIT-LT1 (Mirus). 30 minutes prior to transfection LT1 reagent was combined at a ratio of 3:1 with 1 µg Cas9 plasmid or empty vector and Opti-MEM I Reduced-Serum Medium (Thermofisher). Transfected cells were cultured at 37°C for 48 hours prior to DNA extraction. gDNA was extracted using the Wizard gDNA Purification Kit (Promega) following the manufacturers guidelines (Section 2.1.1).

Primers for the genomic region surrounding the CRISPR target site in *OPA1* exon 2 were designed on Primer-Blast and synthesised by Sigma-Aldrich (Table 2.7). The CRISPR target region was amplified via PCR with GoTaq green master mix. Successful PCR amplification was confirmed by running 5 µl of the PCR reaction on a 2 % (w/v) agarose gel containing Safeview nucleic acid stain. The remaining 20 µl of PCR product was subject to DNA heteroduplex formation via a hybridization process on a thermocycler; 95°C for 10 min, 95°C to 85°C at –2°C/s; 85°C to 25°C at –0.25°C/s; and 25°C hold for 1 min. After heteroduplex formation, products were treated with 4 units T7 endonuclease I (NEB) per 15 µl heteroduplex reaction and analysed on 2 % agarose gel. Gels were imaged on a Gel Doc gel imaging system (Bio-Rad). Images were quantified via Image Lab software (Bio-Rad) to determine band intensities.

To determine gRNA targeting and cutting efficiency the fraction of cleaved PCR product (*fcut*) was calculated with the following formula:

$$fcut = (B+C)/(A+B+C)$$

Where A is the intensity of the undigested product, B and C are T7 cleavage products. The *fcut* value was subsequently used to estimate InDel occurrence (InDel %) with the following formula:

$$InDel\ \% = 100 \times (1-\sqrt{(1-fcut)})$$

Consequently, the CRISPR plasmid with the highest InDel % was chosen for generation of OPA1 knockout iPSC lines.

2.2.6.3 Generation of OPA1+/- iPSCs using CRISPR/Cas9

Generation of CRISPR/Cas9 edited human stem cells was conducted using a simultaneous reprogramming and CRISPR/Cas9 editing protocol modified from Howden *et al*. (2015) and similar to the generation of patient-derived iPSCs. In addition to the episomal reprogramming factors 2 µg of CRISPR/Cas9 plasmid was also included within the plasmid mix. Briefly, control HDFn were grown to 90 % confluency in fibroblast growth media and dissociated with 0.05 % Trypsin-EDTA before centrifugation. Cells were resuspended in PBS, counted and 1×10^6 cells were isolated before centrifugation. Cells were resuspended in Nucleofector solution from Cell Line Nucleofector Kit R and 1 µg of each episomal plasmid together with 2 µg of the selected gRNA CRISPR/Cas9 plasmids was added. A further reaction was set up without CRISPR/Cas9 plasmid present to work as a reprogramming control and to generate wild-type isogenic control cell lines. Samples were transferred to a cuvette and electroporated. Immediately after electroporation fibroblasts were plated onto 0.1 % gelatine coated culture dishes and maintained in fibroblast growth media, with the addition of 0.5 mM sodium butyrate from day two. On day seven fibroblasts were dissociated with TrypLE Express and plated into geltrex coated 6-well plates. From days 8-13 cells were maintained in E8 media containing 0.5 mM sodium butyrate. On day nine of simultaneous reprogramming 1 well from a 6-well plate was lysed to extract gDNA and analysed via a T7 endonuclease assay to confirm the presence of gDNA editing. The remaining wells were cultured until OPA1+/- iPSC colonies emerged. Individual colonies were mechanically isolated using a crescent blade, collected with a sterile pipette tip and placed into individual wells of a geltrex-coated 12-well plate. Clonal lines were maintained in E8 media for 5 days until further analysis.

Upon reaching sufficient size for passaging, colonies were cut approximately in half using a sterile pipette tip, 1 half was further divided for passaging and transferred to a fresh 12-well plate whilst the remaining half was scraped and placed into a 1.5 ml Eppendorf tube for DNA extraction. Once collected, OPA1+/- iPSCs were centrifuged at 600 *g* to pellet cells and DNA extracted with QuickExtract™ DNA Extraction Solution (CamBio), cell lysis was performed in a thermocycler at the following temperatures: 65°C for 15 minutes and 95°C for 5 minutes. Cell lysis solution was diluted 1:3 with ddH_2O and 5µl of this solution was used to expand the region surrounding the CRISPR target region using primers OPA1-ex2F and OPA1-ex2R (Table 2.7). Confirmation of PCR amplification was confirmed by running 5 µl of PCR reaction on a 2 % agarose gel. The remaining PCR product was purified on a MultiScreen® plate, as previously described. DNA was quantified via spectrophotometry and samples sent to Source Biosciences for Sanger sequencing using primer OPA1-ex2F.

The presence or absence of CRISPR/induced mutations was determined by aligning sample sequencing data (.ab1 files) to the *OPA1* reference sequence (ENST00000392438, ensemble.org) using the alignment tool on Benchling. Identification of mutations was initially conducted by identifying misaligned gDNA sequences downstream of gRNA targets within Benchling, in which Benchling alignment software fails to align sequencing data to the reference sequence. To further determine CRISPR effects in mutant cell lines, manual analysis of the gDNA sequence was performed to identify distinct DNA motifs within the reference sequence that were out of frame within the mutant cell line. These motifs were then used to identify upstream InDel mutations.

Once CRISPR-induced mutations were confirmed, CRISPR-iPSC were either frozen down or further cultured for analysis of stem cell markers via immunofluorescence and *OPA1* protein expression levels via western blot.

2.2.6.4 Correction of patient-derived iPSC via Homology-Directed Repair with CRISPR/Cas9

Once patient-derived iPSC lines were successfully established each individual mutation loci were assessed for gRNA sites using Benchling to determine suitability for gene correction via homology directed repair (HDR). Both gRNAs and homology templates were designed to previously optimised specifications (Paquet *et al.* 2016; Richardson *et al.* 2016). As such gRNAs were designed to be as close to mutations as possible, with a maximum distance of 30 bp from the mutation to the Cas9 cutting site (Paquet *et al.* 2016). Single stranded oligodeoxynucleotide (ssODN) HDR templates were designed using Benchling HDR template designer, such that they are complimentary to the sense strand of gDNA and overlapped the dsDNA break by 36 bp upstream and 91 bp

downstream (Richardson *et al.* 2016). Additionally, synonymous point mutations were made in the ssDNA templates to remove gRNA PAM sequences to prevent further dsDNA breaks. Once designed templates were modified to include phosphorothioate bonds between the first 3 and last 3 base pairs. All reagents were purchased from Integrated DNA Technologies (Integrated DNA Technologies, IDT), gRNAs were purchased as crRNAs and tracrRNAs respectively and assembled into complete gRNAs on the day of experimentation.

On the day of transfection iPSC media was changed for StemFlex (Invitrogen) with 4 µM ROCKi at least 2 hours prior to dissociation. During this time, all other transfection reagents were prepared according to the manufacturer's instructions. In brief crRNA, tracrRNA and ssDNA donors were resuspended in nuclease-free ddH_2O to 100 µM. After resuspension, tracrRNA and crRNA were combined to form a 50 µM gRNA complex solution, heated to 95°C for 5 min and allowed to cool to RT on the bench top. Then 3 µL of gRNA complexes were combined with 2 µL of 61 µM Alt-R Cas9 enzyme (IDT) to generate Ribonucleoprotein (RNP) complexes, before incubation at RT for 20 minutes. During this incubation, iPSCs were washed with DPSB and dissociated to single cells using TrypLE express for 15 minutes at 37°C. Cells were resuspended in StemFlex with ROCKi and triturated multiple times with a P1000 Gilson pipette to ensure single cell dissociation. Cells were counted and 200,000 centrifuged at 1000 RPM for 5 minutes. After centrifugation, supernatants were removed and cells were resuspended in P3 Primary cell nucleofector solution (Lonza) before being combined with 5 µL of RNP solution, 2 µL of 100 µM ssDNA and 4 µM Electroporation Enhancer. iPSC-RNP mixes were subsequently nucleofected using a Lonza 4D-nucleofector with X-unit (Lonza), using program CA-137. After nucleofection, iPSCs were incubated at RT for 10 minutes before being resuspended StemFlex with ROCKi, with or without 30 µM HDR enhancer (HDRe, IDT; Table 2.9). Cells were seeded onto 24 well plate coated with 0.5 µg/cm^2 rhLaminin 521 and allowed grow for 5-6 days, until reaching approximately 80 % confluency. Upon reaching confluency, iPSCs were dissociated to single cells using TrypLE express and subsequently split in two: half pelleted for gDNA extraction and half replated into a fresh 6 well plate coated with rhLaminin. Re-plated cells were allowed to grow for a further 5-6 days.

Table 2.9. Nucleofection conditions for CRISPR/Cas9 correction of patient-derived iPSCs.

Nucleofection reaction	RNP	ssDNA	HDR enhancer
Untransfected	-	-	-
gRNA 1	+	+	-
gRNA 1	+	+	+
gRNA 2	+	+	-
gRNA 2	+	+	+

During the second expansion of cells, gDNA was utilised to estimate the efficiency of HDR within the nucleofected cell population. TIDER (https://tider.deskgen.com), an online webtool, was used to estimate the efficiency of HDR gene correction (Brinkman and van Steensel 2019). TIDER utilises Sanger sequencing data from control, reference and edited DNA samples to allow rapid assessment of HDR-mediated gDNA repair. gDNA was extracted from untransfected and a mixed pool of edited cells to generate PCR reactions for control and edited samples respectively, using primers OPA1 exon 14 forward and OPA1 exon 14 reverse. To generate a reference sample, or a sample representative of correctly edited gDNA, primers were designed for a multi-step overlap PCR (Figure 2.1, Table 2.10) that centred on the gRNA site and included identical base changes to those found in the ssDNA HDR template.

Table 2.10. Primers used for generation of TIDER reference template by overlap PCR.

Gene	Primer		Product size
	Forward	Reverse	
OPA1 ex 14	GCATTTTTGCCTTCTCTTCGT	TGCTTTCCTTTTGGGAGTATG	732
OPA1 ex 14 gRNA 1 C	-	GCGTTCAGCATCGACAGATCCATC	268
OPA1 ex 14 gRNA 1 D	GATGGATCTGTCGATGCTGAACGCAGTATTGTTAC	-	488
OPA1 ex 14 gRNA 2 C	-	GTCCATTTGACTGACAAGGTCTGTAACAATACTGCGTTCAGCATCCACAGATCC	301
OPA1 ex 14 gRNA 2 D	TTGTTACAGACCTTGTCAGTCAAATGGAC	-	460

Subsequently two PCR reactions were completed using Q5 2X hot-start master mix (NEB), each generating a PCR product containing the desired point mutations at the 3' end. These two PCR reactions were subsequently mixed together, in the absence of primers, to complete an overlap PCR in which the 3' tails would anneal and allow extension (Figure 2.1). Once extended, primers OPA1-ex14F and OPA1-ex14R (Table 2.7) were added to the reaction to generate full-length PCR products for Sanger sequencing. The overlap PCR was cycled through the following parameters:

1. 98°C for 30 seconds.
2. 10 cycles: 98°C for 20 seconds.
   60°C for 25 seconds.
   72°C for 30 seconds.

At this time PCR reactions were paused and 10 µM forward and reverse primers added (Figure 2.1). The complete reaction mix was then incubated at the following conditions: 30 cycles of of 98°C for 20 seconds, 60°C for 25 seconds, 72°C for 30 seconds and a final extension of 72°C for 2 minutes. Once generated, all PCR product reactions were sent for Sanger sequencing (Section 2.1.7) and .abi files uploaded to TIDER. After TIDER analysis, data were analysed and the nucleofection condition (Table 2.9) with highest HDR estimation and efficiency selected for clonal iPSC selection.

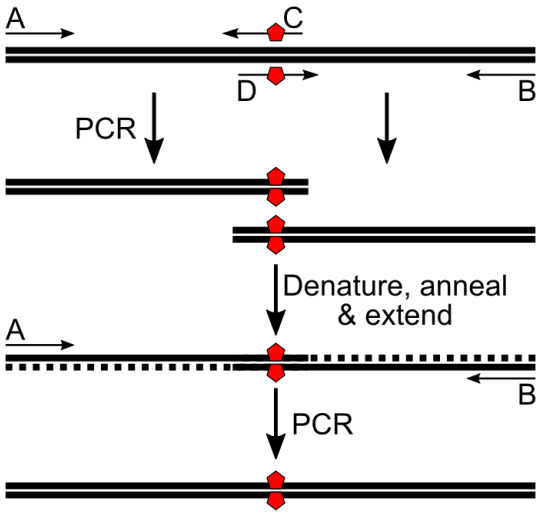

Figure 2.1. Overlap PCR for generation of HDR corrected samples.

Two complimentary halves of the final desired reference sequence are generated through PCRs using primer A + C and B + D, primers C and D are designed to overlap and include the desired base changes (Red pentagons). Each product is purified by gel extraction before being mixed together for annealing and extension to generate a final PCR template. Finally, primers A and B are added to the final PCR reaction to amplify the reference sequence before Sanger sequencing.

After selection of the HDR with highest editing frequency, and approximately 5-6 days of growth, cells were again dissociated to single cells, counted and resuspended in StemFlex with ROCKi. Cells were then plated in a serial dilution at 4000, 2000, 1000, 500, 250 and 125 cells per well of a rhLaminin coated plate to enable single cell clones to establish. After approximately 5-7 days, small isolated colonies that had a clear single cell origin were isolated and re-plated into new wells of a 12 well plate coated with rhLaminin. Once isolated, individual colonies were allowed to grow until large enough to split, approximately 5-6 days, with half of each colony isolated and replated and the other half used for gDNA extraction (Section 2.1.1).

To determine if gene correction had taken place, PCR reactions were completed using primers OPA1-ex14F and OPA1-ex14R (Table 2.7), purified using MultiScreen filter plates (Section 2.1.6.2) and sent for sanger sequencing along with unedited patient and control samples. Clones were aligned to the unedited patient sequence on Benchling and correctly edited clones identified through homozygous G bases at position cDNA 1334 and homozygous ssDNA PAM site mutations at positions cDNA 1362 and 1364. Correctly edited clones were subsequently expanded and selected for further analysis or stored in liquid nitrogen (Section 2.2.7).

2.2.6.5 Analysis of off-target effects

To determine if CRISPR/Cas9 had generated off-target DNA mutations gRNAs were analysed with Offspotter to identify potential off-target DNA regions with closely matched sequences to the gRNAs of choice. Once analysed the top ten off-target regions were

selected and primers to amplify the region of interest designed via Primer-Blast (Table 2.11). OPA1+/- samples and non-edited control DNA were amplified via PCR and the presence of the amplified region was confirmed via 2 % gel electrophoresis. PCR reactions were subsequently purified using MultiScreen filter plates. To confirm the lack of mutations PCR products were sequenced and aligned using Benchling to the non-CRISPR control DNA sequence and wild-type sequences were confirmed.

Table 2.11. CRISPR/Cas9 off-target primers.

Guide	Gene	Primer		Product size
		Forward	Reverse	
InDel gRNA	ACAN	CAGAGAGGGGAGAGATTGATG	ATTTTGGAGGAGGGGGTTC	871
	ADCY2	GGACTGCTGGATTTCTCCGT	TTTCCTAGCCTTCCCAGCAG	600
	CDH20	GACTATCCTCTTTCCTTCCTACACC	GCCTCACTCTACCACCTTTTG	443
	CHRNB2	CTCACGCACACCCTACCAC	CTCTCCCCTAACCTCCAGCA	576
	MMP16	AGATGTACCAAGAACCCCAAC	TGAGAAAAGAAAATGACTGCCAA	788
	PHYKPL	CACGAAGGGAAAGCAGAGG	CCAAGGAACAGAGGAGGAAT	753
	POMP	CCATTTTTGCTGTTGACTTCC	TCCCTTGACTGACCCATTTG	918
	SPTBN2	GAAACCCCGTCTCCACTAAA	GGTGCCCAGCCAAAATAAT	775
	UPB1	AAATGCAAGTGGTTGCTCTGAC	TACTGCCACCTGACACACAAA	756
	ZFAND6	ACTGTGTCCATCGTGCCTG	TTCCTCATTTCTGCCCTTCCTTA	946
HDR gRNA	CLSTN2	CTTGCCTTACAGGGTTGTGGT	GCCTCCCTGACATGACTTCTC	569
	DMD	ACCATCTTCATTCCCTCTCCA	AGCCTCCACGTAAGTTGCATT	511
	INTS9	AACCTGTAGACCCCTTTGCC	TCTGTGAGGGAGGAAGAAGCC	501
	UGGT1	ACATGCTAACAGATGCCCAG	TCCCAACTCCCACTGAACAA	458
	ZNF516	TAGGTGTGTAGGCGATGGTC	TCCTCCTGTACTAAGTGTGCAA	628

2.2.7 Maintenance and storage of iPSCs

Once generated, undifferentiated iPSCs were maintained in 1 % (v/v) Geltrex Coated T25 NUNC flasks or 6 well plates using E8 flex media (Gibco). iPSCs were passaged every 3-4 days with enzyme free cell dissociation buffer (Gibco) until utilisation in experimentation. Fresh iPSCs were defrosted after cells reached approximately 15-20 passages of usage in order to maintain genetic stability and a normal karyotype.

Generated iPSCs were banked in liquid nitrogen at multiple passages. iPSCs were cultured until 70-80 % confluency and dissociated using enzyme free cell dissociation buffer (Gibco). Subsequently, BamBanker freezing medium (Nippon Genetics Europe) was added to cultures and iPSCs broken into small clumps similar to the process of splitting. Once resuspended in BamBanker, iPSCs were transferred to cryovials and frozen at -80°C before transfer to liquid nitrogen storage tanks.

iPSCs were thawed by warming cryovials to RT and transferring the contents into a 50 mL falcon tube containing StemFlex medium (Thermofisher). Cells were pelleted at 0.7 *g,* before resuspension in StemFlex with 4 µM Y-27632, Rho-associated coiled coil forming protein serine/threonine kinase inhibitor (ROCKi, Sigma). The following day, StemFlex media was replenished without ROCKi. Once iPSCs had attached media was

changed every other day until colonies reached sufficient size and confluency to passage.

2.2.8 iPSC self-renewal and pluripotency assay: TaqMan hPSC Scorecard

Patient-derived iPSC, OPA1+/- iPSC and isogenic controls were analysed for their self-renewal and pluripotency potential with the TaqMan® hPSC Scorecard™ Assay (ThermoFisher). iPSC cultures were grown for 3 days before splitting, half grown for four days for iPSC self-renewal assessment and half used to generate embryoid bodies (EBs) after a further seven days of culture. EBs were grown for seven days following an adapted protocol from ThermoFisher (MAN0008384). On day 1 of differentiation, iPSCs were dissociated for 20 seconds in enzyme free cell dissociation buffer and scraped into E8 medium with 10 µM blebbistatin (Sigma) and plated into Ultra-low attachment 6-well plates to promote EB formation. On day 2 of differentiation, EBs were collected and sedimented by gravity for 15 minutes at RT before resuspension in 1:1 E8:EB media (DMEM/F12 with 10 % KnockOut Serum, 1 % NEAA and 0.1 % β-mercaptoethanol) with 10 µM blebbistatin. Day 3, media was exchanged for EB media alone and changed every other day thereafter. On day 8, EBs were collected for RNA extraction.

On the day of collection both iPSC and EB total RNA was extracted using the RNeasy Mini Kit (QIAGEN) as described (Section 2.1.2). EBs were collected and pelleted at 500 *g* before washing with PBS and re-pelleting and lysis.

After total RNA extraction, first strand synthesis was performed using the High Capacity cDNA RT kit with RNase Inhibitor (ThermoFisher) as per manufacturer's instructions. A 2X RT master mix was prepared by mixing the following components: 10X TaqMan® RT Buffer, 25X dNTP Mix, 10X Random Primers, MultiScribe™ Reverse Transcriptase (50 U/µl), RNase Inhibitor (20 U/µl) and RNase-free water. Simultaneously, RNA samples were prepared by diluting 1 µg of total RNA in 225 µl of RNase-free water. The 2X RT master mix and total RNA were then mixed 1:1 and aliquoted into eight PCR tubes. First strand synthesis was performed on a thermal cycler using the following conditions: 10 minutes at 25°C, 120 minutes at 37°C and 5 minutes at 85°C.

Immediately after first strand synthesis, qPCR was performed using the TaqMan® hPSC Scorecard™ Panel FAST 96w (ThermoFisher) with TaqMan® FAST Advanced Master Mix (Thermo Fisher). Each cDNA sample was diluted with 20 µl of PCR grade water and combined with 70 µl of 2X TaqMan® Fast Advanced Master Mix before loading into a TaqMan® hPSC Scorecard™ Panel 96w FAST plate. The plate was centrifuged at 600 *g* for 2 minutes before loading into a StepOnePlus™ Real-Time PCR System (Thermofisher) and cycled through the following conditions: 50°C for 20 seconds, 40

cycles at 95°C for 1 second followed by 60°C for 20 seconds. Once completed, scorecard analysis was performed using ThermoFisher's online cloud-based software.

2.3 RGC differentiation protocols

2.3.1 2D-RGC differentiation

Differentiation of RGCs through 2D methods (2D-RGCs) was based on a previously published protocol by Sluch *et al*. (2017) with small adjustments. iPSCs were maintained in Geltrex-coated T25 flasks in E8 flex media until the day before the differentiation began, known as day (D) -1 (D-1) of the differentiation protocol. On D-1, iPSCs were washed with PBS and dissociated to single cells using TrypLE Express for 10 minutes at 37°C. Cells were scraped and resuspended in E8 flex media with 5 mM blebbistatin before seeding onto 1 % matrigel coated plates at 52 K/cm^2. The day after plating, designated as D0, media was changed for N2B27 media consisting of 1:1 mix of DMEM/F12 and Neurobasal media (Gibco) with 1X GlutaMAX Supplement (Gibco), 1X (v/v) antibiotic-antimycotic (Gibco), 1 % N2 Supplement (Gibco), and 2 % B27 Supplement (Gibco). N2B27 was kept at 4°C for a maximum of 1 week. The following day, D1, small molecules were added to cells in fresh N2B27 media. Subsequently, cells were fed every other day with a complete exchange of N2B27 media, except if a small molecule was required to be added or removed. Small molecules were added on the following days at the concentrations indicated: Dorsomorphin (1 mM, Stratech) and IDE2 (2.5 mM, Peprotech), for D1 to D6, Nicotinamide (10 mM, Sigma) for D1 to D10, Forskolin (25 mM, Peprotech) for D1 to D30 and DAPT (10 mM, Abcam). Differentiation cultures were maintained 37°C in 5 % CO_2.

Upon reaching day 35 of differentiation, Sluch *et al*. (2017) utilized an RGC specific fluorescent reporter to purify differentiated cells by FACS. However, the CRISPR/engineered reporter cell line was not available due to variety of patient cell lines required in this study, therefore, an alternative purification strategy was utilized. Upon reaching day 35 of culture presumptive RGCs were purified for "neuronal clusters". Cells were washed once with PBS and dissociated with Accutase (Sigma) for 30-45 minutes at 37°C. Cultures were subsequently resuspended in N2B27 media, triturated and strained twice using a 70 µm nylon strainer (Falcon) to remove single cells. Cell clusters were retained and washed with PBS before suspension in N2B27 media and centrifugation at 0.7 *g.* Afterwards, neuronal clusters were plated on 1 % matrigel in N2B27 media and cultured for a further 5-10 days.

2.3.2 3D retinal organoid culture

3D RGC differentiation was based on a previously published protocol by Capowski *et al*. (2019) with minor modifications. As with 2D cultures, iPSCs were maintained in Geltrex-coated T25 flasks in E8 flex media. Upon reaching 70 % confluency, termed as D0, iPSCs were lifted with 2 mg/ml dispase (Thermo Fisher) for 4 minutes at 37°C to promote EB formation. Dispase was subsequently removed and cells washed twice with PBS before being diluted in E8 flex media and gently cell scraped to maintain colony morphology. Cells were then centrifuged at 0.7 *g* and resuspended in E8 flex media with 10 mM blebbistatin (Sigma). EBs were transitioned into Neural Induction Medium (NIM; 1:1 DMEM:F12, 1 % N2 supplement, 1X NEAA, 1X GlutaMAX (Thermo Fisher) and 2 mg/ml heparin (Sigma)) through media mixes, D1 E8 flex:NIM 2:1, D2 E8 flex:NIM 1:2 and D3 100 % NIM. On D6, 55 ng/ml BMP4 (Peprotech) was added to EBs in fresh NIM media before plating on 1 % matrigel coated plates on D7 at an approximate density of 200 EBs per well of a 6–well plate. Half media changes were completed on D9, D12 and D15 to dilute the BMP4 concentration. On D16 media was changed for Retina Differentiation Medium (RDM; DMEM:F12 3:1, 2 % B27 supplement without vitamin A, 1X MEM NEAA, 1x antibiotic, anti-mycotic (A/A; Thermo Fisher) and 1X GlutaMAX). On D30-35, 3D optic vesicle (OVs) like structures were dissected using crescent blades and transfer to 25 well plates (Thermofisher) and maintained in RDM until D42, with twice weekly media changes. On D43, suspension media was changed to Retinal Maturation Medium (RMM; 3:1 DMEM:F12, 2 % B27 without vitamin A, 1 % NEAA, 1 % A/A, 10 % FBS, 100 μM taurine and 2mM Glutamax). Cultures were maintained at 37°C in 5 % CO_2 until D90 and monitored using an Olympus GX41 inverted phase microscope (Olympus) to monitor development of retinal lamination.

2.3.2.1 3D retinal organoid fixation and processing

Upon reaching specific time points OVs were processed for total RNA, total gDNA or immunohistochemistry (IHC). For IHC, organoids were washed once with PBS before fixation in 4 % PFA at 4°C for 25 minutes. Subsequently organoids were washed once with PBS and transferred to 30 % (w/v) sucrose (Sigma) solution for cryo-protection. Fixed organoids were embedded in Optimal Cutting Temperature compound (O.C.T; VWR), frozen in dry ice and stored at -80°C until the day of processing. Organoids were cryosectioned at 8 μm using a Leica CM1850 cryostat (Leica) and stored at -20°C until further processing. Organoid IHC sections were allowed to warm to RT in PBS before further IHC processing (Section 2.1.10).

2.4 Mitochondrial phenotyping

2.4.1 Mitochondrial DNA analysis

2.4.1.1 Long range PCR (LR-PCR)

To detect possible mtDNA deletions in cell culture populations LR-PCR was used to target the major arc of the mitochondrial genome, as previously described (Hudson *et al.* 2008; Reeve *et al.* 2008; Yu-Wai-Man *et al.* 2010). Total DNA was isolated from cell cultures (Section 2.1.1) and 50 ng combined with a 2X master mix consisting of 12.5 µl GoTaq Long PCR (Promega) and 0.2 µM of both forward and reverse primers targeting a 10 kb mtDNA fragment (Table 2.12). Amplifications were incubated in a thermocycler at the following conditions: 2 min at 95°C; 35 cycles of 95°C for 30 s, 58°C for 30 s, and 68°C for 10 min and a final extension of 11 min at 68°C. LR-PCR reaction products were analysed on a 0.7 % agarose gel containing SafeView and visualised on BioRad ChemiDoc XRS+.

Table 2.12. Primers used to expand mtDNA via LR-PCR.

Gene	Primer		Product size	Source
	Forward	Reverse		
mtDNA 10kb	CCCTCTCTCCTACTCCTG	CAGGTGGTCAAGTATTTATGG	9932	-

2.4.1.2 MtDNA deletion and copy number assay via qPCR

Quantification of mtDNA copy number and deletion levels was modified from previous studies by He *et al.* (2002), Rooney *et al.* (2015), Markaryan *et al.* (2009) and Yu-Wai-Man *et al.* (2010). The qPCR reaction was completed as described in Section 2.1.5 using primers designed to enable quantification of mtDNA genes, *MTND1* and *MTDN4* (Table 2.13), and nuclear DNA encoded genes, *B2M* and *GAPDH* (Table 2.13). In brief, a final volume mastermix of 15 µl was prepared, loaded into MicroAmp™ Optical 96-Well Reaction Plates in triplicate for each sample and combined with 50 ng of DNA. Reaction plates were centrifuged and placed into a Quantstudio 6 Flex real-time PCR system (Thermofisher) and cycled with the following conditions:

1. 3 min at 95°C.
2. 40 cycles: 10 seconds at 95°C.
   1 minute at 62.5°C.

Finally, amplified reactions were incubated at the following conditions for 30 cycles to generate a melt curve:

1. 15 seconds at 95°C.
2. 15 seconds at 60°C.

The following equations were subsequently used to calculate the relative mtDNA copy number per cell:

$$\Delta Ct = Ct\ target\ gene - Ct\ reference\ gene$$

$$\text{Copy number} = 2(2^{-\Delta Ct})$$

The following equations were used to calculate the relative wild type mtDNA copies per sample:

$$\Delta Ct = Ct\ target\ gene - Ct\ reference\ gene$$

$$\Delta\Delta Ct = \Delta Ct\ test\ samples - \Delta Ct\ reference\ sample$$

$$Wild\ type\ \% = (2^{-\Delta\Delta Ct}) \times 100$$

Table 2.13. MtDNA qPCR primers.

Gene	Primer		Product size
	Forward	Reverse	
B2M	CACTGAAAAAGATGAGTATGCC	AACATTCCCTGACAATCCC	231
GAPDH	CTCATCCAAGACTGGCTCCTCC	CAGCGTACTCCCCACATCAC	243
ND1	ACGCCATAAAACTCTTCACCAAAG	GGGTTCATAGTAGAAGAGCGATGG	111
ND4	ACCTTGGCTATCATCACCCGAT	AGTGCGATGAGTAGGGGAAGG	107

2.4.1.3 Mitochondrial network analysis

Mitochondrial network analysis was based on previously published studies (Valente *et al.* 2017; Machiraju *et al.* 2019; Chaudhry *et al.* 2020). Prior to analysis fibroblasts were grown to approximately 80-90 % confluency in fibroblast growth media, dissociated using 0.05 % Trypsin-EDTA and resuspended in fibroblast growth media. Subsequently 50,000 cells were plated in 6 well dishes containing a 22 x 22 mm^2 glass coverslip and cultured at 37°C in 5 % CO_2 for 48 hours. For fragmentation analysis staining was completed as previously described (Section 2.1.10) using mitochondrial TOMM20 antibody (Santa-Cruz) to identify network morphology.

Fragmentation analysis was completed using a Leica SP8 inverted Laser Scanning Confocal Microscope (Leica Microsystems), with a 63X oil immersion lens and automated image deconvolution through Huygens software (Scientific Volume Imaging). Quantification was completed in at least 30 cells from 3 individual cell preparations using a combination of the Mitochondrial Network Analysis (MiNa) toolset, a semi-automated image-processing system in ImageJ (Valente *et al.* 2017), and an image pre-processing pipeline (Valente *et al.* 2017; Chaudhry *et al.* 2020). Briefly, after acquisition cells were individually cropped and pre-processed by using ImageJ functions Subtract background (Radius 50 pixels), CLAHE (Block size = 299, slope = 10), median filtering (radius = 10),

unsharp mask (Radius = 2, mask weight = 0.6), make binary, despeckle and remove outliers (Radius = 2, threshold = 50). MiNa raw data, including mean network size (Branches), mean fragment length (µm), number of networks (networks and individuals) and mitochondrial footprint (µm^2), was transferred to Microsoft Excel before analysis.

2.4.2 Seahorse bioenergetic assessment

Live assessment of cellular bioenergetics was performed using the Seahorse XFe96 extracellular flux analyser (Seahorse Bioscience) following the manufacturers instructions. Cells were seeded in the following conditions at the stated densities: fibroblasts were seeded at 20,000 cells per well 24 hours prior to analysis, 25,000 iPSCs were seeded onto laminin coated (3.33 µg/mL) plates 48 hours prior to analysis and RGCs were seeded to ensure cell adhesion without over growth. All cells were maintained at 37°C with 5 % CO2 until the day of analysis. The night before analysis Seahorse sensor cartridges were hydrated in H_2O at 37°C and both sensor cartridge calibrant and XF base media were warmed to 37°C, all performed in a CO_2 free incubator. On the day of experimentation, cell media was changed to XF base media approximately 60 minutes before analysis and incubated at 37°C in a CO_2 free incubator to allow media temperature and pH to equilibrate. Subsequently the seahorse machine was calibrated before beginning the simultaneous measurement of mitochondrial respiration by oxygen consumption rate (OCR) and extracellular acidification rate (ECAR). After baseline measurements cells were treated with 3 compounds to modulate mitochondrial respiration and glycolysis, all compounds provided by Seahorse Bioscience. First, oligomycin was used to inhibit OXPHOS through blocking complex V. Secondly, carbonyl cyanide p-triflouromethoxyphenylhydrazone (FCCP) was used to uncouple the mitochondrial membrane and increase respiration rate. Finally, rotenone and antimycin-A, were used to inhibit mitochondrial respiration and determine non-respiratory oxygen consumption of the cells. Once completed, cells were lysed with RIPA buffer plus 2 % PIC and total protein determined with a BCA assay (Section 2.1.8). Data were subsequently analysed using Wave software (Seahorse Bioscience) and raw data exported to Microsoft Excel where calculations were performed as described in Table 2.14.

Table 2.14. Parameter calculations for Seahorse bioenergetics assay.

Parameter	Equation
Basal respiration	(Last rate measurement before first injection [time point 3]) - (Non-mitochondrial respiration rate [time point 12])
Maximal respiration	(Maximum rate measurement after FCCP injection [time point 8]) - (Non-mitochondrial respiration [time point 12])
ATP production	(Last rate measurement before Oligomycin injection [time point 3]) - (Minimum rate measurement after Oligomycin injection [time point 6])
Average basal OCR	Average OCR from first 3 time points
Average basal ECAR	Average ECAR from first 3 time points

2.4.3 Induction of mitochondrial stress – oligomycin A treatment of cells

To generate a positive control sample to enable quantification of the mitochondrial stress response, WT iPSCs were treated with 2.5 μM oligomycin A (Abcam), to induce respiratory chain dysfunction by inhibiting ATP synthase function and induce mitochondrial stress. WT iPSCs were treated for 18 hours at 37°C before RNA extraction (Section 2.1.2) and first strand cDNA synthesis (Section 2.1.3). Subsequently, mitochondrial stress associated with genes were quantified via qPCR (Section 2.1.5).

2.5 Statistical analysis

Statistical analysis was completed with GraphPad Prism 6 software (GraphPad Inc.) using an ordinary One-way AVONA with Tukey's multiple comparison test and Two-way ANOVA with a Sidaks multiple comparison test. Results are represented as arithmetic mean with upper and lower SEM unless otherwise stated.

2.6 Software list

Benchling (Benchling.com) – primarily used for analysis of genetic sequences; including alignment of Sanger sequencing data, primer design and CRISPR/Cas9 gRNA or ssDNA templates.

Graphpad Prism v6 (Graphpad Software Inc.) – used for statistical analysis and the generation of graphs for data presentation.

Inkscape (Inkscape.org) – used for the generation of thesis figures.

Image Lab (Bio-Rad) – western blot and DNA gel imaging and analysis.

FIJI (ImageJ, National institute of health) – confocal image processing and mitochondrial network analysis.

Leica Application Suite X (LASX; Leica Biosystems) – software to capture confocal images on the Leica microscopes.

Microsoft Word (Microsoft) – word processing.

Microsoft Excel (Microsoft) – data processing and analysis.

ND-2000 Nanodrop software (Thermofisher) – quantification of DNA or RNA samples.

QuantStudio Real-Time PCR software (Applied Biosystems) – qPCR assay design and analysis.

Zen Black 2011 (Zeiss) – imaging software for the acquisition of confocal images using Zeiss microscopes.

Chapter 3: Generation and characterisation of *OPA1* iPSCs

3.1 Introduction

To date, the primary source for experimental data surrounding *OPA1* mutations has been obtained from patient-derived cell lines, from non-physiological cell models or from mouse models. Our ability to model disease was radically improved, however, through the isolation of human embryonic stem cells (ESCs; Thomson *et al.* 1998). This work was built upon and further developed through the advent of iPSCs, in which terminally differentiated somatic cells are converted into naïve ESC-like cells with the potential for downstream differentiation and disease modelling. Takahashi and Yamanaka (2006) demonstrated that by forcibly expressing 4 genes, notably *Oct4*, *Sox2*, *Klf4*, and c-*Myc*, mouse fibroblasts could be reverted to a pluripotent and ESC-like state. Crucially, iPSCs maintain an identical genetic profile to that of their parent population, which provides an excellent opportunity to analyse specific mutations and their associated disease phenotypes. Furthermore, iPSCs demonstrate a number of characteristics identical to that of ESCs that has catalysed a disease modelling revolution.

3.1.1 Reprogramming technologies

Although Takahashi and Yamanaka (2006) demonstrated the concept of somatic cell reprogramming with exogenous factors, and numerous studies quickly followed their seminal work (Maherali *et al.* 2007; Takahashi *et al.* 2007; Lowry *et al.* 2008; Park *et al.* 2008). The field has since expanded greatly, enabling efficient reprogramming of a significant number of adult cell populations using a wide variety of methods. Early reprogramming methods, like that used by Takahashi and Yamanaka (2006), utilised integrative DNA methods. That is, transduction of somatic cells with retrovirus or lentivirus that integrate into the host DNA. However, viral integration is largely random and may cause insertional mutagenesis or alter transcription (Zhou and Freed 2009), thus significantly altering the genetic landscape of the host cells. Subsequent technologies have utilised non-integrative technologies, preventing the reprogramming vector from inducing wholescale genetic changes, by using non-integrating vectors such as Adenovirus or Sendai virus (Fusaki *et al.* 2009; Zhou *et al.* 2009) and non-integrating episomal plasmid vectors (Okita *et al.* 2011). Further new methods have moved away from the use of DNA constructs entirely, thus preventing DNA integration, by using reprogramming proteins (Kim *et al.* 2009) and synthetic mRNA constructs (Yoshioka *et al.* 2013). Ultimately, reprogramming technologies aim to have ever increasing levels of reprogramming efficiency, whilst generating iPSCs as characteristically close to ESCs as possible.

In addition to new reprogramming technologies, the array of somatic cell types that are reprogrammable has also expanded. Developing the work of Takahashi and Yamanaka (2006), early successful efforts to reprogram human cells focused on the use of human dermal fibroblasts (Maherali *et al.* 2007; Takahashi *et al.* 2007). However, since initial reports the range of reprogrammable somatic cells has greatly expanded, with efforts focused on finding somatic cells that are easier to obtain and have higher reprogramming efficiency. In addition to fibroblasts, keratinocytes derived from skin biopsies and hair follicles as well as liver hepatocytes and gastric epithelial cells have been successfully reprogrammed (Aasen *et al.* 2008; Aoi *et al.* 2008; Petit *et al.* 2012). Furthermore, minimally invasive and non-invasive methods for acquiring reprogrammable cells have been devised. Both renal tubular epithelial cells, which are found in urine, and peripheral blood mononuclear cells (PBMCs; Okita *et al.* 2017), acquirable from a simple finger-prick blood sample (Tan *et al.* 2014), have been utilised to successfully generate iPSCs. Importantly, generation of iPSCs from these cell sources has opened the door for disease modelling of conditions where it was previously impractical or difficult to receive ethical approval for taking a skin biopsy (Shi *et al.* 2016), for example conditions involving young patients.

3.1.2 Characteristics of iPSCs

Although the invention of iPSCs was once regarded as the next step to 'personalised medicine' through cell/organ replacement, one of their greatest attributes is their ability to facilitate disease modelling. In particularly, iPSCs possess a number of specific characteristics akin to ESCs that make them ideally suited to further our understanding of the pathological mechanisms that are driven by specific genetic mutations. Firstly, generation of iPSCs from adult somatic cells removes many of the religious and ethical concerns often associated with ESC research, which are highly controlled for scientific use in numerous countries. Thus, reducing the limitations and hurdles of scientific research, in particular the studies of developmental processes in which stem cells are key, to enable a greater scope of research worldwide.

Secondly, iPSCs provide a near unlimited source of patient derived material due to their inherent ability to self-renew in a constant state of pluripotency (Takahashi *et al.* 2007), for an almost indefinite period of time (Amit *et al.* 2000). These two characteristics are regulated by a core set of transcription factors, RNAs and signalling pathways that modulate gene expression (Marson *et al.* 2008), through autoregulatory circuitry in a similar mechanism to ESCs. Notably, the transcription factors *OCT4*, *NANOG* and *SOX2*, which are key to early developmental processes, are regarded as core stemness factors and facilitate self-renewal by preventing differentiation towards somatic cells and by promoting proliferation (Boyer *et al.* 2005; Niwa 2007). In addition, signalling

pathways, including the LIF/STAT3, Wnt/β-catenin and FGF/ERK pathways, have been shown to be crucial to ESC maintenance and further modulate self-renewal (Huang *et al.* 2015). Crucially, a number of studies have shown that inhibition or disruption of these key transcription factors and pathways prevents self-renewal and promotes terminal differentiation (Nichols *et al.* 1998; Avilion *et al.* 2003; Huang *et al.* 2015). It is therefore possible to qualitatively assess cellular reprogramming and induction, and thus iPSC quality, by determining the levels of ESC associated proteins. Ultimately ensuring generation of high-grade iPSCs to provide a near unlimited source of mutant *OPA1* material for further research.

Additionally, Thomson *et al*. (1998), demonstrated that human ESCs (hESCs) possessed the potential to derive cells from all three germ layers; the ectoderm, mesoderm and endoderm. Importantly, high quality iPSCs have the same hypothetical potential and as such have been used extensively to model a significant number of cells and tissues from the human body, including cardiomyocytes (Chanana *et al.* 2016), gut epithelia (Zhang *et al.* 2018) and diverse types of neurons (Schwab and Ebert 2015; Fuller *et al.* 2016). Importantly, our ability to determine iPSCs differentiation potential has developed throughout the past decade, enabling rapid qualification of iPSC quality. Until recently assessing iPSC pluripotency was primarily completed through *in vivo* teratoma formation, injecting iPSCs into immunodeficient mice and determining if the resulting teratomas consisted of cells from all 3 germ layers. More recently *in vitro* assays have been developed by using undirected differentiation of iPSCS into EBs which recapitulate early germ layer development (Sheridan *et al.* 2012). Once generated EBs can be analysed via gene expression, such as qPCR with the TaqMan Scorecard (MacVicar *et al.* 2014), and immunohistochemistry to determine the presence of cells originating from each germ layer. Ultimately *in vitro* quality control increases the speed and efficiency of iPSC pluripotency assessment to further support generation of bona fide iPSC clones, whilst also reducing the unnecessary use of animals for iPSC quality control.

Despite the incredible promise of iPSCs and the apparent similarities with ESCs in protein expression and pluripotency, due to the nature of their derivation iPSCs retain inherent differences to ESCs. Importantly, a number of studies have demonstrated that iPSCs can retain both gene expression and DNA methylation profiles of their somatic cell of origin, in a state known as partially reprogrammed iPSCs, and reprogramming events favours their expansion over fully committed iPSCs (Marchetto *et al.* 2009; Ghosh *et al.* 2010; Kim *et al.* 2010; Ma *et al.* 2014; Teshigawara *et al.* 2017). Partially reprogrammed cells exhibit a number of morphological and protein expression signatures similar to ESCs but have distinct differentiate deficits, inhibiting their ability to differentiate or limiting them to cell fates of the germ line of origin (Kim *et al.* 2014).

Furthermore, although it has been suggested that iPSCs and ESCs may be distinct populations of pluripotent cells (Chin *et al.* 2009), overall gene expression analysis suggests fully reprogrammed iPSCs and ESCs have relatively identical gene expression profiles, chromatin structure and similar epigenetic status, with few major consistent differences (Takahashi *et al.* 2007; Lowry *et al.* 2008; Guenther *et al.* 2010; Mattout *et al.* 2011; Marei *et al.* 2017). Analysis of microRNA (miRNA) expression amongst 49 hESC and iPSC lines also suggests that both iPSCs and ESCs form a continual spectrum of pluripotent cells. Both ESCs and iPSCs show variable miRNA expression levels and as such cluster due to expression levels rather than cellular origin (Neveu *et al.* 2010). Similarly, meta-analysis of microarray gene expression for iPSCs and ESCs maintained in different labs demonstrated that there were marginal differences between the cell populations and the majority of differences arise due to the lab-specific microenvironment (Newman and Cooper 2010). Thus, with high enough levels of quality control iPSCs represent an ideal candidate for efficient disease modelling.

Collectively, the characteristics of iPSCs make them ideal for disease modelling, especially when patient tissues are incredibly difficult to obtain, as with DOA. However, although the depth of iPSC disease modelling has accelerated rapidly since their invention, at the time of writing there are a remarkably limited number of papers studying *OPA1* mutations within iPSCs and their derived tissues (Galera-Monge *et al.* 2016; Zurita-Díaz *et al.* 2017; Iannielli *et al.* 2018; Jonikas *et al.* 2018; Iannielli *et al.* 2019; Caglayan *et al.* 2020). As such, generation of *OPA1* mutant iPSCs provides an excellent opportunity to further understand DOA and its associated pathogenic mechanisms.

3.1.3 CRISPR/Cas9 gene editing technology

In conjunction to iPSC technologies, the discovery of the bacterial Clustered Regularly Interspaced Short Palindromic Repeats (CRISPR) and CRISPR associated protein 9 (Cas9) has accelerated our ability to perform precise genomic editing (Jinek *et al.* 2012). Initially identified as prokaryotic bacterial immune system to prevent integration of bacteriophage genetic elements (Garneua *et al.* 2010), the CRISPR/Cas9 system has since been modified for genetic manipulation of mammalian systems (Cong *et al.* 2013; Ran *et al.* 2013). It is therefore now feasible to accurately develop disease models by genetically engineering healthy cells to encode disease-associated mutations with genetically matched, un-edited isogenic control cells.

Though multiple CRISPR/Cas9 systems have been identified, the most well characterised is the type II CRISPR/Cas9 system from Streptococcus pyogenes that utilises a guide RNA (gRNA) in combination with a tracrRNA to target Cas9 nuclease protein to gDNA (Figure 3.1; Ran *et al.* 2013). In addition, a downstream Protospacer

Associated Motif (PAM) site is required for Cas9 gDNA recognition, binding and cleavage. It is therefore possible to target genetic regions of interest through identification of PAM sites and their associated gRNA sequences within target loci. Once expressed within cells gRNAs, tracrRNAs and Cas9 form ribonucleoprotein complexes which target gDNA through Watson-Crick base pairing and induce double strand DNA (dsDNA) breaks through cleavage by RuvC and HNH nuclease domains (Figure 3.1; Sapranauskas *et al.* 2011; Gasiunasa *et al.* 2012).

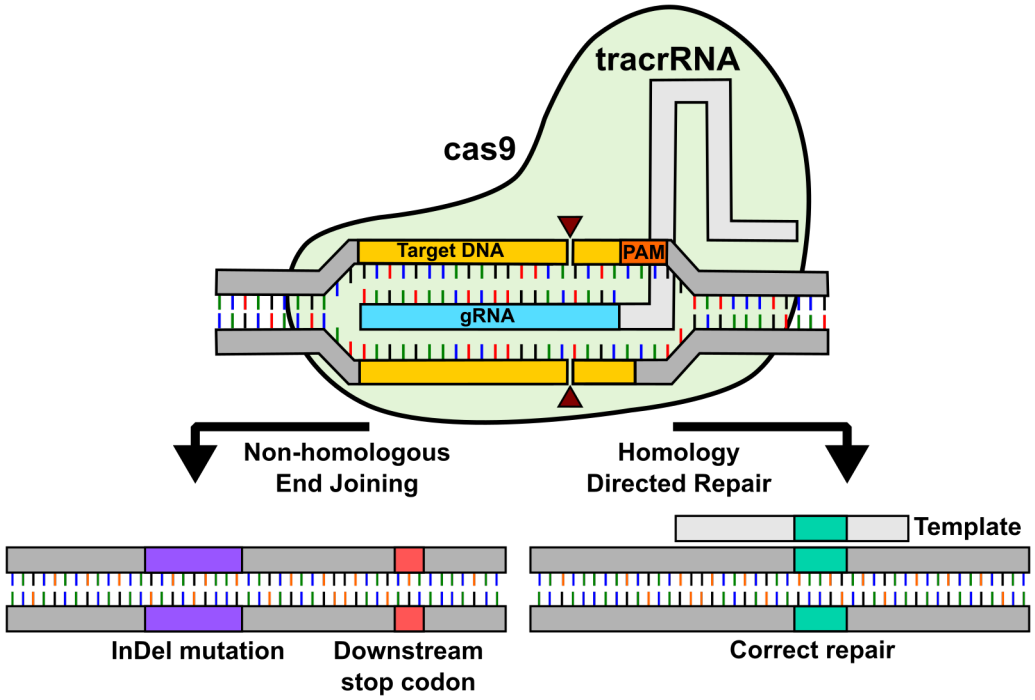

Figure 3.1. Using CRISPR/Cas9 for mammalian genomic engineering.

Cas9 (light green) is targeted to genetic loci by forming nucleoprotein complexes with tracrRNA (light grey) and gRNA (light blue). Once bound to the target Cas9 induces double strand breaks (red arrow) through RuvC and HNH nucleases. Double strand breaks are repaired via one of two pathways. Non-homologous end joining rapidly repairs DNA but is highly error prone, thus inducing random InDel mutations during repair. InDel mutations cause downstream frameshifts and premature stop codons, and can thus be used to manipulate protein expression. Homology directed repair uses a repair template, such as plasmid DNA or a single stranded DNA template, to accurately repair and precisely edit gDNA, enabling the correction of disease-associated genetic defects.

Generation of dsDNA breaks is a gateway to achieving gene editing and activates one of two primary DNA repair pathways: Non-Homologous End Joining (NHEJ) or Homology Directed Repair (HDR; Figure 3.1). When lacking a repair template, NHEJ rapidly repairs dsDNA breaks, however this occurs with remarkably high error frequency (Barnes 2001). Due to its inherent inaccuracy, NHEJ can thus be exploited to induce insertions or deletions (InDels) into gDNA, create downstream frameshift mutations and thus alter protein expression. Conversely, HDR utilises repair templates to precisely, but inefficiently, repair dsDNA breaks. Typically, HDR repair templates take 1 of 2 forms; either dsDNA, such as plasmids, or ssDNA (Ran *et al.* 2013). Although both have their

advantages ssDNA templates have been shown to have greater repair efficiency and reduced off-target integration (Miura *et al.* 2015; Li *et al.* 2017; Won and Dawid 2018). HDR can thus be manipulated to induce specific mutations within a region of interest (Lin *et al.* 2014; Maruyama *et al.* 2015), and enables genetic correction of mutated alleles.

Here, HDR will be utilised to correct patient-derived iPSCs whilst NHEJ will be exploited to alter OPA1 protein expression levels by inducing frameshift mutations in iPSCs through simultaneous reprogramming of otherwise healthy control cell lines. Ultimately, generation of *OPA1* isogenic disease models through CRISPR/Cas9 based gene editing will increase our understanding of *OPA1* disease mechanisms by facilitating direct cellular comparisons and reducing inter-individual genetic variation within RGC cell models.

3.1.4 Chapter aims

Previous data that has established OPA1 cellular function has primarily focused on model cell lines or patient derived fibroblasts. To overcome the limitations of these cell models it is necessary to develop improved model systems that more accurately represent the context of DOA to garner greater understanding of the pathogenic mechanisms that drive this disease. Approximately 60-70 % of DOA is caused by mutation with *OPA1*, yet there is a distinct lack of *OPA1* mutant iPSCs within the published literature. As such, the current study aimed to establish a comprehensive biobank of *OPA1* mutant iPSCs that span the diverse range of DOA causing *OPA1* mutations within the UK population. Additionally, isogenic control cell lines would be established using CRISPR/Cas9 gene editing to allow specific analysis of *OPA1* mutations, irrespective of other genetic differences.

Thus, the primary aims of Chapter 3 were:

1. Generate a comprehensive biobank of DOA patient-derived iPSCs covering the spectrum of *OPA1* mutation.
2. Utilise CRISPR/Cas9 gene editing technology to generate isogenic cell lines for the specific study of *OPA1* mutation.
3. Conduct iPSC quality control: validate iPSC differentiation and self-renewal potential to ensure the iPSC biobank is of sufficient quality for downstream applications.

3.2 Results

3.2.1 Generation of patient-derived iPSC

To investigate the effects of *OPA1* mutations on RGC biology a biobank of *OPA1* mutant iPSCs was generated from six DOA patient-derived fibroblast cell lines (Table 3.1), kindly provided by Dr Yu Wai Man.

Table 3.1. Patient derived cell lines with *OPA1* mutations.

M = male, F = female, AA = amino acid. Gene mutational data are described using the nomenclature of the Human Genome Variation Society (http://varnomen.hgvs.org; human *OPA1*, RefSeq: NM_015560.2).

Cell line	Age	M/F	Diagnosis	*OPA1* mutation		Domain
				Genetic change	Predicted AA change	
M0174KR	48	M	DOA+	c.1334G>A	p.(R445H)	GTPase
M178-8GF	49	M	DOA	c.2708_2711delTTAG	p.(R905*)	GTPase effector
F0014WP	51	M	DOA	c.2708_2711delTTAG	p.(R905*)	GTPase effector
F041CC	51	F	DOA	c.3G>A	p.(M1I)	Basic
				c.113_130del	p.(38_44delRSIYHSH)	
MkI	64	M	DOA+	c.768C>G	p.(S256R)	GTPase
				c.854A>G	p.(Q285R)	
F176SC	62	F	DOA+	c.2356-1G>T	-	Middle

Briefly, all 6 patient fibroblast cell lines were expanded *in vitro* and reprogrammed via electroporation with episomal vectors containing *OCT4*, short hairpin RNA for *P53*, *SOX2*, *KLF4*, *L-MYC*, *LIN28* and micro RNA cluster 302/367 (Okita *et al.* 2011; Schwarz *et al.* 2015). Individual iPSC colonies were isolated through manual selection and expanded to generate at least 6 clonal cell lines per patient. Subsequently, two cell lines were selected for further characterisation due to their clinical relevance, *OPA1*: c.2708_2711delTTAG (henceforth referred to as 2708del) is the most prevalent mutation within the UK population (Yu-Wai-Man *et al.* 2013) and *OPA1*: c.1334G>A (henceforth referred to as 1334G>A) represents a clinically severe DOA+ phenotype (Yu-Wai-Man *et al.* 2010). 2708del and 1334G>A iPSC colonies exhibited classical iPSC morphology, with smooth borders and tightly clustered, nuclear dense cells. The presence of the patient specific mutations was confirmed via PCR using primers OPA1-ex14F and OPA1-ex14R for 1334G>A iPSCs (Table 2.7), and OPA1-ex27F and OPA1-ex27R for 2708del iPSCs (Table 2.7), followed by Sanger sequencing with primers OPA1-ex14F and OPA1-ex27F respectively (Figure 3.2A,B).

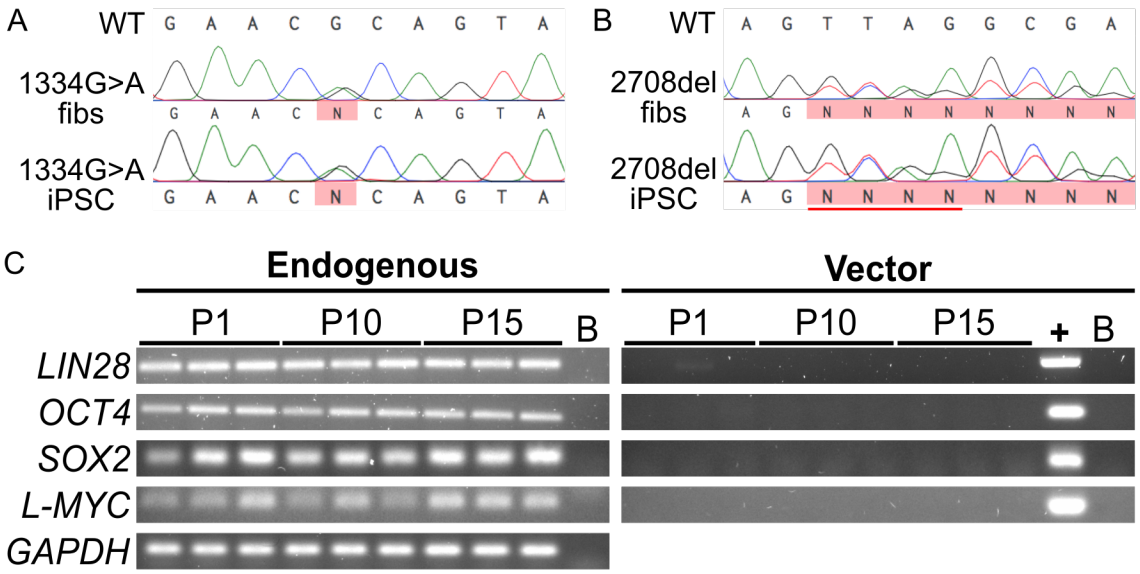

Figure 3.2. Characterisation of patient derived iPSC.

(A, B) Patient mutations from both 1334G>A and 2708del were confirmed in derived iPSCs using Sanger sequencing.

(C) Temporal RT-PCR analysis of 1334G>A iPSC determined induction of endogenous reprogramming factors and loss of episomal vector expression. **+** = episomal vector containing corresponding gene. B = no DNA control.

RT-PCR analysis of 1334G>A iPSCs confirmed the induction of endogenous self-renewal genes *OCT4, L-MYC, SOX2* and *LIN28,* whilst episomal vector expression was negligible at passage 1 (see Lin28 P1 lane 2 Figure 3.2C) and eliminated completely by passage 10 and 15 (Figure 3.2C). Due to the negligible levels of vector expression at the first passage of 1334G>A iPSCs, analysis was not conducted for the other iPSC lines. Subsequently, immunofluorescent staining confirmed that both 1334G>A and 2708del iPSC colonies expressed embryonic stem cell specific markers at the protein level, with nuclear localisation of both NANOG and OCT4 and membrane localisation of SSEA4, TRA-1-60 and TRA-1-81 (Figure 3.3).

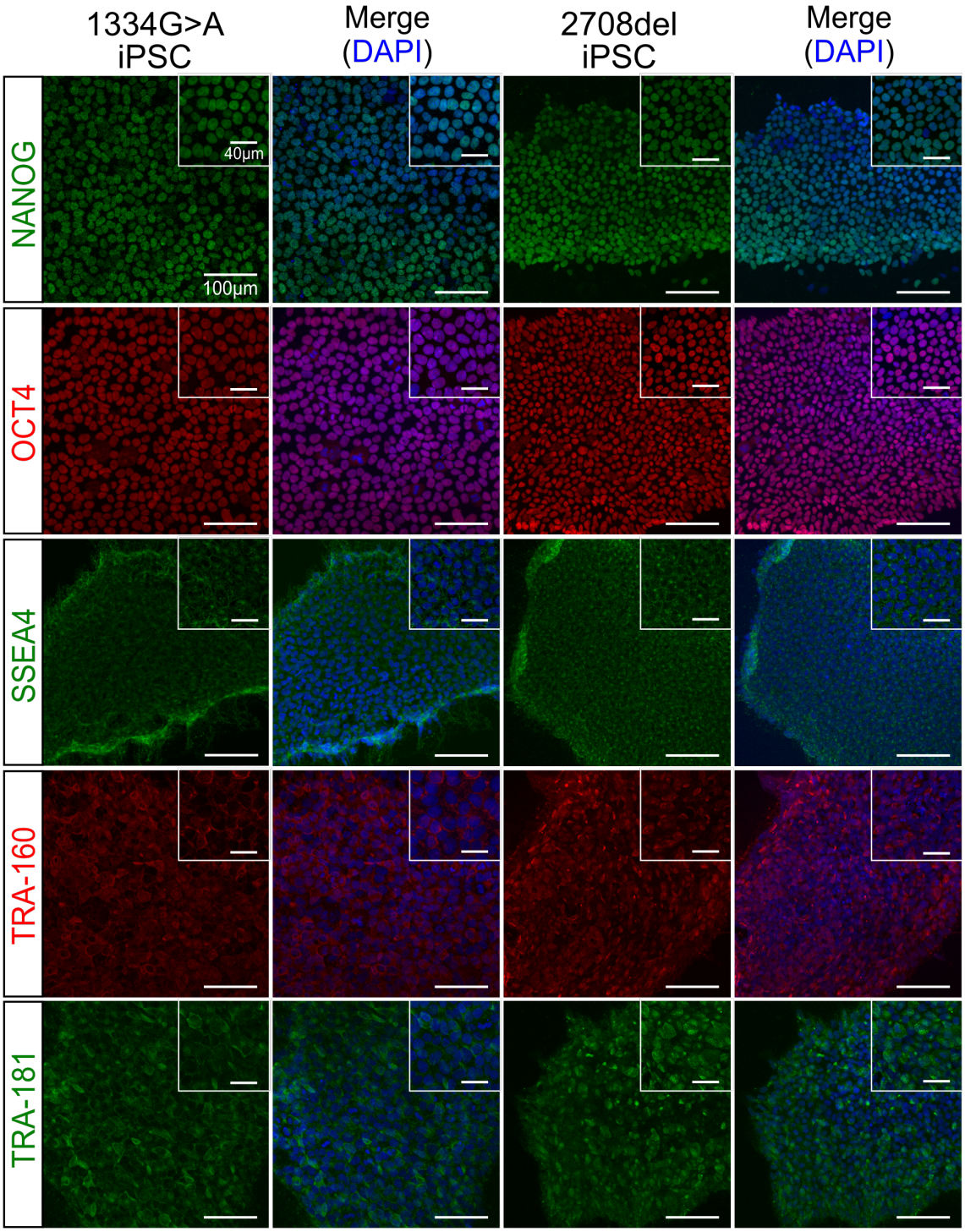

Figure 3.3. Analysis of ESC marker expression in patient-derived iPSC.

iPSC derived from patient fibroblasts carrying *OPA1* 1334G>A and 2708del mutations showed nuclear localisation of embryonic stem cell markers NANOG and OCT4 with membrane/cytoplasmic localisation of SSEA4, TRA-1-60 and TRA-1-81. Scale bars = 100 μm and 40 μm for inset.

3.2.2 Simultaneous reprogramming and *OPA1* gene editing of human control fibroblasts using CRISPR/Cas9

Simultaneous reprogramming and CRISPR/Cas9 gene editing was utilised to generate an isogenic knock-out cell line with reduced OPA1 protein expression by inducing InDels within the *OPA1* gDNA sequence in an otherwise healthy cell line. Experiment design and implementation of CRISPR/Cas9 technology was completed following the protocols of Ran *et al.* (2013) and Howden *et al.* (2015). Initial design of gRNAs was completed on Benchling.com, the MIT CRISPR design tool and Off-spotter, targeting exon 2 of *OPA1* protein due to its large size and incorporation in all splice isoforms (Delettre *et al.* 2001; Figure 3.4A). A 150 base pair sequence centred on the end of exon 2 was analysed for PAM sites and up-stream gRNA sequences, with gRNAs selected for minimal off-target effects, a high CRISPR design tool quality score, high Benchling cutting efficiency and approximately 50 % GC content (Table 3.2). Once designed, guide oligonucleotides were synthesised, modified with 5' overhangs following the protocol provided by Ran *et al.* (2013; Figure 3.4B) and cloned into the PX458 plasmid for transfection (See Appendix B for plasmid map). Successful incorporation of gRNAs into the PX458 plasmid was confirmed with Sanger sequencing using the U6 forward primer, followed by alignment to the PX458 reference sequence on Benchling (Figure 3.4C).

Table 3.2. CRISPR/Cas9 guide oligonucleotide sequences targeting *OPA1* exon 2.

3 guide sequences were selected from Benchling for further analysis. Off-target gDNA regions were analysed by the CRISPR design tool and Off-spotter programs, presented as number of genes predicted per gRNA by each program. On-target efficiency was analysed by the CRISPR design tool quality scorer and Benchling on-target cutting efficiency, with a higher score demonstrating greater cutting efficiency at the gRNA target site.

Guide RNA (gRNA)	Guide oligonucleotide sequence	GC (%)	Off-target gDNA regions		CRISPR design tool quality score	On-target cutting efficiency
			CRISPR design tool	Off-spotter		
gRNA 1	AATATGGCTACCAGCCTCGC	55	65	35	90	56.4
gRNA 2	TCGCTATCTCATACTAGGAT	40	44	85	92	60.5
gRNA 3	CATACTAGGATCGGCTGTTG	50	42	105	93	48.2

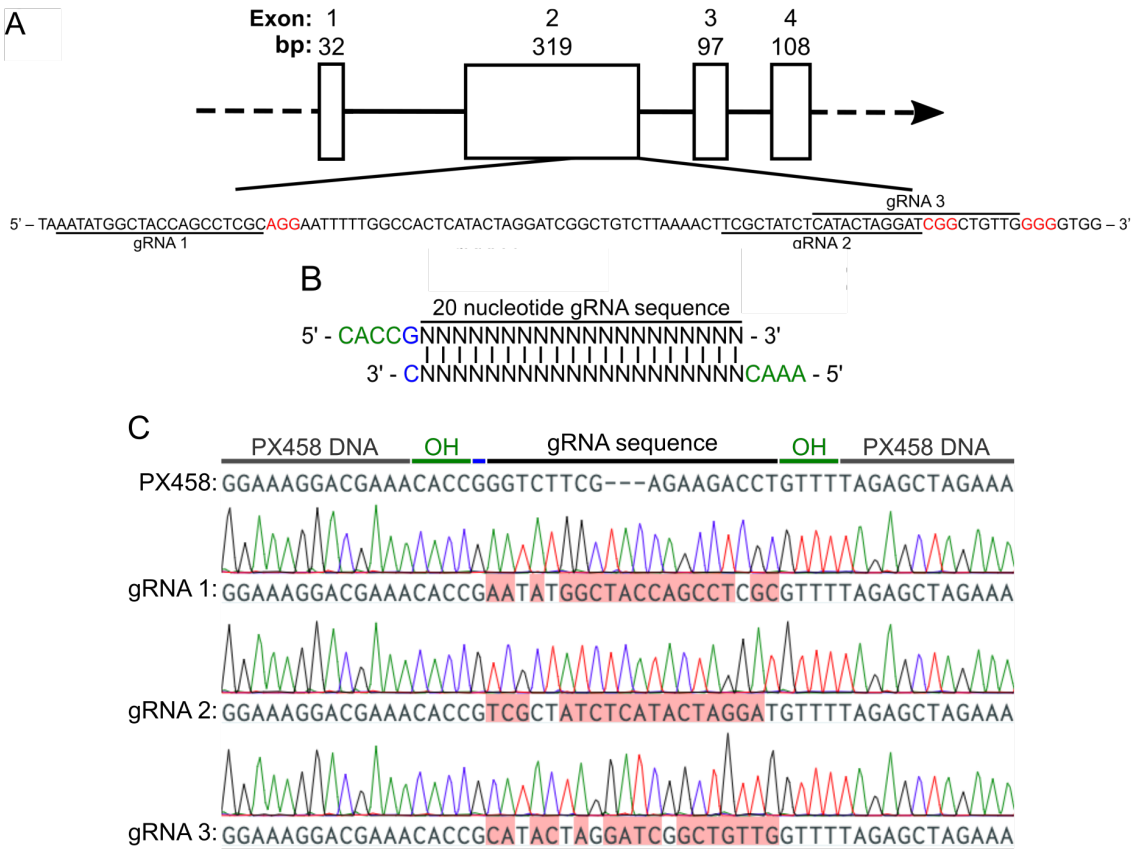

Figure 3.4. Generation of CRISPR/Cas9 PX458 plasmids with *OPA1* specific guide sequences.

(A) Schematic of *OPA1* exons 1-4 and expanded exon 2 sequence showing location of gRNA target sequences (underlined) and PAM sites (red).

(B) gRNAs were modified and synthesised with the addition of plasmid ligation overhangs (green) to the forward and reverse oligonucleotide**.** A single G base (blue) is added at the 5′ end of the sequence for U6 transcription.

(C) Sanger sequencing confirmed successful ligation of each gRNA into the PX458 plasmid. Bases highlighted in red denote gRNA oligonucleotide mismatches to the PX458 reference sequence. OH = overhang sequence.

To determine the efficiency of individual gRNAs for targeting *OPA1*, plasmids encoding each gRNA were transfected in triplicate into HEK-293 cells. 48 hours post transfection gDNA was extracted and the gRNA target region amplified by PCR using primers OPA1-ex2F and OPA1-ex2R (Table 2.7). Successful amplification of the target region was confirmed via gel electrophoresis (Figure 3.5A). The remaining PCR product was subject to heteroduplex formation in a thermocycler to generate mismatch DNA complexes incorporating both WT and CRISPR mutant DNA strands. Heteroduplex complexes were subsequently digested with T7 endonuclease I, which cleaves mismatched DNA strands, and analysed by gel electrophoresis (Figure 3.5B). To determine gRNA cutting efficiency DNA band intensities were quantified using Image Lab software and the fraction of cleaved PCR product (f_{cut}, Figure 3.5B), which is an estimate of InDel occurrence (InDel occurrence %) calculated. Analysis demonstrated a mean InDel occurrence of 16.12 %, 24.73 % and 21.91 % for gRNA 1, 2 and 3, respectively (Figure 3.5C). Due to their higher

efficiency, gRNA 2 and 3 were chosen for further use in simultaneous reprogramming and editing.

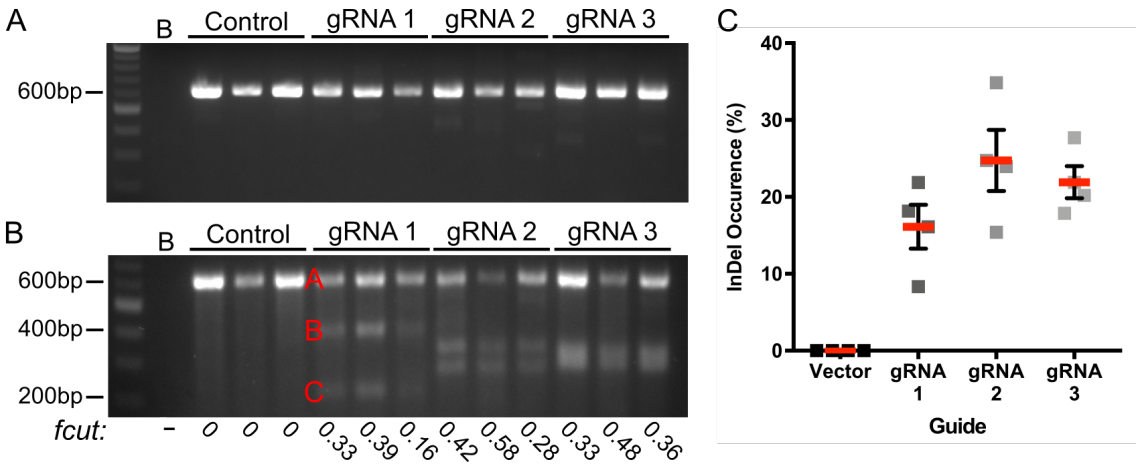

Figure 3.5. Quantification of exon 2 gRNA efficiency with T7 endonuclease I assay.

(A) CRISPR/Cas9 target region was expanded by PCR and confirmed via gel electrophoresis (B – water only control).

(B) PCR products are incubated to form heteroduplexes and then incubated with T7 endonuclease I to cleave mismatched DNA strands. Successful targeting of exon 2 with CRISPR/Cas9 gRNAs generates multiple DNA bands. gRNA targeting efficiency is calculated as the *Fcut* ratio [*fcut* = (B+C)/(A+B+C)].

(C) InDel occurrence estimations calculated (InDel % = (1-[√(1-*fcut*)]*100), for gRNA 2 and gRNA 3 show marginally higher InDel occurrence %. Mean in red ± SEM.

To generate OPA1 knockout and isogenic control cell lines HDFn fibroblasts were simultaneously electroporated with episomal reprogramming vectors and the respective CRISPR/Cas9 plasmids (Figure 3.6A). 52 individual CRISPR-iPSC colonies were manually isolated before gDNA was extracted and the CRISPR target region amplified using primer OPA1-ex2F and OPA1-ex2R before sequencing with OPA1-ex2F (Table 2.7). CRISPR/Cas9 mutated cell lines were initially identified through misalignment to the reference sequence on Benchling (Figure 3.6B). In total 7/52 clones exhibited CRISPR/Cas9 induced mutations (Figure 3.6C), equivalent to a knockout efficiency of 13.5 %.

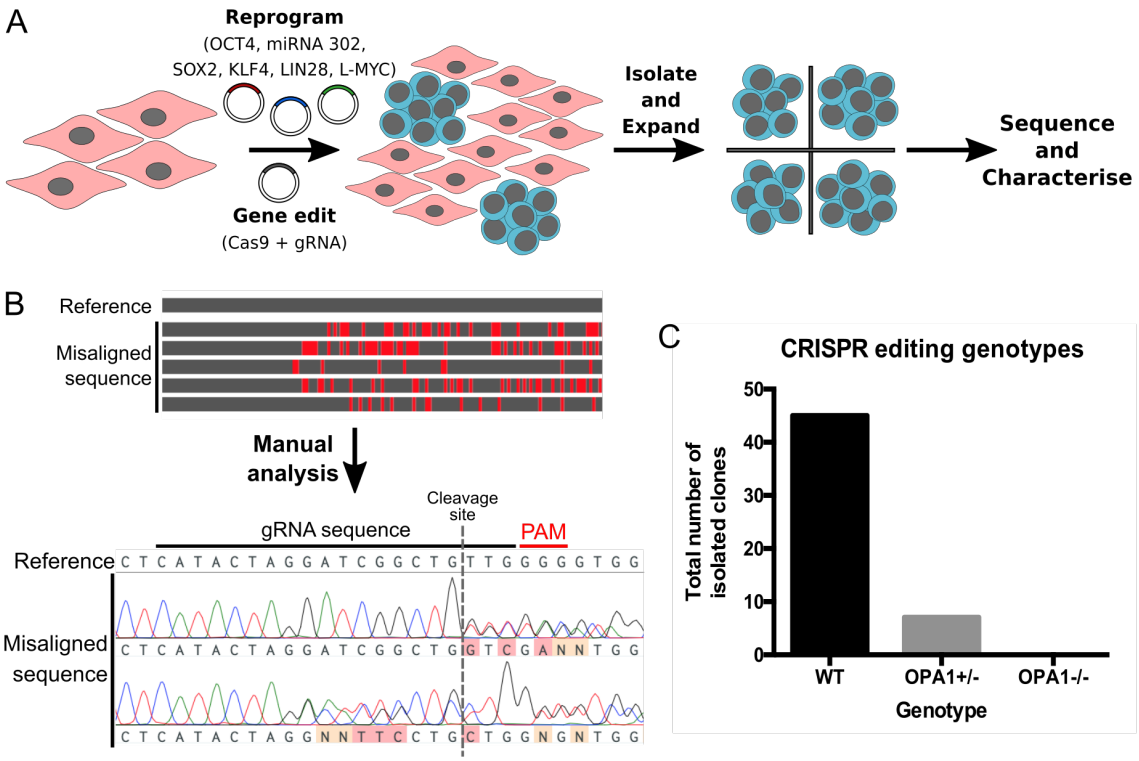

Figure 3.6. Generation of OPA1+/- cell lines via simultaneous CRISPR/Cas9 editing and reprogramming.

(A) Schematic of simultaneous reprogramming methods utilised to knock out *OPA1* at the genomic level. A CRISPR/Cas9 plasmid is utilised at the same time as episomal reprogramming vectors to induce iPSC formation and gene editing. Colonies are then isolated, expanded and sequenced.

(B) Schematic of initial steps used to identify CRISPR-edited cell lines. Benchling software detects mismatched sequences (red bars) during sequence alignment. Detailed manual sequence analysis of genetic traces allows for identification of CRISPR/Cas9 induced InDels centred on the Cas9 cleavage site.

(C) CRISPR/Cas9 editing generated 7 heterozygous WT/mutant *OPA1* cell lines and zero homozygous cell lines.

Detailed examination of *OPA1* exon 2 through manual analysis (Figure 3.6B) further revealed the exact nature of induced mutations, with all clones exhibiting a heterozygous InDel centring on the gRNA cleavage site (Table 3.3). In silico analysis confirmed the presence of downstream premature termination codons for all 6 clonal lines (Figure 3.7). Due to the mutation complexity of clone 7 it was not possible to predict the downstream protein effects. Interestingly, no homozygous or compound heterozygous CRISPR-iPSC colonies were identified, suggesting OPA1 function may be vital to iPSC viability.

Table 3.3. Confirmed CRISPR/Cas9-induced *OPA1* mutations.

Confirmation of CRISPR-induced mutations for 6 generated OPA1+/- iPSC lines. Analysis predicts all mutations will induce downstream premature stop codons. Line 5 also shows a predicted splice site mutation.

OPA1+/- iPSC line	CRISPR induced mutation	Predicted protein effect
1	TTGGGGGT del	p.(V109Gfs*9)
2	T ins	p.(G110Vfs*11)
3	G del	p.(G106Dfs*19)
4	AT ins	p.(G110Ffs*17)
5	40 bp del	Splice variant/p.(G106Dfs*2)
6	AGGATCGGCT del	p.(G106Lfs*17)

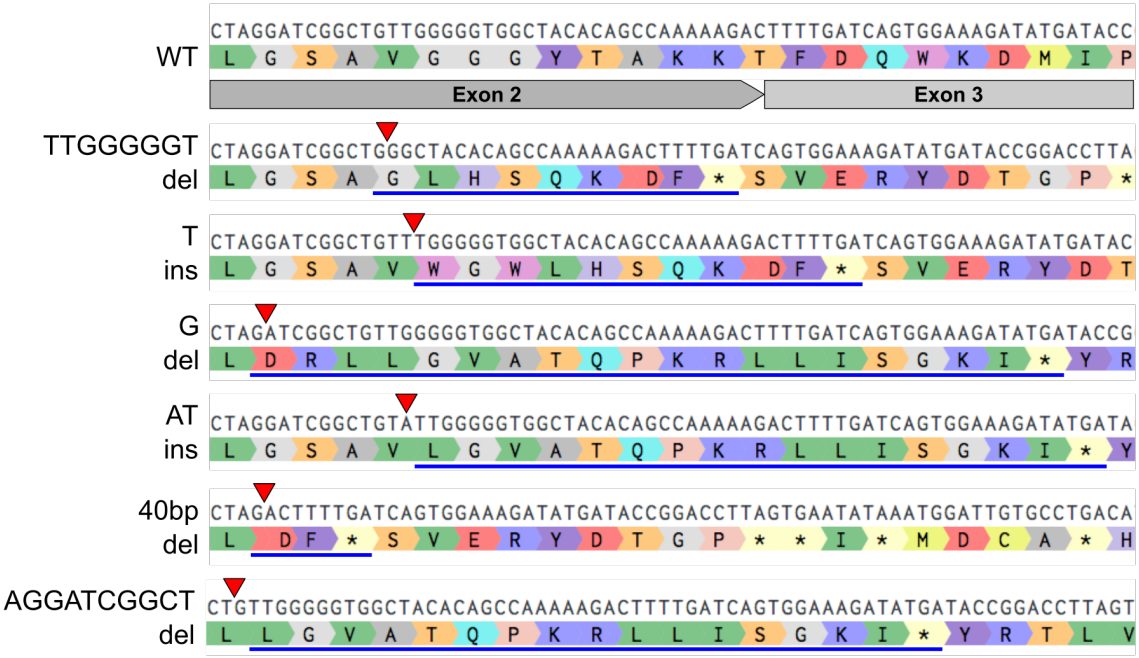

Figure 3.7. Predicted protein changes in six OPA1+/- iPSC lines.

WT cDNA sequence showing amino acid and corresponding junction between *OPA1* exon 2 and exon 3. All CRISPR/Cas9 induced breaks (red arrows) induce downstream amino acid changes (underlined in blue) before a premature termination codon (*) compared to the WT sequence.

In order to reduce the complexity of the knockout system, CRISPR/Cas9 iPSC lines 1, 2 and 3 (hence forth OPA1+/- iPSC) were taken forward due their simpler mutations, compared to mutants with larger deletions or splice site changes. Similarly, three HFDn isogenic control lines that had been through the editing process (now known as control iPSC) were also selected. OPA1+/- iPSC and isogenic control iPSC lines were subsequently analysed for stem cell quality, via immunohistochemistry and Scorecard analysis, and mutation effects via qPCR and western blot. Immunofluorescence analysis of control and OPA1+/- iPSC lines enabled identification of lines with the most consistent expression of embryonic stem cell marker proteins. Importantly, OPA1+/- iPSC line 3 and control iPSC line 3 had the most reliable expression of NANOG and OCT4 throughout the colony whilst also exhibiting strong SSEA4, TRA-1-60 and TRA-1-81 expression within cell membranes (Figure 3.8), and as such were selected for further study.

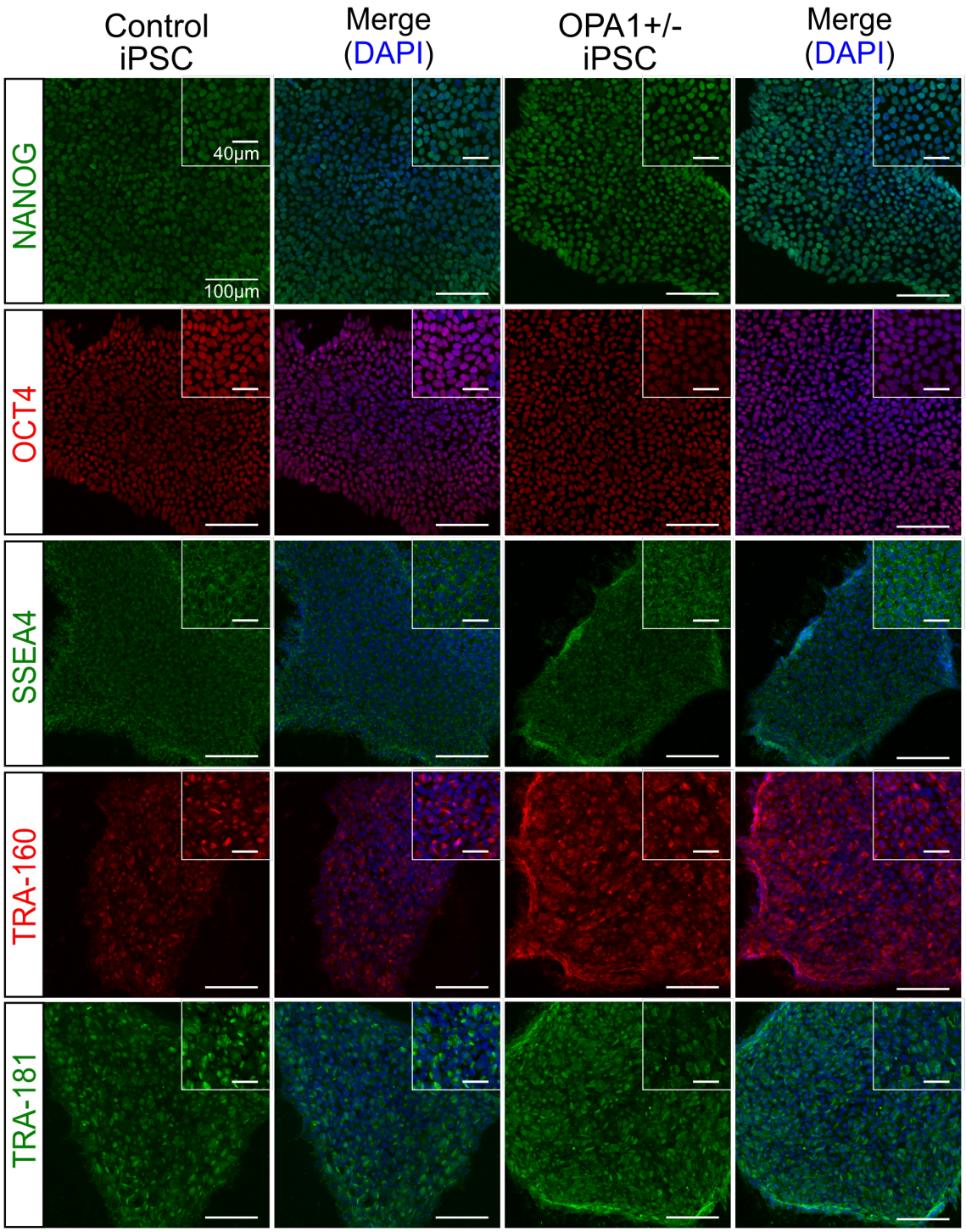

Figure 3.8. Characterisation of OPA1+/- cell lines via immunofluorescence.

Control iPSC and isogenic OPA1+/- iPSCs showed nuclear localisation of embryonic stem cell markers NANOG and OCt4 with membrane/cytoplasmic localisation of SSEA4, TRA-1-60 and TRA-1-81. Scale bars = 100 µm and 40 µm for inset.

Finally, to determine if CRISPR/Cas9 gene editing introduced off-target effects during reprogramming gRNAs were analysed via the Off-Spotter program for regions with sequence-homology to the gRNA target. The top 10 off-target sites were determined and amplified via PCR for both OPA1+/- and unedited control iPSCs. PCR products were sequenced and aligned on Benchling. OPA1+/- iPSCs showed no evidence of off-target mutations when compared to unedited control iPSC (Table 3.4; Appendix C).

Table 3.4. Top 10 predicted off-target genes for OPA1+/- CRISPR/Cas9 gRNA 3.

The top 10 off-target genes were determined on Off-Spotter and amplified by PCR before Sanger sequencing. No off-target CRISPR/Cas9 induced mutations were identified.

Gene	Chromosome	Position	gRNA mistmatches	CRISPR-induced mutation
ACAN	15	Intronic	5	No
ADCY2	5	Intronic	5	No
CHRNB2	1	5' UTR	5	No
CDH20	18	Exon 11	5	No
MMP16	8	Intronic	4	No
PHYKPL	5	Intronic	5	No
POMP	13	Intronic	4	No
SPTBN2	11	Intronic	5	No
UPB1	2	Exon 5	4	No
ZFAND6	15	Intronic	4	No

3.2.3 Correction of *OPA1* 1334G>A patient-derived stem cells using CRISPR/Cas9 and an ssDNA HDR template

In addition to the generation of an OPA1+/- isogenic cell line through targeted *OPA1* mutation, correction of patient-derived iPSCs by CRISPR/Cas9 gene editing and ssODN template (also known as a single stranded DNA (ssDNA) template) guided HDR was also utilised to generate isogenic cell lines. Individual mutation loci were thus assessed for their potential for HDR gene correction using Benchling. gRNAs were identified for suitability for HDR by being located in a region 1-30 bp upstream or downstream of the mutation, whilst having high on-target and low off-target cutting efficiencies. The 1334G>A mutation proved particularly promising for two primary reasons. Firstly, due to the close proximity of two gRNA target sequences, 15 bp upstream and 14 bp downstream respectively (Figure 3.9), thus improving the likelihood of HDR occurring, whilst both guides had suitable on-target cutting efficiencies and low off-target scores. Secondly, the OPA1+/- and the respective HDFn isogenic control iPSCs provide a perfect paradigm for modelling DOA associated with haploinsufficiency. Therefore, correction of 1334G>A iPSCs was chosen to further expand the range of isogenic control iPSCs and enable direct study of the effect dominant-negative *OPA1* mutations have on DOA. Subsequently complementary ssDNA HDR templates, which are typically less toxic and have reduced off-target integration (Li *et al.* 2017), were designed using Benchling HDR template design tool. Templates were designed such that they overlapped the Cas9-induced dsDNA break by 36bp upstream and 91bp downstream and to correct the A>G mutation at position 1334. Finally, synonymous mutations at each gRNA PAM site were included to prevent re-targeting of the CRISPR/Cas9 system after correct HDR (Figure 3.9).

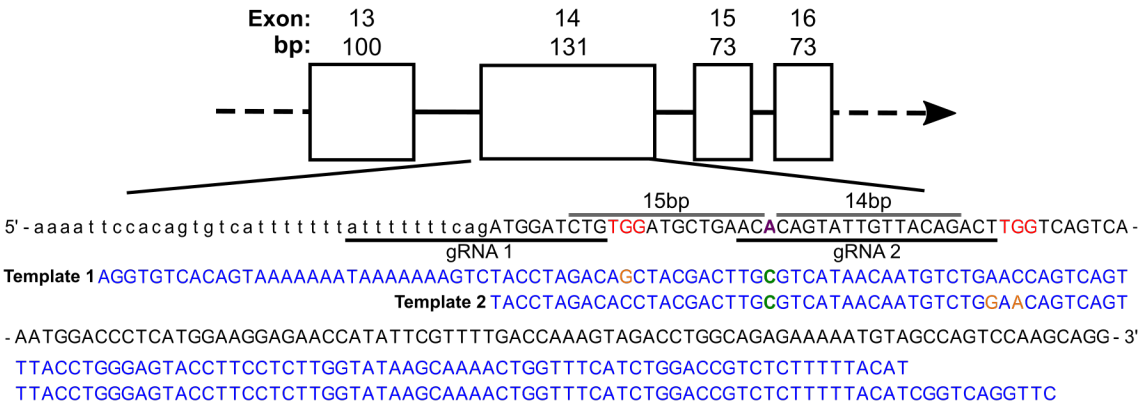

Figure 3.9. HDR gRNA and ssODN template design.

The region surrounding 1334G>A mutation (purple) was analysed on Benchling for suitable gRNAs. Two gRNAs (underlined) with suitable PAM recognition sites (red) were identified 15 bp upstream and 14 bp downstream of the mutation site respectively. Complementary ssODN HDR templates (blue) were designed, using Benchling HDR design tool, to be 36 bp upstream and 91 bp downstream of the Cas9 cut site to correct A>G base change (green), and to include synonymous base changes to remove PAM sites (orange).

Once designed, selected gRNA target sequences, manufactured as CRISPR-RNAs (crRNAs), and ssODN templates were synthesized by Integrated DNA Technologies (IDT) and resuspended in RNase-free water. crRNAs were then mixed with tracrRNAs to generate functional gRNA complexes before incubation with Cas9 protein at RT to generate RNP complexes. Subsequently, 1334G>A iPSCs were dissociated to single cells and nucleofected with RNP complexes and the corresponding ssODN templates. iPSCs were allowed to grow for 7 days and then dissociated into single cells. At this time, half of the cells were reserved for gDNA extraction and half replated into individual wells of a 6-well plate. During the next expansion step of 5-7 days, gDNA was amplified using primers OPA1-ex14F and OPA1-ex14R (Table 2.7) to expand the HDR target region surrounding *OPA1* exon 14, before Sanger sequencing with OPA1-ex14F. Sanger sequencing data was subsequently inputted into the TIDER online algorithm to estimate the frequency of HDR editing and total RNP cutting efficiencies in all transfection conditions. This analysis demonstrated that gRNA 1 had an HDR editing efficiency of approximately 24 %, whereas, gRNA 2 had a notably higher HDR editing efficiency of 60 % (Figure 3.10A). Both gRNAs had increased editing efficiency with the use of HDRe, and increased to 40 % and 70 % for gRNA 1 and 2 respectively (Figure 3.10A). Similarly, the total CRISPR/Cas9 cutting efficiency, an estimation of all gDNA changes around the dsDNA break from either HDR or NHEJ events, of gRNA 2 (73 %) was significantly higher than gRNA 1 (41 %; Figure 3.10B). However, HDRe significantly improved the efficiency of gRNA 1, up to 73 %, whereas it had little to no effect on gRNA 2. As such iPSCs transfected with both gRNA 2 and template 2, with and without HDRe, were selected for further clonal isolation due to the significantly higher levels of HDR editing frequency.

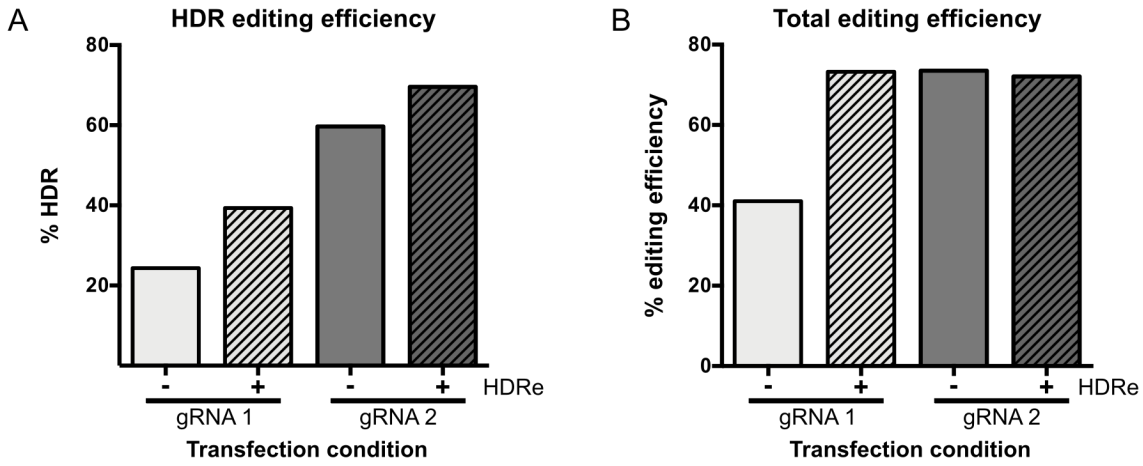

Figure 3.10. CRISPR/Cas9 HDR TIDER analysis.

TIDER analysis compares CRISPR/Cas9 edited sample sequences with a wild-type and a reference sequence containing ssODN base changes to estimate the effectiveness of HDR in iPSCs.

(A) Total HDR editing efficiency determined as the percentage of sequences within each sample with HDR events (ssODN template induced base changes).

(B) Total editing efficiency of each nucleofection condition, estimated by number of base changes (HDR or NHEJ induced) surrounding CRISPR/Cas9 dsDNA break sites.

Subsequently, 2 rounds of clone isolation and sequencing were completed. From the first round of sequencing a total of 8 out of 13 clones were confirmed as successfully edited, and 5 out of 11 for the second round: editing efficiencies of 67 % for round 1, 46 % for round 2 and a combined efficiency of 57 % (Figure 3.11A). Sanger sequences were aligned on Benchling to both WT control and un-transfected patient sequences and correctly edited clones identified by G homozygosity at position c.1334 (Figure 3.11B, purple box). Analysis of all isolated clones demonstrated homozygosity for HDR template induced PAM site changes, demonstrating editing of both the mutated and WT allele (Figure 3.11B, blue box). All correctly edited clones were further expanded, whilst 2 clones were maintained for further experimentation.

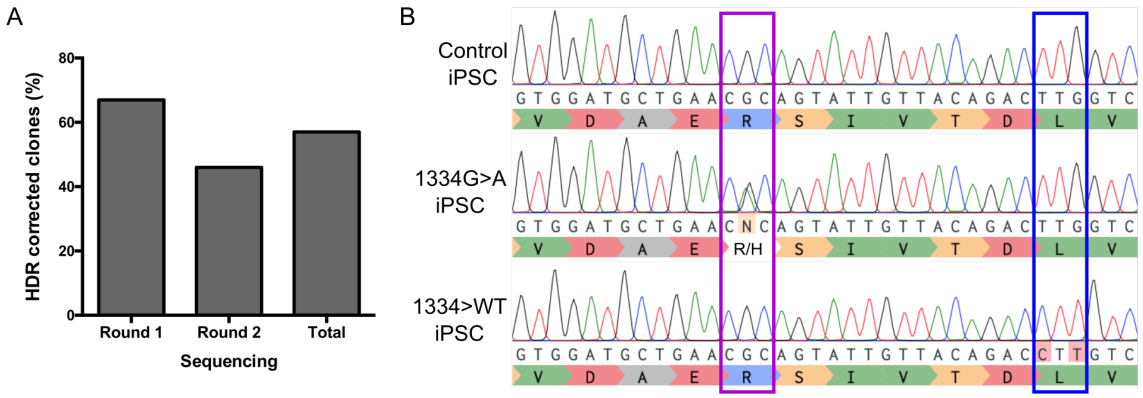

Figure 3.11. Identification of HDR corrected iPSCs.

(A) Sanger sequencing enabled identification of HDR corrected iPSCs. 8/13 (67 %) corrected iPSCs were identified in round 1 and 5/11 (46 %) in round 2. A total editing efficiency of 57 %.

(B) WT iPSC, 1334G>A patient iPSC and HDR edited clones were Sanger sequenced and aligned on Benchling. Correctly edited 1334G>A clones were identified through G homozygosity at position 1334 (purple box) and homozygous synonymous PAM site.

Lastly, to determine if CRISPR/Cas9 editing of patient-derived iPSCs introduced off-target effects during culture gRNA 2 was analysed via the Off-Spotter program for regions with sequence-homology to the gRNA target. The top 5 off-target sites were determined and amplified through PCR for both 1334G>A and edited WT iPSC. PCR products were Sanger sequenced and aligned on Benchling. Both edited iPSC lines showed no evidence of off-target mutations when compared to unedited 1334G>A iPSCs (Table 3.5, sequencing data in Appendix D).

Table 3.5. Top 5 predicted off-target genes for 1334G>A gRNA 2.

The top 5 off-target genes were determined on Off-Spotter and amplified by PCR before Sanger sequencing and sequence alignment. No off-target CRISPR/Cas9 induced mutations were identified.

Gene	Chromosome	Position	gRNA mistmatches	CRISPR-induced mutation
CLSTN2	3	Intronic	3	No
DMD	X	Intronic	5	No
INTS9	8	Intronic	4	No
UGGT1	2	Intronic	3	No
ZNF516	18	Intronic	5	No

3.2.4 Analysis of *OPA1* transcript and protein expression

Once established, the effects of *OPA1* patient mutations, CRISPR/Cas9 heterozygous mutation and correction of the c.1334G>A mutation were validated through qPCR. Initial analysis of *OPA1* transcripts in patient derived fibroblasts demonstrated an approximate 25 % increase in expression for 1334G>A cells when compared to WT controls, whilst there was a significant reduction of approximately 38 % in 2708del cells (Figure 3.12A). Previous reports have identified non-sense mediated decay (NMD) as a possible cause for reduced *OPA1* expression levels in patients with mutations generating premature termination codons (PTCs; Schimpf *et al.* 2008; Ścieżyńska *et al.* 2017). Thus, to determine if NMD was degrading *OPA1* transcripts fibroblasts were treated with 25 µg/ml of emetine, a translation inhibitor that blocks NMD and increases mRNA half-life, for 4 hours at 37°C. Inhibition of NMD caused increased *OPA1* levels across all cell lines (Figure 3.12A), with significantly higher transcript levels in both control and 2708del cells. Notably, NMD inhibition restored 2708del *OPA1* expression back to untreated control cell levels (Figure 3.12A).

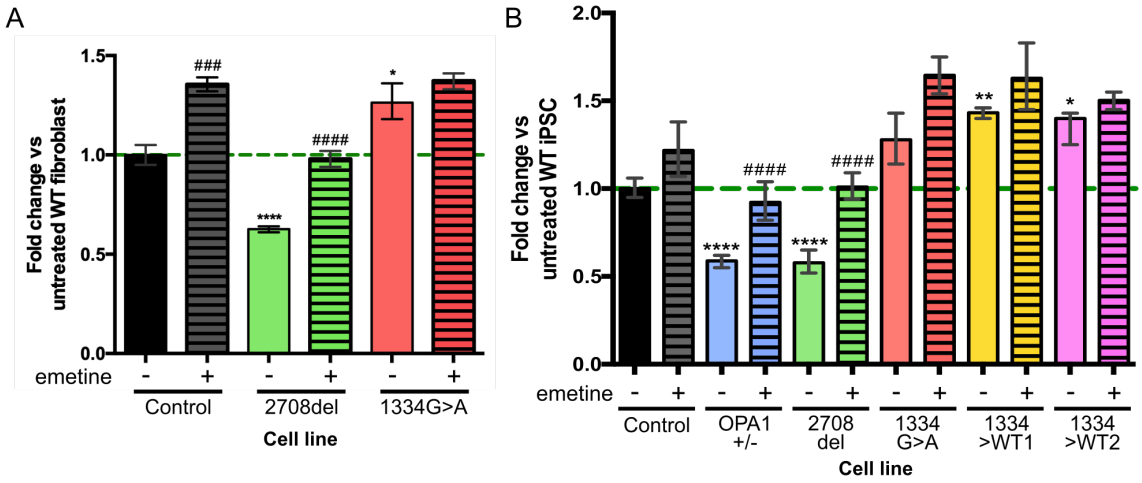

Figure 3.12. Inhibition of NMD via emetine treatment increases *OPA1* transcript levels.

Control, CRISPR edited and patient derived fibroblasts **(A)** and iPSCs **(B)** were treated with either vehicle or emetine for 4 hours to block NMD. Emetine treatment inhibited *OPA1* transcript degradation causing increased transcript retention when compared to both WT and untreated cells. Fibroblasts, N=4 individual treatments. iPSCs, N=3-4 individual samples. * p<0.05, ** p<0.01, **** p<0.0001 vs WT cells. ### p<0.001, #### p<0.0001 vs untreated cells.

qPCR analysis demonstrated that 2708del and 1334G>A iPSCs maintained the same expression pattern as their parent fibroblast lines, with an approximate 43 % reduction and 30 % expression increase respectively (Figure 3.12B). Importantly, OPA1+/- iPSCs, with a G base deletion in e PTC in exon 3, also showed a reduction of approximately 41 % when compared to controls, thus mimicking 2708del patient derived cells. Both 1334>WT1 and 1334>WT2 iPSCs had *OPA1* levels equivalent to that of 1334G>A (Figure 3.12B), suggesting that the G>A mutation is not driving increased expression in the patient cell lines. Again, NMD inhibition via emetine in all iPSCs increased transcript levels, with both OPA1+/- and 2708del cells showing a significant return to WT levels (Figure 3.12B). In addition to qPCR, the regions spanning both OPA1+/- and 2708del *OPA1* mutations were amplified by RT-PCR using primer pairs OPA1-ex2F and OPA1-ex6R; and OPA1-ex25 and OPA1-ex29R, respectively. Sanger sequencing and alignment of RT-PCR reactions for emetine treated OPA1+/- and 2708del iPSCs revealed retention of non-sense transcripts downstream of the respective deleted bases when compared to untreated iPSCs or WT cells (Figure 3.13A,B).

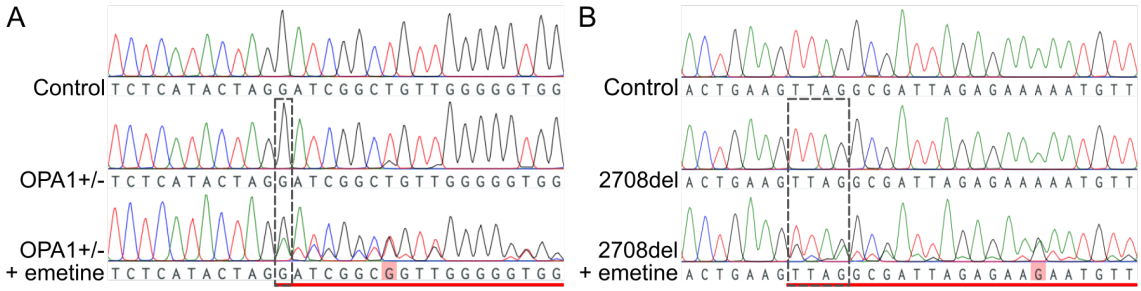

Figure 3.13. Sanger sequencing analysis of emetine treated OPA1+/- and 2708del iPSCs.

Treatment with emetine for 4 hours causes retention of both CRISPR edited OPA1+/- **(A)** and patient-derived 2708del **(B)** transcripts in Sanger sequence traces. Cell line specific deleted bases highlighted in dashed grey box. Retained mutant transcripts underlined in red.

Finally, western blot analysis of 3 individual OPA1+/- iPSCs, lines 1, 2 and 3, was used to validate the downstream effects of mRNA reduction. OPA1+/- iPSCs were cultured to 80 % confluency, lysed and equal protein loaded into gels. Detection of OPA1 showed two clear bands, corresponding to both S-OPA1 and L-OPA1 isoforms (Alavi *et al.* 2007; Lee *et al.* 2017), at approximately 100kDa (Figure 3.14A). After normalisation of OPA1 expression to β-tubulin, there was a statistically significant reduction in OPA1 protein levels, with OPA1+/- iPSCs 1, 2 and 3 expressing 35.6 ± 6.4 % ($p<0.001$), 64.0 ± 9.9 % ($p<0.05$) and 44.6 ± 8.7 % ($p<0.01$) respectively when compared to control iPSC samples (Figure 3.14B).

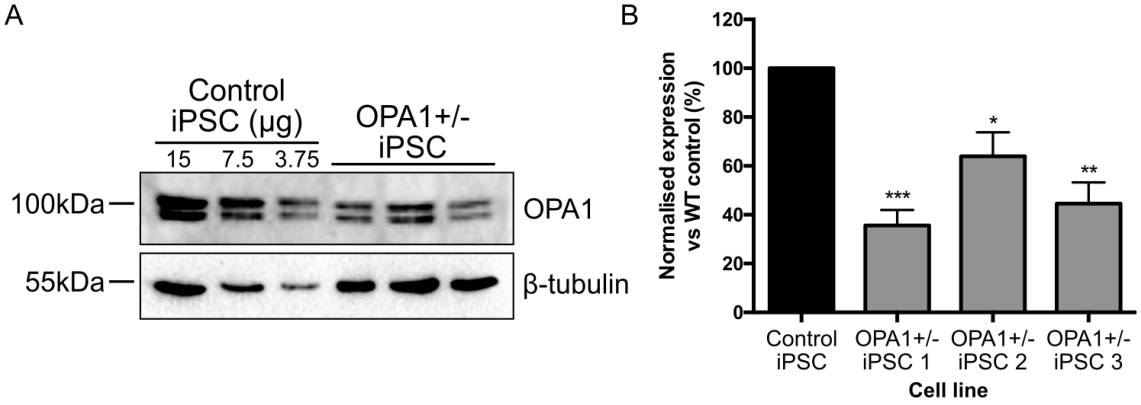

Figure 3.14. CRISPR/Cas9 edited OPA1+/- cell lines show reduced OPA1 protein levels compared to WT cells.

OPA1+/- and WT iPSCs were cultured for 3-4 days before lysis with RIPA buffer.

(A) OPA1 antibody detects short and long isoforms of OPA1 at ~100kDa. β-tubulin reference protein, 55kDa, used for normalisation of OPA1 expression.

(B) Three OPA1+/- iPSC cell lines show significantly reduced levels of OPA1 protein expression compared to the WT control iPSC, after normalisation to reference protein β-tubulin. * $p<0.05$, ** $p<0.01$, *** $p<0.001$, values are mean ± SEM, N = 3 biological replicates from 3 independent western blots.

3.2.5 Validation of iPSC pluripotency

Finally, the self-renewal ability and pluripotency of 1334G>A, 2708del, OPA1+/- and control iPSC were evaluated through the quantitative PCR (qPCR). The Taqman hPSC Scorecard Panel analyses the expression of 93 genes, including nine genes for self-renewal, 74 germ lineage specific genes and 10 qPCR internal controls. All four cell lines were cultured as pure iPSC colonies and through an eight-day undirected EB differentiation protocol to randomly produce cells from all three germ layers. Pure iPSCs and EBs were lysed and RNA extracted and quantified before individual samples were analysed via the Scorecard qPCR. Gene expression patterns were subsequently compared to that of 13 pluripotent stem cell lines to determine an algorithm 'score' for the ability for self-renewal or to generate germ lineage cells.

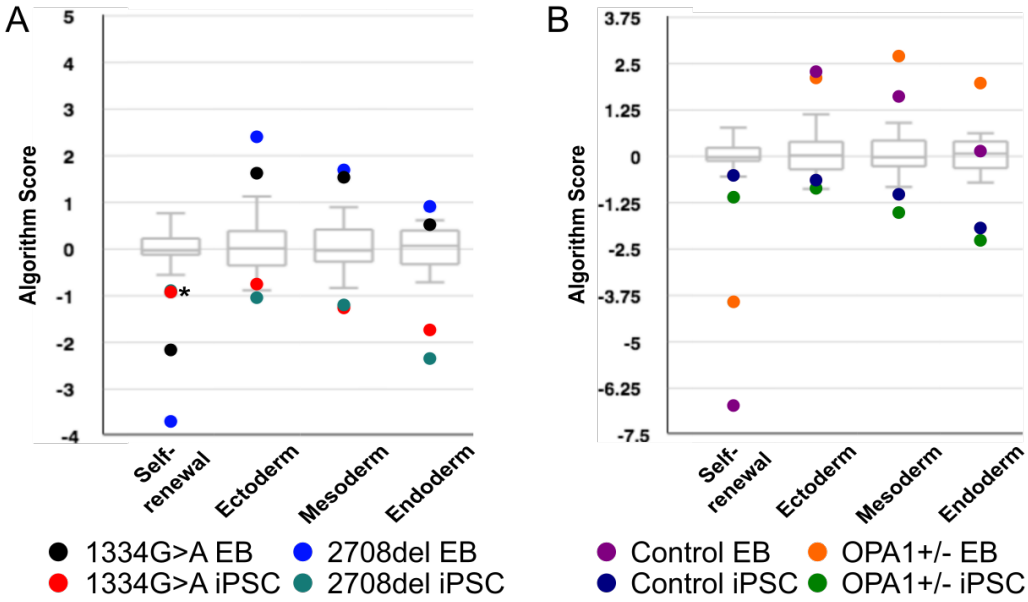

Figure 3.15. Quantification of iPSC self-renewal and pluripotency ability via the Taqman Scorecard Algorithm.

iPSCs were cultured either as naïve iPSCs or differentiated into embryoid bodies (EB) using an 8-day undirected differentiation protocol. Each sample is analysed for the expression of 96 genes via qPCR to determine iPSC quality. Algorithm scores for patient-derived 1334 G>A and 2708del iPSCs **(A**; * denotes overlapping results**)** and OPA1+/- iPSC and isogenic controls **(B)**.

Surprisingly, only the WT control iPSCs returned a positive result for self-renewal, whilst the three *OPA1* mutant cell lines 1334G>A, 2708del and OPA1+/- iPSC returned a negative score, falling below the reference score (Figure 3.15A,B). However, all iPSC lines showed significant downregulation of tri-lineage genes in comparison to EBs, particularly those within endodermal lineages suggesting they have lost the initial fibroblast gene expression profile. Additionally, despite being designated 'mesoendoderm' lineage markers within the scorecard panel, all iPSC lines showed upregulation of *NR5A2* and *GDF3* relative to the undifferentiated reference stem cells, both genes have been shown to be upregulated in iPSCs and ESCs (Clark *et al.* 2004; International Stem Cell Initiative 2007; Wang *et al.* 2011; Rasmussen *et al.* 2016).

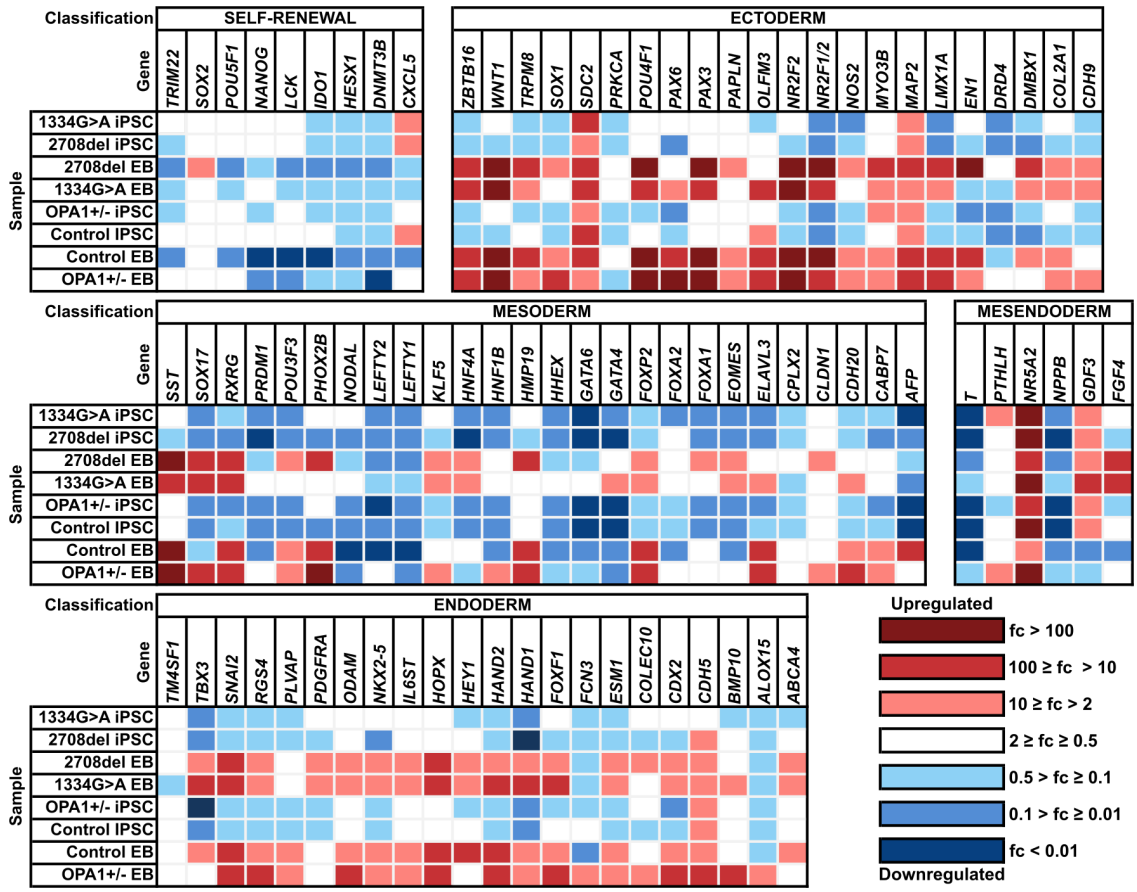

Figure 3.16. Scorecard iPSC differentiation potential heat-plot.

Taqman Scorecard determines up and down regulation of expression for key embryonic stem cell and germ layer markers in patient derived, CRISPR edited and control iPSCs and following 8 days of undirected EB differentiation. Relative fold change vs reference stem cells.

Undirected differentiation confirmed the pluripotent state and ability for tri-lineage differentiation of all iPSCs, with significant increase in the 'score' for each cell line across the three germ layers. All three mutant *OPA1* cell lines cleared the threshold for achieving a positive 'score' for each germ layer (Figure 3.16), demonstrating a robust pluripotent ability. However, although control iPSC showed a significant upregulation in ectoderm and mesoderm score it did not meet the required threshold for the endodermal lineage, despite a score increase when compared to control iPSCs (Figure 3.16). Importantly, EB generation caused significant down regulation of self-renewal genes after differentiation in all iPSC lines (Figure 3.16) demonstrating development away from a pluripotent state. All cell lines showed an excellent propensity to differentiate towards an ectodermal lineage with significant upregulation of *POU4F1* (*BRN3A)* and *PAX6* (Figure 3.16), which are both crucial to the development and survival of RGCs (Marquardt *et al.* 2001; Badea *et al.* 2009). Taken with the strong protein expression of iPSC markers, and noting retinal ganglion cells originate from an ectodermal lineage, these results suggest that 1334G>A, 2708del, OPA1+/- and control iPSC are of high enough quality for further experimentation and use in RGC differentiation protocols.

3.3 Discussion

The principal evidence for the pathogenic mechanisms of *OPA1* mutation originates from studies of out of context non-retinal cell types, including studies of patient derived fibroblasts, RNAi knockdown of *OPA1* in model cell lines and *Opa1*+/- mouse models. As such, there is little evidence from human retinal studies and the disease mechanisms leading to the preferential loss of RGCs remain unclear; however, the advent of iPSC technology and the ability to differentiate to disease specific cell types has significantly increased our ability to accurately and specifically model clinically relevant diseases that have previously been difficult to model. To that end, a biobank of iPSCs was created using 6 DOA patient derived fibroblast cell lines, encompassing the *OPA1* genetic and clinical disease spectrum. Concurrently, CRISPR/Cas9 gene editing technology was utilised to generate isogenic cell lines through *OPA1* knockout and correction of 1334G>A iPSCs back to a WT genotype. This biobank provides the basis to investigate *OPA1* disease mechanisms through context-specific disease modelling, whilst understanding the phenotypic heterogeneity seen within DOA.

Although a genetic spectrum of *OPA1* iPSCs was generated, two specific patient lines were prioritised for in-depth characterisation, notably *OPA1*: c.2708_2711delTTAG (2708del iPSC), the most common *OPA1* mutation in the UK (Yu-Wai-Man *et al.* 2013), and *OPA1*: c.1334G>A (1334G>A iPSC), a clinically severe phenotype (Yu-Wai-Man *et al.* 2010), due to their clinical relevance. Prioritisation was necessary to reduce the extent of iPSC maintenance and characterisation. Once generated, Sanger sequencing confirmed the presence of both *OPA1* mutations within iPSC lines, matching those of the parent fibroblast population. Subsequently, RT-PCR analysis of 1334G>A iPSCs was used to determine the expression of reprogramming vectors and endogenous iPSC genes. Since the first papers describing somatic cell reprogramming, multiple methods including viral transduction, direct protein delivery and mRNA transfection (Fusaki *et al.* 2009; Kim *et al.* 2009; Zhou *et al.* 2009; Yoshioka *et al.* 2013) have been established to generate iPSCs. Here, integration free episomal vectors were used to induce the endogenous expression of 4 genes, *OCT4, LIN28, SOX2 and L-MYC,* required for fibroblast reprogramming (Okita *et al.* 2011). RT-PCR analysis of 1334G>A iPSCs showed induction of endogenous self-renewal genes from the first cell passage. Likewise, there was no evidence of episomal vector expression from the first cell passage, suggesting that vector expression has been lost and the self-renewal and undifferentiated state of the patient-derived iPSCs is being driven by the expression of endogenous factors. Interestingly, Okita *et al.* (2011) found approximately 200 copies of episomal vector at D6 of reprogramming, but by passage 10 or approximately D80 post nucleofection the vector expression was undetectable within this study. It is therefore

feasible that approximately 14-20 days of reprogramming culture can reduce vector expression to untraceable expression levels, particularly in rapidly dividing cells such as iPSCs. Due to the negligible expression of episomal vectors and endogenous gene induction in 1334G>A iPSCs after 1 passage of culture, RT-PCR analysis was not conducted for other generated lines.

In addition to generating patient-derived iPSC, healthy control fibroblasts were genetically edited using simultaneous CRISPR/Cas9 gene editing and reprogramming to create isogenic iPSC cell lines, one with the selective knockout of *OPA1* and an isogenically matched WT control line. Despite the initial estimates of approximately 24 % editing efficiency, only 7 of 52 isolated CRISPR iPSC lines were successfully target, an editing efficiency of 13 %. Intriguingly, all 7 successfully engineered cell lines had heterozygous mutations in *OPA1*, with no homozygous or compound heterozygous mutations, resulting in downstream frameshift mutations and PTCs. This may result for two reasons: *OPA1* is crucial to iPSC viability, or due to low editing efficiency and insufficient clone isolation. *OPA1* is a biallelic gene and thus requires two simultaneous editing events to create an OPA1 null cell line, as such the probability of isolating a homozygous null cell line from 52 clones is less than 1 (0.13 x 0.13 x 52 = 0.88). Therefore, to isolate homozygous null clones a larger sample of clones would need to be screened, or a more efficient editing method would be required. Within mouse models of DOA, *OPA1*-null embryos die in utero between days 9 and 14 (Alavi *et al.* 2007; Davies *et al.* 2007; Sarzi *et al.* 2012), yet, it takes approximately 3 weeks to reprogram fibroblasts and select clonal iPSC lines, a time period in which *OPA1*-null iPSC lines may no longer be viable. Furthermore, the predicted CRISPR knock out efficiency of 24 % within this study is lower than a number of papers that demonstrated CRISPR editing efficiency between 50 and 80 % (Ding *et al.* 2013; Hou *et al.* 2013; Chua *et al.* 2016) and may explain the lack of homozygous or compound heterozygous mutants. Furthermore, although an OPA1-null cell line would provide an extreme paradigm for the function of OPA1 within cells, it would be largely unrepresentative of the DOA genetic spectrum.

Although CRISPR/Cas9 technology allows disease modelling by the generation of knockout cell lines via NHEJ, perhaps its most promising application is to enable correction or generation of specific genetic mutations. Although correction through HDR events often occur at lower frequencies than NHEJ, use of a ssODN repair template enables precise genetic engineering and for the correction of pathogenic mutations. Thus, CRISPR/Cas9 was used to target 1334G>A patient mutations for correction with a ssODN repair template in previously generated 1334G>A iPSCs. TIDER algorithmic analysis of 2 designed gRNAs, and corresponding ssODN templates, demonstrated an editing efficiency between 25 and 70 % suggesting the potential for a high yield of

corrected clones. Surprisingly, all isolated lines showed PAM site changes in both OPA1 alleles, thus demonstrating that gene correction has also altered the original WT allele sequence. In stark contrast to the OPA1+/- generation that had editing efficiency of just 13 %, HDR correction of 1334G>A iPSCs demonstrated an editing efficiency of 52 %. This is likely due to the use of CRISPR/Cas9 RNPs instead of CRISPR/Cas9 expression plasmids, which provide three primary advantages. Firstly, by generating RNPs the CRISPR/Cas9 system is primed for gene targeting once delivered into the cell resulting in more efficient DNA cleavage. Secondly, cellular RNP activity is highly transient, providing a rapid cleavage of DNA but once the proteins are degraded they will not be resynthesized to induce further DNA cleavage, unlike plasmid expression (Sun and Zhao 2014). And lastly, RNPs have been shown to have significantly higher DNA cleavage and editing efficiencies in mammalian cells (Okamoto *et al.* 2019), with editing efficiencies of 94 % in Jukart cells and between 75 and 87 % for stem cell populations (Kim *et al.* 2014; Liang *et al.* 2015; Gundry *et al.* 2016).

Although, the homozygous PAM changes may demonstrate how efficient CRISPR/ca9 editing can be, it could also be indicative of 'genetic selection' within the heterogeneous pool of nucleofected cells, in which the changes introduced by the ssODN template prevent re-cleavage of *OPA1* by PAM site removal. Ultimately, inhibition of Cas9 cleavage could confer greater genetic stability by preventing continual Cas9 cutting, reducing cellular stress by preventing free DNA ends and perhaps provide a mitochondrial bioenergetic advantage, compared to those cells that have not incorporated the ssODN template changes.

Once established corrected iPSCs (henceforth referred to as 1334G>WT1 or WT2) were expanded in culture and exhibited normal iPSC morphology, similar to their parent iPSC population. Thus, this study has established novel isogenic cell lines for the study of c.1334G>A *OPA1* mutations, which will prove invaluable for understanding the dominant-negative disease mechanisms associated with this mutation type. Ultimately, this work has demonstrated how modern gene engineering technologies, such as CRISPR/Cas9, will prove instrumental in understanding *OPA1* biology and its associated pathogenic disease mechanisms in DOA and DOA+.

Although there have been wide reports of excessive off-target activity when using CRISPR/Cas9 gene editing (Cradick *et al.* 2013; Fu *et al.* 2013) in this study there were no off-target effects in the top 10 off-target sites in OPA1+/- iPSCs. Of particular note, there were no mutations in *TAMM41*, a protein required for normal mitochondrial function (Blunsom *et al.* 2018), or *NETRIN-1*, a key RGC axonal guidance protein (de la Torre *et al.* 1997). Similarly, the top 5 off-target sites for the gRNA used to correct 1334G>A

iPSCs were also assessed and demonstrated no off-target mutations. Although this method allows for prediction and assessment of the most likely off-target sites, it does not allow in-depth screening due to the laborious methodologies used. A number of studies have analysed off-target effects through Whole Genomes Sequencing (WGS) demonstrating that in CRISPR/Cas9 engineered monkeys (Wang *et al.* 2018), iPSCs (Smith *et al.* 2014; Li *et al.* 2015) and mice (Iyer *et al.* 2015; Anderson *et al.* 2018) gene editing is highly specific and causes few off-target mutations. While this method is likely significantly more thorough than analysing individual targets via sanger sequencing, it was not deemed cost-effective or feasible within the time frame of this project. Reassuringly, the collective data surrounding CRISPR/Cas9 gene editing suggest it is highly specific for the desired target, maintaining the overall health of the genome and not introducing additional background mutations into the iPSCs that may impact the ability for RGC differentiation or affect disease phenotypes.

The level of *OPA1* expression was subsequently quantified for all iPSCs via qPCR. There are few reports that have established the expression levels of *OPA1* across the mutational disease spectrum. In particular, there are few reports for the effects of non-synonymous point mutations on *OPA1* levels. These mutations are hypothesised to cause disease through loss of function or a dominant negative mechanism, rather than through haploinsufficiency (Amati-Bonneau *et al.* 2008), and 1334G>A patient fibroblasts have normal protein levels compared to healthy individuals (Agier *et al.* 2012). Here, qPCR analysis demonstrated that both patient fibroblast lines had altered *OPA1* expression levels, with a significant 40 % decrease in 2708del fibroblasts and a 25 % increase in 1334G>A fibroblasts. Additionally, both patient-derived iPSC lines had analogous *OPA1* expression levels to their parent fibroblast line, whilst CRISPR edited OPA1+/- iPSC expression was akin to 2708del iPSCs with an approximate 40 % reduction. This analysis is in accordance with a number of previous studies of *OPA1* expression. During the write up of this thesis, Caglayan *et al.* (2020) published data showing OPA1+/- iPSCs generated through CRISPR/Cas9 gene editing and an independent 2708del mutation demonstrated a 50 % reduction in total *OPA1* mRNA expression. A previous report of mice harbouring an *Opa1* c.1051C>T/p.((Q285STOP); hence forth referred to as Opa1^{Q285STOP}) mutation that demonstrated significant reduction in total *Opa1* expression levels within the retina (Williams *et al.* 2012), supporting the theory that both OPA1+/- and 2708del cell lines undergo NMD that likely drives haploinsufficiency. Schimpf *et al*. (2008), have previously demonstrated that *OPA1* mutations that cause downstream PTCs, notably c.2708_2711del and c.2708-1G>T, have reduced levels of mutant transcript when compared to mutations which do not induce downstream frame shifts (Schimpf *et al.* 2008). Interestingly, they note that patients with identical *OPA1* mutations show varying levels of mutant transcripts,

suggesting that there are genetic modifiers that further fine-tune *OPA1* expression. This may explain the significantly elevated levels of *OPA1* within 1334G>A patients, which was not reduced to WT levels upon gene correction, suggesting that there is an additional genetic modifier increasing its expression and it is not being driven by the mutation. However, further analysis of the effect of non-synonymous mutations on *OPA1* expression should be conducted to determine the true effects on expression.

Due to the nature of PTCs within both OPA1+/- and 2708del mutant transcripts it is perhaps unsurprising they have reduced expression levels. Crucially, both 2708del and OPA1+/- PTCs are in accordance with the general NMD rules, featuring PTCs that are over 55bp away from the presumptive exon-exon junction (Kurosaki and Maquat 2016), at approximately 99bp and 75bp respectively. However, there is conflicting evidence for *OPA1* transcript NMD. Indeed, Schimpf *et al*. (2008) demonstrated reduced mutant transcripts when compared to total *OPA1* levels. Yet it is worth noting that analysis of cells harbouring p.Q31*, p.R52* and p.W2* *OPA1* mutations, which all induce a hypothetical PTC, maintained normal levels of OPA1 expression when compared to WT controls (Ścieżyńska *et al.* 2017). To determine the probable cause of *OPA1* reduction NMD was blocked with emetine, a translation inhibitor that causes accumulation of all mRNA transcripts. NMD-blockage increased levels of *OPA1* across all cell lines, with a significant return to WT levels of expression for both OPA1+/- and 2708del cell lines, suggesting NMD is the likely mechanism of reduced *OPA1* transcript levels. To further confirm the effects of reduced *OPA1* levels, western blot analysis was completed on three generated OPA1+/- iPSC lines. This confirmed OPA1 reduction at the protein level; with an approximately 50 % reduction in OPA1 levels compared to WT controls supporting haploinsufficiency as the primary disease mechanism, demonstrating that the CRISPR-edited model therefore represents a model of DOA more closely related to 2708del iPSC (Sarzi *et al.* 2012) rather than the potential dominate-negative effect seen in 1334G>A iPSC. Collectively, the data presented here show a comprehensive analysis of *OPA1* expression patterns for both patient, WT and CRISPR-corrected cell lines, indicating haploinsufficiency as the most probable disease mechanism for both OPA1+/- and 2708del cell lines.

To establish the overall quality of the generated iPSCs immunofluorescence staining was used to determine the expression of ESC pluripotency markers, whilst qPCR was utilised to establish their pluripotency ability. iPSCs demonstrated consistent protein expression of all evaluated ESC markers. Notably, there was prominent nuclear expression of both OCT4 and NANOG at the protein level. *OCT4* is well regarded as a key factor regulating iPSC self-renewal and differentiation potential (Boyer *et al.* 2005), and studies have demonstrated expression of *OCT4* alone can drive somatic cells to an

iPSC fate (Kim *et al.* 2009). Although NANOG has previously been shown to be dispensable for reprogramming (Schwarz *et al.* 2014), and was not episomally expressed during reprogramming, it is highly upregulated in both mouse and hESCs and associated with sustaining self-renewal and stabilising ESC gene expression patterns (Chambers *et al.* 2003; Chambers *et al.* 2007). Additionally, reprogramming induced surface expression of SSEA4, TRA-1-60 and TRA-1-81 in all iPSCs, proteins that are all regarded as defining surface markers of ESCs (Draper *et al.* 2002; International Stem Cell Initiative 2007). Collectively, the endogenous protein expression of NANOG, SSEA4, TRA-1-60 and TRA-1-81 demonstrate downstream upregulation of pluripotency markers induced by reprogramming events. In conjunction with the confirmation of the original patient mutations and the RT-PCR expression of endogenous reprogramming genes, the protein marker expression suggests both all iPSC lines have the relevant expression of pluripotency markers to be considered bona fide WT and DOA-iPSCs.

To fully confirm the pluripotency of all generated iPSC lines, the TaqMan Scorecard was utilised to assay the expression of 93 genes, including nine self-renewal and 74 lineage specific genes. Now considered an important tool for assessing iPSC pluripotency, the TaqMan Scorecard assay was designed to replace the need for invasive and aggressive mouse teratoma formation assays to determine the self-renewal and pluripotency potential of iPSCs, whilst also providing a considerably quicker method of assessment. Despite all iPSC lines strongly expressing five ESC proteins by IF, only control iPSC returned a positive score for self-renewal. Interestingly, all 3 mutant OPA1 iPSC lines returned a sub-threshold score for self-renewal. Despite an in-depth literature search there is no evidence to suggest that OPA1 interacts directly with any of the self-renewal markers within the Scorecard panel, so it is altered levels of OPA1 expression prevents self-renewal in this way. It is therefore plausible that the downstream effects of *OPA1* mutation, such as increased apoptosis (Chen *et al.* 2016), reduce or mask overall expression of self-renewal markers within iPSC colonies.

While the Scorecard assay is becoming increasingly useful for rapidly determining pluripotency, it has inherent limitations. Firstly, the self-renewal assay within the Scorecard is highly sensitive to contamination of differentiated cells. Although all efforts were taken to maintain a 100 % pure iPSC population, small levels of non-renewing differentiated cells can offset the self-renewal potential of a relative iPSC population and thus reduce the relative score. Additionally, there are genes within the panel regarded as tri-lineage differentiation genes that are highly expressed within iPSC populations. Both *NR5A2* and *GDF3* are noted as mesoendoderm markers within the scorecard panel but all four iPSC lines *NR5A2* showed a relative fold change of 10-100 and *GDF3* showed a 2-100 fold change vs reference stem cells. Importantly, *NR5A2* has been

utilised in to reprogram murine cells to iPSC in the place of *Oct4* (Heng *et al.* 2010), and also enhances iPSC reprogramming efficiency (Wang *et al.* 2011). Moreover, *GDF3* is known to be specifically upregulated in hESC lines (Caricasole *et al.* 1998; Clark *et al.* 2004; International Stem Cell Initiative 2007) and has been used to quantify pluripotency in multiple iPSC lines (Rasmussen *et al.* 2016). These data, taken with the consistent ESC protein marker expression and length of time each iPSC line has been cultured (approximately 3-4 months), suggest that each iPSC line is capable of self-renewal, despite not passing the Scorecard self-renewal criteria.

Of more importance is the Scorecards ability to determine iPSC pluripotency ability, which establishes each cell lines ability for tri-lineage differentiation. A previous study of *OPA1* mutant iPSCs carrying a c.1861C>T (p.Q621*) mutation demonstrated through IF the feasibility of heterozygous *OPA1* cells to differentiate into all 3 germ layers during EB development (Galera-Monge *et al.* 2016). The three mutant *OPA1* iPSC lines presented here demonstrated clear ability for tri-lineage differentiation, producing a positive algorithm score for all three germ layers and suggesting they are fully pluripotent stem cell lines. However, the WT control cell line only exhibited partial pluripotency, with significant upregulation of both ectoderm and mesoderm markers but a sub-threshold score for endoderm. This is most likely due to a number of endoderm genes showing significant downregulation when compared to the three other cell lines. Despite the poor endodermal differentiation, control iPSCs showed the most significant downregulation of self-renewal markers perhaps indicating that they have differentiated the furthest away from their naïve self-renewing stem cell population.

In spite of the partial negative result from the pluripotency assay, further analysis of the Scorecard data provides valuable details regarding the iPSC ability for retinogenesis. An ability for ectodermal differentiation is of vital importance as the emerging retina, and thus RGCs, originate within this germ layer (Lamb *et al.* 2007). As such, it is vital that all cell lines demonstrate significant capability for ectodermal differentiation. All 4 cell lines showed significantly upregulated expression of ectoderm genes, with only *PRKCA* and *DRD4* showing minimal upregulation out of the 22 ectoderm genes assayed across the 4 cells lines. Crucially, the Scorecard assay analysed a number of genes that are indispensable for retinal development. *PAX6* is well regarded as an “eye field transcription factor” (EFTF) that is fundamental to early retinogenesis (Zuber *et al.* 2003) and showed upregulation across all 4 cell lines. In *Pax6* mutant mice, the absence of Pax6 fails to induce expression of downstream genes required for RGC specification and an absence of RGCs is observed (Marquardt *et al.* 2001; Philips *et al.* 2005; Riesenberg *et al.* 2009).

Likewise, *BRN3A* (*POU4F1*), was also shown to be significantly upregulated across all 4 derived iPSC lines. Within the retina *BRN3* transcription factors selectively identify RGCs (Xiang *et al.* 1995) and are crucial to RGC development and survival (Liu *et al.* 2001; Yang *et al.* 2003). Furthermore, *SOX2* is regarded as a key regulator in the maintenance of neural stem cells (Pevny and Nicolis 2010), and thus the presumptive retina. Within the Scorecard panel *SOX2* falls in the self-renewal genes panel, but shows no reduction during EB formation. Studies of *Sox2* dosage experiments in mice demonstrated that *Sox2* ablation significantly impaired retinal progenitor cell proliferation and differentiation, whilst heterozygous *Sox2* null mutants had severe microphthalmia (Taranova *et al.* 2006). Collectively the Scorecard data, in particularly the high levels of expression of retinogenesis and RGC associated genes, combined with the expression of ESC markers suggests that all generated iPSC lines are pluripotent with the potential for RGC differentiation.

Although the data presented here suggest the generation of bona fide iPSCs, it is worth noting that other avenues of experimentation could have been utilised to further characterise the quality of the generated cell lines and that iPSCs also have their inherent limitations for *in vitro* disease modelling. Perhaps of most significance is the lack of karyotyping analysis of individual iPSC clones to determine if large scale rearrangements within the genome have occurred. Analysis by Taapken *et al.* (2011) suggest that large scale genomic rearrangements occur in approximately 12.5 % of iPSCs and ESCs, with trisomy of chromosome 12 and 8 the predominant rearrangements. Interestingly, rearrangements of chromosome 12 are associated with enrichment of cell cycle genes, including overexpression of both *NANOG* and *GDF3* (Mayshar *et al.* 2010). Analysis of *NANOG* and *GDF3* expression were quantitatively assessed using the Taqman Scorecard, demonstrating consistent expression amongst the 4 analysed iPSC clones and no significant fold change was detected when compared to the 13 reference lines used in the Scorecard panel analysis, perhaps indicating a lack of chromosome 12 rearrangement within these clones.

Furthermore, Mayshar *et al.* (2010) suggested that aneuploidy within iPSC populations can limit their differentiation potential due to the over expression of cell cycle genes preventing cell-cycle exit and cell type specific differentiation, which has also been demonstrated within other studies (Enver *et al.* 2005; Blum and Benvenisty 2009; Fazeli *et al*. 2009; Taapken *et al.* 2011; Mills *et al.* 2013). Interestingly, Fazeli *et al.* (2009) highlight the lack of induction of *AFP* expression within iPSC-derived EBs as a signature of karyotypically abnormal cells, that fail to generate endodermal cell lineages. Again, *AFP* expression was quantified via the Taqman Scorecard, with 2708del iPSCs demonstrating no clear induction of *AFP* within EBs, potentially suggesting a possible

genomic rearrangement within these cells. Although 2708del iPSCs did demonstrate competence to generate endoderm cell lineages, with significant upregulation of other endoderm genes in EBs and a positive score increase when compared to naïve 2708del iPSCs. Thus, although not conclusive, the data presented within this chapter suggest that the most common chromosomal rearrangements that occur within iPSCs have not happened within the generated cell lines as all control and *OPA1* mutant iPSCs showed a propensity to differentiation. More recently, qPCR analysis has allowed the rapid, cost effective screening of common genomic rearrangements within stem cell populations (Baker *et al.* 2016), thus providing an effective tool to effectively assess genomic instability before iPSCs are utilised for further downstream applications. As such, in future, karyotyping analysis should be routinely conducted on iPSC populations to confirm the integrity of the nuclear genome, especially given the impact rearrangements can have on differentiation capacity and gene expression levels (Mayshar *et al.* 2010; Harewood and Fraser 2014), which is of particular importance given the nDNA association with DOA.

In addition to the effect of aneuploidy, intra-clonal genetic heterogeneity is known to exist within iPSC populations, primarily due to their long-term culture and repeat passaging. Although it is believed the majority of genetic variation between iPSC lines is due to donor-specific differences, such as methylation profiles (Kyttälä *et al.* 2016; Burrows *et al.* 2016), intra-clonal genetic variability and differentiation capacity can be altered due to the acquisition of sub-clonal mutations during routine iPSC culture (Volpato and Webber 2020). However, recent studies by Merkle *et al.* (2017) and Thompson *et al.* (2020) suggested the acquisition of genetic mosaicism is generally rare in stem cell lines, indicating that long term culture of iPSCs does not promote mutation away from the original isolated clone. Interestingly, Merkle *et al.* (2017) demonstrated the acquisition of *TP53* mutations in 5 out of 140 unrelated ESC lines, and suggested these mutations inferred a selective advantage as the *TP53* mutant allelic fraction increased during prolonged culture. Similar work by D'Antonio *et al.* (2018), suggested that subclonal mutations tend to affect gene promoters but these tend not to be generated during passaging, as they found a consistent level of mutations throughout multiple passages. Although this work suggests that subclonal mutations, or iPSC genetic mosaicism, can be generated through long-term culture, it is hoped that simple steps, such as continual use of low passage iPSCs, can abrogate their generation. As such, short-term culture of iPSCs and experimental replication with different cultures of iPSCs should be conducted to ensure consistency within cellular populations, *in vitro* differentiation and disease phenotypes associated with *OPA1* mutation.

In summary, this work has established a biobank of *OPA1* mutant and isogenic control cell lines to enable the further study of DOA associated disease mechanisms. The generated iPSCs cover the genetic and phenotypic disease spectrum, whilst the generation of isogenic control cell lines through CRISPR/Cas9 gene editing allows for *OPA1* mutations to be studied in isolation independent of other co-founding genetic factors. Once established, qPCR analysis demonstrated substantial reduction in *OPA1* expression for both 2708del and OPA1+/- iPSCs, signifying haploinsufficiency as the most probably disease mechanism. Interestingly, 1334G>A and 1334G>WT1/2 iPSCs had upregulated *OPA1* expression when compared to control iPSCs. This is most likely due to a genetic modifier within the genome, as other groups have shown *OPA1* expression can vary significantly even when comparing identical genotypes, yet this requires further investigation of other patients with the 1334G>A mutation. Finally, iPSCs were validated at both the gene and protein level, demonstrating clear expression of ESC markers and the capability for tri-lineage differentiation; crucially showing significant upregulation of genes required for RGC differentiation. Overall, these results demonstrate that *OPA1* mutation does not impact the quality of iPSCs, whilst providing an excellent foundation for further understanding the role of *OPA1* in RGCs by generating a near-unlimited source of patient derived cells to enable *in vitro* modelling of DOA.

Chapter 4: *In vitro* modelling of DOA: generation of retinal ganglion cells through 2D and 3D methods

4.1 Introduction

As described in Chapter 1, the current models of DOA have provided invaluable knowledge surrounding OPA1 function despite their inherent flaws. The discovery of iPSCs has transformed our ability to model patient-specific mutations, providing a crucial source of patient material for further study in a field in which it is challenging to obtain patient tissues (Johnston *et al.* 1979; Kjer *et al.* 1983). Additionally, research into RGC biology has become ever more pertinent over the past decade due to their involvement in a range of debilitating optic neuropathies, in particular glaucoma, which is becoming an ever more prominent societal burden due to an aging populous (Tham *et al.* 2014; Li *et al.* 2019). It has therefore become imperative to develop improved RGC models to facilitate our understanding of their fundamental biological processes and how these are affected during disease, especially for conditions such as DOA that currently lack comprehensive treatment options.

4.1.1 Methods to generate retinal ganglion cells *in vitro*

Currently there are remarkably few research publications that have specifically modelled RGC differentiation, despite the growing burden that RGC associated diseases place on global health systems. Predominantly RGC modelling methods fall into two categories: the differentiation of RGCs through the formation of 3D retinal organoids (Tanaka *et al.* 2015; Maekawa *et al.* 2016; Ohlemacher *et al.* 2016; Aparicio *et al.* 2017) or direct differentiation of stem cells towards RGC lineages through 2D adherent culture (Riazifar *et al.* 2014; Sluch *et al.* 2015; Chen *et al.* 2016; Deng *et al.* 2016; Gill *et al.* 2016; Teotia *et al.* 2016; Sluch *et al.* 2017; Teotia *et al.* 2017). Although it is becoming increasingly common to use multiple methods during culture, there is currently no consensus on the best methodology to use and there is no standardised or consistent protocol, with both 2D and 3D culture methods providing advantages for understanding RGC biology.

4.1.2 3D models of retinogenesis

Although the study of model organisms has provided indisputable insights into retinal biology, they often lack key features of human disease pathology and require further model systems to provide clarity over key biological and disease processes. Our ability to generate retinal organoids, 3D retina-like structures, has drastically improved our understanding of retinal biology and a diverse range of pathogenic retinal disease mechanisms. Meyer *et al*. (2009, 2011) initially demonstrated the feasibility of generating 3D optic vesicle-like structures from human stem cells, which contained retinal precursor

cells expressing early EFTFs, with the ability to differentiate into multiple retinal lineages when dissociated into single cells. Simultaneously, Eiraku *et al*. (2011) and Nakano *et al*. (2012) demonstrated the feasibility of generating retinal-like, multi-layered tissue through serum-free floating culture of embryoid-body-like aggregates with quick reaggregation (SFEBq) from both mouse and human stem cells. Subsequent advancements have significantly improved our ability to recapitulate the developmental processes seen in the mammalian eye, with diverse protocols now established that generate all major retinal cell types in stratified retinal layers in a temporal, self-organising method of development (Nakano *et al.* 2012; Zhong *et al.* 2014; Kaewkhaw *et al.* 2015; Kuwahara *et al.* 2015; Parfitt *et al.* 2016; Volkner *et al.* 2016; Capowski *et al.* 2019; Sridhar *et al.* 2020). Furthermore, long-term analysis of retinal organoids has demonstrated they develop mature retinal features, including advanced photoreceptor structures (Phillips *et al.* 2012; Parfitt *et al.* 2016). Some studies even suggest the ability to respond to light (Zhong *et al.* 2014; Deng *et al.* 2018; Hallam *et al.* 2018), suggesting that they generate bona fide retinal tissues suitable for modelling retinal disease.

In addition to understanding retinal development, organoid generation has been used extensively for disease modelling. Generation of patient-derived iPSCs containing mutations associated with degenerative retinal diseases followed by differentiation into retinal organoids has illuminated retinal specific disease mechanisms, such as ciliation defects and disrupted alternative splicing (Parfitt *et al.* 2016; Buskin *et al.* 2018; Kallman *et al.* 2020). Additionally, CRISPR/Cas9 gene correction of genes associated with X-linked Juvenile Retinoschisis (*RS1*) and Retinitis Pigmentosa (*RPGR*) followed by retinal organoid modelling have brought further insight into the effects of mutations on retinal function (Deng *et al.* 2018; Huang *et al.* 2019), whilst also providing an extreme end-point paradigm for what potential treatment strategies might aim to achieve.

The derivation of retinal organoids has also enabled analysis of potential therapeutic strategies. Parfitt *et al*. (2016) demonstrated the rescue of Leber Congenital Amaurosis (LCA), retinal degeneration due to ciliation defects, within organoids by an antisense oligonucleotide to reduce expression of mutant transcripts causing disease. Additionally, a number of studies have attempted to optimise the delivery of therapeutics through either Lentivirus or AAV transduction of retinal organoid derived cells, although the downstream functional implications were not assessed (Gonzalez-Cordero *et al.* 2018; Garita-Hernandez *et al.* 2020; Kallman *et al.* 2020), providing a foundation of understanding for further developing gene therapy strategies for retinal diseases. Furthermore, generation of photoreceptor precursors through retinal organoids has enabled investigation into the feasibility of photoreceptor transplantation (Shirai *et al.* 2016; Chao *et al.* 2017; Gonzalez-Cordero *et al.* 2017; Gagliardi *et al.* 2018; McLelland

et al. 2018). As such, organoid studies have proven remarkably useful for understanding photoreceptor biology and may also have the potential to help understand the diverse biology mechanisms associated with RGCs.

Collectively, organoid studies have established the development of retinal cell lineages in multiple organoid protocols. Temporal analysis of retinal organoid growth has shown the gene expression pattern during RGC development, although the majority of studies have focused on a small range of developmental and terminal differentiation markers. Crucially, IHC and qPCR analysis has revealed early (D20-30) upregulation of EFTFs, including *VSX2, PAX6* and *RAX,* required for RPC generation during organoid retinogenesis, followed by downstream (D40-50) induction of RGCs, primarily determined by the expression of *BRN3* genes (Nakano *et al.* 2012; Zhong *et al.* 2014; Kuwahara *et al.* 2015; Tanaka *et al.* 2015; Volkner *et al.* 2016; Fligor *et al.* 2018; Langer *et al.* 2018; Capowski *et al.* 2019). Additionally, analysis of mature neuronal markers has demonstrated retinal organoid RGCs express *ELAVL3* (*HUC*), *ISL1*, *TUBB3* and *NEUN*, genes required for neuronal function (Nakano *et al.* 2012; Zhong *et al.* 2014; Tanaka *et al.* 2015; Fligor *et al.* 2018; Langer *et al.* 2018). Interestingly, multiple reports suggest a significant loss of RGCs within organoids from approximately D100 (Zhong *et al.* 2014; Kobayashi *et al.* 2018). In particular, Capowski *et al*. (2019) utilised a BRN3B:tdTomato reporter cell line to establish temporal RGC loss, demonstrating a significant reduction in RGCs as organoids matured from D90 to D160. Although this suggests long-term study of organoid derived RGCs could be problematic, it is analogous to processes in both chick and mammalian retinal development. An excess number of RGCs are present during the initial stages of retinogenesis, which is followed by phases of programmed cell death to reduce overall RGC number and facilitate the development and refinement of both retinal and cortical RGC synaptic connections (Provis *et al.* 1985; Sernagor *et al.* 2001; Isenmann *et al.* 2003). Crucially, establishing correct cortical connections also regulates RGC number, and RGCs that initially develop axonal projections to incorrect cortical regions are known to be eliminated during development (O'Leary *et al.* 1986; Isenmann *et al.* 2003). Additionally, severing RGC-cortical connections, and thus removing terminal axonal target connections, through optic nerve injury, induces mass programmed cell death within RGCs (Villegas-Pérez *et al.* 1993; Berkelaar *et al.* 1994). It is therefore likely that failure of organoid-derived RGCs to find a terminal axonal target and establish synaptic connections that are required for long-term survival results in their programmed cell death and degeneration within organoids. In addition, their localisation within the inner cell layers of 3D retinal organoids severely reduces nutrient availability, and likely impairs their survival (Zhong *et al.* 2014; Brooks *et al.* 2019). Consequently, there is a clear time frame of RGC development in retinal organoids, providing a window

of opportunity for the analysis of RGC disease associated mechanisms during the development of retinal organoids.

Although 3D retinal organoids have primarily been studied in suspension culture, RGC focused studies have combined 3D development with 2D adhesion cultures by plating organoids onto tissue culture plates. Adhered organoids develop significant numbers of axonal projections whilst expressing genes required for axonal compartmentalisation and function, including *TUBB3, TAU* and neurofilament light (*NFL*) and heavy (*NFH*; Tanaka *et al.* 2015; Maekawa *et al.* 2016; Yang *et al.* 2017). Furthermore, 2D-cultured organoids demonstrated the ability to generate axon potentials, as shown by patch-clamp electrophysiology assessment, and the ability for axonal cargo transport, including mitochondria (Tanaka *et al.* 2015; Ohlemacher *et al.* 2016; Yang *et al.* 2017). Interestingly, Yang *et al.* (2017) also demonstrated that RGC axons could be promoted to grow within grooved scaffolds, suggesting a plausible mechanism for developing a model of optic nerve development. Thus, 2D cultures of 3D generated organoids provide a suitable model of axonal elongation to enable further study of RGC biology.

Furthermore, dissociation of retinal organoids followed by single cell isolation has provided further experimental opportunity for RGC study. Fligor *et al.* (2018) demonstrated the feasibility of dissociating 3D retinal organoids into single cells to allow adhesion culture of RGCs, ultimately promoting axonal outgrowth to enable the study of responses to RGC chemoattractants, including netrin-1 and BDNF. Additionally, dissociation of retinal organoids at D30 followed by 2D culture demonstrated that organoids generate a diverse range of RGC subtypes expressing a range of terminal RGC markers. Single cell RNA sequencing (RNA-seq) enabled classification of RGCs and facilitated further characterisation of definitive RGC markers, suggesting *DCX* as a plausible marker of RGCs (Langer *et al.* 2018).

Dissociation of 3D organoids has also been utilised to identify suitable markers for RGC purification. Previous studies of mouse, rat and human RGCs have utilised THY1 to purify RGCs from retinal tissue (Barres *et al.* 1988; Zhang *et al.* 2010; Hong *et al.* 2012). Koboyashi *et al.* (2018) repeated this process for iPSC derived retinal organoids, using a two-step immunopanning processing with THY1. Downstream analysis of purified RGCs confirmed expression of *BRN3B*, *ISL1* and *ATOH7*, indicating that immunopanning for RGCs may provide a suitable method for generating pure populations. Despite this promising result, Aparicio *et al.* (2017) suggested THY1 is an imperfect marker of RGCs in retinal organoids, with IF analysis confirming THY1 expression throughout different cell layers of retinal organoids. Further analysis of retinal organoids indicated that CD171 (L1CAM) and CD184 (CXCR4) can be used to isolate

RGCs from organoids at different development stages, but a combination of both markers enables identification and purification of RGCs from organoids (Aparicio *et al.* 2017). It is therefore clear that greater work needs to be undertaken to understand the marker expression of RGCs that may enable specific isolation, in particular due to the diverse nature and subtypes of RGCs that 3D organoids may generate.

4.1.3 2D models of RGCs

Although 3D retinal organoids demonstrated a comprehensive recapitulation of retinogenesis, they generate many other cells that are not the primary focus when studying RGC pathobiology. As such, to compliment 3D studies, a diverse variety of 2D *in vitro* differentiation methods have been devised with the primary aim of generating enriched populations of RGCs. Analysis via IHC and qPCR of 2D differentiations has demonstrated that they replicate the primary stages of retinogenesis. Importantly, they demonstrate upregulated expression of EFTFs, notably *VSX2*, *PAX6*, *RAX* and *LHX2,* during the early stages (D3-D21) of culture (Riazifar *et al.* 2014; Sluch *et al.* 2015; Deng *et al.* 2016; Gill *et al.* 2016; Teotia *et al.* 2017; Chavali *et al.* 2020; Zhang *et al.* 2020). Following EFTF expression, 2D cultures upregulate genes known to be required for RGC induction and specification, including *ATOH7*, *BRN3B*, *ISL1* and *THY1* (Riazifar *et al.* 2014; Sluch *et al.* 2015; Deng *et al.* 2016; Gill *et al.* 2016; Teotia *et al.* 2016; Chavali *et al.* 2020; Zhang *et al.* 2020). Lastly, a number of studies have also demonstrated the upregulation of cytoskeletal components indicative of mature neuronal populations and required for RGC biology, including *TUBB3* and neurofilament genes (Riazifar *et al.* 2014; Sluch *et al.* 2015; Deng *et al.* 2016; Gill *et al.* 2016; Teotia *et al.* 2016; Chavali *et al.* 2020; Zhang *et al.* 2020).

To further develop a comprehensive phenotype, functional studies of 2D-RGCs have demonstrated that they exhibit a number of characteristics representative of *in vivo* RGCs. Importantly, 2D-RGCs have demonstrated the ability to respond to neurochemical stimuli, with the ability to generate Ca^{2+} fluxes (Deng *et al.* 2016; Teotia *et al.* 2017; Zhang *et al.* 2020) and the generation of action potentials (Sluch *et al.* 2015; Gill *et al.* 2016; Teotia *et al.* 2016; Teotia *et al.* 2017; Chavali *et al.* 2020; Zhang *et al.* 2020). In addition, *in vitro* derived RGCs have been shown to respond to chemoattractant stimuli, including explants of rat visual cortex (Teotia *et al.* 2016), and the ability to transport axonal cargo, including mitochondria (Sluch *et al.* 2015; Gill *et al.* 2016). Furthermore, RNA-seq analysis has enabled comparisons of *in vitro* RGCs with RGCs derived from both mouse and human retina, with significant enrichment of RGC associated genes in iPSC-derived RGCs (Gill *et al.* 2016; Teotia *et al.* 2016).

Although characterisation suggests that 2D differentiation methods generate populations of mature RGCS, a number of studies have analysed the use of purification steps during differentiation to generate an enriched population. Unsurprisingly, small molecule induction of retinal and RGC differentiation induces the generation of superfluous cell types. Sluch *et al.* (2015) demonstrated significant expression of non-RGC associated retinal genes within D40 cultures prior to purification, including markers of photoreceptors, amacrine cells and retinal pigment epithelium. To reduce this heterogeneity, a hESC reporter cell line was generated with mCherry expression driven by expression *BRN3B*. Subsequently, an improved reporter line was generated with bi-cistronic expression of tdTomato-Thy1.2, again driven by *BRN3B*. FACS purification with mCherry resulted in a RGC population with significantly reduced expression of RPE, bipolar, amacrine, horizontal and photoreceptor cell associated genes, when compared to the mCherry negative population. Gill *et al.* (2017) again demonstrated the generation of additional cell lines with significant expression of *RPE65*, a gene required for RPE function, at D25. As such, the study utilised THY1 in an effort to generate pure RGC cultures. Post-purification, RGCs were maintained in culture for a further 15 days with transcriptome analysis demonstrating that purified RGCs showed expression patterns consistent with *in vivo* RGCs and with no significant expression of genes related to other retinal cell populations, including rod photoreceptor, bipolar or amacrine cells. Ultimately, purification of RGCs through cell surface markers or reporter constructs expression will facilitate improved modelling via the rapid, accurate purification, further allowing the study of RGC specific disease mechanisms.

Crucially, the development of *in vitro* RGC modelling provides a near infinite source of context-specific tissue to study; further enabling the development of diverse therapeutic strategies to tackle RGC associated disease. Sluch *et al.* (2015) demonstrated the feasibility of generating an optic nerve-like model by utilising aligned nanofiber scaffolds to culture purified RGCs, causing the isolation of axonal projections and axonal alignments reminiscent of fasciculated nerves. Furthermore, Zhang *et al.* (2020) performed a proof-of-concept study by differentiating RGCs from hESCs and subsequently transplanting presumptive RGCs into rat retinas via intravitreal injection. Analysis demonstrated integration of human RGCs into the rat GCL and short-term survival approximately 1 week after injection. Besides therapy design, 2D-RGC modelling also provides an excellent opportunity for understanding RGC disease mechanisms. Teotia *et al.* (2018) generated patient-derived iPSCs from individuals suffering from primary open angle glaucoma associated with the genetic mutation in *SIX6*, a gene required for retinogenesis. *SIX6* mutant iPSCs demonstrated a differentiation deficit compared to WT cells, with reduced expression of the EFTFs, including *RAX* and *PAX6*, and less developed neuronal projections. Assessment of

mutant RGCs also confirmed increased expression of glaucoma-associated genes, thus clearly identifying molecular disease mechanisms that may contribute to glaucoma pathogenesis.

To-date, one report has demonstrated the feasibility of modelling DOA by generating RGCs from iPSCs. Chen *et el* (2016) derived iPSCs from patients with an *OPA1* splice site mutation, *OPA1* c.2496+1G>T, which is predicted to cause mis-splicing of *OPA1* transcripts. Chen *et al.* suggested that *OPA1* mutant cells had a development deficiency compared to healthy controls, with an inability to form NPCs in the form of neural rosettes, yet with the addition of noggin *OPA1* mutant cells could be driven towards a RPC and RGC lineage. However, in agreement with the Scorecard data presented in Chapter 3, a previous report on the generation of *OPA1* mutant iPSCs suggested cells carrying a heterozygous c.1861C>T mutation could efficiently differentiate towards all three germ layers (Galera-Monge *et al.* 2016). Nevertheless, the differentiation of *OPA1* mutant iPSCs to RGCs has not yet been replicated within the literature and there is therefore a substantial knowledge gap surrounding the effects of *OPA1* mutation on the development of RGCs, and its further downstream implications on their function and survival.

4.1.4 Chapter aims

Current models of OPA1 dysfunction are yet to provide a clinical breakthrough for treating DOA. *In vitro* disease modelling has developed rapidly since the invention of iPSCs, which provide an excellent platform for understanding disease mechanisms associated with specific mutations. In particular, retinal disease modelling through the generation of 3D retinal organoids, which recapitulates retinogenesis, has revealed disease mechanisms associated with a variety of inherited retinal diseases. Importantly, retinal disease modelling has also enabled the efficient analysis of potential therapeutic treatment strategies, such as gene therapy, facilitating their development and advancement towards the clinic. Recently, methods for specifically differentiating RGCs *in vitro* have rapidly expanded, enabling accurate and efficient modelling of RGC-associated diseases. However, these technologies have yet to be applied to DOA research, despite its lack of therapeutic options. Therefore, this study aimed to determine the feasibility of modelling DOA through *in vitro* differentiation technologies to facilitate the study of RGC specific *OPA1* disease mechanisms.

The primary aims of Chapter 4 were:

1. Optimise a 2D differentiation protocol to generate RGC-enriched cultures from WT and *OPA1* mutant cell lines.
2. Use established methods to generate RGCs in 3D retinal organoids to analyse *OPA1* mutations in a context specific model.
3. Investigate the effect of *OPA1* mutation on the development of RGCs.
4. Compare 2D and 3D differentiation strategies to determine the optimal differentiation protocol for modelling DOA.

4.2 Results

At the commencement of this PhD there were a number of previous reports devoted to establishing efficient generation of RGCs (Riazifar *et al.* 2014; Sluch *et al.* 2015; Tanaka *et al.* 2015; Deng *et al.* 2016; Gill *et al.* 2016; Ohlemacher *et al.* 2016; Sluch *et al.* 2017; Teotia *et al.* 2017; Fligor *et al.* 2018; Langer *et al.* 2018; Chavali *et al.* 2020; Zhang *et al.* 2020). As such it was beyond the scope of this thesis to effectively experimentally compare every established RGC protocol. Therefore, two protocols established by Gill *et al.* (2016) and Sluch *et al.* (2015) were prioritised to ascertain their potential and reproducibility. These were selected based on their reported findings, relative ease of use and RGC selection methods. Initially, protocol optimisation was conducted using WT cell lines with analysis via IHC to determine if RGC-like cells could be generated. In addition to testing both basic protocols, the effectiveness of RGC enrichment through THY1 magnetic-associated cell sorting (MACS) isolation was assessed. This proved highly unreliable as an RGC selection marker, with different cell enrichments demonstrating variability and inconsistency for neuronal and non-neuronal cell types. During the initial optimisation stages, Sluch *et al.* (2017) released an enhanced differentiation protocol which was compared to the previously selected protocols. Initial assessment suggested this revised protocol demonstrated increased RGC differentiation efficiency, determined by IHC, when compared to the other two protocols, and formed the basis for the final established method that is further characterised in depth within this chapter.

4.2.1 Generation of 2D-RGCs through *in vitro* differentiation

iPSCs were differentiated towards an RGC lineage over 42 days using N2B27 media with small molecule compounds added during specific time periods (Figure 4.1A). On D-1, iPSCs were dissociated to single cells and plated onto Matrigel-coated plates (Figure 4.1B). In order to determine the efficiency of iPSC differentiation towards a retinal and RGC lineage, a time course of retinal and RGC associated gene expression was determined for the differentiation protocol. By D7, iPSCs had expanded, generating a confluent sheet of cells (Figure 4.1B). qPCR analysis of D7 differentiations demonstrated a rapid increase of important EFTFs *RAX*, *PAX6* and *LHX2* (Figure 4.2; Chen *et al.* 1997; Mathers *et al.* 1997; Mathers *et al.* 2000; Marquardt *et al.* 2001; Tétreaulta *et al.* 2009), however, the EFTF *VSX2* showed a slower onset, with a more moderate induction at D7 (Figure 4.2). EFTF expression was maintained at D21, with a moderate reduction in *RAX* expression and further increases in *VSX2, LHX2* and *PAX6* expression.

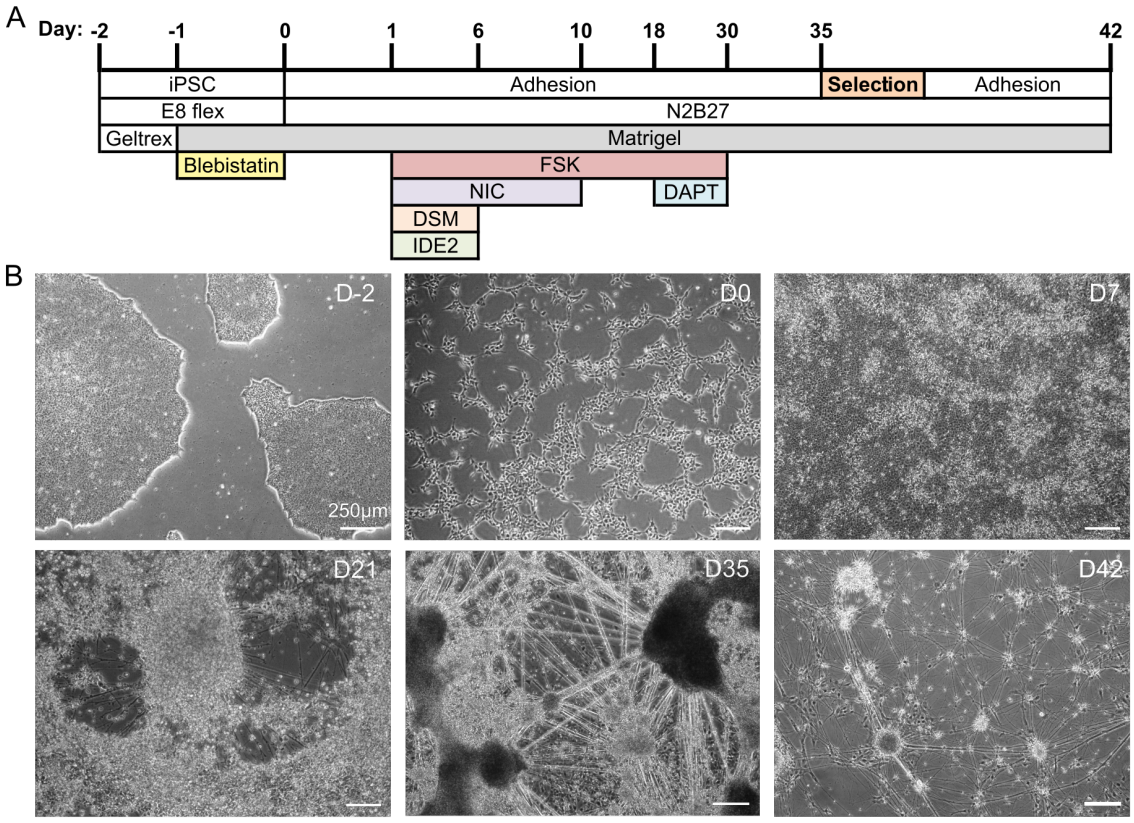

Figure 4.1. 2D-RGC differentiation of iPSCs.

(A) Schematic timeline of RGC differentiation protocol. FSK = forskolin, NIC = nicotinamide, DSM = dorsomorphin.

(B) Representative images of RGC differentiation showing cellular morphology at distinct time points. Scale bars inset. D-2, iPSC colonies have tightly packed cells with distinct boarders. D0, single cell iPSCs begin to re-form colonies. D7, cellular proliferation produces a confluent sheet of precursor cells. D21, neuronal cells begin to cluster and generate early axonal projections. D35, RGCs become tightly clustered and produce extensive axonal networks. D42, purified RGCs generate neuronal clusters with axonal network connections. Scale bars = 250 µm.

By D21, axonal projections began to appear in cultures in conjunction with cell contraction into clusters (Figure 4.1B). Additionally, when compared to D-1 iPSCs, there was significant upregulation of *ATOH7*, a pro-neural gene required for RGC specification that results in RGC depletion when ablated (Figure 4.2; Brown *et al.* 2001; Liu *et al.* 2001; Wang *et al.* 2001; Moshiri *et al.* 2008). By D35, substantial axonal projections had developed, coupled with further bunching or contraction of cells into dense clusters. This morphology was used to isolate presumptive-RGC and neuronal clusters by dissociating heterogeneous cultures to single cells and isolating clusters of neurons that do not dissociate for replating. Isolated neuronal clusters were subsequently cultured for a further 7 days. At D42, neurons had developed into small neuronal clusters with extensive axonal networks (Figure 4.1B). Analysis of terminal RGC differentiation markers demonstrated a slower induction compared to EFTFs (Figure 4.2), indicative of downstream activation during differentiation. γ-synuclein (*SNCG*), a gene identified as a specific marker of RGCs (Surgucheva *et al.* 2008), was initially reduced at D7, before a significant increase in expression at D21 and D42. Both *ISl1* and *BRN3B,* synergistic

genes required for RGC development (Pan *et al.* 2008; Li *et al.* 2014; Wu *et al.* 2015), showed moderate reduction in expression at D7 compared to D-1 iPSCs followed by a significant increase at D21 and a further increase at D42 (Figure 4.2).

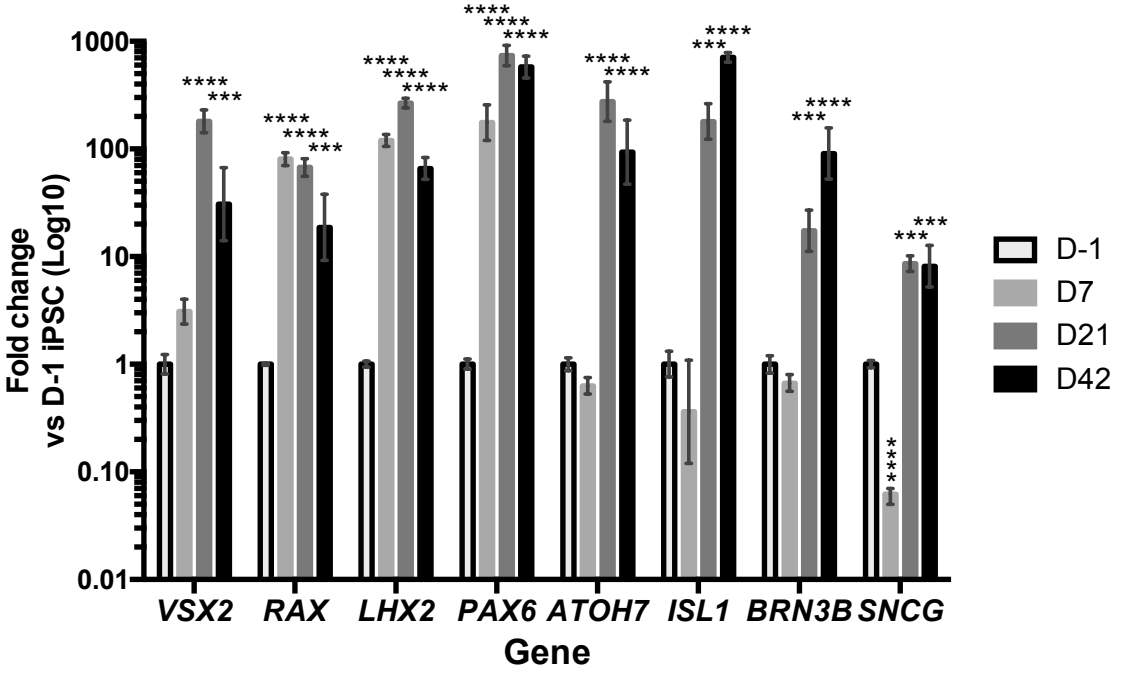

Figure 4.2. 2D-RGC differentiation temporal gene expression.

Total RNA was extracted at D-1, D7, D21 and D42 of control RGC differentiation cultures to determine expression of key RGC genes. Gene expression was first normalised to *GAPDH* and *ACTIN*, and then normalised to D-1 undifferentiated iPSCs. Error bars ± SEM. N=3-4 independent samples. *** p<0.001, **** p<0.0001 versus D-1 iPSCs.

4.2.2 *OPA1* mutation is not detrimental to 2D-RGC differentiation

To test if *OPA1* mutation has an effect on RGC generation, OPA1+/- iPSCs were differentiated in parallel with the isogenic control line to allow for direct comparison of their differentiation capability. Analysis of early RGC associated genes, *VSX2* and *PAX6,* demonstrated clear protein expression on IF staining, whilst qPCR analysis showed no statistical differences throughout the time course of differentiation (Figure 4.3).

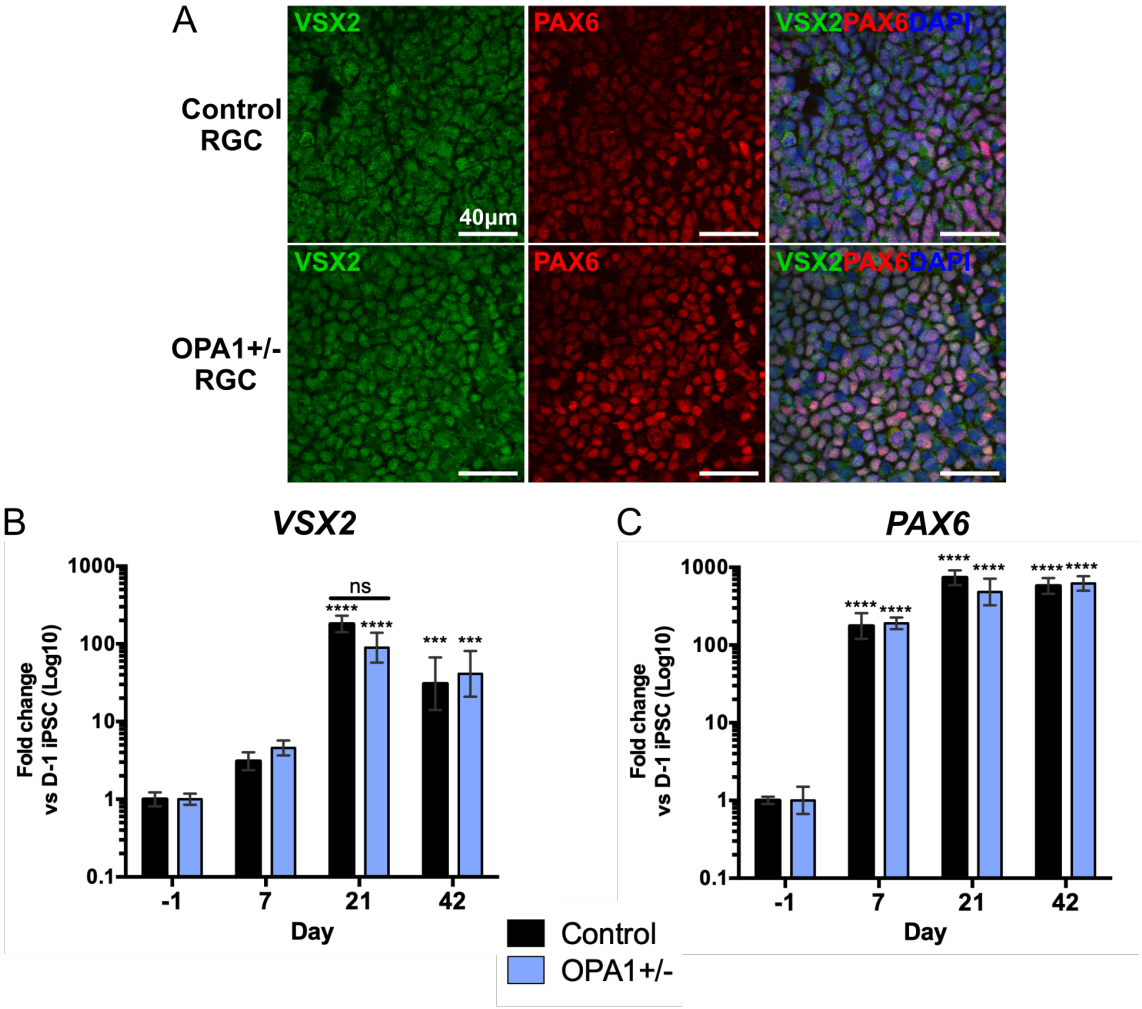

Figure 4.3. *OPA1* mutation does not impair expression of *PAX6* or *VSX2* during RGC differentiation

(A) Representative IHC analysis of D7 control and OPA1+/- differentiations show consistent expression of VSX2 and PAX6. Nuclei identified with DAPI. Scale bar inset.

(B-C) Temporal qPCR analysis of early transcription factors *VSX2* and *PAX6*. Gene expression was first normalised to *GAPDH* and *ACTIN*, and then normalised to D-1 undifferentiated iPSCs. N=3-4 independent samples. Scale bars = 40 µm. *** p<0.01, **** p<0.001 versus D-1 cultures.

Similarly, IF analysis demonstrated consistent expression of both *CRX* and *RAX* (Figure 4.4A) at D7 with no distinct difference in protein expression for either gene between the isogenic cell lines. Similarly, qPCR analysis demonstrated significant upregulation of *LHX2* and *RAX* at D7 for both isogenic cell lines, with consistent expression throughout the differentiation time course (Figure 4.4B,C).

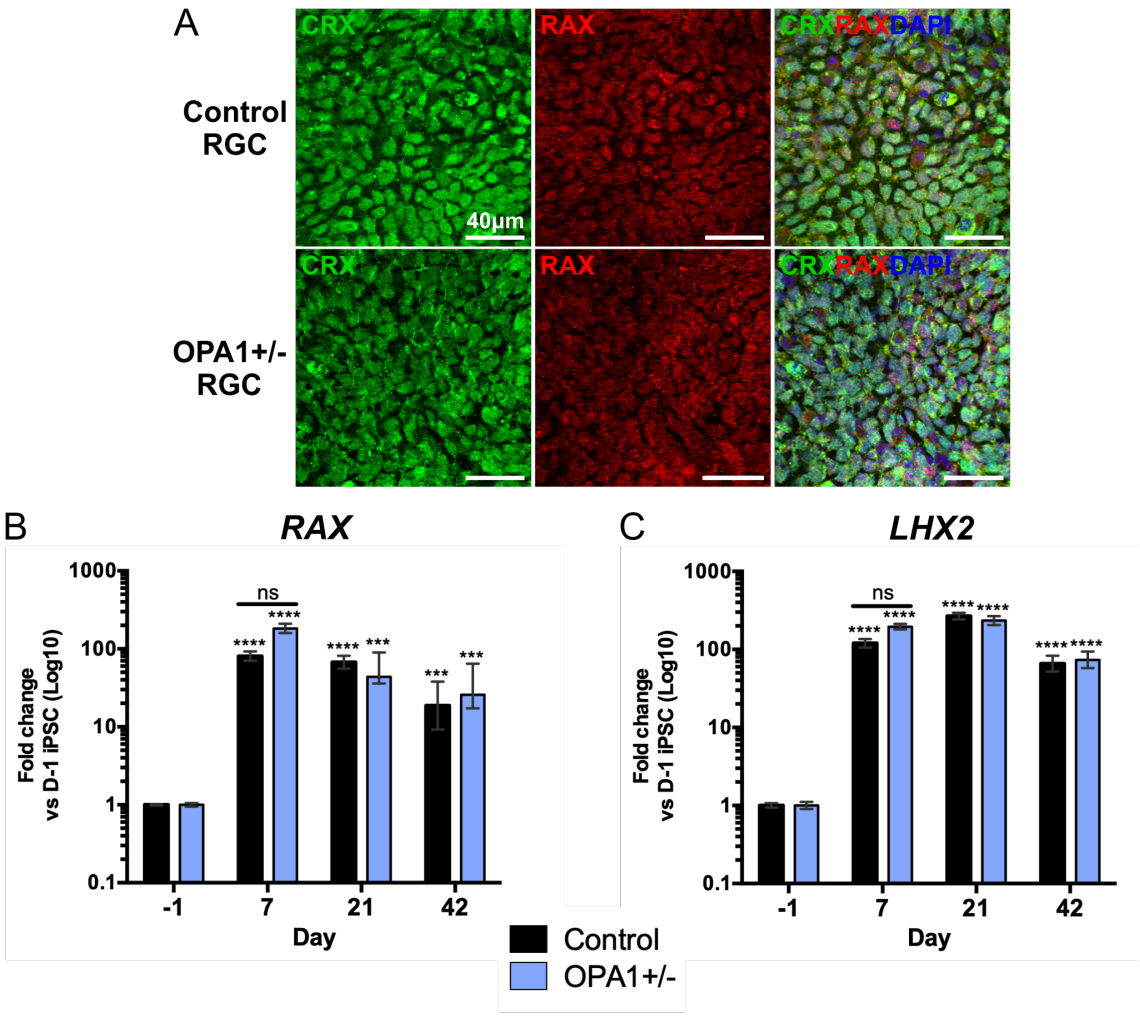

Figure 4.4. CRX, RAX and LHX2 are unaffected by OPA1 mutation during RGC differentiation.

(A) IHC analysis of D7 control and OPA1+/- differentiations show consistent expression of CRX and RAX. Nuclei identified with DAPI. Scale bar inset.

(B-C) Temporal qPCR analysis of early transcription factors *RAX* and *LHX2*. Gene expression was first normalised to *GAPDH* and *ACTIN*, and then normalised to D-1 undifferentiated iPSCs. N=3-4 independent samples. Scale bars = 40 µm. *** p<0.001, **** p<0.0001 versus D-1 iPSCs.

Furthermore, there was no significant difference in expression of the developmental marker *ATOH7* throughout the differentiation. Analysis via qPCR demonstrated significant upregulated *ATOH7* expression at D21 versus D-1 iPSCs with moderate reduction at D42 (Figure 4.5C), whilst IF analysis confirmed expression of ATOH7 at the protein level at D21 (Figure 4.5A). IF also identified early expression of terminal RGC markers, demonstrating isolated expression of BRN3A and consistent expression of SNCG at D21 (Figure 4.5A,B), indicating induction of RGC specific genes. D21 cultures also showed the expression of neuron specific cytoskeletal protein βIII tubulin (TUBB3), with clear axonal projections emanating from neuronal cell clusters (Figure 4.5B).

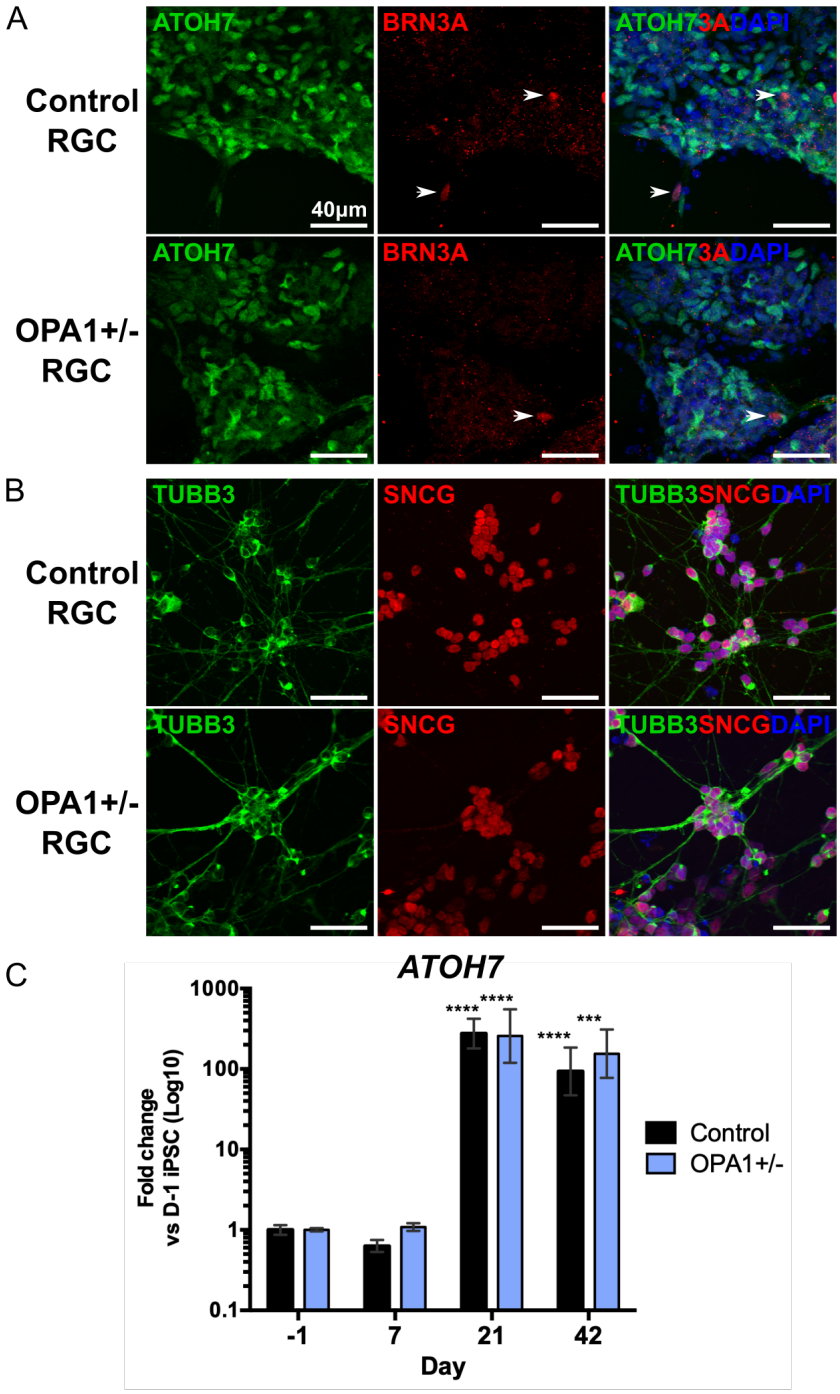

Figure 4.5. 2D-RGCs express ATOH7, BRN3A, SNCG and βIII tubulin (TUBB3) at D21.

(A-B) IHC analysis of D21 control and OPA1+/- differentiations show consistent expression of ATOH7, βIII tubulin (TUBB3) and SNCG with early isolated expression of BRN3A (A, white arrow). Nuclei identified with DAPI. Scale bar inset.

(C) Temporal qPCR analysis of *ATOH7* at D-1, D7, D21 and D42. Gene expression was first normalised to *GAPDH* and *ACTIN*, and then normalised to D-1 undifferentiated iPSCs. N=3-4 independent samples. Scale bars = 40 µm. *** p<0.001, **** p<0.0001 versus D-1 iPSCs.

Finally, IHC analysis of D42 RGC differentiations demonstrated expression of the RGC transcription factors BRN3A, BRN3B, SNCG and ISL1 (Figure 4.6A,B,C), co-localising to cellular nuclei. Additionally, RGCs had prominent expression of mature neuronal markers βIII tubulin (TUBB3; Figure 4.6C) and neurofilament (NFH; Figure 4.6B), which localised to both cell soma and axonal projections.

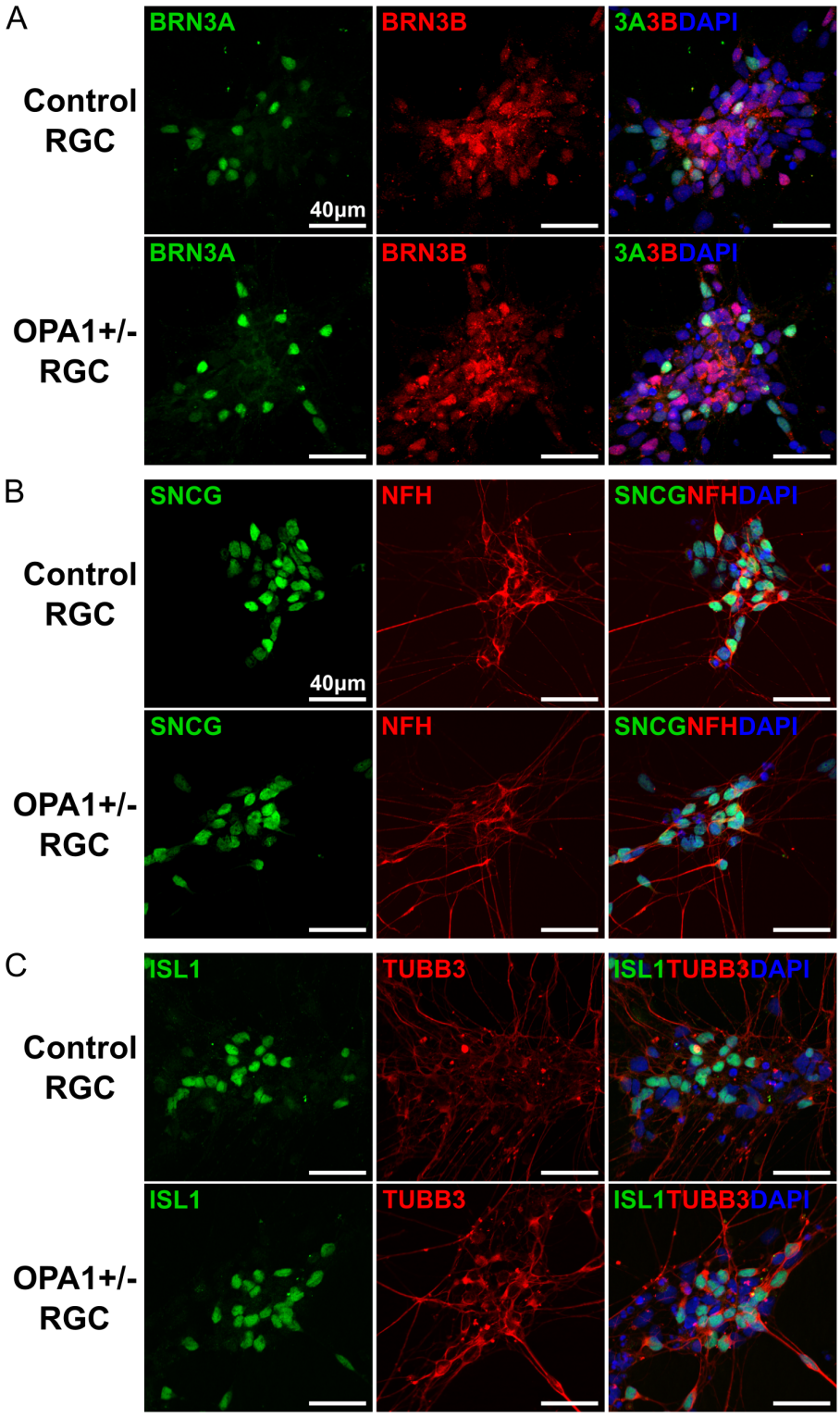

Figure 4.6. IHC analysis of D42 2D-RGCs.

OPA1+/- and control RGCs were isolated at D42 and analysed by immunofluorescent staining to detect expression of terminal differentiation markers. RGCs express transcription factors BRN3A and BRN3B **(A)**, neuronal markers SNCG and ISL1 **(B/C)** and cytoskeletal proteins NFH and TUBB3 **(B/C)**. Nuclei identified with DAPI. Scale bar inset. Scale bars = 40 µm.

To determine the percentage of RGCs within D42 cell populations cell counts were performed on IHC confocal images. Importantly, this analysis demonstrated 54.8 ± 8.1 % of cells were ISL1+, 55.7 ± 6.7 % BRN3+, and 94.2 ± 5.4 % SNCG+ for WT controls.

For OPA1+/- RGC differentiations, 51.8 ± 8.2 % of cells were ISL1+, 54.9 ± 8.6 % BRN3+ and 95.2 ± 3.6 % SNCG+, showing expression was consistent with that observed in control differentiations, with no significant protein expression differences between these two cell lines (Figure 4.7).

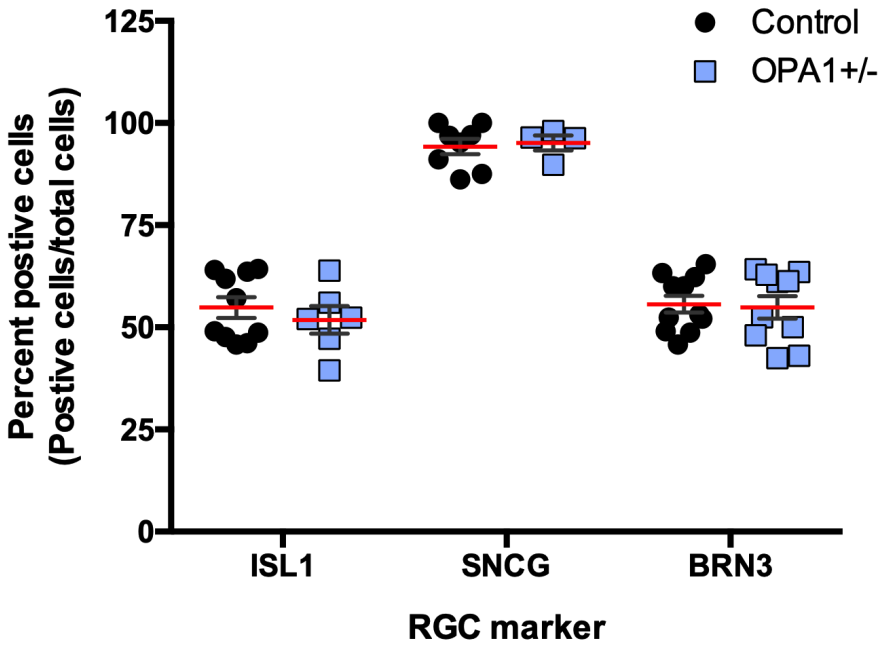

Figure 4.7. Quantification of RGC marker expression in D42 RGCs.

Confocal images were analysed for expression of RGC markers ISL1, SNCG and BRN3, total cell counts were determined from nuclei DAPI staining. Percentage of positive cells calculated as positive marker staining/total cells. N=4-12 individual confocal fields from 4 independent differentiations.

qPCR temporal analysis further demonstrated no significant differences between control and OPA1+/- RGCs for any of the terminal markers, *BRN3B, ISL1* and *SNCG* (Figure 4.8A-C), with both WT control and OPA1+/- differentiations showing moderate reductions in *ISl1* and *BRN3B* and significant reduction of *SNCG* at D7 before significantly increasing expression from D21 onwards (Figure 4.8A-C). By D42, there was significant expression of all three markers with control differentiations demonstrating 99.1 ± 27.1, 559.4 ± 144 and 9.4 ± 2.6-fold change for *BRN3B*, *ISL1* and *SNCG* respectively when compared to naïve iPSCs (Figure 4.8A-C). Similarly, OPA1+/- differentiations demonstrated 74.6 ± 25.8, 593.4 ± 143.1 and 9.2 ± 4.8-fold change, respectively, for the aforementioned genes when compared to OPA1+/- iPSCs (Figure 4.8A-C). To further confirm that *OPA1* mutation does not have a detrimental impact on RGC differentiation both 1334G>A and 2708del iPSCs were also differentiated towards an RGC lineage and analysed at D42. qPCR analysis further supported the analysis of the isogenic cell lines, demonstrating no significant differentiation shortfalls for either 2708del and 1334G>A iPSCs compared to WT controls for *BRN3B* (82.5 ± 47.7 and 83.6 ± 2.1 and respective fold change), *ISl1* (469.7 ± 77.9 and 494.1 ± 91.7 respective fold

change) or *SNCG* (12.8 ± 2.9 and 5.3 ± 1.5 respective fold change; Figure 4.8A-C), confirming that *OPA1* mutation does not inhibit RGC differentiation. Although 1334G>A showed moderately reduced expression of *SNCG*, this proved to be non-significant versus the control cell line.

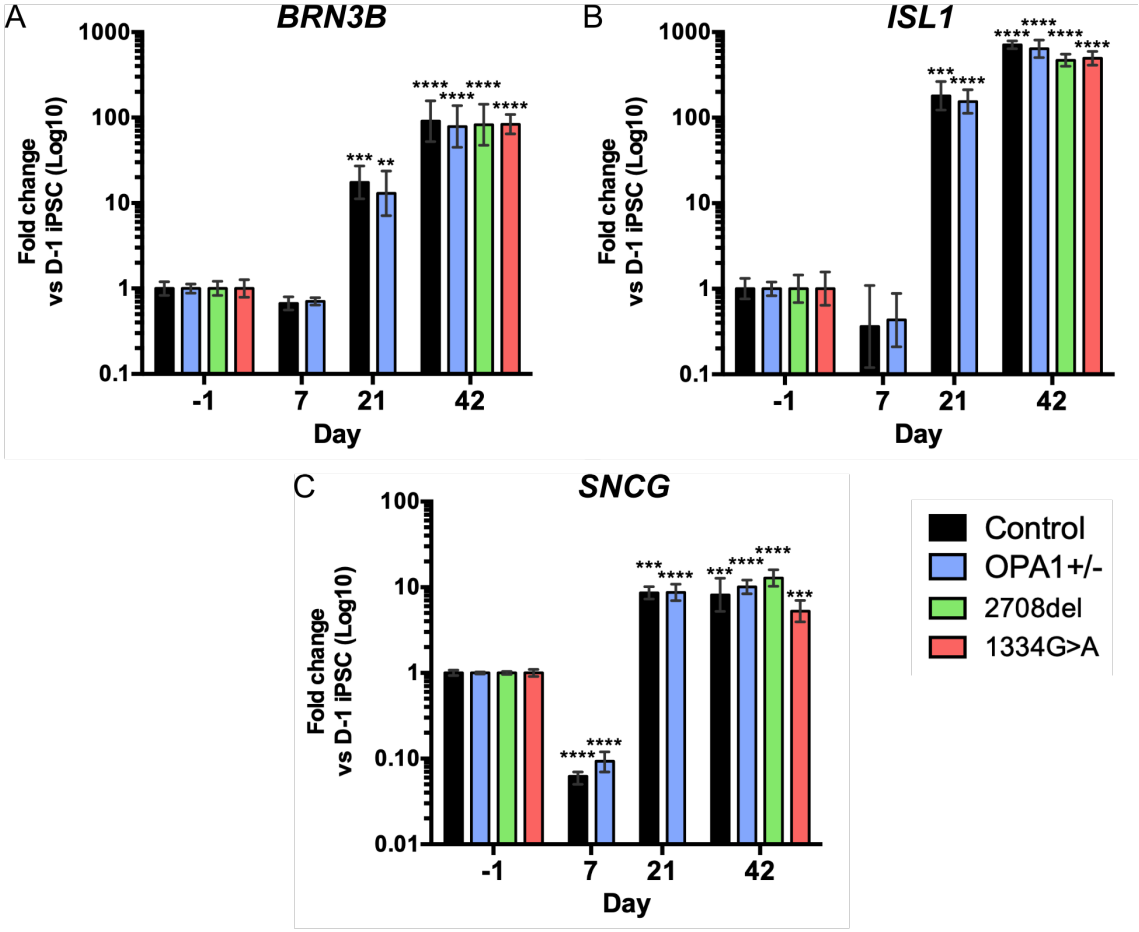

Figure 4.8. *OPA1* mutation does not affect terminal differentiation of RGCs.
Temporal qPCR analysis of *BRN3B* **(A)**, *ISL1* **(B)** and *SNCG* **(C)** at D-1, D7, D21 and D42. Gene expression was first normalised to *GAPDH* and *ACTIN*, and then normalised to D-1 undifferentiated iPSCs. N=3-8 independent samples. ** p<0.005, *** p<0.001, **** p<0.0001 versus D-1 iPSCs.

4.2.3 3D RGC differentiation

Although 2D differentiation methods provide an exciting model to study the pathogenesis of DOA, 3D retinal organoids provide a more physiologically accurate model by recapitulating retinal development (Meyer *et al.* 2009; Nakano *et al.* 2012; Zhong *et al.* 2014; Capowski *et al.* 2019).

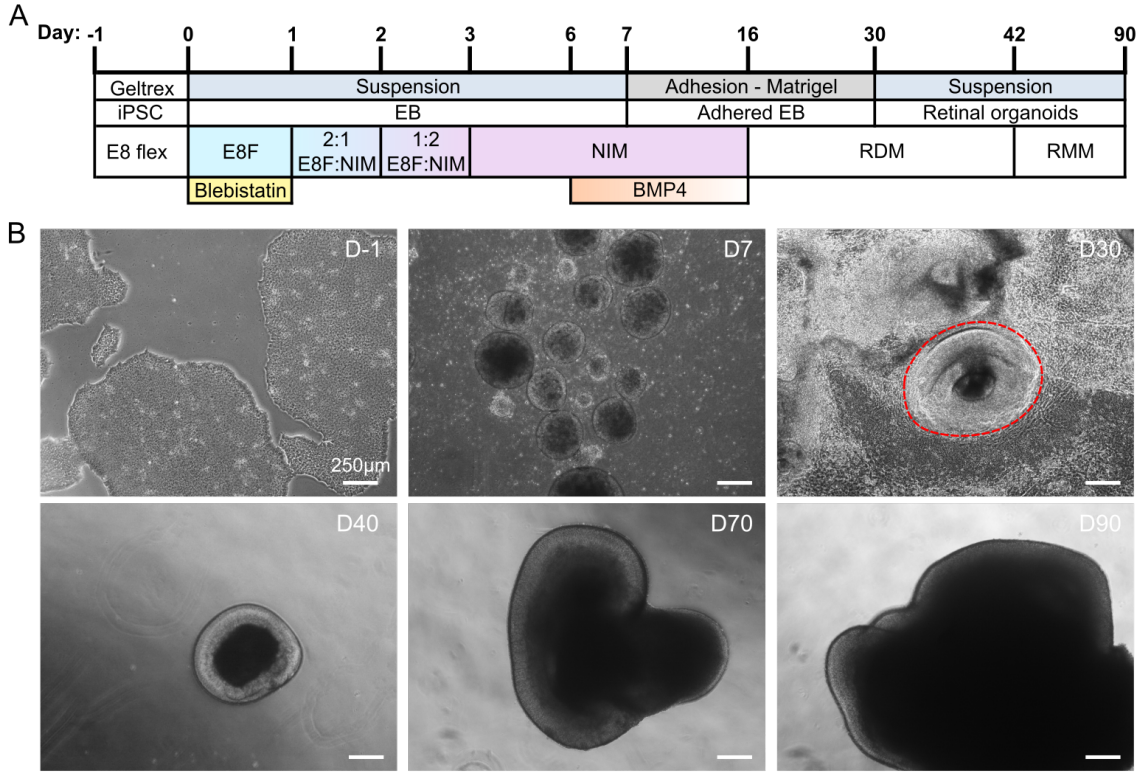

Figure 4.9. Generation of RGCs from iPSCs via long-term culture to 3D retinal organoids.

(A) Schematic timeline of retinal organoid differentiation from iPSCs.

(B) Representative phase contrast images of 3D organoid differentiation showing morphology at distinct time points. D-2, iPSC colonies have tightly packed, nuclear dense cells with distinct borders. D7, embryoid bodies form dense spheres of cells in suspension. By D30, Matrigel plated embryoid bodies begin to develop presumptive optic vesicle-like structures (red dashed line). D40, neural-retinal vesicles are dissected and cultured in suspension as 3D retinal organoids. D70 & D90, retinal organoids continue to grow and develop generating continuous regions of laminated retina-like structures. Scale bars = 250 µm.

3D retinal organoid differentiation (Figure 4.9A) was based on previously published protocols by Zhong *et al.* (2014) and Capowski *et al.* (2019), in which iPSCs were first differentiated into EBs before adhesion to Matrigel coated plates (Figure 4.9B). Once attached, EBs are cultured in neural induction medium (NIM) to develop distinct areas of optic vesicle-like structures (Figure 4.9B). Optic or neural-retinal, vesicles were subsequently dissected and cultured in suspension culture where they develop into 3D retinal organoids with a distinct translucent laminated neuroretina-like outer structure (Figure 4.9B). Due to the early differentiation (Nakano *et al.* 2012; Zhong *et al.* 2014; Kuwahara *et al.* 2015), but also apparent loss (Zhong *et al.* 2014; Capowski *et al.* 2019), of RGCs during culture retinal organoids were maintained until D90 to allow for development of the retinal niche but also retention of any developed RGCs. Thus,

providing a window of assessment to determine the effects of OPA1 mutation on 3D generated RGCs.

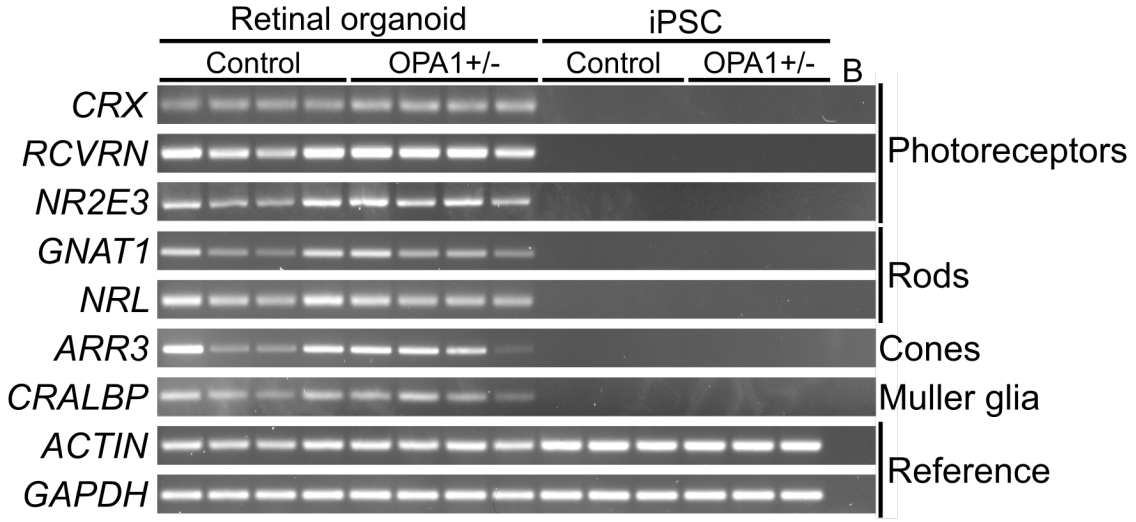

Figure 4.10. D90 retinal organoids express retina associated genes.

RT-PCR analysis confirmed expression of genes associated with retinal development, including *CRX*, *RECOVERIN* (*RCVRN*) and *NR2E3* required for photoreceptor precursor development, *GNAT1* and *NRL* required for rod development, cone arrestin (*ARR3*) required for cone function and *CRALBP* required for muller glia cell function. *ACTIN* and *GAPDH* reference genes confirmed equal cDNA loading. B = no cDNA control.

RT-PCR analysis of retinal organoids demonstrated successful differentiation of both mutant OPA1+/- and WT cell lines towards a retinal cell lineage. D90 retinal organoids showed significant upregulated expression of genes associated with photoreceptor precursor cells, including *CRX* and *NR2E3* (Figure 4.10), required for early specification of the photoreceptor lineage (Chen *et al.* 1997; Milam *et al.* 2002; Haider *et al.* 2009) and *RECOVERIN* (*RCVRN*; Figure 4.10), a photoreceptor specific protein required for phototransduction (McGinnis *et al.* 1997; Koch and Dell'Orco 2015). Although all 3 genes showed variation in expression between individual organoids, there was a significant and robust upregulation compared to D-1 iPSCs (Figure 4.10). Further analysis of rod and cone photoreceptor specific genes confirmed D90 retinal organoids had begun specifying photoreceptor lineages. Notably, retinal organoids expressed both *NRL* (Figure 4.10), required to specify rod photoreceptors (Mitton *et al.* 2000; Mears *et al.* 2001), and *GNAT1* (Figure 4.10), a rod specific gene variant required for phototransduction (Naeem *et al.* 2012). Additionally, there was significant upregulation of cone arrestin (*ARR3*, also known as X-arrestin), required for cone cell signal transduction (Craft *et al.* 1994; Sakuma *et al.* 1996), when compared to D-1 iPSCs (Figure 4.10). Lastly, D90 organoids expressed *CRALBP*, a gene indicative of Muller glia cells (Rowan *et al.* 2004). These genes showed variable expression across individual organoids, but they demonstrated significant upregulation against naïve iPSCs, demonstrating clear differentiation towards a retinal lineage.

In addition, IF analysis confirmed expression of the pan-photoreceptor marker RCVRN in both WT and isogenic OPA1+/- D90 organoids, showing prominent expression on the outer aspect of the retinal organoid (Figure 4.12), indicative of photoreceptor precursor cells. In addition, a number of RCVRN+ cells presented within the inner cell layers of organoids, perhaps indicating displaced or migrating photoreceptor cells (Figure 4.12). Retinal organoids also showed expression of TUBB3 (Figure 4.12).

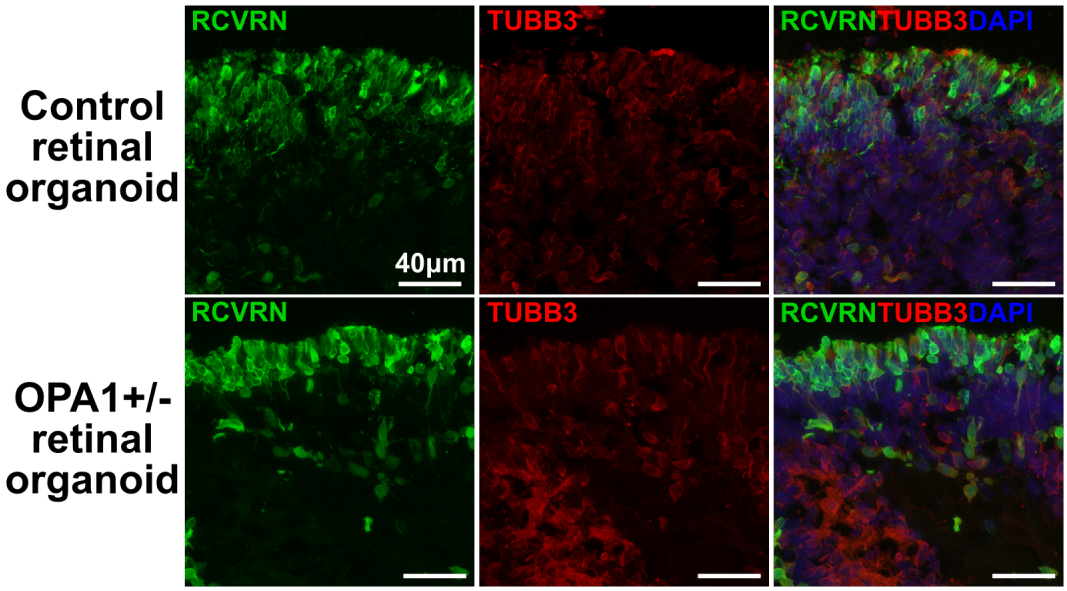

Figure 4.12. D90 retinal organoids contain developing photoreceptors.

IF analysis identified maturing RCVRN+ photoreceptor cells at the outer regions of both WT and isogenic OPA1+/- retinal organoids, with prominent expression of neuron specific TUBB3. Scale bars = 40 µm.

Subsequently, qPCR and IF analysis were used to determine if 3D retinal organoids had led to the successful differentiation of RGCs at D90. qPCR analysis revealed significant upregulation of terminal RGC markers *BRN3B*, *ISL1* and *SNCG* at D90 when compared to D-1 iPSCs (Figure 4.11). Similarly, to 2D-RGC cultures, *OPA1* mutant cell lines did not show any significant differences in expression of terminal RGC differentiation markers compared to WT D90 organoids (Figure 4.11).

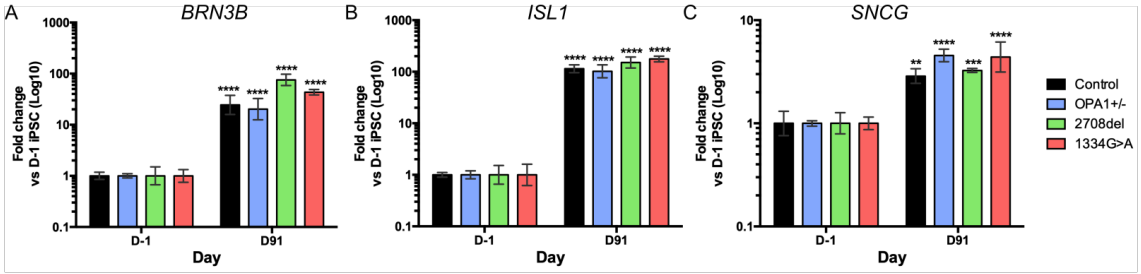

Figure 4.11. qPCR analysis of RGC markers in D90 retinal organoids.

Temporal qPCR analysis of *BRN3B* **(A)**, *ISL1* **(B)** and *SNCG* **(C)** in D-1 iPSCs and D90 retinal organoids. Gene expression was first normalised to *GAPDH* and *ACTIN*, and then normalised to D-1 undifferentiated iPSCs. N=3-5 independent samples. ** p<0.005, *** p<0.001, **** p<0.0001 versus naïve iPSCs.

To confirm the expression of RGC associated genes, protein expression of terminal RGC markers were evaluated in OPA1+/- and isogenic WT organoids by IF staining. D90 organoids demonstrated significant expression of ISL1 within the inner cell layers (ICL; Figure 4.13A). Interestingly, ISL1+ cells were also identified within the organoid periphery, or outer cell layers (OCL; Figure 4.13A), although this is not surprising given that ISL1 has previously been shown to have a dynamic spatiotemporal expression within the retina and regulates the development of a number of cell types, including bipolar, horizontal and amacrine cells, before becoming a terminal RGC marker (Elshatory *et al.* 2007; Bejarano-Escobar *et al.* 2015). As such, D90 retinal organoids were co-stained with BRN3A revealing a number of ISL1+ BRN3A+ RGCs in the ICL of both WT control and OPA1+/- organoids (Figure 4.13A), further identifying the ICL as the presumptive ganglion cell layer.

To further understand the distribution of RGCs, D90 organoids were further analysed for the expression of SNCG and neurofilament proteins (NFH). Similarly to ISL1, SNCG staining identified a large number of cells within the ICL of organoids that also co-localised with neurofilament expression (Figure 4.13B). Although SNCG has been identified as definitive marker of RGCs (Surgucheva *et al.* 2008), within D90 organoids SNCG+ cells within D90 retinal organoids appeared more widely distributed throughout the retina layers, although cells within the presumptive GCL showed the most prominent staining (Figure 4.13B). In particularly, SNCG+ NFH+ cells formed a distinct layer in the ICL of OPA1+/- organoids, indicative of the presumptive GCL, when compared to the isogenic WT control organoids that had a more disorganised distribution (Figure 4.13B). Final analysis of D90 organoids determined the expression of BRN3B and TUBB3. Again, BRN3B+ cells were identified within the ICL of both WT and OPA1+/- organoids, co-localising with prominent TUBB3 staining (Figure 4.13C). Collectively, IF analysis of D90 retinal organoids supports qPCR analysis demonstrating robust expression of RGC terminal markers and thus differentiation towards a retinal cell fate.

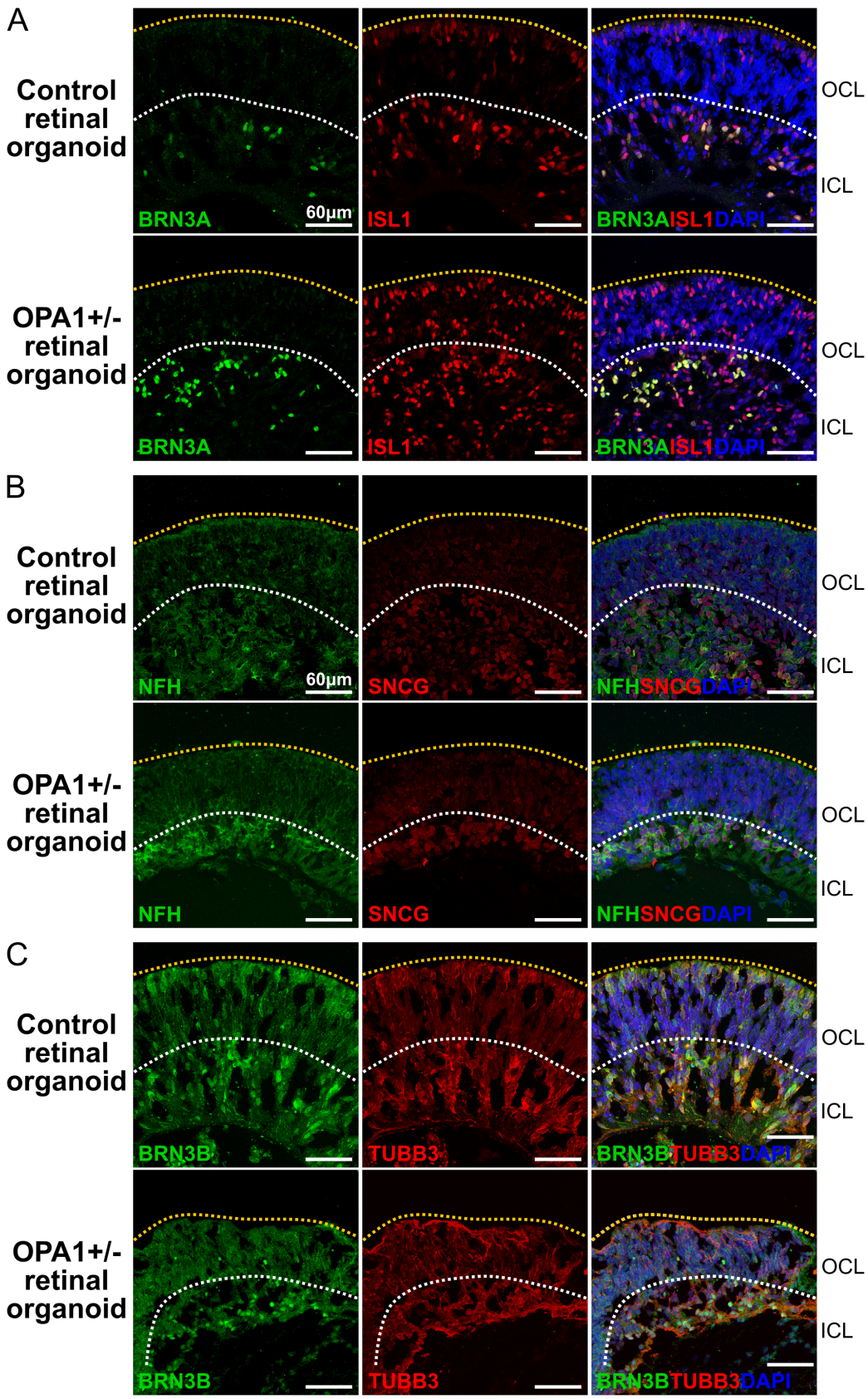

Figure 4.13. D90 retinal organoids express RGC terminal markers BRN3A, BRN3B, ISL1 and SNCG.

Representative IF images of D90 organoids to determine protein expression of RGC markers within the outer cell layer (OCL) and inner cell layer (ICL) of organoid sections.D90 organoids show expression of: BRN3A and ISL1 **(A)**, SNCG and neurofilament (NFH) **(B)**, and BRN3B and TUBB3 **(C)**. Yellow dotted line represents outer edge of organoids, white dotted line the presumptive boundary between inner cells (including RGCs) and outer cells (e.g. presumptive photoreceptors). Scale bars = 60 µm.

4.2.4 2D versus 3D differentiation

Although both 2D and 3D differentiations are versatile options for studying DOA, they have inherent differences due to the methods, compounds and factors required to generate RGCs. Thus, qPCR and RT-PCR were performed to determine if either methodology provided a significant differentiation advantage, for example, by generating RGCs with greater maturation or a culture with greater enrichment of RGC cells. Analysis of terminal differentiation markers in both D42 RGCs and D91 retinal organoids by qPCR demonstrated that there was a moderate enrichment of RGCs within 2D cultures. *ISL1* showed significant upregulation within 2D cultures compared to 3D cultures for WT control, OPA1+/-, 2708del and 1334G>A differentiations (Figure 4.14A). Similarly, *SNCG* showed significant levels of upregulation for control, OPA1+/- and 2708del cells within 2D cultures (Figure 4.14B). Although 1334G>A 2D cultures showed a slight upregulation this was not significantly different compared to 3D organoids (Figure 4.14B). Similarly, *BRN3B* only demonstrated a statistically significant upregulation of expression in WT and OPA1+/- 2D-RGC cultures (Figure 4.14C), whereas 1334G>A 2D cultures showed a trends towards higher mean expression and 2708del 2D cultures only showed a marginal increase versus 3D organoids (Figure 4.14C).

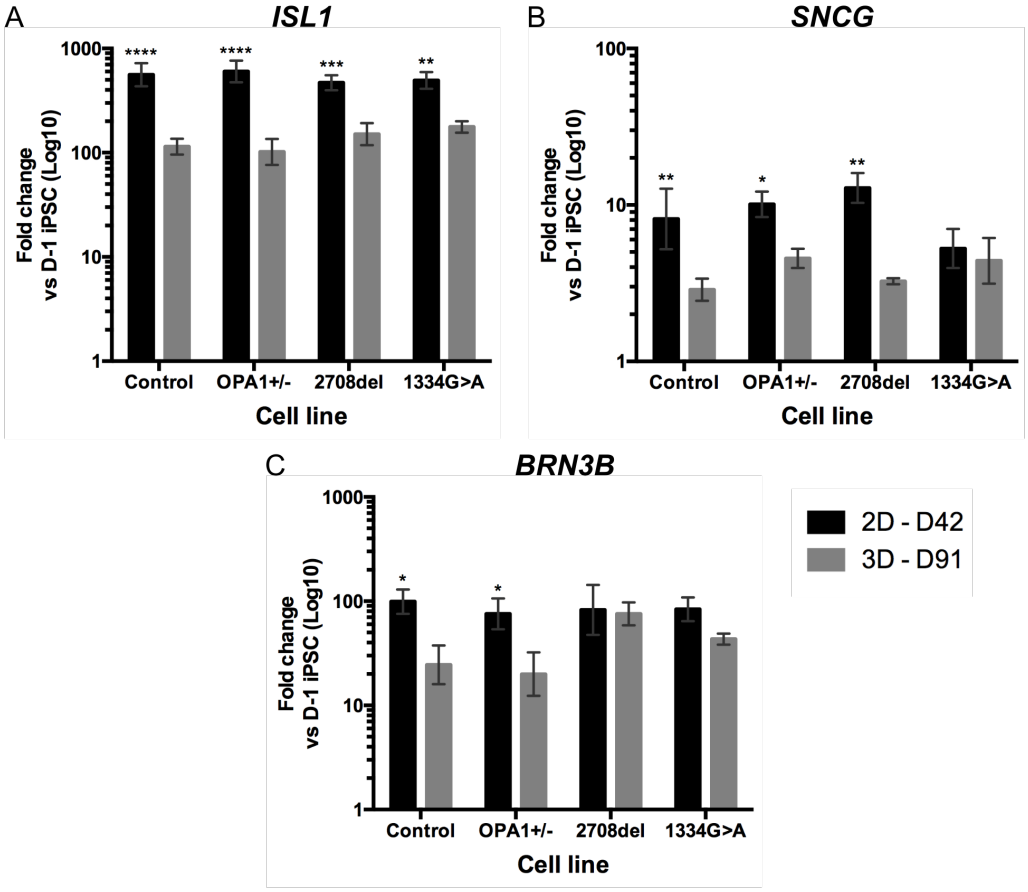

Figure 4.14. qPCR comparisons of 2D and 3D differentiation.

D42 2D-RGCs and D91 3D retinal organoids were compared for the expression of terminal RGC differentiation markers *ISL1* **(A)**, *BRN3B* **(B)** and *SNCG* **(C)** within WT and *OPA1* mutant cell lines. Expression was first normalised to *ACTIN* and *GAPDH* then to naïve iPSCs. N=6-8 individual D42 differentiations. N=5 individual retinal organoids. * $p<0.05$, ** $p<0.01$, *** $p<0.001$.

To further assess the quality of both 2D and 3D RGC differentiations RT-PCR analysis was completed for a diverse range of auxiliary pan-neuronal markers to determine the maturation state of RGCs and allow further comparisons between the two differentiation methods (Figure 4.15). Both WT control and OPA1+/- 2D-RGCs showed significant upregulation of all genes required for neuronal health and function when compared to naïve iPSCs, whilst D90 retinal organoids showed varying levels of upregulation across the range of genes analysed.

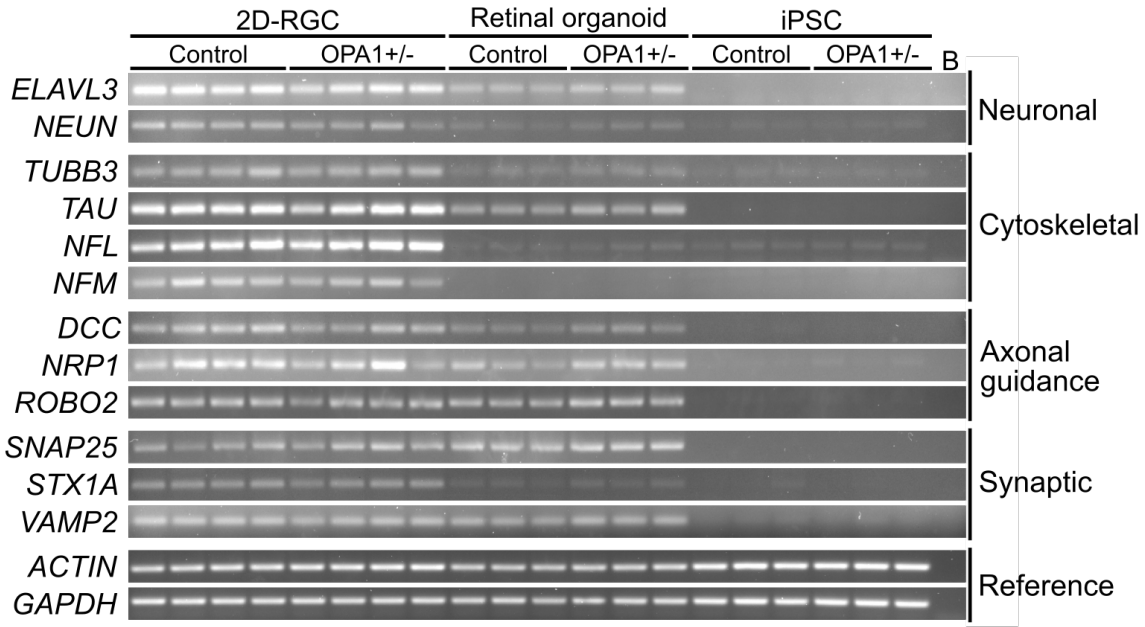

Figure 4.15. Quantification of pan-neuronal genes in D42 RGCs, D90 retinal organoids and D-1 iPSCs.

Comparison of expression of genes required for neuronal form and function in D-1 iPSCs, D42 RGCs and D90 retinal organoids by RT-PCR. Each lane represents an independent 2D-RGC differentiation, retinal organoid or iPSC culture. *ACTIN* and *GAPDH* for reference. B = water only control.

RT-PCR analysis demonstrated that D42 RGCs and D90 organoids both expressed *NEUN* and *ELAVL3* (also known as *HUC*, Figure 4.15), two genes required for neuronal mRNA splicing regulation (Mullen *et al.* 1992; Kim *et al.* 2009; Ince-Dunn *et al.* 2012), with notably higher levels of expression within 2D-RGC cultures and little to no expression detected in D-1 iPSCs (Figure 4.15). Additionally, D42 RGCs expressed a range of genes required for axonal structure and function. RT-PCR analysis supported D42 RGC and D90 retinal organoids IF staining, confirming the expression of *TUBB3* (Figure 4.15). Analysis also established 2D-RGC expression of *TAU* and the neurofilament genes *NFM* and *NFL*, which are required for axonal structure and compartmentalisation (Shahani and Brandt 2002; Ruiz-Ederra *et al.* 2004; Yuan *et al.* 2017). Interestingly, D90 retinal organoids had noticeably reduced expression for all 4 cytoskeletal genes when compared to D42 RGCs, with both *TAU, NFL* and *NFM* expression significantly reduced and remarkably similar to D-1 iPSCs (Figure 4.15),

contrary to the positive IF staining for neurofilament proteins, suggesting there is upregulation of both genes.

In addition to analysing genes related to axonal structural proteins, RT-PCR analysis revealed expression of genes required for axonal and dendritic outgrowth during development (Erskine *et al.* 2007). *ROBO2* expression, a slit protein receptor, is required for RGC axonal outgrowth and the branching of dendrites (Hocking *et al.* 2010). *DCC*, a netrin-1 receptor, is required for guiding RGC axons into the optic nerve head during development (Deiner *et al.* 1997) and *NRP1*, a VEGF and semaphorin receptor, is required for dendritic patterning and axonal guidance (Neufeld *et al.* 2002; Erskine *et al.* 2011). Both 2D-RGCs and D90 retinal organoids showed significant upregulation versus naïve iPSCs (Figure 4.15), with marginally greater expression of *DCC* and *NRP1* in D42 RGCs compared to retinal organoids. *ROBO2* did not show any clear differences in expression levels between the two differentiation protocols. D42 RGC cultures also showed significant upregulation of transcripts involved in synaptic function with notable upregulated expression of vesicular and cell membrane bound SNARE complex genes including *SNAP25, VAMP2* and *SYNTAXIN* (*STX1A*; Figure 4.15; Südhof and Rizo 2011; Ramakrishnan *et al.* 2012). D90 organoids showed comparable levels of expression of *SNAP25* and *VAMP2* when compared to D42 RGCs, however, although *SYNTAXIN* was upregulated compared to iPSCs, it had lower expression levels compared to 2D-RGCs.

Finally, RT-PCR was used to determine the presence of transcripts associated with other retinal cell lineages within D42 cultures. Analysis demonstrated no significant upregulation of genes required for photoreceptror diferentiation and function, including *RECOVERIN*, *ARR3* (Cone arrestin) and *NRL* (Figure 4.16). Analysis of *CRALBP*, a Muller glia cell marker, demonstrated minor expression in 1 differentiation of OPA1+/- iPSCs (Figure 4.16, 2D-RGC OPA1+/- lane 1), but no expression in the remaining differentiations. Importantly, this RT-PCR analyis suggests there is an enriched population of RGCs in 2D cultures, with little to no differentiation of additional retinal cell lineages.

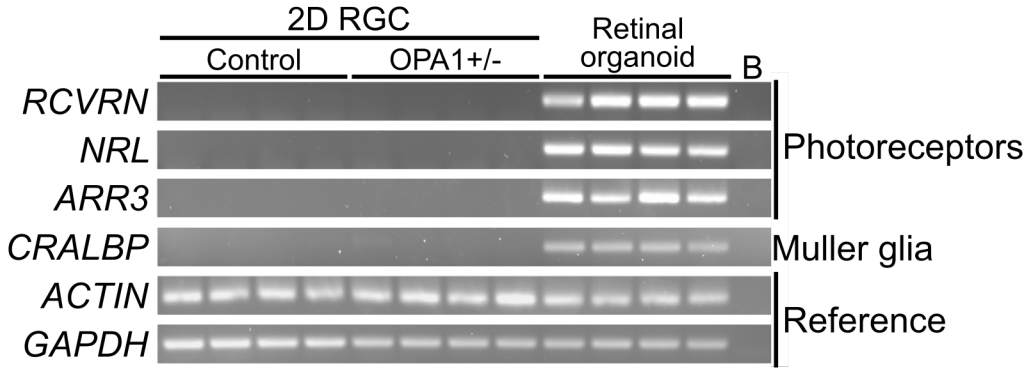

Figure 4.16. 2D-RGCs do not express markers of retinal cell lineages.

RT-PCR analysis of 2D-RGCs using markers of photoreceptors (*RCVRN*, *NRL*, *ARR3*) and muller glia cells (*CRALBP*). D90 retinal organoids used as positive control. *ACTIN* and *GAPDH* confirmed equal loading of cDNA.

Collectively the qPCR and RT-PCR comparisons indicate that 2D-RGCs may provide a moderate enrichment of RGCs when compared to D90 retinal organoids. Importantly, RT-PCR data support both qPCR and IF data demonstrating that *OPA1* mutation does not have a substantial impact on RGC differentiation, with no significant differences in expression of neuronal associated genes between OPA1+/- and control 2D-RGCs or D90 retinal organoids.

4.3 Discussion

Developing improved models to study RGC biology is important to understanding their role in both physiological states and a variety of retinal diseases. Although early research studying *in vitro* retinal models began over a decade ago (Meyer *et al.* 2009), little work has been focused on RGC health and their associated disease mechanisms for conditions such as DOA. Previous studies have begun to expand our knowledge surrounding RGC biology by developing protocols to recapitulate RGC development, through either induction with small molecule compounds or via 3D self-organising organoids. Here, 2D and 3D *in vitro* differentiation methods were used to generate iPSC-derived RGCs from WT and *OPA1* mutant cell lines. Both 2D and 3D methodologies proved proficient at generating *in vitro* RGCs, characterised through temporal qPCR analysis, IF staining and RT-PCR.

4.3.1 2D differentiation of RGCs

In this study, 2D differentiation of RGCs was based on a previously published protocol by Sluch *et al.* (2017), in which iPSCs are differentiated towards a retinal and RGC lineage with small molecule compounds. Initial temporal qPCR analysis of RGC differentiations was used to determine a time course of genes associated with retinal development. In accordance with previous studies (Sluch *et al.* 2015; Deng *et al.* 2016; Gill *et al.* 2016; Teotia *et al.* 2017; Chavali *et al.* 2020; Zhang *et al.* 2020), qPCR analysis demonstrated significant upregulation of genes associated with RPC development during the early stages of differentiation. Crucially, there was upregulation of *PAX6*, *LHX2*, *RAX* and *VSX2,* all of which have been shown to be vital to retinogenesis. Generation of mice containing mutations in *Pax6*, *Rax* or *Vsx2* causes significant retinal developmental defects (Mathers *et al.* 2000; Marquardt *et al.* 2001; Philips *et al.* 2005; Riesenberg *et al.* 2009; Zou and Levine 2012), in particularly, *Rax* null mice lack development of the apparent eye field (Mathers *et al.* 1997). Furthermore, *Pax6* is known to maintain the multipotent state of retinal progenitor cells and regulates timings of retinal progenitor differentiation, whilst its absence prevents induction of downstream genes, such as *Math5* (*ATOH7*)*,* required for RGC specification and an absence of RGCs is observed (Marquardt *et al.* 2001). Similarly, generation of *Lhx2* null mice demonstrated significantly impaired induction of *Rax* and *Pax6* expression during embryonic development, suggesting *Lhx2* is a key regulator of retinogenesis (Tétreaulta *et al.* 2009). Collectively, analysis of early retinal differentiation markers suggests that this differentiation protocol generates a high percentage of RPCs for further RGC differentiation.

Analysis of genes downstream of initial EFTFs demonstrated a significant upregulation of *ATOH7* at D21. Studies of *Math5*, the mouse *ATOH7* orthologue, have demonstrated that it is required for determining the RGC differentiation competence of RPCs. Ablation of *Math5* significantly reduces expression of downstream genes, including *Brn3b*, required for RGC differentiation (Wang *et al.* 2001; Yang *et al.* 2003). Furthermore, although *Math5* mutant mice are genetically viable they have negligible development of RGCs and absent optic nerves (Brown *et al.* 2001).

ATOH7 upregulation also coincided with initiation of expression of genes that have classically been used to detect RGCs. Initial studies of RGCs *in vivo* utilised the *BRN3* family of transcription factors, consisting of *BRN3A*, *BRN3B* and *BRN3C*, to specifically identify the presence and development of RGCs within the retina (Xiang *et al.* 1993; Gan *et al.* 1999). Subsequent analysis of all 3 *BRN3* isoforms demonstrated their function within the developing retina. Deletion of *Brn3b* within mice causes a dramatic reduction in RGC number due to misspecification of precursor cells, poorly formed axonal projections and loss of the optic nerve, ultimately leading to RGC apoptosis (Erkman *et al.* 1996; Xiang 1998; Gan *et al.* 1999; Wang *et al.* 2000; Qiu *et al.* 2008; Badea *et al.* 2009). Although deletion of *BRN3A* does not cause significant RGC loss, it does reduce their dendritic distribution (Badea *et al.* 2009). In double *Brn3b* and *Brn3c* knockout mice, there is greater loss of RGCs and further reductions in optic nerve axonal projections (Wang *et al.* 2002). Thus, although *BRN3A* and *BRN3C* ablation does not cause dramatic RGC loss, they can be considered to facilitate RGC development through neuronal process outgrowth. Within this study, the expression of *BRN3B* was determined due to its integral role within RGC specification. qPCR demonstrated significantly increased *BRN3B* expression compared to naïve iPSCs throughout the differentiation time course, whilst double IF staining of BRN3B and BRN3A confirmed the expression of both isoforms. Interestingly, IF staining indicated a greater number of BRN3B positive cells, perhaps confirming its greater requirement in RGC development over BRN3A. Collectively, the analysis of *BRN3* expression is indicative of generation of RGCs.

Although early studies primarily focused on *BRN3*, additional genetic markers of RGCs have subsequently been identified. Temporal analysis of *ISL1* throughout mouse retinal development demonstrated a diverse pattern of expression, with expression throughout RGC, amacrine and bipolar cell development, which is maintained in mature RGCs (Elshatory *et al.* 2007). Subsequent studies have demonstrated that *ISL1* and *BRN3B* form a molecular complex to regulate gene expression within developing RGCs (Li *et al.* 2014). Deletion of *Isl1* in mice causes apoptosis of RGCs and optic nerve defects, which are further exacerbated in *Isl1* and *Brn3b* double null mutants (Pan *et al.* 2008). Furthermore, ectopic expression of both *Brn3b* and *Isl1* in *Math5* null mice, which

generate few RGCs, restores the development of RGCs and results in a near normal GCL in the mature retina (Wu *et al.* 2015), suggesting expression of *Isl1* and *Brn3b* alone can specify RGCs. In addition, *Snc*g has been identified as a specific marker of RGCs within the mature retina, co-localising with expression of BRN3A (Surgucheva *et al.* 2008). Within this study, there was significant upregulation of both *SNCG* and *ISL1* from D21, with a further increase in *ISL1* expression by D42. Protein analysis via IF staining also confirmed expression of both RGC markers, which was in keeping with previous studies that have used a diverse panel of markers to determine RGC generation and all show significant expression of both genes at their designated terminal time point (Riazifar *et al.* 2014; Sluch *et al.* 2015; Gill *et al.* 2016; Teotia *et al.* 2016; Teotia *et al.* 2017).

Nevertheless, it is important to note that although markers of RGCs are specific within the retina, they have more diverse expression when analysing other tissue expression. Analysis of the *BRN3* family of transcription factors has shown that they have roles in the development of neural circuitry throughout the body. Both *Brn3b* and *Brn3a* are required for early development of the central nervous system (CNS), but later become selectively expressed within specific populations of post-mitotic CNS neurons (Turner *et al.* 1994; Xiang *et al.* 1996). Additionally, *Brn3c* is required for auditory nerve development, with *Brn3c* null mice exhibiting deafness and impaired balance (Erkman *et al.* 1996; Xiang *et al.* 1997). As previously mentioned, *ISL1* expression shows a dynamic pattern of expression throughout retinogenesis (Elshatory *et al.* 2007), whilst *ISL1* expression has been identified in pancreatic islet cells (Ahlgren *et al.* 1997), specific cardiac lineages (Sun *et al.* 2007), and it is required for the generation of motor neurons (Thor *et al.* 1991; Plaff *et al.* 1996). Due to the diverse cellular expression of genes regarded as definitive RGC markers, analysis must consider the expression of multiple genes to identify presumptive RGCs within culture.

In this study, a substantial upregulation of *BRN3B*, *ISL1* and *SNCG* transcripts was observed within RGC cultures when compared to naïve iPSCs, but immunofluorescence analysis demonstrated that these markers were only detectable in 55 %, 50 % and 95 % of cells, respectively, with other cells being either negative for expression or too weak for detection. In comparison, Riazifar *et al.* (2014) demonstrated that approximately 30 % of hESCs converted into presumptive RGCs. While this suggests that 2D cultures generated in this study contain a higher proportion of RGCs, there is also a significant level of variability with RGC marker expression throughout a purified population. Indeed, Langer *et al.* (2018) demonstrated the diversity of stem cell derived RGCs by assessing the co-expression of ISL1, BRN3 and SNCG via IF staining, demonstrating that there are bespoke populations of both single and double immunoreactive positive cell lineages

generated within retinal organoids. It is worth noting that within the early stages of differentiation there were significant, consistent expression of RPC genes, suggesting that although later time points show variable expression of RGCs, the derived cells have most likely been generated from RPCs and are thus of retinal origin. Although work to date has successfully identified multiple RGC markers, it is important to further expand the pool of RGC specific markers, such as the work of Langer *et al.* (2018). Cross comparisons of RGC expression patterns in 2D and 3D cultures and *in vivo* will increase our ability to specifically identify RGCs in heterogeneous cultures and enable study of their biological processes.

Furthermore, post-enrichment RT-PCR analysis confirmed the absence of genes associated with other retinal cell lineages. Sluch *et al.* (2015) showed that their 2D-RGC cultures had significant upregulation of genes associated with other retinal cell lineages, including *RECOVERIN* (photoreceptors), *PROX1* (amacrine cells) and *RPE65* (RPE cells), suggesting that 2D-RGC cultures generate additional cell types. Gill *et al.* (2017) utilised RNA-seq to show significant downregulation of genes associated with rod and bipolar cells in D45 cultures. Although the assessment conducted here was far from comprehensive, with a relatively small number of genes analysed, in accordance with previous studies, it suggests that the isolation methods used here are generating enriched RGC cultures with limited generation of other retinal cell lineages.

Although the RT-PCR analysis conducted here analysed expression of non-RGC associated retinal genes, this analysis failed to determine the overall level of cellular heterogeneity within the cultures at the terminal differentiation time point. Importantly, this may impact the phenotypic characterisation of *OPA1* mutant cell lines given that for many patients RGCs are the sole affected cell type exhibiting mutant phenotypes in DOA. While this is likely an oversight in characterisation of the 2D model presented within this chapter, it is in line with the current publications demonstrating *in vitro* RGC differentiation as these predominantly focus on understanding the generation of RGCs rather than the possible contaminating cell populations. Of note, Riazifar *et al.* (2014), Chen *et al.* (2016) Teotia *et al.* (2016) and Gill *et al.* (2017) present IF data demonstrating fields of view containing numerous cells solely identified by DAPI staining and lacking protein RGC markers, suggesting that these cell populations also contain non-RGC contaminating cells. Interestingly, Schwartzentruber *et al.* (2018) have previously suggested that iPSC culture conditions drastically affect the ability of iPSCs to generate neuronal or non-neuronal (contaminating) cell types. It is therefore imperative to maintain consistent culture conditions of healthy iPSCs to ensure reproducibility within the modelling system and prevent generation of non-RGC cell lineages.

Furthermore, whether the generation of contaminating cell populations affects the downstream characterisation of *OPA1* mutant phenotypes remains to be investigated, especially given that cells typically unaffected in DOA (such as patient-derived fibroblasts) display mutant phenotypes in culture. Importantly, VanderWall *et al.* (2019) recently demonstrated that co-culture of astrocytes and RGCs generate cultures of *in vitro* RGCs with greater maturity, although the presence of this cell type was not analysed in the cultures presented within this chapter, it suggests that a level of culture heterogeneity is required for maturation of *in vitro* RGCs. As such, generating 100 % pure populations of RGCs may be detrimental to disease modelling and prevent the development of mature RGCs exhibiting phenotypes associated with DOA. In addition, the advancement of single cell sequencing has enabled the study of specific cell types within heterogeneous cultures. Within an iPSC-derived neuron model of PD single-cell sequencing was utilised to identify therapeutic targets in dopamine neurons from heterogenous cultures, which were subsequently rescued through therapeutic targeting (Lang *et al.* 2019). This is a technique that has yet to be utilised in understanding the disease mechanisms associated to DOA and would facilitate the specific understanding of aberrant transcripts in *OPA1* mutant RGCs. It is therefore imperative that methods to reduce the heterogeneity of cellular populations, such as developing *in vitro* differentiation methods with higher purity or identifying selective RGC surface markers for purification, should be further developed to enable the specific study of DOA-RGCs and to facilitate single-cell studies of the specific cells of interest.

An important difference between the work presented in this chapter and the work of Sluch *et al.* (2015, 2017), which provided the basis for the 2D-RGC differentiation protocol, was the lack of a mCherry or tDTomato and Thy1.2 reporter driven by *BRN3B* expression. Due to time constraints associated with this project, it was not feasible to generate reporter cell lines for all *OPA1* genotypes. In addition, RGC isolation by endogenous markers and commercially available methods, such as MACS purification via THY1, is not thought to generate pure populations of RGCs (Aparicio *et al.* 2017). Indeed, THY1 isolation proved highly variable, isolating varying proportions of neuronal and non-neuronal looking cells, when trying to purify RGCs for assessment of the two initial protocols in this study and as such was not utilised further. Instead, the propensity of neuronal cells to contract into clusters during differentiation was exploited through a simple isolation step by using cell strainers to isolate clustered presumptive-RGCs from the differentiation culture. The cluster panning method enabled generation of enriched RGC cultures, as seen by significant upregulation of terminal RGC markers when compared to naïve iPSCs and other differentiation time points.

Although generation of RGC reporter cell lines would not be without its own limitations, they would facilitate the investigation of DOA disease mechanisms by enabling highly specific RGC cellular enrichment. As noted previously, markers known to be RGC specific within the eye, such as *BRN3* and *ISL1*, are known to be expressed within other neuronal cell populations throughout the body (Ahlgren *et al.* 1997; Elshatory *et al.* 2007; Badea *et al.* 2012). Thus, purifying RGCs with such markers may also isolate non-RGC populations for further culture. In addition, RGC-associated genes are known to have varying levels of expression throughout RGC populations, for example each *BRN3* isoform is differentially expressed within RGC development and mature populations (Wang *et al.* 2002; Badea *et al.* 2009; Nadal-Nicolás *et al.* 2009) and would thus not allow complete isolation of RGCs from heterogeneous differentiations. Therefore, there are also clear considerations when selecting which RGC-associated gene to use for reporter expression, and the generation of a reporter cell line does not solve all the problems associated with other purification protocols.

4.3.2 3D differentiation of RGCs

3D retinal organoids are now well regarded as a key tool for developing our understanding of retinal development and the associated disease mechanisms that occur in a diverse range of retinal cell lineages. Although multiple differentiation methods have been devised, they have been relatively underutilised to study RGCs and disease mechanisms. In this study, retinal organoid generation was based on previous work by Zhong *et al.* (2014) and Capowski *et al.* (2019), in which iPSCs are differentiated through EBs, adhesion and suspension phases. RT-PCR analysis and IF staining were conducted to verify the ability of *OPA1* mutant cell lines to differentiate towards a retinal lineage. In accordance with a number of other studies (Zhong *et al.* 2014; Kaewkhaw *et al.* 2015; Kuwahara *et al.* 2015; Deng *et al.* 2018; Capowski *et al.* 2019; Kallman *et al.* 2020), D90 retinal organoids demonstrated significant expression of both *CRX* and *RCVRN*, early indicators of photoreceptor differentiation. RT-PCR was supported by prominent IF staining of RCVRN in the outer layers of retinal organoids, indicative of the outer nuclear layer of mature retinas. In addition, RT-PCR showed expression of diverse retinal cell lineages, including both rod (*NRL*) and cone (*ARR3*) photoreceptors and Muller glia cells (*CRALBP*). This analysis confirmed similar levels of expression for both WT control and OPA1+/- cell lines, suggesting that *OPA1* haploinsufficiency does not hinder differentiation towards a retinal phenotype.

In terms of retinal maturation, D90 retinal organoids are considered to be at a relatively immature stage of development, with retinal organoids often cultured for significantly longer periods of time to understand terminal photoreceptor biology (Kaewkhaw *et al.* 2015; Parfitt *et al.* 2016; Volkner *et al.* 2016; Schwarz *et al.* 2017; Capowski *et al.* 2019;

Sridhar *et al.* 2020). Analysis of ISL1 IF staining confirmed the immature state of retinal organoids with positive cells distributed throughout the retinal tissue, indicative of maturing non-RGC populations (Elshatory *et al.* 2007). However, co-localisation of BRN3A with a number of ISL1 positive cells confirmed the developing GCL within the inner mass of retinal organoids. Again, in agreement with previous retinal organoid studies (Nakano *et al.* 2012; Zhong *et al.* 2014; Kuwahara *et al.* 2015; Ohlemacher *et al.* 2016; Fligor *et al.* 2018; Capowski *et al.* 2019), IF staining also demonstrated SNCG and BRN3B expression within the inner cells of retinal organoids, whilst qPCR established significant upregulation of *ISL1*, *SNCG* and *BRN3B* transcripts. Collectively the data demonstrate that it is plausible to study the disease mechanisms associated with *OPA1* mutation and DOA through generation of RGCs via retinal organoids.

4.3.3 *OPA1* mutation does not impair RGC differentiation

Although this study established through the Scorecard qPCR assay that OPA1+/-, 2708del and 1334G>A iPSCs have no differentiation deficit when compared to WT control cells, it has previously been suggested that *OPA1* mutant cell lines have a reduced capability for RGC differentiation. Chen *et al.* (2016) generated iPSCs from patient-derived cells carrying an *OPA1* c.2496+1G>T mutation, demonstrating that they were unable to efficiently generate neural rosettes, and ultimately RGCs, through *in vitro* differentiation. However, upon the inclusion of noggin within the differentiation cocktail, *OPA1* mutant iPSCs could be directed towards an RGC phenotype. However, research from other groups and data gathered in this study contradict this argument. A number of published RGC differentiation studies have included noggin, or an equivalent agonist, in their initial differentiation protocols and successfully utilised these protocols to efficiently generate RGC-like cells (Deng *et al.* 2016; Gill *et al.* 2016; Sluch *et al.* 2017). In addition, studies of animal models further confirm the requirement of noggin during retinal development. Treatment of ectodermal explants or stem cells extracted from frog (*Xenopus)* and mouse with noggin induces a retinal fate and drastically increases the expression of EFTFs, including *Pax6* and *Lhx2* (Zuber *et al.* 2003; Lan *et al.* 2009). Furthermore, studies of mice, zebrafish and frogs have demonstrated clear expression of noggin in the mature adult retina, including RGCs (Messina *et al.* 2014). Thus, it can be argued that noggin is an essential requirement for RGC differentiation.

Here, isogenic *OPA1* mutant and WT cell lines were differentiated simultaneously through both differentiation protocols. Isogenic cell lines remove genetic heterogeneity from differentiation systems, allowing the study of isolated genetic changes and their impacts on developmental processes. Crucially, temporal analysis of 2D-RGC differentiations demonstrated that isogenic OPA1+/- cells are not developmentally delayed. Chen *et al.* (2016), demonstrated *OPA1* mutant cells were unable to generate

neural rosettes, a process in part regulated by *PAX6* and *LHX2* (Zhang *et al.* 2010; Hou *et al.* 2013). However, in this study OPA1+/- differentiations had equal expression of early differentiation markers including *PAX6* and *VSX2*, *RAX* and *LHX2* when compared to WT cells.

Importantly, analysis of terminal differentiation markers in both D42 RGCs and D90 retinal organoids across all *OPA1* mutant genotypes confirmed no differentiation deficit, demonstrating that regardless of the type of mutation OPA1 dysfunction does not impact differentiation ability. Additionally, both control and *OPA1* mutant RGCs expressed a wide range of neuronal markers, including *ELAVL3, SYNTAXIN* and *TAU,* indicative of mature neurons with no clear deficits amongst either 2D-RGCs or D90 organoids. In conjunction with the Scorecard differentiation assessment, the data presented here suggests that *OPA1* mutant cell lines are equally as capable of differentiation as their WT counterparts.

4.3.4 2D versus 3D RGC differentiation

Although both 2D and 3D methodologies proved capable of generating *OPA1* mutant RGCs, showing significant upregulation of RGC associated markers, an additional aim of this study was to validate if either differentiation method provided an enrichment of RGCs to study DOA. qPCR comparison of both differentiated methods demonstrated a significant upregulation of terminal RGC genes *ISL1* and *SNCG* in D42 cultures when compared to retinal organoids. *BRN3B* showed significant upregulation within WT and OPA1+/- 2D-RGCs versus D90 retinal organoids. However, there was no significant difference between the 2D and organoid methods for the 2708del or 1334G>A cell lines, which is most likely due to the higher levels of *BRN3B* expression within D90 organoids for these two cell lines when compared to the isogenic pair. When considering the expression of RGC associated genes, it is important to consider where this difference may originate, namely, either the 2D culture method is generating a greater population of RGCs, or they are generating cells with greater expression of the respective markers. IF analysis demonstrated that both methodologies generated non-RGC cell populations, suggesting that total RGC gene expression is being diluted within both differentiation protocols. Taking this into consideration, it is therefore more likely that 2D differentiations are generating a greater proportion of RGCs that is causing higher overall expression patterns.

Although analysis of terminal RGC markers demonstrates significant upregulation of general RGC related genes, it does not provide insight into the diversity of RGC subtypes within the differentiation protocols. Approximately 30 different subtypes of RGCs are known to be present in the mammalian eye (Sanes *et al.* 2015; Rheaume *et al.* 2018).

However, few published studies have completed in-depth analysis of RGC subtype specification within differentiation protocols, with the primary focus being the expression of melanopsin (*OPN4*), a specific marker for ipRGCs (Sluch *et al.* 2015; Gill *et al.* 2016; Ohlemacher *et al.* 2016). The most thorough study to date by Langer *et al.* (2018) demonstrated significant RGC diversity in cultures when generated through a combination of 3D and 2D cultures, using single cell RNA-seq to identify ipRGCs alongside α-RGCs and direction sensitive-RGCs. Within this study the diversity of RGCs was not analysed as the primary aim was to demonstrate the feasibility of modelling DOA, rather than developing specific protocols for generating the diverse RGC subtypes. Additionally, although RGC loss within DOA appears to affect the majority of RGC subtypes (Majander *et al.* 2017), so generating protocols to generate specific RGC subtypes may be unnecessary. However, it is worth noting that research suggests that ipRGCs may be resistant to neurodegeneration associated with mitochondrial dysfunction, with post-mortem tissue analysis suggesting a sparing of these cells when compared to the mass loss of total RGC number in both LHON and DOA tissues (La Morgia *et al.* 2010). As such, further investigation of RGC subtype specification should be completed to determine if *OPA1* mutation significantly impacts the development of these diverse cells, with a particular focus on ipRGCs due to their apparent resistance to mitochondrial dysfunction.

To further supplement the qPCR temporal analysis of RGC differentiations, RT-PCR was completed on both D42 and D90 cultures to determine the maturation state of presumptive RGCs. Within the mammalian retina, both *NEUN* and *ELAVL3* are predominantly expressed in mature RGCs (Mullen *et al.* 1992; Lin *et al.* 2018), whilst previous studies of RGC differentiation have demonstrated consistent expression in RGCs in both 2D and 3D protocols (Gill *et al.* 2016; Volkner *et al.* 2016; Fligor *et al.* 2018; Sridhar *et al.* 2020). Here, both *NEUN* and *ELAVL3* demonstrated upregulation within D42 and D90 RGCs. However, D42 RGCs demonstrated higher levels of expression, particularly of *ELAVL3,* indicating that 2D-RGCs may present a more advanced maturation state. This is of particular importance when considering the characteristics of DOA, in which mature RGCs are progressively lost from the retina. It is thus important to develop populations of RGCs with a mature phenotype to accurately model the disease mechanisms associated with DOA RGCs.

In addition, analysis demonstrated a difference in expression of axonal cytoskeletal components, with reduced levels of *TUBB3* and negligible expression of neurofilament components *NFL* and *NFM* within D90 retinal organoids. Interestingly, one of the most striking differences between 2D and 3D models was the level of axonal generation observed. In 3D retinal organoids RGCs have a remarkably limited capacity for axonal

generation due to the small internal volume of each individual organoid and a lack of final axonal targets. In comparison, 2D adherent cultures enable a greater capacity for axonal projections and network connections to form due to the greater culture surface area and the underlying extracellular matrix. This is of vital importance for the study of optic neuropathies, such as DOA, in which there is preferential degeneration of RGCs and their axonal projections within the optic nerve, whilst the other retinal layers remain unaffected. Previous studies of the Opa1^{Q285STOP} and *Opa1*^{delTTAG} mouse models have demonstrated that axonal structural changes occur within the optic nerve before the actual loss of RGCs within the inner retina becomes evident (White *et al.* 2009; Williams *et al.* 2010; Sarzi *et al.* 2012), whilst initial charactersiation of DOA by Johnson *et al.* (1979) and Kjer *et al.* (1983) suggested changes in optic nerve structure. Although this was not replicated in an *Opa1* mouse model with a heterozygous splice site mutation (Alavi *et al.* 2007), it is possible that axonal structural or biochemical changes could precede RGC death in DOA. Thus, generating a DOA model that has superior axonal generation may provide increased insight into the disease mechanisms associated with axonal changes that lead to RGC and vision loss.

Here, RT-PCR confirmed the differential expression of axonal cytoskeletal genes between the differentiation methods, suggesting that 2D-RGC cultures may provide a superior model to study axonal generation and pathophysiology. A number of late-onset complex neurological diseases, including AD and PD, have also noted that axonal changes and neuronal dysfunction may preclude the complete loss of neurons (Tammineni *et al.* 2017; Czaniecki *et al.* 2019). As such, methods are now being developed to specifically study axonal structure and function in neurological diseases. Axonal micro-dissection in rats enabled the specific study of axonal transcripts (Farias *et al.* 2020), whilst growth of neurons in microfluidic devices, which separate neuronal axons and soma, now makes it possible to study the specific transcripts in both health and disease states (Bigler *et al.* 2017; Nijssen *et al.* 2019). Deep sequencing of ribosome-bound mRNAs in rat RGCs has demonstrated the diverse evolution of axonal mRNAs throughout development, initially showing expression of mRNAs required for axonal elongation and synaptogenesis, as expected, followed by those involved in axonal survival and neurotransmission (Shigeoka *et al.* 2016). Furthermore, analysis of a model of amyotrophic lateral sclerosis via axonal RNA-seq found 121 significant changes to axonal transcripts when compared to WT cells (Nijssen *et al.* 2018). Therefore, 2D cultures of *OPA1* mutant RGCs may enable greater understanding of the DOA axonal transcriptome via specific RNA-seq of axonal processes, illuminating the axonal disease mechanisms associated with OPA1 dysfunction and how this may impact RGC loss in the patients with DOA.

To further analyse the generation of axonal projections, RT-PCR was completed on D42 RGCs to determine the expression of axonal guidance and synaptic function transcripts. Teotia *et al.* (2016) demonstrated 2D-RGCs expressed chemoattractant receptor transcripts and could respond to appropriate chemoattractant stimuli, including sections of mouse visual cortex. Additionally, Fligor *et al.* (2018) demonstrated the responsiveness of RGCs to soluble chemoattractant factors, demonstrating that netrin 1 can improve RGC neurite outgrowth. Here, RT-PCR analysis demonstrated the expression of transcripts for axonal guidance receptors and presynaptic proteins within 2D-RGC cultures. Although not indicative of function, the expression of transcripts indicated that 2D-RGCs are likely using axonal growth cones to project towards targets and likely forming neuronal connections once found. D90 retinal organoids also expressed similar levels of both sets of transcripts, demonstrating that synaptic formation and axonal guidance is likely occurring within the inner cell mass of organoid cultures. Importantly, analysis within Opa1^{Q285STOP} mouse model of DOA demonstrated that Opa1 is vital for synaptic connectivity, with loss of Opa1 function reducing RGC post-synaptic connections with bipolar cells (Williams *et al.* 2012). In addition, analysis of *ex vivo* cortical neurons using *OPA1* siRNA demonstrated that *OPA1* reduction impairs neuronal maturation, including the reduced synaptic development and both pre- and post-synaptic protein expression (Bertholet *et al.* 2013). It is therefore important to develop models of DOA that express transcripts associated with mature neuronal form and function, such as synaptic formation, to be able to ascertain if there are DOA disease mechanisms associated with these neuronal traits. Confirmation of expression of these transcripts in both 2D-RGCs and retinal organoids suggests that both differentiation methods would be suitable for investigating axonal related processes in DOA-associated mutant cell lines.

The final aspect to consider regarding the differentiation protocols is the methods used to generate RGCs. Derivation of retinal organoids is primarily driven by retinogenesis through self-formation, i.e. organoids are spontaneously generated via inherent pathways resulting from cellular interactions (Meyer *et al.* 2009; Meyer *et al.* 2011; Nakano *et al.* 2012; Zhong *et al.* 2014). Conversely, in 2D differentiation methods stem cells, are driven towards a RGC fate using chemicfally defined media, often with the use of small molecule compounds (Riazifar *et al.* 2014; Gill *et al.* 2016; Teotia *et al.* 2016; Sluch *et al.* 2017). Although both methods are technically feasible, it can be argued that organoid generation more accurately portrays the temporal and architectural development of the retina, whilst the use of small molecules forces stem cells through specific differentiation stages. Although the majority of these molecules are known to activate specific receptors, their complete downstream effects have not been fully ascertained. Thus, the use of small molecules could potentially impact the development

of specific characteristics or mechanisms associated with certain diseases. However, the spontaneous derivation of RGCs within 3D retinal organoids also produces a number of challenges for further downstream applications. Retinal organoids provide an excellent model system to enable the study and optimisation of treatment strategies for photoreceptor-related retinal degeneration, including the use of antisense oligonucleotides and viral transduction, due to the apical localisation of organoid photoreceptors (Parfitt *et al.* 2016; Gonzalez-Cordero *et al.* 2018; Garita-Hernandez *et al.* 2020; Kallman *et al.* 2020). However, unlike in the mammalian retina where RGCs develop as the Innermost and most accessible layer, RGCs develop within the internal cellular mass of retinal organoids, reducing their accessibility and physical exposure to assessing potential therapeutic agents. As such, 2D models of RGCs may prove more versatile for investigating therapeutic strategies than 3D retinal organoids may not be able to. It is clear that both 2D and 3D RGC models both have distinct advantages and disadvantages for studying *OPA1* mutations, and they thus must be considered complimentary models for further defining the disease mechanisms and therapeutic pathways in DOA.

In summary, the data presented in this chapter provide a methodological framework for the generation of *in vitro* RGCs from *OPA1* mutant cell lines and isogenically-matched WT controls. Generated RGCs showed a clear developmental induction of retinal and RGC associated genes, with comparable gene and protein expression profiles to previously published literature. Analysis of pan-neuronal markers showed expression of genes required for neuronal health and function, including splicing, axonal guidance and synaptic proteins. In contrast to previous reports, isogenic OPA1+/-, 2708del and 1334G>A cell lines showed no clear differentiation deficit compared to WT cell lines in 2D or 3D RGC cultures, suggesting that mutations with dominant-negative effects or resulting in haploinsufficiency do not impair RGC differentiation. Crucially, the models developed within this chapter will enable the downstream consequences of *OPA1* mutations to be directly investigated in RGCs, providing a crucial resource for developing our understanding of DOA-associated disease mechanisms.

Chapter 5: Effect of *OPA1* mutation on mitochondrial homeostasis

5.1 Introduction

As described in Chapter 1, OPA1 is now regarded as an essential mitochondrial protein, contributing to the diverse cellular functions of the mitochondrial network. Most notably, OPA1 is essential to mitochondrial dynamics, facilitating the constant remodelling of the mitochondrial network through the coordination of IMM fusion (Olichon *et al.* 2007; Agier *et al.* 2012; Ban *et al.* 2017; Del Dotto *et al.* 2017). In addition, numerous studies have demonstrated how OPA1 maintains the integrity of the mitochondrial genome, energetic output and biosynthetic pathways (Yu-Wai-Man *et al.* 2010; Sarzi *et al.* 2012; Patten *et al.* 2014; Millet *et al.* 2016; Bocca *et al.* 2018; Yang *et al.* 2020). Although it is unclear why these mitochondrial deficits result in the specific loss of RGCs in DOA, direct comparisons with clinically related conditions provides insight into the disease mechanisms associated with mitochondrial disease and RGC loss.

5.1.1 Comparisons to related conditions

Understanding RGC biology has gained significant traction over the past two decades due to the increasing prevalence of glaucoma within the global population, predicted to cause irreversible blindness in 110 million individuals by 2040 (Tham *et al.* 2014). Although glaucoma typically has multiple aetiologies, and is commonly associated with increased intraocular pressure (IOP), understanding its associated disease mechanisms may translate to understanding DOA given they are both conditions in which RGCs are the primary affected cell type. As with DOA, access to physiologically relevant tissue samples from glaucoma patients is remarkably difficult to come by. As such, the vast majority of knowledge about glaucoma disease mechanisms has originated from non-physiological human samples and animal models. Analysis of lymphocytes derived from primary open angle glaucoma (POAG) patients has also revealed disease mechanisms typically associated with mitochondrial optic neuropathies, most notably POAG patients demonstrate reduced levels of ETC complexes, OXPHOS inhibition and accumulation of mtDNA mutations, when compared to healthy controls (Abu-Amero *et al.* 2006; Lee *et al.* 2012; Van Bergen *et al.* 2015).

In addition to respiratory defects, analysis of mtDNA extracted from POAG patients demonstrated significantly higher levels of mtDNA variants when compared to healthy controls, predominantly in mtDNA complex I genes (Abu-Amero *et al.* 2006; Banerjee *et al.* 2013; Jeoung *et al.* 2014; Sundaresan *et al.* 2015). Similarly, analysis of aqueous humour samples and post-operative extracted RGCs indicated greater levels of lipid

peroxidation, suggesting glaucoma-patients have higher incidence of cellular oxidative stress (Zanon-Moreno *et al.* 2008; McElnea *et al.* 2011). Interestingly, single nucleotide polymorphisms (SNPs) in *OPA1* intron 8 are associated with higher risk of developing normal tension glaucoma and developing high tension glaucoma at an earlier age (Mabuchi *et al.* 2007), whilst SNPs within *MFN1* and *MFN2* have been associated with development of normal tension glaucoma (Wolf *et al.* 2009). Collectively these studies indicate mitochondrial dysfunction as a plausible driver of glaucoma development, suggesting a possible link between well-known mitochondrial optic neuropathies and age-related glaucoma.

As with human samples, animal models have provided invaluable insight into the disease mechanisms driving RGC loss in glaucoma, demonstrating involvement of mitochondrial dysfunction. Assessment of mitochondrial morphology and function in the DBA/2J mouse model of glaucoma, which spontaneously generates high IOP and RGC degeneration, have consistently demonstrated accumulation of morphologically abnormal mitochondria. Glaucomatous mice typically present with smaller more fragmented mitochondria containing abnormal IMM cristae morphology (fragmented, swollen or absent) when compared to control mice (Ju *et al.* 2008; Coughlin *et al.* 2015; Williams *et al.* 2017). Interestingly, increased IOP is associated with alteration to mitochondrial fusion and fission machinery, driving the aforementioned morphological changes. Ju *et al.* (2008) demonstrated increased IOP promotes reduction in *Opa1* expression and an increase in *Dnm1* (a murine homologue of the pro-fission gene *DRP1*) expression, coupled with reduced Opa1 protein levels and release of Opa1 from the mitochondrial network. A more recent study confirmed these findings, suggesting high IOP causes increased oxidative stress, which results in the upregulation of *Drp1* and induction of mitochondrial fragmentation associated with reduced mitochondrial mass in RGC axons in glaucomatous mice (Kim *et al.* 2015). Mitochondrial changes within glaucomatous mice are associated with decreased levels of NAD^+ (Williams *et al.* 2017), required for ETC function, and reduced ATP production in the optic nerve (Baltan *et al.* 2010). Importantly, supplementation with nicotinamide (vitamin B_3) can reduce NAD^+ associated deficits and prevent RGC loss (Williams *et al.* 2017). Ultimately, these changes demonstrate how mitochondrial fragmentation and reduced functionality contribute to RGC loss in glaucoma, and confirms how alterations to OPA1 function may drive RGC death in DOA.

More recently, a handful of studies have begun to analyse glaucoma-associated disease pathways through *in vitro* differentiation of glaucoma-patient derived iPSCs towards RGCs. 3D differentiation of glaucoma patient-derived iPSCs carrying an *OPTN* gene mutation, typically associated with familial forms of glaucoma, demonstrated glaucoma-

RGCs had higher levels of apoptosis that could be reduced when treated with neuroprotective factors (Ohlemacher *et al.* 2016). Similarly, 2D differentiation of glaucoma patient-derived iPSCs carrying a *SIX6* gene mutation, a known glaucoma risk allele, suggested glaucoma-iPSCs had development abnormalities and global dysregulation of genes associated with signalling pathways required for metabolic function and cell survival (Teotia *et al.* 2017). Although no studies to date have analysed DOA-RGC global gene regulation, studies have indicated cells carrying *OPA1* mutations have increased levels of apoptosis (Olichon *et al.* 2003; Arnoult *et al.* 2005; Olichon *et al.* 2007; Chen *et al.* 2016), perhaps indicating overlapping disease mechanisms with glaucoma.

Furthermore, as mentioned in Chapter 1, DOA is most commonly associated with LHON, a clinically similar optic neuropathy caused by specific mutations in mtDNA encoded genes, namely *MTND1*, *MTND4* and *MTND6* (Yu-Wai-Man *et al.* 2002). Therefore, direct comparisons of LHON and DOA provide an excellent opportunity to understand the impact of mitochondrial dysfunction of RGC health. Studies of LHON-associated mutations have helped to illuminate the mutant mitochondrial phenotypes associated with mtDNA mutation. Early studies of cybrid cell lines carrying LHON patient-derived mitochondria demonstrated increased levels of ROS production (Wong *et al.* 2002) and reduced ATP synthesis (Carelli *et al.* 2004), both associated with defective complex I function. These findings were confirmed in a LHON mouse model, carrying mutation in *MTND6*. Analysis of mice carrying mutations in *MTND6* demonstrated accumulation of morphologically abnormal mitochondria within the axon, defects in complex I and mitochondrial respiration and demyelination. However, analysis of synaptosomes demonstrated no reduction in ATP, but increased ROS accumulation (Lin *et al.* 2012). Most recently, two studies have conducted RGC modelling utilising LHON patient-derived iPSCs. Both studies demonstrated impaired mitochondrial function, indicating decreased basal respiration and reduced spare respiratory capacity (Wu *et al.* 2018) and increased levels of ROS production and RGC apoptosis, alongside increased retrograde mitochondrial transport and reduced stationary axonal mitochondria (Yang *et al.* 2020), when compared to control RGCs. Thus, analysis of LHON tissues, and *in vitro* derived RGCs demonstrates that mitochondrial deficiencies, particularly those associated with mitochondrial morphology and respiration, are commonly associated with RGC loss.

In addition to LHON there are a number of diverse syndromic optic neuropathies that are also caused by mutations within mitochondrial-associated genes, including hereditary spastic paraplegia 7 (HSP7), Charcot-Marie-Tooth type 2A and Mitochondrial Encephalomyopathy Lactic Acidosis Stroke-like (MELAS). As with DOA and LHON, these conditions are caused by mutations in both nDNA and mtDNA encoded genes that

result in loss of RGCs, alongside their syndromic symptoms such as peripheral neuropathy and brain dysfunction (Carelli *et al.* 2009). HSP7 is caused by mutation to *SPG7* (paraplegin), a mitochondrial associated AAA-metalloprotease (Casari *et al.* 1998) that is also associated with development of DOA (Klebe *et al.* 2012). Defects in paraplegin are associated with reduced OXHPOS output, with reduced levels of cellular ATP content (Casari *et al.* 1998; Ferreirinha *et al.* 2004; Pareek *et al.* 2018; Wali *et al.* 2020), whilst mouse models of HSP7 demonstrate axonal degeneration associated with mitochondrial abnormalities, including hypertrophic mitochondrial and abnormal cristae morphology (Ferreirinha *et al.* 2004). Interestingly, paraplegin is known to proteolytically process L-OPA1 into S-OPA1, suggesting HSP7 and DOA may be closely related in their disease mechanisms (Ishihara *et al.* 2006).

Like HSP7, mutation to the nDNA encoded *MFN2* is associated with Charcot-Marie-Tooth type 2A (Züchner *et al.* 2004; Chung *et al.* 2006). Alongside MFN1, MFN2 coordinates the fusion of the OMM (Chen *et al.* 2003), and as such, defects in MFN2 function result in abnormal mitochondrial morphology in patient-derived fibroblasts (Rouzier *et al.* 2012), iPSC-derived neurons (Fang *et al.* 2016) and muscle cells (Bach *et al.* 2003). Furthermore, dysfunctional MFN2 is also associated with impaired mtDNA maintenance, with studies showing both accumulation of mtDNA mutations (Rouzier *et al.* 2012) and increased proliferation of mtDNA (Sitarz *et al.* 2012). Lastly, impaired MFN2 function results in mitochondrial respiratory defects, associated with reduction in total ATP levels (Bach *et al.* 2003; Fang *et al.* 2016; Wolf *et al.* 2019).

As with *OPA1* mutations, which are now associated with a spectrum of neurodegenerative disorders (Carelli *et al.* 2015; Spiegel *et al.* 2016; Iannielli *et al.* 2018), mutations in mtDNA encoded genes that are typically associated with LHON are now associated with a wider range of neurological conditions. Mutations in mitochondrial transfer RNAs and to both *MTND1* and *MTND5,* encoding components of ETC complex I, are associated with MELAS (Pulkes *et al.* 1999; Blakely *et al.* 2005; Carelli *et al.* 2009). Like with other mitochondrial associated conditions, MELAS is associated with ETC abnormalities, notably complex I deficiency, reduced OXPHOS and ATP reduction (Dubeau *et al.* 2000; Rodan *et al.* 2015; Frey *et al.* 2017; Nukui *et al.* 2020).

Importantly, the defects exhibited in POAG, LHON and the related syndromic mitochondrial conditions confirm the susceptibility of RGCs to mitochondrial dysfunction, including reduced energy production and secondary mtDNA changes, and highlight it as a mechanism that can promote the loss of neuronal viability.

5.1.2 The pros and cons of current DOA models

Although it is clear that defects in mitochondrial proteins cause significant impairment to mitochondrial homeostasis, due to their unique morphology and energy requirements it is unclear how mutation in *OPA1* affects human RGC health. As mentioned in Chapter 1, access to DOA patient tissue is remarkably rare (Johnston *et al.* 1979; Kjer *et al.* 1983) and although the study of model cell lines, mouse models and patient-derived cells has provided invaluable insight into DOA disease mechanisms, it is important to consider the main differences of these system when compared to the biology of RGCs.

Studies of patient-derived fibroblasts have provided key insights into the specific effects of clinically relevant *OPA1* mutations, demonstrating how these mutations affect mitochondrial network morphology, cristae structure and respiratory output (Amati-Bonneau *et al.* 2005; Frezza *et al.* 2006; Amati-Bonneau *et al.* 2008; Chevrollier *et al.* 2008; Zanna *et al.* 2008; Agier *et al.* 2012; Patten *et al.* 2014; Liao *et al.* 2017). Similarly, use of RNAi to reduce *OPA1* expression has provided key insights into the effect of OPA1 reduction on IMM cristae morphology, Ca^{2+} homeostasis and OPA1 isoform specific regulation of mtDNA maintenance (Olichon *et al.* 2003; Arnoult *et al.* 2005; Olichon *et al.* 2007; Elachouri *et al.* 2011; Kushnareva *et al.* 2013; Patten *et al.* 2014). Both of these cell models have inherent advantages for understanding OPA1 function. In particular, fibroblasts provide an ideal 2D system for understanding the diverse dynamics of mitochondrial networks, whilst RNAi studies demonstrate the adverse effects of ablating *OPA1* expression. Furthermore, both of these model systems are relatively cost-effect, easy to biologically manipulate and have high rates of replication, enabling high-throughput studies to be conducted on OPA1 dysfunction.

However, these methods also pose a number of problems for understanding the impact of *OPA1* mutation on RGC health. Firstly, these cell systems have significantly different cellular morphology when compared to RGCs, which are specialised to transmit neuronal signals within both myelinated and unmyelinated axons (Perry and Lund 1990). As such, they have expansive mitochondrial networks, with both biogenesis and clearance of mitochondrial occurring within the cell soma and distally in the axonal projections alongside with focal points of mitochondrial bioenergetics require for neuronal transmission (Amiri and Hollenbeck 2008). This is in direct comparison to fibroblasts and cell lines used for RNAi studies, which typically have highly interconnected, branched mitochondrial networks. Therefore, whether the dispersed nature of RGC mitochondrial networks plays a role in DOA pathogenesis remains to be seen. Furthermore, these models are typically unrepresentative of the levels of *OPA1* expression within DOA. Most notably, RNAi typically causes significantly higher levels of OPA1 protein reduction when compared to DOA associated *OPA1* mutations, given the majority of *OPA1* mutations

result in haploinsufficiency (Pesch *et al.* 2001; Marchbank *et al.* 2002; Schimpf *et al.* 2008; Ścieżyńska *et al.* 2017), whilst point mutations are typically associated with dominant-negative effects (Olichon *et al.* 2007; Amati-Bonneau *et al.* 2008; Huang *et al.* 2009; Yu-Wai-Man *et al.* 2010; Barboni *et al.* 2014; Kane *et al.* 2017). Therefore, it is unlikely RNAi represents the physiological levels of OPA1 dysfunction and is therefore unrepresentative of the disease mechanisms associated with OPA1 loss. Lastly, both fibroblasts and cells used in RNAi experiments do not face the same metabolic challenges as *in vivo* RGCs. Within the retina, RGCs have highly dynamic cell-cell interactions required for transmitting visual information to the brain (Levin *et al.* 2011). Integrating extrinsic signals received from bipolar cells and amacrine cells and subsequently transmitting signals through action potentials is an incredibly energy demanding process (Wong-Riley 2010). As such, these neuronal processes place high levels of demand on the mitochondrial network in order to maintain ionic and protein signalling cascades (Nelson and Jenkins 2017). Therefore, studying the impact of *OPA1* mutation in cells with rudimentary signal integration fails to recapitulate the impacts of these process on RGC health.

As with model cell lines, animal models have provided valuable insights into DOA, highlighting deficits in mtDNA maintenance, respiratory complex instability, mitochondrial morphology and bioenergetics (Alavi *et al.* 2007; Davies *et al.* 2007; Yu-Wai-Man *et al.* 2009; Chen *et al.* 2012; Cogliati *et al.* 2013; Millet *et al.* 2016; Sarzi *et al.* 2016). It is believed most rodent models of DOA provide a relatively accurate representation of the disease, resulting in optic nerve degeneration and visual impairment, whilst also providing a physiological relevant model of RGC loss and enabling modelling of common *OPA1* mutations, including the c.2708_2711delTTAG mutation (Sarzi *et al.* 2012). However, rodent modelling of DOA also has its inherent drawbacks. Of significant note, the c.2708_2711delTTAG mouse model exhibits syndromic features, including auditory failure, encephalomyopathy, ataxia and peripheral neuropathy. Although there is evidence of DOA+ associating with deletion mutations, these phenotypes typically associate with missense mutations within the GTPase domain (Yu-Wai-Man *et al.* 2010), suggesting loss of Opa1 function within this mouse model generates a severer form of optic nerve degeneration unrepresentative of the human condition. Furthermore, there is significant difference in *OPA1* expression between rodents and humans, with rodents expressing 4 distinct Opa1 isoforms compared to the 8 human OPA1 isoforms, suggesting an increase in diversity of expression in humans when compared to rodents (Akepati *et al.* 2008). How the differences in isoform expression affect disease progression in animal models is unclear, and may need further investigating when planning to understand the translation of therapeutics from these models.

Unlike the aforementioned disease models, most recently concerted efforts have been made to study the disease mechanisms associated with *OPA1* mutation through *in vitro* neuronal disease modelling. These studies have provided key insights into the effects *OPA1* mutation has on neuronal health, demonstrating increased levels of apoptosis, reduced axonal mitochondrial transport and impaired OXPHOS (Chen *et al.* 2016; Galera-Monge *et al.* 2016; Iannielli *et al.* 2018; Jonikas *et al.* 2018; Iannielli *et al.* 2019; Caglayan *et al.* 2020). Although these models provide a more physiologically relevant model for studying OPA1 function, only 20 % of all clinically diagnosed OPA1-DOA patients exhibit extraocular features (Yu-Wai-Man *et al.* 2010), suggesting that *OPA1* mutation does not have equal impact on the health of the majority of neurons. Therefore, whether the disease mechanisms discovered in these *in vitro* systems are truly representative of those associated with RGC death in DOA is unclear.

5.1.3 Aims

Although *OPA1* is constitutively expressed throughout the body, genetic mutations preferentially effect RGCs and other neuronal populations. Previous studies of model and patient-derived cell lines have demonstrated significant impairments in mitochondrial network dynamics, with both patient mutations and siRNA knockdown of OPA1 causing fragmented, dysfunctional networks (Olichon *et al.* 2003; Amati-Bonneau *et al.* 2005; Zanna *et al.* 2008). Additionally, research has demonstrated that OPA1 plays an important role in regulation of mitochondrial energy output, with impaired OPA1 function reducing levels of mitochondrial ATP synthesis (Lodi *et al.* 2004; Kushnareva *et al.* 2013). In addition, *OPA1* has been shown to facilitate mtDNA quality control, regulating the integrity and copy number of mtDNA. Research has demonstrated that *OPA1* mutation impairs this function, however current research provides conflicting evidence for this effect, with evidence for both normal and irregular mtDNA copy number. Finally, a limited number of studies have aimed to determine the effects of *OPA1* on overall mitochondrial stress, with limited evidence for increased chaperone/proteases/stress levels. However, current cell lines fail to accurately represent DOA and fail to illuminate the specific disease mechanisms effecting RGCs. Therefore, this chapter aimed to determine the effects of *OPA1* mutations on mitochondrial homeostasis, examining the effects on mitochondrial network morphology, bioenergetic capability, mtDNA integrity and the mitochondrial stress response.

Thus, the primary aims of Chapter 5 were:

1. Characterise cell type specific expression of *OPA1*.
2. Establish the effects of *OPA1* mutation on mitochondrial form through network analysis.
3. Investigate how *OPA1* mutation alters cellular bioenergetics within all generated cell lines.
4. Investigate the effects of OPA1 dysfunction on mtDNA quality control.
5. Establish a qPCR assay to assess mitochondrial stress markers.
6. Investigate the effects of *OPA1* mutation on mitochondrial stress within iPSCs and differentiated cells.

5.2 Results

5.2.1 Expression of *OPA1*

As previously reported in the literature 2708del cells have altered expression of *OPA1* when compared to WT control samples (Schimpf *et al.* 2008; Ścieżyńska *et al.* 2017). Analysis of *OPA1* expression in Chapter 3 further confirmed this effect demonstrating reduced *OPA1* levels for both 2708del cells and *OPA1*+/- iPSCs, likely driven by NMD. In addition, 1334G>A fibroblasts and iPSCs demonstrated elevated expression of *OPA1* when compared to WT control levels. However, this analysis determined expression of total *OPA1* levels rather than that of specific isoforms. Previous reports have analysed isoform specific expression of *OPA1,* demonstrating diverse expression of *OPA1* in a variety of tissues, including retina, heart and skin (Delettre *et al.* 2001). Thus, RT-PCR and qPCR were conducted to further characterise the expression of *OPA1* in fibroblasts, iPSCs, D42 RGCs and D90 retinal organoids.

Here, qPCR data sets were re-analysed by normalising all cell types to baseline expression in control WT fibroblasts, demonstrating a diverse expression pattern of *OPA1* throughout all cell and mutational types. Fibroblasts retained the expression pattern from Chapter 3, with significant reduction of 2708del *OPA1* expression and raised expression in 1334G>A cells (Figure 5.1). Comparison of iPSCs to WT fibroblasts demonstrated elevated *OPA1* expression for all cell lines relative to their corresponding fibroblast line, with an approximate 50 % increase in expression for WT, 1334G>A and 2708del iPSCs (Figure 5.1). Again, CRISPR/Cas9 edited cell lines maintained the expression pattern as seen in Chapter 3, with OPA1+/- iPSCs showing a statistically significant reduction when compared to WT iPSCs and 1334>WT1/2 iPSCs mirroring 1334G>A expression (Figure 5.1). Interestingly, both D91 retinal organoids and 2D-RGCs demonstrated a further increase in *OPA1* expression when compared to both fibroblasts and iPSCs. Retinal organoids demonstrated the largest increase in *OPA1* expression; with WT cells expressing a near 3-fold expression increase when compared to fibroblasts and a 2-fold increase when compared to WT iPSCs (Figure 5.1). Similarly, OPA1+/-, 2708del and 1334G>A retinal organoids demonstrated significant increases in *OPA1* mRNA levels (Figure 5.1). These results thus demonstrate a clear difference in *OPA1* levels across the four analysed cell types.

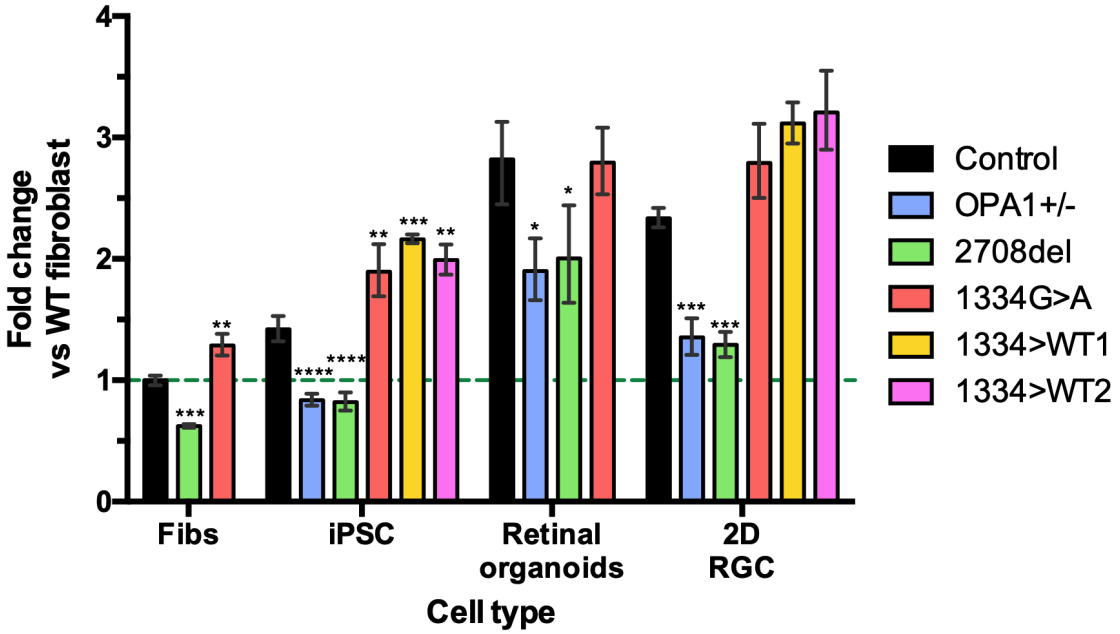

Figure 5.1. qPCR analysis of cell line and cell type specific *OPA1* expression.

RNA was extracted from fibroblasts (Fibs), iPSCs, D91 retinal organoids and D42 2D-RGCs to determine expression of total *OPA1* mRNA for each cell line. Gene expression was first normalised to *GAPDH* and *ACTIN*, and then normalised to WT fibroblasts. Error bars ± SEM. N=3-4 independent iPSC and fibroblast samples, N=5 retinal organoid and N=5-9 2D-RGC samples. Mean fold change ± SEM. ** p<0.01, *** p<0.001, **** p<0.0001 vs genotype matched fibroblasts.

To further investigate *OPA1* expression, RT-PCR primers were designed to span *OPA1* exons 3 to 9, the region of *OPA1* alternative splicing and thus generate RT-PCR products of varying sizes depending on cellular splicing events. Due to the near identical size of exons 4 (108 bp) and 5b (111 bp), only 6 distinct bands are generated by RT-PCR. Fibroblasts demonstrated consistent isoform expression across all three genotypes with *OPA1* expression dominated by transcripts at 470/473 bp (Δ4/4b and Δ4b/5b; Figure 5.2B), whilst there was also moderate expression of transcripts at 581 bp (Δ4b), 524/527 bp (Δ4 and Δ5b; Figure 5.2B). The maximal PCR product, at 635 bp (No Δ), and bands at 416bp (Δ4/5b) and 362 (Δ4/4b/5b) showed minimal levels of expression.

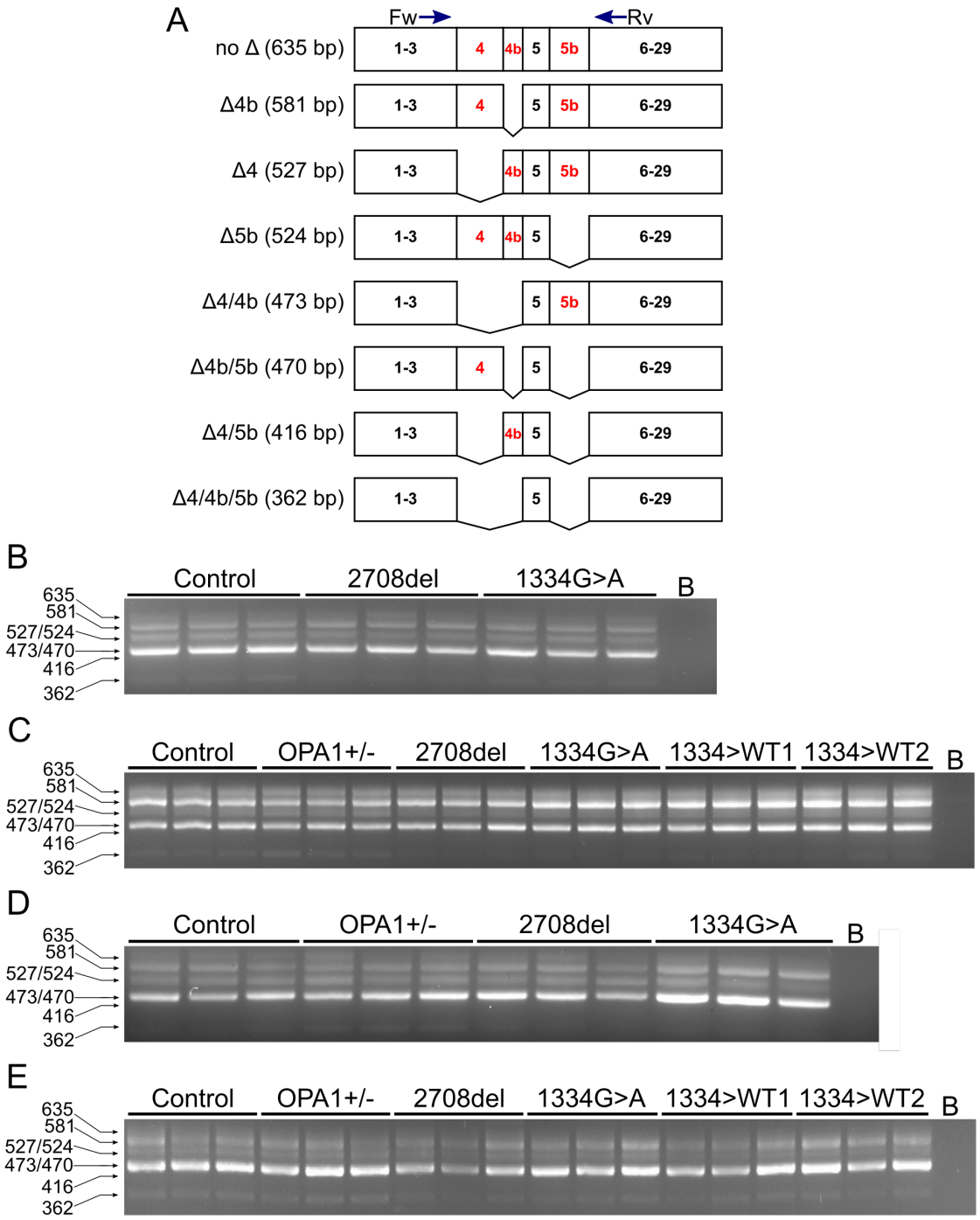

Figure 5.2. *OPA1* alternative splicing generates 8 distinct isoforms

(A) Schematic representation of *OPA1* alternative splicing events (Inspire by Delettre *et al.* (2001)), denoting PCR fragment size generated by RT-PCR. Forward (Fw) and reverse (Rv) primers were located in exon 3 and on the junction of exon 8-9, respectively.

(B-E) RT-PCR analysis of *OPA1* isoform expression in WT control, patient derived and CRISPR/Cas9 generated cell lines: fibroblasts **(B)**, iPSCs **(C)**, D91 retinal organoids **(D)** and D42 RGCs **(E)**. Each lane represents an individual cDNA sample prepared from separate RNA isolations. B = no cDNA control.

Interestingly, there was a shift in alternative splicing in iPSCs, although they retained similar expression of transcripts at 470/473bp (Δ4/4b and Δ4b/5b; Figure 5.2C) when compared to fibroblasts, there was also prominent expression of transcripts at 581 bp (Δ4b; Figure 5.2C) and a marginal increase in expression of transcripts at 635 bp (No Δ;

Figure 5.2C). iPSCs also showed negligible expression of the bands at 416 bp (Δ4/5b) and 362 bp (Δ4/4b/5b). Both D91 retinal organoids and D42 2D-RGCs showed comparable expression to that of fibroblasts, primarily expressing transcripts at 470/473 bp (Δ4/4b and Δ4b/5b; Figure 5.2D,E). However, expression appeared more variable, with some samples suggesting an increase in expression of bands at 581 bp (Δ4b).

5.2.2 *OPA1* mutation causes mitochondrial network fragmentation in fibroblasts

A number of previous reports have demonstrated dysfunctional mitochondrial networks within *OPA1* mutant cell lines (Amati-Bonneau *et al.* 2005; Zanna *et al.* 2008). Here, a semi-automated mitochondrial network pipeline was established to enable network quantification (Figure 5.3). Firstly, fibroblasts were identified with IHC using anti-TOMM20, an OMM protein, antibody. The cells were imaged on a Leica SP8 confocal microscope using Huygens deconvolution software to generate high resolution images of mitochondrial networks for image analysis (Figure 5.3A). Images were subsequently processed through FIJI image software (Figure 5.3B,C) and assessed with MiNa (Figure 5.3D-F), a semi-automated ImageJ plugin, to quantify total levels of mitochondrial fragmentation through network analysis by identifying mitochondrial networks, as well as average number of network branches and branch length and numbers of individual rod and punctae mitochondria (Figure 5.3F).

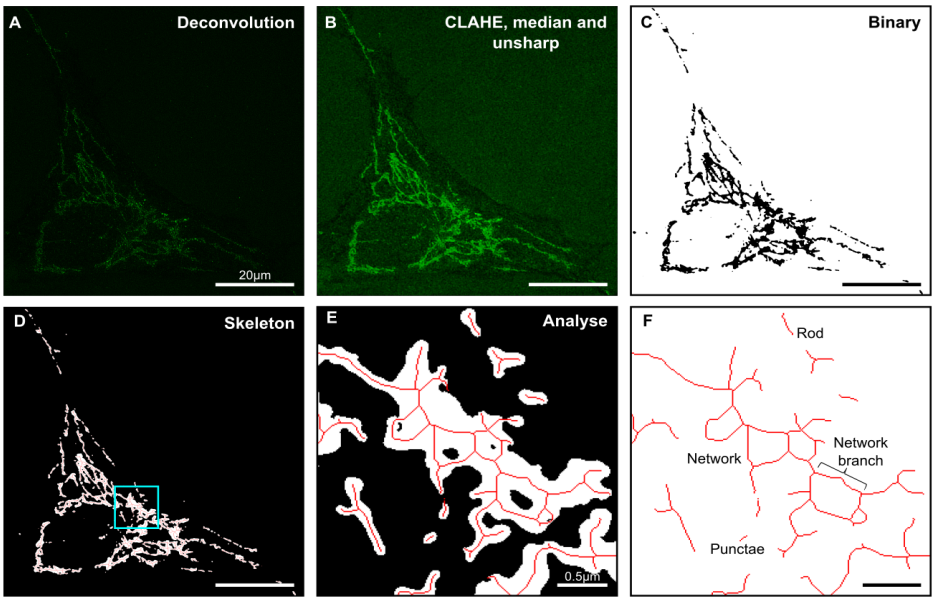

Figure 5.3. Fibroblast mitochondrial network analysis pipeline.

(**A)** Individual fibroblasts are labelled with TOMM20 antibodies and imaged via confocal microscopy before processing with image deconvolution to generate high resolution mitochondrial network images.

(B-E) Images are processed in FIJI image software to generate a skeleton of the mitochondrial network.

(E) Zoomed image of the mitochondrial network defined by the blue square in **(D)**.

(F) Skeletonised networks are analysed for the presence of networks and individual mitochondria (rod or punctae) to determine the connectivity state of the mitochondrial network. A-D, scale bars = 20 µm, E and F scale bar = 0.5 µm.

Initial qualitative assessment of fibroblasts suggested that both 1334G>A and 2708del networks were more fragmented, with a visibly greater number of small mitochondrial in contrast to control mitochondrial networks, that were typically more tubular and interconnected (Figure 5.4).

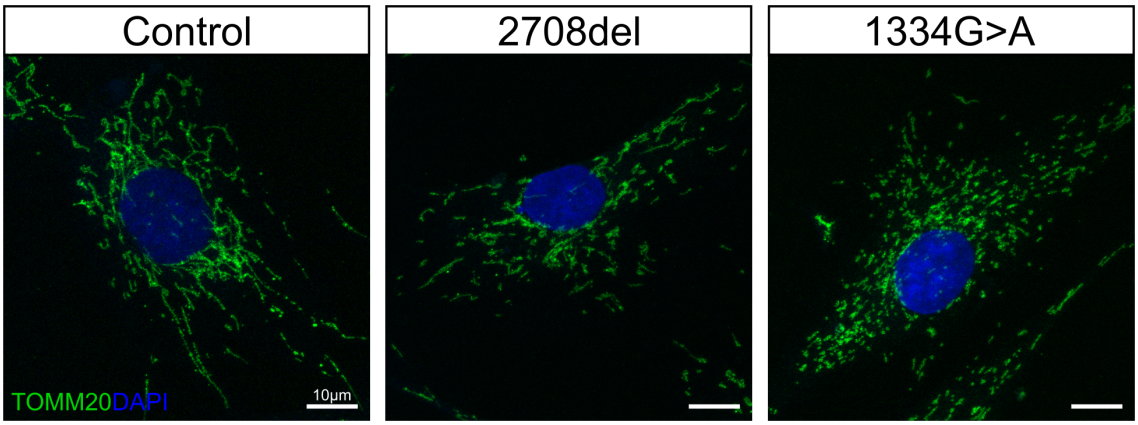

Figure 5.4. *OPA1* mutation causes disrupted mitochondrial network dynamics in patient-derived fibroblasts.

Representative confocal images of anti-TOMM20 (green) labelled control, 2708del and 1334G>A fibroblast cell lines. DAPI identifies nuclei, scale bar = 10 µm.

Subsequent analysis via the semi-automated MiNa pipeline demonstrated both 2708del and 1334G>A fibroblasts had significant levels of mitochondrial fragmentation with a greater number of total components (WT = 62.5 ± 5.4, 2708del = 99.7 ± 4.4 & 1334G>A = 121.7 ± 7.2; Figure 5.5B), individual mitochondria (WT = 47.1 ± 4.1, 2708del = 62.2 ± 3.2 & 1334G>A = 89.2 ± 4.8; Figure 5.5B) and mitochondrial networks (WT = 15.4 ± 1.9, 2708del = 37.5 ± 2.5 & 1334G>A = 32.5 ± 3.2; Figure 5.5B). Additionally, 1334G>A fibroblasts had significantly more total components and individuals when compared to 2708del fibroblasts (Figure 5.5C), suggesting the fragmentation is more severe within 1334G>A cells. Despite having more fragmented networks, both patient fibroblast lines showed no significant differences in their mitochondrial footprint when compared to control cells, suggesting fragmentation does not impact mitochondrial biogenesis (Figure 5.5A). MiNa analysis further confirmed fragmentation with both 2708del and 1334G>A fibroblasts having a reduced number of branches per network (WT = 35.9 ± 1.2, 2708del = 23.9 ± 1.2 & 1334G>A = 26.8 ± 1.1; Figure 5.5C) and a shorter length of branch (WT = 19.1 ± 2.0, 2708del = 8.6 ± 0.7 & 1334G>A = 6.8 ± 0.4; Figure 5.5D) than WT controls, indicative of a network that has fragmented into smaller pieces.

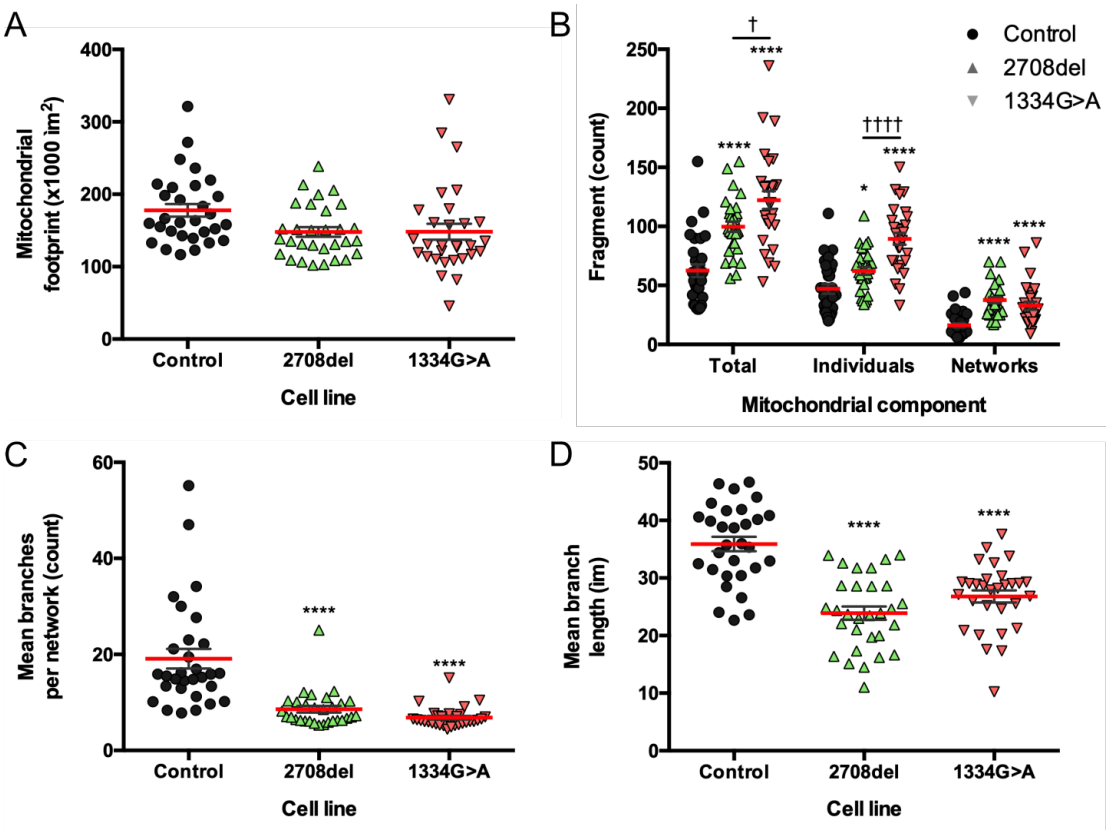

Figure 5.5. MiNa semi-automated analysis of *OPA1* mutant mitochondrial networks.

Fibroblast mitochondrial networks were identified with anti-TOMM20 immunofluorescence before analysis with MiNA to determine:

(A) Total mitochondrial network footprint.

(B) The type of mitochondrial component, determined as total components, individual mitochondria (no branches) or mitochondrial networks (branched mitochondria).

(C) The mean number of branches per mitochondrial network.

(D) Mean network branch length, the distance between two branch points.

Red bar denotes mean ± SEM. N=30 individual fibroblasts from at least 3 separate cell preparations. * $p<0.05$, **** $p<0.0001$ versus control fibroblasts. † $p<0.05$, †††† $p<0.0001$ between patient cell lines.

5.2.3 Analysis of iPSC and RGC mitochondrial networks

Following analysis of patient derived fibroblasts, assessment of all generated iPSCs was conducted using anti-TOMM20 IHC and confocal imaging. This analysis was performed to determine the downstream effects of CRISPR/Cas9 gene editing on mitochondrial networks. However, unfortunately due to the complex and compact nature of iPSC mitochondrial networks (Figure 5.6), identifying individual cellular networks and assessment through the semi-automated MiNa pipeline was not possible. As such, quantification of the iPSC mitochondrial network was not feasible.

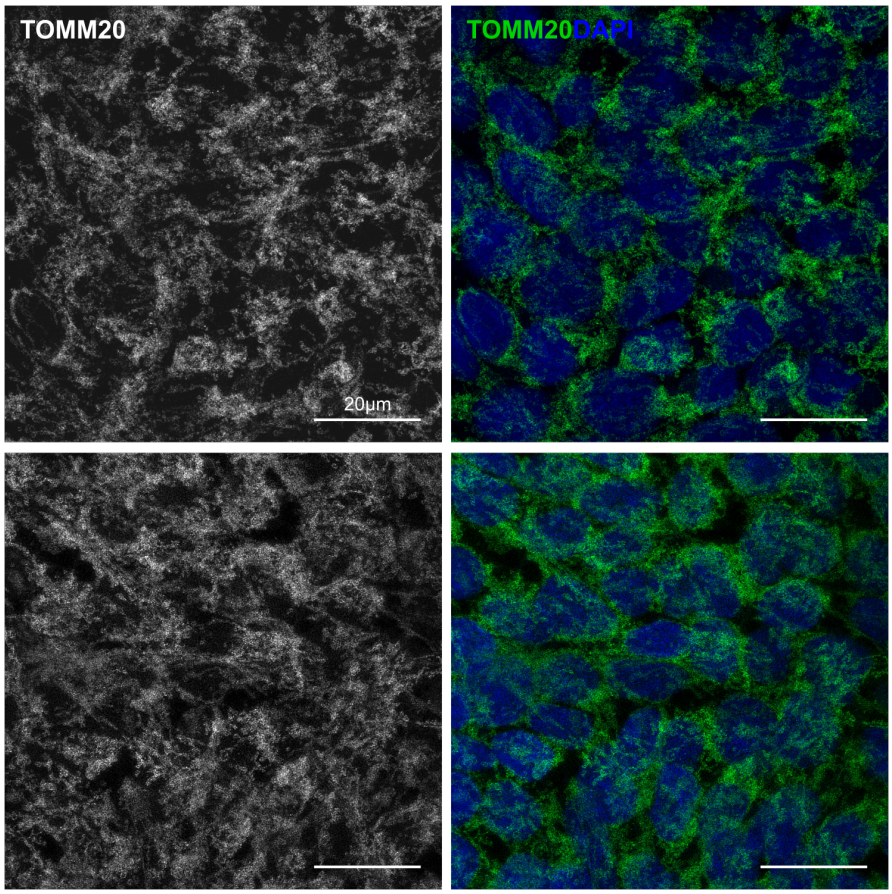

Figure 5.6. iPSC analysis of mitochondria.

Representative deconvoluted confocal images of anti-TOMM20 labelled control iPSCs. Merge with DAPI identifies nuclei, scale bar = 20 µm.

Unfortunately, due to Covid-19 it was not possible to complete characterisation of mitochondrial networks in 2D-RGC cultures.

5.2.4 Bioenergetic assessment of *OPA1* mutant cell lines

Bioenergetic profiles were generated using Seahorse XFe96 Analyser and the Seahorse Cell mito stress test kit, which measures mitochondrial respiration by determining the cellular oxygen consumption rate. Seahorse analysis enables high throughput analysis of mitochondrial respiration, and has been extensively used for the analysis of *OPA1* mutations (Chen *et al.* 2012; Samant *et al.* 2014; Millet *et al.* 2016; Del Dotto *et al.* 2017; Bocca *et al.* 2018). Thus, Seahorse bioenergetic profiling was employed within this study to determine the downstream effects of *OPA1* mutation on the respiratory function of mitochondria, enabling the determination of basal respiration, maximal respiration and ATP production through the injection of compounds that modulate mitochondrial OXPHOS. Following determination of basal respiration (the steady state of oxygen consumption before mitochondrial manipulation), cells were treated with oligomycin A, FCCP and rotenone with antimycin-A to modulate mitochondrial co (Table 5.1) and enable quantification of maximal respiration (the maximum ETC OCR when electron

transport is uncoupled from ATP production), and ATP production (OCR driven by ATP synthase activity, equivalent to ATP production).

Table 5.1. Effect of test compounds on mitochondrial ETC activity and OCR.

Compound	Affect on mitochondria	Affect on OCR
Oligomycin A	ATP synthase inhibition	Reduced electron flow through the ETC, resuting in reduced mitochondrial OCR linked to ATP production
FCCP	Mitochondrial uncoupling	Unihibited electron flow through the ETC, resulting in maximum oxygen consumption by complex IV
Rotenone & Antimycin A	Complex I & III inhibition	Total ETC inhibition, enabling determinaton of non-mitochondrial OCR

Initial assessment was completed using WT and patient-derived fibroblasts, plated at 25,000 cells per well, to determine a basal bioenergetic profile for each corresponding genotype (Figure 5.7). Analysis demonstrated significant differences between the WT control and both 2708del and 1334G>A fibroblasts bioenergetic profiles, with initial levels of OCR lower for both 2708del and 1334G>A fibroblasts. Oligomycin injection induced reduced levels of OCR whilst FCCP injection caused rapid induction of increased OCR, with both *OPA1* mutant cell lines having a lower level of maximal OCR after FCCP injection (Figure 5.7). Finally, antimycin A and rotenone injection caused a final reduction in OCR level (Figure 5.7).

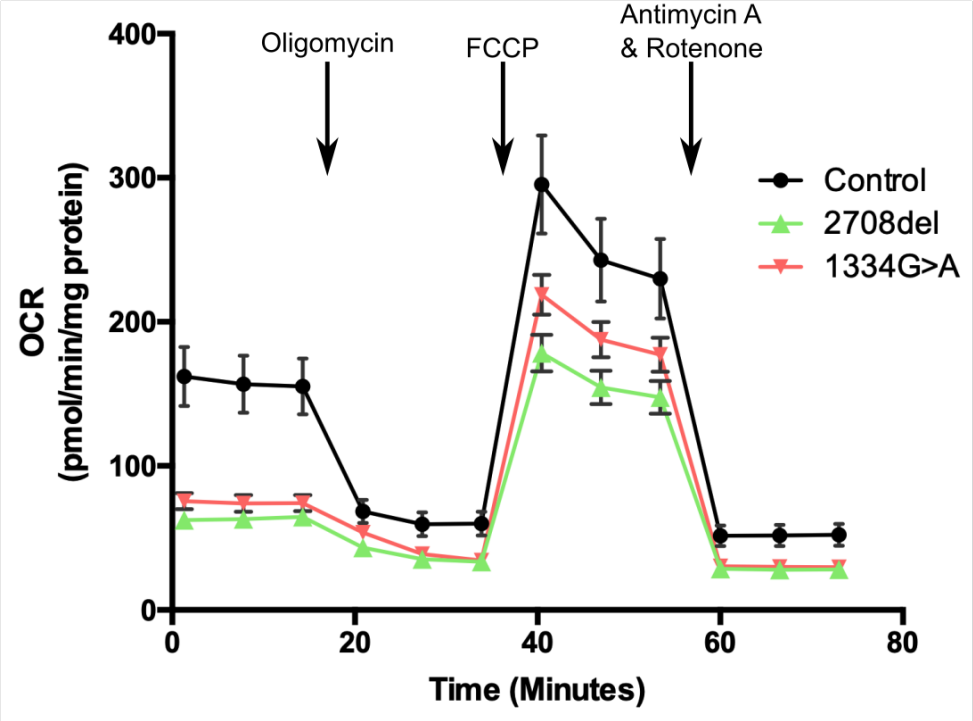

Figure 5.7. Seahorse bioenergetic profiling of *OPA1* mutant fibroblasts.

The oxygen consumption rate (OCR) was determined using the Seahorse XFe96 Analyzer for WT, 2708del and 1334G>A fibroblast lines. 1 µM oligomycin, 1 µM FCCP and 1 µM antimycin A and 1 µM rotenone were injected at designated time points. Following Seahorse analysis data was normalised to total protein via Pierce BCA assay. N=38-42 replicates per cell line, from 2 separate experiments. Symbols represent mean OCR ± SEM.

Subsequent analysis of bioenergetic profiles demonstrated that WT fibroblasts had significantly higher levels of basal respiration (Figure 5.8A), maximal respiration (Figure 5.8B) and total ATP production (Figure 5.8C), when compared to both 2708del and 1334G>A fibroblasts. Furthermore, there were no significant differences between 2708del and 1334G>A fibroblasts for any of the Seahorse assessed characteristics.

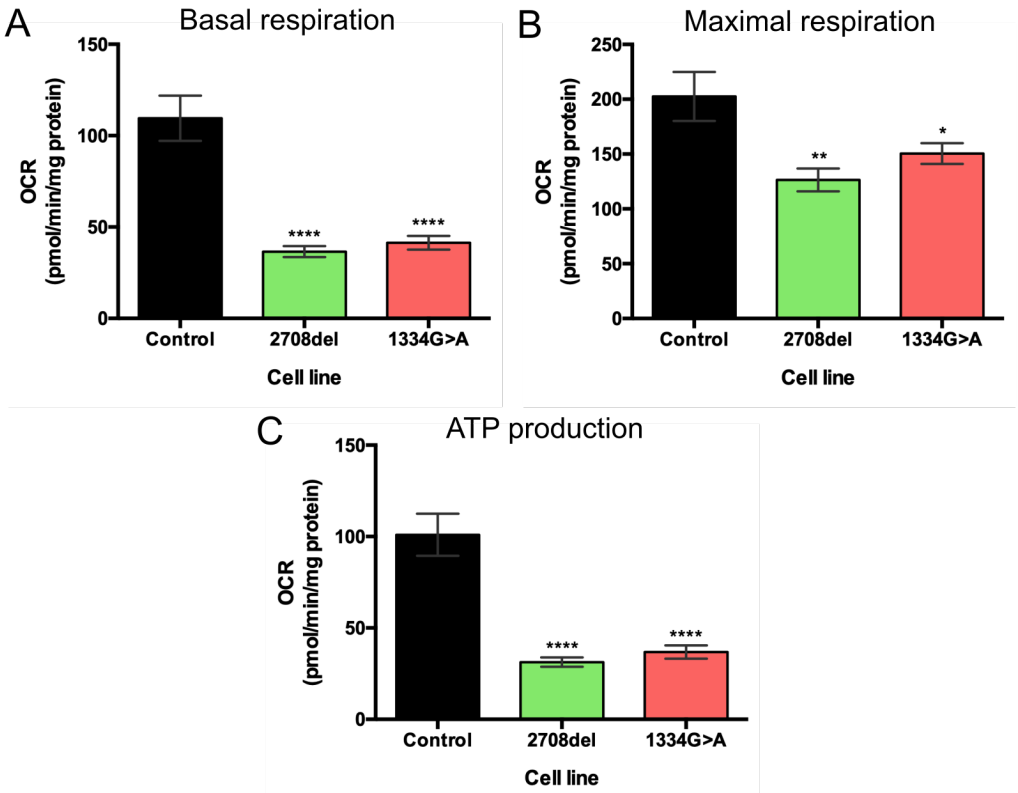

Figure 5.8. Seahorse analysis of *OPA1* mutant and control fibroblasts.

Analysis of bioenergetic profiles demonstrates the mitochondrial respiratory phenotype of fibroblasts. *OPA1* mutant cell lines have lower levels of basal respiration **(A)**, maximal respiration **(B)** and ATP production **(C)**. N=38-42 replicates per cell line, from 2 separate experiments. Bars represent mean OCR ± SEM. * p<0.05, ** p<0.01 **** p<0.0001 versus control cells.

Following fibroblast analysis, Seahorse bioenergetic profiles were generated for WT, patient-derived and CRISPR edited iPSCs, plated at 20,000 cells per well (Figure 5.9). Analysis demonstrated significant differences between the WT iPSC (control and 1334G>WT1/2) and *OPA1* mutant iPSC (OPA1+/-, 2708del and 1334G>A) bioenergetic profiles, with initial levels of OCR lower for all *OPA1* mutant cell lines (Figure 5.9). In similar fashion to the fibroblasts, oligomycin injection caused dramatic reduction in OCR level whilst FCCP caused a rapid increase in OCR. Both OPA1+/- and 1334G>A iPSCs showed reduced levels of OCR after FCCP when compared to WT and 2708del iPSCs, whilst 1334G>WT1/2 iPSCs showed increased rates when compared to WT controls (Figure 5.9). Again, antimycin A and rotenone injection caused a rapid decline in OCR rate for all iPSCs (Figure 5.9).

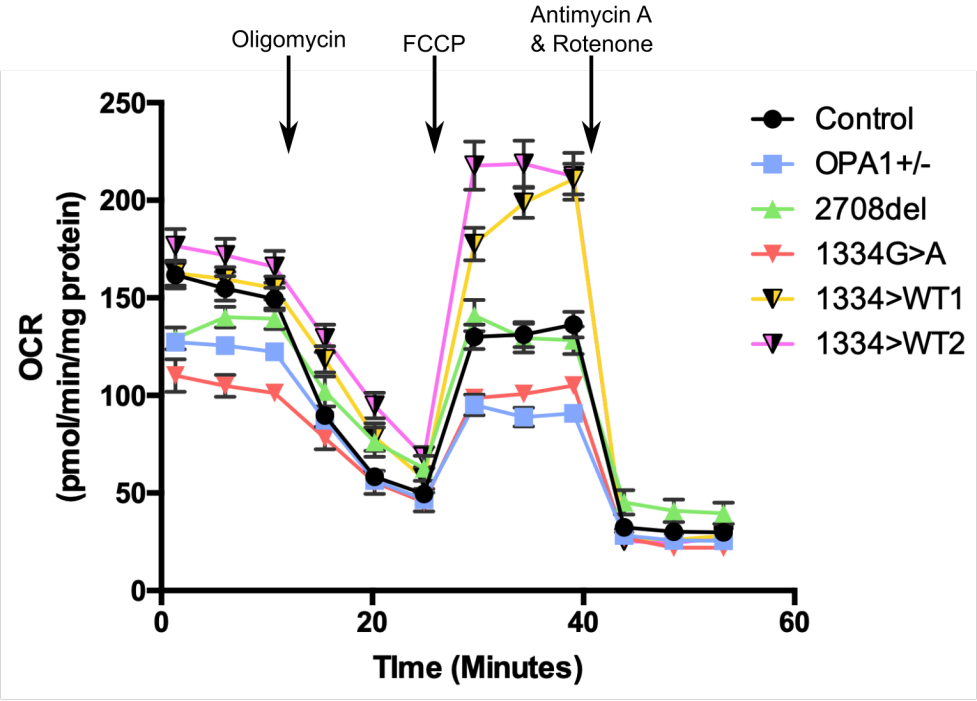

Figure 5.9. Seahorse bioenergetic analysis of iPSCs.

The oxygen consumption rate (OCR) was determined using the Seahorse XFe96 Analyzer for WT, OPA1+/-, 2708del, 1334G>A, 1334>WT1 and 1334>WT2 iPSCs. 1 µM oligomycin, 1 µM FCCP and 1 µM antimycin A and 1 µM rotenone were injected at the indicated time points. N=30-43 replicates per cell line, from 4 separate cultures. Symbols represent mean OCR ± SEM.

Analysis of bioenergetic profiles demonstrated that *OPA1* mutation caused significant deficits in iPSC basal respiration, with all three mutant iPSC cell lines showing statistically significant reductions in basal OCR levels when compared to WT iPSCs (Figure 5.10A). Interestingly, mutation type seemed to have an effect on basal OCR, with 1334G>A iPSCs also showing a reduced level of basal respiration when compared to 2708del iPSCs, and a non-significant reduction when compared to OPA1+/- iPSCs (Figure 5.10A). Correction of 1334G>A iPSCs also had a significant impact on basal respiration, with both 1334G>WT1 and WT2 iPSCs showing a significant higher level of basal OCR when compared to the patient-derived 1334G>A iPSCs, and a level equivalent to that of WT controls (Figure 5.10A). Analysis of maximal respiration demonstrated significant reductions for both OPA1+/- and 1334G>A iPSCs, but not 2708del iPSCs compared to control WT (Figure 5.10B). Of note, corrected 1334G>WT1 and WT2 iPSCs had a significant higher level of maximal respiration when compared to 1334G>A iPSCs and to the control iPSCs (Figure 5.10B). Assessment of ATP production confirmed the phenotypes found within basal and maximal respiration assessment, with OPA1+/-, 2708del and 1334G>A iPSCs having significantly reduced levels of ATP production when compared to controls (Figure 5.10C). 1334G>A iPSCs also showed significant reduced ATP production when compared to 2708del and OPA1+/- iPSCs (Figure 5.10C), whilst corrected 1334G>WT1 and WT2 iPSCs showed similar levels of

ATP production to that of WT controls and significantly increased when compared to 1334G>A iPSCs (Figure 5.10C).

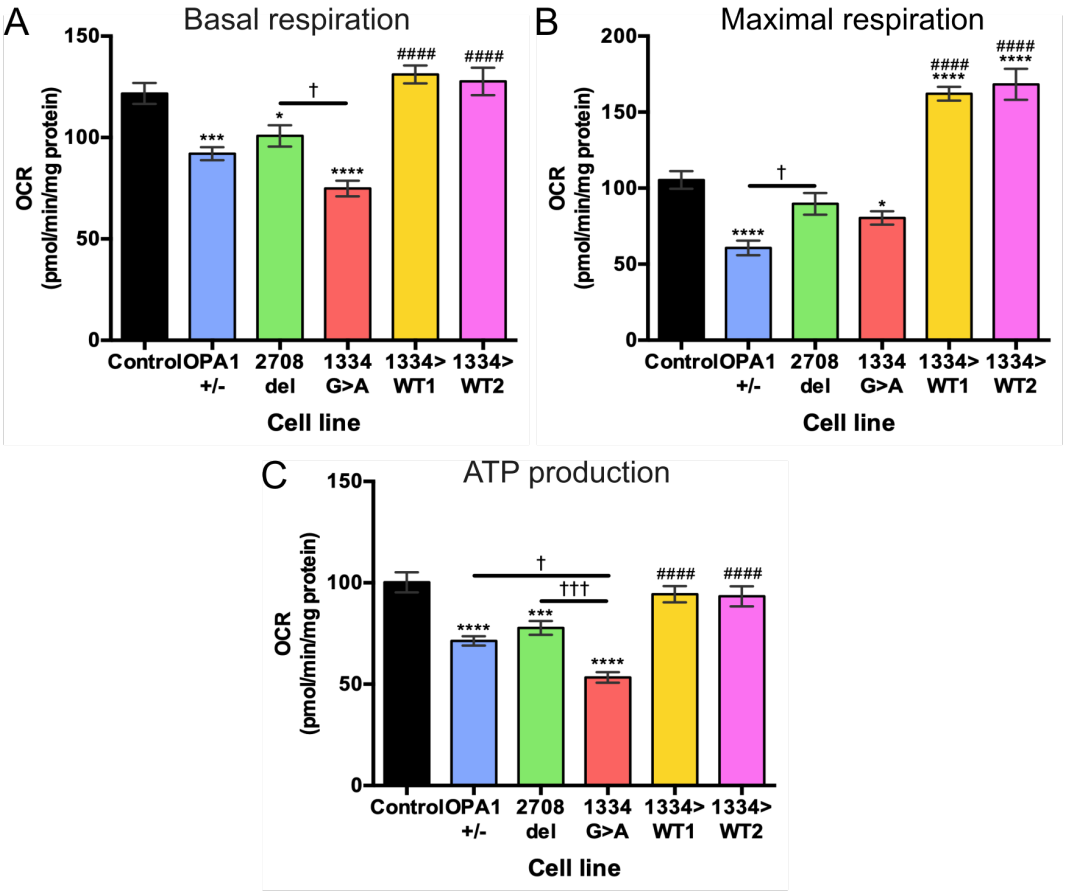

Figure 5.10. Seahorse analysis of control, patient-derived and CRISPR/Cas9 edited iPSCs.
Analysis of bioenergetic profiles reveals the respiratory phenotype of all generated iPSC lines.
(A) *OPA1* mutant cell lines have lower levels of basal respiration, OCR pre-compound injection.
(B) The level of maximal respiration, determined as the maximal OCR after FCCP injection.
(**C**) ATP production, determined as the difference between basal OCR and minimum OCR after oligomycin injection.
N=34-48 replicates per cell line, from 4 separate experiments. Bars represent mean OCR ± SEM. * p<0.05, *** p<0.001, **** p<0.0001 versus control iPSCs. #### p<0.0001 versus 1334G>A iPSCs. † p<0.05, ††† p<0.001 between cell lines as indicated.

As described in Chapter 2, upon reaching D35 of *in vitro* differentiation presumptive RGCs were enriched via neuronal cluster isolation. To enable RGC bioenergetic characterisation, RGC clusters were cultured until D40-42 in Seahorse 96-well plates coated with 1 % Matrigel. 2D-RGCs demonstrated similar trends to both fibroblasts and iPSCs, with all *OPA1* mutant cell lines demonstrating reduced OCR levels when compared to WT cell lines (Figure 5.11). Interestingly, RGCs demonstrated a less severe drop in OCR level following oligomycin injection when compared to fibroblasts and iPSCs. OCR level demonstrated a rapid increase after FCCP injection for all cell lines (Figure 5.11), with the most prominent increases in WT control, 1334>WT2 and 2708del RGCs. Intriguingly, 1334>WT1 RGCs demonstrated a lower increase in OCR level than

1334>WT2 (Figure 5.11), although this was still higher than 1334G>A RGCs. Both OPA1+/- and 1334G>A RGCs demonstrated the smallest increase in OCR level following FCCP injection (Figure 5.11). Finally, antimycin A and rotenone injection caused a decline in OCR rate for all 2D-RGCs (Figure 5.11).

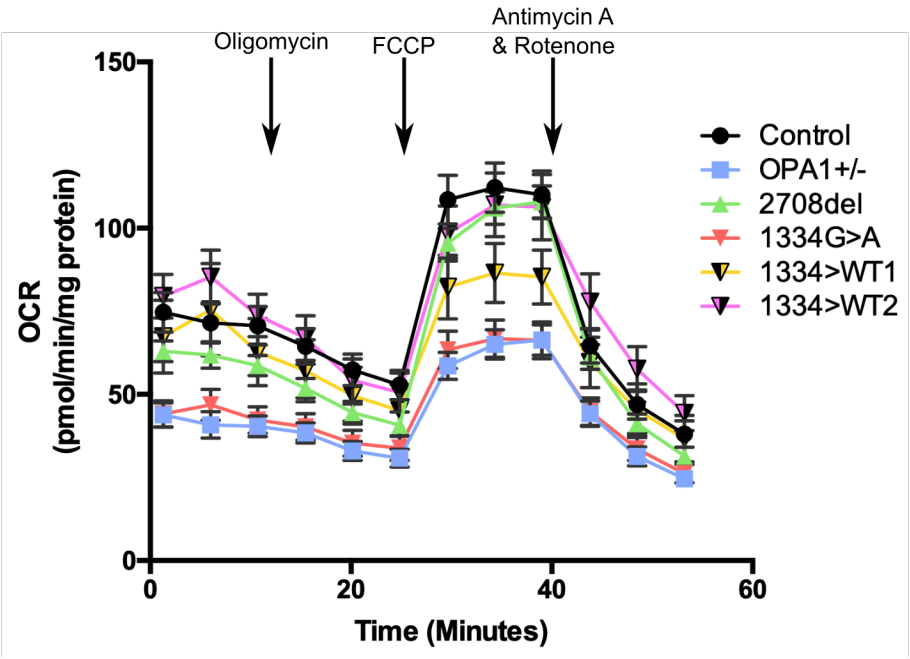

Figure 5.11. 2D-RGC bioenergetic profiling.

Oxygen consumption rate (OCR) was determined using the Seahorse XFe96 Analyzer for WT control, OPA1+/-, 2708del, 1334G>A, 1334>WT1 and 1334>WT2 iPSCs. 1.5 µM oligomycin, 1 µM FCCP and 1 µM antimycin A and 1 µM rotenone were injected at the indicated time points. N=39-66 replicates per cell line, from 3 separate *in vitro* differentiations. Symbols represent mean OCR ± SEM.

Analysis of 2D-RGC bioenergetic profiles demonstrated that *OPA1* mutation caused significant deficits in basal respiration, with all three mutant RGC lines showing statistically significant reductions in basal OCR levels when compared to WT controls (Figure 5.12A). Interestingly, 2708del RGCs also demonstrated a significantly higher level of basal respiration than both OPA1+/- and 1334G>A RGCs (Figure 5.12A). CRISPR correction of the 1334G>A mutation also had a significant impact on basal RGC respiration, both 1334>WT1 and WT2 RGCs demonstrated a significantly higher basal OCR when compared to 1334G>A RGCs (Figure 5.12A), however, 1334>WT2 RGCs maintained a reduced basal respiratory rate when compared to WT RGCs (Figure 5.12A).

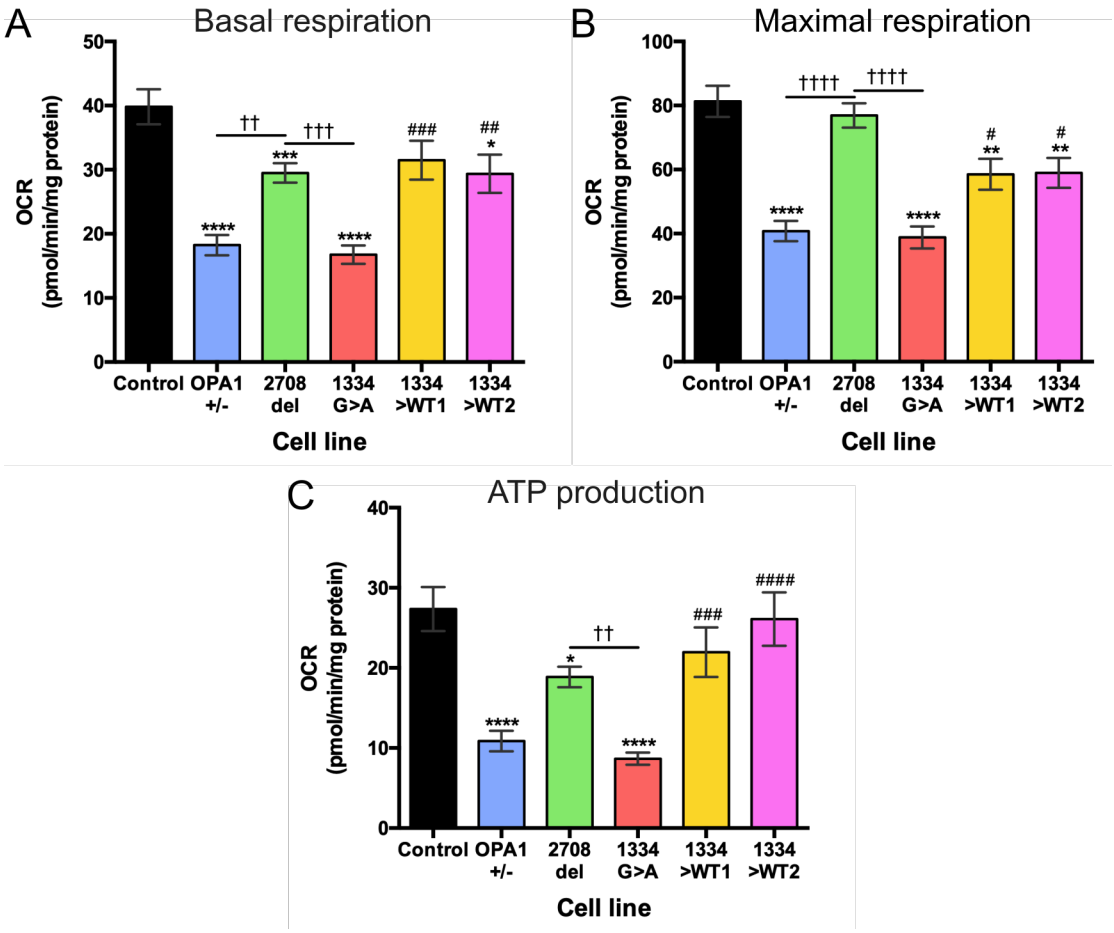

Figure 5.12. Seahorse bioenergetic analysis of control, patient-derived and CRISPR/Cas9 edited 2D-RGCs.

Analysis of bioenergetic profiles revealed the respiratory phenotype of all generated RGCs after 40-42 days of *in vitro* differentiation.

(A) *OPA1* mutant cell lines have lower levels of basal respiration when compared to WT cells.

(B) Isogenic *OPA1* mutant cell lines show reduced levels of maximal respiration, the level of OCR after FCCP injection, when compared to WT cell lines.

(C) ATP production is reduced in *OPA1* mutant cell lines, and restored with CRISPR/Cas9 gene correction of 1334G>A mutations.

N=39-66 replicates per cell line, from 3 separate differentiations. Bars represent mean OCR ± SEM. * p<0.05, ** p<0.01, *** p<0.001, **** p<0.0001 versus control RGCs. # p<0.05, ## p<0.001, ### p<0.001, #### p<0.0001 versus 1334G>A RGCs. †† p<0.01, ††† p<0.001, †††† p<0.0001 between cell lines.

Similar to iPSCs, analysis of maximal respiration demonstrated significant deficits for both OPA1+/- and 1334G>A RGCs, but no significant reduction 2708del for RGCs (Figure 5.12B). 2708del showed no significant reductions when compared to WT control RGCs, and also demonstrated significantly higher levels than both OPA1+/- and 1334G>A RGCs (Figure 5.12B). Again, 1334>WT1 and WT2 RGCs displayed significantly higher levels of maximal respiration compared to 1334G>A RGCs, however, this was significantly lower than WT control RGCs (Figure 5.12B). Analysis of ATP production further confirmed the effects of *OPA1* mutation on RGC bioenergetics, with OPA1+/-, 2708del and 1334G>A RGCs having significantly reduced levels of ATP production when compared to WT control RGCs (Figure 5.12B), whilst 2708del RGCs

also demonstrated higher levels of ATP production than 1334G>A RGCs (Figure 5.12C). CRISPR corrected 1334>WT1 and WT2 RGCs both demonstrated significantly higher levels of ATP production when compared to the patient-derived 1334G>A RGCs and unlike both basal and maximal respiration this was not significantly inferior to WT controls (Figure 5.12C).

Once Seahorse OCR profiles were established for all cell types analysis was completed to determine differences between the bioenergetic outputs. Analysis of basal respiration demonstrated significant differences between the three cell types, with iPSCs displaying the highest levels of basal respiration (Figure 5.13A). Across all six genotypes 2D-RGCs demonstrated significantly lower levels of basal OCR when compared to their genotype specific iPSCs (Figure 5.13A). Both control and 1334G>A RGCs also demonstrated significantly reduced basal respiration levels when compared to their genotype specific fibroblast lines (Figure 5.13A). Furthermore, 2708del and 1334G>A iPSCs showed significant differences to their equivalent patient-derived fibroblast cell line (Figure 5.13A).

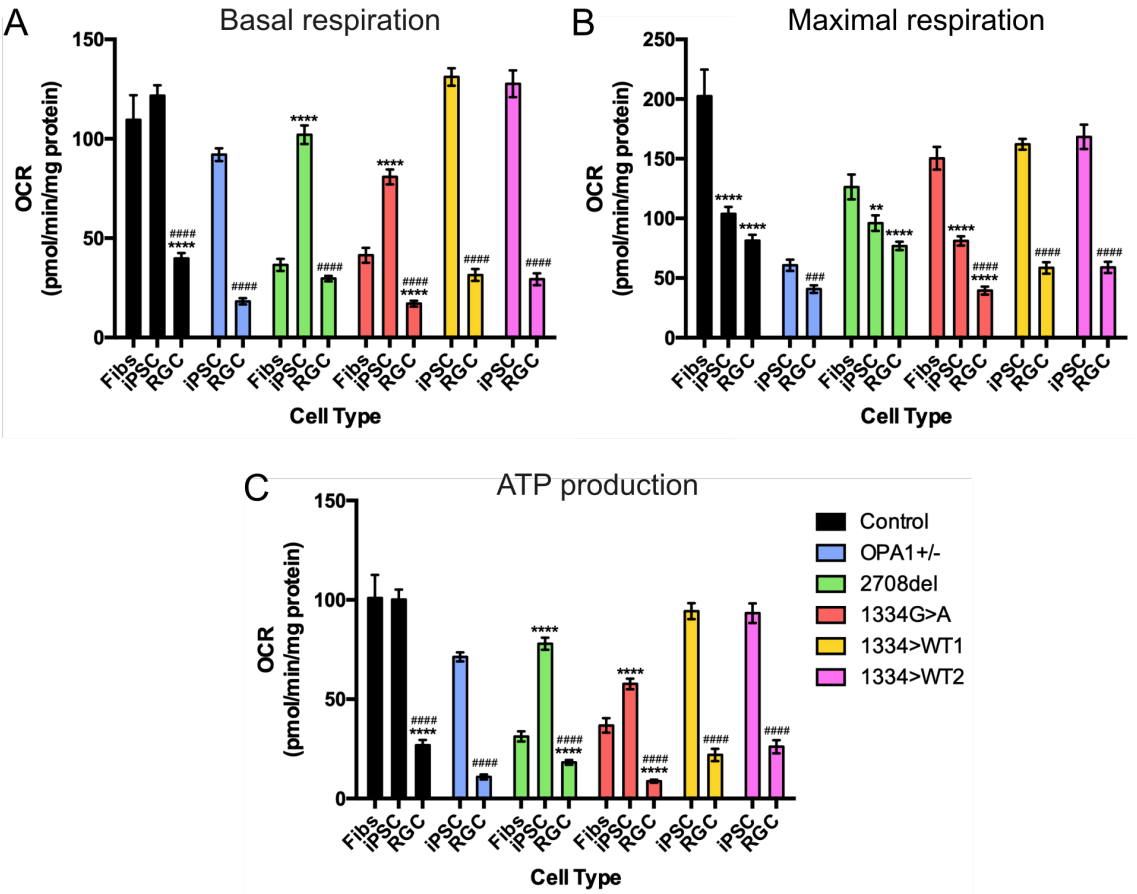

Figure 5.13. *In vitro* RGCs show lower levels of respiration and ATP production when compared to fibroblasts and iPSCs.

Seahorse bioenergetic outputs were cross-compared to determine changes to bioenergetic outputs across different cell types.

(A) Basal respiration, the level of OCR before compound injection.

(B) Maximal respiration, OCR level after injection of FCCP to uncouple mitochondrial respiration.

(C) ATP production, the difference between basal OCR and the level OCR after injection of oligomycin.

N=33-66 replicates per cell line. Bars represent mean OCR ± SEM. ** p<0.01, **** p<0.0001 versus cell line fibroblasts. ### p<0.001, #### p<0.0001 versus cell line iPSCs.

Maximal respiratory output also showed similar trends to that of basal respiration. Analysis of control, 2708del and 1334G>A genotypes demonstrated that both iPSCs and 2D-RGCs had significantly reduced maximal respiration in comparison to fibroblasts (Figure 5.13B). In addition, OPA1+/-, 1334G>A, 1334>WT1 and 1334>WT2 RGCs demonstrated significantly reduced levels of maximal respiration when compared to their genotype specific iPSC line (Figure 5.13B), whilst both control and 2708del RGCs showed a trend to reduced maximal respiration levels (Figure 5.13B). Finally, comparisons of ATP production revealed significantly lower levels of ATP production in 2D-RGCs for all genotypes when compared to their genotype specific iPSCs (Figure 5.13C). In addition, control, 2708del and 1334G>A RGCs also demonstrated significantly reduced ATP synthesis when compared to their genotype specific fibroblast lines (Figure 5.13C).

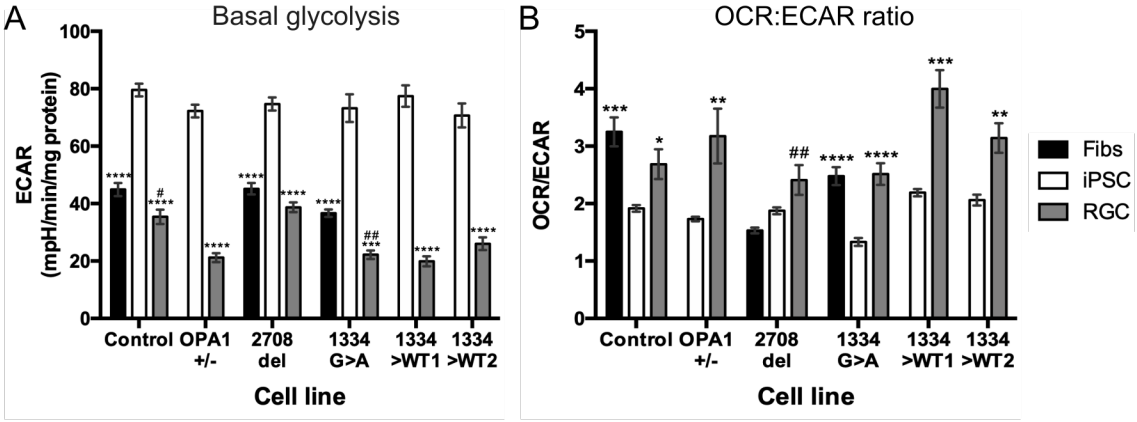

Figure 5.14. *In vitro* cell lines demonstrate differing levels of glycolysis.

(A) Seahorse determines levels of Extracellular acidification rate (ECAR), in parallel to OCR, as a measure of basal glycolytic activity. N=33-66 replicates per cell line. Bars represent mean OCR ± SEM. *** p<0.001, **** p<0.0001 versus cell line iPSCs. # p<0.05, ## p<0.01, versus cell line fibroblasts.

(B) Basal OCR:ECAR ratio was calculated to determine the levels of glycolysis and oxidative phosphorylation for each cultured cell type. N=33-66 replicates per cell line. Bars represent mean OCR ± SEM. * p<0.05, ** p<0.01, *** p<0.001, **** p<0.0001 versus cell line iPSCs. ## p<0.01, versus cell line fibroblasts.

In addition to analysis mitochondrial respiration Seahorse profiling also determines the basal levels of cellular glycolysis, measured as extracellular acidification rate (ECAR), in parallel to OCR. Analysis of ECAR for all three 2D cultured cell types demonstrated significantly higher levels of basal glycolysis for iPSCs across all genotypes, when compared to fibroblasts and 2D-RGCs (Figure 5.14A). In addition, control and 1334G>A 2D-RGCs showed a lower level of ECAR when compared to their respective fibroblast cells (Figure 5.14A). Following analysis of ECAR, the ratio of mitochondrial respiration versus glycolysis was determined by calculating the OCR:ECAR ration. This analysis demonstrated a significant shift away from glycolysis and a predominance for OXPHOS, with all genotypes except 2708del showing statistically significant OCR:ECAR changes for both fibroblasts and 2D-RGCs (Figure 5.14B). Interestingly, 2708del 2D-RGCs showed a trend to an increased OCR:ECAR ratio (p=0.066) against iPSCs, whilst fibroblasts demonstrated a non-significant reduction (Figure 5.14B).

5.2.5 Effect of *OPA1* on mtDNA

To further understand the downstream effects of *OPA1* mutation on mitochondrial homeostasis the quality and quantity of mtDNA was assessed through LR-PCR, to detect large scale deletions within the major arc of mtDNA (Figure 5.15A), and qPCR, which is more sensitive to smaller scale mtDNA alterations and enables mtDNA copy number assessment. LR-PCR assessment of fibroblast mtDNA demonstrated no detectable levels of deletion within the WT control and both 2708del and 1334G>A cells (Figure 5.15B). In addition, a mitochondrial cybrid cell line (a kind gift from Dr. Angela Pyle) was used as a positive control, demonstrating significant levels of mtDNA deletion with the

majority of the PCR product presenting at less than 3 kb and a faint band at 10 kb (Figure 5.15), indicative of mtDNA with a substantial level of deletion in the major arc.

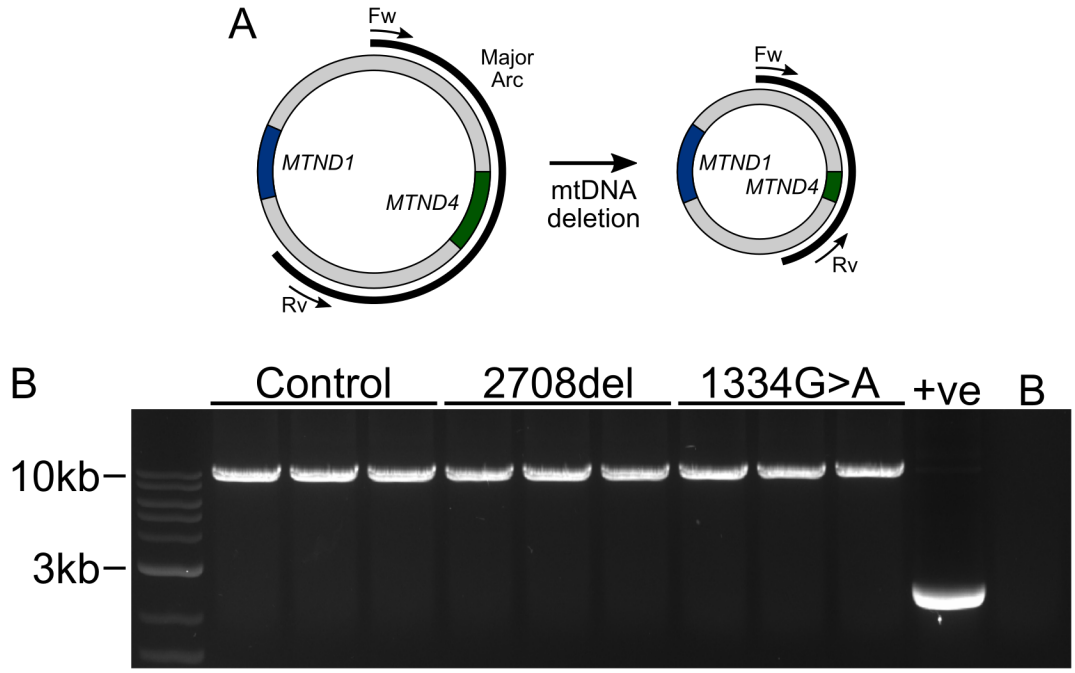

Figure 5.15. LR-PCR analysis of WT and *OPA1* mutant fibroblasts.

(A) Schematic of LR-PCR mtDNA analysis. Forward (Fw) and reverse (Rv) primers target the major arc of mtDNA. mtDNA deletion commonly occurs within the major arc, large scale mutations or deletions significantly reduce its size enabling detection of unstable mtDNA. Inspired by Yu-Wai-Man *et al.* (2009).

(B) MtDNA was expanded with primers targeting a 9.9 kb region in the major arc of mtDNA. No significant levels of deletion were detected in WT control or either 2708del or 1334G>A fibroblast cell lines. Each lane represents an individual sample of DNA. +ve denotes cybrid cell DNA. B = no DNA control.

In addition to LR-PCR, qPCR analysis was utilised to further assess the quality of mtDNA by determining the ratio of WT mtDNA copies to deleted mtDNA copies (henceforth the WT mtDNA percentage) through comparison of *MTND1* (WT mtDNA) and *MTND4* (deleted mtDNA) gene quantities (Figure 5.16A). In addition, the total mtDNA copy number (number of mtDNA per nuclear genome) was determined through comparisons of *MTND1* and nDNA quantity, determined from the geometric mean of *GAPDH* and *B2M* (He *et al.* 2002; Markaryan *et al.* 2010; Yu-Wai-Man *et al.* 2010; Rooney *et al.* 2015). To determine if mtDNA qPCR could accurately detect mtDNA deletion, or reduced WT mtDNA percentage, WT fibroblast and iPSC lines were compared to cybrid mtDNA. Similar to LR-PCR, qPCR analysis demonstrated significant levels of mtDNA deletion in the cybrid cell line, with only 27.2 ± 1.9 % WT mtDNA when compared to both the WT fibroblasts (100.0 ± 29.5 % WT mtDNA) and iPSCs (102.8 ± 16.8 % WT mtDNA; Figure 5.16B).

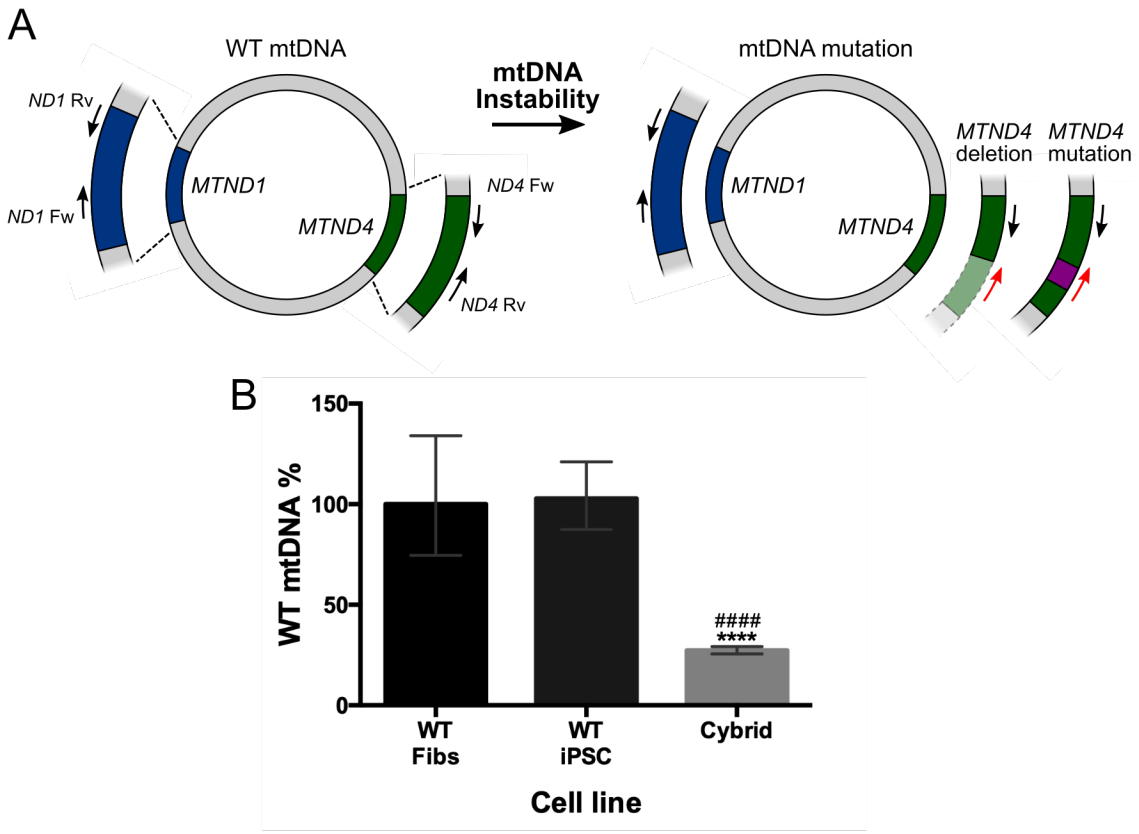

Figure 5.16. Mitochondrial cybrid cells display high levels of mtDNA deletion.

(A) Schematic of mtDNA quantification by qPCR. Both *MTND1* and *MTND4* are analysed to determine the level of WT mtDNA molecules. The mitochondrial major arc commonly acquires mutations, disrupting mtDNA sequence through deletion or mutation preventing primer binding (red arrows) and reduced quantification by qPCR.

(B) qPCR analysis of *MTND1* and *MTND4* genes enabled quantification of WT mtDNA percentage (%). Bars represent average WT mtDNA % ± SEM. N=4 samples per cell line, **** $p<0.0001$ versus WT fibs, #### $p<0.0001$ versus WT iPSCs.

Subsequent analysis of patient-derived fibroblasts demonstrated both 2708del and 1334G>A fibroblasts demonstrated a significant level of mtDNA deletion, with a reduction to 86.3 ± 6.3 % and 87.3 ± 1.8 % WT mtDNA levels in 2708del and 133G>A cells respectively, when compared to WT controls (Figure 5.17B). Copy number analysis, the total number of mtDNA copies per nDNA, demonstrated no significant changes amongst the three cell lines (Figure 5.17B).

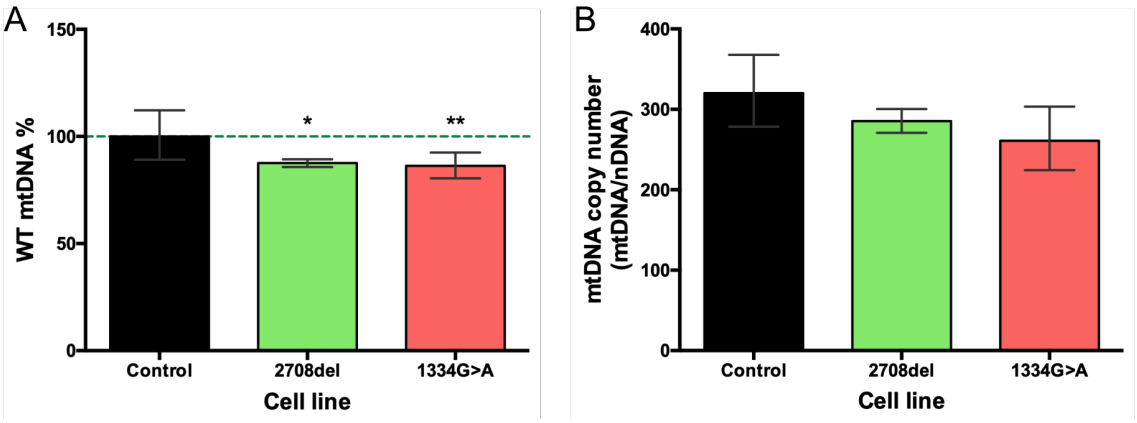

Figure 5.17. qPCR analysis of mtDNA in *OPA1* mutant fibroblasts.

(A) Analysis of *MTND1* and *MTND4* genes a reduced level of WT mtDNA in 2708del and 1334G>A cell lines. Bars represent mean mtDNA ± SEM. N=5-6 individual DNA samples per cell line. *p<0.05, **p<0.01 versus control cells.

(B) qPCR quantification of mtDNA copy number via determination of *MTND1* and nDNA (Geometric mean) levels. Bars represent mean mtDNA ± SEM. N=5-6 individual DNA samples per cell line.

LR-PCR analysis of control, patient-derived and CRISPR-edited iPSCs demonstrated no apparent mtDNA deletion, with no clear mtDNA PCR products visible below the 10 kb WT product (Figure 5.18A). qPCR analysis demonstrated significant levels of mtDNA deletion in 2708del and 1334G>A iPSCs when compared to control iPSCs, with a reduction to 86.6 ± 5.5 % and 83.8 ± 5.5 % WT mtDNA levels respectively (Figure 5.18B). Interestingly, CRISPR/Cas9 gene editing of *OPA1* had a significant impact on mtDNA quality. Both CRISPR-corrected 1334G>WT1 and WT2 iPSC lines showed restored levels of WT mtDNA back to that of WT control cells, showing 98.5 ± 4,3 % and 99.4 ± 6.7 % WT mtDNA levels respectively, a significant increase when compared to 1334G>A iPSCs (Figure 5.18B). Furthermore, OPA1+/- iPSCs showed a trend to reduced WT mtDNA levels, with 90.4 ± 9.5 % WT mtDNA respectively, although this did not show a statistically significance against WT control iPSCs ($p = 0.07$). Copy number analysis of all 6 iPSC cell lines demonstrated no significant differences amongst the cell lines (Figure 5.18C).

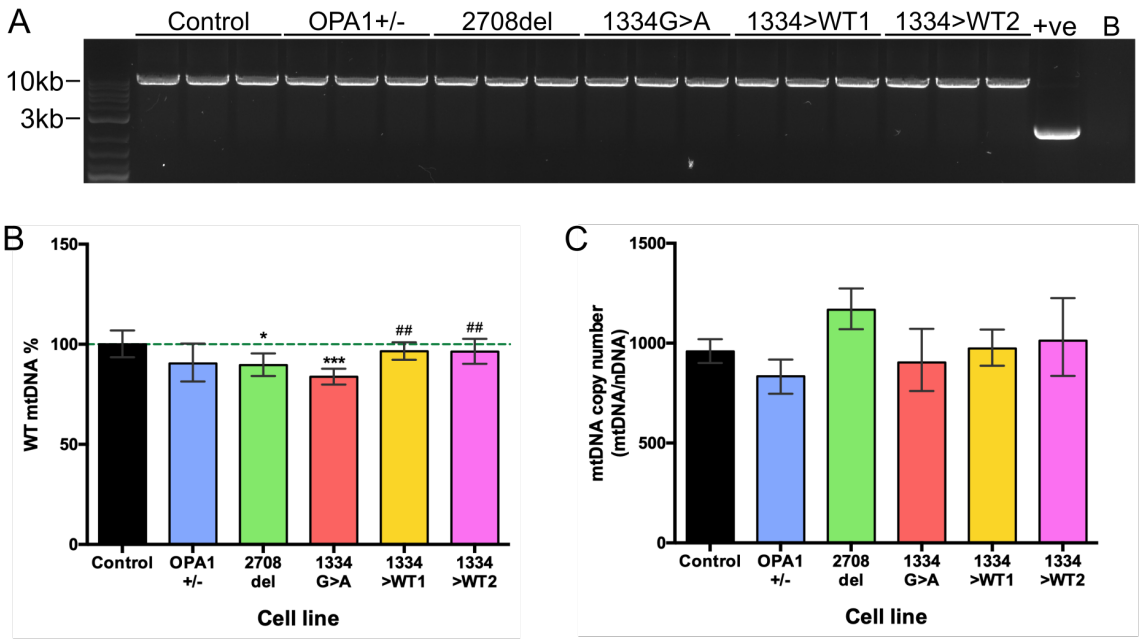

Figure 5.18. Analysis of iPSC mtDNA quantity and quality by LR-PCR and qPCR.

(A) LR-PCR analysis shows no clear evidence of large scale mtDNA deletions for any of the 6 iPSC cell lines.

(B) Patient derived 2708del and 1334G>A iPSCs show evidence of reduced WT mtDNA levels when compared to WT controls. Correction of 1334G>A mutation via CRISPR/Cas9 restores mtDNA quality back to WT levels. Bars represent mean ± SEM. * $p<0.05$, *** $p<0.001$ versus control iPSCs. ## $p<0.01$ versus 1334G>A iPSCs.

(C) *OPA1* mutation has no effect on mtDNA copy number in iPSCs. N=6 samples per cell line. Bars represent mean ± SEM.

To determine the effect of *OPA1* mutation on mtDNA in RGCs both D90 retinal organoids and D42 2D-RGCs were analysed via LR-PCR and qPCR. LR-PCR analysis confirmed the absence of larger scale mtDNA mutations, with a clear band produced at 10 kb and no further PCR products observed in the gel (Figure 5.19A). Following LR-PCR, qPCR analysis demonstrated significant levels of mtDNA deletion in both 2708del and 1334G>A RGCs when compared to WT RGCs (Figure 5.19A), with 92.7 ± 19.3 % and 91.8 ± 22.3 % versus 100.0 ± 15.5 % WT mtDNA levels respectively (Figure 5.19C). No significant differences were detected in OPA1+/- RGCs. As with iPSC mtDNA levels, CRISPR/Cas9 corrected 2D-RGCs showed restored levels of WT mtDNA, with 1334>WT1 and 1334>WT2 RGCs showing 99.3 ± 19.7 % and 101.4 ± 43.2 % WT mtDNA levels respectively (Figure 5.19C). Retinal organoids also exhibited similar WT mtDNA levels. WT retinal organoids showed a WT mtDNA level of 100.0 ± 21.45 % (Figure 5.19E). OPA+/- retinal organoids showed no evidence of reduced WT mtDNA levels. Both 2708del and 1334G>A retinal organoids demonstrated reduced levels of WT mtDNA levels, exhibiting 88.9 ± 10.9 % and 89.3 ± 9.2 % respectively (Figure 5.19E). There were no significant changes to mtDNA copy number in either 2D-RGCs or 3D retinal ganglion cells (Figure 5.19D,F).

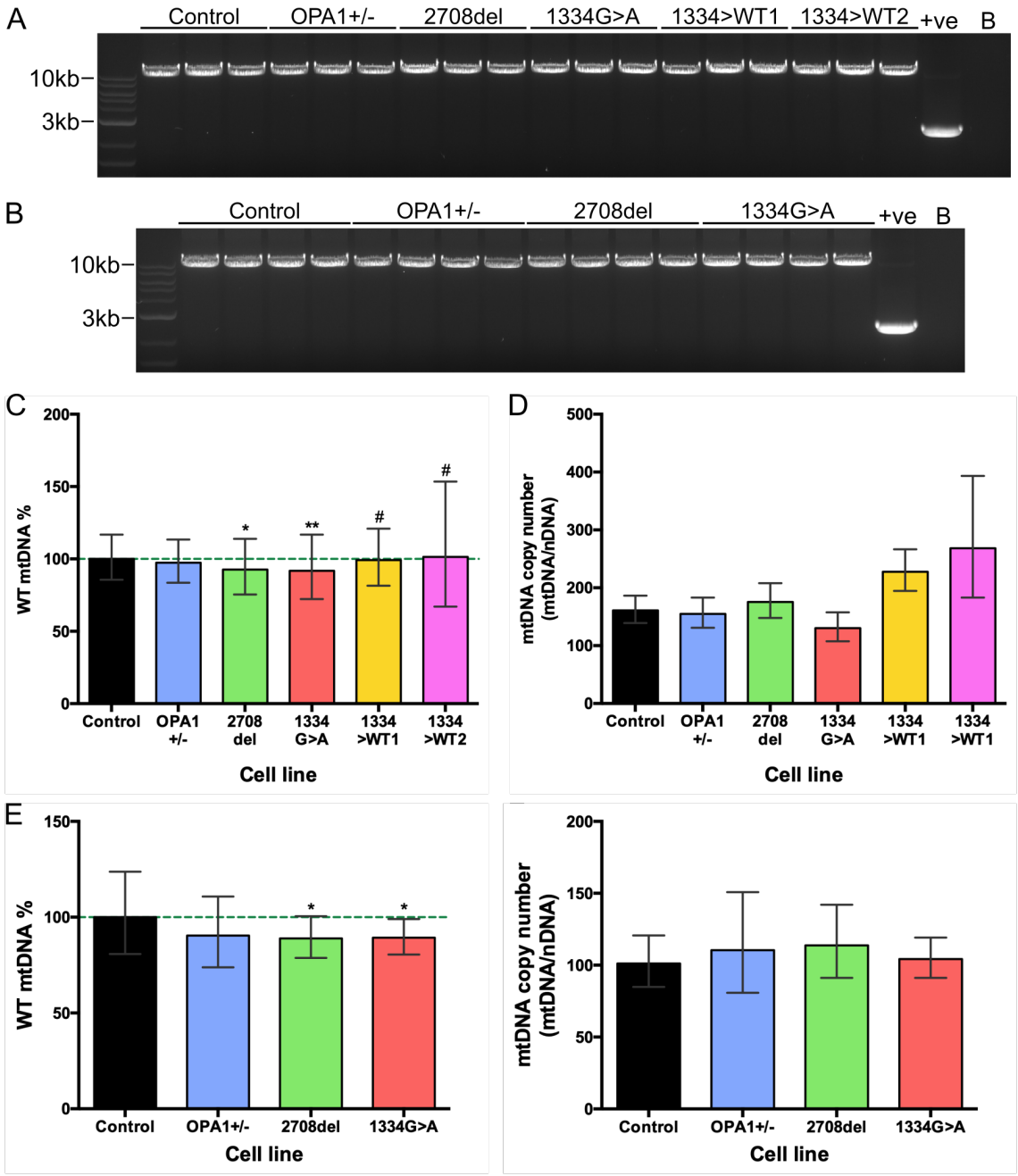

Figure 5.19. Analysis of mtDNA in WT, patient-derived and CRISPR edited 2D-RGCs and retinal organoids.

(A,B) A 9.9 kb region spanning the major arc of mtDNA was expanded via LR-PCR. No significant levels of mtDNA deletion were detected in either D42 2D-RGCs **(A)** or D91 retinal organoids **(B)**. Each lane represents an individual DNA sample. +ve denotes cybrid cell line with known mtDNA deletion.

(C) qPCR analysis of 2D-RGCs revealed reduced levels of WT mtDNA in 270del and 1334G>A cells, whilst CRISPR corrected 1334>WT1 and WT2 returned to WT levels.

(D) No significant changes in mtDNA copy number were detected in 2D-RGCs.

(E) Analysis of WT mtDNA levels in D91 retinal organoids revealed significant reductions in both 2708del and 1334G>A organoids.

(F) Analysis of D91 retinal organoids revealed no changes in mtDNA copy number.

Bars represent mean ± SEM. N=3-8 individual 2D-RGC. N=5 individual 3D retinal organoids. * $p<0.05$, ** $p<0.01$ versus control cell lines. # $p<0.05$ versus 1334G>A samples.

5.2.6 Dysfunctional OPA1 and the mitochondrial stress response

To determine if it was possible to assess the mitochondria stress response *in vitro*, mitochondrial stress was induced within WT iPSCs through treatment with 2.5 µM oligomycin A, to induce respiratory chain dysfunction by inhibiting ATP synthase function, for 18 hours before RNA extraction and first strand cDNA synthesis. Subsequently a panel of genes associated with mitochondria stress signal transduction, notably *ATF4*, *ATF5*, *DDIT3*, *CEBPB* and *NRF1*, and downstream effector proteins, *HSPA9*, *HSP60* (*HSPD1*), *SIRT3*, *SOD2* and *HTRA2*, were assessed by qPCR to determine their fold change compared to untreated iPSCs (Figure 5.20). Oligomycin treatment of iPSCs caused significant levels of upregulation in 10 out of 11 genes assessed, with only *HSP60* not demonstrating significant levels of fold change in oligomycin treated cells. Interestingly, genes involved in mitochondrial stress signalling, including *ATF5*, *DDIT3* and *CEBPB,* showed a more marked response when compared to downstream effector genes, such as *SIRT3*, *HSPA9*, *SOD2* and *HTRA2* (Figure 5.20), suggesting that Oligomycin treatment causes greater changes at the transcriptional level before promoting changes in effector proteins. Importantly, these data suggest assaying mitochondrial stress responses is feasible via qPCR.

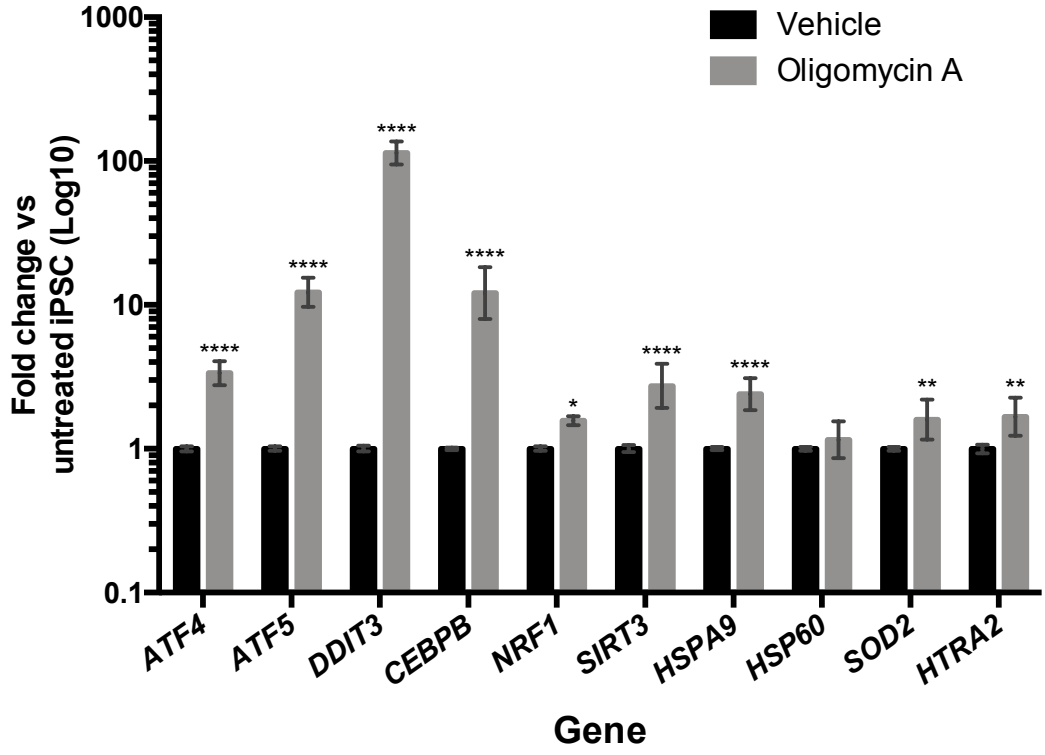

Figure 5.20. Treatment of iPSCs with oligomycin induces the mitochondrial stress response.

WT iPSCs were treated with 2.5 µM Oligomycin A or vehicle for 18 hours before assessment of mitochondrial stress associated genes by qPCR. Expression was first normalised to the geometric mean of two reference genes, *GAPDH* and *ACTIN*, before normalisation to untreated iPSCs. N=3 samples from 2 individual treatments. Bars represent mean fold change ± SEM. * $p<0.05$, ** $p<0.01$, **** $p<0.0001$ versus untreated iPSCs.

Following assessment of oligomycin induced stress, all 6 generated iPSCs were analysed via qPCR to determine if *OPA1* mutation induced mitochondrial stress and whether CRISPR/Cas9 gene editing had any detrimental or beneficial impacts. Analysis demonstrated a significant level of increased expression for the majority of genes for 1334G>A iPSCs when compared to both endogenous WT and CRISPR corrected 1334>WT1 and WT2 iPSCs. Notably, there was significant upregulated expression for signal cascade genes *ATF4*, *ATF5*, *CEBPB*, *SIRT3* and *DDIT3* versus WT cell lines (Figure 5.21A,B,C,D,I). In addition, 1334G>A iPSCs also showed increased expression compared to 2708del and OPA1+/- iPSCs, suggesting missense mutations may drive higher levels of mito-stress than mutations primarily causing haploinsufficiency (Figure 5.21A,B,C,D,I). Interestingly, 1334G>A iPSCs also showed increased expression of mitochondrial chaperones and proteases, including *HSPA9*, *HSP60* and *HTRA2*, versus WT cell lines, although these changes were of lower magnitude when compared to those of signalling transcription factors (Figure 5.21E,F,G). *SOD2* expression did not show expression patterns consistent with the other assessed genes, with significantly elevated expression for 2708del iPSCs when compared to WT control iPSCs, whilst it showed no significant increase for any other cell line (Figure 5.21J).

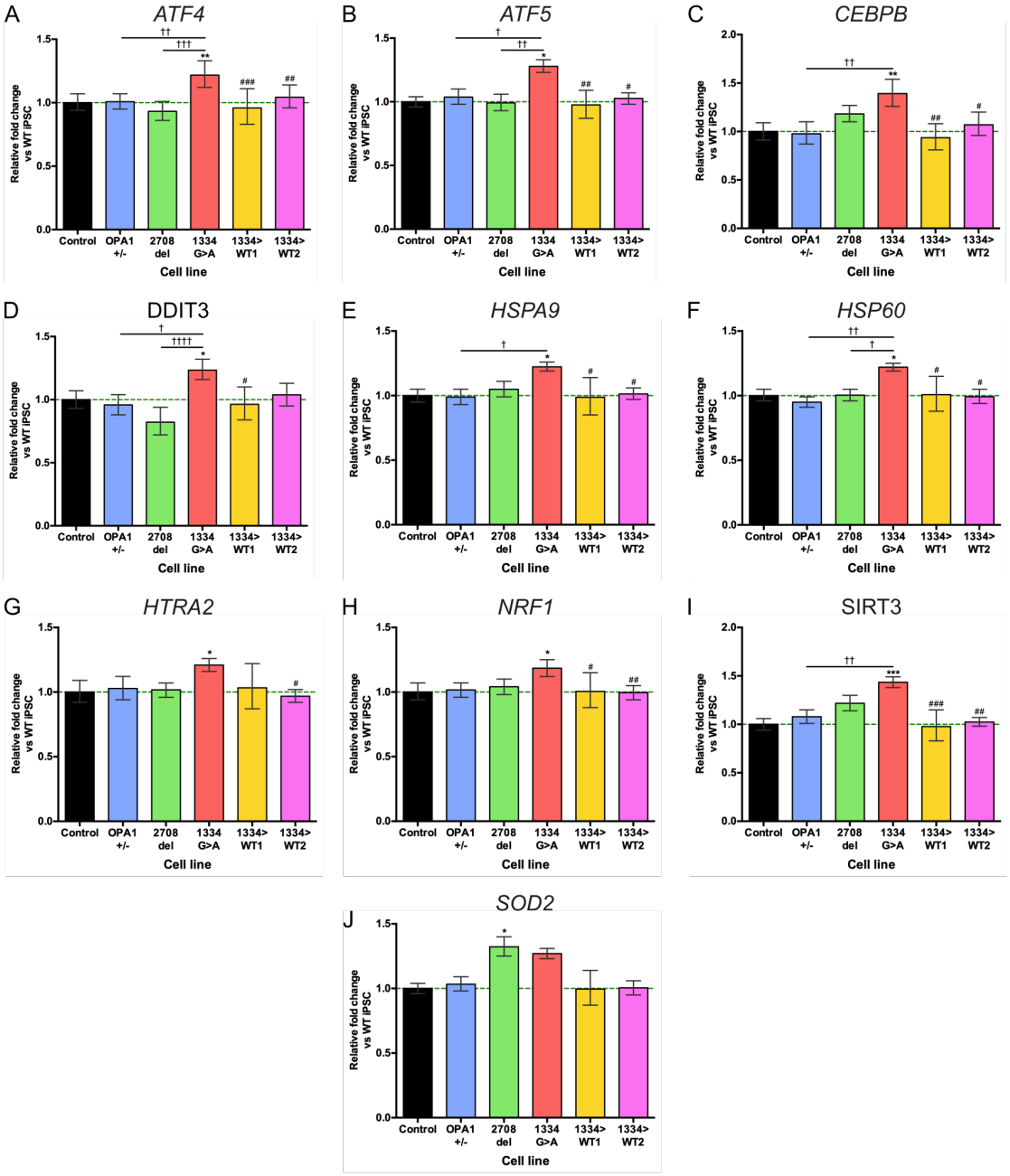

Figure 5.21. qPCR assessment of mito-stress associated genes in iPSCs.

iPSCs were assessed for expression of mito-stress associated genes **(A-J)**. Expression was first normalised to the geometric mean of two reference genes, *GAPDH* and *ACTIN*, before normalisation to isogenic WT cell lines. 1334G>A iPSCs were normalised to the average expression of both 1334>WT1 and WT2 cells. 2708del iPSCs were normalised to the average expression of WT control, 1334>WT1 and 1334>WT2 cells. N=6 individual RNA samples per cell line. Bars represent mean fold change ± SEM. * p<0.05, ** p<0.01, *** p<0.001 versus control iPSCs. # p<0.05, ## p<0.01, ### p<0.001, versus 1334G>A iPSCs. † p<0.05, †† p<0.01, ††† p<0.001, †††† p<0.0001 between cell lines.

To assess the effect of *OPA1* mutation on RGC mitochondrial stress responses, RNA was extracted from D91 retinal organoids for qPCR. Analysis of mito-stress genes demonstrated a significant level of increased expression for a number of genes, although not as many as in iPSCs. Unlike iPSCs, *ATF4*, *DDIT3*, *HTRA2*, *NRF1* and *SIRT3* all showed no statistically significant changes in expression for *OPA1* mutant retinal organoids versus WT controls. However, *ATF5*, *HSPA9*, and *HSP60* all showed

significantly higher levels of expression in 1334G>A organoids than the WT control (Figure 5.22B,E,F). In addition, 1334G>A retinal organoids also showed a trend towards upregulated *CEBPB* expression against WT controls, although this was not significant (p=0.0549; Figure 5.22C). Furthermore, 2708del retinal organoids showed a significant upregulation of *CEBPB* and *HSPA9* against WT organoids (Figure 5.22C,E), whilst *SOD2* showed a similar pattern to that of iPSCs, with significantly higher levels of expression in 2708del organoids compared to WT, OPA1+/- and 1334G>A organoids (Figure 5.22J).

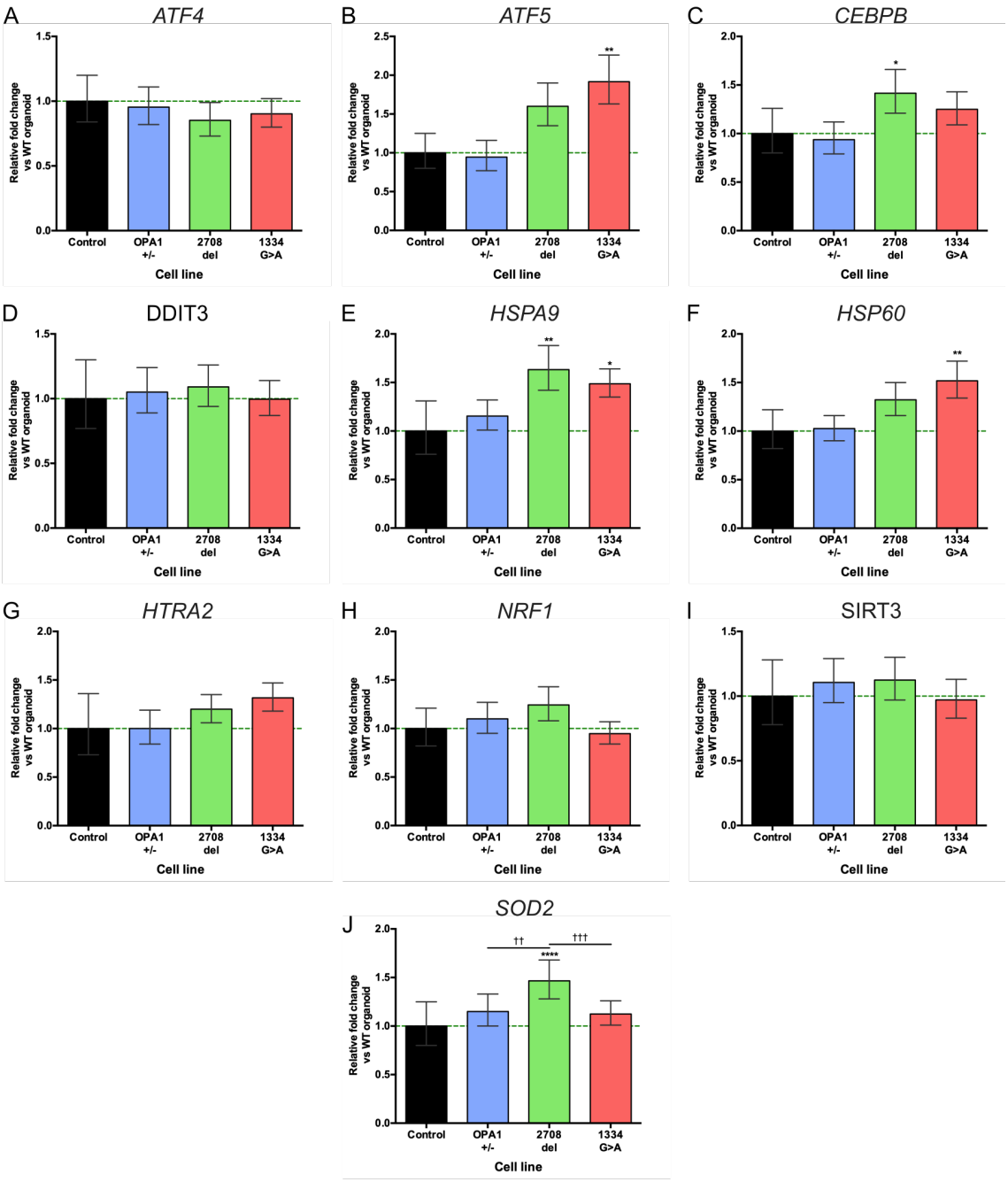

Figure 5.22. qPCR assessment of mito-stress genes in retinal organoids.

D91 retinal organoids were assessed for expression of mito-stress associated genes **(A-J)**. Expression was first normalised to the geometric mean of two reference genes, *GAPDH* and *ACTIN*, before normalisation to WT retinal organoids. N=4-7 individual retinal organoids per cell line. Bars represent mean fold change ± SEM. * p<0.05, ** p<0.01, **** p<0.0001 versus control retinal organoids. †† p<0.01, ††† p<0.001 between cell lines.

Although retinal organoids represent a more physiologically holistic model of retinal physiology, 2D-RGC cultures were also analysed via qPCR to further establish if *OPA1*-induced mito-stress preferentially impacts RGCs. Interestingly, 2D-RGCs showed the lowest number of significantly upregulated genes, with overall expression markedly more variable than both iPSCs and retinal organoids for the panel of genes assessed. Although the majority of genes showed no significant upregulation for *OPA1* mutant cell lines, two genes did show changes. 1334G>A RGCs demonstrated significant upregulation for both *CEBPB* and *HSP60* when compared to WT and 1334>WT1 and WT2 RGCs (Figure 5.23C,F). In addition, *CEBPB* was significantly upregulated against 2708del RGCs whilst *HSP60* showed significantly increased expression against OPA1+/- RGCs.

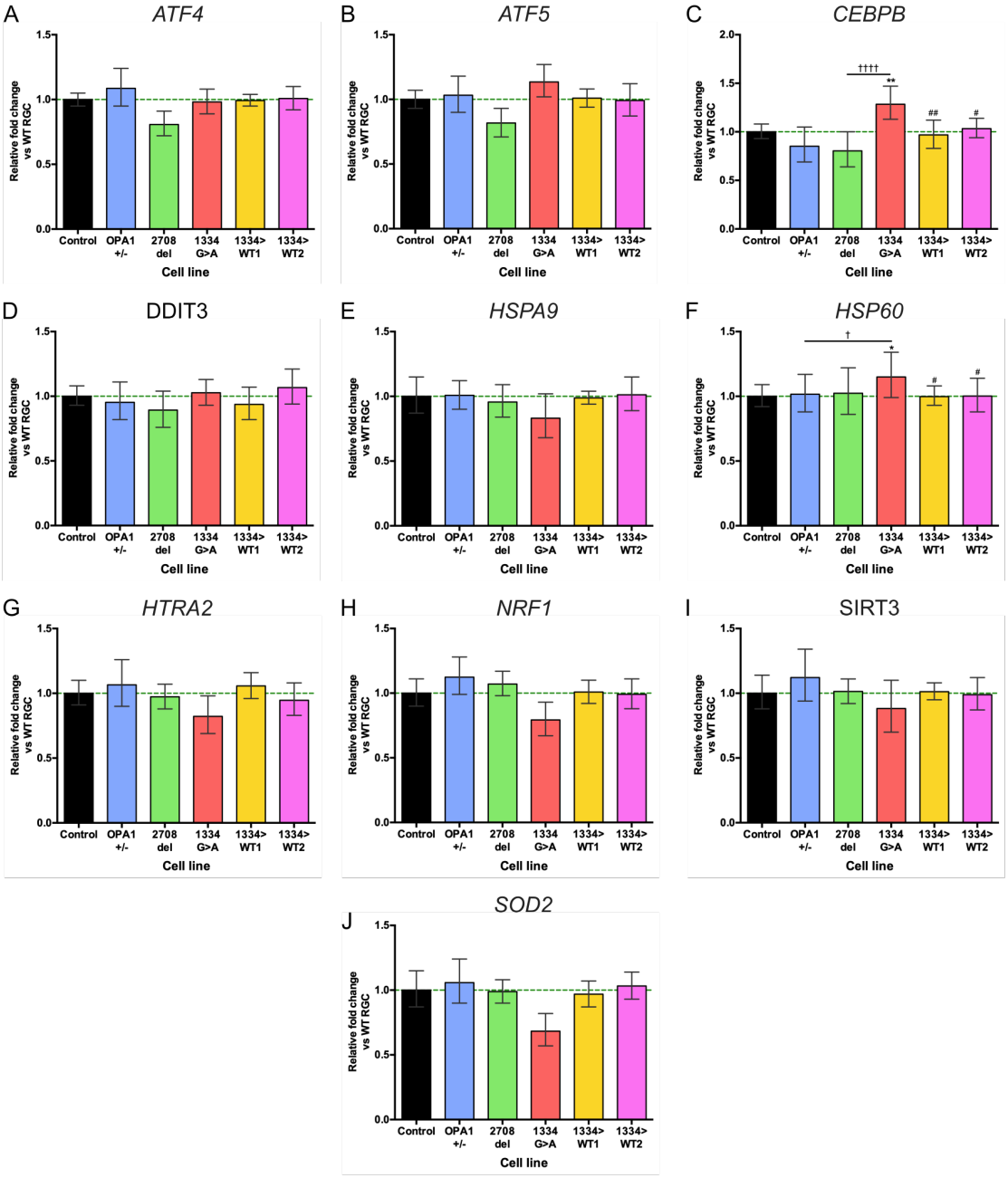

Figure 5.23. qPCR assessment of mito-stress associated genes in *OPA1* mutant and isogenic 2D-RGC.

D42 2D-RGCs were assessed for expression of mito-stress associated genes **(A-J)**. Gene expression was first normalised to the geometric mean of two reference genes, *GAPDH* and *ACTIN*, before normalisation to isogenic WT RGCs. 1334G>A RGCs were normalised to the average expression of both 1334>WT1 and WT2 RGCs. 2708del RGCs were normalised to the average expression of control 1334>WT1 and WT2 RGCs. N=3-5 individual RNA samples per cell line. Bars represent mean fold change ± SEM. * p<0.05, ** p<0.01 versus control 2D-RGCs. # p<0.05, ## p<0.01 versus 1334G>A 2D-RGCs. † p<0.05, †††† p<0.0001 between cell lines.

5.3 Discussion

Since its discovery as the primary genetic cause of DOA, research has established OPA1 as a multifunctional protein, central to maintaining mitochondrial homeostasis. The diverse isoforms of OPA1 are vital for maintaining the integrity of mitochondrial networks by enabling IMM fusion (Amati-Bonneau *et al.* 2005; Agier *et al.* 2012; Ban *et al.* 2017; Ban *et al.* 2018), whilst also regulating mitochondrial bioenergetic output by facilitating dynamic and specific responses to rapidly changing cellular metabolic demands (Mishra *et al.* 2014; Patten *et al.* 2014). More recently, OPA1 exon 4b has been shown to be integral to the maintenance of mtDNA (Yang *et al.* 2020), with dysfunctional OPA1 resulting in impaired mtDNA maintenance, the accumulation of mtDNA deletions and reduced mtDNA copy number quality control (Hudson *et al.* 2008; Yu-Wai-Man *et al.* 2010; Elachouri *et al.* 2011; Chen *et al.* 2012). Furthermore, although it is clear that *OPA1* mutation significantly impairs mitochondrial homeostasis there is no clear relation between *OPA1* mutation and the induction of mito-stress and the associated stress response pathways. Here, molecular characterisation was completed on fibroblasts and iPSCs, including isogenic knockout and control cell lines, to determine baseline phenotypes for each *OPA1* mutation type, followed by analysis of 2D and 3D RGCs to determine its effects on mitochondrial form and function in *in vitro* cell models of DOA. *OPA1* mutation resulted in impaired mitochondrial metabolism and mtDNA maintenance across all cell types assayed. Investigation of mito-stress revealed moderate levels of mito-stress associated with the *OPA1* c.1334G>A mutation, however, this appeared inconsistent across the cell models analysed. As such, the results presented here demonstrate previously uncharacterised deficits, particularly pertaining to human *in vitro* RGCs, which will further elaborate the molecular mechanisms associated to RGC loss in DOA.

5.3.1 Analysis of *OPA1* expression

OPA1 expression patterns have previously been studied in human tissue samples, with the high levels of expression in the retina, brain and heart (Alexander *et al.* 2000; Delettre *et al.* 2001); however, these have failed to specifically determine expression patterns within RGCs and what effect *OPA1* mutation has on isoform expression. Here, qPCR and RT-PCR were used to determine total *OPA1* and isoform specific expression across patient derived fibroblasts, iPSCs, 2D-RGCs and 3D retinal organoids. qPCR analysis demonstrated significantly different levels of expression between the four cell types analysed, with retinal organoids featuring the highest levels of expression followed by 2D-RGCs and iPSCs. This result is surprising given the nature of DOA, with *OPA1* mutations preferentially affecting RGCs, it may be expected that RGCs feature the highest level of *OPA1* expression. However, recent single-cell RNA-seq of mouse and

human retinal tissue suggests that *OPA1* expression varies greatly throughout the diverse retinal cell types (Macosko *et al.* 2015; Orozco *et al.* 2020). RNA-seq of human cells demonstrated that bipolar cells and horizontal cells both have greater mean and maximal expression of *OPA1* when compared to RGCs (Orozco *et al.* 2020). Furthermore, analysis of mouse cells confirmed the higher levels of *Opa1* expression within bipolar cells, and also suggests amacrine cells have greater expression than RGCs too (Macosko *et al.* 2015). Therefore, it is plausible that cells generated during retinogenesis within 3D retinal organoids contribute to higher *OPA1* expression levels than 2D-RGCs. Again, these results further highlight the importance of investigating disease appropriate models. Although these are novel studies which require further support, they further demonstrate the differences between mouse and human retina gene expression.

RT-PCR demonstrated further *OPA1* expression differences with fibroblasts, 2D-RGCs and retinal organoids demonstrating similar isoform expression patterns, predominantly expressing isoforms containing exon 4 and 5b. On the other hand, iPSCs expressed isoforms containing exon 4 and 5b alongside an isoform containing exons 4, 5 and 5b. Importantly, these data are consistent with the *OPA1* isoform patterns demonstrated for retinal tissue by Delettre *et al.* (2001) and throughout *in vitro* differentiation presented by Caglayan *et al.* (2020), suggesting that *in vitro* modelling accurately represents the *in vivo* physiological niche. Furthermore, this data confirmed that mutation type does not affect isoform expression, although this is unsurprising given the mutations are not located in alternatively spliced regions or associated with splice defects.

This work further demonstrates the requirement for developing improved human RGC models of DOA to further understand relevant disease mechanisms. Due to their ease of culture and isolation from patient-derived fibroblasts are routinely studied to understand OPA1 function, however, although RT-PCR demonstrates that fibroblasts exhibit isoform expression akin to the retina they demonstrate significantly reduced levels of total *OPA1* expression when compared to RGC cultures. Furthermore, although mouse models of DOA have provided key RGC-specific knowledge of *OPA1*, analysis of mouse *Opa1* expression demonstrated reduced alternative splicing, with only four isoforms, when compared to human cells (Akepati *et al.* 2008). Despite the clear *OPA1* expression differences, these models are extensively used for understanding the effects of therapeutics yet it is important to replicate tissue specific expression to fully understand the effects of therapeutics. More recently, analysis of *OPA1* expression during *in vitro* neural differentiation demonstrated significant increases over time as cells progressed from iPSCs, through NPCs and finally to neurons, confirming the upregulation of *OPA1* in neuronal populations (Caglayan *et al.* 2020). Thus, the work

presented here alongside past analysis of human and mouse *OPA1* isoforms demonstrates the need for further improved modelling due to the differences in expression level and the need to study models with relatable isoform expression.

Although, distinct functions are now being associated with specific exons, such as exon 4b binding mtDNA (Yang *et al.* 2020), further understanding of specific isoform function is needed. RT-PCR analysis demonstrated that 2D-RGCs and retinal organoids express high levels of isoforms with exon 5b, suggesting a requirement for its specific function for maintaining normal RGC health. Previous studies of OPA1 have demonstrated that exon 5b encodes a proteolytic cleavage site required for OPA1 processing (Song *et al.* 2007), whilst analysis in cell lines and patient-derived fibroblasts carrying an exon 5b mutation demonstrated its requirement for sequestration of cytochrome *c*, with dysfunction resulting in increased apoptosis (Olichon *et al.* 2007; Cornille *et al.* 2008). Yet whether this function is replicated in RGCs is unknown. Thus, further understanding the role of alternative splicing, cleavage of exon 5b and its involvement in IMM structure may illuminate if exon 5b isoforms are imperative to RGC health, facilitate understanding of the pathogenic mechanisms behind preferential RGC loss in DOA.

Creation of iPSCs carrying mutations within or deletions of specific exons would facilitate our understanding of the role alternative splicing plays in RGC biology. The work presented in this thesis has established the downstream consequences of heterozygous OPA1 expression by generating OPA1+/- iPSCs using CRISPR/Cas9 gene editing technology. Recent comprehensive analysis of *OPA1* mutations demonstrated there are no known mutations within exons 4 or 4b, whilst there is only one known mutation with *OPA1* exon 5b (Ferre *et al.* 2015). Thus CRISPR/Cas9 editing could be further employed to generate iPSCs carrying deletions of exon 4, 4b and 5b (Mou *et al.* 2017), to further study the effects of alternative splicing on RGC biology and health. Crucially, the OPA1+/- iPSCs generated here provide a definitive paradigm demonstrating the effect of OPA1 haploinsufficiency, enabling clarification of the effect alternative splicing has on mitochondrial homeostasis.

In addition, the analysis presented here also demonstrated higher levels of expression across all 1334G>A cell lines when compared to endogenous WT cells. Although this is an isolated cell line carrying this mutation it raises the question of what may be driving higher levels of expression and whether this could influence disease progression, particularly due to the diagnosis of DOA+ for this patient. Higher levels of expression are known to have detrimental impacts on mitochondrial homeostasis, with overexpression of WT *OPA1* shown to induce fragmentation in mitochondrial networks (Misaka *et al.* 2002; Griparic *et al.* 2004; Olichon *et al.* 2007) and apoptosis in cardio-myoblasts (Chen

et al. 2009). However, given that approximately 50 % of OPA1 in 1334G>A cell is likely dysfunctional this could be a compensatory mechanism to upregulate WT *OPA1* expression, and, as such requires further clarification. Of note, the overexpression is unlikely to be driven by the mutation itself as expression was not reduced to WT levels upon correction with CRISPR/Cas9. Additionally, previous analysis of 2708del patients demonstrated considerable variation in expression of *OPA1* mutant transcripts, demonstrating the variability of *OPA1* expression (Schimpf *et al.* 2008). As such, it is likely other mechanisms are driving differential *OPA1* expression. The presumptive promoter region for *OPA1* is known to be located approximately 40 to 600 bp upstream of the translation start site (Delettre *et al.* 2003; Müller-Rischart *et al.* 2013), however, to-date the promoter region has not been comprehensively sequenced within DOA patients, suggesting there may be uncovered polymorphisms further contributing to the pathogenic mechanisms of mutations.

Furthermore, investigation into the ratio of expression between mutant and WT alleles may increase understanding of why there is phenotypic variation amongst individuals with the same mutation. Although point mutations are associated with higher risk of developing DOA+ (Yu-Wai-Man *et al.* 2010), there is no direct relationship between genotype and phenotype. Recent RNA-seq analysis of healthy retinal tissues suggested genes associated with autosomal dominant inherited retinal diseases undergo allelic expression imbalance, with one allele expressed at a higher level than the other, suggesting a mechanism for incomplete penetrance and variable clinical expression (Llavona *et al.* 2017). Further analysis of transcriptome datasets for Mendelian inherited retinal diseases demonstrated significant levels of expression variation in genes commonly associated with incomplete penetrance, suggesting gene expression analysis should be completed alongside genetic screening (Green *et al.* 2020). Although this analysis has not been conducted on *OPA1* point mutations, determining the ratio of WT:mutant allele expression may further illuminate mechanisms that drive DOA penetrance, specifically the increased association of DOA+ and GTPase mutations. Unfortunately, the expression pattern of *OPA1* determined here in 1334G>A cells could not be replicated in other biological samples as there are no other patients with this mutation in the biobank or Moorfields DOA patient cohort. Nevertheless, analysis of *OPA1* promoter regions should be conducted, particularly in patients with DOA+, to determine if polymorphisms are further contributing to disease mechanisms.

5.3.2 Effects of OPA1 mutation of mitochondrial networks

To establish a baseline for investigating RGC phenotypes, 2708del and 1334G>A fibroblasts were analysed through a semi-automated mitochondrial network analysis pipeline. Both 1334G>A and 2708del fibroblasts showed signs of significant levels of

mitochondrial fragmentation with a greater number of total, individual and networked mitochondria when compared to WT controls. Further analysis of the networked mitochondria demonstrated they had fewer branches and those branches were significantly shorter in length than WT fibroblasts. As such, this analysis is in accordance with a number of previously published studies that have determined the impact of OPA1 dysfunction on mitochondrial networks using a variety of different methods to assess network quality (Olichon *et al.* 2003; Cipolat *et al.* 2004; Amati-Bonneau *et al.* 2005; Olichon *et al.* 2007; Zanna *et al.* 2008; Agier *et al.* 2012). In particular, this work agrees with previous studies of both 2708del and 1334G>A fibroblast that demonstrated significant levels of mitochondrial fragmentation with dysfunctional network fusion (Amati-Bonneau *et al.* 2005; Zanna *et al.* 2008). However, the data presented here also underline potential mutation differences, with 1334G>A fibroblasts containing greater numbers of total and individual mitochondria when compared to 2708del cells, suggesting that mutations with the potential for a dominant-negative disease mechanism cause a greater level of fusion dysfunction when compared to mutations primarily driven by haploinsufficiency alone. This would agree with the clinical characterisation of DOA in which mutations associated with DOA+, such as 1334G>A point mutations, demonstrate greater severity of symptoms including greater visual decline and greater mtDNA instability (Amati-Bonneau *et al.* 2008; Yu-Wai-Man *et al.* 2010). Thus, it is evident that both haploinsufficiency and dominant-negative mutations impact the function of OPA1 as a pro-fusion protein, with indication that 1334G>A mutations cause greater OPA1 dysfunction when compared to haploinsufficiency mutations.

Although the initial objectives of this thesis incorporated mitochondria network analysis of all generated cell types, including iPSCs and RGCs, this was sadly not completed due to the coronavirus pandemic. Imagining mitochondrial networks within iPSC colonies proved particularly problematic due to their nuclear dense morphology and highly compact nature of their mitochondrial networks. Although Caglayan *et al.* (2020) demonstrated the ability to assess ESC mitochondrial morphology, this was completed using ESCs dissociated into single cells. Although this method was considered for this study, it was not utilised given the high levels of stress single-cell dissociation typically places on iPSCs (Chen and Pruett-Miller 2018). Thus, further methods for assessing iPSC mitochondrial morphology are required to fully understand the effect of *OPA1* mutation, or CRISPR/Cas9 gene correction, on iPSC mitochondrial morphology.

Whilst imaging of RGC mitochondrial networks was not possible, it is important to consider the potential effect of *OPA1* mutation within RGC networks. Given their unique and elongated cell morphology, neuronal cell populations have very distinct mitochondrial networks, typically featuring more complex networks within the cell body

and smaller, more sparsely distributed mitochondria within axonal projections (Seager *et al.* 2020). Previous studies of *in vitro* neuronal populations with *OPA1* mutations have begun to illuminate the effect of neuronal mitochondrial morphology. Jonikas *et al.* (2018) demonstrated significant levels of mitochondrial fragmentation within dopaminergic neurons carrying a 9 bp insertion in *OPA1* exon 2 associated with PD, resulting in haploinsufficiency. Similar analysis completed by Iannielli *et al.* (2018, 2019) confirmed these findings, demonstrating fragmented mitochondrial networks and significantly reduced numbers of mitochondria per axonal projections within neurons and NPCs carrying heterozygous mutations within the *OPA1* GTPase domain. However, whether these findings would be replicated in RGCs remains to be confirmed, given the differential clinical presentation of *OPA1* mutations associated with PD and DOA. Furthermore, more recent analysis of hESC derived neurons did not confirm this morphological difference, with no mitochondrial morphological aberrations detected in OPA1 haploinsufficient neurons when compared to WT controls (Caglayan *et al.* 2020). Similarly, treatment of *ex vivo* rat RGCs with *Opa1* siRNA caused no morphological abnormalities in axonal mitochondria, with mitochondrial characteristics equal to those cells treated with scrambled siRNA (Kushnareva *et al.* 2013). Thus, more in-depth studies are required to illuminate the effects of *OPA1* mutation on axonal mitochondrial networks and to determine their impact on RGC health.

Mitochondrial fusion is also essential for maintaining homeostasis by enabling metabolite, protein and mtDNA transfer within the mitochondrial network (Chan 2020), thus impaired fusion likely prevents the successful mixing of mitochondrial components resulting in accumulation of dysfunctional mitochondria. This may have significant impacts on axonal mitochondrial populations, causing an accumulation of dysfunctional or morphologically impaired (smaller) mitochondrial within the axon and synaptic terminal. Signal transduction and synaptic transmission demand high levels of energy, typically generated through OXPHOS (Zheng *et al.* 2016; Ito and Di Polo 2017; Seager *et al.* 2020). Ultimately, transport of functionally compromised mitochondria within axonal projections may impair RGC function and prevent neuron signal transduction. Indeed, this is a hypothesis also proposed by Iannielli *et al.* (2019), in which accumulation of dysfunctional mitochondria causes reduced bioenergetic output and synaptic degeneration. Furthermore, mitochondrial biogenesis occurs within both the cell body and axonal projections of neuronal populations (Davis and Clayton 1996; Amiri *et al.* 2008). Thus, transport of dysfunctional mitochondria with the axonal projections may drive an accumulation of dysfunctional mitochondrial components, further impairing RGC function. Whether there are greater levels of dysfunctional mitochondria within the neuronal axons given mitochondrial network fragmentation and an impairment for

metabolite and protein transfer between mitochondria remains to be confirmed, and is an important disease mechanism to clarify in DOA.

5.3.3 Cellular bioenergetics in *OPA1* mutant cell lines

Following confirmation of a fragmented mitochondrial network in patient-derived fibroblasts Seahorse bioenergetic profiling was conducted to determine if *OPA1* mutation resulted in mitochondrial bioenergetic dysfunction. Comparison of WT with both 2708del and 1334G>A fibroblasts demonstrated significant reductions in basal and maximal respiration and ATP production for both mutant cell lines. These data confirm numerous previous reports examining the effect of OPA1 dysfunction on overall mitochondrial metabolism, which demonstrated significant reductions in ATP production due to reduced OXPHOS (Lodi *et al.* 2004; Amati-Bonneau *et al.* 2005; Zanna *et al.* 2008).

Subsequent analysis of iPSCs enabled the assessment of isogenic cell lines, reducing cell genetic variability to isolate the effects of *OPA1* mutation on respiratory output. Although a number of studies report the generation of *OPA1* mutant iPSCs (Chen *et al.* 2016; Galera-Monge *et al.* 2016; Jonikas *et al.* 2018; Iannielli *et al.* 2019), to date only one report has examined the effect of *OPA1* mutation on iPSC bioenergetic output. Surprisingly, OPA1+/- ESCs generated by Caglayan *et al.* (2020) demonstrated no significant deficits in basal respiration or ATP production versus WT ESCs when measured by Seahorse profiling. In addition, Caglayan *et al.* suggested OPA1+/- ESCs have higher levels of maximal respiration when compared to WT controls. The data presented within this study contradict these findings. Analysis demonstrated significant reductions in basal respiration and ATP production for OPA1+/-, 2708del and 1334G>A iPSCs, with significantly lower maximal respiration for OPA1+/- and 1334G>A iPSCs. In addition, 1334G>A iPSCs showed reduced ATP production compared to both OPA1+/- and 2708del. CRISPR/Cas9 mediated correction of 1334G>A iPSCs had a significant impact on bioenergetic output, with both 1334>WT cell lines having significantly higher levels of basal and maximal respiration and ATP output, profiles resembling that of endogenous WT iPSCs. Importantly, the data presented here demonstrate a more comprehensive analysis of OPA1 dysfunction, through the analysis of three independent iPSC lines carrying distinct *OPA1* mutations alongside isogenic control cell lines. Importantly, these data are also further supported by analysis of the original fibroblast cell lines within this study that confirmed respiration deficiencies for *OPA1* mutants and previous literature that established ATP production deficits due to dysfunctional OXPHOS (Lodi *et al.* 2004; Amati-Bonneau *et al.* 2005; Zanna *et al.* 2008). It is therefore important to further establish how *OPA1* mutation effects stem cell biology, and to clarify the effects of different mutation types, given these opposing results.

As previously mentioned, although a number of studies have generated *OPA1* mutant iPSCs, to date no study has analysed the bioenergetic consequences of *OPA1* mutation in human RGCs. Analysis of *OPA1* mutant patient-derived iPSCs differentiated into dopaminergic neurons and in NPCs demonstrated significant reductions in basal respiration, maximal respiration and ATP output for haploinsufficient mutant cells when compared to WT controls (Iannielli *et al.* 2018; Jonikas *et al.* 2018). Furthermore, knockdown of *Opa1* within *ex vivo* rat primary cortical neurons revealed a significant reduction in basal and maximal respiration, associated with an approximate 70 % reduction in protein level (Millet *et al.* 2016). The work presented in this chapter further expands on these studies by analysing the effect of multiple *OPA1* mutation types in human 2D-RGCs, demonstrating deficiencies in basal respiration and ATP production for all mutations, and reduced maximal respiration for OPA1+/- and 1334G>A 2D-RGCs. Importantly, corrected 1334>WT1 and WT2 RGCs also demonstrated significant improvements in mitochondrial respiration when compared to 1334G>A RGCs.

Although it is hard to cross compare Seahorse data amongst studies due to variable normalisation methods, the Seahorse profiles presented here replicate those previously published by Lorenz *et al.* (2017), which demonstrated reduced levels of OCR for both NPCs and dopaminergic neurons when compared to pure iPSCs. However, the recent study by Caglayan *et al.* (2020) presented data contradicting these findings, demonstrating increased OCR levels for *in vitro* forebrain neurons when compared to ESCs, whilst also suggesting that heterozygous *OPA1* knockout does not impair mitochondrial respiration of *in vitro* neurons. Although the increase in OCR is not surprising given the dependence of neurons on OXPHOS (Zheng *et al.* 2016), the lack of difference in basal and maximal respiration for heterozygous *OPA1* neurons is unexpected. Caglayan *et al.* (2020) suggested that the lack of difference is due to ESCs and *in vitro* neurons retaining approximately 50 % OPA1 expression when compared to total reduction caused by RNAi, however, both haploinsufficiency cell lines within this study showed similar levels of *OPA1* mRNA reduction whilst OPA1+/- iPSCs demonstrated an approximate 50 % reduction in protein. It is therefore unclear what is causing the disparity in bioenergetic output, given the use of isogenic cell lines in both studies and the work by Jonikas *et al.* (2018) and Ianielli *et al.* (2018) that demonstrated reduced bioenergetic output in haploinsufficient dopaminergic neurons and missense mutations in NPCs, respectively.

It is interesting to postulate why the Caglayan *et al.* (2020) study did not find significant differences in the respiratory phenotype for OPA1 knockout cell lines given the consistency of previous work on *OPA1* mutation and the impact on OXPHOS. Interestingly, Caglayan *et al.* did not detect any gross morphological abnormalities within

their OPA1 haploinsufficient ESCs, with only moderate changes to cristae structure. Importantly, Jonikas *et al.* (2018) also found no significant differences in mitochondrial cristae structure, however, there were significant differences in mitochondrial network structure with fragmented networks in *OPA1* mutant neurons. This may indicate why there were no dramatic alterations to the mitochondrial respiratory phenotype within the Caglayan *et al.* paper, given that mitochondrial structure is tightly linked to OXPHOS function (Chen *et al.* 2005; Suárez-Rivero *et al.* 2017), thus mitochondrial respiration may not be impaired without significant alterations to network morphology. Although it was not possible to assess iPSC mitochondrial morphology within this study, fibroblast analysis confirmed significant mitochondrial network fragmentation in both 1334G>A and 2708del fibroblasts. Importantly, the disparities between this work and studies in the literature demonstrate the importance of conducting context specific modelling for understanding the preferential loss of RGCs during DOA progression.

Importantly, the work presented within this Chapter demonstrates a previously uncharacterised bioenergetic deficit (reduced mitochondrial respiration and ATP production) within human RGCs and thus provides greater understanding to the specific disease mechanisms leading to RGC loss in DOA. Due to their unique morphology neurons have high metabolic demands, and produce the majority of their required energy through efficient OXPHOS (Zheng *et al.* 2016; Ito *et al.* 2017), thus making neuronal populations highly susceptible to impaired OXPHOS and reduced ATP production. Deficits in OXPHOS are commonly associated with both genetic and sporadic neurodegenerative diseases, including Leigh syndrome, PD and multiple sclerosis (MS; Wallace *et al.* 1991; Finsterer 2008; de Barcelos *et al.* 2019). In particular, RGCs are believed to have remarkably high metabolic need due to their lack of myelination in the retina (Wong-Riley 2010) and related optic neuropathies, including LHON and glaucoma, demonstrate deficits in OXPHOS (Yu-Wai-Man *et al.* 2002; Lee *et al.* 2012; Van Bergen *et al.* 2015; Catarino *et al.* 2017). It is therefore likely that dysfunctional mitochondrial bioenergetics is a significant contributor to RGC degeneration. Further understanding why specific neuronal populations are impacted by *OPA1* mutation whilst increasing understanding of the specific downstream effects of energy deficit may benefit diseases associated with RGC loss.

In addition to identifying RGC disease mechanisms, this study sought to highlight differences between haploinsufficient and dominant-negative mutational types, given the association of GTPase point mutations with higher risk of DOA+ (Amati-Bonneau *et al.* 2008; Yu-Wai-Man *et al.* 2010). Although Seahorse bioenergetic profiling of fibroblasts revealed no differences between patient-derived lines, subsequent examination of both iPSCs and 2D-RGCs demonstrated notable differences between 2708del and 1334G>A

cell lines. Interestingly, 2708del iPSCs and 2D-RGCs demonstrated significantly higher levels of basal respiration and ATP production when compared to 1334G>A cells, whilst in 2D-RGCs 2708del cells also demonstrated significantly higher maximal respiration. Although, this was not replicated in isogenic OPA1+/- cells, it may demonstrate differences between clinically important mutation types. 1334G>A mutations clinically present with greater visual decline when compared to haploinsufficient mutations. Given the high metabolic demand of RGCs (Wong-Riley 2010) a greater reduction in ATP production would have more severe consequences for RGC health and potentially result in a greater speed of optic nerve degeneration, thus providing insight into the potential disease mechanisms driving syndromic features.

The final comparisons of Seahorse data compared all 2D culture cell types to determine the relevance of each model for investigating DOA disease mechanisms. These data demonstrated significant reductions in OCR across all parameters for 2D-RGCs when compared to fibroblasts and iPSCs, confirming the need for context specific modelling as the current *in vitro* models of DOA have drastically different bioenergetics when compared to the primary pathologically affected cells. Notably, control 2D-RGCs had lower levels of maximal respiration and ATP production when compared to iPSCs and fibroblasts, perhaps indicating how RGCs have a reduced ability to respond to the changing metabolic requirements associated with neuronal function due to their lower levels of maximal energy output (Watts *et al.* 2018). This effect would be further exasperated in *OPA1* mutant cells that showed further reductions in maximal respiration and ATP synthesis, further reducing their ability to respond to metabolic change. Therefore, understanding the specific metabolic demands of RGCs may facilitate the development of treatments to reduce RGC death.

In addition to quantifying mitochondrial respiration through OCR, Seahorse profiling also quantifies basal glycolysis rate through the measurement of ECAR, enabling the analysis of overall metabolic output. Within this study, quantification of ECAR demonstrated significantly higher levels for iPSCs against fibroblasts and 2D-RGCs for all cell lines, whilst analysis of the OCR:ECAR ratio demonstrated significantly higher ratio for 2D-RGCs and fibroblasts, except for 2708del cells, confirming an increase in OXPHOS when compared to glycolytic metabolism. Previous studies of iPSCs have demonstrated that undifferentiated stem cells predominantly rely on glycolysis for energy production, rather than mitochondrial respiration, and glycolytic function is required for maintaining pluripotency (Kondoh *et al.* 2007; Prigione *et al.* 2010; Folmes *et al.* 2011; Lisowski *et al.* 2018). Thus, the elevated iPSC ECAR presented here suggest the cells have undergone appropriate metabolic changes during reprogramming, further confirming the generation of genuine stem cell-like cells.

Due to their unique morphology neurons have high metabolic demands and thus produce the majority of their required energy through OXPHOS (Wong-Riley 2010; Ito *et al.* 2017), with RGCs particularly susceptible to hypoxic conditions (Kaur *et al.* 2008; Tulsawani *et al.* 2010). Previous studies of *in vitro* neuronal differentiation, including mtDNA disorders, have demonstrated a significant shift from glycolysis to OXPHOS during neural induction (Zheng *et al.* 2016; Lorenz *et al.* 2017). As such, analysis of the basal glycolytic level and change in OCR:ECAR ratio can enable the investigation of two aspects of DOA modelling, the determination of differentiation quality and cellular heterogeneity as OXPHOS induction and a low change in ratio suggests a retention of cells relying on glycolysis. In accordance with the literature (Zheng *et al.* 2016; Lorenz *et al.* 2017), within this study all RGCs demonstrated an increase in OCR:ECAR ratio when compared to naïve stem cells, suggesting neural and RGC induction. However, both WT control and 2708del cell lines demonstrated a significantly lower level of OCR:ECAR ratio change when compared to the other four genotypes, potentially suggesting both a reduced quality of differentiation and a potential heterogenous culture retaining cells favouring glycolytic energy metabolism. This may be of particular importance given the high level of maximal respiration for 2708del 2D-RGCs, which may be due to the retention of cells with higher levels of OCR. It is therefore important to consider the ECAR values when assessing the effects of *OPA1* on mitochondrial OCR, ensuring low levels of ECAR to focus study on RGC OXPHOS. Analysis of OCR:ECAR ratio can also supplement comparisons of differentiation protocols to enable rapid determination of differentiation protocol ability for generating high quality neuronal populations.

5.3.4 OPA1 and mtDNA maintenance

Further to the analysis of bioenergetic, the quality of the mtDNA was analysed in *in vitro* cell lines to understand the effect *OPA1* mutation has on mtDNA maintenance in 2D-RGCs. Analysis of OPA1 function has demonstrated its role in maintaining the mitochondrial genome by anchoring mtDNA through direct interaction of exon 4b and the mtDNA D-loop (Elachouri *et al.* 2011; Yang *et al.* 2020). Initial analysis of cybrid DNA demonstrated the feasibility for mtDNA quality assessment, with an approximate 70 % reduction in WT mtDNA copies in cybrid cells when compared to WT cells, further confirmed by LR-PCR analysis. In accordance with a number of previous studies (Amati-Bonneau *et al.* 2008; Hudson *et al.* 2008; Yu-Wai-Man *et al.* 2010; Chen *et al.* 2012), analysis of mtDNA in *in vitro* cultured cells demonstrated a significant reduction in mtDNA WT levels for both 2708del and 1334G>A cells, across all analysed cell types. Interestingly, although CRISPR/Cas9 mutation of *OPA1* resulted in a trend to reduced WT mtDNA this was not significant, however, correction of 1334G>A cells significantly restored mtDNA quality in iPSCs and 2D-RGCs. Although a number of previous studies

have demonstrated altered mtDNA copy number associated with *OPA1* mutation (Kim *et al.* 2004; Zanna *et al.* 2008; Yu-Wai-Man *et al.* 2010; Chen *et al.* 2012; Kushnareva *et al.* 2013), within this study there were no statistical differences in mtDNA copy number amongst the cultured cell types.

The data presented in this chapter is in accordance with the majority of the literature, however, one previous study by Liao *et al.* (2017) suggested only mutations associated with DOA+ drive mtDNA defects. Within this study both 2708del and 1334G>A mutations were associated decreased WT mtDNA levels suggesting that both missense and haploinsufficient mutations reduce mtDNA quality control. In addition, restoration of GTPase function through CRISPR/Cas9 gene correction restored mtDNA quality, further indicating the importance of a functional GTPase domain in mitochondrial homeostasis and mtDNA maintenance. Importantly, this agrees with previous analysis of OPA1 indicating that a functional GTPase domain is required for mtDNA stability, as expression of OPA1 variants incapable GTP hydrolysis do not restore mtDNA content in Opa1-/- cells (Del Dotto *et al.* 2017), whilst mtDNA deletions are also evident in tissue from patients carrying 1334G>A mutations (Amati-Bonneau *et al.* 2008). Thus, the data presented here supports the theory that missense point mutation within the GTPase domain impact the ability of OPA1 to maintain mtDNA integrity, further supporting the theory that GTPase point mutations infer a dominant-negative effect, reducing the functional capabilities of WT OPA1 for maintaining mtDNA stability.

Importantly, this study demonstrates the functional restoration of mtDNA quality control through correction of a nuclear encoded gene using CRISPR/Cas9 gene editing technology. Although mtDNA only encodes 37 genes, these encode core proteins required for mitochondrial function (Holt *et al.* 2007) and loss of mtDNA integrity is a common phenotype associated with neurodegenerative conditions, including PD and AD (de la Monte *et al.* 2000; Bender *et al.* 2006; Sanders *et al.* 2014). In particularly, LHON is caused by specific mutations within the mitochondrial genome, resulting in a phenotypically similar disease to DOA (Yu-Wai-Man *et al.* 2002), demonstrating the importance of mtDNA maintenance for RGC health. Thus, the ability to restore mtDNA integrity is a favourable therapeutic strategy for a range of genetic and sporadic neurodegenerative conditions. Interestingly, Sanders *et al.* (2014) previously demonstrated that correction of *LRRK2* mutations, associated with PD, with ZFNs reduced mtDNA lesions in both iPSCs and neural cells. Whilst numerous studies have also now demonstrated the feasibility of selectively targeting mtDNA for gene editing, yet, mtDNA editing remains problematic due to inefficient mitochondrial nucleotide import efficiency (Jo *et al.* 2015; Gammage *et al.* 2018; Mok *et al.* 2020). However, due to their spontaneous development, mtDNA mutations associated with DOA are heterogeneous

in nature and thus impractical to selectively target for correction. Therefore, demonstrating the ability to correct a monoallelic nuclear mutation to restore mtDNA integrity proves an exciting prospect for DOA, and a range of other neurological conditions.

Improved mtDNA maintenance likely occurs due to increased OPA1 function and thus improved mtDNA quality control. As discussed in Chapter 1, OPA1 binds to mtDNA via exon 4b, anchoring it to the IMM (Yang *et al.* 2020), whilst previous studies have confirmed GTPase activity is essential to maintaining the integrity of mtDNA (Amati-Bonneau *et al.* 2008; Hudson *et al.* 2008; Yu-Wai-Man *et al.* 2010; Del Dotto *et al.* 2017). Crucially, cells can remove dysfunctional mitochondria through mitophagy, including those that carry abnormal mtDNA (Chan 2020). A number of studies have confirmed this process, demonstrating the removal of mutated mtDNA through mitophagy in *Drosophila* and *in vitro* cell lines (Malena *et al.* 2009; Suen *et al.* 2010; Kandul *et al.* 2016). It is therefore reasonable to deduce that restoring GTPase function within 1334G>WT cells would increase their ability to bind and sequester abnormal mtDNA to the IMM and enable the increased clearance of abnormal mtDNA through clearance of dysfunctional mitochondria.

5.3.5 *OPA1* mutation effect on mitochondrial stress

Further to analysing the effects of *OPA1* mutation on previously described mitochondrial functions, this chapter describes the effect of *OPA1* mutation on overall mitochondrial stress through analysis of a panel of stress response associated genes. A number of previous studies have previously demonstrated increased levels of mito-stress related proteins in association with *OPA1* dysfunction, demonstrating involvement of SIRT3 for upregulating OPA1 GTPase activity, changes in HSP60 and SOD2 expression and a role for DDIT3 and ATF4 activation caused by *OPA1* knockout (Samant *et al.* 2014; Millet *et al.* 2016; Tezze *et al.* 2017), however, these studies have not analysed the diverse pathway changes that occur at a transcriptional level. Within this chapter, mito-stress associated gene expression was analysed through qPCR, demonstrating significant upregulated expression upon ATP synthase inhibition with oligomycin. Analysis of mutant cell lines demonstrated upregulated expression for a number of mito-stress genes within 1334G>A iPSCs, 2D-RGCs and retinal organoids, suggesting a possible association with dominant-negative mutations rather than those caused by haploinsufficiency.

Within this study oligomycin was utilised to provide a positive control for evaluating mito-stress gene expression, demonstrating inhibition of the ETC causes significant upregulation mito-stress associated genes. However, although 1334G>A iPSCs,

organoids and 2D-RGCs showed higher levels of gene expression than WT cells these changes were moderate when compared to oligomycin induced stress. Previous studies of mito-stress pathways have demonstrated that various types of mitochondrial dysfunction drive mito-stress, including mtDNA damage or depletion, respiratory chain complex inhibition or inactivation of mitochondrial protein-handling machinery (Martinus *et al.* 1996; Zhao *et al.* 2002; Yoneda *et al.* 2004; Baker *et al.* 2012; Runkel *et al.* 2013). Here, OPA1+/-, 2708del and 1334G>A iPSCs demonstrated dysfunctional mtDNA quality control and inhibited respiratory output and thus exhibit phenotypes associated with increased mito-stress. Nevertheless, only 1334G>A cells displayed a mito-stress phenotype when compared to WT cells suggesting that not all mutations drive mito-stress. Importantly, molecular phenotyping also revealed mutational differences, 1334G>A iPSCs and 2D-RGCs demonstrated significantly reduced levels of basal respiration and ATP production when compared to 2708del cells, whilst 1334G>A cells also showed a trend to lower WT mtDNA levels when compared to 2708del cells, suggesting this increased level of mitochondrial dysfunction may be inducing greater levels of mito-stress. However, whether this effect is associated with 1334G>A GTPase mutations or DOA+ clinical phenotype is unclear. Mito-stress thus requires further validation in other DOA+ cell lines with different mutations alongside understanding the specific mitochondrial dysfunction causing elevated gene expression.

Furthermore, this analysis demonstrated that there are different levels of mito-stress response across different cell types, with greater quantities of upregulated stress genes in iPSCs when compared to 2D-RGCs. Interestingly, this may demonstrate that different disease mechanisms caused by *OPA1* mutation may affect different tissues or specific time points throughout retinal development. Although data in chapter 3 and 4 demonstrated that *OPA1* mutation does not impact iPSC differentiation ability, establishing if mito-stress levels impact cell viability during early development may help to ascertain if DOA or DOA+ has a developmental involvement. Interestingly, analysis of *in vitro* neural differentiation suggests *ATF5* expression blocks the progression of NPCs to post-mitotic neurons (Angelastro *et al.* 2003), and, in the presence of sonic hedgehog, constitutive expression of *ATF5* promotes NPC proliferation and delays cell cycle exit and differentiation to cerebellar granule neurons (Lee *et al.* 2012). These studies therefore demonstrate the importance of *ATF5* regulation in developing neuronal circuits, which is of further significance given the association of 1334G>A mutations with extraocular DOA+ symptoms, highlighting potential differentiation deficits caused by increased mito-stress that may lead to extraocular features like ataxia.

It is also worth noting that several reports suggest that DOA patients with *OPA1* mutations have fewer total RGCs at birth, which contributes to their rapid vision decline

(Barboni *et al.* 2010; Milea *et al.* 2010; Barboni *et al.* 2011), however, the cause for potential reduced RGC number is not clear. Although previous research by Chen *et al.* (2016) demonstrated a reduced ability for RGC differentiation in *OPA1* mutant cells, this was not consistent with the results presented in this study. Nevertheless, analysis of mito-stress associated genes may indicate why some patients have fewer RGCs at birth. Given that RGCs are generated early during retinogenesis (Cepko *et al.* 1996; Centanin and Wittbrodt 2014), increased expression of *ATF5* in conjunction with sonic hedgehog expression, a known regulator of RGC differentiation (Wang *et al.* 2005), may reduce RPCs exiting the cell cycle to generate RGCs and thus drive them to a later developmental cell type and reducing total RGC number. Importantly, this is an effect demonstrated in *Xenopus* retinogenesis, where inhibition of cell cycle exit causes increased number of late-stage cell types, such as photoreceptors (Ohnuma *et al.* 2002). Thus, further research is required to understand the impact elevated levels of stress related genes have on the generation and survival of neuronal populations associated with dominant-negative mutations.

In addition to the effect on neural development, mito-stress associated factors have been implicated in neurodegenerative disease progression. Of most importance here is the elevated levels of *HSP60* in 2D-RGC and retinal organoids, a factor which has previously been associated with both a neuroprotective function and increased disease progression in neurodegenerative conditions (Campanella *et al.* 2018). Although primarily functioning as a mitochondrial chaperone, studies of primary neuronal cultures treated with exogenous HSP60 demonstrated its ability to induce apoptosis and compound the effect of neurotoxic insults (Noelker *et al.* 2014). Further studies of HSP60 have demonstrated its ability to accelerate the activation of caspase 3 and increase the initiation of apoptosis induction cascades (Xanthoudakis *et al.* 1999), whilst analysis of PD models has established HSP60 as an immunomodulatory factor, demonstrating its upregulation and release from neurons during degeneration to activate microglia inflammatory response (Feng *et al.* 2013; Kuter *et al.* 2016; Sun *et al.* 2018). Given that previous studies have demonstrated that OPA1 dysfunction results in increased apoptosis due to cytochrome *c* release and caspase cascade activation (Olichon *et al.* 2003; Frezza *et al.* 2006; Olichon *et al.* 2007; Chen *et al.* 2009) increased *HSP60* expression may compound the effects of *OPA1* mutation driving RGC cell death.

Further to its association with neurodegenerative diseases, increased HSP60 expression has been associated with glaucoma. Initial analysis of blood samples from glaucoma patients demonstrated increased levels of anti-HSP60 antibodies in patient samples (Wax *et al.* 1998; Wax *et al.* 2001), indicative of an autoimmune response to endogenous proteins. Further analysis of post-mortem glaucoma retinal tissues demonstrated

increased expression in the of HSP60 in RGCs when compared to healthy control tissues (Tezel *et al.* 2000), whilst inoculation of rats with HSP60 induced retinal degeneration through activation of T-cells and induction of RGC apoptosis (Wax *et al.* 2008). Although the authors studying the association of HSP60 and glaucoma postulate increased expression of HSP60 as a neuroprotective strategy it is plausible that *HSP60* expression is inducing further retinal damage. Indeed, activation of microglia is associated with disease progression in other RGC degenerative conditions, including glaucoma (Ebneter *et al.* 2010; Williams *et al.* 2017), suggesting un-checked inflammatory responses may contribute to and accelerate retinal degeneration. Thus, increased expression of HSP60 within RGCs may further exacerbate the progression of DOA through induction of detrimental inflammatory processes. Although the roles of other mito-stress related genes in differentiation and neuronal function are not well studied, it is clear that fine-tuned regulation of mito-stress associated factors is required for RGC health. As such, the role mito-stress plays in early development of RGCs and progression of DOA or DOA+ should be further investigated.

It is also important to consider the reasons behind elevated expression and any potential benefits increased expression may have. Interestingly, analysis of ATF5 function demonstrated its role in maintaining mitochondrial function. Knockdown of *ATF5* in HEK293T cells caused significant reductions in mitochondrial bioenergetic output, reducing basal and maximal respiration as determined by Seahorse profiling (Fiorese *et al.* 2016) demonstrating its ability to regulate OXPHOS. Furthermore, analysis of the yeast orthologue of *ATF5*, *atfs-1*, demonstrated its importance in coordinating the bioenergetic response to mitochondrial stress through regulating expression of both nuclear and mitochondrial encoded ETC components, preventing the unnecessary accumulation of proteins during stress by reducing overall gene expression to match mitochondrial protein biogenesis to proteostasis levels (Nargund *et al.* 2015). In addition, knockdown of *HSP60* in pancreatic cancer cells caused reduced levels of basal respiration and ATP production that were subsequently restored through ectopic *HSP60* expression, thus demonstrating its function in mitochondrial respiration likely due to its role regulating proteostasis and stabilising mtDNA (Zhou *et al.* 2018). This therefore may indicate that *ATF5* and/or *HSP60* upregulation acts as a compensatory mechanism to support dysfunctional mitochondrial respiration in *OPA1* mutant cells, in addition to coordinating mitochondrial proteostasis. However, upregulated expression of either gene in 1334G>A iPSCs was not sufficient to compensate for the deficits caused by *OPA1* mutation, as demonstrated by the reduced Seahorse bioenergetic profiles. Given these results, further experimentation to investigate the role HSP60 and ATF5 play in mitochondrial respiratory compensation should be conducted. Knockdown of *ATF5* and/or *HSP60* expression through RNAi followed by assessment of mitochondrial

respiration with Seahorse would reveal if either gene is supporting mitochondrial respiratory function given the deficit caused by *OPA1* mutation. This work would illuminate if HSP60 and/or ATF5 have a functional role within *OPA1* mutant cell lines, potentially providing an opportunity for further therapeutic approaches that modulate compensatory factors to alleviate disease phenotypes.

Finally, it is also important to consider the reasons for variability of mito-stress gene expression within the different *in vitro* cultures. Firstly, it is worth noting that 1334G>A iPSCs demonstrated greater impairment of mitochondrial function when compared to their RGC counterparts. 1334G>A iPSCs demonstrated a mean reduction of 38.5 % for basal respiration when compared to WT control cells, whereas RGCs exhibited a reduction of 58.1 %. Similarly, 1334G>A iPSCs exhibited a reduction of 16.3 % for WT mtDNA percentage, whilst 1334G>A 2D-RGCs only demonstrated a reduction of 8.2 %. Given that both mitochondrial OXPHOS dysfunction and impaired mtDNA quality control are known induces of mitochondrial stress (Martinus *et al.* 1996; Yoneda *et al.* 2004; Baker *et al.* 2012; Runkel *et al.* 2013), it is unsurprising 1334G>A iPSCs exhibited a greater induction of mito-stress associated genes.

It is also worth noting that this analysis offers a single time point of mitochondrial stress within RGC cultures. It is likely that mitochondrial stress fluctuates throughout development and within mature RGCs due to their diverse activity and function, as seen by the differences between iPSCs and RGCs, and thus may impact disease progression. This is of particular importance given the heterogeneity in both 2D and 3D *in vitro* RGC cultures. Previous studies of RGC differentiation protocols have demonstrated generation of non-RGC cells within cultures, identified through IF by RGC marker negative cells and gene expression via qPCR (Riazifar *et al.* 2014; Sluch *et al.* 2015; Tanaka *et al.* 2015; Gill *et al.* 2016; Teotia *et al.* 2016). RT-PCR and IF analysis of retinal organoids demonstrated consistent expression of other retinal cell lineage associate genes, including those of precursor cells, photoreceptors and Muller glia. Similarly, cell counts in 2D-RGC studies demonstrated approximately 50 – 60 % of cells expressing RGC associated markers, including BRN3B and ISL1, indicting other cell lineages are present within cultures. Furthermore, 1334G>A RGCs demonstrated reduced OCR:ECAR ratio when compared to 1334>WT1 and >WT2 RGCs, suggesting that 1334G>A RGCs may have a more heterogeneous culture when compared to both corrected WT RGCs. It is therefore clear, that although offering increased accuracy of DOA modelling, 2D and 3D cultures retain populations of cells that may be clinically unaffected by *OPA1* mutation (Ito *et al.* 2007; Lenears *et al.* 2012) and retain normal mitochondrial homeostasis, thus likely masking both upregulated and downregulated expression patterns associated with RGC mito-stress.

Furthermore, analysis via RT-PCR demonstrated expression of synaptic function associated genes, indicating the development of neuronal networks connected through synapses within *in vitro* cultures. However, given that synaptic transmission is a highly energy demanding process (Wong-Riley 2010; Watts *et al.* 2018), cultures with different synaptic maturation will undoubtedly have greater metabolic demands when compared to cultures with immature synaptic connections. Given that OXPHOS powers synaptic transmission (Hall *et al.* 2012), increased metabolic demand may increase generation of intrinsic stresses, such as ROS, thus driving mito-stress gene expression. Despite the potential pitfalls of cellular heterogeneity, the analysis of mito-stress gene expression further establishes potential RGC disease mechanisms associated with DOA, whilst demonstrating the relevance of studying physiological relevant disease models for understanding DOA pathogenic mechanisms. A study of *OPA1* mutant iPSCs alone would deduce that mito-stress is a significant contributor to DOA pathogenesis, however, *in vitro* differentiation of RGCs revealed lower expression of mito-stress genes perhaps indicating it has less of an impact on disease progression. It is therefore important to further develop *in vitro* RGC models to provide a clearer picture of the effects mito-stress has on the progression of DOA.

5.3.6 Alternative strategies to assess mitochondrial phenotypes

Although the methods presented within this chapter illuminated the potential disease mechanisms associated with *OPA1* mutation in RGCs, there are a broad range of additional techniques that could be utilised to characterise mitochondrial phenotypes and further clarify the effects of *OPA1* mutation on RGC biology.

Within this chapter, bioenergetic analysis of all cell models was completed using the Seahorse extracellular flux analyser, which enables the analysis of respiratory competence of cells in conjunction with their ability to produce ATP. However, OPA1 is known to regulate many different aspects of mitochondrial energy production, including cristae junction tightening, the ability to form mitochondrial ETC supercomplexes and ATP synthase dimerisation, and *OPA1* mutation is known to negatively effect many of these functions (Gomes *et al.* 2011; Sarzi *et al.* 2012; Cogliati *et al.* 2013; Patten *et al.* 2014). Importantly, the aforementioned previous studies have demonstrated that these mitochondrial parameters can be quantitively assessed through western blot analysis, enabling the quantification of OPA1 oligomerisation (a feature of cristae junction tightening) and the levels of respiratory supercomplexes within cells (Cogliati *et al.* 2013; Patten *et al.* 2014). In addition to quantification of protein complexes, analysis of specific metabolites required for mitochondrial bioenergetics or ETC complex functionality may reveal the deficits or cellular compensation being driven by *OPA1* mutation. Analysis of ETC complex functionality through either polarographic or spectrophotometric assays

(Barrientos 2002) would demonstrate if *OPA1* mutation is driving specific deficits in ETC enzymatic activity, a feature previously identified in complex I within patient-derived fibroblasts (Zanna *et al.* 2008). It is therefore possible to quantify additional parameters of mitochondrial bioenergetics in *OPA1* mutant cell lines, enabling the generation of a more comprehensive picture of ETC competency in human RGCs, and the impact any ETC deficits may have in DOA disease progression.

Further to additional studies of mitochondrial bioenergetics, multiple additional methods are available for studying mitochondrial dynamics that would further illuminate the potential disease mechanisms caused by *OPA1* mutation. Importantly, previous studies have utilised live cell imaging to demonstrate that OPA1 dysfunction results in impaired mitochondrial fusion and morphological abnormalities (Zanna *et al.* 2008; Anand *et al.* 2014; Del Dotto *et al.* 2017; Hu *et al.* 2020). Of note, studying the diffusion of photoactivable mitochondrial targeted proteins, such as mtPAGFP, throughout the mitochondrial network enables the accurate quantification of IMM fusion dynamics and competency (Zanna *et al.* 2008; Del Dotto *et al.* 2017). As such, live cell imaging presents an effective tool for studying mitochondrial IMM dynamics and the effects impaired OPA1 function on the mitochondrial network. In addition, although TOMM20 IF analysis demonstrated fragmentation within both 2708del and 1334G>A cells within this chapter, this may present an incomplete picture of the level of mitochondrial fragmentation occurring within these cells given that OMM fusion machinery is unaffected. Therefore, additional analysis using markers of the IMM, such as identifying the IMM encapsulated matrix with mtHSP70 or the IMM itself with AIF and OPA1 antibodies (Ouellet *et al.* 2017; Reinhardt *et al.* 2020), would demonstrate if there are significantly greater levels of impaired IMM fusion, and thus network fragmentation, in *OPA1* mutant cells when compared to WT counterparts.

In conjunction to further analysing mitochondrial dynamics, analysis of IMM integrity would enable determination of overall mitochondrial health. IMM integrity is integral to mitochondrial function by creating an electrochemical gradient which is required for ATP synthesis and protein quality control (Kühlbrandt 2015; Zorova *et al.* 2018). Previous studies have demonstrated the importance of OPA1 for maintaining IMM structure and integrity (Olichon *et al.* 2002; Olichon *et al.* 2003; Alavi *et al.* 2007; Song *et al.* 2007; Agier *et al.* 2012). As such loss of the IMM electrochemical gradient can be considered a hallmark of dysfunctional OPA1 (Olichon *et al.* 2002; Olichon *et al.* 2007; Williams *et al.* 2012), a characteristic that can be assessed through the mitochondrial dye JC-1, which accumulates within healthy mitochondria but when the electrochemical potential is lost predominantly accumulates within the cytoplasm, or the dyes TMRM and TMRE that specifically accumulate in mitochondria with healthy electrochemical gradients.

Analysis with mitochondrial fluorescent dyes would enable the determination of the effect *OPA1* mutation has on overall mitochondrial quality rather than focusing on specific mitochondrial characteristics, such as ATP production or mtDNA maintenance.

In addition to analysis of mitochondrial dynamics and health, there are alternative strategies for the assessment of mtDNA quality and quantity. Importantly, OPA1 is known to anchor mtDNA nucleoids to the IMM within mitochondria, thus facilitating its distribution throughout the mitochondrial network (Elachouri *et al.* 2011; Yang *et al.* 2020). As such, analysis of fibroblasts, iPSCs and RGCs using mtDNA specific dyes or antibodies, such as PicoGreen or anti-mtTFA (Ashley *et al.* 2005), would enable the determination of how *OPA1* mutation effects mtDNA distribution within cells, or if RGCs are actively transporting mitochondria with reduced mtDNA content along axonal projections. Although qPCR was utilised within this chapter to analyse mtDNA mutation and deletion, advances in next generation sequencing (NGS) technology have enabled screening of the entire mitochondrial genome with higher throughput and greater sensitivity to mtDNA variants (Bris *et al.* 2018). Given that no large scale mtDNA deletions were identified by LR-PCR within this chapter, it suggests that the majority of mtDNA abnormalities causing reduced WT mtDNA levels in *OPA1* mutant cell lines are small scale InDels. As such, NGS of mtDNA may provide greater sensitivity to determine the effects *OPA1* mutation is having on mtDNA integrity, and reveal the types of mtDNA mutations that are accumulating as a result of impaired OPA1 interaction with mtDNA.

Although the mito-stress qPCR panel allowed the assessment of changes in gene expression, in addition WB and IF analysis could be conducted to determine alterations to protein quantity or cellular localisation. Previous studies of both AKT and ERα have demonstrated how their function and activation is regulated through phosphorylation, which is required for downstream activation of *NRF1* (Papa and Germain 2011; Papa and Germain 2014). In addition, translocation of mito-stress associated proteins is key for their signalling cascade induction, with ATF5 imported in mitochondria under normal homeostatic conditions but translocated to the nucleus during induction of mito-stress (Fiorese et al. 2016). Both phosphorylation and protein translocation can be analysed through WB and IF, which would provide a greater level of clarity for the mito-stress associated protein changes occurring in *OPA1* mutant cells and whether these significantly contribute to RGC death and the progression of DOA.

In summary, this study aimed to utilise *in vitro* cell lines to deduce the molecular disease mechanisms associated with OPA1 dysfunction, and determine if RGCs show particular deficits that make them prone to preferential death in DOA. Analysis of all cultured cells demonstrated significantly altered *OPA1* expression levels for mutations associated with

haploinsufficiency, however, mutations did not affect isoform expression patterns that were consistent with previously published literature. Furthermore, mitochondrial phenotyping demonstrated deficits in mitochondrial bioenergetics and mtDNA quality control in *OPA1* mutant cell lines, within fibroblasts, iPSCs and 2D-RGCs respectively. Analysis of mito-stress associated gene expression revealed significantly upregulated expression for numerous genes, including *ATF5*, *CEBPB*, *DDIT3* and *HSP60*, in 1334G>A cells, suggesting dominant-negative mutations drive increased mitochondrial stress. Importantly, CRISPR/Cas9 genetic correction of 1334G>A iPSCs restored mitochondrial homeostasis, including re-establishing WT mtDNA levels, improved mitochondrial ATP production and reduced mito-stress gene expression. Overall, these results highlight disease mechanisms associated with *OPA1* mutation in previously un-evaluated models of DOA.

Chapter 6: General discussion

The identification of *OPA1* as the primary genetic cause of DOA led to a significant progress over the past 2 decades on identifying the molecular disease mechanisms that drive the preferential loss of RGCs. Analysis of the various available *in vitro* and *in vivo* disease models has rapidly developed our understanding of the key functions OPA1 plays in maintaining mitochondrial homeostasis, yet, due to its complex multi-function role the exact disease mechanisms causing RGC loss are not fully understood and a successful therapeutic strategy is still to be developed. As such, greater understanding of the specific disease mechanisms associated with RGC loss is imperative to drive DOA research forward. The work described in this thesis aimed to develop a context specific understanding of DOA through generation of improved *in vitro* disease models utilising a biobank of clinically relevant *OPA1* mutant iPSCs and isogenic controls. Additionally, this thesis details the molecular defects associated with *OPA1* mutations across a variety of cell types, generating a comprehensive disease phenotype associated with different *OPA1* mutation types and explores how these disease mechanisms may result in the premature death of RGCs.

6.1 Understanding DOA through improved RGC modelling

The initial objective of this thesis was to establish a biobank of *OPA1* mutant iPSCs with isogenically matched WT control cells. To-date the majority of studies utilising *OPA1* mutant iPSCs for disease modelling have focused on small range of mutational types, either those associated with OPA1 haploinsufficiency or mutations associated with PD (Galera-Monge *et al.* 2016; Iannielli *et al.* 2018; Jonikas *et al.* 2018; Iannielli *et al.* 2019; Caglayan *et al.* 2020). Although two mutations were prioritised for the work presented within this thesis, a biobank of 6 patient-derived iPSC lines has been generated encompassing 5 different *OPA1* mutations. This biobank therefore expands the range of *OPA1* mutations available for study, encompassing a greater spectrum of DOA clinical presentation and its associated range of *OPA1* mutations.

Furthermore, there is a growing level of interest in OPA1 given its relevance to the broader field of neurodegeneration, with a growing list of clinical phenotypes associated with its dysfunction. In particular, *OPA1* has become associated with multisystem developmental conditions (Bonneau *et al.* 2014; Carelli *et al.* 2014; Spiegel *et al.* 2016; Nasca *et al.* 2017) and there is a growing body of evidence surrounding OPA1 dysfunction in PD (Carelli *et al.* 2015; Lynch *et al.* 2017; Iannielli *et al.* 2018; Jonikas *et al.* 2018; Iannielli *et al.* 2019). The biobank of iPSCs therefore presents a vital resource for developing our understanding of the effect of OPA1 dysfunction on neuronal health

particularly given the relationship of OPA1 with PD, which is a major cause of morbidity in the elderly population, affecting approximately 1-2 individuals per 1000 people (Tysnes and Storstein 2017).

The advent of iPSC technology revolutionised our ability to accurately model specific genetic abnormalities and their associated disease mechanisms. More recently, the discovery of the CRISPR/Cas9 system and its application for gene editing in eukaryotic organisms has further advanced the disease modelling world. Together, these two technologies allow for accurate, gene specific investigation into a multitude of conditions with known genetic causes. In this thesis, CRISPR/Cas9 gene editing was successfully used to alter the *OPA1* genotype in both WT and patient-derived cell lines, allowing the specific study of *OPA1* mutations with isogenically matched cell lines. Further application of CRISPR/Cas9 technology within *OPA1* would further facilitate the investigation of its function within RGC health. Notably, homozygous and compound heterozygous *OPA1* mutations have been identified (Bonneau *et al.* 2014; Carelli *et al.* 2014; Spiegel *et al.* 2016; Nasca *et al.* 2017). Although these mutations are typically associated with severe neurological conditions rather than pure DOA, selectively targeting and editing the different mutations within compound heterozygous *OPA1* mutant cells may provide insight into the contribution of each mutation to the associated disease mechanisms.

Similarly, our knowledge surrounding the specific function of *OPA1* exons is gradually increasing, with greater understanding of how exon 4b regulates OPA1 proteolytic cleavage and interacts with mtDNA (Song *et al.* 2007; Yang *et al.* 2020). CRISPR/Cas9 has been utilised for the removal of specific exons in a number of genes, demonstrating both the rescue and alteration of gene function in mice and model cell lines (Nelson *et al.* 2016; Mou *et al.* 2017; Li *et al.* 2020). Therefore, manipulation with CRISPR/Cas9 to selectively remove OPA1 alternatively spliced exons may provide insights into the roles these play in *OPA1* function and RGC biology. This would further demonstrate if alternatively spliced exons are vital to RGC function and facilitate the development of targeted OPA1 gene therapy.

Similar to the growing interesting in OPA1, there is increasing body of evidence in the literature surrounding the *in vitro* differentiation of RGC through 2D and 3D methods. Since the start of this PhD, multiple publications have reported the feasibility of generating RGCs to understand their biology and the drive to understand the effects of pathogenic disease mechanisms (Sluch *et al.* 2015; Deng *et al.* 2016; Ohlemacher *et al.* 2016; Teotia *et al.* 2016; Sluch *et al.* 2017; Teotia *et al.* 2017; Yang *et al.* 2017; Fligor *et al.* 2018; Langer *et al.* 2018; Capowski *et al.* 2019; VanderWall *et al.* 2019; Chavali *et al.* 2020; Sridhar *et al.* 2020). Understanding RGC biology is applicable to multiple

neurodegenerative conditions, as optic nerve degeneration is a common comorbidity in classical neurodegenerative conditions including AD, PD and Huntington disease (La Morgia *et al.* 2017). Furthermore, RGCs are the primary affected cell type in glaucoma (Tham *et al.* 2014). Therefore, understanding the disease mechanisms that affect RGCs within neurodegenerative conditions is imperative to furthering our ability to solve these aetiologically complex conditions.

Although the differentiation method developed during this PhD and described in this thesis was modified from a previous publication, we hope it will provide the foundation for understanding and accelerating *OPA1*-RGC context specific research by demonstrating the feasibility of such approaches. Furthermore, the additional insight gained about OPA1 function within human 2D-RGCs, with a number of readily assayable phenotypes, can facilitate the development of novel therapeutic strategies to treat DOA.

6.1.1 Current limitations to DOA and RGC modelling

Despite the advancements in 2D and 3D *in vitro* RGC modelling, as discussed in Chapter 4, the DOA models presented in this thesis carry a number of inherent limitations that require further development to facilitate our understanding of RGC associated disease mechanisms.

Firstly, it is worth noting that DOA is a progressive disease with the initial clinical diagnosis in the second decade of life, however, the majority of patients experience a gradual decline in visual function, thus suggesting that RGCs gradually acquire disease phenotypes that ultimately contribute to their death. As such, examining the *in vitro* models presented within this thesis at a single time point demonstrates a significant limitation, given that RGCs likely undergo gradual decline in health and viability that may alter the phenotypes associated with *OPA1* mutation. Although the majority of studies utilising *OPA1* mutant iPSCs have focused on a single time point of analysis (Chen *et al.* 2016; Iannelli *et al.* 2018; Iannelli *et al.* 2019; Caglayan *et al.* 2020), Jonikas *et al.* (2018) demonstrated the effects of *OPA1* mutation, associated with PD, at multiple time points following differentiation towards dopaminergic neurons. Interestingly, Jonikas *et al.* illustrated significant reduction in mitochondrial OCR and increased mitochondrial fragmentation when comparing D65 *OPA1* mutant neurons to those at D25, but not for WT neurons, clearly demonstrating that long term culture of cells carrying *OPA1* mutations results in progressive deterioration of mitochondrial function. As such, future experimental approaches analysing *in vitro* RGCs should aim to incorporate multiple analysis time points to determine if *OPA1* mutation results in gradual acquisition of compromised phenotypes and a decline in RGC health, rather than focusing on one specific time point.

In addition, a major oversight within the molecular phenotyping of *OPA1* mutant cell lines was the failure to quantify the number or volume of mitochondria, and their integrity, within the analysed iPSC-derived cell models. Although analysis of fibroblast mitochondrial content within chapter 5 demonstrated no significant differences between *OPA1* mutant and WT cells, indicating that *OPA1* mutant cells do not have significantly reduced mitochondrial number, it is unclear whether this picture remains in *in vitro* RGCs. However, there are conflicting theories within the literature surrounding the effect of *OPA1* mutation on mitochondria mass, with studies of DOA associated *OPA1* mutant fibroblasts carrying p.S545R or p.R445H mutations exhibiting reduced mitochondrial volume, but those carrying a p.R733X mutation demonstrating similar mitochondrial volume to WT cells (Chevrollier *et al.* 2012; Kane *et al.* 2017). Similarly, in HeLa cells treated with *OPA1* siRNA mitochondrial number is increased due to fragmentation, which was also associated with a non-statistically significant increase in mitochondrial volume. Whilst in *ex vivo* mouse RGCs, mitochondrial length and number were maintained after siRNA knockdown of OPA1 (Kushnavera *et al.* 2013). Interestingly, studies of zebrafish and cardiomyocytes suggest mitochondria biogenesis is increased in response to Opa1 depletion, potentially in an attempt to restore mitochondrial homeostasis (Rahn *et al.* 2013; Xin *et al.* 2020), however, the effect of this on mitochondrial number or volume was not determined. It is therefore unclear what the direct impact of *OPA1* mutation is on mitochondrial volume and whether this contributes to the phenotypes associated with *OPA1* mutation in the cell models presented within this thesis. As such, quantification of mitochondrial number or volume should be conducted in all cell models to confirm that disease phenotypes associated with *OPA1* mutation are not being driven by reduced mitochondrial content and are a downstream result of OPA1 dysfunction.

Alongside the unclear picture of mitochondrial quantity, an additional oversight of the studies performed within this thesis is a lack of clarity surrounding mitochondrial integrity, a characteristic predominantly assessed through quantification of mitochondria membrane potential. Maintenance of the mitochondrial IMM potential is essential to mitochondrial function; required for the generation of ATP, mitochondrial protein import and overall mitochondrial quality control through mitophagy (Kühlbrandt 2015; Nguyen *et al.* 2016; Zorova *et al.* 2018). Importantly, previous studies of *OPA1* mutations have highlighted how OPA1 dysfunction results in loss of the IMM potential (Olichon *et al.* 2003; Zhang *et al.* 2017). Given that mitochondrial integrity is essential to mitochondrial function, it is therefore likely that impaired or reduced mitochondrial integrity is in part driving the phenotypes associated with OPA1 dysfunction demonstrated in chapter 5. Therefore, future studies of *OPA1* mutation should aim to clarify its effect on RGC mitochondrial integrity to investigate how the loss of integrity affects disease progression in DOA.

Although all efforts were made within this thesis to generate *in vitro* cultures with high RGC purity, unsurprisingly, there was heterogeneity within 2D cultures at the assessed time points. This was predominately evidenced through cell count assessment of IF images, which demonstrated that approximately 60 % of generated cells expressed the RGC markers BRN3B, ISI1 and SNCG at D42. This heterogeneity has also been highlighted in the published literature (Riazifar *et al.* 2014; Aparicio *et al.* 2017; Fligor *et al.* 2018) and several groups have attempted to generate enriched or pure populations of RGCs through isolation methods (Sluch *et al.* 2015; Gill *et al.* 2016; Aparicio *et al.* 2017; Sluch *et al.* 2017). In this thesis, CRISPR/Cas9 gene editing was utilised for *OPA1* genetic manipulation, demonstrating efficient generation of edited cell lines. However, it also poses an exciting instrument for generating tools to improve RGC purification and identification through the incorporation of reporter cassettes in RGC-associated genes. During the course of this PhD, a number of publications (Fligor *et al.* 2018; Langer *et al.* 2018; Capowski *et al.* 2019; VanderWall *et al.* 2019; Chavali *et al.* 2020; Sridhar *et al.* 2020) have reported utilising the *BRN3B*-reporter cell line initially reported by Sluch *et al.* (2017). *BRN3B* is expressed by approximately 70 % of all RGCs (Badea *et al.* 2009), and this reporter cell line therefore enables the isolation and purification of RGCs throughout *in vitro* differentiation, improving the purity of cultures to specifically understand RGC biology. Expanding the range of RGC-associated gene driven reporter cassettes, for example, by incorporating different fluorescent reporters into the *BRN*3 genes or into *ISL1* or *SNCG*, would also further facilitate RGC modelling, given the variability in expression of RGC-associated genes within these cultures. This would also be further advanced by identifying additional RGC specific markers, such as the work of Langer *et al.* (2018), to increase the range of RGC subtypes (Sanes *et al.* 2015) that can be analysed through RGC purification. Due to the large number of individual iPSC clones utilised within this thesis it was not feasible to generate reporter cell lines for each individual cell line. However, development and application of this reporter method within the biobank of iPSCs generated within this thesis would further allow the study of *OPA1* mutations in enriched RGC cultures to further highlight the disease mechanisms specifically associated with this cell type.

Another overlooked aspect of RGC biology in this thesis was the generation of specific RGC subtypes. Previous studies have aimed to quantify the development of RGC subtypes within *in vitro* differentiations (Sluch *et al.* 2015; Gill *et al.* 2016; Ohlemacher *et al.* 2016). These studies predominantly focus on the expression of *OPN4* to identify the presence of ipRGCs, however, all three studies confirmed the absence of ipRGCs within their cultures. More recently a study used single-cell RNA-seq to understand the diversity

of RGC populations within retinal organoids (Langer *et al.* 2018), whilst multiple RGC subtypes were also identified in 2D-RGC cultures (Chavali *et al.* 2020). However, the majority of current protocols still aim to differentiate general RGC populations rather than specifically generating RGC subtypes. However, RGC subtypes, most notably ipRGCs, have been shown to be preserved LHON and DOA (La Morgia *et al.* 2010; Perganta *et al.* 2013), whilst they have also been shown to survive in models of glaucomatous neurodegeneration (Li *et al.* 2006; Li *et al.* 2008; Zhang *et al.* 2013; Struebing *et al.* 2016), optic nerve injury (Robinson *et al.* 2004; Pérez de Sevilla Müller *et al.* 2014) and chemical excitotoxicity (DeParis *et al.* 2012). Understanding why these RGC subtypes are resistant to injury may provide insight into the deficit's vulnerable populations experience and, in turn, guide the development of therapeutic strategies to prevent RGC loss. Thus, future work on RGC *in vitro* differentiation should aim to characterise the conditions that further define RGC subtype patterning, improving overall RGC knowledge.

Another potential deficiency within this *in vitro* model of DOA is the lack of axonal myelination within the cell cultures. Although the initial projections of the RGCs are un-myelinated, once the projections leave the retina through the optic nerve head they become myelinated beyond the lamina cribosa to facilitate more rapid and efficient saltatory nerve conduction (Perry *et al.* 1990). As such, mitochondrial localisation within the axon becomes highly specialised to regions surrounding the nodes of Ranvier to enable cellular energy generation to be focused in regions of highest energetic demand (Bristow *et al.* 2002; Barron *et al.* 2004). Future modelling of DOA should therefore look to utilise models in which axonal projections become myelinated, for example, with the use of RGC-oligodendrocyte co-cultures, to understand the importance of these interactions and the effect *OPA1* mutation has on the maintenance of axonal myelination. A number of studies have demonstrated the feasibility of using microfluidic chambers to study the interactions of neurons and their myelinating cells, demonstrating the successful myelination of axonal projections in such co-cultures (Taylor *et al.* 2005; Park *et al.* 2009; Yang *et al.* 2012). Importantly, microfluidic chambers allow the isolated culture of specific cell populations whilst facilitating their interactions through microgrooves, which are only accessible for axonal projections. Use of this model system would therefore more accurately represent the morphology of RGCs and the optic nerve, designating regions of unmyelinated and myelinated projections (Figure 6.1), to study the effect of myelination on mitochondrial function and RGC biology.

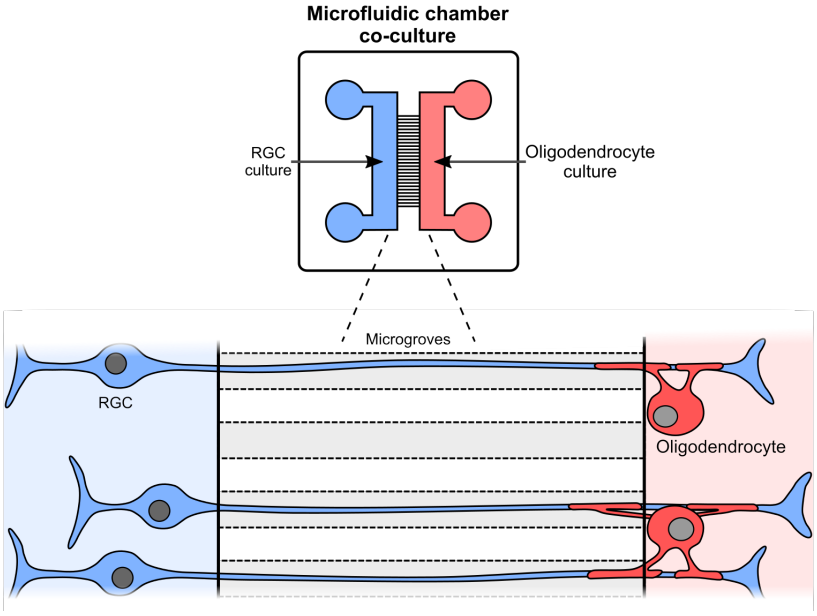

Figure 6.1. Proposed mechanism of RGC-oligodendrocyte co-culture.

Co-culture of *In vitro* generated RGCs and oligodendrocytes in microfluidic chambers separated by microgrooves generates regions of axonal projections with and without myelination, more accurately representing the axonal projections of RGCs within the retina and once they transition through the optic nerve head to form the optic nerve. This would enable the study of the effect *OPA1* mutation has on myelination maintenance, to determine if OPA1 dysfunction promotes axonal dysfunction through impaired node of Ranvier formation.

In addition to generating fluorescent reporter iPSCs for improved RGC modelling, fluorescent mitochondrial reporter proteins have been developed to enable the precise study of mitochondrial biology. Most notably MitoTimer, a version of the “Timer” protein that changes fluorescence upon oxidation fused to an MTS sequence from cytochrome *c* oxidase subunit VIII, has been demonstrated to be effective for studying mitochondrial biogenesis and dynamics (Ferree *et al.* 2013; Hernandez *et al.* 2013; Laker *et al.* 2014). Importantly, this system has been utilised to study the age and transport of mitochondria within hippocampal neurons, demonstrating its effectiveness for understanding mitochondrial biology in neurodegenerative conditions (Ferree *et al.* 2013). Combining MitoTimer and CRISPR/Cas9 gene editing, as demonstrated by Sluch *et al.* (2017), with the biobank of iPSCs generated in this thesis, would enable the production of MitoTimer-reporter iPSCs carrying both WT *OPA1* and mutant *OPA1* (Figure 6.2). MitoTimer expression would therefore be driven by *BRN3B* expression, generating increasing levels of fluorescent mitochondria as RGCs differentiate and mature (Figure 6.2). As such, the generation of CRISPR/Cas9 edited *OPA1* mutant iPSCs carrying the MitoTimer mitochondrial fluorescent reporter driven by *BRN3B* expression would remove the necessity to purify RGCS from heterogeneous cultures and aid the understanding of mitochondrial biology.

To summarise, iPSC and CRISR/Cas9 gene editing technologies now provide an excellent platform for studying DOA and its associated genetic mutations. Within this thesis, both technologies have been demonstrated to be highly effective for studying

OPA1 and the differentiation of *in vitro* RGCs, ultimately improving our ability to understand the effect of mitochondrial dysfunction in a context specific disease model.

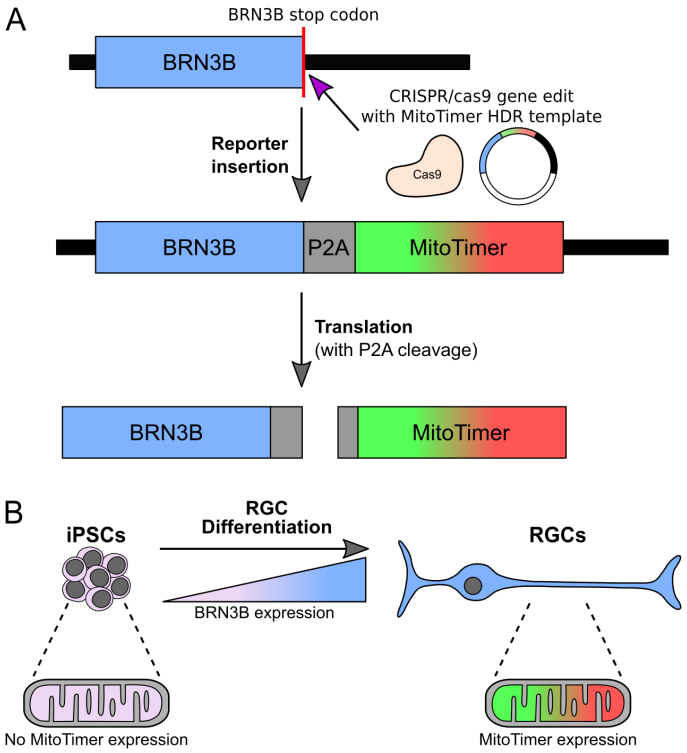

Figure 6.2. Generation of mitochondrial fluorescent reporter cell lines.

(A) Schematic of the method to generate MitoTimer-reporter iPSCs. CRISPR/Cas9 cleavage of the 3' end of the *BRN3B* gene enables insertion of the P2A-MitoTimer reporter protein downstream of the *BRN3B* coding sequence, using an HDR template carrying P2A-MitoTimer coding sequence flanked by BRN3B and BRN3B 3' UTR homology arms. Once expressed, BRN3B and MitoTimer localise to the nucleus or mitochondria due to cleave of the P2A peptide.

(B) Effect of BRN3B expression on MitoTimer expression during *in vitro* RGC differentiation. iPSCs have little to no expression of BRN3B, however, during RGC differentiation *BRN3B* expression gradually increases, inducing expression of MitoTimer, resulting in terminal RGC populations expressing fluorescently labelled mitochondria.

6.2 DOA pathogenic disease mechanisms

The initial aims of this study were to establish an *OPA1* mutant iPSCs biobank and establish an *in vitro* DOA disease model. Subsequent aims were to understand specific disease mechanisms associated with RGC biology. The data presented here demonstrate that loss of OPA1 function trigger a number of detrimental effects that likely contribute to the preferential loss of RGCs in DOA. Notably, we found evidence of dysfunctional mitochondrial bioenergetics, including reduced basal respiration and ATP synthesis, together with mitochondrial genome instability and moderate induction of mitochondrial stress related genes. Although it was hoped *in vitro* RGC disease modelling would provide clues into RGC specific disease mechanisms, most disease phenotypes established here were consist across all *in vitro* cell types studied (fibroblasts and iPSC), and it is therefore important to consider these findings in the

context of previously demonstrated molecular deficits and other neurodegenerative conditions.

Although DOA is predominantly caused by mutations to mitochondrial genes (Kerrison *et al.* 1999; Reynier *et al.* 2004; Barbet *et al.* 2005; Eiberg *et al.* 2006; Carelli *et al.* 2011; Klebe *et al.* 2012; Charif *et al.* 2015; Colavito *et al.* 2017; Gerber *et al.* 2017; Jurkute *et al.* 2019), mitochondrial dysfunction is now implicated in the aetiology and progression of age-related neurodegenerative diseases. In this thesis, mitochondrial bioenergetic failure, typified by reduced ATP levels, was consistent across all generated mutant genotypes in all studied cell types. Importantly, this phenotype was rescued when *OPA1* mutation was corrected via CRISPR/Cas9 gene editing, suggesting that restoration of WT OPA1 can rescue mitochondrial bioenergetics within previously dysfunctional networks. Although it is not known if energy failure is the primary defect causing neuronal death, it has emerged as a prominent contributory factor in models of classical neurodegenerative conditions, including PD, AD, ALS and MS (Milakovic and Johnson 2005; Finsterer 2008; Reddy 2009; Rhein *et al.* 2009; Lazzarino *et al.* 2010; Calkins *et al.* 2011; Pérez *et al.* 2017; Ludtmann *et al.* 2018; de Barcelos *et al.* 2019). Although these disorders are aetiologically complex and mostly sporadic, rather than caused directly by mitochondrial defects, collectively this body of work demonstrates the role energy failure plays in neuronal death in diverse neuronal populations.

Furthermore, energy failure is known to play a direct role in the loss of RGCs in other inherited optic neuropathies and syndromic mitochondrial diseases, in particular LHON, due to failure of complex I to drive ATP synthesis (Carelli *et al.* 2004; Lin *et al.* 2012; Wu *et al.* 2018). Similarly, HSP7, Charcot-Marie-Tooth type 2A and MELAS exhibit reduced OXPHOS capacity and ATP levels (Dubeau *et al.* 2000; Bach *et al.* 2003; Rodan *et al.* 2015; Fang *et al.* 2016; Frey *et al.* 2017; Pareek *et al.* 2018; Wolf *et al.* 2019; Nukui *et al.* 2020; Wali *et al.* 2020). The analysis of POAG patients, a disease also caused by RGC death, has also revealed ETC complex and OXPHOS inhibition in age-related RGC conditions (Abu-Amero *et al.* 2006; Lee *et al.* 2012; Van Bergen *et al.* 2015). Importantly, the defects exhibited in LHON, syndromic mitochondrial diseases and POAG confirm the susceptibility of RGCs to reduced energy production, and underline energetic failure as a key disease mechanism associated with the loss of neuronal viability.

Neuronal populations have very high metabolic requirements due to their unique morphology and the sustained energy demands arising from processes such neurotransmitter synthesis, neurotransmission and maintaining ionic gradients. RGCs in particular require high levels of energy generation due to the lack of axonal myelination in the retina (Wong-Riley 2010; Zheng *et al.* 2016; Ito *et al.* 2017). Unsurprisingly,

neuronal cells are especially susceptible to OXPHOS deficits and energy failure. Analysis of how energy failure drives neurodegeneration indicates that loss of synaptic function, due to impaired ATP synthesis, may drive neuronal death due to an inability to regulate vesicular transport (Pathak *et al.* 2015). However, given the central role of ATP for neuronal cellular function and metabolism, including the synthesis of macromolecules, cytoskeletal organisation, maintenance of ionic gradients, cell signalling cascades and cellular repair (including proteins and DNA), it is clear that energy failure has a global impact on cellular health (Shetty *et al.* 2012). Clarifying if RGCs undergo a period of neuronal dysfunction before degeneration would further illuminate the impact bioenergetic failure has on RGC loss in DOA.

In addition to reducing total cellular ATP, OXPHOS deficits are also directly coupled to the excessive generation of intrinsic cellular insults, most notably the induction of oxidative stress through the generation of ROS via electron leak from complex I and III (Nissanka and Moraes 2018). Although ROS are key second messenger molecules, excessive accumulation of ROS has significant detrimental molecular effects (Hamanaka and Chandel 2010). Due to its proximity to the source, mtDNA is frequently oxidised by ROS driving the accumulation of somatic mtDNA mutations (Chan 2006). In addition, increased ROS are known to drive mitochondrial fragmentation (Dagda *et al.* 2009; Wu *et al.* 2011) whilst also altering the organisation and permeability of the IMM, due to peroxidation of membrane phospholipids (Paradies *et al.* 2010; Guo *et al.* 2013). Furthermore, ETC proteins are also susceptible to oxidation and nitration, which reduces their enzymatic functionality (Guo *et al.* 2013), likely compounding the effects of the alterations to the IMM. ROS also impair mitochondrial OXPHOS inhibiting ATP synthesis and further promoting ROS production in a vicious feedback cycle. Studies of OPA1 have indicated that its dysfunction promotes the formation of ROS (Tang *et al.* 2009; Chen *et al.* 2012), whilst increases in ROS production have been associated with neurodegeneration in both AD and MS (Pérez *et al.* 2017; Choi *et al.* 2018). Thus, ROS present a plausible driver of RGC degeneration, perpetuating the effects of already defective cellular and mitochondrial processes.

Although these studies, and the data presented within Chapter 5, demonstrates how cellular energy failure plays a significant role within neurodegeneration, energy failure alone cannot solely be attributed to RGC death in DOA. Photoreceptor cells also rely heavily on OXPHOS to generate ATP for opsin signalling, however, these cells appear unaffected in DOA (Ito *et al.* 2007; Lenears *et al.* 2012). In addition, treatments that support mitochondrial OXPHOS function, such as idebenone, have not been show to completely rescue mitochondrial function (Haefeli *et al.* 2011) and RGC health. Notably, although idebenone is approved for clinical use in LHON patients, it demonstrated

inconsistent results for DOA in clinical trials with some patients demonstrating no improvement in visual function (Carelli *et al.* 2011; Klopstock *et al.* 2011), Most recently, an off-label cohort study of idebenone treatment in DOA patients demonstrated the majority of patients exhibited stabilisation or recovery of visual acuity when compared to un-treated patients. However, the study also reported worsening visual acuity for a number of idebenone treated individuals (Romagnoli *et al.* 2020), suggesting there are additional factors that drive optic neuropathy and treatments that provide greater benefit are required.

Another 3.didigm in neurodegenerative diseases is impaired maintenance of the mitochondrial genome. In this thesis, *OPA1* mutant cell lines were associated with reduced mtDNA integrity. Although no large-scale mtDNA rearrangements were detected by LR-PCR, qPCR analysis demonstrated the accumulation of mtDNA mutations that reduced the percentage of WT mtDNA copies. MtDNA defects have been identified in PD, ALS, MS, AD and glaucoma (Ikebe *et al.* 1990; Gu *et al.* 1998; de la Monte *et al.* 2000; Dhaliwal and Grewal 2000; Bender *et al.* 2006; Keeney and Bennett 2010; Campbell *et al.* 2011; Artuso *et al.* 2013; Sundaresan *et al.* 2015), many of which were identified before the identification of OPA1 function as a key mtDNA regulator (Elachouri *et al.* 2011). Since this initial discovery, a number of studies have linked *OPA1* mutations with impaired mtDNA maintenance (Amati-Bonneau *et al.* 2008; Hudson *et al.* 2008; Yu-Wai-Man *et al.* 2010; Chen *et al.* 2012). Although the generation of mtDNA defects is associated with ageing, the aforementioned neurodegenerative conditions exhibit significantly greater accumulation of somatic mtDNA mutations when compared to healthy individuals (Bender *et al.* 2006). Importantly, although it is believed that these mtDNA defects are secondary to the initial sporadic disease stimulus, impaired mtDNA maintenance in these disorders emphasizes how mtDNA maintenance is crucial for sustaining neuronal health (Compagnoni *et al.* 2020). Impaired mitochondrial genome maintenance undoubtedly contributes to neuronal demise given its central role in encoding ETC and mitochondrial translation components. As such, it is unsurprisingly that a defect within a mitochondrial protein such as *OPA1*, with a known role in mtDNA preservation, impacts the ability for RGCs to sustain WT mtDNA molecules and contributes to the disease mechanisms within DOA.

In addition to the direct links between OPA1 function and the maintenance of mtDNA, reduced fusion competence driven by *OPA1* mutations further perpetuate the deficiencies created by mtDNA mutation. Within this study, analysis of mitochondrial networks demonstrated significant fragmentation associated with *OPA1* mutations, confirming the effect found in a number of previous studies have investigated this phenomenon in fibroblasts (Amati-Bonneau *et al.* 2005; Zanna *et al.* 2008) and RNAi

studies (Amati-Bonneau *et al.* 2005; Arnoult *et al.* 2005; Zanna *et al.* 2008; Kushnareva *et al.* 2013). Unfortunately, analysis of RGC mitochondrial networks was not completed due to the COVID-19 pandemic. Analysis of mouse models of DOA and iPSC-derived neurons has suggested that these cell populations exhibit mitochondrial fragmentation (Davies *et al.* 2007; Jonikas *et al.* 2018; Iannielli *et al.* 2019). However, siRNA treatment to reduce *Opa1* expression in *ex vivo* rat RGCs contradicted these findings (Kushnareva *et al.* 2013). Mitochondrial fusion is key to maintaining the distribution of mtDNA, protein and metabolites through the mitochondrial network. As such, the loss of fusion capability prevents the distribution of mtDNA within the mitochondrial network (Harman 1992; Taylor *et al.* 2005; Chen *et al.* 2007; Liu *et al.* 2009; Chen *et al.* 2010; Yu-Wai-Man *et al.* 2010; Chan 2020).

Furthermore, OPA1 functions within the IMM to both maintain cristae structure and bind mtDNA nucleoids (Olichon *et al.* 2003; Alavi *et al.* 2007; Song *et al.* 2007; Agier *et al.* 2012; Yang *et al.* 2020). Loss of OPA1 function within the IMM therefore plays a dual role in the reduction of WT mtDNA quantity. Firstly by reducing the IMM structure (Frezza *et al.* 2006) and thus reducing the surface area for OPA1 membrane integration to bind and stabilise mtDNA, and secondly, due to its reduced ability to directly interact with mtDNA through exon 4b (Elachouri *et al.* 2011; Yang *et al.* 2020). As such, the reduction of WT mtDNA in *OPA1* mutant RGCs within this study is likely partly being propagated by fusion reduction, impaired IMM structure and failure of mtDNA network distribution and clearance, thus driving RGC death in DOA.

As discussed earlier, the model of DOA presented in this thesis lacks a primary characteristic of the optic nerve required for efficient neuronal conduction, namely, RGC axonal myelination (Perry *et al.* 1990). A number of studies have demonstrated how mitochondria are precisely distributed throughout RGCs, primarily due to the differing energetic demands of unmyelinated and myelinated axonal projections (Bristow *et al.* 2002; Barron *et al.* 2004; Ohno *et al.* 2011). The initial characterisation of DOA by Johnson *et al.* (1979) and Kjer *et al.* (1983) demonstrated that DOA patients have abnormal myelination within the optic nerve, exhibiting regions of reduced myelin sheath and expansive regions of demyelination. In addition, analysis of the Opa1^{Q285STOP} mouse model of DOA demonstrated significantly abnormalities in optic nerve myelination alongside noticeable regions of demyelination (Davies *et al.* 2007; White *et al.* 2009). Furthermore, reduced ETC activity through inhibition of complex I has been demonstrated to induce disorganization of the nodes of Ranvier along the optic nerve due to loss of function of node structural proteins, ultimately inducing significant visual impairment (Marella *et al.* 2013). It is, therefore, plausible that reduced basal respiration and ATP production in RGCs due to *OPA1* mutation results in abnormal myelin sheath

structure, or complete optic nerve demyelination. Previous reports have associated both DOA and LHON with an MS-like phenotype, suggesting that *OPA1* mutations can contribute to the underlying pathophysiological process that drives demyelination (Harding *et al.* 1992; Verny *et al.* 2008; Yu-Wai-Man *et al.* 2016). In a mouse model of MS, demyelination of the RGC axons was found to precede cell death, suggesting that demyelination and/or axonal degeneration may induce the activation of cell death pathways, resulting in the loss of RGCs (Shindler *et al.* 2008).

Loss of the myelin sheath, and thus the nodes of Ranvier, has significant downstream implications for axonal health due to their primary role in axonal membrane organisation. These nodes of Ranvier are characterised by the localisation of key proteins, including sodium (Na^+) and potassium (K^+) channels and the ATP demanding Na^+/K^+-ATPase pumps, which are required for maintaining the ionic gradients essential for saltatory conduction during action potential transmission (Nelson *et al.* 2017). Although saltatory conduction along myelinated axons is thought to require relatively minimal energy (Wong-Riley 2010), the breakdown of node structure results in ion pump redistribution within the axonal membrane to enable the continuation of action potential propagation, as evidenced by the redistribution of Na^+ channels in the optic nerve in a model of inflammatory demyelination (Craner *et al.* 2003; Alrashdi *et al.* 2019) and in MS (Kornek *et al.* 2001; Craner *et al.* 2004). Dysregulation of ion channels within the axon has two main effects. Firstly, an increased energy demand is induced in the axonal projection to facilitate the maintenance of membrane ion homeostasis due to the expanding region of ion flux. This promotes a loop of negative feedback whereby neurons cannot match the energetic demand of the axon, which is compounded given that energy shortage was the initial stimulus for demyelination (van den Berg *et al.* 2017; Campbell and Mahad 2018). Secondly, demyelination induces aberrant signalling cascades due to the diminished ability to maintain ion gradients, primarily through the Na^+/K^+ ATPase, resulting in the accumulation of axonal Na^+. Increasing levels of axonal Na^+ induces reversal of Na^+/Ca^{2+} exchanger and drives the influx of Ca^{2+} into the axoplasm (Campbell and Mahad 2011; van den Berg *et al.* 2017; Campbell *et al.* 2018). Ultimately this results in toxic levels of Ca^{2+}, impairing its function as a second messenger molecule and stimulating the degradation of the axon (Trapp and Stys 2009), an effect that is likely exasperated by *OPA1* mutation given their apparent inability to modulate Ca^{2+} flux (Kushnareva *et al.* 2013). Given the association of *OPA1* with an MS-like clinical presentation and the contribution of reduced ATP to axonal demyelination and ion dysregulation, it is possible that reduced mitochondrial respiration in RGCs results in aberrant axonal morphology and function, which potentially proceeds RGC death but ultimately contributes to their demise.

6.2.1 Disease mechanisms associated with DOA+

In addition to identifying specific disease mechanisms driving RGC death, the studies presented within this thesis also aimed to compare the detrimental effects of the different *OPA1* mutation subtypes given their different associations with DOA and DOA+ (Yu-Wai-Man *et al.* 2010; Ham *et al.* 2019). Analysis demonstrated the c.1334G>A point mutation within the OPA1 GTPase domain causes increased mitochondrial fragmentation (1334G>A vs 2708del fibroblasts), worse basal respiration and ATP production (in iPSC and RGC; 1334G>A vs 2708del) and moderately increased mito-stress response (1334G>A vs all genotypes). Patients diagnosed with DOA+ typically have greater levels of visual impairment compared to those with DOA (Yu-Wai-Man *et al.* 2010). Given the data presented here, and the known impact mitochondrial fragmentation and increased energetic stress have on the viability of RGCs, it is easy to appreciate how these combined mechanisms can magnify the detrimental impact on RGC survival.

However, analysis of mito-stress associated genes identified a previously unreported phenotype within 1334G>A cells, with elevated gene expression when compared to WT and haploinsufficiency associated mutations. Although these data may suggest that mito-stress is potentially driving the more severe phenotype, the picture surrounding the detrimental or beneficial expression of these genes is unclear. It has been suggested that increased levels of HSP60 drives disease progression in PD (Xanthoudakis *et al.* 1999; Feng *et al.* 2013; Noelker *et al.* 2014; Kuter *et al.* 2016; Campanella *et al.* 2018; Sun *et al.* 2018) and glaucoma (Wax *et al.* 1998; Tezel *et al.* 2000; Wax *et al.* 2001; Wax *et al.* 2008; Ebneter *et al.* 2010; Williams *et al.* 2017). Whilst the activation of the mito-stress response in yeast is known to promote the proliferation of mtDNA mutations, with reduction of *Atfs-1* (orthologue of human *ATF5*) reducing the amount of mutated mtDNA and increasing the WT percentage (Lin *et al.* 2016). Conversely, both ATF5 and HSP60 have also been demonstrated to support mitochondrial respiratory function (Nargund *et al.* 2015; Fiorese *et al.* 2016; Zhou *et al.* 2018), suggesting their upregulation may support cellular health. As such, the picture surrounding the impact of mito-stress on the progression of DOA+ is unclear, although logical routes of investigation through inhibition of mito-stress factors via RNAi, may provide greater insight into its impact.

Most notably, DOA+ is commonly associated with development of extraocular neuronal features that include sensorineural hearing loss, ataxia and peripheral neuropathy (Votruba *et al.* 1998; Amati-Bonneau *et al.* 2005; Amati-Bonneau *et al.* 2008; Yu-Wai-Man *et al.* 2010; Lenears *et al.* 2012). Therefore, mutations associated with pure DOA should not directly impact these neuronal populations to the same extent as DOA+ associated mutations. As such, modelling DOA+ associated neuronal populations, in

addition to RGCs, would provide a tool for investigating the impact of these mutations and the impact of mito-stress gene induction.

6.2.2 RGC death: the downward spiral

Based on the experimental evidence gathered over the past 2 decades about the multifaceted role OPA1 plays in mitochondrial homeostasis, it is clear that RGC loss in DOA is not driven by a single molecular defect, but rather, it is the result of multiple mitochondrial functional defects (Figure 6.3). Collectively, the inability to maintain mtDNA integrity, impaired mitochondrial dynamics, reduced bioenergetics for maintaining overall cellular function, and the failure to regulate cell signalling cascades all contribute to neuronal dysfunction and eventually, a feed forward downward spiral of progressive neurodegeneration culminating in RGC death.

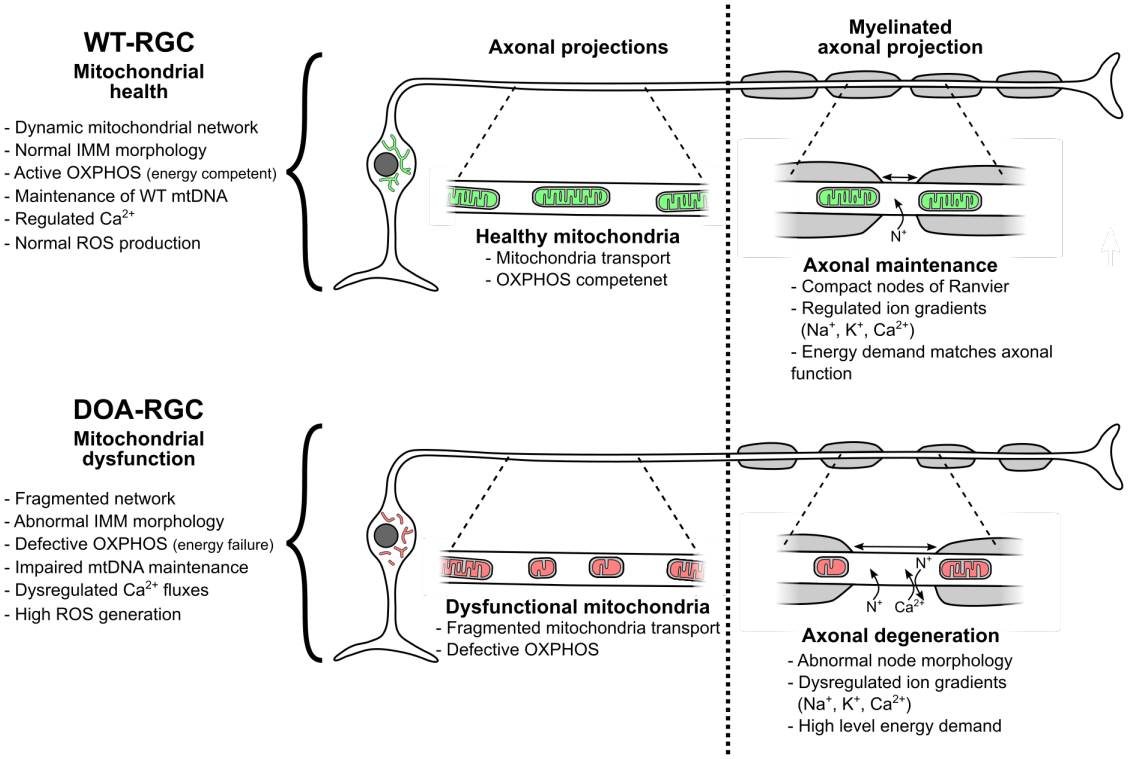

Figure 6.3. DOA disease hypothesis.

Schematic representation of the disease process in DOA related to *OPA1* mutation. WT cells have functional mitochondrial dynamics involving fission and fusion, regulate the integrity of the mitochondrial genome and are energetically competent. Loss of OPA1 function results in a fragmented mitochondrial network with impaired mtDNA maintenance and defective OXPHOS.

OPA1 mutant neurons transport morphologically abnormal mitochondria along the axonal projections, impairing axonal function. Within the myelinated optic nerve impaired mitochondrial function disrupts myelination and the nodes of Ranvier, inducing demyelination of RGC axons and causing abnormal ion gradients that induce Ca^{2+} stress and greater energy demand, which further exasperate the energetic shortfalls.

6.3 The future of DOA therapeutics

Although developing novel therapeutic strategies for DOA was not an aim of this thesis, it is hoped that the work presented here provides the foundation for future progress in

this area of unmet clinical need. It is interesting to postulate what the future of DOA therapeutics may look like given the RGC-associated disease mechanisms investigated in Chapter 5. As mentioned in Chapter 1, the current therapeutic options to treat DOA are incredibly limited with much of the focus on the use of idebenone, a cytochrome *c* analogue capable of supporting ETC function (Yu-Wai-Man *et al.* 2014; Yu-Wai-Man 2015), due to its approval for treating LHON (Mashima *et al.* 2000; Carelli *et al.* 2011; Klopstock *et al.* 2011; Klopstock *et al.* 2013; Lloria *et al.* 2019; Zhao *et al.* 2020). Unfortunately, idebenone has proven inconsistent within DOA (Barboni *et al.* 2013; Smith *et al.* 2016; Romagnoli *et al.* 2020) and its suitability as a therapy remains uncertain. The data presented in this thesis indicate that *OPA1* mutations impair mitochondrial bioenergetics in RGCs and idebenone could, therefore, have a beneficial effect. However, whether the function of idebenone is sufficient to restore RGC health given the multi-faceted function of *OPA1* in the mitochondrial network requires further investigation to further support or rule-out its use a therapy. Furthermore, as with most other therapeutic strategies, idebenone fails to correct the underlying disease mechanisms in DOA. *OPA1* mutations can result in haploinsufficiency or dominant-negative effects, and as such the development of alternative therapeutic strategies is likely to be challenging requiring different approaches depending on the underlying mechanism of action.

Most recently, gene replacement or gene therapy has been demonstrated as a viable therapeutic strategy for DOA (Figure 6.4; Del Dotto *et al.* 2017; Sarzi *et al.* 2018), given that the majority of *OPA1* mutations result in haploinsufficiency (Pesch *et al.* 2001; Marchbank *et al.* 2002; Schimpf *et al.* 2008; Ścieżyńska *et al.* 2017). However, *OPA1* gene therapy poses a number of problems that must be overcome to optimise it as a therapy. Firstly, overexpression of OPA1 has been suggested to promote mitochondrial fragmentation (Misaka *et al.* 2002; Cipolat *et al.* 2004; Griparic *et al.* 2004; Olichon *et al.* 2007). Secondly, as demonstrated in chapter 5 and by Delettre *et al.* (2001), *OPA1* is expressed in 8 isoforms due to alternative splicing of exons 4, 4b and 5b. Although the exact molecular functions of all isoforms are not entirely understood, it is becoming clearer that specific isoforms are associated with defined mitochondrial functions, such as exon 4b binding mtDNA (Yang *et al.* 2020), whilst isoforms containing exon 4b are entirely processed in S-OPA1 (Song *et al.* 2007). It its therefore imperative that the chosen cDNA utilised in gene therapy is capable of replicating the diverse isoform and functional spectrum of endogenous *OPA1* required to promote and maintain mitochondrial homeostasis.

As such, alternative therapeutic strategies to alleviate the molecular deficits caused by *OPA1* are an exciting prospect. Here, CRISPR/Cas9 gene correction of *OPA1* restored mitochondrial homeostasis, promoting a return of OXPHOS function and restored levels

of WT mtDNA. Although this study provides a proof-of-concept in rapidly dividing mitotic cells, which would likely facilitate the activity of DNA repair mechanisms and reduction of dysfunctional mitochondria, it demonstrates that restoration of endogenous gene expression provides a viable alternative to that of exogenous expression. Importantly, this approach capitalises on the endogenous cell machinery to regulate both total expression and alternative splicing, exhibited by the identical expression profiles of 1334G>A and the WT corrected cells in Chapter 5. Importantly, this approach also allows cells to regulate specific isoform expression to facilitate specific mitochondrial functions, given the diverse patterns of expression demonstrated here and by Delettre *et al.* 2001. Recent data has demonstrated the feasibility of editing post-mitotic neuronal populations, demonstrating the feasibility of *in vivo* editing genes associated with PD and AD. Targeted mutation using CRISPR/Cas9 of *Bace1*, a gene required for the generation of amyloid beta (Aβ) and thus the Aβ accumulation associated with AD, and *Snca,* encoding α-synuclein which classically aggregates in PD, prevented the adherent accumulation of protein and improved mice behavioural characteristics (Park *et al.* 2019; Yoon *et al.* 2020).

In vivo CRISPR/Cas9 gene editing has also been explored for the treatment of other inherited retinal diseases, determining the feasibility of editing genes associated with LCA and X-linked retinitis pigmentosa (XLRP). Subretinal delivery of vectors carrying CRISPR/Cas9 targeting *Cep290* caused significant levels of gene editing, reducing expression of isoforms that are known to drive LCA (Maeder *et al.* 2019). Similarly, CRISPR/Cas9 editing of *Rpgr* in a mouse model of XLRP demonstrated accurate and precise gene correction and restoration of retinal structure and function (Hu *et al.* 2020). Unlike LCA and XLRP, which affect the photoreceptors within the retina, the primary disease tissue within DOA is the RGCs, which exhibit significantly greater accessibility for treatment given their location adjacent to the vitreous humour. Therefore, *in vivo* retinal or neuronal gene editing is gradually becoming more feasible and requires further investigation for its application to DOA.

Although predominantly known for its ability to induce dsDNA breaks, the CRISPR/Cas9 field is rapidly evolving and new gene augmentation strategies are continually being developed to enable diverse strategies of genetic manipulation. CRISPR/Cas9 technology has been adapted to function as a transcriptional modifier, inactivating its nuclease activity to prevent DNA cleavage, but retaining its site-specific targeting through gRNAs to either activate (CRISPR activation or CRISPRa) or inhibit gene expression (CRISPR interference or CRISPRi). Although there are multiple CRISPRa strategies, the overarching aim of CRISPRa poses an enticing prospect for treating DOA given its dominant mode of inheritance, with the majority of patients carrying a WT copy

of *OPA1* whilst the mutated copy is likely degraded by NMD (Pesch *et al.* 2001; Schimpf *et al.* 2008). Crucially, CRISPRa has advantages over traditional gene therapy as it activates endogenous *OPA1* gene expression and thus capitalises on the splicing machinery to enable expression of the 8 *OPA1* isoforms (Figure 6.4). Importantly, CRISPRa has been demonstrated to induce gene expression across a range of genes in human, mouse and fly cell lines (Chavez *et al.* 2016). CRISPRa has also previously been shown to efficiently, and specifically, cause upregulation of gene transcripts in both *ex vivo* and *in vivo* rat neuronal populations (Savell *et al.* 2019). Furthermore, a recent study in a rhodopsin-deficient mouse model of retinitis pigmentosa demonstrated that CRISPRa induction of opsin genes reduced retinal degeneration and improved retinal function (Böhm *et al.* 2020). Collectively the data supporting CRISPRa demonstrate its feasibility as a therapeutic strategy, with excellent potential for treating DOA and other inherited retinal diseases caused by dominant mutations.

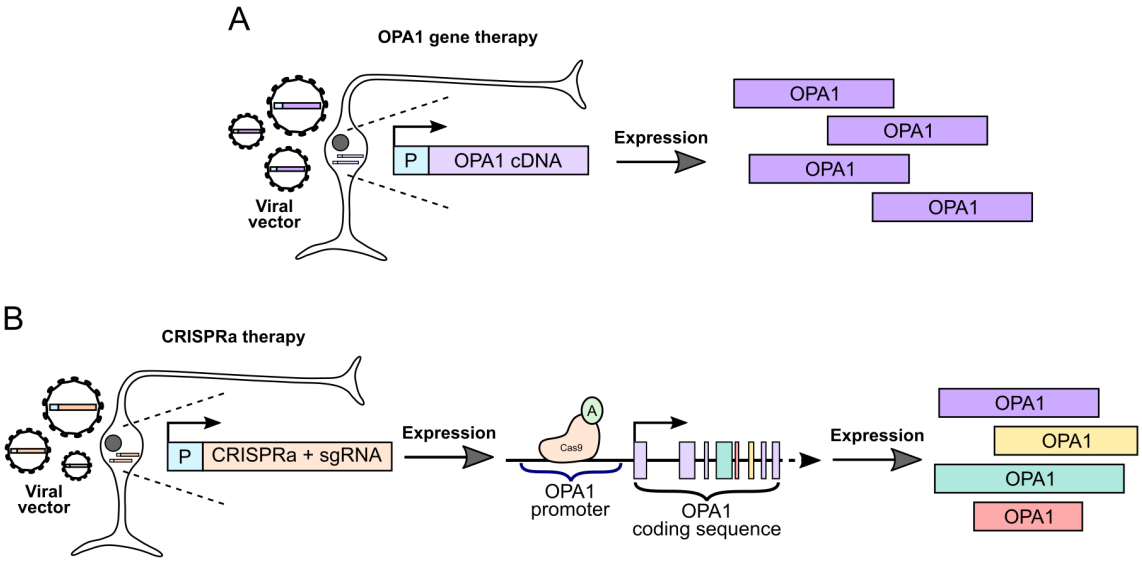

Figure 6.4. Schematics of potential therapeutic strategies for treating *OPA1*-related DOA.

(A) OPA1 gene therapy utilises *OPA1* cDNA encapsulated in viral vectors. Transduction of cells induces expression of a single isoform of OPA1. Expression of *OPA1* rescues mitochondrial homeostasis.

(B) OPA1 CRISPRa therapy. Transduction of target cells with viral vectors containing coding sequences for the CRISPRa proteins and sgRNAs targeting the *OPA1* promoter region. CRISPRa binds to the target region in the *OPA1* promoter, inducing expression of the endogenous gene. Target cells express multiple isoforms of OPA1 required for correct cellular function and restoration of mitochondrial network homeostasis.

Collectively there are now a number of diverse and effective therapeutic strategies that may be optimal for treating the underlying cause of DOA, increasing WT gene expression, whilst there are also options for reducing mutant *OPA1* transcripts. However, significant further investigation is required for optimising these strategies for treating DOA, which can hopefully capitalise on the iPSC biobank resource generated in this thesis to maximise therapeutic understanding.

6.4 Concluding remarks

Although we now have a greater understanding of OPA1 function and its role in both health and disease states, an effective treatment to halt the progressive visual loss in DOA remains elusive. The work in this thesis focused on the generation of a morphologically relevant disease model through the use of innovative stem cell and CRISPR/Cas9 gene editing technologies to understand the pathogenic disease mechanisms driving RGC loss. *In vitro* RGC disease modelling proved an effective method to understand defects associated with *OPA1* mutation, demonstrating that *OPA1* mutation has no impact on the development and differentiation of RGCs in 2D or 3D cultures. Utilising both stem cell technologies and CRISPR/Cas9 provides a near endless resource of *OPA1* mutant and isogenic control cell lines for understanding the impact of *OPA1* mutations in DOA. Importantly, CRISPR/Cas9 gene editing provides a perfect paradigm to screen and understand the effects of novel therapeutics on the restoration of mitochondrial homeostasis.

To-date, research has demonstrated that OPA1 has a multifaceted function, responsible for regulating mitochondrial dynamics, morphology and functional output. The work presented here confirms these findings in RGCs and further work will clarify whether RGC specific disease mechanisms is driving optic nerve degeneration and visual loss in DOA. A far deeper understanding of the effects of OPA1 dysfunction on RGC mitochondrial morphology, transport and bioenergetic function is thus required to unravel the disease mechanisms associated with RGC loss. We need to disentangle how, when and where these primary defects occur, together with understanding the thresholds at which these deficits drive RGC dysfunction. Only then will we be in a stronger position to develop targeted therapies to rescue RGCs in DOA.

Although there are still numerous questions that remain unanswered surrounding the process of RGC loss and visual loss in DOA, the work presented in this thesis demonstrates the usefulness of an *in vitro* iPSC-RGC model to dissect OPA1-related mechanisms and importantly, it provides a powerful model for investigating novel therapeutic strategies to prevent irreversible blindness in affected individuals.

Chapter 7: References

Aasen, T., Raya, A., Barrero, M.J., Garreta, E., Consiglio, A., Gonzalez, F., ... and Belmonte, C.J.I. (2008). "Efficient and rapid generation of induced pluripotent stem cells from human keratinocytes." Nature Biotechnology **26**: 1276-1284.

Abu-Amero, K.K., Morales, J. and Bosley, T.M. (2006). "Mitochondrial Abnormalities in Patients with Primary Open-Angle Glaucoma." Investigative Ophthalmology & Visual Science **47**(6): 2533-2541.

Adler, R. and Canto-Soler, M.V. (2007). "Molecular mechanisms of optic vesicle development: Complexities, ambiguities and controversies." Developmental Biology **305**(1): 1-13.

Agier, V., Oliviero, P., Lainé, J., L'Hermitte-Stead, C., Girard, S., Fillaut, S., ... and Lombès, A. (2012). "Defective mitochondrial fusion, altered respiratory function, and distorted cristae structure in skin fibroblasts with heterozygous OPA1 mutations." Biochimica et Biophysica Acta (BBA) - Molecular Basis of Disease **1822**(10): 1570-1580.

Ahlgren, U., Pfaff, S.L., Jessell, T.M., Edlund, T. and Edlund, H. (1997). "Independent requirement for ISL1 in formation of pancreatic mesenchyme and islet cells." Nature **385**: 257-260.

Ahn, C.S. and Metallo, C.M. (2015). "Mitochondria as biosynthetic factories for cancer proliferation." Cancer & Metabolism **3**: 1.

Aijaz, S., Erskine, L., Jeffery, G., Bhattacharya, S.S. and Votruba, M. (2004). "Developmental Expression Profile of the Optic Atrophy Gene Product: OPA1 Is Not Localized Exclusively in the Mammalian Retinal Ganglion Cell Layer." Biochemistry and Molecular Biology **45**(6).

Akepati, V.R., Muller, E.-C., Otto, A., Stauss, H.M., Portwich, M. and Alexander, C. (2008). "Characterization of Opa1 isoforms isolated from mouse tissues." Journal of Neurochemistry **106**(1).

Alavi, M.V., Bette, S., Schimpf, S., Schuettauf, F., Schraermeyer, U., Wehrl, H.F., ... and Wissinger, B. (2007). "A splice site mutation in the murine Opa1 gene features pathology of autosomal dominant optic atrophy." Brain **130**(4): 1029-1042.

Aldridge, J.E., Horibe, T. and Hoogenraad, N.J. (2007). "Discovery of Genes Activated by the Mitochondrial Unfolded Protein Response (mtUPR) and Cognate Promoter Elements." PLOS ONE **2**(9): e874.

Alexander, C., Votruba, M., Pesch, U.E.A., Thiselton, D.L., Mayer, S., Moore, A.T., ... and Wissinger, B. (2000). "OPA1, encoding a dynamin-related GTPase, is mutated in autosomal dominant optic atrophy linked to chromosome 3q28." Nature Genetics **26**: 211-215.

Alexeyev, M., Shokolenko, I., Wilson, G. and LeDoux, S. (2013). "The Maintenance of Mitochondrial DNA Integrity—Critical Analysis and Update." Cold Spring Harb Perspect Biol **5**(5): a012641.

Alrashdi, B., Dawod, B., Schampel, A., Tacke, S., Kuerten, S., Marshall, J.S. and Côté, P.D. (2019). "Nav1.6 promotes inflammation and neuronal degeneration in a mouse model of multiple sclerosis." Journal of Neuroinflammation **16**(1): 215.

Alston, C.L., Rocha, M.C., Lax, N.Z., Turnbull, D.M. and Taylor, R.W. (2017). "The genetics and pathology of mitochondrial disease." J. Pathol. **241**: 236-250.

Amati-Bonneau, P., Guichet, A., Olichon, A., Chevrollier, A., Viala, F., Miot, S., ... and Reynier, P. (2005). "OPA1 R445H mutation in optic atrophy associated with sensorineural deafness." Annals of Neurology **58**(6): 958-963.

Amati-Bonneau, P., Odent, S., Derrien, C., Pasquier, L., Malthiéry, Y., Reynier, P. and Bonneau, D. (2003). "The association of autosomal dominant optic atrophy and moderate deafness may be due to the R445H mutation in the OPA1 gene." American Journal of Ophthalmology **136**(6): 1170-1171.

Amati-Bonneau, P., Valentino, M.L., Reynier, P., Gallardo, M.E., Bornstein, B., Boissiere, A., ... and Carelli, V. (2008). "OPA1 mutations induce mitochondrial DNA instability and optic atrophy 'plus' phenotypes." Brain **131**(2): 338-351.

Amiri, M. and Hollenbeck, P.J. (2008). "Mitochondrial biogenesis in the axons of vertebrate peripheral neurons." Developmental Neurobiology **68**(11): 1348-1361.

Amit, M., Carpenter, M.K., Inokuma, M.S., Chiu, C.P., Harris, C.P., Waknitz, M.A., ... and Thomson, J.A. (2000). "Clonally Derived Human Embryonic Stem Cell Lines Maintain Pluripotency and Proliferative Potential for Prolonged Periods of Culture." Developmental Biology **227**(2): 271-278.

Anand, R., Wai, T., Baker, M.J., Kladt, N., Schauss, A.C., Rugarli, E. and Langer, T. (2014). "The i-AAA protease YME1L and OMA1 cleave OPA1 to balance mitochondrial fusion and fission." J Cell Biol **204**(6): 919–929.

Anderson, K.R., Haeussler, M., Watanabe, C., Janakiraman, V., Lund, J., Modrusan, Z., ... and Warming, S. (2018). "CRISPR off-target analysis in genetically engineered rats and mice." Nature Methods **15**(7): 512-514.

Andersson, S.G.E. and Kurland, C.G. (1998). "Reductive evolution of resident genomes." Trends in Microbiology **6**(7): 263-268.

Andreazzoli, M. (2009). "Molecular Regulation of Vertebrate Retina Cell Fate." Birth defects research **87**(3): 284-295.

Angelastro, J.M., Ignatova, T.N., Kukekov, V.G., Steindler, D.A., Stengren, G.B., Mendelsohn, C. and Greene, L.A. (2003). "Regulated Expression of ATF5 Is Required for the Progression of Neural Progenitor Cells to Neurons." The Journal of Neuroscience **23**(11): 4590.

Aoi, T., Yae, K., Nakagawa, M., Ichisaka, T., Okita, K., Takahashi, K., ... and Yamanaka, S. (2008). "Generation of Pluripotent Stem Cells from Adult Mouse Liver and Stomach Cells." Science **321**(5889): 699-702.

Aparicio, J.G., Hopp, H., Choi, A., Mandayam Comar, J., Liao, V.C., Harutyunyan, N. and Lee, T.C. (2017). "Temporal expression of CD184 (CXCR4) and CD171 (L1CAM) identifies distinct early evelopmental stages of human retinal ganglion cells in embryonic stem cell derived retina." Experimental Eye Research **154**(177-189).

Arnoult, D., Grodet, A., Lee, Y.-J., Estaquier, J. and Blackstone, C. (2005). "Release of OPA1 during Apoptosis Participates in the Rapid and Complete Release of Cytochrome c and Subsequent Mitochondrial Fragmentation." The Journal of Biological Chemistry **280**: 35742-35750.

Artuso, L., Zoccolella, S., Favia, P., Amati, A., Capozzo, R., Logroscino, G., ... and Petruzzella, V. (2013). "Mitochondrial genome aberrations in skeletal muscle of patients with motor neuron disease." Amyotrophic Lateral Sclerosis and Frontotemporal Degeneration **14**(4): 261-266.

Ashley, N., Harris, D. and Poulton, J. (2005). "Detection of mitochondrial DNA depletion in living human cells using PicoGreen staining." Experimental Cell Research **303**(2): 432-446.

Avilion, A.A., Nicolis, S.K., Pevny, L.H., Perez, L., Vivian, N. and Lovell-Badge, R. (2003). "Multipotent cell lineages in early mouse development depend on SOX2 function." Genes Dev. **17**: 126-140.

Bach, D., Pich, S., Soriano, F.X., Vega, N., Baumgartner, B., Oriola, J., ... and Zorzano, A. (2003). "Mitofusin-2 Determines Mitochondrial Network Architecture and Mitochondrial Metabolism: A NOVEL REGULATORY MECHANISM ALTERED IN OBESITY." Journal of Biological Chemistry **278**(19): 17190-17197.

Badea, T.C., Cahill, H., Ecker, J., Hattar, S. and Nathans, J. (2009). "Distinct Roles of Transcription Factors Brn3a and Brn3b in Controlling the Development, Morphology, and Function of Retinal Ganglion Cells." Neuron **61**(6): 852-864.

Badea, T.C., Williams, J., Smallwood, P., Shi, M., Motajo, O. and Nathans, J. (2012). "Combinatorial expression of Brn3 transcription factors in somatosensory neurons: genetic and morphologic analysis." Journal of Neuroscience **32**(3): 995-1007.

Bailey, T.J., El-Hodiri, H., Zhang, L., Shah, R., Mathers, P.H. and Jamrich, M. (2004). "Regulation of vertebrate eye development by Rx genes." Int. J. Dev. Biol. **48**: 761-770.

Baird, L. and Dinkova-Kostova, A.T. (2011). "The cytoprotective role of the Keap1–Nrf2 pathway." Archives of Toxicology **85**(4): 241-272.

Baker, B.M., Nargund, A.M., Sun, T. and Haynes, C.M. (2012). "Protective Coupling of Mitochondrial Function and Protein Synthesis via the eIF2α Kinase GCN-2." PLOS Genetics **8**(6): e1002760.

Baker, D., Hirst, Adam J., Gokhale, Paul J., Juarez, Miguel A., Williams, S., Wheeler, M., ... and Barbaric, I. (2016). "Detecting Genetic Mosaicism in Cultures of Human Pluripotent Stem Cells." Stem Cell Reports **7**(5): 998-1012.

Baltan, S., Inman, D.M., Danilov, C.A., Morrison, R.S., Calkins, D.J. and Horner, P.J. (2010). "Metabolic Vulnerability Disposes Retinal Ganglion Cell Axons to Dysfunction in a Model of Glaucomatous Degeneration." The Journal of Neuroscience **30**(16): 5644-5652.

Ban, T., Ishihara, T., Kohno, H., Saita, S., Ichimura, A., Maenaka, K., ... and Ishihara, N. (2017). "Molecular basis of selective mitochondrial fusion by heterotypic action between OPA1 and cardiolipin." Nature Cell Biology **19**: 856-863.

Ban, T., Kohno, H., Ishihara, T. and Ishihara, N. (2018). "Relationship between OPA1 and cardiolipin in mitochondrial inner-membrane fusion." Biochimica et Biophysica Acta (BBA) - Bioenergetics **1859**(9): 951-957.

Banerjee, D., Banerjee, A., Mookherjee, S., Vishal, M., Mukhopadhyay, A., Sen, A., ... and Ray, K. (2013). "Mitochondrial Genome Analysis of Primary Open Angle Glaucoma Patients." PLOS ONE **8**(8): e70760.

Bao, X.R., Ong, S., Goldberger, O., Peng, J., Sharma, R., Thompson, D.A., ... and Mootha, V.K. (2016). "Mitochondrial dysfunction remodels onecarbon metabolism in human cells." eLife **5**: e10575.

Bao, Z.Z. (2008). "Intraretinal projection of retinal ganglion cell axons as a model system for studying axon navigation." Brain Research **1192**: 165-177.

Barbet, F., Hakiki, S., Orssaud, C., Gerber, S., Perrault, I., Hanein, S., ... and Rozet, J.-M. (2005). "A third locus for dominant optic atrophy on chromosome 22q." Journal of Medical Genetics **42**: e1.

Barboni, P., Carbonelli, M., Savini, G., Foscarini, B., Parisi, V., Valentino, M.L., ... and Carelli, V. (2010). "OPA1 Mutations Associated with Dominant Optic Atrophy Influence Optic Nerve Head Size." Ophthalmology **117**(8): 1547-1553.

Barboni, P., Savini, G., Cascavilla, M.L., Caporali, L., Milesi, J., Borrelli, E., ... and Carelli, V. (2014). "Early Macular Retinal Ganglion Cell Loss in Dominant Optic Atrophy: Genotype-Phenotype Correlation." American Journal of Ophthalmology **158**(3): 628-636.e623.

Barboni, P., Savini, G., Parisi, V., Carbonelli, M., La Morgia, C., Maresca, A., ... and Carelli, V. (2011). "Retinal Nerve Fiber Layer Thickness in Dominant Optic Atrophy: Measurements by Optical Coherence Tomography and Correlation with Age." Ophthalmology **118**(10): 2076-2080.

Barboni, P., Valentino, M.L., La Morgia, C., Carbonelli, M., Savini, G., De Negi, A., ... and Carelli, V. (2013). "Idebenone treatment in patients with OPA1-mutant dominant optic atrophy." Brain **136**: 1-5.

Barnes, D.E. (2001). "Non-homologous end joining as a mechanism of DNA repair." Current Biology **11**(12): R455-R457.

Barnils, N., Mesa, E., Munoz, S., Ferrer-Artola, A. and Arruga, J. (2007). "Response to Idebenone and multivitamin therapy in Leber's Hereditary Optic Neuropathy." Arch Soc Esp Oftalmol **82**: 377-380.

Barres, B.A., Silverstein, B.E., Corey, D.P. and Chun, L.L.Y. (1988). "Immunological, Morphological, and Electrophysiological Variation among Retinal Ganglion Cells Purified by Panning." Neuron **1**: 791-803.

Barrientos, A. (2002). "In vivo and in organello assessment of OXPHOS activities." Methods **26**(4): 307-316.

Barron, M.J., Griffiths, P., Turnbull, D.M., Bates, D. and Nichols, P. (2004). "The distributions of mitochondria and sodium channels reflect the specific energy requirements and conduction properties of the human optic nerve head." British Journal of Ophthalmology **88**(2): 286-290.

Bejarano-Escobar, R., Álvarez-Hernán, G., Morona, R., González, A., Martín-Partido, G. and Francisco-Morcillo, J. (2015). "Expression and function of the LIM-homeodomain transcription factor Islet-1 in the developing and mature vertebrate retina." Experimental Eye Research **138**: 22-31.

Belenguer, P. and Pellegrin, L. (2013). "The dynamin GTPase OPA1: More than mitochondria?" Biochimica et Biophysica Acta (BBA) - Molecular Cell Research **1833**: 176-183.

Ben-Sahra, I., Hoxhaj, G., Ricoult, S.J.H., Asara, J.M. and Manning, B.D. (2016). "mTORC1 induces purine synthesis through control of the mitochondrial tetrahydrofolate cycle." Science **351**(6274): 728-733.

Bender, A., Krishnan, K.J., Morris, C.M., Taylor, G.A., Reeve, A.K., Perry, R.H., ... and Turnbull, D.M. (2006). "High levels of mitochondrial DNA deletions in substantia nigra neurons in aging and Parkinson disease." Nature Genetics **38**: 515-517.

Berkelaar, M., Clarke, D.B., Wang, Y.C., Bray, G.M. and Aguayo, A.J. (1994). "Axotomy results in delayed death and apoptosis of retinal ganglion cells in adult rats." J Neurosci. **14**(7): 4368-4374.

Bertholet, A.M., Millet, A.M.E., Guillermin, O., Daloyau, M., Davezac, N., Miquel, M.C. and Belenguer, P. (2013). "OPA1 loss of function affects in vitro neuronal maturation." Brain **136**(5): 1518-1533.

Bigler, R.L., Kamande, J.W., Dumitru, R., Niedringhaus, M. and Taylor, A.M. (2017). "Messenger RNAs localized to distal projections of human stem cell derived neurons." Scientific Reports **7**: 611.

Blakely, E.L., de Silva, R., King, A., Schwarzer, V., Harrower, T., Dawidek, G., ... and Taylor, R.W. (2005). "LHON/MELAS overlap syndrome associated with a mitochondrial MTND1 gene mutation." European Journal of Human Genetics **13**(5): 623-627.

Bleazard, W., McCaffery, J.M., King, E.J., Bale, S., Mozdy, A., Tieu, Q., ... and Shaw, J.M. (1999). "The dynamin-related GTPase Dnm1 regulates mitochondrial fission in yeast." Nature Cell Biology **1**(5): 298-304.

Blum, B. and Benvenisty, N. (2009). "The tumorigenicity of diploid and aneuploid human pluripotent stem cells." Cell Cycle **8**(23): 3822-3830.

Blunsom, N.J., Gomez-Espinosa, E., Ashlin, T.G. and Cockcrof, S. (2018). "Mitochondrial CDP-diacylglycerol synthase activity is due to the peripheral protein, TAMM41 and not due to the integral membrane protein, CDP-diacylglycerol synthase 1." Biochimica et Biophysica Acta (BBA) - Molecular and Cell Biology of Lipids **1863**(3): 294-298.

Bocca, C., Kane, M.S., Veyrat-Durebex, C., Chupin, S., Alban, J., Kouassi Nzoughet, J., ... and Reynier, P. (2018). "The Metabolomic Bioenergetic Signature of Opa1-Disrupted Mouse Embryonic Fibroblasts Highlights Aspartate Deficiency." Scientific Reports **8**(1): 11528.

Bocca, C., Kouassi Nzoughet, J., Leruez, S., Amati-Bonneau, P., Ferré, M., Kane, M.-S., ... and Reynier, P. (2018). "A Plasma Metabolomic Signature Involving Purine Metabolism in Human Optic Atrophy 1 (OPA1)-Related Disorders." Investigative Ophthalmology & Visual Science **59**(1): 185-195.

Bodick, N. and Levinthal, C. (1980). "Growing optic nerve fibers follow neighbors during embryogenesis." Proc. Nati. Acad. Sci. USA. **77**(7): 4374-4378.

Böhm, S., Splith, V., Riedmayr, L.M., Rötzer, R.D., Gasparoni, G., Nordström, K.J.V., ... and Becirovic, E. (2020). "A gene therapy for inherited blindness using dCas9-VPR–mediated transcriptional activation." Science Advances **6**(34): eaba5614.

Bonneau, D., Colin, E., Oca, F., Ferré, M., Chevrollier, A., Guéguen, N., ... and Reynier, P. (2014). "Early-onset Behr syndrome due to compound heterozygous mutations in OPA1." Brain **137**(10): e301-e301.

Bonneau, D., Souied, E., Gerber, S., Rozet, J.M., D'Haens, E., Journel, H., ... and Kaplan, J. (1995). "No evidence of genetic heterogeneity in dominant optic atrophy." Journal of Medical Genetics **32**: 951-953.

Bosanquet, N. and Mehta, P. (2009). Evidence Base to Support the UK Vision Strategy. London, RNIB.

Boyer, L.A., Lee, T.I., Cole, M.F., Johnstone, S.E., Levine, S.S., Zucker, J.P., ... and Young, R.A. (2005). "Core Transcriptional Regulatory Circuitry in Human Embryonic Stem Cells." Cell **122**(6): 947-956.

Brinkman, E.K. and van Steensel, B. (2019). Rapid Quantitative Evaluation of CRISPR Genome Editing by TIDE and TIDER. CRISPR Gene Editing: Methods and Protocols. Y. Luo. New York, NY, Springer New York**:** 29-44.

Bris, C., Goudenege, D., Desquiret-Dumas, V., Charif, M., Colin, E., Bonneau, D., ... and Procaccio, V. (2018). "Bioinformatics Tools and Databases to Assess the Pathogenicity of Mitochondrial DNA Variants in the Field of Next Generation Sequencing." Frontiers in Genetics **9**(632).

Bristow, E.A., Griffiths, P.G., Andrews, R.M., Johnson, M.A. and Turnbull, D.M. (2002). "The Distribution of Mitochondrial Activity in Relation to Optic Nerve Structure." Archives of Ophthalmology **120**(6): 791-796.

Brooks, M.J., Chen, H.Y., Kelley, R.A., Mondal, A.K., Nagashima, K., De Val, N., ... and Swaroop, A. (2019). "Improved Retinal Organoid Differentiation by Modulating Signaling Pathways Revealed by Comparative Transcriptome Analyses with Development In Vivo." Stem Cell Reports **13**: 891-905.

Brown, N.L., Patel, S., Brzezinski, J. and Glaser, T. (2001). "Math5 is required for retinal ganglion cell and optic nerve formation." Development **128**(13): 2497-2508.

Bulthuis, E.P., Adjobo-Hermans, M.J.W., Willems, P.H.G.M. and Koopman, W.J.H. (2019). "Mitochondrial Morphofunction in Mammalian Cells." Antioxid. Redox Signal. **30**(18): 2066-2109.

Burrows, C.K., Banovich, N.E., Pavlovic, B.J., Patterson, K., Gallego Romero, I., Pritchard, J.K. and Gilad, Y. (2016). "Genetic Variation, Not Cell Type of Origin, Underlies the Majority of Identifiable Regulatory Differences in iPSCs." PLOS Genetics **12**(1): e1005793.

Buskin, A., Zhu, L., Chichagova, V., Basu, B., Mozaffari-Jovin, S., Dolan, D., ... and Lako, M. (2018). "Disrupted alternative splicing for genes implicated in splicing and ciliogenesis causes PRPF31 retinitis pigmentosa." Nature Communications **9**(1): 4234.

Caglayan, S., Hashim, A., Cieslar-Pobuda, A., Jensen, V., Behringer, S., Talug, B., ... and Staerk, J. (2020). "Optic Atrophy 1 Controls Human Neuronal Development by Preventing Aberrant Nuclear DNA Methylation." iScience **23**(6): 101154.

Calkins, M.J., Manczak, M., Mao, P., Shirendeb, U. and Reddy, P.H. (2011). "Impaired mitochondrial biogenesis, defective axonal transport of mitochondria, abnormal mitochondrial dynamics and synaptic degeneration in a mouse model of Alzheimer's disease." Human Molecular Genetics **20**(23): 4515-4529.

Campanella, C., Pace, A., Bavisotto, C.C., Marzullo, P., Gammazza, A.M., Buscemi, S. and Piccionello, A.P. (2018). "Heat Shock Proteins in Alzheimer's Disease: Role and Targeting." Int J Mol Sci. **19**(9): 2603.

Campbell, G. and Mahad, D.J. (2018). "Mitochondrial dysfunction and axon degeneration in progressive multiple sclerosis." FEBS Letters **592**(7): 1113-1121.

Campbell, G.R. and Mahad, D.J. (2011). "Mitochondria as Crucial Players in Demyelinated Axons: Lessons from Neuropathology and Experimental Demyelination." Autoimmune Diseases **2011**: 262847.

Campbell, G.R., Ziabreva, I., Reeve, A.K., Krishnan, K.J., Reynolds, R., Howell, O., ... and Mahad, D.J. (2011). "Mitochondrial DNA deletions and neurodegeneration in multiple sclerosis." Annals of Neurology **69**(3): 481-492.

Capowski, E.E., Samimi, K., Mayerl, S.J., Phillips, M.J., Pinilla, I., Howden, S.E., ... and Gamm, D.M. (2019). "Reproducibility and staging of 3D human retinal organoids across multiple pluripotent stem cell lines." Human Development **146**.

Carelli, V., Ghelli, A., Zanna, C., Baracca, A., Sgarbi, G. and Martinuzzi, A. (2004). "Severe Defect of Complex I–Dependent ATP Synthesis Shapes the Mitochondria–Driven Path of Apoptotic Cell Death in Leber's Hereditary Optic Neuropathy (LHON)." Investigative Ophthalmology & Visual Science **45**(13): 1624-1624.

Carelli, V., La Morgia, C., Valentino, M.L., Barboni, P., Ross-Cisneros, F.N. and Sadun, A.A. (2009). "Retinal ganglion cell neurodegeneration in mitochondrial inherited disorders." Biochimica et Biophysica Acta (BBA) - Bioenergetics **1787**(5): 518-528.

Carelli, V., La Morgia, C., Valentino, M.L., Rizzo, G., Carbonelli, M., De Negri, A.M., ... and Barboni, P. (2011). "Idebenone Treatment In Leber's Hereditary Optic Neuropathy." Brain **134**(9): e188-e188.

Carelli, V., Musumeci, O., Caporali, L., Zanna, C., La Morgia, C., Del Dotto, V., ... and Zeviani, M. (2015). "Syndromic parkinsonism and dementia associated with OPA1 missense mutations." Annals of Neurology **78**(1): 21-38.

Carelli, V., Sabatelli, M., Carrozzo, R., Rizza, T., Schimpf, S., Wissinger, B., ... and Bertini, E. (2014). "'Behr syndrome' with OPA1 compound heterozygote mutations." Brain **138**(1): e321-e321.

Carelli, V., Schimpf, S., Fuhrmann, N., Valentino, M.L., Zanna, C., Iommarini, L., ... and Wissinger, B. (2011). "A clinically complex form of dominant optic atrophy (OPA8) maps on chromosome 16." Human Molecular Genetics **20**(10): 1893-1905.

Caricasole, A.A., van Schaik, R.H., Zeinstra, L.M., Wierikx, C.D., van Gurp, R.J., van den Pol, M., ... and van den Eijnden-van Raaij, A.J. (1998). "Human growth-differentiation factor 3 (hGDF3): developmental regulation in human teratocarcinoma cell lines and expression in primary testicular germ cell tumours." Oncogene **16**(1): 95-103.

Casari, G., De Fusco, M., Ciarmatori, S., Zeviani, M., Mora, M., Fernandez, P., ... and Ballabio, A. (1998). "Spastic Paraplegia and OXPHOS Impairment Caused by Mutations in Paraplegin, a Nuclear-Encoded Mitochondrial Metalloprotease." Cell **93**(6): 973-983.

Catarino, C., Ahting, U., Gusic, M., Arcangela, I., Repp, B., Peters, K., ... and Klopstock, T. (2017). "Characterization of a Leber's hereditary optic neuropathy (LHON) family harboring two primary LHON mutations m.11778G>A and m.14484T>C of the mitochondrial DNA." Mitochondrion **36**: 15-20.

Centanin, L. and Wittbrodt, J. (2014). "Retinal neurogenesis." Development **141**: 241-244.

Cepko, C.L., Austin, C.P., Yang, X., Alexiades, M. and Ezzeddine, D. (1996). "Cell fate determination in the vertebrate retina." Proc. Natl. Acad. Sci. USA **93**: 589-595.

Chaban, Y., Boekema, E.J. and Dudkina, N.V. (2014). "Structures of mitochondrial oxidative phosphorylation supercomplexes and mechanisms for their stabilisation." Biochimica et Biophysica Acta (BBA) - Bioenergetics **1837**(4): 418-426.

Chambers, I., Colby, D., Robertson, M., Nichols, J., Lee, S., Tweedie, S. and Smith, A. (2003). "Functional Expression Cloning of Nanog, a Pluripotency Sustaining Factor in Embryonic Stem Cells." Cell **113**(5): 643-655.

Chambers, I., Silva, J., Colby, D., Nichols, J., Nijmeijer, B., Robertson, M., ... and Smith, A. (2007). "Nanog safeguards pluripotency and mediates germline development." Nature **450**: 1230-1234.

Chan, D.C. (2006). "Mitochondria: Dynamic Organelles in Disease, Aging, and Development." Cell **125**(7): 1241-1252.

Chan, D.C. (2020). "Mitochondrial Dynamics and Its Involvement in Disease." Annual Review of Pathology: Mechanisms of Disease **15**(1): 235-259.

Chanana, A.M., Rhee, J.W. and Wu, J.C. (2016). "Human Induced Pluripotent Stem Cell Approaches to Model Inborn and Acquired Metabolic Heart Diseases." Curr Opin Cardiol. **31**(3): 266-274.

Chao, J.R., Lamba, D.A., Klesert, T.R., La Torre, A., Hoshino, A., R.J., T., ... and Reh, T.A. (2017). "Transplantation of Human Embryonic Stem Cell-Derived Retinal Cells into the Subretinal Space of a Non-Human Primate." Translational Vision Science & Technology **6**(4).

Charif, M., Roubertie, A., Salime, S., Mamouni, S., Goizet, C., Hamel, C.P. and Lenears, G. (2015). "A novel mutation of AFG3L2 might cause dominant optic atrophy in patients with mild intellectual disability." Front Genet **6**(311).

Chau, L.-Y. (2015). "Heme oxygenase-1: emerging target of cancer therapy." Journal of Biomedical Science **22**(1): 22.

Chaudhry, A., Shi, R. and Luciani, D.S. (2020). "A pipeline for multidimensional confocal analysis of mitochondrial morphology, function and dynamics in pancreatic β-cells." American Journal of Physiology-Endocrinology and Metabolism **318**(2): E87-E101.

Chavali, V.R.M., Haider, N., Rathi, S., Alapati, T., He, J., Gill, K., ... and Mills, J.A. (2020). "Dual SMAD inhibition and Wnt inhibition enhances the differentiation of induced pluripotent stem cells into Retinal Ganglion cells (iPSC-RGCs)." Scientific Reports **10**.

Chavez, A., Tuttle, M., Pruitt, B.W., Ewen-Campen, B., Chari, R., Ter-Ovanesyan, D., ... and Church, G. (2016). "Comparison of Cas9 activators in multiple species." Nature Methods **13**(7): 563-567.

Chen, H., Chomyn, A. and Chan, D.C. (2005). "Disruption of Fusion Results in Mitochondrial Heterogeneity and Dysfunction." The Journal of Biological Chemistry **280**.

Chen, H., Detmer, S.A., Ewald, A.J., Griffin, E.E., Fraser, S.E. and Chan, D.C. (2003). "Mitofusins Mfn1 and Mfn2 coordinately regulate mitochondrial fusion and are essential for embryonic development." Journal of Cell Biology **160**(2): 189-200.

Chen, H., McCaffery, J.M. and Chan, D.C. (2007). "Mitochondrial Fusion Protects against Neurodegeneration in the Cerebellum." Cell **130**(3): 548-562.

Chen, H., Vermulst, M., Wang, Y.E., Chomyn, A., Prolla, T.A., McCaffery, J.M. and Chan, D.C. (2010). "Mitochondrial fusion is required for mtDNA stability in skeletal muscle and tolerance of mtDNA mutations." Cell. **141**(2): 280-289.

Chen, J., Riazifar, H., Guan, M.-X. and Huang, T. (2016). "Modeling autosomal dominant optic atrophy using induced pluripotent stem cells and identifying potential therapeutic targets." Stem Cell Research & Therapy **7**(2).

Chen, L., Gong, Q., Stice, J.P. and Knowlton, A.A. (2009). "Mitochondrial OPA1, apoptosis, and heart failure." Cardiovascular Research **84**(1): 91–99.

Chen, L., Liu, T., Tran, A., Lu, X., Tomilov, A.A., Davies, V., ... and Knowlton, A.A. (2012). "OPA1 Mutation and Late-Onset Cardiomyopathy: Mitochondrial Dysfunction and mtDNA Instability." Journal of the American Heart Association **1**: e003012.

Chen, S., Wang, Q.L., Nie, Z., Sun, H., Lennon, G., Copeland, N.G., ... and Zack, D.J. (1997). "Crx, a Novel Otx-like Paired-Homeodomain Protein, Binds to and Transactivates Photoreceptor Cell-Specific Genes." Neuron **19**(5): 1017-1030.

Chen, Y.-H. and Pruett-Miller, S.M. (2018). "Improving single-cell cloning workflow for gene editing in human pluripotent stem cells." Stem Cell Research **31**: 186-192.

Chevrollier, A., Guillet, V., Loiseau, D., Gueguen, N., Pou de Crescenzo, M.-A., Verny, C., ... and Reynier, P. (2008). "Hereditary optic neuropathies share a common mitochondrial coupling defect." Annals of Neurology **63**(6): 794-798.

Chevrollier, A., Cassereau, J., Ferré, M., Alban, J., Desquiret-Dumas, V., Gueguen, N., ... and Reynier, P. (2012). "Standardized mitochondrial analysis gives new insights into mitochondrial dynamics and OPA1 function." The International Journal of Biochemistry & Cell Biology **44**(6): 980-988.

Chin, M.H., Mason, M.J., Xie, W., Volinia, S., Singer, M., Peterson, C., ... and Lowry, W.E. (2009). "Induced Pluripotent Stem Cells and Embryonic Stem Cells Are Distinguished by Gene Expression Signatures." Cell Stem Cell **5**(1): 111-123.

Choi, I.-Y., Lee, P., Adany, P., Hughes, A.J., Belliston, S., Denney, D.R. and Lynch, S.G. (2018). "In vivo evidence of oxidative stress in brains of patients with progressive multiple sclerosis." Multiple Sclerosis Journal **24**(8): 1029-1038.

Chow, R.L., Altmann, C.R., Lang, R.A. and Hemmati-Brivanlou, A. (1999). "Pax6 induces ectopic eyes in a vertebrate." Development **126**(19): 4213-4222.

Chow, R.L. and Lang, R.A. (2001). "Early Eye Development in Vertebrates." Annual Review of Cell and Developmental Biology **17**(1): 255-296.

Chua, V.T., Grafa, R., Wirtza, T., Webera, T., Favreta, J., Lia, X., ... and Rajewskya, K. (2016). "Efficient CRISPR-mediated mutagenesis in primary immune cells using CrispRGold and a C57BL/6 Cas9 transgenic mouse line." PNAS **113**(44): 12514-12519.

Chun, B.Y. and Rizzo III, J.F. (2017). "Dominant Optic Atrophy and Leber's Hereditary Optic Neuropathy: Update on Clinical Features and Current Therapeutic Approaches." Seminars in Pediatric Neurology **24**(2): 129-134.

Chung, K.W., Kim, S.B., Park, K.D., Choi, K.G., Lee, J.H., Eun, H.W., ... and Choi, B.O. (2006). "Early onset severe and late-onset mild Charcot–Marie–Tooth disease with mitofusin 2 (MFN2) mutations." Brain **129**(8): 2103-2118.

Cipolat, S., Martins de Brito, O., Zillo, B.D. and Scorrano, L. (2004). "OPA1 requires mitofusin 1 to promote mitochondrial fusion. ." PNAS **101**(45): 15927-15932.

Clark, A.T., Rodriguez, R.T., Bodnar, M.S., Abeyta, M.J., Cedars, M.I., Turek, P.J., ... and Reijo Pera, R.A. (2004). "Human STELLAR, NANOG, and GDF3 Genes Are Expressed in Pluripotent Cells and Map to Chromosome 12p13, a Hotspot for Teratocarcinoma." Stem Cells **22**(2): 160-179.

Cogliati, S., Frezza, C., Soriano, M.E., Varanita, T., Quintana-Cabrera, R., Corrado, M., ... and Scorrano, L. (2013). "Mitochondrial Cristae Shape Determines Respiratory Chain Supercomplexes Assembly and Respiratory Efficiency." Cell **155**(1): 160-171.

Cohn, A.C., Toomes, C., Potter, C., Towns, K.V., Hewitt, A.W., C.F., I., ... and Mackey, D.A. (2007). "Autosomal Dominant Optic Atrophy: Penetrance and Expressivity in Patients With OPA1 Mutations." American Journal of Ophthalmology **143**(4): 656-662.e651.

Colavito, D., Maritan, V., Suppiej, A., Del Giudice, E., Mazzarolo, M., Miotto, S., ... and Leon, A. (2017). "Non-syndromic isolated dominant optic atrophy caused by the p.R468C mutation in the AFG3 like matrix AAA peptidase subunit 2 gene." Biomed Rep **7**(5): 451-454.

Compagnoni, G.M., Di Fonzo, A., Corti, S., Comi, G.P., Bresolin1 and Masliah, E. (2020). "The Role of Mitochondria in Neurodegenerative Diseases: the Lesson from Alzheimer's Disease and Parkinson's Disease." Molecular Neurobiology **57**: 2959–2980.

Cong, L., Ann Ran, F., D., C., Lin, S., Barretto, R., Habib, N., ... and Zhang, F. (2013). "Multiplex Genome Engineering Using CRISPR/Cas Systems." Science **339**(6121).

Cornille, K., Milea, D., Amati-Bonneau, P., Procaccio, V., Zazoun, L., Guillet, V., ... and Lenaers, G. (2008). "Reversible optic neuropathy with OPA1 exon 5b mutation." Annals of Neurology **63**(5): 667-671.

Coronado, M., Fajardo, G., Nguyen, K., Zhao, M., Kooiker, K., Jung, G., ... and Bernstein, D. (2018). "Physiological Mitochondrial Fragmentation Is a Normal Cardiac Adaptation to Increased Energy Demand." Circulation Research **122**(2): 282-295.

Coughlin, L., Morrison, R.S., Horner, P.J. and Inman, D.M. (2015). "Mitochondrial Morphology Differences and Mitophagy Deficit in Murine Glaucomatous Optic Nerve." Investigative Ophthalmology & Visual Science **56**(3): 1437-1446.

Cradick, T.J., Fine, E.J., Antico, C.J. and Bao, G. (2013). "CRISPR/Cas9 systems targeting β-globin and CCR5 genes have substantial off-target activity." Nucleic Acids Research **41**(20): 9584-9592.

Craft, C.M., Whitmore, D.H. and Wiechmann, A.F. (1994). "Cone arrestin identified by targeting expression of a functional family." J Biol Chem. **269**: 4613-4619.

Craner, M.J., Lo, A.C., Black, J.A. and Waxman, S.G. (2003). "Abnormal sodium channel distribution in optic nerve axons in a model of inflammatory demyelination." Brain **126**(7): 1552-1561.

Craner, M.J., Newcombe, J., Black, J.A., Hartle, C., Cuzner, M.L. and Waxman, S.G. (2004). "Molecular changes in neurons in multiple sclerosis: Altered axonal expression of Nav1.2 and Nav1.6 sodium channels and Na+/Ca2+ exchanger." Proceedings of the National Academy of Sciences of the United States of America **101**(21): 8168-8173.

Czaniecki, C., Ryan, T., Stykel, M.G., Drolet, J., Heide, J., Hallam, R., ... and Ryan, S.D. (2019). "Axonal pathology in hPSC-based models of Parkinson's disease results from loss of Nrf2 transcriptional activity at the Map1b gene locus." PNAS **116**(28): 14280-14289.

Dagda, R.K., Cherra, S.J., Kulich, S.M., Tandon, A., Park, D. and Chu, C.T. (2009). "Loss of PINK1 Function Promotes Mitophagy through Effects on Oxidative Stress and Mitochondrial Fission." Journal of Biological Chemistry **284**(20): 13843-13855.

Danese, A., Patergnani, S., Bonora, M., Wieckowski, M.R., Previati, M., Giorgi, C. and Pinton, P. (2017). "Calcium regulates cell death in cancer: Roles of the mitochondria and mitochondria-associated membranes (MAMs)." Biochimica et Biophysica Acta (BBA) - Bioenergetics **1858**(8): 615-627.

D'Antonio, M., Benaglio, P., Jakubosky, D., Greenwald, W.W., Matsui, H., Donovan, M.K.R., ... and Frazer, K.A. (2018). "Insights into the Mutational Burden of Human Induced Pluripotent Stem Cells from an Integrative Multi-Omics Approach." Cell Reports **24**(4): 883-894.

David, G. and Barrett, E.F. (2003). "Mitochondrial Ca2+ uptake prevents desynchronization of quantal release and minimizes depletion during repetitive stimulation of mouse motor nerve terminals." The Journal of Physiology **548**(2): 425-438.

Davies, V.J., Hollins, A.J., Piechota, M.J., Yip, W., Davies, J.R., White, K.E., ... and Votruba, M. (2007). "OPA1 deficiency in a mouse model of autosomal dominant optic atrophy impairs mitochondrial morphology, optic nerve structure and visual function." Human Molecular Genetics **16**(11): 1307-1318.

Davis, A.F. and Clayton, D.A. (1996). "In situ localization of mitochondrial DNA replication in intact mammalian cells." Journal of Cell Biology **135**(4): 883-893.

de Barcelos, I.P., Troxell, R.M. and Graves, J.S. (2019). "Mitochondrial Dysfunction and Multiple Sclerosis." Biology (Basel). **8**(2): 37.

de la Monte, S.M., Luong, T., Neely, T.R., Robinson, D. and Wands, J.R. (2000). "Mitochondrial DNA Damage as a Mechanism of Cell Loss in Alzheimer's Disease." Laboratory Investigation **80**(8): 1323-1335.

de la Torre, J.R., Höpker, V.H., Guo-li Ming, G.-L., Poo, M.-M., Tessier-Lavigne, M., Hemmati-Brivanlou, A. and Holt, C.E. (1997). "Turning of Retinal Growth Cones in a Netrin-1 Gradient Mediated by the Netrin Receptor DCC." Neuron **19**(6): 1211-1224.

Deas, E., Wood, N.W. and Plun-Favreau, H. (2011). "Mitophagy and Parkinson's disease: The PINK1–parkin link." Biochimica et Biophysica Acta (BBA) - Molecular Cell Research **1813**(4): 623-633.

Deiner, M.S., Kennedy, T.E., Fazeli, A., Serafini, T., Tessier-Lavigne, M. and Sretavan, D.W. (1997). "Netrin-1 and DCC Mediate Axon Guidance Locally at the Optic Disc: Loss of Function Leads to Optic Nerve Hypoplasia." Neuron **19**(3): 575-589.

Del Dotto, V., Mishra, P., Vidoni, S., Fogazza, M., Maresca, A., Caporali, L., ... and Zanna, C. (2017). "OPA1 Isoforms in the Hierarchical Organization of Mitochondrial Functions." Cell Reports **19**: 2557-2571.

Delettre, C., Griffoin, J.-M., Kaplan, J., Dollfus, H., Lorenz, B., Faivre, L., ... and Hamel, C.P. (2001). "Mutation spectrum and splicing variants in the OPA1 gene." Hum Genet **109**: 584-591.

Delettre, C., Lenaers, G., Belenguer, P. and Hamel, C.P. (2003). "Gene structure and chromosomal localization of mouse Opa1 : its exclusion from the Bst locus." BMC Genetics **4**(1): 8.

Delettre, C., Lenears, G., Griffoin, J.-M., Gigarel, N., Lorenzo, N., Belenguer, P., ... and Hamel, C.P. (2000). "Nuclear gene OPA1, encoding a mitochondrial dynamin-related protein, is mutated in dominant optic atrophy." Nature Genetics **26**(207-210).

Deng, F., Chen, M., Liu, Y., Hu, H., Xiong, Y., Xu, C., ... and Ge, J. (2016). "Stage-specific differentiation of iPSCs toward retinal ganglion cell lineage." Molecular Vision **22**: 536-547.

Deng, W.-L., Gao, M.-L., Lei, X.-L., Lv, J.-N., Zhao, H., He, K.-W., ... and Jin, Z.-B. (2018). "Gene Correction Reverses Ciliopathy and Photoreceptor Loss in iPSC-Derived Retinal Organoids from Retinitis Pigmentosa Patients." Stem Cell Reports **10**(4): 1267-1281.

DeParis, S.W., Caprara, C. and Grimm, C. (2012). "Intrinsically photosensitive retinal ganglion cells are resistant to N-methyl-D-aspartic acid excitotoxicity." Mol Vis. **18**: 2814–2827.

Detmer, S.A. and Chan, D.C. (2007). "Functions and dysfunctions of mitochondrial dynamics." Nature Reviews Molecular Cell Biology **8**: 870-879.

Dhaliwal, G.K. and Grewal, R.P. (2000). "Mitochondrial DNA deletion mutation levels are elevated in ALS brains." NeuroReport **11**(11): 2507-2509.

Ding, Q., Regan, S.N., Xia, Y., Oostrom, L.A., Cowan, C.A. and Musunuru, K. (2013). "Enhanced Efficiency of Human Pluripotent Stem Cell Genome Editing through Replacing TALENs with CRISPRs." Cell Stem Cell **12**(4): 393–394.

Diot, A., Guillou, E., Daloyau, M., Arnauné-Pelloquin, L., Emorine, L.J. and Belenguer, P. (2009). "Transmembrane segments of the dynamin Msp1p uncouple its functions in the control of mitochondrial morphology and genome maintenance." Journal of Cell Science **122**(15): 2632.

Drago, I., De Stefani, D., Rizzuto, R. and Pozzan, T. (2012). "Mitochondrial Ca2+ uptake contributes to buffering cytoplasmic Ca2+ peaks in cardiomyocytes." Proceedings of the National Academy of Sciences **109**(32): 12986-12991.

Draper, J.S., Pigott, C., Thomson, J.A. and Andrews, P.W. (2002). "Surface antigens of human embryonic stem cells: changes upon differentiation in culture." Journal of Anatomy **200**(3): 249-258.

Dubeau, F., De Stefano, N., Zifkin, B.G., Arnold, D.L. and Shoubridge, E.A. (2000). "Oxidative phosphorylation defect in the brains of carriers of the tRNAleu(UUR) A3243G mutation in a MELAS pedigree." Annals of Neurology **47**(2): 179-185.

Duvezin-Caube, S., Jagasia, R., Wagener, J., Hofmann, S., Trifunovic, A., Hansson, A., ... and Reichert, A.S. (2006). "Proteolytic Processing of OPA1 Links Mitochondrial Dysfunction to Alterations in Mitochondrial Morphology." The Journal of Biological Chemistry **281**: 37972-37979.

Ebneter, A., Casson, R.J., Wood, J.P.M. and Chidlow, G. (2010). "Microglial Activation in the Visual Pathway in Experimental Glaucoma: Spatiotemporal Characterization and Correlation with Axonal Injury." Invest. Ophthalmol. Vis. Sci. **51**(12): 6448-6460.

Ecker, J.L., Dumitrescu, O.D., Wong, K.Y., Alam, N.M., Chen, S.K., Le Gates, T., ... and Hatta, S. (2010). "Melanopsin-Expressing Retinal Ganglion-Cell Photoreceptors: Cellular Diversity and Role in Pattern Vision." Neuron **67**(1): 49-60.

Eiberg, H., Hansen, L., Kjer, B., Hansen, T., Pedersen, O., Bille, M., ... and Tranebjærg, L. (2006). "Autosomal dominant optic atrophy associated with hearing impairment and impaired glucose regulation caused by a missense mutation in the WFS1 gene." Journal of Medical Genetics **43**: 435-440.

Eiberg, H., Kjer, B., Kjer, P. and Rosenberg, T. (1994). "Dominant optic atrophy (OPA1) mapped to chromosome 3q region. I. Linkage analysis." Human Molecular Genetics **3**(6): 977-980.

Eikaru, M., Takata, N., Ishibashi, H., Kawada, M., Sakaura, E., Okuda, S., Sekiguchi, K., Adachi, T., and Sasai, Y. (2011). “Self-organising optic-cup morphogenesis in three-dimensional culture.” Nature **472**: 51-56.

Elachouri, G., Vidoni, S., Zanna, C., Pattyn, A., H., B., Gaget, K., ... and Lenaers, G. (2011). "OPA1 links human mitochondrial genome maintenance to mtDNA replication and distribution." Genome Res. **21**(1): 12-20.

Eliott, D., Traboulsi, E.I. and Maumenee, I.H. (1993). "Visual Prognosis in Autosomal Dominant Optic Atrophy (Kjer Type)." American Journal of Ophthalmology **115**(3): 360-367.

Elshatory, Y., Deng, M., Xie, X. and Gan, L. (2007). "Expression of the LIM-homeodomain protein Isl1 in the developing and mature mouse retina." The Journal of Comparative Neurology **503**(1): 182-197.

Enver, T., Soneji, S., Joshi, C., Brown, J., Iborra, F., Orntoft, T., ... and Andrews, P.W. (2005). "Cellular differentiation hierarchies in normal and culture-adapted human embryonic stem cells." Human Molecular Genetics **14**(21): 3129-3140.

Erkman, L., McEvilly, R.J., Luo, L., Ryan, A.K., Hooshmand, F., O'Connell, S.M., ... and Rosenfeld, M.G. (1996). "Role of transcription factors Brn-3.1 and Brn-3.2 in auditory and visual system development." Nature **381**(6583): 603-606.

Erskine, L. and Herrera, E. (2007). "The retinal ganglion cell axon's journey: Insights into molecular mechanisms of axon guidance." Developmental Biology **308**(1): 1-14.

Erskine, L., Reijntjes, S., Pratt, T., Denti, L., Schwarz, Q., Vieira, J.M., ... and Ruhrberg, C. (2011). "VEGF Signaling through Neuropilin 1 Guides Commissural Axon Crossing at the Optic Chiasm." Neuron **70**(5): 951-965.

Fang, D., Yan, S., Yu, Q., Chen, D. and Yan, S.S. (2016). "Mfn2 is Required for Mitochondrial Development and Synapse Formation in Human Induced Pluripotent Stem Cells/hiPSC Derived Cortical Neurons." Scientific Reports **6**(1): 31462.

Farias, J., Holt, C.E., Sotelo, J.R. and Sotelo-Silveira, J.R. (2020). "Axon micro-dissection and transcriptome profiling reveals the in vivo RNA content of fully differentiated myelinated motor axons." RNA **26**(3).

Farrar, G.J., Carrigan, M., Dockery, A., Millington-Ward, S., Palfi, A., Chadderton, N., ... and Humphries, P. (2017). "Toward an elucidation of the molecular genetics of inherited retinal degenerations." Human Molecular Genetics **26**(R1): R2-R11.

Fazeli, A., Liew, C.G., Matin, M.M., Elliott, S., Jeanmeure, L.F.C., Wright, P.C., ... and Andrews, P.W. (2011). "Altered patterns of differentiation in karyotypically abnormal human embryonic stem cells." Int. J. Dev. Biol. **55**: 175-180.

Feng, M.J., Zhang, L., Liu, Z., Zhou, P. and Lu, X. (2013). "The Expression and Release of Hsp60 in 6-OHDA Induced In Vivo and In Vitro Models of Parkinson's Disease." Neurochemical Research **38**: 2180–2189.

Ferre, M., Amati-Bonneau, P., Tourmen, Y., Malthièry, Y. and Reynier, P. (2005). "eOPA1: An Online Database for OPA1 Mutations." Human Mutation **25**: 423-428

Ferre, M., Caignard, A., Milea, D., Leruez, S., Cassereau, J., Chevrollier, A., ... and Reynier, P. (2015). "Improved Locus-Specific Database for OPA1 Mutations Allows Inclusion of Advanced Clinical Data." Human Mutation **36**(1): 20-25.

Ferree, A.W., Trudeau, K., Zik, E., Benador, I.Y., Twig, G., Gottlieb, R.A. and Shirihai, O.S. (2013). "MitoTimer probe reveals the impact of autophagy, fusion, and motility on subcellular distribution of young and old mitochondrial protein and on relative mitochondrial protein age." Autophagy **9**(11): 1887-1896.

Ferreirinha, F., Quattrini, A., Pirozzi, M., Valsecchi, V., Dina, G., Broccoli, V., ... and Rugarli, E.I. (2004). "Axonal degeneration in paraplegin-deficient mice is associated with abnormal mitochondria and impairment of axonal transport." The Journal of Clinical Investigation **113**(2): 231-242.

Finsterer, J. (2008). "Leigh and Leigh-Like Syndrome in Children and Adults." Pediatric Neurology **39**(4): 223-235.

Fiorese, Christopher J., Schulz, Anna M., Lin, Y.-F., Rosin, N., Pellegrino, Mark W. and Haynes, Cole M. (2016). "The Transcription Factor ATF5 Mediates a Mammalian Mitochondrial UPR." Current Biology **26**(15): 2037-2043.

Fligor, C.M., Langer, K.B., Sridhar, A., Ren, Y., Shields, P.K., Edler, M.C., ... and Meyer, J.S. (2018). "Three-Dimensional Retinal Organoids Facilitate the Investigation of Retinal Ganglion Cell Development, Organization and Neurite Outgrowth from Human Pluripotent Stem Cells." Scientific Reports **8**: 14520.

Fluegge, D., Moeller, L.M., Cichy, A., Gorin, M., Weth, A., Veitinger, S., ... and Spehr, M. (2012). "Mitochondrial Ca2+ mobilization is a key element in olfactory signaling." Nature Neuroscience **15**(5): 754-762.

Folmes, Clifford D.L., Nelson, Timothy J., Martinez-Fernandez, A., Arrell, D.K., Lindor, Jelena Z., Dzeja, Petras P., ... and Terzic, A. (2011). "Somatic Oxidative Bioenergetics Transitions into Pluripotency-Dependent Glycolysis to Facilitate Nuclear Reprogramming." Cell Metabolism **14**(2): 264-271.

Frank, M., Duvezin-Caubet, S., Koob, S., Occhipinti, A., Jagasia, R., Petcherski, A., ... and Reichert, A.S. (2012). "Mitophagy is triggered by mild oxidative stress in a mitochondrial fission dependent manner." Biochimica et Biophysica Acta (BBA) - Molecular Cell Research **1823**(12): 2297-2310.

Fraser, J.A., Biousse, V. and Newman, N.J. (2010). "The Neuro-ophthalmology of Mitochondrial Disease." Survey of Ophthalmology **55**(4): 299-334.

Frey, S., Geffroy, G., Desquiret-Dumas, V., Gueguen, N., Bris, C., Belal, S., ... and Procaccio, V. (2017). "The addition of ketone bodies alleviates mitochondrial dysfunction by restoring complex I assembly in a MELAS cellular model." Biochimica et Biophysica Acta (BBA) - Molecular Basis of Disease **1863**(1): 284-291.

Frezza, C., Cipolat, S., de Brito, O.M., Micaroni, M., Beznoussenko, G.V., Rudka, T., ... and Scorrano, L. (2006). "OPA1 Controls Apoptotic Cristae Remodeling Independently from Mitochondrial Fusion." Cell **126**(1): 177-189.

Fu, Y., Foden, J.A., Khayter, C., Maeder, M.L., Reyon, D., Joung, J.K. and Sander, J.D. (2013). "High-frequency off-target mutagenesis induced by CRISPR-Cas nucleases in human cells." Nature Biotechnology **31**: 822-826.

Fuhrmann, N., Alavi, M.V., Bitoun, P., Woernie, S., Auburger, G., Leo-Kottler, B., ... and Wissinger, B. (2009). "Genomic rearrangements in OPA1 are frequent in patients with autosomal dominant optic atrophy." Journal of Medical Genetics **46**: 136-144.

Fuller, H.R., Mandefro, B., Shirran, S.L., Gross, A.R., Kaus, A.S., Botting, C.H., ... and Sareen, D. (2016). "Spinal Muscular Atrophy Patient iPSC-Derived Motor Neurons Have Reduced Expression of Proteins Important in Neuronal Development." Front. Cell. Neurosci. **9**: 506.

Fusaki, N., Ban, H., Nishiyama, A., Saeki, K. and Hasegawa, M. (2009). "Efficient induction of transgene-free human pluripotent stem cells using a vector based on Sendai virus, an RNA virus that does not integrate into the host genome." Proc Jpn Acad Ser B Phys Biol Sci. **85**: 348-362.

Gagliardi, G., Ben M'Barek, K., Chaffiol, A., Slembrouck-Brec, A., Conart, J.-B., Nanteau, C., ... and Goureau, O. (2018). "Characterization and Transplantation of CD73-Positive Photoreceptors Isolated from Human iPSC-Derived Retinal Organoids." Stem Cell Reports **11**(3): 665-680.

Galera-Monge, T., Zurita-Díaz, F., Moreno-Izquierdo, A., Fraga, M.F., Fernández, A.F., Ayuso, C., ... and Gallardo, M.E. (2016). "Generation of a human iPSC line from a patient with an optic atrophy 'plus' phenotype due to a mutation in the OPA1 gene." Stem Cell Research **16**(3): 673-676.

Galloway, N.R., Amoaku, W.M.K., Galloway, P.H. and Browning, A.C. (2006). Basic anatomy and physiology of the eye. Common eye diseases and their management. London, Springer**:** 7–15.

Gammage, P.A., Moraes, C.T. and Minczuk, M. (2018). "Mitochondrial Genome Engineering: The Revolution May Not Be CRISPR-Ized." Trends Genet. **34**(2): 101-110.

Gan, L., Wang, S.W., Huang, Z. and Klein, W.H. (1999). "POU domain factor Brn-3b is essential for retinal ganglion cell differentiation and survival but not for initial cell fate specification." Dev Biol. **210**(2): 469-480.

Garita-Hernandez, M., Routet, F., Guibbal, L., Khabou, H., Toualbi, L., Riancho, L., ... and Dalkara, D. (2020). "AAV-Mediated Gene Delivery to 3D Retinal Organoids Derived from Human Induced Pluripotent Stem Cells." Int. J. Mol. Sci. **21**: 994.

Garneua, J.E., Dupulus, M.-E., Villion, M., Romero, D.A., Barrangou, R., Boyaval, P., ... and Moineau, S. (2010). "The CRISPR/Cas bacterial immune system cleaves bacteriophage and plasmid DNA." Nature **468**: 67-71.

Gasiunasa, G., Barrangoub, R., Horvathc, P. and Siksnysa, V. (2012). "Cas9–crRNA ribonucleoprotein complex mediates specific DNA cleavage for adaptive immunity in bacteria." PNAS **109**(39): E2579–E2586.

Geisler, S., Holmström, K.M., Skujat, D., Fiesel, F.C., Rothfuss, O.C., Kahle, P.J. and Springer, W. (2010). "PINK1/Parkin-mediated mitophagy is dependent on VDAC1 and p62/SQSTM1." Nature Cell Biology **12**(2): 119-131.

Gerber, S., Charif, M., Chevrollier, A., Chaumette, T., Angebault, C., Kane, M.S., ... and Lenaers, G. (2017). "Mutations in DNM1L, as in OPA1, result in dominant optic atrophy despite opposite effects on mitochondrial fusion and fission." Brain **140**(10): 2586-2596.

Ghosh, Z., Wilson, K.D., Wu, Y., Hu, S., Quertermous, T. and Wu, J.C. (2010). "Persistent Donor Cell Gene Expression among Human Induced Pluripotent Stem Cells Contributes to Differences with Human Embryonic Stem Cells." PLOS ONE **5**(2): e8975.

Gilkerson, R.W., Selker, J.M.L. and Capaldi, R.A. (2003). "The cristal membrane of mitochondria is the principal site of oxidative phosphorylation." FEBS Letters **546**(2): 355-358.

Gill, K.P., Hung, S.S.C., Sharov, A., Lo, C.Y., Needham, K., Lidgerwood, G.E., ... and Wong, R.C.B. (2016). "Enriched retinal ganglion cells derived from human embryonic stem cells." Scientific Reports **6**: 30552.

Gillespie, R.L., Hall, G. and Black, G.C. (2014). "Genetic testing for inherited ocular disease: delivering on the promise at last?" Clinical & Experimental Ophthalmology **42**(1): 65-77.

Giorgi, C., Marchi, S. and Pinton, P. (2018). "The machineries, regulation and cellular functions of mitochondrial calcium." Nature Reviews Molecular Cell Biology **19**(11): 713-730.

Gomes, L.C., Benedetto, G.D. and Scorrano, L. (2011). "During autophagy mitochondria elongate, are spared from degradation and sustain cell viability." Nature Cell Biology **13**(5): 589-598.

Gonzalez-Cordero, A., Goh, D., Kruczek, K., Naeem, A., Fernando, M., Kleine Holthaus, S.M., ... and Ali, R.R. (2018). "Assessment of AAV Vector Tropisms for Mouse and Human Pluripotent Stem Cell-Derived RPE and Photoreceptor Cells." Hum Gene Ther. **29**(10): 1124-1139.

Gonzalez-Cordero, A., Kruczek, K., Naeem, A., Fernando, M., Kloc, M., Ribeiro, J., ... and Ali, R.R. (2017). "Recapitulation of human retinal development from human pluripotent stem cells generates transplantable populations of cone photoreceptors." Stem Cell Reports **9**: 820-837.

Graw, J. (2010). Chapter Ten - Eye Development. Current Topics in Developmental Biology. P. Koopman, Academic Press. **90:** 343-386.

Green, D.J., Sallah, S.R., Ellingford, J.M., Lovell, S.C. and Sergouniotis, P.I. (2020). "Variability in Gene Expression is Associated with Incomplete Penetrance in Inherited Eye Disorders." Genes **11**(2): 179.

Griffiths, E.J. and Rutter, G.A. (2009). "Mitochondrial calcium as a key regulator of mitochondrial ATP production in mammalian cells." Biochimica et Biophysica Acta (BBA) - Bioenergetics **1787**(11): 1324-1333.

Griparic, L., van der Wel, N.N., Orozco, I.J., Peters, P.J. and van der Bliek, A.M. (2004). "Loss of the Intermembrane Space Protein Mgm1/OPA1 Induces Swelling and Localized Constrictions along the Lengths of Mitochondria." The Journal of Biological Chemistry **279**: 18792-18798.

Gu, M., Cooper, J.M., Taanman, J.W. and Schapira, A.H.V. (1998). "Mitochondrial DNA transmission of the mitochondrial defect in Parkinson's disease." Annals of Neurology **44**(2): 177-186.

Guan, K., Farh, L., Marshall, T.K. and Deschenes, R.J. (1993). "Normal mitochondrial structure and genome maintenance in yeast requires the dynamin-like product of the MGM1 gene." Curr Genet **24**: 141-148.

Guenther, M.G., Frampton, G.M., Soldner, F., Hockemeyer, D., Mitalipova, M., Jaenisch, R. and Young, R.A. (2010). "Chromatin Structure and Gene Expression Programs of Human Embryonic and Induced Pluripotent Stem Cells." Cell Stem Cell **7**(2): 249-257.

Gundry, Michael C., Brunetti, L., Lin, A., Mayle, Allison E., Kitano, A., Wagner, D., ... and Nakada, D. (2016). "Highly Efficient Genome Editing of Murine and Human Hematopoietic Progenitor Cells by CRISPR/Cas9." Cell Reports **17**(5): 1453-1461.

Gunter, T.E., Buntinas, L., Sparagna, G. and Eliseev, R.G., K. (2000). "Mitochondrial calcium transport: mechanisms and functions." Cell Calcium **28**(5/6): 285–296.

Guo, C., Sun, L., Chen, X. and Zhang, D. (2013). "Oxidative stress, mitochondrial damage and neurodegenerative diseases." Neural regeneration research **8**(21): 2003-2014.

Gutiérrez-Aguilar, M. and Baines, C.P. (2013). "Physiological and pathological roles of mitochondrial SLC25 carriers." Biochem J. **454**(3): 371-386.

Haefeli, R.H., Erb, M., Gemperli, A.C., Robay, D., Courdier Fruh, I., Anklin, C., ... and Gueven, N. (2011). "NQO1-Dependent Redox Cycling of Idebenone: Effects on Cellular Redox Potential and Energy Levels." PLOS ONE **6**(3): e17963.

Haider, N.B., Mollema, N., Gaule, M., Yuan, Y., Sachs, A.J., Nystuen, A.M., ... and Nishina, P.M. (2009). "Nr2e3-directed transcriptional regulation of genes involved in photoreceptor development and cell-type specific phototransduction." Experimental eye Research **89**(3): 365-372.

Halfter, W., Dong, S., Balasubramani, M. and Bier, M.E. (2001). "Temporary Disruption of the Retinal Basal Lamina and Its Effect on Retinal Histogenesis." Developmental Biology 238, 79–96 (2001) **238**: 79-96.

Hall, C.N., Klein-Flügge, M.C., Howarth, C. and Attwell, D. (2012). "Oxidative Phosphorylation, Not Glycolysis, Powers Presynaptic and Postsynaptic Mechanisms Underlying Brain Information Processing." Journal of Neuroscience **32**(26): 8940-8951.

Hallam, D., Hilgen, G., Dorgau, B., Zhu, L., Yu, M., Bojic, S., ... and Lako, M. (2018). "Human-Induced Pluripotent Stem Cells Generate Light Responsive Retinal Organoids with Variable and Nutrient-Dependent Efficiency." Stem Cells **36**: 1535-1551.

Ham, M., Han, J., Osann, K., Smith, M. and Kimonis, V. (2019). "Meta-analysis of genotype-phenotype analysis of OPA1 mutations in autosomal dominant optic atrophy." Mitochondrion **46**: 262-269.

Hamanaka, R.B. and Chandel, N.S. (2010). "Mitochondrial reactive oxygen species regulate cellular signaling and dictate biological outcomes." Trends in Biochemical Sciences **35**(9): 505-513.

Harding, A.E., Sweeney, M.G., Miller, D.H., Mumford, C.J., Kellar-Wood, H., Menard, D., ... and Compston, D.A. (1992). "Occurrence of a multiple sclerosis-like illness in women who have a Leber's hereditary optic neuropathy mitochondrial DNA mutation. ." Brain **115**(979-989).

Harewood, L. and Fraser, P. (2014). "The impact of chromosomal rearrangements on regulation of gene expression." Human Molecular Genetics **23**(R1): R76-R82.

Harman, D. (1992). "Free radical theory of aging." Mutation Research **275**: 257-266.

He, L., Chinnery, P.F., Durham, S.E., Blakely, E.L., Wardell, T.M., Borthwick, G.M., ... and Turnbull, D.M. (2002). "Detection and quantification of mitochondrial DNA deletions in individual cells by real-time PCR." Nucleic Acids Research **30**(14): e68.

He, X., HongKan, H., LuCai, L. and Ma, Q. (2009). "Nrf2 is critical in defense against high glucose-induced oxidative damage in cardiomyocytes." Journal of Molecular and Cellular Cardiology **46**(1): 47-58.

Heavner, W. and Pevny, L. (2012). "Eye Development and Retinogenesis." Cold Spring Harb Perspect Biol. **4**: a008391.

Heng, J.-C.D., Feng, B., Han, J., Jiang, J., Kraus, P., Ng, J.-H., ... and Ng, H.-H. (2010). "The Nuclear Receptor Nr5a2 Can Replace Oct4 in the Reprogramming of Murine Somatic Cells to Pluripotent Cells." Cell Stem Cell **6**(2): 167-174.

Herlan, M., Vogel, F., Bornhövd, C., Neupert, W. and Reichert, A.S. (2003). "Processing of Mgm1 by the Rhomboid-type Protease Pcp1 Is Required for Maintenance of Mitochondrial Morphology and of Mitochondrial DNA." Journal of Biological Chemistry **278**(30): 27781-27788.

Hermann, G.J., Thatcher, J.W., Mills, J.P., Hales, K.G., Fuller, M.T., Nunnari, J. and Shaw, J.M. (1998). "Mitochondrial Fusion in Yeast Requires the Transmembrane GTPase Fzo1p." Journal of Cell Biology **143**(2): 359-373.

Hernandez, G., Thornton, C., Stotland, A., Lui, D., Sin, J., Ramil, J., ... and Gottlieb, R.A. (2013). "MitoTimer: A novel tool for monitoring mitochondrial turnover." Autophagy **9**: 1852-1861

Herst, P.M., Rowe, M.R., Carson, G.M. and Berridge, M.V. (2017). "Functional Mitochondria in Health and Disease." Frontiers in Endocrinology **8**(296).

Hocking, J.C., Hehr, C.L., Bertolesi, G.E., Wu, J.Y. and McFarlane, S. (2010). "Distinct roles for Robo2 in the regulation of axon and dendrite growth by retinal ganglion cells." Mechanisms of Development **127**(1-2): 36-48.

Holmström, K.M., Baird, L., Zhang, Y., Hargreaves, I., Chalasani, A., Land, J.M., ... and Abramov, A.Y. (2013). "Nrf2 impacts cellular bioenergetics by controlling substrate availability for mitochondrial respiration." Biology Open **2**: 761-770.

Holt, I.J., He, J., Mao, C.-C., Boyd-Kirkup, J.D., Martinsson, P., Sembongi, H., ... and Spelbrink, J.N. (2007). "Mammalian mitochondrial nucleoids: Organizing an independently minded genome." Mitochondrion **7**(5): 311-321.

Holt, I.J. and Reyes, A. (2012). "Human Mitochondrial DNA Replication." Cold Spring Harb Perspect Biol **4**: a012971.

Hong, S., Iizuka, Y., Kim, C.Y. and Seong, G.J. (2012). "Isolation of primary mouse retinal ganglion cells using immunopanning-magnetic separation." Mol Vis. **18**(2922-2930).

Horsford, D.J., Nguyen, M.-T.T., Sellar, G.C., Kothary, R., Arnheiter, H. and McInnes, R.R. (2005). "Chx10 repression of Mitf is required for the maintenance of mammalian neuroretinal identity." Development **132**(177-187).

Hou, P.S., Chuang, C.Y., Kao, C.F., Chou, S.J., Stone, L., Ho, H.N., ... and Kuo, H.C. (2013). "LHX2 regulates the neural differentiation of human embryonic stem cells via transcriptional modulation of PAX6 and CER1." Nucleic Acids Res. **41**(6): 7753-7770.

Hou, Z., Zhang, Z.Y., Propson, N.E., Howden, S.E., Chu, L.-F., Sontheimer, E.J. and Thomson, J.A. (2013). "Efficient genome engineering in human pluripotent stem cells using Cas9 from Neisseria meningitidis." Proc Natl Acad Sci U S A. **110**(39): 15644-15649.

Hu, S., Du, J., Chen, N., Jia, R., Zhang, J., Liu, X. and Yang, L. (2020). "In Vivo CRISPR/Cas9-Mediated Genome Editing Mitigates Photoreceptor Degeneration in a Mouse Model of X-Linked Retinitis Pigmentosa." Investigative Ophthalmology & Visual Science **61**(4): 31-31.

Hu, C., Shu, L., Huang, X., Yu, J., Li, l., Gong, L., ... and Song, Z. (2020). "OPA1 and MICOS Regulate mitochondrial crista dynamics and formation." Cell Death & Disease **11**(10): 940.

Huang, G., Ye, S., Zhou, X., Liu, D. and Ying, Q.-L. (2015). "Molecular basis of embryonic stem cell self-renewal: from signaling pathways to pluripotency network." Cellular and Molecular Life Sciences **72**: 1741–1757.

Huang, T., Santarelli, R. and Starrc, A. (2009). "Mutation of OPA1 gene causes deafness by affecting function of auditory nerve terminals." Brain Research **1300**: 97-104.

Hudson, G., Amati-Bonneau, P., Blakely, E.L., Stewart, J.D., He, L., Schaefer, A.M., ... and Taylor, R.W. (2008). "Mutation of OPA1 causes dominant optic atrophy with external ophthalmoplegia, ataxia, deafness and multiple mitochondrial DNA deletions: a novel disorder of mtDNA maintenance." Brain **131**(2): 329-337.

Iannielli, A., Bido, S., Folladori, L., Segnali, A., Cancellieri, C., Maresca, A., ... and Broccoli, V. (2018). "Pharmacological Inhibition of Necroptosis Protects from Dopaminergic Neuronal Cell Death in Parkinson's Disease Models." Cell Reports **22**(8): 2066-2079.

Iannielli, A., Ugolini, G.S., Cordiglieri, C., Bido, S., Rubio, A., Colasante, G., ... and Broccoli, V. (2019). "Reconstitution of the Human Nigro-striatal Pathway on-a-Chip Reveals OPA1-Dependent Mitochondrial Defects and Loss of Dopaminergic Synapses." Cell Reports **29**: 4646–4656.

Ikebe, S.-i., Tanaka, M., Ohno, K., Sato, W., Hattori, K., Kondo, T., ... and Ozawa, T. (1990). "Increase of deleted mitochondrial DNA in the striatum in Parkinson's disease and senescence." Biochemical and Biophysical Research Communications **170**(3): 1044-1048.

Ince-Dunn, G., Okano, H.J., Jensen, K.B., Woong-Park, Y., Zhong, R., Ule, J., ... and Darnell, R.B. (2012). "Neuronal Elav-like (Hu) Proteins Regulate RNA Splicing and Abundance to Control Glutamate Levels and Neuronal Excitability." Neuron **75**(6): 1067-1080.

International Stem Cell Initiative, T. (2007). "Characterization of human embryonic stem cell lines by the International Stem Cell Initiative." Nature Biotechnology **25**: 803-816.

Isenmann, S., Kretz, A. and Cellerina, A. (2003). "Molecular determinants of retinal ganglion cell development, survival, and regeneration." Progress in Retinal and Eye Research **22**(4): 483-543.

Ishihara, N., Fujita, Y., Oka, T. and Mihara, K. (2006). "Regulation of mitochondrial morphology through proteolytic cleavage of OPA1." The EMBO Journal **25**(13): 2966-2977.

Ito, Y., Nakamura, M., Yamakoshi, T., Lin, J., Yatsuya, H. and Terasaki, H. (2007). "Reduction of Inner Retinal Thickness in Patients with Autosomal Dominant Optic Atrophy Associated with OPA1 Mutations." Invest. Ophthalmol. Vis. Sci. **48**(9): 4079-4086.

Ito, Y.A. and Di Polo, A. (2017). "Mitochondrial dynamics, transport, and quality control: A bottleneck for retinal ganglion cell viability in optic neuropathies." Mitochondrion **36**: 186-192.

Iyer, V., Shen, B., Zhang, W., Hodgkins, A., Keane, T., Huang, X. and Skarnes, W.C. (2015). "Off-target mutations are rare in Cas9-modified mice." Nature Methods **12**: 479.

Jacoby, J. and Schwartz, G.W. (2017). "Three Small-Receptive-Field Ganglion Cells in the Mouse Retina Are Distinctly Tuned to Size, Speed, and Object Motion." J. Neurosci. **37**(3): 610-625.

Jefcoate, C.R., McNamara, B.C., Artemenko, I. and Yamazaki, T. (1992). "Regulation of cholesterol movement to mitochondrial cytochrome P450scc in steroid hormone synthesis." The Journal of Steroid Biochemistry and Molecular Biology **43**(8): 751-767.

Jeoung, J.W., Seong, M.-W., Park, S.S., Kim, D.M., Kim, S.H. and Park, K.H. (2014). "Mitochondrial DNA Variant Discovery in Normal-Tension Glaucoma Patients by Next-Generation Sequencing." Investigative Ophthalmology & Visual Science **55**(2): 986-992.

Jinek, M., Chylinksi, K., Fonfara, I., Hauer, M., Doudna, J.A. and Charpentier, E. (2012). "A Programmable Dual-RNA–Guided DNA Endonuclease in Adaptive Bacterial Immunity." Science **337**(6096): 816-821.

Jo, A., Ham, S., Lee, G.H., Lee, Y.-I., Kim, S., Lee, Y.-S., ... and Lee, Y. (2015). "Efficient Mitochondrial Genome Editing by CRISPR/Cas9." BioMed Research International **2015**: 305716.

Johnston, P.B., Gaster, R.N., Smith, V.C. and Tripathi, R.C. (1979). "Clinicopathological study of autosomal dominant atrophy." American Journal of Ophthalmology **88**(5): 868-875.

Jones, B.A. and Fangman, W.L. (1992). "Mitochondrial DNA maintenance in yeast requires a protein containing a region related to the GTP-binding domain of dynamin." Genes & Dev. **6**: 380-389.

Jonikas, M., Madill, M., Mathy, A., Zekoll, T., Zois, C.E., Wigfield, S., ... and Tofaris, G.K. (2018). "Stem cell modeling of mitochondrial parkinsonism reveals key functions of OPA1." Annals of Neurology **83**(5): 915-925.

Jouaville, L.S., Pinton, P., Bastianutto, C., Rutter, G.A. and Rizzuto, R. (1999). "Regulation of mitochondrial ATP synthesis by calcium: Evidence for a long-term metabolic priming." Proceedings of the National Academy of Sciences **96**(24): 13807-13812.

Ju, W.-K., Kim, K.-Y., Lindsey, J.D., Angert, M., Duong-Polk, K.X., Scott, R.T., ... and Weinreb, R.N. (2008). "Intraocular Pressure Elevation Induces Mitochondrial Fission and Triggers OPA1 Release in Glaucomatous Optic Nerve." Investigative Ophthalmology & Visual Science **49**(11): 4903-4911.

Jurkute, N., Leu, C., Pogoda, H.-M., Arno, G., Robson, A.G., Nürnberg, G., ... and Votruba, M. (2019). "SSBP1 mutations in dominant optic atrophy with variable retinal degeneration." Annals of Neurology **86**(3): 368-383.

Kaewkhaw, R., Kaya, K.D., Brooks, M., Homma, K., Zou, J., Chaitankar, V., ... and Swaroop, A. (2015). "Transcriptome Dynamics of Developing Photoreceptors in Three-Dimensional Retina Cultures Recapitulates Temporal Sequence of Human Cone and Rod Differentiation Revealing Cell Surface Markers and Gene Networks." Stem Cells **33**(12): 3504-3518.

Kallman, A., Capowski, E.E., Wang, J., Kaushik, A.M., Jansen, A.D., Edwards, K.L., ... and Zack, D.J. (2020). "Investigating cone photoreceptor development using patient-derived NRL null retinal organoids." Communications Biology **3**: 82.

Kamei, S., Chen-Kuo-Chang, M., Cazevieille, C., Lenaers, G., Olichon, A., Belenguer, P., ... and Hamel, C.P. (2005). "Expression of the Opa1 Mitochondrial Protein in Retinal Ganglion Cells: Its Downregulation Causes Aggregation of the Mitochondrial Network." Investigative Ophthalmology & Visual Science **46**(11).

Kandul, N.P., Zhang, T., Hay, B.A. and Guo, M. (2016). "Selective removal of deletion-bearing mitochondrial DNA in heteroplasmic Drosophila." Nature Communications **7**(1): 13100.

Kane, M.S., Alban, J., Desquiret-Dumas, V., Gueguen, N., Ishak, L., Ferre, M., ... and Chevrollier, A. (2017). "Autophagy controls the pathogenicity of OPA1 mutations in dominant optic atrophy." Journal of Cellular and Molecular Medicine **21**(10): 2284-2297.

Huang, K.C., Wang, M.L., Chen, S.J., Kuo, J.C., Wang, W.J., Nguyen, P.N.N., ... and S.H., C. (2019). "Morphological and Molecular Defects in Human Three-Dimensional Retinal Organoid Model of X-Linked Juvenile Retinoschisis." Stem Cell Reports **13**: 906-923.

Kaur, C., Foulds, W.S. and Ling, E.-A. (2008). "Hypoxia-ischemia and retinal ganglion cell damage." Clinical ophthalmology (Auckland, N.Z.) **2**(4): 879-889.

Kay, J.N., De la Huerta, I., Kim, I.J., Zhang, Y., Yamagata, M., Chu, M.W., ... and Sanes, J.R. (2011). "Retinal Ganglion Cells with Distinct Directional Preferences Differ in Molecular Identity, Structure, and Central Projections." The Journal of Neuroscience **31**(21): 7753-7762.

Keeney, P.M. and Bennett, J.P. (2010). "ALS spinal neurons show varied and reduced mtDNA gene copy numbers and increased mtDNA gene deletions." Molecular Neurodegeneration **5**(1): 21.

Kenny, T.C., Manfredi, G. and Germain, D. (2017). "The Mitochondrial Unfolded Protein Response as a Non-Oncogene Addiction to Support Adaptation to Stress during Transformation in Cancer and Beyond." Frontiers in Oncology **7**(159).

Kerrison, J.B., Arnould, V.J., Ferraz Sallum, J.M., Vagefi, M.R., Michael Barmada, M.M., Li, Y., ... and Maumenee, I.H. (1999). "Genetic Heterogeneity of Dominant Optic Atrophy, Kjer Type: Identification of a Second Locus on Chromosome 18q12.2-12.3." Arch Ophthalmol. **117**(6): 805–810.

Kim, D., Kim, C.H., Moon, J.I., Chung, Y.G., Chang, M.Y., Han, B.S., ... and Kim, K.S. (2009). "Generation of Human Induced Pluripotent Stem Cells by Direct Delivery of Reprogramming Proteins." Cell Stem Cell **4**(6): 472–476.

Kim, H.-S., Patel, K., Muldoon-Jacobs, K., Bisht, K.S., Aykin-Burns, N., Pennington, J.D., ... and Gius, D. (2010). "SIRT3 Is a Mitochondria-Localized Tumor Suppressor Required for Maintenance of Mitochondrial Integrity and Metabolism during Stress." Cancer Cell **17**(1): 41-52.

Kim, J.B., Greber, B., Araúzo-Bravo, M.J., Meyer, J., In Park, K., Zaehres, H. and Schöler, H.R. (2009). "Direct reprogramming of human neural stem cells by OCT4." Nature **461**: 649-653.

Kim, J.S., Choi, H.W., Choi, S., Seo, H.G., Moon, S.H., Chung, H.M. and Do, J.T. (2014). "Conversion of Partially Reprogrammed Cells to Fully Pluripotent Stem Cells Is Associated with Further Activation of Stem Cell Maintenance- and Gamete Generation-Related Genes." Stem Cells and Development **23**(21): 2637-2648.

Kim, J.Y., Hwang, J.-M., Ko, H.S., Seong, M.-W., Park, B.-J. and Park, S.S. (2004). "Mitochondrial DNA content is decreased in autosomal dominant optic atrophy." Neurology **64**(6).

Kim, K., Doi, A., Wen, B., Ng, K., Zhao, R., Cahan, P., ... and Daley, G.Q. (2010). "Epigenetic memory in induced pluripotent stem cells." Nature **467**(7313): 285-290.

Kim, K.K., Adelstein, R.S. and Kawamoto, S. (2009). "Identification of Neuronal Nuclei (NeuN) as Fox-3, a New Member of the Fox-1 Gene Family of Splicing Factors." The Journal of Biological Chemistry **284**: 31052-31061.

Kim, K.Y., Perkins, G.A., Shim, M.S., Bushong, E., Alcasid, N., Ju, S., ... and Ju, W.K. (2015). "DRP1 inhibition rescues retinal ganglion cells and their axons by preserving mitochondrial integrity in a mouse model of glaucoma." Cell Death & Disease **6**(8): e1839-e1839.

Kim, S., Kim, D., Cho, S.W., Kim, J. and Kim, J.S. (2014). "Highly efficient RNA-guided genome editing in human cells via delivery of purified Cas9 ribonucleoproteins." Genome Res. **24**: 1012-1019.

Kim, Y., Park, J., Kim, S., Song, S., Kwon, S.-K., Lee, S.-H., ... and Chung, J. (2008). "PINK1 controls mitochondrial localization of Parkin through direct phosphorylation." Biochemical and Biophysical Research Communications **377**(3): 975-980.

Kjer, B., Elberg, H., Kjer, P. and Rosenberg, T. (1996). "Dominant optic atrophy mapped to chromosome 3q region. II Clinical and epidemiological aspects." Acta Ophthalmol Scand. **74**(1): 3-7.

Kjer, P. (1959). "Infantile optic atrophy with dominant mode of inheritance. A clinical and genetic study of 19 Danish families." Acta Ophthalmol **164**: 1-147.

Kjer, P., Jensen, O.A. and Klinken, L. (1983). "Histopathology of the eye, optic nerve and brain in a case of dominant optic atrophy." Acta Ophthalmologica **61**(2): 300-312.

Klebe, S., Depienne, C., Gerber, S., Challe, G., Pelloquin, L., Mathieu, A., ... and Durr, A. (2012). "Spastic paraplegia gene 7 in patients with spasticity and/or optic neuropathy." Brain **135**(10): 2980-2993.

Klopstock, T., Metz, G., Yu-Wai-Man, P., Buchner, B., Gallenmuller, C., Bailie, M., ... and Chinnery, P.F. (2013). "Persistence of the treatment effect of idebenone in Leber's hereditary optic neuropathy." Brain **136**(2): e230.

Klopstock, T., Yu-Wai-Man, P., Dimitriadis, K., Rouleau, J., Heck, S., Bailie, M., ... and Chinnery, P.F. (2011). "A randomized placebo-controlled trial of idebenone in Leber's hereditary optic neuropathy." Brain **134**(9): 2677-2686.

Kobayashi, W., Onishi, A., Tu, H.Y., Takihara, Y., Matsumura, M., Tsujimoto, K., ... and Takahashi, M. (2018). "Culture Systems of Dissociated Mouse and Human Pluripotent

Stem Cell–Derived Retinal Ganglion Cells Purified by Two-Step Immunopanning." Investigative Ophthalmology & Visual Science **59**: 776-787.

Koch, K.-W. and Dell'Orco, D. (2015). "Protein and Signaling Networks in Vertebrate Photoreceptor Cells." Frontiers in Molecular Neuroscience **8**(67).

Kondapalli, C., Kazlauskaite, A., Zhang, N., Woodroof, H.I., Campbell, D.G., Gourlay, R., ... and Muqit, M.M.K. (2012). "PINK1 is activated by mitochondrial membrane potential depolarization and stimulates Parkin E3 ligase activity by phosphorylating Serine 65." Open Biology **2**(5): 120080.

Kondoh, H., Lleonart, M.E., Nakashima, Y., Yokode, M., Tanaka, M., Bernard, D. and Beach, J.G.D. (2007). "A High Glycolytic Flux Supports the Proliferative Potential of Murine Embryonic Stem Cells." Antioxid. Redox Signal. **9**: 293-299.

Kornek, B., Storch, M.K., Bauer, J., Djamshidian, A., Weissert, R., Wallstroem, E., ... and Lassmann, H. (2001). "Distribution of a calcium channel subunit in dystrophic axons in multiple sclerosis and experimental autoimmune encephalomyelitis." Brain **124**(6): 1114-1124.

Kovac, S., Angelova, P.R., Holmström, K.M., Zhang, Y., Dinkova-Kostova, A.T. and Abramova, A.Y. (2015). "Nrf2 regulates ROS production by mitochondria and NADPH oxidase." Biochimica et Biophysica Acta (BBA) - General Subjects **1850**(4): 794-801.

Kühlbrandt, W. (2015). "Structure and function of mitochondrial membrane protein complexes." BMC Biology **13**.

Kurosaki, T. and Maquat, L.E. (2016). "Nonsense-mediated mRNA decay in humans at a glance." Journal of Cell Science **129**: 461-467.

Kushnareva, Y.E., Gerencser, A.A., Bossy, B., Ju, W.-K., White, A.D., Waggoner, J., ... and Bossy-Wetzel, E. (2013). "Loss of OPA1 disturbs cellular calcium homeostasis and sensitizes for excitotoxicity." Cell Death and Differentiation **20**: 353-365.

Kuter, K., Kratochwil, M., Marx, S.-H., Hartwig, S., Lehr, S., Sugawa, M.D. and Dencher, N.A. (2016). "Native DIGE proteomic analysis of mitochondria from substantia nigra and striatum during neuronal degeneration and its compensation in an animal model of early Parkinson's disease." Archives of Physiology and Biochemistry **122**(5): 238-256.

Kuwahara, A., Ozone, C., Nakano, T., Saito, K., Eiraku, M. and Sasai, Y. (2015). "Generation of a ciliary margin-like stem cell niche from self-organizing human retinal tissue." Nature Communications **6**: 6286.

Kyttälä, A., Moraghebi, R., Valensisi, C., Kettunen, J., Andrus, C., Pasumarthy, Kalyan K., ... and Trokovic, R. (2016). "Genetic Variability Overrides the Impact of Parental Cell Type and Determines iPSC Differentiation Potential." Stem Cell Reports **6**(2): 200-212.

La Morgia, C., Di Vito, L., Carelli, V. and Carbonelli, M. (2017). "Patterns of Retinal Ganglion Cell Damage in Neurodegenerative Disorders: Parvocellular vs Magnocellular Degeneration in Optical Coherence Tomography Studies." Frontiers in Neurology **8**(710).

La Morgia, C., Ross-Cisneros, F.N., Sadun, A.A., Hannibal, J., Munarini A, M., V., Barboni, P., ... and Carelli, V. (2010). "Melanopsin retinal ganglion cells are resistant to neurodegeneration in mitochondrial optic neuropathies." Brain **133**: 2426-2438.

Laboissonniere, L.A., Goetz, J.J., Martin, G.M., Bi, R., Lund, T.J.S., Ellson, L., ... and Trimarchi, J.M. (2019). "Molecular signatures of retinal ganglion cells revealed through single cell profiling." Scientific Reports **9**(1): 15778.

Laker, R.C., Xu, P., Ryall, K.A., Sujkowski, A., Kenwood, B.M., Chain, K.H., ... and Yan, Z. (2014). "A novel MitoTimer reporter gene for mitochondrial content, structure, stress, and damage in vivo." The Journal of biological chemistry **289**(17): 12005-12015.

Lamb, T.D., Collin, S.P. and Pugh Jr, E.N. (2007). "Evolution of the vertebrate eye: opsins, photoreceptors, retina and eye cup." Nature Reviews Neuroscience **8**: 960-976.

Lan, L., Vitobello, A., Bertacchi, M., Cremisi, F., Vignali, R., Andreazzoli, M., ... and Casarosa, S. (2009). "Noggin Elicits Retinal Fate in Xenopus Animal Cap Embryonic Stem Cells." Stem Cells **27**(9): 2146-2152.

Lang, C., Campbell, K.R., Ryan, B.J., Carling, P., Attar, M., Vowles, J., ... and Wade-Martins, R. (2019). "Single-Cell Sequencing of iPSC-Dopamine Neurons Reconstructs Disease Progression and Identifies HDAC4 as a Regulator of Parkinson Cell Phenotypes." Cell Stem Cell **24**(1): 93-106.e106.

Langer, K.B., Ohlemacher, S.K., Phillips, M.J., Fligor, C.M., Jiang, P., Gamm, D.M. and Meyer, J.S. (2018). "Retinal Ganglion Cell Diversity and Subtype Specification from Human Pluripotent Stem Cells." Stem Cell Reports **10**(4): 1282-1293.

Lazzarino, G., Amorini, A., Eikelenboom, M., Killestein, J., Belli, A., Di Pietro, V., ... and Petzold, A. (2010). "Cerebrospinal fluid ATP metabolites in multiple sclerosis." Multiple Sclerosis Journal **16**(5): 549-554.

Lee, H., Smith, S.B. and Yoon, Y. (2017). "The short variant of the mitochondrial dynamin OPA1 maintains mitochondrial energetics and cristae structure." J Biol Chem. **292**(17): 7115-7130.

Lee, H.Y., Angelastro, J.M., Kenney, A.M., Mason, C.A. and Greene, L.A. (2012). "Reciprocal actions of ATF5 and Shh in proliferation of cerebellar granule neuron progenitor cells." Developmental Neurobiology **72**(6): 789-804.

Lee, S., Sheck, L., Crowston, J.G., Van Bergen, N.J., O'Neill, E.C., O'Hare, F., ... and Trounce, I.A. (2012). "Impaired Complex-I-Linked Respiration and ATP Synthesis in Primary Open-Angle Glaucoma Patient Lymphoblasts." Investigative Ophthalmology & Visual Science **53**(4): 2431-2437.

Lee, S., Sheck, L., Crowston, J.G., Van Bergen, N.J., O'Neill, E.C., O'Hare, F., ... and Trounce, I.A. (2012). "Impaired complex-I-linked respiration and ATP synthesis in primary open-angle glaucoma patient lymphoblasts." Invest Ophthalmol Vis Sci. **53**(4): 2431-2437.

Lemasters, J.J. (2005). "Selective Mitochondrial Autophagy, or Mitophagy, as a Targeted Defense Against Oxidative Stress, Mitochondrial Dysfunction, and Aging." Rejuvination Research **8**(1).

Lemasters, J.J., Theruvath, T.P., Zhong, Z. and Nieminen, A.-L. (2009). "Mitochondrial calcium and the permeability transition in cell death." Biochimica et Biophysica Acta (BBA) - Bioenergetics **1787**(11): 1395-1401.

Lenears, G., Hamel, C., Delettre, C., Amati-Bonneau, P., Procaccio, V., Bonneau, D., ... and Milea, D. (2012). "Dominant optic atrophy." Orphanet Journal of Rare Diseases **7**(46).

Levin, L.A., Nilsson, S.F.E., Hoeve, J.V., Wu, S.M., Kaufman, P.L. and Alm, A. (2011). Alder's physiology of the eye, Elsevier Health Sciences.

Li, D., Wang, J., Jin, Z. and Zhang, Z. (2019). "Structural and evolutionary characteristics of dynamin-related GTPase OPA1." PeerJ **7**: e7285.

Li, H., Beckman, K.A., Pessino, V., Huang, B., Weissman, J.S. and Leonetti, M.D. (2017). "Design and specificity of long ssDNA donors for CRISPR-based knock-in." bioRxiv.

Li, Hongmei L., Fujimoto, N., Sasakawa, N., Shirai, S., Ohkame, T., Sakuma, T., ... and Hotta, A. (2015). "Precise Correction of the Dystrophin Gene in Duchenne Muscular Dystrophy Patient Induced Pluripotent Stem Cells by TALEN and CRISPR-Cas9." Stem Cell Reports **4**(1): 143-154.

Li, J.Q., Welchowski, T., Schmid, M., Mauschitz, M.M., Holz, F.G. and Finger, R.P. (2019). "Prevalence and incidence of age-related macular degeneration in Europe: a systematic review and meta-analysis." British Journal of Ophthalmology: bjophthalmol-2019-314422.

Li, R., Wu, F., Ruonala, R., apkota, D., Hu, Z. and Xiuqian Mu, X. (2014). "Isl1 and Pou4f2 Form a Complex to Regulate Target Genes in Developing Retinal Ganglion Cells." PLOS ONE **9**(3): e92105.

Li, R.S., Chen, B.Y., Tay, D.K., Chan, H.H.L., Pu, M.L. and So, K.F. (2006). "Melanopsin-Expressing Retinal Ganglion Cells Are More Injury-Resistant in a Chronic Ocular Hypertension Model." Investigative Ophthalmology & Visual Science **47**: 2951-2958.

Li, S.Y., Yau, S.Y., Chen, B.Y., Tay, D.K., Lee, V.W.H., Pu, M.L., ... and So, K.F. (2008). "Enhanced Survival of Melanopsin-expressing Retinal Ganglion Cells After Injury is Associated with the PI3 K/Akt Pathway." Cell Mol Neurobiol **28**: 1095-1107.

Li, Z., Zhang, M., Zheng, S., Song, Y., Cheng, X., Yu, D., ... and Zhao, Y. (2020). "Genetic removal of the CH1 exon leads to the production of hypofunctional heavy chain-only IgG2a in rats." Transgenic Research **29**(2): 199-213.

Liang, X., Potter, J., Kumar, S., Zou, Y., Quintanilla, R., Sridharan, M., ... and Chesnut, J.D. (2015). "Rapid and highly efficient mammalian cell engineering via Cas9 protein transfection." J Biotechnol. **208**: 44-53.

Liao, C., Ashley, N., Diot, A., Morten, K., Phadwal, K., Williams, A., ... and Poulton, J. (2017). "Dysregulated mitophagy and mitochondrial organization in optic atrophy due to OPA1 mutations." Neurology **88**(2).

Liesa, M., Palacín, M. and Zorzano, A. (2009). "Mitochondrial Dynamics in Mammalian Health and Disease." Physiological Reviews **89**(3): 799-845.

Liew, G., Michaelides, M. and Bunce, C. (2014). "A comparison of the causes of blindness certifications in England and Wales in working age adults (16–64 years), 1999–2000 with 2009–2010." BMJ Open **4**: e004015.

Lin, C.S., Sharpley, M.S., Fan, W., Waymire, K.G., Sadun, A.A., Carelli, V., ... and Wallace, D.C. (2012). "Mouse mtDNA mutant model of Leber hereditary optic neuropathy." Proceedings of the National Academy of Sciences **109**(49): 20065-20070.

Lin, S., Staahl, B.T., Alla, R.K. and Doudna, J.A. (2014). "Enhanced homology-directed human genome engineering by controlled timing of CRISPR/Cas9 delivery." eLife **3**: e04766.

Lin, Y.-F., Schulz, A.M., Pellegrino, M.W., Lu, Y., Shaham, S. and Haynes, C.M. (2016). "Maintenance and propagation of a deleterious mitochondrial genome by the mitochondrial unfolded protein response." Nature **533**(7603): 416-419.

Lin, Y.S., Kuo, K.T., Chen, S.K. and Huang, H.S. (2018). "RBFOX3/NeuN is dispensable for visual function." PLOS ONE **13**(2): e0192355.

Lisowski, P., Kannan, P., Mlody, B. and Prigione, A. (2018). "Mitochondria and the dynamic control of stem cell homeostasis." EMBO Rep **19**: e45432.

Liu, W., Mo, Z. and Xiang, M. (2001). "The Ath5 proneural genes function upstream of Brn3 POU domain transcription factor genes to promote retinal ganglion cell development." PNAS **98**(4): 1649-1654.

Liu, X., Weaver, D., Shirihai, O. and Hajnóczky, G. (2009). "Mitochondrial 'kiss-and-run': interplay between mitochondrial motility and fusion–fission dynamics." EMBO J **28**(3074-3089).

Livak, K.J. and Schmittgen, T.D. (2001). "Analysis of Relative Gene Expression Data Using Real-Time Quantitative PCR and the ddCT Method." Methods **25**: 402-408.

Llavona, P., Pinelli, M., Mutarelli, M., Marwah, V.S., Schimpf-Linzenbold, S., Thaler, S., ... and Wissinger, B. (2017). "Allelic Expression Imbalance in the Human Retinal Transcriptome and Potential Impact on Inherited Retinal Diseases." Genes **8**(10): 283.

Lloria, X., Silva, M., Lawrence, C., Rudolph, G., Lob, F., von Livonius, B., ... and Klopstock, T. (2019). "Maintenance of idebenone treatment results in continued improvement in LHON patients." Journal of Neurology, Neurosurgery and Psychiatry **90**(12): e1-e65.

Lodi, R., Tonon, C., Valentino, M.L., Lotti, S., Clementi, V., Malucelli, E., ... and Carelli, V. (2004). "Deficit of in vivo mitochondrial ATP production in OPA1-related dominant optic atrophy." Annals of Neurology **56**(5): 719-723.

Löffler, M., Fairbanks, L.D., Zameitat, E., Marinaki, A.M. and Simmonds, H.A. (2005). "Pyrimidine pathways in health and disease." Trends in Molecular Medicine **11**(9): 430-437.

Lorenz, C., Lesimple, P., Bukowiecki, R., Zink, A., Inak, G., Mlody, B., ... and Prigione, A. (2017). "Human iPSC-Derived Neural Progenitors Are an Effective Drug Discovery Model for Neurological mtDNA Disorders." Cell Stem Cell **20**(5): 659-674.e659.

Losón, O.C., Song, Z., Chen, H. and Chan , D.C. (2013). "Fis1, Mff, MiD49, and MiD51 mediate Drp1 recruitment in mitochondrial fission." Molecular Biology of the Cell **24**(5): 659-667.

Lowry, W.E., Richter, L., Yachechko, R., Pyle, A.D., Tchieu, J., Sridharan, R., ... and Plath, K. (2008). "Generation of human induced pluripotent stem cells from dermal fibroblasts." PNAS **105**(8): 2883-2888.

Ludtmann, M.H.R., Angelova, P.R., Horrocks, M.H., Choi, M.L., Rodrigues, M., Baev, A.Y., ... and Gandhi, S. (2018). "α-synuclein oligomers interact with ATP synthase and open the permeability transition pore in Parkinson's disease." Nature Communications **9**(1): 2293.

Lynch, D.S., Loh, S.H.Y., Harley, J., Noyce, A.J., Martins, L.M., Wood, N.W., ... and Plun-Favreau, H. (2017). "Nonsyndromic Parkinson disease in a family with autosomal dominant optic atrophy due to OPA1 mutations." Neurology Genetics **3**(5): e188.

Lyseng-Williamson, K.A. (2016). "Idebenone: A Review in Leber's Hereditary Optic Neuropathy." Drugs **76**: 805-813.

Ma, H., Morey, R., O'Neil, R.C., He, Y., Daughtry, B., Schultz, M.D., ... and Mitalipov, S. (2014). "Abnormalities in human pluripotent cells due to reprogramming mechanisms." Nature **511**(7508): 177-183.

Maack, C., Cortassa, S., Aon, M.A., Ganesan, A.N., Liu, T. and O'Rourke, B. (2006). "Elevated Cytosolic Na+ Decreases Mitochondrial Ca2+ Uptake During Excitation-Contraction Coupling and Impairs Energetic Adaptation in Cardiac Myocytes." Circulation Research **99**(2): 172-182.

Mabuchi, F., Tang, S., Kashiwagi, K., Yamagata, Z., Iijima, H. and Tsukahara, S. (2007). "The OPA1 Gene Polymorphism is Associated With Normal Tension and High Tension Glaucoma." American Journal of Ophthalmology **143**(1): 125-130.e122.

Machiraju, P., Wang, X., Sabouny, R., Huang, J., Zhao, T., Iqbal, F., ... and Greenway, S.C. (2019). "SS-31 Peptide Reverses the Mitochondrial Fragmentation Present in Fibroblasts From Patients With DCMA, a Mitochondrial Cardiomyopathy." Front Cardiovasc Med **6**: 167.

Macosko, Evan Z., Basu, A., Satija, R., Nemesh, J., Shekhar, K., Goldman, M., ... and McCarroll, Steven A. (2015). "Highly Parallel Genome-wide Expression Profiling of Individual Cells Using Nanoliter Droplets." Cell **161**(5): 1202-1214.

MacVicar, T.D.B. and Lane, J.D. (2014). "Impaired OMA1-dependent cleavage of OPA1 and reduced DRP1 fission activity combine to prevent mitophagy in cells that are dependent on oxidative phosphorylation." Journal of Cell Science **127**: 2313-2325.

MacVicar, T.D.B. and Langer, T. (2016). "OPA1 processing in cell death and disease – the long and short of it." Journal of Cell Science **129**: 2297-2306.

Maeder, M.L., Stefanidakis, M., Wilson, C.J., Baral, R., Barrera, L.A., Bounoutas, G.S., ... and Jiang, H. (2019). "Development of a gene-editing approach to restore vision loss in Leber congenital amaurosis type 10." Nature Medicine **25**(2): 229-233.

Maekawa, Y., Onishi, A., Matsushita, K., Koide, N., Mandai, M., Suzuma, K., ... and Takahashi, M. (2016). "Optimized Culture System to Induce Neurite Outgrowth From Retinal Ganglion Cells in Three-Dimensional Retinal Aggregates Differentiated From Mouse and Human Embryonic Stem Cells." Current Eye Research **41**(4): 558-568.

Maherali, N., Sridharan, R., Xie, W., Utikal, J., Eminli, S., Arnold, K., ... and Hochedlinger, K. (2007). "Directly Reprogrammed Fibroblasts Show Global Epigenetic Remodeling and Widespread Tissue Contribution." Cell Stem Cell **1**(1): 55-70.

Majander, A., João, C., Rider, A.T., Henning, G.B., Votruba, M., Moore, A.T., ... and Stockman, A. (2017). "The Pattern of Retinal Ganglion Cell Loss in OPA1-Related Autosomal Dominant Optic Atrophy Inferred From Temporal, Spatial, and Chromatic Sensitivity Losses." Invest. Ophthalmol. Vis. Sci. **58**(1): 502-516.

Malena, A., Loro, E., Di Re, M., Holt, I.J. and Vergani, L. (2009). "Inhibition of mitochondrial fission favours mutant over wild-type mitochondrial DNA." Human Molecular Genetics **18**(18): 3407-3416.

Marchbank, N.J., Craig, J.E., Leek, J.P., Toohey, M., Churchill, A.J., Markham, A.F., ... and C.F., I. (2002). "Deletion of the OPA1 gene in a dominant optic atrophy family: evidence that haploinsufficiency is the cause of disease." J Med Genet **39**: e47.

Marchetto, M.C.N., Yeo, G.W., Kainohana, O., Marsala, M., Gage, F.H. and Muotri, A.R. (2009). "Transcriptional Signature and Memory Retention of Human-Induced Pluripotent Stem Cells." PLOS ONE **4**(9): e7076.

Marei, H.E., Althani, A., S., L., Cenciarelli, C. and Hasan, A. (2017). "Genetically unmatched human iPSC and ESC exhibit equivalent gene expression and neuronal differentiation potential." Scientific Reports **7**: 17504.

Marella, M., Patki, G., Matsuno-Yagi, A. and Yagi, T. (2013). "Complex I inhibition in the visual pathway induces disorganization of the node of Ranvier." Neurobiology of Disease **58**: 281-288.

Markaryan, A., Nelson, E.G. and Hinojosa, R. (2010). "Major arc mitochondrial DNA deletions in cytochrome c oxidase-deficient human cochlear spiral ganglion cells." Acta Oto-Laryngologica **130**(7): 780-787.

Marquardt, T., Ashery-Padan, R., Andrejewski, Scardigli, R., Guillemot, F. and Gruss, P. (2001). "Pax6 Is Required for the Multipotent State of Retinal Progenitor Cells." Cell **105**(1): 43-55.

Marson, A., Levine, S.S., Cole, M.F., Frampton, G.M., Brambrink, T., Johnstone, S., ... and Young, R.A. (2008). "Connecting microRNA Genes to the Core Transcriptional Regulatory Circuitry of Embryonic Stem Cells." Cell **134**(3): 521-533.

Martínez-Reyes, I. and Chandel, N.S. (2020). "Mitochondrial TCA cycle metabolites control physiology and disease." Nature Communications **11**: 102.

Martinus, R.D., Garth, G.P., Webster, T.L., Cartwright, P., Naylor, D.J., Høj, P.B. and Hoogenraad, N.J. (1996). "Selective Induction of Mitochondrial Chaperones in Response to Loss of the Mitochondrial Genome." European Journal of Biochemistry **240**(1): 98-103.

Maruyama, T., Dougan, S.K., Truttmann, M.C., Bilate, A.M., Ingram, J.R. and Ploegh, H.L. (2015). "Increasing the efficiency of precise genome editing with CRISPR-Cas9 by inhibition of nonhomologous end joining." Nature Biotechnology **33**: 538-542.

Mashima, Y., Kigasawa, K., Wakakura, M. and Oguchi, Y. (2000). "Do Idebenone and Vitamin Therapy Shorten the Time to Achieve Visual Recovery in Leber Hereditary Optic Neuropathy?" Journal of Neuw-Ophthalmology **20**(3): 166-170.

Mathers, P.H., Grinberg, A., Mahon, K.A. and Jamrich, M. (1997). "The Rx homeobox gene is essential for vertebrate eye development." Nature **387**: 603-607.

Mathers, P.H. and Jamrich, M. (2000). "Regulation of eye formation by the Rx and pax6 homeobox genes." Cellular and Molecular Life Sciences **57**(2): 186-194.

Matsuda, N., Sato, S., Shiba, K., Okatsu, K., Saisho, K., Gautier, C.A., ... and Tanaka, K. (2010). "PINK1 stabilized by mitochondrial depolarization recruits Parkin to damaged mitochondria and activates latent Parkin for mitophagy." Journal of Cell Biology **189**(2): 211-221.

Mattout, A., Biran, A. and Meshorer, E. (2011). "Global epigenetic changes during somatic cell reprogramming to iPS cells." Journal of Molecular Cell Biology **3**(6).

Mayshar, Y., Ben-David, U., Lavon, N., Biancotti, J.-C., Yakir, B., Clark, A.T., ... and Benvenisty, N. (2010). "Identification and Classification of Chromosomal Aberrations in Human Induced Pluripotent Stem Cells." Cell Stem Cell **7**(4): 521-531.

McElnea, E.M., Quill, B., Docherty, N.G., Irnaten, M., Siah, W.F., Clark, A.F., ... and Wallace, D.M. (2011). "Oxidative stress, mitochondrial dysfunction and calcium overload in human lamina cribrosa cells from glaucoma donors." Molecular vision **17**: 1182-1191.

McGinnis, J.F., Stepanik, P.L., Jariangprasert, S. and Lerious, V. (1997). "Functional Significance of RecoverinLocalization in Multiple Retina Cell Types." Journal of Neuroscience Research **50**: 487-495.

McLelland, B.T., B., L., Mathur, A., Aramant, R.B., Thomas, B.B., Nistor, G., ... and Seiler, M.J. (2018). "Transplanted hESC-Derived Retina Organoid Sheets Differentiate, Integrate, and Improve Visual Function in Retinal Degenerate Rats." Investigative Ophthalmology & Visual Science **59**: 2586-2603.

Mears, A.J., Kondo, M., Swain, P.K., Takada, Y., Bush, R.A., Saunders, T.L., ... and Swaroop, A. (2001). "Nrl is required for rod photoreceptor development." Nature Genetics **20**: 447-452.

Melber, A. and Haynes, C.M. (2018). "UPRmt regulation and output: a stress response mediated by mitochondrial-nuclear communication." Cell Research **28**: 281-295.

Merkle, F.T., Ghosh, S., Kamitaki, N., Mitchell, J., Avior, Y., Mello, C., ... and Eggan, K. (2017). "Human pluripotent stem cells recurrently acquire and expand dominant negative P53 mutations." Nature **545**(7653): 229-233.

Messina, A., Incitti, T., Bozza, A., Bozzi, Y. and Casarosa, S. (2014). "Noggin Expression in the Adult Retina Suggests a Conserved Role during Vertebrate Evolution." J Histochem Cytochem. **62**(7): 532-540.

Meyer, J.S., Howden, S.E., Wallace, K.A., Verhoenven, A.D., Wright, L.S., Capowski, E.E., ... and Gamm, D.M. (2011). "Optic vesicle-like structures derived from human pluripotent stem cells facilitate a customized approach to retinal disease treatment." Stem Cells **29**: 1206-1218.

Meyer, J.S., Shearer, R.L., Capowski, E.E., Wright, L.S., Wallace, K.A., McMillan, E.L., ... and Gamm, D.M. (2009). "Modeling early retinal development with human embryonic and induced pluripotent stem cells." PNAS **106**(39): 16698-16703.

Milakovic, T. and Johnson, G.V. (2005). "Mitochondrial respiration and ATP production are significantly impaired in striatal cells expressing mutant huntingtin." J Biol Chem. **280**(35): 3077330782.

Milam, A.H., Rose, L., Cideciyan, A.V., Barakat, M.R., Tang, W.X., Gupta, N., ... and Jacobson, S.G. (2002). "The nuclear receptor NR2E3 plays a role in human retinal photoreceptor differentiation and degeneration." Proc Natl Acad Sci USA. **99**(1): 473-478.

Milea, D., Sander, B., Wegener, M., Jensen, H., Kjer, B., Jørgensen, T.M., ... and Larsen, M. (2010). "Axonal loss occurs early in dominant optic atrophy." Acta Ophthalmologica **88**(3): 342-346.

Miller, W.L. (2013). "Steroid hormone synthesis in mitochondria." Molecular and Cellular Endocrinology **379**(1): 62-73.

Millet, A.M.C., Bertholet, A.M., Daloyau, M., Reynier, P., Galinier, A., Devin, A., ... and Davezac, N. (2016). "Loss of functional OPA1 unbalances redox state: implications in dominant optic atrophy pathogenesis." Annals of Clinical and Translational neurology **3**(6): 408-421.

Mills, J.A., Wang, K., Paluru, P., Ying, L., Lu, L., Galvão, A.M., ... and Gadue, P. (2013). "Clonal genetic and hematopoietic heterogeneity among human-induced pluripotent stem cell lines." Blood **122**(12): 2047-2051.

Misaka, T., Miyashitall, T. and Kubo, Y. (2002). "Primary Structure of a Dynamin-related Mouse Mitochondrial GTPase and Its Distribution in Brain, Subcellular Localization, and Effect on Mitochondrial Morphology." The Journal of Biological Chemistry **277**: 15834-15842.

Mishra, P., Carelli, V., Manfredi, G. and Chan, D.C. (2014). "Proteolytic Cleavage of Opa1 Stimulates Mitochondrial Inner Membrane Fusion and Couples Fusion to Oxidative Phosphorylation." Cell Metabolism **19**(4): 630-641.

Mishra, P. and Chan, D.C. (2016). "Metabolic regulation of mitochondrial dynamics." J Cell Biol **212**(4): 379-387.

Mitton, K.P., Swain, P.K., Chen, S., Xu, S., Zack, D.J. and Swaroop, A. (2000). "The Leucine Zipper of NRL Interacts with the CRX Homeodomain: A possible mechanism of transcriptional synergy in rhodopsin regulation." J Biol Chem. **275**: 29794.

Miura, H., Gurumurthy, C.B., Sato, T., Sato, M. and Ohtsuka, M. (2015). "CRISPR/Cas9-based generation of knockdown mice by intronic insertion of artificial microRNA using longer single-stranded DNA." Scientific Reports **5**.

Mok, B.Y., de Moraes, M.H., Zeng, J., Bosch, D.E., Kotrys, A.V., Raguram, A., ... and Liu, D.R. (2020). "A bacterial cytidine deaminase toxin enables CRISPR-free mitochondrial base editing." Nature **583**: 631-637.

Moshiri, A., Gonzalez, E., Tagawa, K., Maeda, H., Wang, M., Frishman, L.J. and Wang, S.W. (2008). "Near complete loss of retinal ganglion cells in the math5/brn3b double knockout elicits severe reductions of other cell types during retinal development." Developmental Biology **316**(2): 214-227.

Mou, H., Smith, J.L., Peng, L., Yin, H., Moore, J., Zhang, X.-O., ... and Xue, W. (2017). "CRISPR/Cas9-mediated genome editing induces exon skipping by alternative splicing or exon deletion." Genome Biology **18**(1): 108.

Mouchiroud, L., Houtkooper, R.H., Moullan, N., Katsyuba, E., Ryu, D., Cantó, C., ... and Auwer, J. (2013). "The NAD+/Sirtuin Pathway Modulates Longevity through Activation of Mitochondrial UPR and FOXO Signaling." Cell **154**(2): 430-441.

Mullen, R.J., Buck, C.R. and Smith, A.M. (1992). "NeuN, a neuronal specific nuclear protein in vertebrates." Development **116**: 201-211.

Müller-Rischart, Anne K., Pilsl, A., Beaudette, P., Patra, M., Hadian, K., Funke, M., ... and Winklhofer, Konstanze F. (2013). "The E3 Ligase Parkin Maintains Mitochondrial Integrity by Increasing Linear Ubiquitination of NEMO." Molecular Cell **49**(5): 908-921.

Münch, C. (2018). "The different axes of the mammalian mitochondrial unfolded protein response." BMC Biology **16**: 81.

Münch, C. and Harper, J.W. (2016). "Mitochondrial unfolded protein response controls matrix pre-RNA processing and translation." Nature **534**: 710–713.

Murphy, E., Ardehali, H., Balaban, R.S., DiLisa, F., Dorn, G.W., Kitsis, R.N., ... and Youle, R.J. (2016). "Mitochondrial Function, Biology, and Role in Disease." Circulation Research **118**(12): 1960-1991.

Nadal-Nicolás, F.M., Jiménez-López, M., Sobrado-Calvo, P., Nieto-López, L., Cánovas-Martínez, I., Salinas-Navarro, M., ... and Agudo, M. (2009). "Brn3a as a Marker of Retinal Ganglion Cells: Qualitative and Quantitative Time Course Studies in Naïve and Optic Nerve–Injured Retinas." Retina **50**(8).

Naeem, M.A., Chavali, V.R.M., Ali, S., Iqbal, M., Riazuddin, S., Khan, S.N., ... and Riazuddin, S.A. (2012). "GNAT1 Associated with Autosomal Recessive Congenital Stationary Night Blindness." Retina **53**(3).

Nakano, T., Ando, S., Takata, N., Kawada, M., Muguruma, K., Sekiguchi, K., ... and Sasai, Y. (2012). "Self-Formation of Optic Cups and Storable Stratified Neural Retina from Human ESCs." Cell Stem Cell **10**(6): 771-785.

Namani, A., Li, Y., Wang, X.J. and Tang, X. (2014). "Modulation of NRF2 signaling pathway by nuclear receptors: Implications for cancer." Biochimica et Biophysica Acta (BBA) - Molecular Cell Research **1843**: 1875-1885.

Narendra, D., Kane, L.A., Hauser, D.N., Fearnley, I.M. and Youle, R.J. (2010). "p62/SQSTM1 is required for Parkin-induced mitochondrial clustering but not mitophagy; VDAC1 is dispensable for both." Autophagy **6**(8): 1090-1106.

Nargund, A.M., Fiorese, C.J., Pellegrino, M.W., Deng, P. and Haynes, C.M. (2015). "Mitochondrial and Nuclear Accumulation of the Transcription Factor ATFS-1 Promotes OXPHOS Recovery during the UPRmt." Molecular Cell **58**: 123-133.

Nargund, A.M., Pellegrino, M.W., Fiorese, C.J., Baker, B.M. and Haynes, C.M. (2012). "Mitochondrial Import Efficiency of ATFS-1 Regulates Mitochondrial UPR Activation." Science **337**(6094): 587-590.

Nasca, A., Rizza, T., Doimo, M., Legati, A., Ciolfi, A., Diodato, D., ... and Ghezzi, D. (2017). "Not only dominant, not only optic atrophy: expanding the clinical spectrum associated with OPA1 mutations." Orphanet Journal of Rare Diseases **12**(1): 89.

Nelson, A.D. and Jenkins, P.M. (2017). "Axonal Membranes and Their Domains: Assembly and Function of the Axon Initial Segment and Node of Ranvier." Frontiers in Cellular Neuroscience **11**(136).

Nelson, C.E., Hakim, C.H., Ousterout, D.G., Thakore, P.I., Moreb, E.A., Rivera, R.M.C., ... and Gersbach, C.A. (2016). "In vivo genome editing improves muscle function in a mouse model of Duchenne muscular dystrophy." Science **351**(6271): 403-407.

Neufeld, G., Cohen, T., Shraga, N., Lange, T., Kessler, O. and Herzog, Y. (2002). "The Neuropilins: Multifunctional Semaphorin and VEGF Receptors that Modulate Axon Guidance and Angiogenesis." Trends in Cardiovascular Medicine **12**(1): 13-19.

Neveu, P., Kye, M.J., Qi, S., Buchholz, D.E., Clegg, D.O., Sahin, M., ... and Kosik, K.S. (2010). "MicroRNA Profiling Reveals Two Distinct p53-Related Human Pluripotent Stem Cell States." Cell Stem Cell **7**(6): 671-681.

Newman, A.M. and Cooper, J.B. (2010). "Lab-Specific Gene Expression Signatures in Pluripotent Stem Cells." Cell Stem Cell **7**(2): 258-262.

Newman, N.J. and Biousse, V. (2004). "Hereditary optic neuropathies." Eye **18**: 1144-1160.

Nguyen, T.N., Padman, B.S. and Lazarou, M. (2016). "Deciphering the Molecular Signals of PINK1/Parkin Mitophagy." Trends in Cell Biology **26**(10): 733-744.

Nichols, J., Zevnik, B., Anastassiadis, K., Niwa, H., Klewe-Nebenius, D., Chambers, I., ... and Smith, A. (1998). "Formation of Pluripotent Stem Cells in the Mammalian Embryo Depends on the POU Transcription Factor Oct4." Cell **95**(3): 379-391.

Nijssen, J., Aguila, J. and Hedlund, E. (2019). "Axon-seq for in Depth Analysis of the RNA Content of Neuronal Processes." Bio-protocol **9**(14): e3312.

Nijssen, J., Aguila, J., Hoogstraaten, R., Kee, N. and Hedlund, E. (2018). "Axon-Seq Decodes the Motor Axon Transcriptome and Its Modulation in Response to ALS." Stem Cell Reports. **11**(6): 1565-1578.

Nissanka, N. and Moraes, C.T. (2018). "Mitochondrial DNA damage and reactive oxygen species in neurodegenerative disease." FEBS Letters **592**(5): 728-742.

Niwa, H. (2007). "How is pluripotency determined and maintained?" Development **134**: 635-646.

Noelker, C., Morel, L., Osterloh, A., Alvarez-Fischer, D., Lescot, T., Breloer, M., ... and Hartmann, A. (2014). "Heat shock protein 60: an endogenous inducer of dopaminergic cell death in Parkinson disease." Journal of Neuroinflammation **11**(1): 86.

Nukui, T., Matsui, A., Niimi, H., Yamamoto, M., Matsuda, N., Piao, J.-L., ... and Nakatsuji, Y. (2020). "Cerebrospinal fluid ATP as a potential biomarker in patients with mitochondrial myopathy, encephalopathy, lactic acidosis, and stroke like episodes (MELAS)." Mitochondrion **50**: 145-148.

O'Leary, D.D., Fawcett, J.W. and Cowan, W.M. (1986). "Topographic targeting errors in the retinocollicular projection and their elimination by selective ganglion cell death." Journal of Neuroscience **6**(12): 3692-3705.

Oh, J.Y., Choi, G.E., Lee, H.J., Y.H., J., Chae, C.W., Kim, J.S., ... and Han, H.J. (2019). "17β-Estradiol protects mesenchymal stem cells against high glucose-induced mitochondrial oxidants production via Nrf2/Sirt3/MnSOD signaling." Free Radical Biology and Medicine **130**: 328-342.

Ohlemacher, S.K., Sridhar, A., Xiao, Y., Hochstetler, A.E., Sarfarazi, M., Cummins, T.R. and Meyer, J.S. (2016). "Stepwise Differentiation of Retinal Ganglion Cells from Human Pluripotent Stem Cells Enables Analysis of Glaucomatous Neurodegeneration." Stem Cells **34**: 1553–1562.

Ohno, N., Kidd, G.J., Mahad, D., Kiryu-Seo, S., Avishai, A., Komuro, H. and Trapp, B.D. (2011). "Myelination and Axonal Electrical Activity Modulate the Distribution and Motility of Mitochondria at CNS Nodes of Ranvier." The Journal of Neuroscience **31**(20): 7249-7258.

Ohnuma, S., Hopper, S., Wang, K.C., Philpott, A. and Harris, W.A. (2002). "Co-ordinating retinal histogenesis: early cell cycle exit enhances early cell fate determination in the Xenopus retina." Development **129**: 2435-2446.

Okamoto, S., Amaishi, Y., Maki, I., Enoki, T. and Mineno, J. (2019). "Highly efficient genome editing for single-base substitutions using optimized ssODNs with Cas9-RNPs." Scientific Reports **9**: 4811.

Okita, K., Matsumura, Y., Sato, Y., Okada, A., Morizane, A., Okamoto, S., ... and Yamanaka, S. (2011). "A more efficient method to generate integration-free human iPS cells." Nature Methods **8**: 409-412.

Okita, K., Yamakawa, T., Matsumura, Y., Sato, Y., Amano, N., Watanabe, A., ... and Yamanaka, S. (2017). "An Efficient Nonviral Method to Generate Integration-Free Human-Induced Pluripotent Stem Cells from Cord Blood and Peripheral Blood Cells." Stem Cells **31**: 458-466.

Olichon, A., Baricault, L., Gas, N., Guillou, E., Valette, A., Belenguer, P. and Lenears, G. (2003). "Loss of OPA1 Perturbates the Mitochondrial Inner Membrane Structure and Integrity, Leading to Cytochrome c Release and Apoptosis." The Journal of Biological Chemistry **278**(10).

Olichon, A., Elachouri, G., Baricault, L., Delettre, C., Belenguer, P. and Lenaers, G. (2007). "OPA1 alternate splicing uncouples an evolutionary conserved function in mitochondrial fusion from a vertebrate restricted function in apoptosis." Cell Death & Differentiation **14**: 682–692.

Olichon, A., T., L., Arnaune-Pelloquin, L., Emorine, L.J., Mils, V., Guichet, A., ... and Belenguer, P. (2007). "Effects of OPA1 mutations on mitochondrial morphology and apoptosis: Relevance to ADOA pathogenesis." Cellular Physiology **211**(2): 423-430.

Orozco, L.D., Chen, H.-H., Cox, C., Katschke, K.J., Arceo, R., Espiritu, C., ... and Hackney, J.A. (2020). "Integration of eQTL and a Single-Cell Atlas in the Human Eye Identifies Causal Genes for Age-Related Macular Degeneration." Cell Reports **30**(4): 1246-1259.e1246.

Osellame, L.D., Blacker, T.S. and Duchen, M.R. (2012). "Cellular and molecular mechanisms of mitochondrial function." Best Pract Res Clin Endocrinol Metab. **26**(6): 711-723.

Oster, S.F., Bodeker, M.O., He, F. and Sretavan, D.W. (2003). "Invariant Sema5A inhibition serves an ensheathing function during optic nerve development." Development **130**(775-784).

Oster, S.F., Deiner, M.S., Birgbauer, E. and Sretavan, D.W. (2004). "Ganglion cell axon pathfinding in the retina and optic nerve." Seminars in Cell & Developmental Biology **15**(1): 125-136.

Oster, S.F. and Sretavan, D.W. (2003). "Connecting the eye to the brain: the molecular basis of ganglion cell axon guidance." Br J Ophthalmol. **87**(5): 639-645.

Ouellet, M., Guillebaud, G., Gervais, V., Lupien St-Pierre, D. and Germain, M. (2017). "A novel algorithm identifies stress-induced alterations in mitochondrial connectivity and inner membrane structure from confocal images." PLOS Computational Biology **13**(6): e1005612.

Pakos-Zebrucka, K., Koryga, I., Mnich, K., Ljujic, M., Samali, A. and Gorman, A.M. (2016). "The integrated stress response." EMBO Rep **17**: 1374-1395.

Pan, L., Deng, M., Xie, X. and Gan, L. (2008). "ISL1 and BRN3B co-regulate the differentiation of murine retinal ganglion cells." Development **135**: 1981-1990.

Papa, L. and Germain, D. (2011). "Estrogen receptor mediates a distinct mitochondrial unfolded protein response." Journal of Cell Science **124**: 1396-1402.

Papa, L. and Germain, D. (2014). "SirT3 Regulates the Mitochondrial Unfolded Protein Response." Molecular and Cellular Biology **34**(4): 699.

Paquet, D., Kwart, D., Chen, A., Sproul, A., Jacob, S., Teo, S., ... and Tessier-Lavigne, M. (2016). "Efficient introduction of specific homozygous and heterozygous mutations using CRISPR/Cas9." Nature volume **533**: 125–129.

Paradies, G., Petrosillo, G., Paradies, V. and Ruggiero, F.M. (2010). "Oxidative stress, mitochondrial bioenergetics, and cardiolipin in aging." Free Radical Biology and Medicine **48**(10): 1286-1295.

Pareek, G., Thomas, R.E. and Pallanck, L.J. (2018). "Loss of the Drosophila m-AAA mitochondrial protease paraplegin results in mitochondrial dysfunction, shortened lifespan, and neuronal and muscular degeneration." Cell Death & Disease **9**(3): 304.

Parfitt, David A., Lane, A., Ramsden, Conor M., Carr, A.-Jayne F., Munro, Peter M., Jovanovic, K., ... and Cheetham, Michael E. (2016). "Identification and Correction of Mechanisms Underlying Inherited Blindness in Human iPSC-Derived Optic Cups." Cell Stem Cell **18**(6): 769-781.

Park, H., Oh, J., Shim, G., Cho, B., Chang, Y., Kim, S., ... and Kim, J. (2019). "In vivo neuronal gene editing via CRISPR–Cas9 amphiphilic nanocomplexes alleviates deficits in mouse models of Alzheimer's disease." Nature Neuroscience **22**(4): 524-528.

Park, I.-H., Zhao, R., West, J.A., Yabuuchi, A., Huo, H., Ince, T.A., ... and Daley, G.Q. (2008). "Reprogramming of human somatic cells to pluripotency with defined factors." Nature **451**(7175): 141-146.

Park, J., Koito, H., Li, J. and Han, A. (2009). "Microfluidic compartmentalized co-culture platform for CNS axon myelination research." Biomedical Microdevices **11**(6): 1145.

Pathak, D., Shields, L.Y., Mendelsohn, B.A., Haddad, D., Lin, W., Gerencser, A.A., ... and Nakamura, K. (2015). "The Role of Mitochondrially Derived ATP in Synaptic Vesicle Recycling." Journal of Biological Chemistry **290**(37): 22325-22336.

Patten, D.A., Wong, J., Khacho, M., Soubannier, V., Mailloux, R.J., Pilon-Larose, K., ... and Slack, R.S. (2014). "OPA1-dependent cristae modulation is essential for cellular adaptation to metabolic demand." EMBO J **33**: 2676-2691.

Paumard, P., Vaillier, J., Coulary, B., Schaeffer, J., Soubannier, V., Mueller, D.M., ... and Velours, J. (2002). "The ATP synthase is involved in generating mitochondrial cristae morphology." The EMBO journal **21**(3): 221-230.

Pérez de Sevilla Müller, L., Sargoy, A., Rodriguez, A.R. and Brecha, N.C. (2014). "Melanopsin Ganglion Cells Are the Most Resistant Retinal Ganglion Cell Type to Axonal Injury in the Rat Retina." PLOS ONE **9**(3): e93274.

Pérez, M.J., Ponce, D.P., Osorio-Fuentealba, C., Behrens, M.I. and Quintanilla, R.A. (2017). "Mitochondrial Bioenergetics Is Altered in Fibroblasts from Patients with Sporadic Alzheimer's Disease." Frontiers in Neuroscience **11**(553).

Perganta, G., Barnard, A.R., Katti, C., Vachtsevanos, A., Douglas, R.H., MacLaren, R.E., ... and Sekaran, S. (2013). "Non-Image-Forming Light Driven Functions Are Preserved in a Mouse Model of Autosomal Dominant Optic Atrophy." PLOS ONE **8**(2): e56350.

Perry, V.H. and Lund, R.D. (1990). "Evidence that the lamina cribrosa prevents intraretinal myelination of retinal ganglion cell axons." Journal of Neurocytology **19**: 265-272.

Pesch, U.E.A., Leo-Kottler, B., Mayer, S., Jurklies, B., Kellner, U., Apfelstedt-Sylla, E., ... and Wissinger, B. (2001). "OPA1 mutations in patients with autosomal dominant optic

atrophy and evidence for semi-dominant inheritance." Human Molecular Genetics **10**(13): 1359-1368.

Petit, I., Salman Kesner, N., Karry, R., Robicsek, O., E.Aberdam, E., Müller, F.J., ... and Ben-Shachard, D. (2012). "Induced pluripotent stem cells from hair follicles as a cellular model for neurodevelopmental disorders." Stem Cell Research **8**(1): 134-140.

Pevny, L.H. and Nicolis, S.K. (2010). "Sox2 roles in neural stem cells." The International Journal of Biochemistry & Cell Biology **42**(3): 421-424.

Pfanner, N., van der Laan, M., Amati, P., Capaldi, R.A., Caudy, A.A., Chacinska, A., ... and Nunnari, J. (2014). "Uniform nomenclature for the mitochondrial contact site and cristae organizing system." Journal of Cell Biology **204**(7): 1083-1086.

Philips, G.T., Stair, C.N., Lee, H.Y., Wroblewski, E., Berberoglu, M.A., Brown, N.L. and Mastic, G.S. (2005). "Precocious retinal neurons: Pax6 controls timing of differentiation and determination of cell type." Developmental Biology **279**(2): 308-321.

Phillips, M.J., Wallace, K.A., Dickerson, S.J., Miller, M.J., Verhoeven, A.D., Martin, J.M., ... and Gamm, D.M. (2012). "Blood-Derived Human iPS Cells Generate Optic Vesicle–Like Structures with the Capacity to Form Retinal Laminae and Develop Synapses." Investigative Ophthalmology & Visual Science **53**(4): 2007-2019.

Pietrocola, F., Galluzzi, L., Bravo-San Pedro, J.M., Madeo, F. and Kroemer, G. (2015). "Acetyl Coenzyme A: A Central Metabolite and Second Messenger." Cell Metabolism **21**(6): 805-821.

Pinton, P., Giorgi, C., Siviero, R., Zecchini, E. and Rizzuto, R. (2008). "Calcium and apoptosis: ER-mitochondria Ca2+ transfer in the control of apoptosis." Oncogene. **27**(50): 6407-6418.

Plaff, S.L., Mendelsohn, M., Stewart, C.L., Edlund, T. and Jessell, T.M. (1996). "Requirement for LIM Homeobox Gene Isl1 in Motor Neuron Generation Reveals a Motor Neuron– Dependent Step in Interneuron Differentiation." Cell **84**(2): 309-320.

Pontikos, N., Arno, G., Jurkute, N., Schiff, E., Ba-Abbad, R., Malka, S., ... and Mahroo, O.A. (2020). "Genetic Basis of Inherited Retinal Disease in a Molecularly Characterized Cohort of More Than 3000 Families from the United Kingdom." Ophthalmology **127**(10): 1384-1394.

Prigione, A., Fauler, B., Lurz, R., Lehrach, H. and Adjaye, J. (2010). "The Senescence-Related Mitochondrial/Oxidative Stress Pathway is Repressed in Human Induced Pluripotent Stem Cells." STEM CELLS **28**(4): 721-733.

Provis, J.M., Van Driel, D., Billson, F.A. and Russell, P. (1985). "Human Fetal Optic Nerve: Overproduction and Elimination of Retinal Axons During Development." The Journal of Comparative Neurology **238**: 92-100.

Pulkes, T., Eunson, L., Patterson, V., Siddiqui, A., Wood, N.W., Nelson, I.P., ... and Hanna, M.G. (1999). "The mitochondrial DNA G13513A transition in ND5 is associated with a LHON/MELAS overlap syndrome and may be a frequent cause of MELAS." Annals of Neurology **46**(6): 916-919.

Puomila, A., Huoponen, K., Mäntyjärvi, M., Hämäläinen, P., Paananen, R., Sankila, E.M., ... and Nikoskelainen, E. (2005). "Dominant optic atrophy: correlation between clinical and molecular genetic studies. ." Acta Ophthalmologica Scandinavica **83**: 337-346.

Qiu, F., Jiang, H. and Xiang, M. (2008). "A Comprehensive Negative Regulatory Program Controlled by Brn3b to Ensure Ganglion Cell Specification from Multipotential Retinal Precursors." Journal of Neuroscience **28**(13): 3392-3403.

Quirós, P.M., Prado, M.A., Zamboni, N., D'Amico, D., Williams, R.W., Finley, D., ... and Auwerx, J. (2017). "Multi-omics analysis identifies ATF4 as a key regulator of the mitochondrial stress response in mammals." J Cell Biol **216**(7): 2027–2045.

Radke, S., Chander, H., Schäfer, P., Meiss, G., Krüger, R., Schulz‖, J.B. and Germain, D. (2008). "Mitochondrial Protein Quality Control by the Proteasome Involves Ubiquitination and the Protease Omi." The Journal of Biological Chemistry **283**: 12681-12685.

Rahn, J.J., Stackley, K.D. and Chan, S.S.L. (2013). "Opa1 Is Required for Proper Mitochondrial Metabolism in Early Development." PLOS ONE **8**(3): e59218.

Ramakrishnan, N.A., Drescher, M.J. and Drescher, D.G. (2012). "The SNARE complex in neuronal and sensory cells." Mol Cell Neurosci. **50**(1): 58-69.

Rambold, A.S., Kostelecky, B., Elia, N. and Lippincott-Schwartz, J. (2011). "Tubular network formation protects mitochondria from autophagosomal degradation during nutrient starvation." PNAS **25**: 10190-10195.

Ran, F.A., Hsu, P.D., Wright, J., Agarwala, V., Scott, D.A. and Zhang, F. (2013). "Genome engineering using the CRISPR-Cas9 system." Nature Protocols **8**: 2281-2308.

Rasmussen, M.A., Lena E.Hjermind, L.E., Hasholt, L.F., Waldemar, G., J.E., N., Clausen, C., ... and Holst, B. (2016). "Induced pluripotent stem cells (iPSCs) derived from a patient with frontotemporal dementia caused by a P301L mutation in microtubule-associated protein tau (MAPT)." Stem Cell Research **16**(1): 70-74.

Reddy, P.H. (2009). "Amyloid beta, mitochondrial structural and functional dynamics in Alzheimer's disease." Experimental Neurology **218**(2): 286-292.

Reeve, A.K., Krishnan, K.J., Elson, J.L., Morris, C.M., Bender, A., Lightowlers, R.N. and Turnbull, D.M. (2008). "Nature of Mitochondrial DNA Deletions in Substantia Nigra Neurons." Am J Hum Genet. **82**(1): 228-235.

Reinhardt, C., Arena, G., Nedara, K., Edwards, R., Brenner, C., Tokatlidis, K. and Modjtahedi, N. (2020). "AIF meets the CHCHD4/Mia40-dependent mitochondrial import pathway." Biochimica et Biophysica Acta (BBA) - Molecular Basis of Disease **1866**(6): 165746.

Reynier, P., Amati-Bonneau, P., Verny, C., Olichon, A., Simard, G., Guichet, A., ... and Bonneau, D. (2004). "OPA3 gene mutations responsible for autosomal dominant optic atrophy and cataract." Journal of Medical Genetics **41**: e110.

Rheaume, B.A., Jereen, A., Bolisetty, M., Sajid, M., Yang, Y., Renna, K., ... and Trakhtenberg, E.F. (2018). "Single cell transcriptome profiling of retinal ganglion cells identifies cellular subtypes." Nature Communications **9**: 2759.

Rhein, V., Song, X., Wiesner, A., Ittner, L.M., Baysang, G., Meier, F., ... and Eckert, A. (2009). "Amyloid-β and tau synergistically impair the oxidative phosphorylation system in triple transgenic Alzheimer's disease mice." Proceedings of the National Academy of Sciences **106**(47): 20057-20062.

Riazifar, H., Yousheng, J., Chen, J., Lynch, G. and Huang, T. (2014). "Chemically Induced Specification of Retinal Ganglion Cells From Human Embryonic and Induced Pluripotent Stem Cells." Stem Cells Translational Medicine **3**(4): 424-432.

Richardson, C.D., Ray, G.J., DeWitt, M.A., Curie, G.L. and Corn, J.E. (2016). "Enhancing homology-directed genome editing by catalytically active and inactive CRISPR-Cas9 using asymmetric donor DNA." Nature Biotechnology **34**: 339-344.

Riesenberg, A.N., Le, T.T., Willardsen, M.I., Blackburn, D.C., Vetter, M.L. and Brown, N.L. (2009). "Pax6 regulation of Math5 during mouse retinal neurogenesis." Genesis **47**(3): 175-187.

Rizzuto, R., De Stefani, D., Raffaello, A. and Mammucari, C. (2012). "Mitochondria as sensors and regulators of calcium signalling." Nature Reviews Molecular Cell Biology **13**(9): 566-578.

Rizzuto, R., Pinton, P., Ferrari, D., Chami, M., Szabadkai, G., Magalhães, P.J., ... and Pozzan, T. (2003). "Calcium and apoptosis: facts and hypotheses." Oncogene **22**(53): 8619-8627.

Robinson, G.A. and Madison, R.D. (2004). "Axotomized mouse retinal ganglion cells containing melanopsin show enhanced survival, but not enhanced axon regrowth into a peripheral nerve graft." Vision Research **44**(23): 2667-2674.

Rodan, L.H., Wells, G.D., Banks, L., Thompson, S., Schneiderman, J.E. and Tein, I. (2015). "L-Arginine Affects Aerobic Capacity and Muscle Metabolism in MELAS (Mitochondrial Encephalomyopathy, Lactic Acidosis and Stroke-Like Episodes) Syndrome." PLOS ONE **10**(5): e0127066.

Romagnoli, M., La Morgia, C., Carbonelli, M., Di Vito, L., Amore, G., Zenesini, C., ... and Carelli, V. (2020). "Idebenone increases chance of stabilization/recovery of visual acuity in OPA1-dominant optic atrophy." Annals of Clinical and Translational Neurology **7**(4): 590-594.

Romagnoli, M., La Morgia, C., Carbonelli, M., Di Vito, L., Amore, G., Zenesini, C., ... and Carelli, V. (2020). "Idebenone increases chance of stabilization/recovery of visual acuity in OPA1-dominant optic atrophy." Ann Clin Transl Neurol. **7**(4): 590-594.

Rooney, J.P., Ryde, I.T., Sanders, L.H., Howlett, E.H., Colton, M.D., Germ, K.E., ... and Meyer, J.N. (2015). PCR Based Determination of Mitochondrial DNA Copy Number in Multiple Species. Mitochondrial Regulation: Methods and Protocols. C.M. Palmeira and A.P. Rolo. New York, NY, Springer New York**:** 23-38.

Ross, D. and Siegel, D. (2017). "Functions of NQO1 in Cellular Protection and CoQ10 Metabolism and its Potential Role as a Redox Sensitive Molecular Switch." Frontiers in Physiology **8**(595).

Rossignol, R., Gilkerson, R., Aggeler, R., Yamagata, K., Remington, S.J. and Capaldi, R.A. (2004). "Energy Substrate Modulates Mitochondrial Structure and Oxidative Capacity in Cancer Cells." Cancer Research **64**(3): 985-993.

Rouzier, C., Bannwarth, S., Chaussenot, A., Chevrollier, A., Verschueren, A., Bonello-Palot, N., ... and Paquis-Flucklinger, V. (2012). "The MFN2 gene is responsible for mitochondrial DNA instability and optic atrophy 'plus' phenotype." Brain **135**(1): 23-34.

Rowan, R., Chen, C.M.A., Young, T.L., Fisher, D.E. and Cepko, C.L. (2004). "Transdifferentiation of the retina into pigmented cells in ocular retardation mice defines a new function of the homeodomain gene Chx10." Development **131**: 5139-5152.

Ruiz-Ederra, J., García, M., Hicks, D. and Vecino, E. (2004). "Comparative study of the three neurofilament subunits within pig and human retinal ganglion cells." Mol Vis. **10**: 83-92.

Runkel, E.D., Liu, S., Baumeister, R. and Schulze, E. (2013). "Surveillance-Activated Defenses Block the ROS–Induced Mitochondrial Unfolded Protein Response." PLOS Genetics **9**(3): e1003346.

Sakuma, H., Inana, G., Murakami, A., Higashide, T. and McLaren, M.J. (1996). "Immunolocalization of X-arrestin in human cone photoreceptors." FEBS Lett. **382**: 105-110.

Samant, S.A., Zhang, H.J., Hong, Z., Pillai, V.B., Sundaresan, N.R., Wolfgeher, D., ... and Gupta, M.P. (2014). "SIRT3 Deacetylates and Activates OPA1 To Regulate Mitochondrial Dynamics during Stress." Molecular and Cellular Biology **34**(5): 807– 819.

Sanders, L.H., Laganière, J., Cooper, O., Mak, S.K., Vu, B.J., Huang, Y.A., ... and Schüle, B. (2014). "LRRK2 mutations cause mitochondrial DNA damage in iPSC-derived neural cells from Parkinson's disease patients: Reversal by gene correction." Neurobiology of Disease **62**: 381-386.

Sanes, J.R. and Masland, R.H. (2015). "The Types of Retinal Ganglion Cells: Current Status and Implications for Neuronal Classification." Annual Review of Neuroscience **38**(1): 221-246.

Santel, A. and Fuller, M.T. (2000). "Control of mitochondrial morphology by a human mitofusin." Journal of Cell Science **114**: 867-887.

Sapranauskas, R., Gasiunas, G., Fremaux, C., Barrangou, R., Horvath, P. and Siksnys, V. (2011). "The Streptococcus thermophilus CRISPR/Cas system provides immunity in Escherichia coli." Nucleic Acids Research **39**(21): 9275-9282.

Sarzi, E., Angebault, I., Seveno, M., Gueguen, N., Chaix, C., Bielicki, G., ... and Lenaers, G. (2012). "The human OPA1delTTAG mutation induces premature age-related systemic neurodegeneration in mouse." Brain **135**(12): 3599-3613.

Sarzi, E., Seveno, M., Angebault, C., Milea, D., Rönnbäck, C., Quilès, M., ... and Müller, A. (2016). "Increased steroidogenesis promotes early-onset and severe vision loss in females with OPA1 dominant optic atrophy." Human Molecular Genetics **25**(12): 2539-2551.

Sarzi, E., Seveno, M., Piro-Mégy, C., Elzière, L., Quilès, M., Péquignot, M., ... and Delettre, C. (2018). "OPA1 gene therapy prevents retinal ganglion cell loss in a Dominant Optic Atrophy mouse model." Scientific Reports **8**: 2468.

Sattler, R. and Tymianski, M. (2000). "Molecular mechanisms of calcium-dependent excitotoxicity." J Mol Med **78**: 3-13.

Savell, K.E., Bach, S.V., Zipperly, M.E., Revanna, J.S., Goska, N.A., Tuscher, J.J., ... and Day, J.J. (2019). "A Neuron-Optimized CRISPR/dCas9 Activation System for Robust and Specific Gene Regulation." eNeuro **6**(1): ENEURO.0495-0418.2019.

Scarpulla, R.C. (2006). "Nuclear control of respiratory gene expression in mammalian cells." J. Cell. Biochem. **97**: 673-683.

Schimpf, S., Fuhrmann, N., Schaich, S. and Wissinger, B. (2008). "Comprehensive cDNA Study and Quantitativetranscript Analysis of Mutant Opa1 Transcripts Containing Premature Termination Codons." Human Mutation **29**(1): 106-112.

Schoenwolf, G.L., Bleyl, S.B., Brauer, P.R. and Francist-West, P.H. (2009). Larsen's human embryology. Philadelphia, Elsevier.

Schwab, A.J. and Ebert, A.D. (2015). "Neurite Aggregation and Calcium Dysfunction in iPSC-Derived Sensory Neurons with Parkinson's Disease-Related LRRK2 G2019S Mutation." Stem Cell Reports **5**(6): 1039-1052.

Schwarz, B.A., Bar-Nur, O., Silva, J.C.R. and Hochedlinger, K. (2014). "Nanog Is Dispensable for the Generation of Induced Pluripotent Stem Cells." Current Biology **24**(3): 347-350.

Schwarz, N., Carr, A.-J., Lane, A., Moeller, F., Chen, L.L., Aguilà, M., ... and Hardcastle, A.J. (2015). "Translational read-through of the RP2 Arg120stop mutation in patient iPSC-derived retinal pigment epithelium cells." Human Molecular Genetics **24**(4): 972-986.

Schwarz, N., Lane, A., Jovanovic, K., Parfitt, D.A., Aguila, M., Thompson, C.L., ... and Cheetham, M.E. (2017). "Arl3 and RP2 regulate the trafficking of ciliary tip kinesins." Human Molecular Genetics **26**(13): 2480-2492.

Ścieżyńska, A., Ruszkowska, E., Szulborski, K., Rydz, K., Wierzbowska, J., Kosińska, J., ... and Ołdak, M. (2017). "Processing of OPA1 with a novel N-terminal mutation in patients with autosomal dominant optic atrophy: Escape from nonsense-mediated decay." PLOS ONE **12**(8): e0183866.

Scorrano, L., Oakes, S.A., Opferman, J.T., Cheng, E.H., Sorcinelli, M.D., Pozzan, T. and Korsmeyer, S.J. (2003). "BAX and BAK Regulation of Endoplasmic Reticulum Ca2+: A Control Point for Apoptosis." Science **300**(5616): 135-139.

Seager, R., Lee, L., Henley, Jeremy M. and Wilkinson, Kevin A. (2020). "Mechanisms and roles of mitochondrial localisation and dynamics in neuronal function." Neuronal Signaling **4**(2).

Sernagor, E., Eglen, S.J. and Wong, R.O.L. (2001). "Development of Retinal Ganglion Cell Structure and Function." Progress in Retinal and Eye Research **20**(2): 139-174.

Sesaki, H., Southard, S.M., Hobbs, A.E.A. and Jensen, R.E. (2003). "Cells lacking Pcp1p/Ugo2p, a rhomboid-like protease required for Mgm1p processing, lose mtDNA and mitochondrial structure in a Dnm1p-dependent manner, but remain competent for mitochondrial fusion." Biochemical and Biophysical Research Communications **308**(2): 276-283.

Shahani, N. and Brandt, R. (2002). "Functions and malfunctions of the tau proteins." Cell. Mol. Life Sci. **59**: 1668-1680.

Sheridan, S.D., Surampudi, V. and Rao, R.R. (2012). "Analysis of Embryoid Bodies Derived from Human Induced Pluripotent Stem Cells as a Means to Assess Pluripotency." Stem Cells International **2012**: 9.

Shetty, P.K., Galeffi, F. and Turner, D.A. (2012). "Cellular Links between Neuronal Activity and Energy Homeostasis." Frontiers in pharmacology **3**: 43.

Shi, L., Cui, Y., Luan, J., Zhou, X. and Han, J. (2016). "Urine-derived induced pluripotent stem cells as a modeling tool to study rare human diseases." Intractable Rare Dis Res. **5**(3): 192-201.

Shigeoka, T., Jung, H., Jung, J., Turner-Bridger, B., Ohk, J., Lin, J.Q., ... and Holt, C.E. (2016). "Dynamic Axonal Translation in Developing and Mature Visual Circuits." Cell **166**(1): 181-192.

Shih, A.Y., Imbeault, S., Barakauskas, V., Erb, H., Jiang, L., Li, P. and Murphy, T.H. (2005). "Induction of the Nrf2-driven Antioxidant Response Confers Neuroprotection during Mitochondrial Stress in Vivo." The Journal of Biological Chemistry **280**: 22925-22936.

Shindler, K.S., Ventura, E., Dutt, M. and Rostami, A. (2008). "Inflammatory demyelination induces axonal injury and retinal ganglion cell apoptosis in experimental optic neuritis." Experimental Eye Research **87**(3): 208-213.

Shirai, H., Mandai, M., Matsushita, K., Kuwahara, A., Yonemura, S., Nakano, T., ... and Takahashi, M. (2016). "Transplantation of human embryonic stem cell-derived retinal tissue in two primate models of retinal degeneration." Proceedings of the National Academy of Sciences **113**(1): E81.

Shokolenko, I.N. and Alexeyev, M.F. (2017). "Mitochondrial transcription in mammalian cells." Front Biosci **22**: 835-853.

Silva, J.M., Wong, A., Carelli, V. and Cortopass, G.A. (2009). "Inhibition of mitochondrial function induces an integrated stress response in oligodendroglia." Neurobiology of Disease **34**(2): 357-365.

Sitarz, K.S., Yu-Wai-Man, P., Pyle, A., Stewart, J.D., Rautenstrauss, B., Seeman, P., ... and Chinnery, P.F. (2012). "MFN2 mutations cause compensatory mitochondrial DNA proliferation." Brain **135**(8): e219-e219.

Sluch, V.M., Chamling, X., Liu, M.M., Berlinicke, C.A., Cheng, J., Mitchell, K.L., ... and Zack, D.J. (2017). "Enhanced Stem Cell Differentiation and Immunopurification of Genome Engineered Human Retinal Ganglion Cells." Stem Cells Translational Medicine **6**: 1972-1986.

Sluch, V.M., Davis, C.-H.O., Ranganathan, V., Kerr, J.M., Krick, K., Martin, R., ... and Zack, D.J. (2015). "Differentiation of human ESCs to retinal ganglion cells using a CRISPR engineered reporter cell line." Scientific Reports **5**: 16595.

Smirnova, E., Griparic, L., Shurland, D.L. and van der Bliek, A.M. (2001). "Dynamin-related Protein Drp1 Is Required for Mitochondrial Division in Mammalian Cells." Molecular Biology of the Cell **12**(8): 2245-2256.

Smith, C., Gore, A., Yan, W., Zhang, K., Cheng, L. and Ye, Z. (2014). "Whole-Genome Sequencing Analysis Reveals High Specificity of CRISPR/Cas9 and TALEN-Based Genome Editing in Human iPSCs." Cell Stem Cell: P12-13.

Smith, T.G., Seto, S., Ganne, P. and Votruba, M. (2016). "A randomized, placebo-controlled trial of the benzoquinone idebenone in a mouse model of OPA1-related dominant optic atrophy reveals a limited therapeutic effect on retinal ganglion cell dendropathy and visual function." Neuroscience **319**: 92-106.

Song, Z., Chen, H., Fiket, M., Alexander, C. and Chan, D.C. (2007). "OPA1 processing controls mitochondrial fusion and is regulated by mRNA splicing, membrane potential, and Yme1L. ." Journal of Cell Biology **178**(5): 749.

Spiegel, R., Saada, A., Flannery, P.J., Burté, F., Soiferman, D., Khayat, M., ... and Yu-Wai-Man, P. (2016). "Fatal infantile mitochondrial encephalomyopathy, hypertrophic cardiomyopathy and optic atrophy associated with a homozygous OPA1 mutation." J Med Genet. **53**(2): 127-131.

Spiegel, R., Saada, A., Flannery, P.J., Burté, F., Soiferman, D., Khayat, M., ... and Yu-Wai-Man, P. (2016). "Fatal infantile mitochondrial encephalomyopathy, hypertrophic

cardiomyopathy and optic atrophy associated with a homozygous *OPA1* mutation." Journal of Medical Genetics **53**(2): 127.

Spinelli, J.B. and Haigis, M.C. (2018). "The multifaceted contributions of mitochondria to cellular metabolism." Nature Cell Biology **20**: 745-754.

Sridhar, A., Hoshino, A., Finkbeiner, C.R., Chitsazan, A., Dai, L., Haugan, A.K., ... and Reh, T.A. (2020). "Single-Cell Transcriptomic Comparison of Human Fetal Retina, hPSC-Derived Retinal Organoids, and Long-Term Retinal Cultures." Cell Reports **30**: 1644-1659.

Struebing, F.L., Lee, R.K., Williams, R.W. and Geisert, E.E. (2016). "Genetic Networks in Mouse Retinal Ganglion Cells." Frontiers in Genetics **7**(169).

Suárez-Rivero, J.M., Villanueva-Paz, M., de la Cruz-Ojeda, P., de la Mata, M., Cotán, D., Oropesa-Ávila, M., ... and Luzón-Hidalgo, R.S.-A., J.A. (2017). "Mitochondrial Dynamics in Mitochondrial Diseases. ." Diseases **5**(1): 1.

Südhof, T.C. and Rizo, J. (2011). "Synaptic Vesicle Exocytosis." Cold Spring Harb Perspect Biol. **3**(12): a005637.

Suen, D.-F., Narendra, D.P., Tanaka, A., Manfredi, G. and Youle, R.J. (2010). "Parkin overexpression selects against a deleterious mtDNA mutation in heteroplasmic cybrid cells." Proceedings of the National Academy of Sciences **107**(26): 11835-11840.

Sümbül, U., Song, S., McCulloch, K., Becker, M., Lin, B., Sanes, J.R., ... and Seung, H.S. (2014). "A genetic and computational approach to structurally classify neuronal types." Nature Communications **5**: 3512.

Sun, N. and Zhao, H. (2014). "Seamless correction of the sickle cell disease mutation of the HBB gene in human induced pluripotent stem cells using TALENs." Biotechnology and Bioengineering **111**(5): 1048-1053.

Sun, Y., Liang, X., Najafi, N., Cass, M., Lin, L., Cai, C.L., ... and Evans, S.M. (2007). "Islet 1 is expressed in distinct cardiovascular lineages, including pacemaker and coronary vascular cells." Developmental Biology **304**(1): 286-296.

Sun, Y., Zheng, J., Xu, Y. and Zhang, X. (2018). "Paraquat-induced inflammatory response of microglia through HSP60/TLR4 signaling. ." Human & Experimental Toxicology **37**(11): 1161–1168.

Sundaresan, P., Simpson, D.A., Sambare, C., Duffy, S., Lechner, J., Dastane, A., ... and Willoughby, C.E. (2015). "Whole-mitochondrial genome sequencing in primary open-angle glaucoma using massively parallel sequencing identifies novel and known pathogenic variants." Genetics in Medicine **17**(4): 279-284.

Surgucheva, I., Weisman, A.D., Goldberg, J.L., Shnyra, A. and Surguchov, A. (2008). "γ-Synuclein as a marker of retinal ganglion cells." Mol Vis. **14**: 1540–1548.

Sweeney, N.T., James, K.N., Nistorica, A., Lorig-Roach, R.M. and Feldheim, D.A. (2019). "Expression of transcription factors divides retinal ganglion cells into distinct classes." The Journal of Comparative Neurology **527**(1): 225-235.

Taanman, J.W. (1999). "The mitochondrial genome: structure, transcription, translation and replication." Biochimica et Biophysica Acta (BBA) - Bioenergetics **1410**(2): 103-123.

Taapken, S.M., Nisler, B.S., Newton, M.A., Sampsell-Barron, T.L., Leonhard, K.A., McIntire, E.M. and Montgomery, K.D. (2011). "Karyotypic abnormalities in human

induced pluripotent stem cells and embryonic stem cells." Nature Biotechnology **29**(4): 313-314.

Takahashi, K., Tanabe, K., Ohnuki, M., Narita, M., Ichisaka, T., Tomoda, K. and Yamanaka, S. (2007). "Induction of pluripotent stem cells from adult human fibroblasts by defined factors." Cell **131**(5): 861-872.

Takahashi, K. and Yamanaka, S. (2006).“Induction of Pluripotent Stem Cells from Mouse Embryonic and Adult Fibroblast Cultures by Defined Factors.” Cell **126**(4): 663-676.

Tammineni, P., Ye, X., Feng, T., Aikal, D. and Cai, Q. (2017). "Impaired retrograde transport of axonal autophagosomes contributes to autophagic stress in Alzheimer’s disease neurons." eLife **6**: e21776.

Tan, H.K., Delon Toh, C.X., Ma, D., Yang, B., Ming Liu, T., Lu, J., ... and Loh, Y.H. (2014). "Human Finger-Prick Induced Pluripotent Stem Cells Facilitate the Development of Stem Cell Banking." Stem Cells Translational Medicine **3**(5): 586-598.

Tanaka, T., Yokoi, T., Tamalu, F., Watanabe, S.-I., Nishina, S. and Azuma, N. (2015). "Generation of retinal ganglion cells with functional axons from human induced pluripotent stem cells." Scientific Reports **5**.

Tang, S., Khanh, P., Tse, S., Wallace, D.C. and Huang, T. (2009). "Heterozygous Mutation of Opa1 in Drosophila Shortens Lifespan Mediated through Increased Reactive Oxygen Species Production." PLOS ONE **4**(2): e4492.

Taranova, O.V., Magness, S.T., Fagan, M., Wu, Y., Surzenko, N., Hutton, S.R. and Pevny, L.H. (2006). "SOX2 is a dose-dependent regulator of retinal neural progenitor competence." Genes & Dev. **20**: 1187-1202.

Taylor, A.M., Blurton-Jones, M., Rhee, S.W., Cribbs, D.H., Cotman, C.W. and Jeon, N.L. (2005). "A microfluidic culture platform for CNS axonal injury, regeneration and transport." Nature Methods **2**(8): 599-605.

Taylor, D. (2005). "Optic nerve axons: life and death before birth." Eye **19**: 499-527.

Taylor, R.W. and Turnbull, D.M. (2005). "Mitochondrial DNA mutations in human disease." Nat Rev Genet. **6**(5): 389-402.

Teotia, P., Chopra, D.A., Dravid, S.M., Van Hook, M.J., Qiu, F., Morrison, J., ... and Ahmad, I. (2016). "Generation of Functional Human Retinal Ganglion Cells with Target Specificity from Pluripotent Stem Cells by Chemically Defined Recapitulation of Developmental Mechanism." Stem Cells **35**: 572-585.

Teotia, P., Van Hook, M.J., Wichman, C.S., Allingham, R.R., Hauser, M.A. and Ahmad, I. (2017). "Modeling Glaucoma: Retinal Ganglion Cells Generated from Induced Pluripotent Stem Cells of Patients with SIX6 Risk Allele Show Developmental Abnormalities." Stem Cells **35**: 2239-2252.

Teshigawara, R., Cho, J., Kameda, M. and Tada, T. (2017). "Mechanism of human somatic reprogramming to iPS cell." Laboratory Investigation **97**: 1152-1157.

Tétreaulta, N., Champagnea, M.P. and Bernier, G. (2009). "The LIM homeobox transcription factor Lhx2 is required to specify the retina field and synergistically cooperates with Pax6 for Six6 trans-activation." Developmental Biology **327**(2): 541-550.

Tezel, G., Hernandez, M.R. and Wax, M.B. (2000). "Immunostaining of Heat Shock Proteins in the Retina and Optic Nerve Head of Normal and Glaucomatous Eyes." Arch Ophthalmol. **118**(4): 511–518.

Tezze, C., Romanello, V., Desbats, M.A., Fadini, G.P., Albiero, M., Favaro, G., ... and Sandri, M. (2017). "Age-Associated Loss of OPA1 in Muscle Impacts Muscle Mass, Metabolic Homeostasis, Systemic Inflammation, and Epithelial Senescence." Cell Metabolism **25**(6): 1374–1389.

Tham, Y.C., Li, X., Wong, T.Y., Quigley, H.A., Aung, T. and Cheng, C.Y. (2014). "Global prevalence of glaucoma and projections of glaucoma burden through 2040: a systematic review and meta-analysis." Ophthalmology **121**(11): 2081-2090.

Thompson, O., von Meyenn, F., Hewitt, Z., Alexander, J., Wood, A., Weightman, R., ... and Andrews, P.W. (2020). "Low rates of mutation in clinical grade human pluripotent stem cells under different culture conditions." Nature Communications **11**(1): 1528.

Thomson, J.A., tskovitz-Eldor, J., Shapiro, S.S., Waknitz, M.A., Swiergiel, J.J., Marshall, V.S. and Jones, J.M. (1998). "Embryonic Stem Cell Lines Derived from Human Blastocysts." Science **282**(5391): 1145-1147.

Thor, S., Ericson, J., Brannstrom, T. and Edlund, T. (1991). "The homeodomain LIM protein Isl-1 is expressed in subsets of neurons and endocrine cells in the adult rat." Neuron **7**(6): 881-889.

Tondera, D., Grandemange, S., Jourdain, A., Karbowski, M., Mattenberger, Y., Herzig, S., ... and Martinou, J.-C. (2009). "SLP-2 is required for stress-induced mitochondrial hyperfusion." The EMBO Journal **28**(11): 1589-1600.

Toyama, E.Q., Herzig, S., Courchet, J., Lewis, T.L., Losón, O.C., Hellberg, K., ... and Shaw, R.J. (2016). "AMP-activated protein kinase mediates mitochondrial fission in response to energy stress." Science **351**(6270): 275-281.

Trapp, B.D. and Stys, P.K. (2009). "Virtual hypoxia and chronic necrosis of demyelinated axons in multiple sclerosis." The Lancet Neurology **8**(3): 280-291.

Tronstad, K.J., Nooteboom, M., Nilsson, L.I.H., Nikolaisen, J., Sokolewicz, M., Grefte, S., ... and Koopman, W.J.H. (2014). "Regulation and quantification of cellular mitochondrial morphology and content." Curr Pharm Des. **20**(35): 5634-5652.

Tulsawani, R., Kelly, L.S., Fatma, N., Chhunchha, B., Kubo, E., Kumar, A. and Singh, D.P. (2010). "Neuroprotective effect of peroxiredoxin 6 against hypoxia-induced retinal ganglion cell damage." BMC Neuroscience **11**(1): 125.

Turner, E.E., Jenne, K.J. and Rosenfeld, M.G. (1994). "Brn-3.2: A Brn-3-related transcription factor with distinctive central nervous system expression and regulation by retinoic acid." Neuron **12**(1): 205-218.

Twig, G., Elorza, A., Molina, A.J.A., Mohamed, H., Wikstrom, J.D., Walzer, G., ... and Shirihai, O.S. (2008). "Fission and selective fusion govern mitochondrial segregation and elimination by autophagy." The EMBO Journal **27**(2): 433-446.

Twig, G. and Shirihai, O.S. (2011). "The interplay between mitochondrial dynamics and mitophagy." Antioxidants & redox signaling **14**(10): 1939-1951.

Tysnes, O.-B. and Storstein, A. (2017). "Epidemiology of Parkinson's disease." Journal of Neural Transmission **124**(8): 901-905.

Valente, A.J., Maddalena, L.A., Robb, E.L., Moradi, F. and Stuart, J.A. (2017). "A simple ImageJ macro tool for analyzing mitochondrial network morphology in mammalian cell culture." Acta Histochem **119**(3): 315-326.

Van Bergen, N.J., Crowston, J.G., Craig, J.E., Burdon, K.P., Kearns, L.S., Sharma, S., ... and Trounce, I.A. (2015). "Measurement of Systemic Mitochondrial Function in Advanced Primary Open-Angle Glaucoma and Leber Hereditary Optic Neuropathy." PLOS ONE **10**(10): e0140919-e0140919.

van den Berg, R., Hoogenraad, C.C. and Hintzen, R.Q. (2017). "Axonal transport deficits in multiple sclerosis: spiraling into the abyss." Acta Neuropathologica **134**(1): 1-14.

Van Wyk, M., Wässle, H. and Taylor, W.R. (2009). "Receptive field properties of ON- and OFF-ganglion cells in the mouse retina." Vis Neurosci. **26**(3): 297-308.

VanderWall, K.B., Vij, R., Ohlemacher, S.K., Sridhar, A., Fligor, C.M., Feder, E.M., ... and Meyer, J.S. (2019). "Astrocytes Regulate the Development and Maturation of Retinal Ganglion Cells Derived from Human Pluripotent Stem Cells." Stem Cell Reports **12**(2): 201-212.

Vanstone, J.R., Smith, A.M., McBride, S., Naas, T., Holcik, M., Antoun, G., ... and Care4Rare, C. (2016). "DNM1L-related mitochondrial fission defect presenting as refractory epilepsy." European Journal of Human Genetics **24**(7): 1084-1088.

Verny, C., Loiseau, D., Scherer, C., Lejeune, P., Chevrollier, A., Gueguen, N., ... and Bonneau, D. (2008). "Multple Sclerosis-Like disorder in OPA1-related Autsomal dominant optic atrophy." Neurology **70**(13 Part 2): 1152-1153.

Villegas-Pérez, M.P., Vidal-Sanz, M., Rasminsky, M., Bray, G.M. and Aguayo, A.J. (1993). "Rapid and protracted phases of retinal ganglion cell loss follow axotomy in the optic nerve of adult rats." Dev Biol. **24**(1): 23-36.

Volkner, M., Zschatzsch, M., Rostovskaya, M., Overall, R.W., Busskamp, V., Anastassiadis, K. and Karl, M.O. (2016). "Retinal Organoids from Pluripotent Stem Cells Efficiently Recapitulate Retinogenesis." Stem Cell Reports **6**(4): 525-538.

Volpato, V. and Webber, C. (2020). "Addressing variability in iPSC-derived models of human disease: guidelines to promote reproducibility." Disease models & mechanisms **13**(1): dmm042317.

Votruba, M., Moore, A.T. and Bhattacharya, S.S. (1998). "Clinical features, molecular genetics, and pathophysiolgy of dominant optic atrophy." J Med Genet. **35**: 793-800.

Votruba, M., Thiselton, D. and Bhattacharya, S.S. (2003). "Optic disc morphology of patients with OPA1 autosomal dominant optic atrophy." British Journal of Ophthalmology **87**(1): 48.

Wali, G., Kumar, K.R., Liyanage, E., Davis, R.L., Mackay-Sim, A. and Sue, C.M. (2020). "Mitochondrial Function in Hereditary Spastic Paraplegia: Deficits in SPG7 but Not SPAST Patient-Derived Stem Cells." Frontiers in Neuroscience **14**(820).

Wallace, D.C., Shoffner, J.M., Watts, R.L., Juncos, J.L. and Torroni, A. (1991). "Mitochondrial oxidative phosphorylation defects in parkinson's disease." Annals of Neurology **30**(3): 332-339.

Wang, S., Ren, S., Bai, R., Xiao, P., Zhou, Q., Zhou, Y., ... and Chen, Y. (2018). "No off-target mutations in functional genome regions of a CRISPR/Cas9-generated monkey model of muscular dystrophy." The Journal of Biological Chemistry **293**: 11654-11658.

Wang, S.W., Gan, L., Martin, S.E. and Klein, W.H. (2000). "Abnormal polarization and axon outgrowth in retinal ganglion cells lacking the POU-domain transcription factor Brn-3b." Mol Cell Neurosci. **16**(2): 141-156.

Wang, S.W., Kim, B.S., Ding, K., Wang, H., Sun, D., Johnson, R.L., ... and Gan, L. (2001). "Requirement for math5 in the development of retinal ganglion cells." Genes Dev. **15**(1): 24-29.

Wang, S.W., Mu, X., Bowers, W.J., Kim, D.S., Plas, D.J., Crair, M.C., ... and Klein, W.H. (2002). "Brn3b/Brn3c double knockout mice reveal an unsuspected role for Brn3c in retinal ganglion cell axon outgrowth." Development **129**: 467-477.

Wang, W., Yang, J., Liu, H., Lu, D., Chen, X., Zenonos, Z., ... and Liu, P. (2011). "Rapid and efficient reprogramming of somatic cells to induced pluripotent stem cells by retinoic acid receptor gamma and liver receptor homolog 1." PNAS **108**(45): 18283-18288.

Wang, Y., Dakubo, G.D., Thurig, S., Mazerolle, C.J. and Wallace, V.A. (2005). "Retinal ganglion cell-derived sonic hedgehog locally controls proliferation and the timing of RGC development in the embryonic mouse retina." Development **132**(22): 5103.

Wang, Z. and Wu, M. (2015). "An integrated phylogenomic approach toward pinpointing the origin of mitochondria." Scientific Reports **5**: 7949.

Watanabe, M., Sawai, H. and Fukuda, Y. (1993). "Number, Distribution, and Morphology of Retinal Ganglion Cells Axons Regenerated into Peripheral Nerve Graft in Adult Cats." The Journal of Neuroscience **13**(5): 2105-2117.

Waterham, H.R., Koster, J., van Roermund, C.W.T., Mooyer, P.A.W., Wanders, R.J.A. and Leonard, J.V. (2007). "A Lethal Defect of Mitochondrial and Peroxisomal Fission." New England Journal of Medicine **356**(17): 1736-1741.

Watts, M.E., Pocock, R. and Claudianos, C. (2018). "Brain Energy and Oxygen Metabolism: Emerging Role in Normal Function and Disease." Front. Mol. Neurosci. **11**: 216.

Wax, M.B., Tezel, G. and Edward, P.D. (1998). "Clinical and Ocular Histopathological Findings in a Patient With Normal-Pressure Glaucoma." Arch Ophthalmol. **116**(8): 993-1001.

Wax, M.B., Tezel, G., Kawase, K. and Kitazawa, Y. (2001). "Serum autoantibodies to heat shock proteins in glaucoma patients from Japan and the United States." Ophthalmology **108**(2): 296-302.

Wax, M.B., Tezel, G., Yang, J., Peng, G., Patil, R.V., Agarwal, N., ... and Calkins, D.J. (2008). "Induced Autoimmunity to Heat Shock Proteins Elicits Glaucomatous Loss of Retinal Ganglion Cell Neurons via Activated T-Cell-Derived Fas-Ligand." Journal of Neuroscience **28**(46): 12085-12096.

Werth, J.L. and Thayer, S.A. (1994). "Mitochondria Buffer Physiological Calcium Loads in Cultured Rat Dorsal Root Ganglion Neurons." The Journal of Neuroscience **14**(1): 348-358.

Westermann, B. (2010). "Mitochondrial fusion and fission in cell life and death." Nature Reviews Molecular Cell Biology **11**: 872–884.

White, K.E., Davies, V.J., Hogan, V.E., Piechota, M.J., Nichols, P.P., Turnbull, D.M. and Votruba, M. (2009). "OPA1 Deficiency Associated with Increased Autophagy in Retinal

Ganglion Cells in a Murine Model of Dominant Optic Atrophy." Invest. Ophthalmol. Vis. Sci. **50**(6): 2567-2571.

Williams, N.C. and O'Neill, L.A.J. (2018). "A Role for the Krebs Cycle Intermediate Citrate in Metabolic Reprogramming in Innate Immunity and Inflammation." Frontiers in Immunology **9**(141).

Williams, P.A., Harder, J.M., Foxworth, N.E., Cochran, K.E., Philip, V.M., Porciatti, V., ... and John, S.W.M. (2017). "Vitamin B3 modulates mitochondrial vulnerability and prevents glaucoma in aged mice." Science **355**(6326): 756-760.

Williams, P.A., Marsh-Armstrong, N. and Howell, G.R. (2017). "Neuroinflammation in glaucoma: A new opportunity." Experimental Eye Research **157**: 20-27.

Williams, P.A., Morgan, J.E. and Votruba, M. (2010). "Opa1 deficiency in a mouse model of dominant optic atrophy leads to retinal ganglion cell dendropathy." Brain **133**(10): 2942-2951.

Williams, P.A., Piechota, M., von Ruhland, C., Taylor, E., Morgan, J.E. and Votruba, M. (2012). "Opa1 is essential for retinal ganglion cell synaptic architecture and connectivity." Brain **135**(2): 493-505.

Willoughby, C.E., Ponzin, D., Ferrari, S., Lobo, A., Landau, K. and Omidi, Y. (2010). "Anatomy and physiology of the human eye: effects of mucopolysaccharidoses disease on structure and function – a review." Clinical & Experimental Ophthalmology **38**(s1): 2-11.

Wilson, J.H. and Wensel, T.G. (2003). "The nature of dominant mutations of rhodopsin and implications for gene therapy." Molecular Neurobiology **28**: 149-158.

Wolf, C., Gramer, E. Müller-Myhsok, B., Pasutto, F., Reinthal, E., Wissinger, B., and Weisschuh, N. (2009). "Evaluation of nine candidate genes in patients with normal tension glaucoma: a case control study." BMC medical genetics **10**(1): 91.

Wolf, C., Zimmermann, R., Thaher, O., Bueno, D., Wüllner, V., Schäfer, M.K., ... and Methner, A. (2019). "The Charcot–Marie Tooth Disease Mutation R94Q in MFN2 Decreases ATP Production but Increases Mitochondrial Respiration under Conditions of Mild Oxidative Stress." Cells **8**: 1289.

Won, M. and Dawid, I.B. (2018). "PCR artifact in testing for homologous recombination in genomic editing in zebrafish. ." PLOS ONE **12**: e0172802.

Wong, A., Cavelier, L., Collins-Schramm, H.E., Seldin, M.F., McGrogan, M., Savontaus, M.-L. and Cortopassi, G.A. (2002). "Differentiation-specific effects of LHON mutations introduced into neuronal NT2 cells." Human Molecular Genetics **11**(4): 431-438.

Wong-Riley, M. (2010). "Energy metabolism of the visual system." Eye Brain. **2**: 99–116.

Wu, F., Kaczynski, T.J., Sethuramanujam, S., Li, R., Jain, V., Slaughter, M. and Mu, X. (2015). "Two transcription factors, Pou4f2 and Isl1, are sufficient to specify the retinal ganglion cell fate." PNAS **112**(13): E1559-E1568.

Wu, S., Zhou, F., Zhang, Z. and Xing, D. (2011). "Mitochondrial oxidative stress causes mitochondrial fragmentation via differential modulation of mitochondrial fission–fusion proteins." The FEBS Journal **278**(6): 941-954.

Wu, Y.-R., Wang, A.-G., Chen, Y.-T., Yarmishyn, A.A., Buddhakosai, W., Yang, T.-C., ... and Chen, S.-J. (2018). "Bioactivity and gene expression profiles of hiPSC-generated

retinal ganglion cells in MT-ND4 mutated Leber's hereditary optic neuropathy." Experimental Cell Research **363**(2): 299-309.

Xanthoudakis, S., Roy, S., Rasper, D., Hennessey, T., Aubin, Y., Cassady, R., ... and Nicholson, D.W. (1999). "Hsp60 accelerates the maturation of pro-caspase-3 by upstream activator proteases during apoptosis." EMBO J. **18**(8): 2049–2056.

Xiang, M. (1998). "Requirement for Brn-3b in early differentiation of postmitotic retinal ganglion cell precursors." Dev Biol. **197**(2): 155-169.

Xiang, M., Gan, L., Li, D., Chen, Z.Y., Zhou, L., O'Malley Jr., B.W., ... and Nathans, J. (1997). "Essential role of POU–domain factor Brn-3c in auditory and vestibular hair cell development." PNAS **94**(17): 9445-9450.

Xiang, M., Gan, L., Zhou, L., Klein, W.H. and Nathans, J. (1996). "Targeted deletion of the mouse POU domain gene Brn-3a causes selective loss of neurons in the brainstem and trigeminal ganglion, uncoordinated limb movement, and impaired suckling." PNAS **93**(21): 11950-11955.

Xiang, M., Zhou, L., Peng, Y.W., Eddy, R.L., Shows, T.B. and Nathans, J. (1993). "Brn-3b: a POU domain gene expressed in a subset of retinal ganglion cells." Neuron **11**(4): 689-701.

Xiang, M., Zhoui, L., Macke, J.P., Yoshioka, T., Hendry, S.H.C., Eddy, R.L., ... and Nathans, J. (1995). "The Brn-3 Family of POU-Domain Factors: Primary Structure, Binding Specificity, and Expression in Subsets of Retinal Ganglion Cells and Somatosensory Neurons." The Journal of Neuroscience **15**(7): 4752-4785.

Xin, T., Lv, W., Liu, D., Jing, Y. and Hu, F. (2020). "Opa1 Reduces Hypoxia-Induced Cardiomyocyte Death by Improving Mitochondrial Quality Control." Frontiers in cell and developmental biology **8**: 853-853.

Yang, I.H., Gary, D., Malone, M., Dria, S., Houdayer, T., Belegu, V., ... and Thakor, N. (2012). "Axon myelination and electrical stimulation in a microfluidic, compartmentalized cell culture platform." Neuromolecular Med **14**(2): 112-118.

Yang, L., Tang, H., Lin, X., Wu, Y., Zeng, S., Pan, Y., ... and Liu, X. (2020). "OPA1-Exon4b Binds to mtDNA D-Loop for Transcriptional and Metabolic Modulation, Independent of Mitochondrial Fusion." Frontiers in Cell and Developmental Biology **8**(180).

Yang, T.-C., Yarmishyn, A.A., Yang, Y.-P., Lu, P.-C., Chou, S.-J., Wang, M.-L., ... and Chiou, S.-H. (2020). "Mitochondrial transport mediates survival of retinal ganglion cells in affected LHON patients." Human Molecular Genetics **29**(9): 1454-1464.

Yang, T.C., Chuang, J.H., Buddhakosai, W., Wu, W.J., Lee, C.J., Chen, W.S., ... and Chen, S.J. (2017). "Elongation of Axon Extension for Human iPSC-Derived Retinal Ganglion Cells by a Nano-Imprinted Scaffold." Int. J. Mol. Sci. **18**(9): 2013.

Yang, W., Nagasawa, K., Münch, C., Xu, Y., Satterstrom, K., Jeong, S., ... and Haigis, M.C. (2016). "Mitochondrial Sirtuin Network Reveals Dynamic SIRT3-Dependent Deacetylation in Response to Membrane Depolarization." Cell **167**(4): 985-1000.e1021.

Yang, Z., Ding, K., Pan, L., Deng, M. and Gan, L. (2003). "Math5 determines the competence state of retinal ganglion cell progenitors." Developmental Biology **264**(1): 240-254.

Yoneda, T., Benedetti, C., Urano, F., Clark, S.G., Harding, H.P. and Ron, D. (2004). "Compartment-specific perturbation of protein handling activates genes encoding mitochondrial chaperones." Journal of Cell Science **116**: 4055-4066.

Yoon, H.H., Ye, S., Lim, S., Lee, S.E., Oh, S.-J., Jo, A., ... and Jeon, S.R. (2020). "CRISPR/Cas9-mediated gene editing induces neurological recovery in an A53T-SNCA overexpression rat model of Parkinson's disease." bioRxiv.

Yoshioka, N., Gros, E., Li, H.R., Kumar, S., Deacon, D.C., Maron, C., ... and Dowdy, S.F. (2013). "Efficient Generation of Human iPSCs by a Synthetic Self-Replicative RNA." Cell Stem Cell **13**(2): 246-254.

Young, M.J., Bay, D.C., Hausner, G. and Court, D.A. (2007). "The evolutionary history of mitochondrial porins." BMC Evolutionary Biology **7**: 31.

Yu, S.B. and Pekkurnaz, G. (2018). "Mechanisms Orchestrating Mitochondrial Dynamics for Energy Homeostasis." J Mol Biol. **430**(21).

Yu-Wai-Man, P. (2015). "Therapeutic Approaches to Inherited Optic Neuropathies." Semin Neurol **30**(5): 578-586.

Yu-Wai-Man, P. and Chinnery, P.F. (2013). "Dominant optic atrophy—Novel OPA1 mutations and revised prevalence estimates." Ophthalmology **120**(8): 1712.

Yu-Wai-Man, P., Davies, V.J., Piechota, M.J., Cree, L.M., Votruba, M. and Chinnery, P.F. (2009). "Secondary mtDNA defects do not cause optic nerve dysfunction in a mouse model of dominant optic atrophy." Invest Ophthalmol Vis Sci. **50**(10): 4561-4566.

Yu-Wai-Man, P., Griffith, P.G. and Chinnery, P.F. (2011). "Mitochondrial optic neuropathies – Disease mechanisms and therapeutic strategies." Progress in Retinal and Eye Research **30**(2): 81-114.

Yu-Wai-Man, P., Griffiths, P.G., Burke, A., Sellar, P.W., Clarke, M.P., Gnanaraj, L., ... and Chinnery, P.F. (2010). "The Prevalence and Natural History of Dominant Optic Atrophy due to OPA1 Mutations." Ophthalmology **117**(8): 1538-1546.e1531.

Yu-Wai-Man, P., Griffiths, P.G., Gorman, G.S., Lourenco, C.M., Wright, A.F., Auer-Grumbach, M., ... and Chinnery, P.F. (2010). "Multi-system neurological disease is common in patients with OPA1 mutations." Brain **133**: 771–786.

Yu-Wai-Man, P., Sitarz, K.S., Samuels, D.C., Griffiths, P.G., Reeve, A.K., Bindoff, L.A., ... and Chinnery, P.F. (2010). "OPA1 mutations cause cytochrome c oxidase deficiency due to loss of wild-type mtDNA molecules." Human Molecular Genetics **19**(15): 3043–3052.

Yu-Wai-Man, P., Soiferman, D., Moore, D.G., Burté, F. and Saada, A. (2017). "Evaluating the therapeutic potential of idebenone and related quinone analogues in Leber hereditary optic neuropathy." Mitochondrion **36**: 36-42.

Yu-Wai-Man, P., Spyropoulos, A., Duncan, H.J., Guadagno, J.V. and Chinnery, P.F. (2016). "A multiple sclerosis-like disorder in patients with OPA1 mutations." Annals of Clinical and Translational Neurology **3**(9): 723-729.

Yu-Wai-Man, P., Turnbull, D.M. and Chinnery, P.F. (2002). "Leber hereditary optic neuropathy." Journal of Medical Genetics **39**: 162-169.

Yu-Wai-Man, P., Votruba, M., Burte, F., La Morgia, C., Barboni, P. and Carelli, V. (2016). "A neurodegenerative perspective on mitochondrial optic neuropathies." Acta Neuropathologica **132**(6): 789-806.

Yu-Wai-Man, P., Votruba, M., Moore, A.T. and Chinnery, P.F. (2014). "Treatment strategies for inherited optic neuropathies: past, present and future." Eye **28**: 521-537.

Yuan, A., Rao, M.V., Veeranna and Nixon, R.A. (2017). "Neurofilaments and Neurofilament Proteins in Health and Disease." Cold Spring Harbor Perspectives in Biology **9**(4).

Zagozewski, J.L., Zhang, Q. and Eisenstat, D.D. (2014). "Genetic regulation of vertebrate eye development." Special Issue: Genetics and Translational Medicine **86**(5): 453-460.

Zanna, C., Ghelli, A., Porcelli, A.M., Karbowski, M., Youle, R.J., Schimpf, S., ... and Carelli, V. (2008). "OPA1 mutations associated with dominant optic atrophy impair oxidative phosphorylation and mitochondrial fusion." Brain **131**(2).

Zanon-Moreno, V., Marco-Ventura, P., Lleo-Perez, A., Pons-Vazquez, S., Garcia-Medina, J.J., Vinuesa-Silva, I., ... and Pinazo-Duran, M.D. (2008). "Oxidative Stress in Primary Open-angle Glaucoma." Journal of Glaucoma **17**(4).

Zhang, J., Liu, X., Liang, X., Lu, Y., Zhu, L., Fu, R., ... and Guan, M.-X. (2017). "A novel ADOA-associated OPA1 mutation alters the mitochondrial function, membrane potential, ROS production and apoptosis." Scientific Reports **7**(1): 5704.

Zhang, Q., Vuong, H., Huang, X., Wang, Y.L., Brecha, N.C., Pu, M.L. and Gao, J. (2013). "Melanopsin-expressing retinal ganglion cell loss and behavioral analysis in the Thy1-CFP-DBA/2J mouse model of glaucoma." Science China Life Sciences **56**: 720-730.

Zhang, R., Koido, M., Tadokoro, T., Ouchi, R., Matsuno, T., Ueno, Y., ... and iTaniguchi, H. (2018). "Human iPSC-Derived Posterior Gut Progenitors Are Expandable and Capable of Forming Gut and Liver Organoids." Stem Cell Reports **10**(3): 780-793.

Zhang, X., Huang, C.T., Chen, J., Pankratz, M.T., Xi, J., Li, J., ... and Zhang, S.C. (2010). "Pax6 is a human neuroectoderm cell fate determinant." Cell Stem Cell. **7**(1): 90-100.

Zhang, X., Tenerelli, K., Wu, S., Xia, X., Yokota, S., Sun, C., ... and Chang, K.C. (2020). "Cell transplantation of retinal ganglion cells derived from hESCs." Restorative Neurology and Neuroscience **38**(2): 131-140.

Zhang, X.-M., Li Liu, D.T., Chiang, S.W.-Y., Choy, K.-W., Pang, C.-P., Lam, D.S.-C. and Yam, G.H.-F. (2010). "Immunopanning purification and long-term culture of human retinal ganglion cells." Mol Vis. **16**: 2867-2872.

Zhao, Q., Wang, J., Levichkin, I.V., Stasinopoulos, S., Ryan, M.T. and Hoogenraad, N.J. (2002). "A mitochondrial specific stress response in mammalian cells." EMBO J **21**: 4411-4419.

Zhao, X., Zhang, Y., Lu, L. and Yang, H. (2020). "Therapeutic Effects of Idebenone on Leber Hereditary Optic Neuropathy." Current Eye Research: 1-9.

Zheng, X., Boyer, L., Jin, M., Mertens, J., Kim, Y., Ma, L., ... and Hunter, T. (2016). "Metabolic reprogramming during neuronal differentiation from aerobic glycolysis to neuronal oxidative phosphorylation." eLife **5**: e13374.

Zhong, X., Gutierrez, C., Xue, T., Hampton, C., Vergara, M.N., Cao, L.-H., ... and M.V., C. (2014). "Generation of three dimensional retinal tissue with functional photoreceptors from human iPSCs." Nat Commun **5**: 4047.

Zhou, C., Sun, H., Zheng, C., Gao, J., Fu, Q., Hu, N., ... and Lyu, J. (2018). "Oncogenic HSP60 regulates mitochondrial oxidative phosphorylation to support Erk1/2 activation during pancreatic cancer cell growth." Cell Death & Disease **9**: 161.

Zhou, W. and Freed, C.R. (2009). "Adenoviral Gene Delivery Can Reprogram Human Fibroblasts toInduced Pluripotent Stem Cells." Stem Cells **27**(11): 2667-2674.

Ziviani, E., Tao, R.N. and Whitworth, A.J. (2010). "Drosophila Parkin requires PINK1 for mitochondrial translocation and ubiquitinates Mitofusin." PNAS **107**(11): 5018-5023.

Zolessi, F.R., Poggi, L., Wilkinson, C.J., C.B., C. and Harris, W.A. (2006). "Polarization and orientation of retinal ganglion cells in vivo." Neural Development **1**.

Zorova, L.D., Popkov, V.A., Plotnikov, E.Y., Silachev, D.N., Pevzner, I.B., Jankauskas, S.S., ... and Zorov, D.B. (2018). "Mitochondrial membrane potential." Anal Biochem. **552**: 50–59.

Zou, C. and Levine, E.M. (2012). "Vsx2 Controls Eye Organogenesis and Retinal Progenitor Identity Via Homeodomain and Non-Homeodomain Residues Required for High Affinity DNA Binding." PLOS Genetics **8**(9): e1002924.

Zuber, M.E., Gestri, G., Viczian, A.S., Barsacchi, G. and Harris, W.A. (2003). "Specification of the vertebrate eye by a network of eye field transcription factors." Development **130**: 5155-5167.

Züchner, S., Mersiyanova, I.V., Muglia, M., Bissar-Tadmouri, N., Rochelle, J., Dadali, E.L., ... and Vance, J.M. (2004). "Mutations in the mitochondrial GTPase mitofusin 2 cause Charcot-Marie-Tooth neuropathy type 2A." Nature Genetics **36**(5): 449-451.

Zurita-Díaz, F., Galera-Monge, T., Moreno-Izquierdo, A., Corton, M., Ayuso, C., Garesse, R. and Gallardo, M.E. (2017). "Establishment of a human DOA 'plus' iPSC line, IISHDOi003-A, with the mutation in the OPA1 gene: c.1635C>A; p.Ser545Arg." Stem Cell Research **24**: 81-84.

Chapter 8: Appendices

8.1 Appendix A

All materials utilised in this thesis are stated below.

0.01 % Poly-L-lysine (PLL) – Sigma, P4707-50ML.

0.05 % Trypsin-EDTA – Gibco, 25300-054.

0.2 mL 8-strip PCR tube, individually attached domed caps – StarLab, S1602-2900.

2X LabTAQ hi-rox green – LabTech, LTSHR-1.

4',6-diamidino-2-phenylindole dilactate (DAPI) dilactate – Sigma, D9564-10MG.

6-well CytoOne plate, TC treated – StarLab, CC7682-7506.

10 % SDS solution – Severn Biotech Ltd, 20-4000-10.

12-well CytoOne plate, TC treated – StarLab, CC7682-7512.

16 % paraformaldehyde (PFA) – ThermoFisher, 28908.

24-well CytoOne plate, TC treated – StarLab, CC7682-7524.

30 % Acrylamide – National diagnostics, EC-890.

35 mm µ-Dish, high Glass Bottom – Ibidi, 81158.

90 mm Fisherbrand asceptic petri dish – Fisher scientific – 12664785.

96-well CytoOne plate, TC treated – StarLab, CC7682-7596.

100 % Ethanol – VWR, 20821.310P.

100 % Methanol – VWR, 20847.320.

Accutase solution – Sigma, A6964-100ML.

Agar powder – Bioline, BIO-41025.

Alt-R® S.p. Cas9 Nuclease V3, 100 µg – IDT, 1081058

Alt-R® Cas9 Electroporation Enhancer, 2 nmol – IDT, 1075915

Alt-R® CRISPR-Cas9 tracrRNA, 20 nmol – IDT, 1072533

Alt-R® HDR Enhancer, 100 µL – IDT, 1081072

Ammonium persulfate – Sigma, A3678.

Ampicillin sodium salt – Sigma, A1066.

Antibiotic-antimycotic (100X) – Gibco, 15240-062.

B27 supplement – Gibco, 17504-044.

Bambanker freeing medium - Nippon Genetics Europe, BB01

BBsI – NEB, R0539S.

Blebbistatin – Sigma, B0560-1MG.

Bone morphogenic protein 4 (BMP4; HeLa derived) – Peprotech, 120-05.

Bovine Serum Albumin – Sigma, A7906-100G.

β-mercaptoethanol – Gibco, 21985-023.

Cell Dissociation Buffer, Enzyme free, PBS – Gibco, 13151-014.

Cell Line Nucleofector® Kit R – Lonza, VCA-1001.

DAKO Fluorescent mounting medium – Dako, S3023.

DAPT – Abcam, Ab120633.

DMEM/F12 with GlutaMAX – Gibco, 31331-028.

DMEM with GlutaMAX – Gibco, 41966-029.

Dorsomorphin – Stratech, B3252-APE.

Dried skimmed milk powder – Marvel.

Dulbecco Phosphate Buffered Saline (DPBS), pH 7-7.3 – Gibco, 14190-094.

Dulbeccos Phosphate Buffers Saline tablets – Oxoid, BR0014G.

Emetine dihydrochloride hydrate – Sigma, E2375-500MG.

Essential 8 (E8) Flex media – Gibco, A2858501.

Falcon 70 µm cell strainer – Fisher scientific, 10788201.

Falcon cell culture flask 75 cm^2 – VWR, 734-0050.

Falcon cell culture flask 175 cm^2 – VWR, 734-0047.

Feather C35 microtome blade – Cellpath, JDA-0700-00A.

Foetal Bovine Serum (FBS) – Labtech, FCS-SA.

Forkskolin – Peprotech, 6652995.

Gelatin – Sigma, G1393-100ML.

Geltrex LDEV-free reduced growth factor basement membrane matrix – Gibco, A1413202.

High Capacity cDNA RT kit with RNase Inhibitor – ThermoFisher, 4374966.

Human Dermal Fibroblast, neonatal – Sigma, 106-05N.

IDE2 – Peprotech, 1139374.

KnockOut serum replacement – Gibco, 10828-010.

Lysogeny broth (LB), Miller – Sigma, L3522-1KG.

LB broth with agar (Lennox) – Sigma, L2897-1KG.

Luminata Crescendo western HRP substrate – Millipore, WBLUR0500.

Luminata Forte western HRP substrate – Millipore, WBLUF05000.

Matrigel®, Growth Factor Reduced Basement Membrane, LDEV-free – Corning, 354230.

MicroAmp Optical 96-well reaction plate – Thermofisher, N8010560.

Mirus TransIT LT1 – Mirus, MR2304.

MitoTracker™ Green FM – Thermofisher, M7514.

MultiScreen® PCRµ96 Filter Plate – Millipore, LSKMPCR10.

N2 supplement – Gibco, 17502-048.

Neurobasal media – Gibco, 21103049.

N,N,N',N'-Tetramethyl-ethylenediamine (TEMED) – Sigma, T9281.

Nitrocelllose Blotting membrane – GE healthcare, 10600002

Non-Essential Amino Acids (NEAA) – Gibco, 11140-035.

Normal donkey serum (NDS) – Sigma, 09663-10ML.

Nunc™ EasYFlask™ 25 cm^2 cell culture flask – Fisher scientific, 12034917.

Oligomycin A, ATP synthase inhibitor – Abcam, ab143423.

PageRulerTM Plus Prestained Protein Ladder – ThermoFisher, 26619.

Penicillin-streptomycin (P/S) – Gibco, 15140122.

Pierce BCA protein assay kit – ThermoFisher, 23227.

Proteinase inhibitor cocktail (PIC) – Sigma, P8340.

QIAshredders – Qiagen, 79656.

Quick-Load® 1 kb plus DNA ladder – NEB, N0550S.

Recombinant human laminin-521 – Thermofisher, 78060.

Recombinant human noggin – Stem Cell Technologies, A29249.

Recombinant human DKK1 – Peprotech, 120-30.

Recombinant Insulin-like Growth Factor (IGF) 1 – Peprotech, 100-11.

RNase-Free DNase Set – Qiagen, 79254.

RNeasy mini kit – Qiagen, 79254.

Safeview nucleic acid stain – NBS Biologicals, NBS-SV.

Seahorse XF base medium, 500 mL – Agilent, 103334-100.

Seahorse XF Cell Mito Stress Test Kit – Agilent, 103015-100.

Seahorse XF 1.0 M glucose solution, 50 mL – Agilent, 103577-100.

Seahorse XF 100 mM pyruvate solution, 50 mL – Agilent, 103578-100.

Seahorse XFe96 FluxPaks (mini) – Agilent, 102601-100.

SOC Media – NEB, B9020S.

Sodium butyrate – Sigma, B5887.

Sodium dodecyl sulphate (SDS) – Sigma, L3771.

StemFlex media™ – Invitrogen, A3349401.

Superfrost plus glass microscope slides – Fisher scientific, 10149870.

T7 DNA Ligase – NEB, M0318.

T7 Endonuclease I – NEB, M0302.

TaqMan® Fast advanced Master Mix – ThermoFisher, 4444964.

TaqMan® hPSC Scorecard Panel, Fast 96-well – ThermoFisher, A15876.

Tetro cDNA Synthesis Kit – Bioline, BIO-65043.

Tris-Glycine 10X solution – Severn Biotech Ltd, 20-6300-50.

Tris-Glycine SDS 10X solution – Severn Biotech Ltd, 20-6400-50.

Triton X100 – Sigma, T8787.

Tryple express – Gibco, 12604-013.

TWEEN 20 – Sigma, P9146.

Vectorshield Vibrance antifade mounting media – Vector laboratories, H-1700-10.

Wizard® Plus SV Minipreps DNA purification system – Promega, A1460.

Wizard® SV Genomic DNA purification system – Promega, A2360.

8.1.1 Buffers and Solutions

10 % acrylamide resolving gels – 370 µM Tris (pH 8.8), 10 % (v/v) acrylamide, 0.1 % (v/v) SDS, 0.1% (v/v) APS, 0.05 % (v/v) TEMED, diluted in ddH_2O.

10 % acrylamide stacking gels – 125 µM Tris (pH 6.8), 4 % (v/v) acrylamide, 0.1 % (v/v) SDS, 0.1 % (v/v) APS, 0.2 % (v/v) TEMED, diluted in ddH_2O.

LB agar plates – 17.5 g/l LB agar (Miller) powder, diluted in ddH_2O with antibiotic as stated in methods.

LB broth – 12.5 g/l LB broth with agar (Lennox) power, diluted in ddH_2O with antibiotic as stated in methods.

Ponceau S stain – 0.5 % (w/v) Ponceau S, 1 % (v/v) acetic acid, diluted in ddH_2O.

Running buffer – 1X Tris-glycine SDS, diluted in ddH_2O.

Transfer buffer – 1X Tris-glycine with 20 % (v/v) methanol, diluted in ddH_2O.

8.2 Appendix B

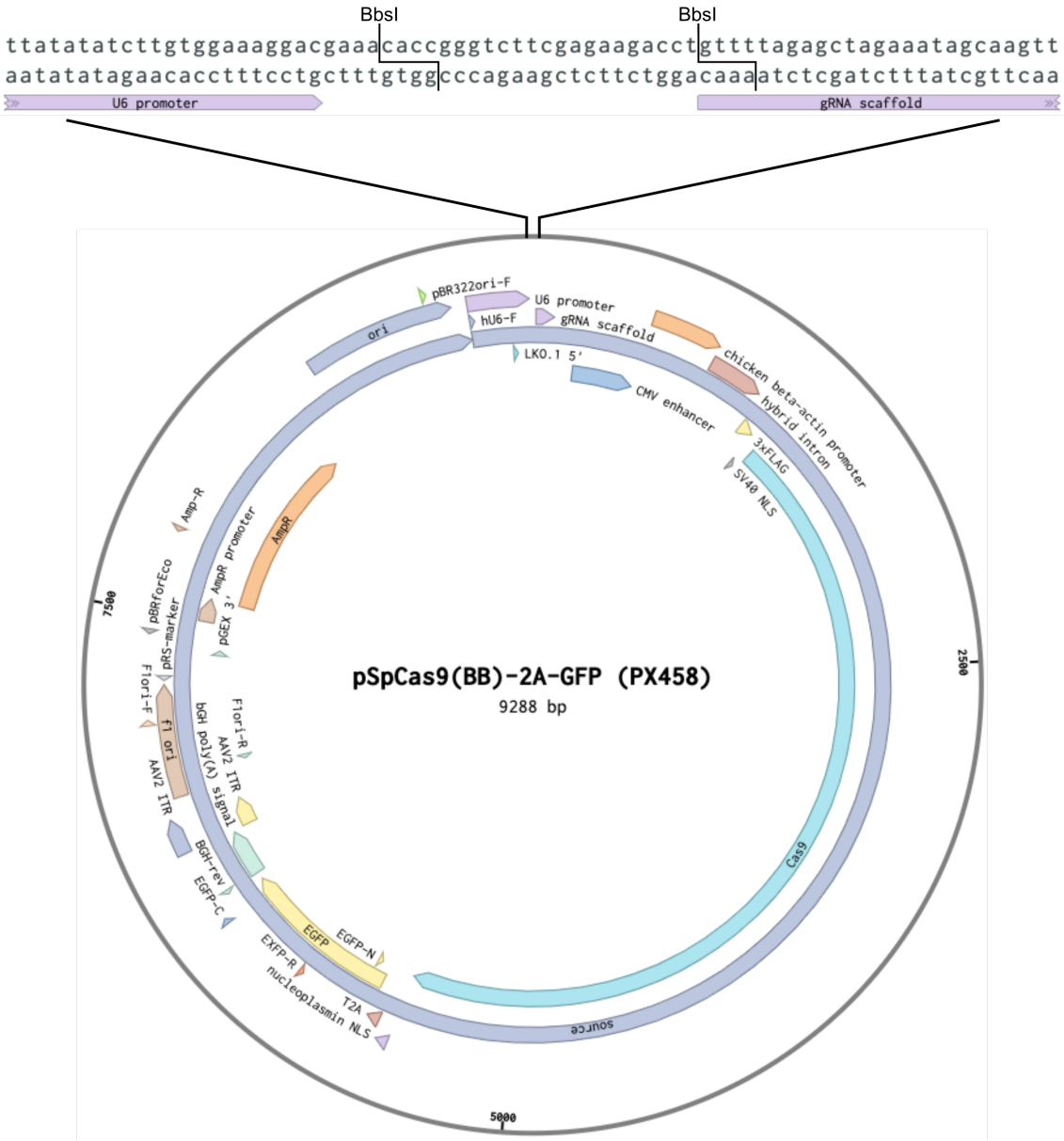

Figure 8.1. pSpCas9 (BB) - 2A - GFP (PX458) plasmid map.

CRISPR/Cas9 plasmid PX458 used for gene editing of *OPA1* in HDF control cells. Expanded region shows area of guide oligonucleotide insertion between 2 BbsI restriction enzyme sites.

8.3 Appendix C

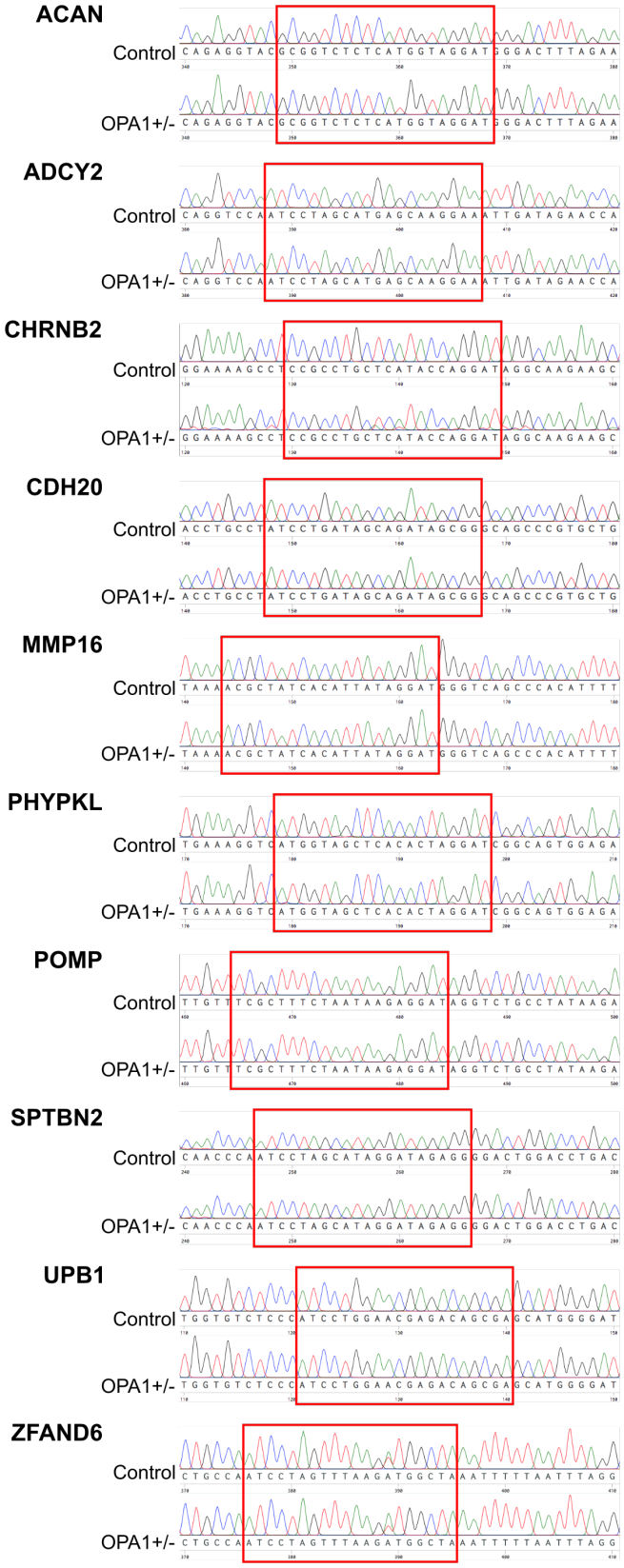

Figure 8.2. Sequence traces for the top 10 off-target genes for heterozygous knockout of *OPA1* gRNA 2.

Sequences corresponding to off-target gRNA sequences boxed in red. No off-target CRISPR/Cas9 mutations are identified in Sanger sequencing traces for *OPA1* edited cells.

8.4 Appendix D

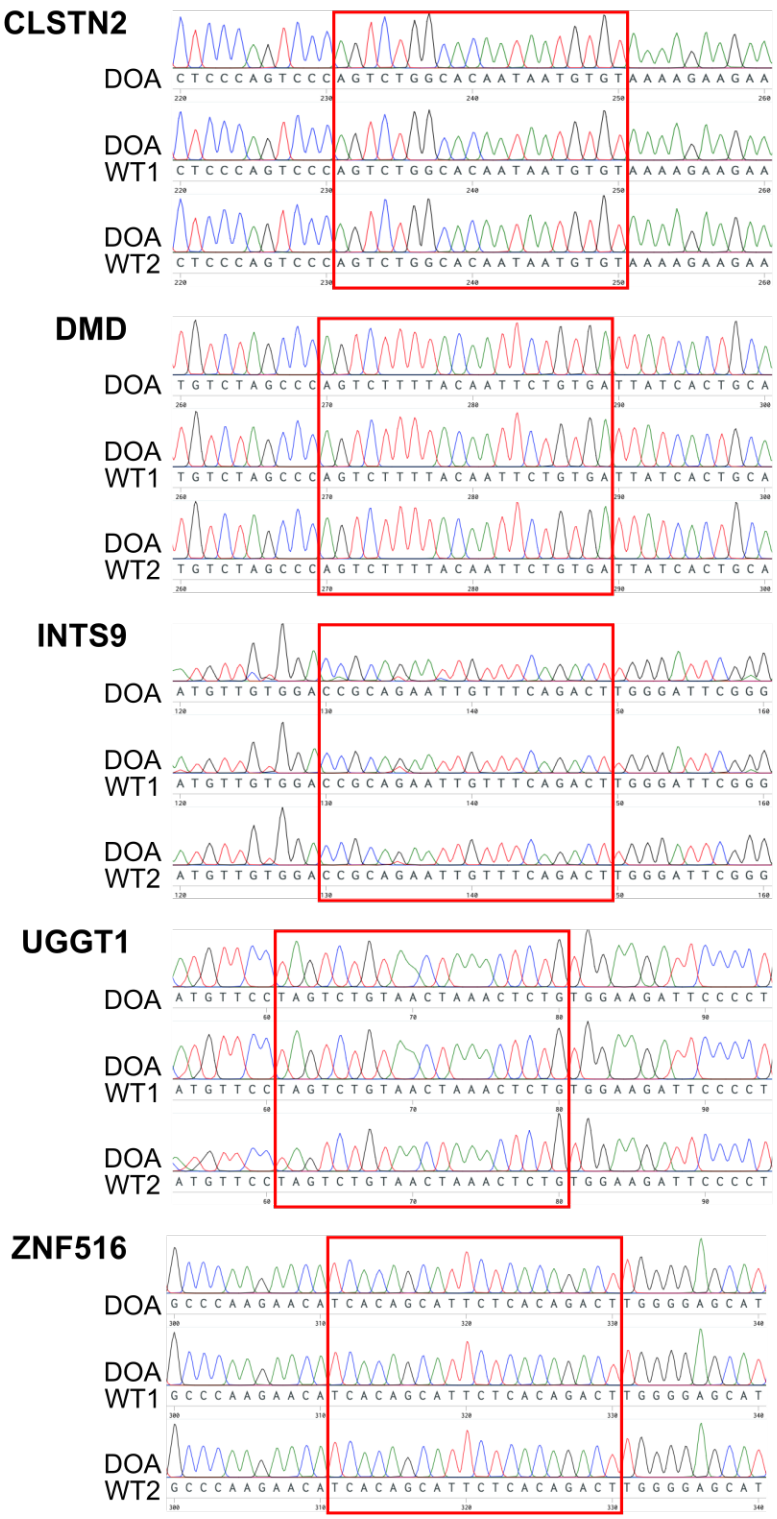

Figure 8.3. Sequence traces for the top 5 off-target genes for HDR gRNA 2.

Sequences corresponding to off-target gRNA sequences boxed in red. No off-target CRISPR/Cas9 mutations are identified in Sanger sequencing traces.